PHYSICAL PROPERTIES OF LIPIDS

edited by

Alejandro G. Marangoni
University of Guelph
Guelph, Ontario, Canada

Suresh S. Narine
University of Alberta
Edmonton, Alberta, Canada

MARCEL DEKKER, INC. NEW YORK • BASEL

Copyright 2002 by Marcel Dekker. All Rights Reserved.

ISBN: 0-8247-0005-8

This book is printed on acid-free paper.

Headquarters
Marcel Dekker, Inc.
270 Madison Avenue, New York, NY 10016
tel: 212-696-9000; fax: 212-685-4540

Eastern Hemisphere Distribution
Marcel Dekker AG
Hutgasse 4, Postfach 812, CH-4001 Basel, Switzerland
tel: 41-61-261-8482; fax: 41-61-261-8896

World Wide Web
http://www.dekker.com

The publisher offers discounts on this book when ordered in bulk quantities. For more information, write to Special Sales/Professional Marketing at the headquarters address above.

Copyright © 2002 by Marcel Dekker, Inc. All Rights Reserved.

Neither this book nor any part may be reproduced or transmitted in any form or by any means, electronic or mechanical, including photocopying, microfilming, and recording, or by any information storage and retrieval system, without permission in writing from the publisher.

Current printing (last digit):
10 9 8 7 6 5 4 3 2 1

PRINTED IN THE UNITED STATES OF AMERICA

Copyright 2002 by Marcel Dekker. All Rights Reserved.

To our children:
Isaac and Joshua Marangoni
and
Rudra, Geetanjali, and Vandana Narine

Copyright 2002 by Marcel Dekker. All Rights Reserved.

Preface

In many ways, the development of a comprehensive understanding of the relationships among molecular compositions, processing conditions, structural levels, and final physical macroscopic functionality of lipid systems is still a work in progress. Although gigantic strides in the elucidation of such relationships have been made in recent years, we are still far away from enjoying the benefits of a comprehensive theoretical understanding of structure formation as it relates to processing conditions, and physical functionality as it relates to final structure, that are perhaps more commonplace in the areas of metallurgy and ceramics.

However, the pursuit of such a theoretical framework not only is of immense academic importance but is paramount in the industrial applications of lipid systems. Among the widely varying industrial uses to which lipids are put are their uses in food systems. This book therefore attempts to provide an update on the advances in the theoretical understanding of such relationships in food lipids.

The book provides a snapshot of current research efforts in four major areas: fat crystallization, structure–rheology–texture relationships, emulsifiers, and processing. The book is intended to augment the excellent food lipid literature that already discusses other important areas of physical properties of lipids. The book is targeted at graduate students and researchers working in lipid research. A deliberate attempt was made to avoid duplication of the information already available in the current literature. For example, in the crystallization section, rather than provide a comprehensive review of this area, we focus on two topics not covered previously in great depth: the modeling of triglyceride crystallization and fat crystallization in O/W emulsions controlled by hydrophobic emulsifier additives.

Copyright 2002 by Marcel Dekker. All Rights Reserved.

The next section, structure–rheology–texture relationships, deals with the quantification and modeling of the structure and the mechanical properties of lipid networks, and then examines cocoa butter and milkfat within this general framework. The chapter on milkfat focuses on the effects of the minor components contained in native milkfat on structure formation and final mechanical properties. This section also contains a chapter on the use of fluorescence depolarization spectroscopy as a tool to determine microviscosity and structural order in lipid systems and an overview of the texture of fat systems.

The penultimate section of the book, dealing with emulsifiers, highlights the use of fat crystals in the stabilization of emulsion systems and the design of emulsifiers in low-fat spreads.

The final section of the book, which examines research efforts in processing, contains review chapters in the important areas of deodorization and fat fractionation. Additionally, chapters are included on the physical effects of hydrogenation (as it applies to sunflower oil) and physical effects of blending and interesterification (both chemical and enzymatic) as they apply to a number of fat systems.

The book is not intended to be read sequentially, although it is our hope that readers—students of lipids as well as current researchers in the field—will find all the information useful. The book is designed to be used as a reference text, either as supplementary material for a senior graduate-level course on the physical properties of lipids or as an introduction to the exciting new areas of research into the theoretical understanding of physical properties of lipids. It is our intention to update the book as needed to include newer advances in the field.

The book itself would not have been possible without the gargantuan efforts of the contributing authors—ours was the relatively easy task of soliciting, editing, and compiling their work and genius. To the contributing authors, we offer our sincere thanks (in order of appearance): Philippe Rousset, Tarek Awad and Kiyotaka Sato, Sara McGauley, Amanda Wright, John deMan, Leny deMan, Dérick Rousseau, Nissim Garti, Alan Brench, David Illingworth and Lidia Herrera. While we can claim no credit for their work, we bear sole responsibility for any errors. We would also like to express our sincere thanks to Marcel Dekker, Inc., for their patience and helpful editing over the time it took to put this book together. Lastly, we would like to thank our wives, Rekha Narine and Dianne Del Zotto, for their continual support of our academic endeavors.

Alejandro G. Marangoni
Suresh S. Narine

Copyright 2002 by Marcel Dekker. All Rights Reserved.

Contents

Copyright 2002 by Marcel Dekker. All Rights Reserved.

Copyright 2002 by Marcel Dekker. All Rights Reserved.

Contributors

Tarek Samir Awad Faculty of Applied Biological Science, Hiroshima University, Higashi-Hiroshima, Japan

W. Alan Brench AB Consulting, Hampstead, Maryland

John M. deMan Department of Food Science, University of Guelph, Guelph, Ontario, Canada

Leny deMan deMan Food Technology Services, Inc., Guelph, Ontario, Canada

Nissim Garti Casali Institute of Applied Chemistry, The Hebrew University of Jerusalem, Jerusalem, Israel

María Lidia Herrera Department of Industries, University of Buenos Aires, Buenos Aires, Argentina

David Illingworth Cheese and Milkfat Technology, New Zealand Dairy Research Institute, Palmerston North, New Zealand

Alejandro G. Marangoni Department of Food Science, University of Guelph, Guelph, Ontario, Canada

Sara E. McGauley Department of Food Science, University of Guelph, Guelph, Ontario, Canada

Copyright 2002 by Marcel Dekker. All Rights Reserved.

Suresh S. Narine Department of Agricultural, Food, and Nutritional Science, University of Alberta, Edmonton, Alberta, Canada

Dérick Rousseau Department of Nutrition, Ryerson University, Toronto, Ontario, Canada

Philippe Rousset Nestlé Research Center, Nestec Ltd., Lausanne, Switzerland

Kiyotaka Sato Faculty of Applied Biological Science, Hiroshima University, Higashi-Hiroshima, Japan

Amanda J. Wright Department of Food Science, University of Guelph, Guelph, Ontario, Canada

Copyright 2002 by Marcel Dekker. All Rights Reserved.

1
Modeling Crystallization Kinetics of Triacylglycerols

Philippe Rousset
Nestlé Research Center, Nestec Ltd., Lausanne, Switzerland

I. INTRODUCTION

Prediction of crystallization with computer modeling may have many applications for the food industry. It would allow a better understanding of the phenomena occurring during manufacturing, making possible the optimization of ancient empirical processes or the development of new, more efficient unit operations. For example, changing the fat source in a food product may completely change the cooling process. Empirical determination of new process parameters is expensive, as many pilot-scale or even production line trials have to be performed. In contrast, computer modeling would quickly, easily, and cheaply determine the best cooling conditions for the new food system.

Nevertheless, much work still has to be done to reach a state of knowledge equivalent to that in the field of metals, where modeling of solidification is widely used to simulate the casting of turbine blades for aircraft reactors or the continuous flow of aluminum or steel. As a matter of fact, the triacylglycerol systems that compose fat are quite complex. Thermodynamic and kinetics data necessary for the models are rarely known and are sometimes too complex to be acquired.

This chapter presents the most recent advances in this domain, divided into two parts. First microscopic models are presented. These use the theory of crystallization kinetics at the crystal level. Second, macroscopic models are detailed. These treat crystallization more globally through its description at the macroscopic scale.

Copyright 2002 by Marcel Dekker. All Rights Reserved.

II. THEORY: KINETICS OF CRYSTALLIZATION

The theory of crystallization is not presented in detail in this chapter. Only the important points necessary for the understanding of crystallization models are mentioned. For a more exhaustive general description of solidification, readers should refer to Strickland-Constable [1]; for lipids, Boistelle [2]; for metals, Chalmers [3], Flemings [4], and Kurz and Fischer [5]; for polymers, Long et al. [6] and Wunderlich [7].

A fat is composed of many triacylglycerols (TAGs), so the correct approach to examining its crystallization would be to consider it as a multicomponent system and describe this system with a phase diagram. If, as in a fat, more than 10 and up to hundreds of thousands of components are present, the resolution of thermodynamics and kinetics becomes completely unrealistic due to the complexity. Therefore, two simplified approaches are used to overcome this problem [2]. If the TAGs composing the fat are relatively similar, it is assumed that only one component is present. Crystallization occurs in the bulk, i.e., in the melt. This theory is described in paragraphs Sections II.A–II.E, where the equations presented focus on crystallization in a pure material. The second option, which is chosen for fats that clearly contain two families of quite different TAGs, is to consider the fat as two separate molecules that are immiscible in the solid state. The TAGs with the lower melting temperature compose the solution, and the TAGs with the higher melting temperature are considered the solute. This approach is often used by researchers in the field of fractionation. Crystallization is assumed to be governed by the solubility of the solute in the solution. The kinetic theory is slightly different than in the first case and is presented in Section II.F.

In the case of a pure component, below the temperature of fusion, T_f, thermodynamics predicts that the stable phase is the solid. In reality, the liquid does not solidify instantaneously. Transition of the molecules from the liquid state to the solid state, which is energetically more stable, is not direct. The system must go through unstable transitory states that require overcoming energy barriers (Fig. 1). Kinetics studies are therefore essential to complete the thermodynamic analysis and to predict the temporal evolution of the systems. The basic theory for nucleation and growth is presented below.

A. Nucleation in Bulk

The first stage of crystallization in an undercooled liquid (i.e., below the melting temperature) is the formation of solid embryos. Transformation of the liquid into a solid generates a decrease in the Gibbs free energy per unit volume, ΔG_v:

$$\Delta G_v = -\frac{\Delta H_{m,f}\,\Delta T}{T_f V_m} \tag{1}$$

Copyright 2002 by Marcel Dekker. All Rights Reserved.

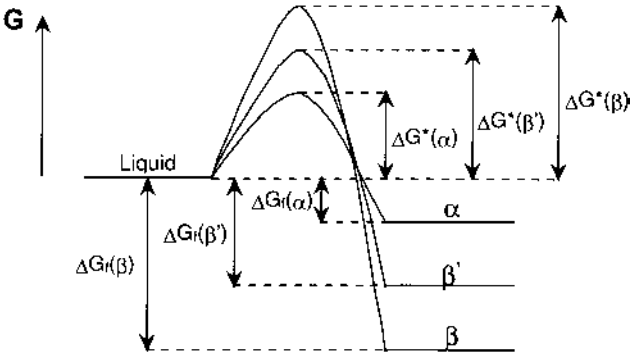

Figure 1 Schematics of the free energy of fusion and of activation for three polymorphic phases of a TAG, at given conditions (P,T) below their temperature of fusion.

where $\Delta H_{m,f}$ is the molar enthalpy of fusion, ΔT is the undercooling ($= T_f - T$), and V_m is the molar volume.

This creation of solid in the liquid generates a solid/liquid interface. It is associated with a change in the surface free energy, ΔG_s:

$$\Delta G_s = \sigma \tag{2}$$

where σ is the surface energy.

In the simple case of a pure substance and homogeneous nucleation in the liquid, the change in the Gibbs free energy due to the creation of a solid embryo is given by

$$\Delta G_{\text{hom}} = \Delta G_v V + \Delta G_s S = -\frac{\Delta H_{m,f}\Delta T}{T_f V_m} V + \sigma S \tag{3}$$

where V and S are the volume and surface, respectively, of the formed embryo. If the solid is isotropic, embryos are spherical and the expressions of S and V are simple. Figure 2 shows the variation of ΔG_{hom} as a function of the radius of the embryo. There is a critical radius r^* (corresponding to n^* molecules composing the embryo) where ΔG_{hom} is maximum:

$$r^* = -\frac{2\sigma}{\Delta G_v} \quad \text{and} \quad \Delta G_{\text{hom}}(n^*) = -\frac{16\pi}{3}\left(\frac{\sigma^3}{\Delta G_v^2}\right) = \frac{16\pi}{3}\left(\frac{\sigma^3 T_f^2 V_m^2}{\Delta H_{m,f}^2 \Delta T^2}\right) \tag{4}$$

Growth of the embryo does not induce a decrease in the free energy up to this critical radius r^*. Therefore, below this radius the embryo is unstable. It becomes a stable nucleus only above r^*.

Copyright 2002 by Marcel Dekker. All Rights Reserved.

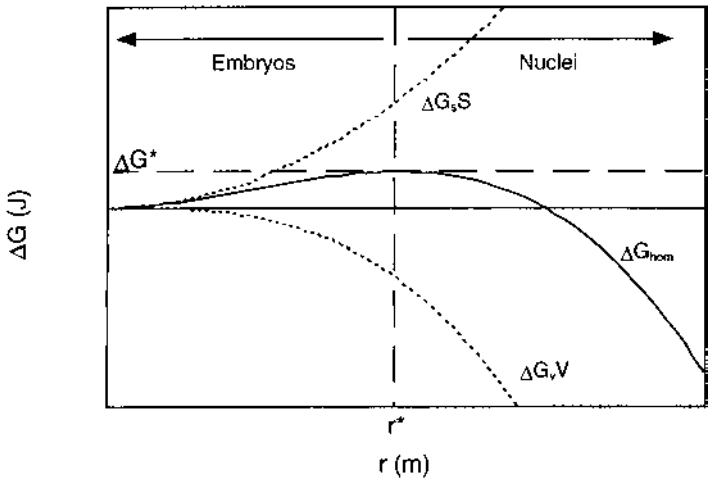

Figure 2 Change in Gibbs free energy, ΔG, generated by the creation of a solid spherical embryo in the liquid, as a function of its radius r. The critical radius r^* determines the limit between the domain of the unstable embryo ($r < r^*$) and that of the stable nucleus ($r > r^*$).

If we suppose that the embryos follow a Boltzmann distribution as a function of their free energy, the density of embryos of each size can be estimated in the stationary state:

$$N_n = N_0 \exp\left[- \frac{\Delta G_{\text{hom}}(n)}{k_B T} \right] \tag{5}$$

where N_n is the number of embryos containing n molecules, N_0 is the number of molecules per unit volume, and k_B is the Boltzmann constant.

From these expressions and from studies on the germination of drops of a liquid in a gas [8,9], Turnbull and Fischer [10] developed a model for homogeneous nucleation of a solid in a liquid. In the simplified case, they expressed the nucleation rate I_{hom} as

$$I_{\text{hom}} = N_0 \nu_0 \, p N_s^0 \exp\left[- \frac{\varepsilon}{k_B T} \right] \exp\left[- \frac{\Delta G_{\text{hom}}(n^*)}{k_B T} \right] \tag{6}$$

where ν_0 is the atomic vibration frequency, p is the adsorption probability of a molecule, N_s^0 is the density of sites on a nucleus, and ε is the activation free energy necessary to incorporate a molecule in the crystalline nucleus.

Copyright 2002 by Marcel Dekker. All Rights Reserved.

Except in the case of an amorphous transformation, the exponential term of the activation energy is usually small and can be considered constant if the temperature does not change much. It is estimated to be about 10^{-5} for TAGs [11].

In reality, nucleation is usually heterogeneous for TAGs and other molecules. This means that nucleation occurs on impurities in the system, requiring less undercooling than homogeneous nucleation. Heterogeneous nucleation can be estimated similarly to homogeneous nucleation [12]. The heterogeneous nucleation rate, I_{het}, is expressed by

$$I_{het} = I_{0,het} \exp\left[- \frac{\Delta G_{het}(n^*)}{k_B T} \right] = I_{0,het} \exp\left[- \frac{\Delta G_{hom}(n^*) f_\theta}{k_B T} \right] \tag{7}$$

where $\Delta G_{het}(n^*)$ is the free energy per unit volume of a heterogeneous nucleus of critical size and f_θ (<1) is a correction factor for the surface energy that derives the expression of the formation energy of a heterogeneous embryo of critical size from the expression of the formation energy of a homogeneous embryo of similar size. The correction factor f_θ is a function of θ, the wetting angle of the nucleus on the impurity substrate.

For polymers, the expression is slightly different because the term $\varepsilon/k_B T$ cannot be considered a constant close to the amorphous transition temperature [13]. Like viscosity, it is a function of the temperature. A simple mathematical approximation [7] is given by

$$\frac{\varepsilon}{k_B T} = a_\varepsilon + \frac{b_\varepsilon}{k_B (T - T_g + C_2)} \tag{8}$$

where a_ε and b_ε are constants and $T_g - C_2$ is the Gibbs–di Marcio temperature of the amorphous transition. C_2 is a constant found experimentally to be close to 30°C.

Finally, the heterogeneous nucleation rate of polymers can be expressed as

$$I_{het,pol} = I_{0,het,pol} \exp\left[- \frac{b_\varepsilon}{k_B (T - T_g + C_2)} \right] \exp\left[- \frac{\Delta G_{hom}(n^*) f_\theta}{k_B T} \right] \tag{9}$$

where ΔG_{hom} is given by

$$\Delta G_{hom}(n^*) = 32 \frac{\sigma^2 \sigma_e T_f^2 V_m^2}{\Delta H_{m,f}^2 \Delta T^2} \tag{10}$$

If we compare Eq. (4) with Eq. (10), we see that the term σ^3 is replaced by $\sigma^2 \sigma_e$. This is due to the anisotropy of the molecules. σ and σ_e are the surface energies of the growing face and the transverse face of the crystal, respectively. TAGs

Copyright 2002 by Marcel Dekker. All Rights Reserved.

are not isotropic. Their behavior is probably close to that of polymers and is likely to follow Eq. (9).

Equations (6), (7), and (9) express the nucleation rate in simple cases. But before nucleation can start, a stationary distribution of solid embryos of all sizes must be established. When a liquid is brought from a temperature well above its melting temperature to a given undercooling, the distribution of embryos comprising more than one molecule is practically empty [14]. The time necessary to establish a stationary distribution of embryos is by definition the induction time or incubation time, t_{ind} [15]. This induction time is virtually equal to zero for metals, because the atoms are highly mobile and the stationary population of embryos is established almost instantaneously. On the other hand, t_{ind} can be quite large for organic molecules of relatively large size such as TAGs. As a matter of fact, these large molecules require complex reorientation mechanisms to incorporate a crystalline network. As a first estimation, t_{ind} is inversely proportional to the heterogeneous nucleation rate I_{het} [16]:

$$t_{\text{ind}} = A \exp\left[\frac{\Delta G(n^*)}{k_B T}\right] = \frac{1}{(4\sigma k_B T)^{1/2}} v_m^{-1/3} h \exp\left[\frac{16\pi\sigma^3 T_f^2 V_m^2 f_\theta}{3k_B T \Delta H_{m,f}^2 \Delta T^2}\right] \tag{11}$$

where v_m is the molecular volume and h is the Planck constant.

Other, more complex expressions have been proposed for t_{ind}. Muchova and Lednicky [17] took into account the initial nucleation on a heterogeneous substance (primary nucleation) and the growth of the solid (by a mechanism of secondary nucleation; see next subsection), in the formation of nuclei of critical size.

B. Growth in Bulk

Below the temperature of fusion of the solid phase, the growth rate of the solid/liquid interface at low undercooling is affected mainly by the undercooling. The entropy of fusion of TAGs, which are quite long molecules, is high ($\Delta H_{m,f}/k_B T_f \approx 60$ [18]). Therefore, the attachment kinetics is the factor that limits growth. The crystal grows layer by layer, by a mechanism of secondary nucleation. This involves a homogeneous bidimensional nucleation of each new layer at the surface of the crystal. The growth rate can be estimated with reasoning similar to that followed for nucleation in the volume, but in a two-dimensional space, the surface of the crystal. At the critical size to be stable, a nucleus has a free energy that is proportional to $1/\Delta T$. With the assumption of an isotropic surface (σ independent of direction), the growth rate of the solid/liquid front, v, is given by the equation [18]

Copyright 2002 by Marcel Dekker. All Rights Reserved.

$$v = K_1 \exp\left[- \frac{\pi a_0 T_f \sigma^2 V_m}{3 k_B T \Delta H_{m,f} \Delta T} \right] \tag{12}$$

K_1 is a constant that depends on the characteristics of the crystal, and a_0 is the radius of the molecules.

For polymers, the formula is more complex. The activation energy term is not constant, and the molecules are nonisotropic [7]:

$$v_{\text{pol}} = v_0 \exp\left[- \frac{b_\varepsilon}{k_B (T - T_g - C_2)} \right] \exp\left[- \frac{\beta b T_f \sigma \sigma_e V_m}{k_B T \Delta H_{m,f} \Delta T} \right] \tag{13}$$

β is a geometric factor equal to 4 or 2 depending on whether the growth regime is I or II [19], and b is the thickness of the molecular layer added to the crystal at each growth step (about 0.4 nm). Other parameters were defined in Eq. (9). Regime I corresponds to growth at low undercooling: The nucleation rate is low, so each new layer grows completely before a new layer is nucleated. Growth rate is then directly proportional to the secondary nucleation rate. Regime II corresponds to higher undercooling. In this case, the nucleation rate is high, so many nuclei appear on the substrate, and the growth rate depends on the secondary nucleation rate at the power 1/2, so β has a value of 2.

TAGs are not isotropic, so Eq. (13) is more likely to describe their growth behavior. Moreover, in the rest of this chapter, we will suppose that they follow growth regime I, because low undercooling is usually used in experiments.

C. Morphology of Crystals

Triacylglycerols often crystallize from the liquid state in the form of spherulites. This morphology is also commonly observed for polymers and some mineral rocks [20,21]. The reasons for the formation of spherulites are not well understood but are linked in particular to solidification from viscous fluids. A spherulite is an aggregate made of many crystalline ribbons (or lamellas) that grow radially from the same central nucleus [22]. Each of these ribbons may branch out when the size of the spherulite increases. Liquid molecules are incorporated perpendicularly to these crystalline ribbons. Spherulites grow through a secondary nucleation mechanism for each layer at the surface of the individual lamellas. Because polymers are molecules of various lengths, their spherulites are only partially crystallized, having many amorphous interlamellar domains. In contrast, spherulites of TAGs can reasonably be considered to be fully crystalline. TAG molecules are all of similar size, so they integrate themselves perfectly to the lamellas.

The size of the spherulites may widely vary depending on the solidification conditions. Spherulites may be very fine and seen as a mass of small particles under the optical microscope. Moreover, observed structures are not regular

Copyright 2002 by Marcel Dekker. All Rights Reserved.

spherical spherulites. Some distortions are possible, and the interface with the liquid may be diffuse.

Depending on the cooling conditions, TAGs do not always grow as spherulites. They can form individual crystalline fibers that are also called needles [23,24]. These needles are, in fact, the primary elements of spherulites, but in this case they grow separately, each from a different nucleus.

D. Competition Between the Polymorphic Forms

Most TAGs exhibit monotropic polymorphism [25]; i.e., below the stability domain of the liquid, there is a single stable phase throughout the temperature range. Other polymorphic forms are not stable, so they never form.

In reality, because the stable phase nucleates and grows very slowly, other less stable phases with quicker kinetics of formation have the opportunity to nucleate and grow from the liquid state. As a matter of fact, according to the theoretical expressions, the induction time [Eq. (11)], nucleation rate [Eq. (6)], and growth rate [Eq. (12)] are functions of the ratio $\sigma^3/\Delta T^2 \Delta H_f^2$ or $\sigma^2/\Delta T \Delta H_f$. There is competition between the surface energy of the solid/liquid interface, which slows down the kinetics, and the undercooling and melting enthalpy, which accelerate it. The term σ varies greatly between an unstable solid phase with a structure close to that of the liquid and a solid phase with a very different structure from that of the liquid. This means that the least stable phases have the fastest formation kinetics, though ΔT and $\Delta H_{m,f}$ increase with the stability of the phases. As soon as the liquid is below the melting temperature of a less stable form, this form generally nucleates and grows the most rapidly. Figure 1 illustrates this phenomenon. The phase with the lowest melting free energy ΔG_f, i.e., the least stable phase, also has the lowest energetic barrier ΔG^* to form from the liquid.

E. Crystallization Under Shear

Polymers and TAGs crystallize far more quickly when they are exposed to a shear. This phenomenon has been observed experimentally [26–30]. Crystallization under shear is still not fully understood on the theoretical side, yet this is a key parameter for the modeling of industrial processes. A first simple idea is that in the presence of shear the chains of the molecules rotate faster in the liquid and are therefore more easily incorporated into the intracrystalline network. Morphologies of polymer crystals vary depending on the shear: They crystallize preferentially in lamellas under shear whereas they are mostly crystallized as spherulites if they solidify statically, i.e., in quiescent conditions.

A theoretically advanced model for polymer crystallization under shear was developed by Eder and Janeschitz-Kriegl [31]. The main hypothesis is that dynamic nucleation (i.e., when nuclei appear due to shear) is different from static

Copyright 2002 by Marcel Dekker. All Rights Reserved.

nucleation. Eder and Janeschitz-Kriegl found that the induction time, t_{ind}, had two domains as a function of the shear. At very low shear rates, static nucleation dominates, with an observed static induction time t_{stat}. At higher shear rates, shear nucleation predominates, and t_{ind} is proportional to $\dot{\gamma}^{-1}$.

F. Crystallization in Solution

Nucleation in a solution can be described using assumptions similar to those for nucleation in the melt [2]. Instead of Eq. (1), transformation of the liquid into solid generates a decrease in the Gibbs free energy per unit volume, ΔG_v:

$$\Delta G_v = -k_B T \ln\left[\frac{c}{c_s}\right]\left(\frac{1}{V_m}\right) \tag{14}$$

where c is the actual concentration of solute and c_s the saturation concentration of solute at temperature T. $\ln[c/c_s]$ is called the supersaturation.

Corresponding to Eq. (3) for a solution, Eq. (15) expresses the change in free energy due to the creation of a solid embryo:

$$\Delta G_{hom} = -k_B T \ln\left[\frac{c}{c_s}\right]\left(\frac{V}{V_m}\right) + \sigma S \tag{15}$$

With the assumptions of homogeneous nucleation and spherical embryos, the maximum of ΔG_{hom} is

$$\Delta G_{hom}(n^*) = \frac{16\pi}{3}\left(\frac{\sigma^3 V_m^2}{(k_B T)^2(\ln[c/c_s])^2}\right) \tag{16}$$

Substituting this into Eq. (6), the nucleation rate is expressed as

$$I_{hom} = N_0 \nu_0 p N_s^0 \exp\left[-\frac{\varepsilon}{k_B T}\right]\exp\left[-\frac{16\pi}{3}\left(\frac{\sigma^3 V_m^2}{(k_B T)^3(\ln\,[c/c_s])^2}\right)\right] \tag{17}$$

In the case of crystallization in a solution, the growth rate depends mainly on the degree of supersaturation, analogous to crystallization in bulk mainly depending on the degree of undercooling. Yet different expressions can be drawn, depending on the growth mechanism. For a two-dimensional nucleation mechanism of growth, the expression is fairly similar to that found in a melt [32]:

$$v = v_0\left(\ln\left[\frac{c}{c_s}\right]\right)^p \exp\left[\frac{A_2}{\ln[c/c_s]}\right] \tag{18}$$

where $p(-3/2 < p < 5/6)$, v_0, and A_2 are constants.

Copyright 2002 by Marcel Dekker. All Rights Reserved.

Van Putte and Bakker [33] observed for palm oil a screw dislocation–like mechanism, where v is given by

$$v = K\frac{c - c_s}{c_s} \tag{19}$$

where K is a constant.

III. MICROSCOPIC MODELING OF CRYSTALLIZATION

This section discusses simulations that use direct microscopic descriptions of crystallization through equations of nucleation and growth to predict kinetics.

A. Deterministic Approach

In the ideal case, where the nucleation rate $I(t)$ and the growth rate $v(t)$ are known, evolution of the solid fraction can be calculated.

The extended solid fraction $f_s^e(t)$ is the solid fraction obtained when the crystals are supposed to never impinge on each other. It is simply written as

$$f_s^e(t) = \int_0^t I(\tau)V_c(t,\tau)\, d\tau \tag{20}$$

where $V_c(t,\tau)$ is the volume at time t of a crystal nucleated at time τ. The time origin is taken as the start of nucleation, just after the induction period.

If we suppose that the sample has an infinite size and that nucleation is random in space, the real solid fraction, f_s, is a simple function of f_s^e [34,35]:

$$f_s(t) = 1 - \exp[-f_s^e(t)] = 1 - \exp\left[-\int_0^t I(\tau)V_c(t,\tau)\, d\tau\right] \tag{21}$$

If in addition, we suppose that solidification is isothermal under the form of perfectly spherical spherulites, then the growth rate of the solid/liquid front, v, is constant [30], and the volume at time t of a spherulite that has been nucleated at time τ is given by

$$V_c(t,\tau) = \frac{4}{3}\pi v^3(t - \tau)^3 \tag{22}$$

Two extreme cases can be considered for nucleation:

1. Nucleation is instantaneous. All nuclei appear simultaneously at time $t = 0$, with a density of sites per unit volume equal to N_f. The solid fraction is then expressed as

$$f_s(t) = 1 - \exp\left[-N_f\frac{4}{3}\pi v^3 t^3\right] \tag{23}$$

Copyright 2002 by Marcel Dekker. All Rights Reserved.

2. The nucleation rate, I_0, is constant. The solid fraction is then written

$$f_s(t) = 1 - \exp\left[-I_0 \frac{\pi}{3} v^3 t^4\right] \tag{24}$$

The general formulation of Avrami [35] for the solid fraction is

$$f_s(t) = 1 - \exp(-bt^n) \tag{25}$$

where b and n are two constants to be determined depending on the system studied. This approximation is very useful for obtaining an analytical expression of real cases, where nucleation is more complicated than the two extreme cases described above.

B. Numerical Approach

As we have seen, Eq. (21) can be solved directly in only a few simple cases. However, often these simple cases use assumptions that are too drastic to be realistic. More complicated expressions of the nucleation and/or growth rates are often necessary to better describe real systems, which must then be solved numerically.

Van Putte and Bakker [33] proposed a first numerical approach to model crystallization kinetics of palm oil. They took the approach of solvent crystallization (see Section II.F) and observed the crystallization of the ''saturated'' part of TAGs in palm oil. For their system, they determined nucleation and growth rates as a function of temperature from microscopic observations at very low percentages of solids (f_s around 0.1%), as shown in Figures 3 and 4, respectively.

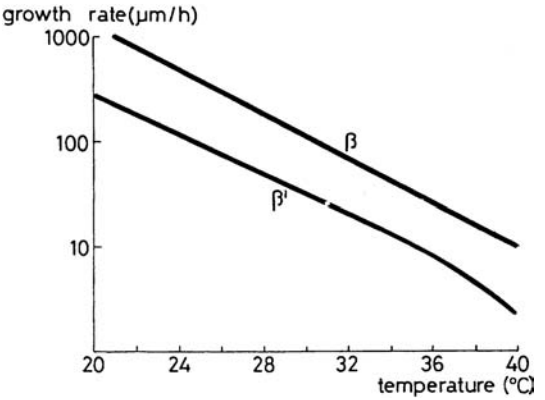

Figure 3 Growth rate of β and β′ crystals of saturated triacylglycerols in refined palm oil as a function of temperature. (Reprinted from Ref. 33, courtesy of the American Oil Chemists' Society.)

Copyright 2002 by Marcel Dekker. All Rights Reserved.

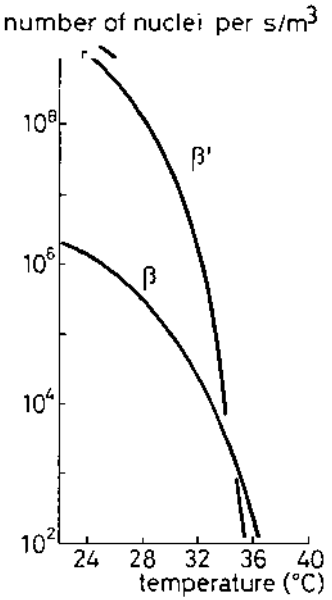

Figure 4 Nucleation rate of β and β′ crystals of saturated triacylglycerols in refined palm oil as a function of temperature. (Reprinted from Ref. 33, courtesy of the American Oil Chemists' Society.)

Then, knowing the evolution of the solubility of the saturated TAG fraction in palm oil with temperature, they expressed the variation of nucleation and growth rates as a function of the degree of supersaturation. They fitted the experimental values of the nucleation rate with the expression given by Eq. (17) and those of the growth rate with Eq. (19), which corresponds to crystallization in solution. In the temperature domain of study [20°C, 40°C], they determined these parameters for both phases β and β′. With these expressions, they calculated numerically the evolution of the volume fraction of solid as a function of time. They did not take into account the impingement between crystals. By solving numerically a simplified population balance equation, they obtained the expression of an extended volume fraction of solid, $f_s^e(t)$. Figure 5 presents calculated and measured evolutions of $f_s^e(t)$. Agreement is quite good, except when the maximum solid is reached (around 8%), certainly because the model does not take into account the impingement between crystals, which becomes important at such low solid fractions.

Kloek et al. [32,36] had a similar approach considering a fat mixture of hydrogenated palm oil in sunflower oil as a solute in a solvent. The soluble fraction is calculated with the Hildebrand equation, which is valid for ideal solutions. They calculated the nucleation rate from the same expression as that used by van

Copyright 2002 by Marcel Dekker. All Rights Reserved.

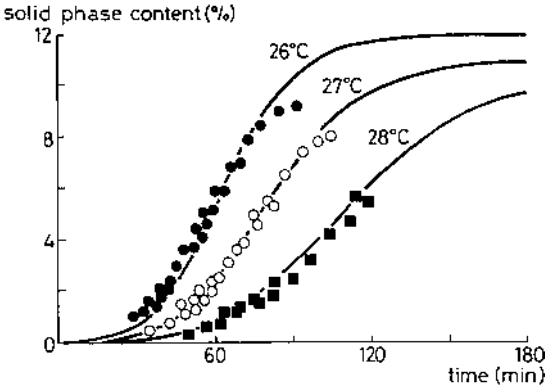

Figure 5 Calculated and measured solid phase curves of refined palm oil. (Reprinted from Ref. 33, courtesy of the American Oil Chemists' Society.)

Putte and Bakker [Eq. (17)]. But they did not fit the expression of homogeneous nucleation rate to experimental values as a function of temperature. They calculated it directly by estimating the value of all parameters in this equation. For this, they neglected the term pN_0^s in the expression for I_{hom}, which is often done because it is close to 1 [10]. They then assumed that ε could be expressed as

$$\varepsilon = \frac{\alpha \, \Delta S}{R} \tag{26}$$

with α being the fraction of molecules that are in a correct conformation for incorporation in a nucleus, ΔS the decrease in entropy on crystallization of 1 mole of TAGs, and R the gas constant. An empirical value of 0.8 for α was found to fit well with the β' crystals. ΔS was calculated as the ratio of the enthalpy of fusion to the temperature of fusion, with both parameters determined from differential scanning calorimetric (DSC) measurements. In the expression of $\Delta G_{\text{hom}}(n^*)$, the only remaining unknown is the surface energy σ. Kloek et al. calculated it from the experimental determination of the induction time. The induction time was estimated from the curves $f_s(t)$ measured by p-NMR, taking the intercept of the tangent line at the inflection point with the time axis. Then, he plotted $\ln(t_{\text{ind}})$ as a function of the supersaturation. Assuming that the first exponential term in Eq. (17) is a constant, the curve is a straight line with a slope from which σ can be calculated.

The experimental curves $f_s(t)$ were fitted to the numerical expression given by a reparametrized Gompertz equation:

$$f_s(t) = f_{s,\max} \exp\left\{-\exp\left[\frac{\mu e}{f_{s,\max}}(t_{\text{ind}} - t) + 1\right]\right\} \tag{27}$$

Copyright 2002 by Marcel Dekker. All Rights Reserved.

with μ the maximum increase rate in solid fraction [i.e., at the inflection point of the curve $f_s(t)$] and e the base of the natural logarithm. The maximum solid fraction is expressed as a function of the initial supersaturation:

$$f_{s,\max} = c_0\left(1 - \frac{c_s}{c_0}\right) \tag{28}$$

where c_0 is the initial concentration of the solute.

Knowing the nucleation rate and having with this expression the increase in nuclei at each time step, Kloek et al. could calculate at each time step the increase in solid fraction due to crystal growth. They obtained a curve of the growth rate as a function of time. Calculating the evolution of supersaturation from the change in $f_s(t)$, they calculated the curve of the growth rate as a function of the supersaturation. They then fitted this curve to the expression

$$v = a\left(\frac{c}{c_s}\right)^b \tag{29}$$

where a and b are constants determined empirically. Then they got the expressions of both the nucleation and the growth rate as a function of the supersaturation. They also made the assumption that there was no impingement between crystals, which they justified by the fact that they considered only small solid fractions lower than 0.1. Then they numerically calculated the evolution of the solid fraction starting from various initial supersaturations (Fig. 6). The agree-

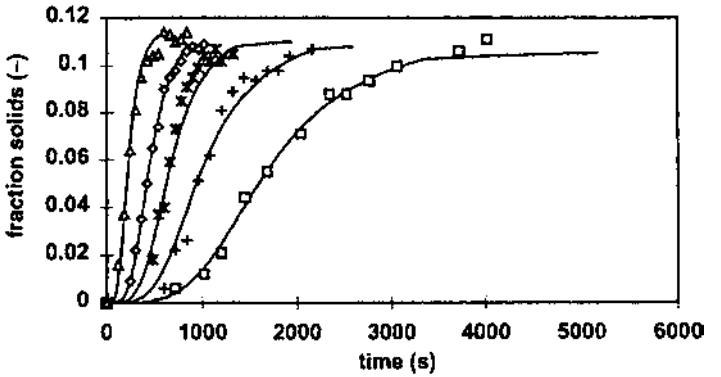

Figure 6 Measured and fitted crystallization curves of 12% hydrogenated palm oil in sunflower oil mixtures crystallized at various initial levels of supersaturation. Fits were obtained from fitted growth rates given by Eq. (29). Initial supersaturation: (□) 2.25; (+) 2.5; (×) 2.75; (◇) 3; (Δ) 3.25. (Reprinted from Ref. 32, courtesy of the American Oil Chemists' Society.)

Copyright 2002 by Marcel Dekker. All Rights Reserved.

ment between the experimental and simulated curves is quite good if we consider all the assumptions made.

C. Stochastic Approach

Another approach consists in simulating the nucleation and growth of crystals in a defined space. A 3-D stochastic model to simulate spherulitic crystallization was developed by Rousset [30], based on a model previously developed for the crystallization of metals by Charbon et al. [37,38]. The software was modified for application to the isothermal static crystallization of TAG spherulites in a small sample such as in a DSC pan. It allows the study of spherulitic crystallization. The principle of the method is to follow the evolution of the solid/liquid interface in the three-dimensional domain representing the volume V_e of the sample. To do so, the surface of each spherulite, assumed to be spherical, is cut into a large number of facets, making a complete paving of the sphere. Each facet is characterized by its direction, originating from the spherulite nucleus and pointing to the center of the facet, by its solid angle, and by its distance from the nucleus. The advance of each facet of all spherulites is calculated at each time step δt. The set of facets completely describes the solid/liquid interface. Their progression at each time step allows calculation of the evolution of the solid fraction in the spatial domain.

Boundary effects are eliminated when the size of the simulated sample, l, is smaller than that of the real one. In such a case, a size slightly larger, $l + 2\delta l$, is chosen for the simulated domain (Fig. 7). This will be the case for the DSC

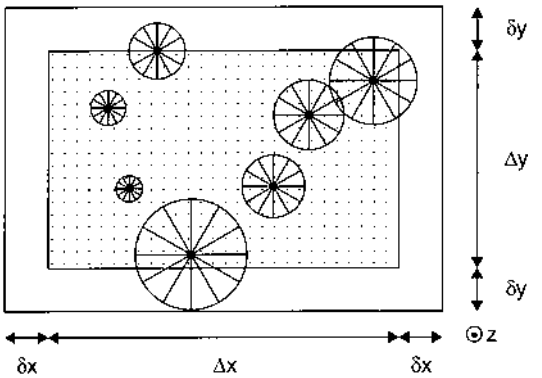

Figure 7 Three-dimensional stochastic modeling applied to DSC. Boundary effects are eliminated in the x and y directions by simulating solidification in a larger domain [$\Delta x + 2\delta x$, $\Delta y + 2\delta y$,Δz], but the evolution of the solid fraction and of heat are calculated only in the domain of desired size [Δx, Δy, Δz].

Copyright 2002 by Marcel Dekker. All Rights Reserved.

pan example shown below. The simulated domain has the same height as the real DSC pan, but it has smaller lateral dimensions. Another technique would consist in taking periodic conditions, but it is more complicated to implement.

The two basic parameters of this model are nucleation and growth rate of the spherulites.

1. Nucleation

The positions of nuclei are chosen randomly in the volume of the sample. The expression of the nucleation rate can be chosen to be a function of time and temperature. Two extreme cases are considered by Rousset:

1. Nucleation is instantaneous. All the nuclei appear at time $t = 0$ (the origin of time corresponding to the end of the induction period), with a given spatial density, N_f, a single function of the solidification temperature.
2. Nucleation is at a constant rate I_0. At each time step, a number of nuclei, $I_0 \delta t V_e$, are activated in the volume of the sample.

If a new nucleus is localized inside an already existing solid spherulite, it is eliminated. This means that the model takes in to account the extinction of nucleation sites by growth of the solid.

2. Growth

Spherulites grow from the center of their nucleus. Their growth rate can be taken as a function of the temperature. In the case considered by Rousset, the growth rate of the solid/liquid front, v, is isotropic, because temperature is assumed to be uniform in the sample. All the spherulites are spherical until there is some impingement. At each time step, a facet still in contact with the liquid moves forward at a radial increment

$$\delta r = v \delta t \tag{30}$$

If a facet of a spherulite is in contact with liquid, its increment in solid volume, δV_s, is given by

$$\delta V_s = r(t)^2 \delta\Omega \delta r \tag{31}$$

where $\delta\Omega$ is the solid angle of the facet and r is the radius of the spherulite it belongs to. If a facet is in contact with another spherulite or the edge of the sample, it is blocked—its increment of solid volume is nonexistent.

The increment of solid fraction in the sample, $\delta f_s(t)$, is calculated by summing the increments of solid volume of each facet of all spherulites present in the volume of the sample.

Copyright 2002 by Marcel Dekker. All Rights Reserved.

The increment of heat, δQ, generated by the solidification in the sample of volume V_e is

$$\delta Q(t) = \delta f_s(t) \Delta H_f \rho V_e \tag{32}$$

where ρ is the density of the sample and ΔH_f is the enthalpy of fusion per unit of mass. This evolution of heat $\delta Q(t)$ corresponds exactly to the peak measured by the DSC apparatus in the case of isothermal treatment. Therefore it can be directly compared to the experimental measurements.

Apart from the release of latent heat, the model also calculates maps of the microstructure of the sample. Unlike microscopic observation by reflection, which is in fact observation of only a section of the sample, TAG samples are often observed by transmission with polarized light microscopy (PLM) [30]. Such a microscopic view is, in fact, a projection of the sample parallel to the light beam, i.e., along the height of the sample. The PLM views in transmission give an erroneous picture of the advancement of the phase transformation, by showing an overestimated solid fraction present, except if the sample height is close to zero. A simulated view must be an integration on the height of the sample of all the horizontal sections if it is to be compared with a microscopic PLM view.

The model described above was applied to the crystallization of γ-POP at 15°C, because γ-POP was observed to occur exclusively as spherulites [39]. Four cases were simulated with different nucleation laws. The first case (S1) supposes an instantaneous nucleation, with a density of nuclei equal to the final number of spherulites determined experimentally. The three other simulations suppose nucleation at constant rate I_0. Case S2 estimates I_0 based on the final crystal density and the growth rate measured experimentally, using the formula of Meijering [40]:

$$I_0 = \left(\frac{\pi}{3}\right)^{1/3} \left[\Gamma\left(\frac{5}{4}\right)^{-1} N_f\right]^{4/3} v \tag{33}$$

where N_f is the final crystal density, v is the growth rate of the solid/liquid interface, and $\Gamma(x)$ is the gamma function:

$$\Gamma(x) = \int_0^\infty u^{x-1} e^{-u} du \tag{34}$$

This calculation is valid in the case of constant crystal nucleation and growth rates. It is based on a probabilistic analysis and is valid under the assumptions of a sample of infinite size and random nucleation in space.

For simulations S3 and S4, two higher values of I_0 were taken. For all four cases, the growth rate of the solid/liquid front was determined experimentally

Copyright 2002 by Marcel Dekker. All Rights Reserved.

Table 1 Parameters Used by the Stochastic Model to Simulate Crystallization of γ-POP at 15°C

Height of the sample, h	50 μm
Observation window, $\Delta x \Delta y$	0.65 mm × 0.496 mm
Enthalpy of fusion, ΔH_f	10^8 J/m^3
Nucleation	
Instantaneous, N_f	1.2×10^{13} m^{-3} (S1)
Constant rate, I_0	0.9×10^{11} m^{-3} s^{-1} (S2)
	2×10^{11} m^{-3} s^{-1} (S3)
	4×10^{11} m^{-3} s^{-1} (S4)
Growth rate, v	0.275 μm/s
Number of facets on each spherulite	732

[30]. Parameters for the simulations are presented in Table 1. Figure 8 presents the view of the sample by transmission, i.e., the projected view of the sample parallel to the light beam, for four different times during the solidification (5, 35, 65, and 125 s). Origin of time $t = 0$ was chosen to be when nucleation starts, once the induction period has elapsed. In the simulations, liquid is represented as black, solid as white. In simulation S1, all the isolated spherulites have the same size, because they nucleate at the same time and the growth rate is constant. This is not the case for the other simulations, where there is a size distribution due to nucleation throughout solidification.

Figure 9 shows the evolution of the latent heat in the sample for the experiment and the four simulations. The assumption of instantaneous nucleation (S1) gives results quite similar to those of the experiment, both for the microscopic view and for the DSC peak. On the other side, the assumption of constant nucleation rate (S2), with the value of I_0 estimated from the experimental measurements, gives results quite different from those of the experiment. Visibly, I_0 is too small, because the number of spherulites present in the microscopic views is too small and solidification is too slow. This is explained by an underestimate of the final number of spherulites measured from the microscopic views: The spherulites, which appear late in the solidification, have little space to grow before impinging on other spherulites and being blocked. These spherulites are too small to be visible and are therefore not counted. The measurement takes into account only spherulites that have nucleated quite early and that could reach a sufficiently large size. It is not representative of all the spherulites that appear during solidification. Two simulations with higher nucleation rates [2×10^{11} m^{-3}s^{-1} (S3) or 4×10^{11} m^{-3}s^{-1} (S4)] were done and gave results closer to reality. In the case of S3, the density was too low at the beginning, but solidification finished on a

Copyright 2002 by Marcel Dekker. All Rights Reserved.

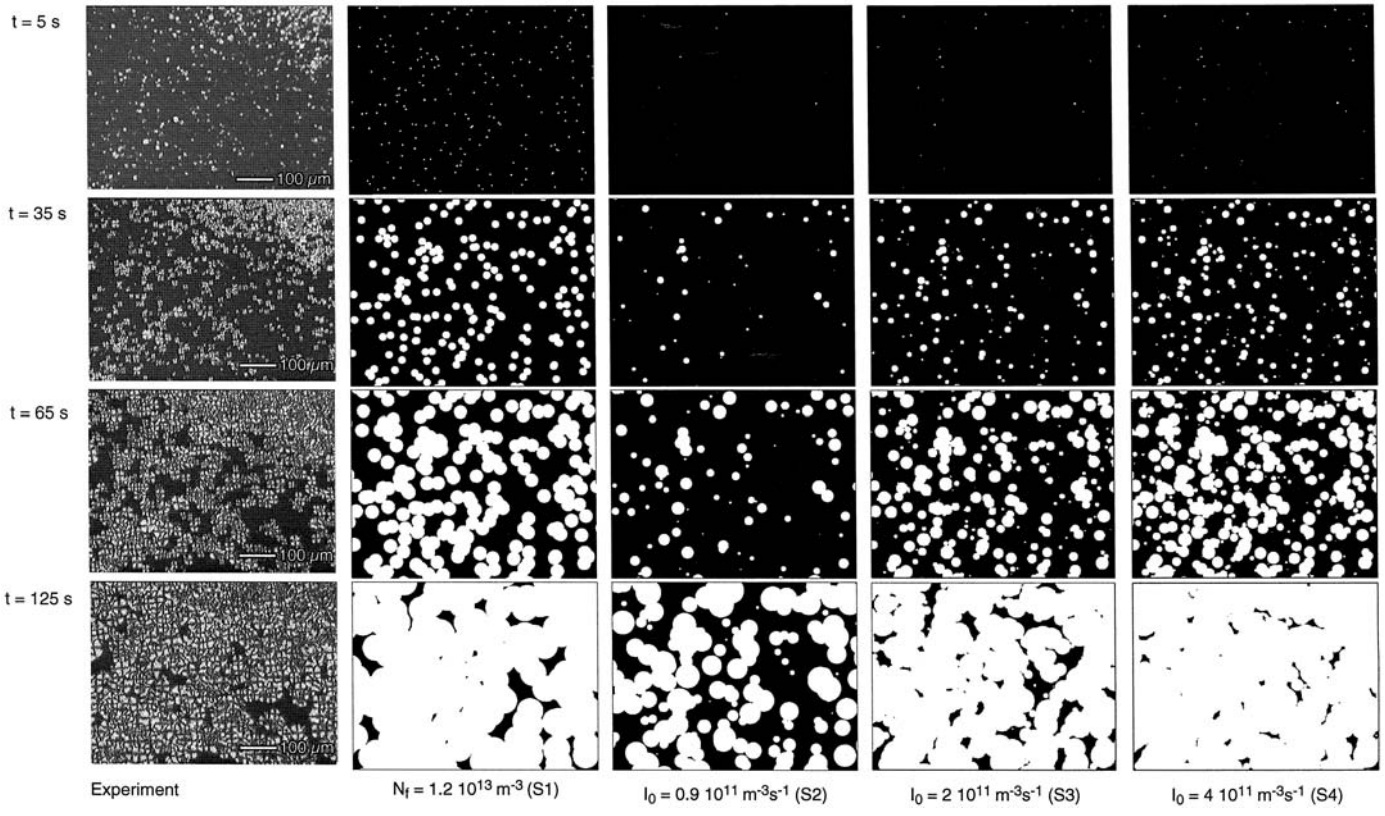

Figure 8 Experimental and simulated views at different times of a glycerol-1,3-dipalmitate-2-oleate (POP) sample solidifying at 15°C. The four simulation cases correspond to various nucleation regimes: S1 is instantaneous, whereas S2, S3, and S4 are three different constant nucleation rates. (From Ref. 30.)

Copyright 2002 by Marcel Dekker. All Rights Reserved.

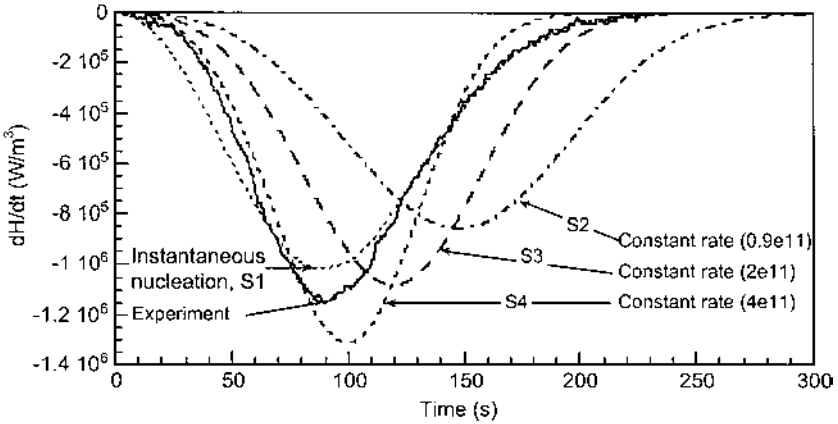

Figure 9 Experimental and simulated DSC peaks of POP solidifying at 15°C. Abbreviations as in Figure 8. (From Ref. 30.)

time scale similar to that of the experiment. In the case of S4, the first part of the solidification was well represented, but completion was too early because there were too many spherulites in the volume. Reality lies in between these two cases, with a huge number of nuclei appearing quickly at the onset of crystallization and then a nucleation rate not equal to zero but low and remaining low for a given time during the solidification. As a matter of fact, the size distribution of isolated spherulites observed in the microscopic pictures is not completely uniform. In conclusion, the approximation of instantaneous nucleation (S1) is the assumption that gives the results closest to experimental ones.

This 3-D stochastic model is very interesting for simulating spherulitic crystallization, because it not only predicts the evolution of latent heat in the sample, but also shows a view of the microstructure in any section and projection of the sample. From these simulated microstructures, all the microstructural parameters can be calculated. This is a great advantage to see the effect of a change in the nucleation law and/or a change in the growth rate on the aspect of the microstructure, the final number of spherulites, and the final crystal size distribution, for example. Moreover, this model may be a tool to validate experimental measurements or theoretical expressions of the nucleation and growth rates, by comparing the simulated and experimental microstructures and peaks of latent heat released.

D. Probabilistic Approach

The probabilistic approach is, in fact, a kind of numerical approach, where a probabilistic theory has been elaborated to eliminate the assumption of an infinite

Copyright 2002 by Marcel Dekker. All Rights Reserved.

size for the sample. Rousset [30] developed a semianalytical probabilistic model that calculates the expression of the solid fraction as a function of time for a sample of finite height z but infinite in x and y (a reasonable approximation for a DSC pan, for example). The model is based on the Avrami reasoning leading to Eq. (21) but is adapted to a noninfinite medium with a finite sample height. Details of this development are given in Ref. 30.

The solid fraction is not uniform in the volume of the sample; it is affected by its finite height h. First the exclusion volume $V_{ex}(d,t)$ must be defined. It is equal to the volume taken at time t by a hypothetical spherical crystal that would have nucleated at $t = 0$ at a height d in the sample (the origin of the z axis is taken at midheight of the sample). The exclusion volume corresponds to the volume in which no nuclei should nucleate, so that a point in the sample at height d is still liquid at time t. By doing a probabilistic reasoning on the number of nuclei activated and the volume they occupy, the solid fraction of the sample can be expressed as a function of the time t and the height d. In the case of instantaneous nucleation, the expression of the solid fraction at a given height d, $f_{s,d}(t)$, is

$$f_{s,d}(t) = 1 - \exp[-N_f V_{ex}(d,t)] \tag{35}$$

where N_f is the number of nuclei activated at time 0.

The expression of the overall solid fraction in the sample is then easily deduced:

$$f_s(t) = \frac{1}{h/2} \int_0^{h/2} f_{s,d}(t)dt \tag{36}$$

In the case of constant rate nucleation, Eq. (35) is replaced by

$$f_{s,d}(t) = 1 - \exp\left(-\int_0^t V_{ex}(d,t,\tau) I_0 d\tau \right) \tag{37}$$

where I_0 is the nucleation rate. The solid fraction $f_s(t)$ is calculated with Eq. (36), using Eq. (37) to get $f_{s,d}(t)$.

Rousset compared the stochastic model and the probabilistic model for cases S1–S4. Curves calculated by the two methods are almost equal. The very slight shift is due to the dimensions of the sample simulated with the stochastic method, which cannot be considered infinite in the x and y directions. The size of the simulated domain (1.5×1.5 mm^2) is very much smaller than the real size of the DSC pan (6 mm diameter). Therefore, the assumption of the DSC pan as a thin strip is valid in the cases studied (size of the crystals very small compared to these dimensions).

With this probabilistic model, a fifth case was considered. It is the combination of instantaneous and constant nucleation rates. For the calculation of $f_s(t)$,

Copyright 2002 by Marcel Dekker. All Rights Reserved.

Eq. (36) was used with $f_{s,d}(t)$ given by

$$f_{s,d}(t) = 1 - \exp\left[-N_f^{\text{inst}} V_{\text{ex}}^{N_f}(d,t) - \int_0^t V_{\text{ex}}^{I_0}(t)(d,t,\tau) I_0 \, d\tau\right] \tag{38}$$

where $V_{\text{ex}}^{N_f}$ and $V_{\text{ex}}^{I_0}$ are the exclusion volumes for the instantaneous nucleation and constant rate nucleation, respectively.

Conditions of nucleation were $N_f^{\text{inst}} = 0.5 \times 10^{13}\text{m}^{-3}$ and $I_0 = 2 \times 10^{11}\text{m}^{-3}\text{s}^{-1}$. The total final number of spherulites was $N_f = 2.5 \times 10^{13}\text{m}^{-3}$, given by the equation

$$N_f = N_f^{\text{inst}} + I_0 \int_0^{\infty} [1 - f_s(t)] dt \tag{39}$$

The experimental $f_s(t)$ was used for the calculation of the integral of the second term of the equation. Figure 10 presents the results obtained. Curve S5 is quite close to the experimental curve. The onset of solidification is well reproduced. The second part after 50 s is a little bit slow, but it finishes too quickly after 170 s. This means that in the experiment the nucleation rate is higher at around 50 s but does not continue until the end, maybe because the number of sites that can be activated at this temperature is saturated.

These simple nucleation models are limited, but they allow us to analyze quite precisely the real behavior of the system. As a complement to a direct

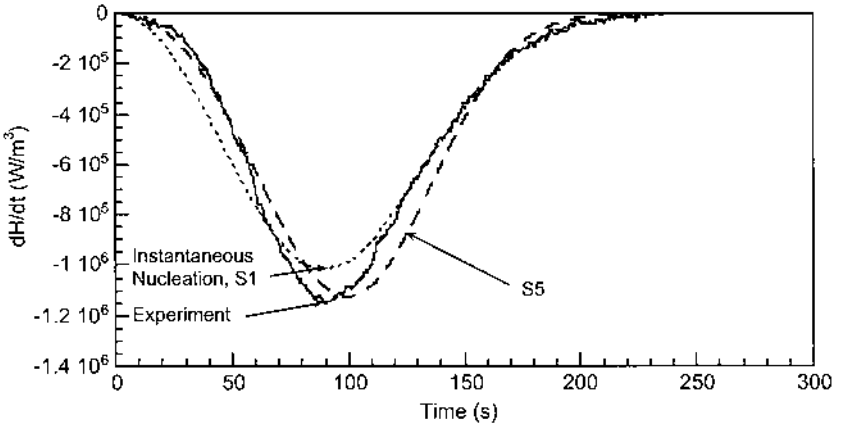

Figure 10 Experimental and simulated DSC peaks of POP solidifying at 15°C. (Simulation S1 is an instantaneous nucleation, with $N_f = 1.2 \times 10^{13}\text{m}^{-3}$; simulation S5 is a combination of instantaneous and constant rate nucleation, with $N_f^{\text{inst}} = 0.5 \times 10^{13}\ \text{m}^{-3}$ and $I_0 = 2 \times 10^{11}\text{m}^{-3}\text{s}^{-1}$.) (From Ref. 30.)

Copyright 2002 by Marcel Dekker. All Rights Reserved.

measurement of the nucleation rate [33,41], this approach is interesting when measurement of the nuclear density is too tedious or not possible.

IV. MACROSCOPIC MODELING OF CRYSTALLIZATION

When the microscopic mechanisms of nucleation and growth are too complex or are not known, a more pragmatic technique that can be used to solve the crystallization kinetics is to obtain an overall view of the evolution of the different phases in the sample and use it to simulate the changes in heat.

Four different approaches are found in the literature. Basically, they all solve the heat flow equation in the sample in the same way, by a finite element method or a finite difference method, to get the thermal evolution. They differ in how the release of the heat due to phase transformation is treated. This means that the authors have considered different theories to describe macroscopically the crystallization and the heat changes it induces, as we will see below. The heat conservation equation is

$$\frac{\partial H}{\partial t} = \text{div}(\kappa\, \mathbf{grad} T) \tag{40}$$

where H is the enthalpy per unit volume, κ is the thermal conductivity of the medium, and T is the temperature. The variation of H is given by

$$\frac{\partial H}{\partial t} = \rho_s\, \Delta H_f \frac{\partial f_s}{\partial t} + [\rho_l c_{p,l}(1 - f_s) + \rho_s c_{p,s} f_s] \frac{\partial T}{\partial t} \tag{41}$$

where ρ_i and $c_{p,i}$ are the density and mass specific heat, respectively, of phase i ($i = l$ for the liquid and s for the solid). A single-phase transformation between the liquid and a solid phase is assumed. On the right-hand side of Eq. (41), the first term corresponds to the latent heat released due to the phase transformation, and the second term corresponds to the change in specific heat due to temperature changes.

A. Linear Crystallization in the Melting Range

Tewkesbury et al. [42] studied the cooling of chocolate from the molten state. The single event that occurs during this step is the crystallization of the fat phase, often mainly cocoa butter. They used commercially available software, FIDAP, to compute the simulations. With it, they solved the heat conservation equation with a finite element method and made a basic assumption for crystallization: The release of latent heat is assumed to be linear in the melting range of the cocoa butter, chosen to be between 21°C and 32°C. With this hypothesis, all parameters present in the equations are known for the liquid and solid phases:

Copyright 2002 by Marcel Dekker. All Rights Reserved.

thermal conductivity, specific heat capacity, density, and latent heat. They did not validate the model with experiment; they just looked at the effect of changing the mold thickness on the cooling rate in the center of a chocolate.

B. Crystallization as a Two-State Transition

Rudnicki and Niezgodka [43] used a model to simulate the melting of cocoa butter in DSC samples. They did not study crystallization from the melt, but they looked at how phases of cocoa butter transform from the most metastable to the most stable and finally to the liquid when the sample is heated. They made the following assumptions: Transitions between phases are given by a bistable thermodynamic potential. The equilibrium distribution between the phases is described by Boltzmann functions, and process dynamics can be calculated by Arrhenius laws where energy levels of each phase are given by thermodynamics.

Thermodynamic parameters of the model were determined from experimental data (heat and temperature of fusion). Missing parameters were calculated by fitting the simulated DSC curves to the experimental curves. As a result, their model provides quite an interesting view of how phase transformation evolves during the heating of a complex system such as cocoa butter and explains the quite complex shape of DSC heating curves (Fig. 11).

C. Empirical Expression for Crystallization

Franke [44] developed a one-dimensional unsteady-state model for the cooling tunnel step in the process of chocolate making. This step of the process takes place between the tempering and the molding. Before cooling, chocolate is tempered to ensure the nucleation of stable fat crystals. At the end of this step, the percentage of crystallized fat is low, around 0.5%. Then, during the cooling stage, most of the fat crystallizes. For modeling the cooling step, Franke assumed that all nuclei were already present at the start of the cooling stage and that only crystal growth would occur during that stage. Therefore, he defined an empirical function for the heat release due to crystallization that is bilinear as a function of the quantity already crystallized and linear as a function of temperature:

$$\rho\ \Delta H_f \left(\frac{\partial f_s}{\partial t}\right) = \rho c_p f_1(Q_m)\, f_2(T) \tag{42}$$

Variation of the two functions $f_1(Q_m)$ and $f_2(T)$ is presented in Figure 12. Q_m is the heat of crystallization already released. The functions f_1 and f_2 depend on three and two empirical parameters, respectively: f_{1m}, maximum heat release rate; $Q_{\max}$, value of Q_m corresponding to f_{1m}; Q_{end}, value of the heat of crystallization; $f_{T'}$, dependence of the rate of crystallization on the undercooling; and T_{crist}, initial

Copyright 2002 by Marcel Dekker. All Rights Reserved.

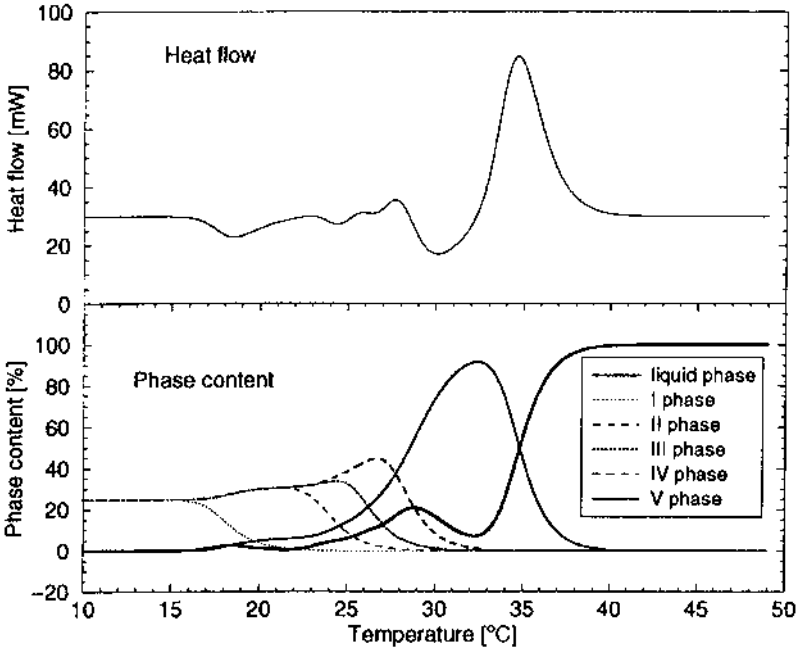

Figure 11 Simulated DSC heating curve of cocoa butter, starting initially at 10°C from 25% each of phases, I, II, III, and IV using the rate model. (Reprinted from Ref. 43, with permission from the authors.)

temperature of crystallization. These parameters are fitted by using experiments done on a lab scale. Figure 13 presents the agreement between the experimental data and the model. Franke used this model to optimize the combination of two cooling processes for cookies, either purely radiative or convective. By such an optimized combination, he could keep the crystallization rate below a maximum level during the overall cooling to ensure optimum gloss of the product.

D. Crystallization Using Isothermal Experimental Data (TTT Diagrams)

Rousset [30] used a model called FEM-TTT. The software, based on a model originally developed for metal solidification [45,46], is able to calculate the kinetics of the phase transformation for any thermal path, using experimental isothermal crystallization kinetics data represented by the time–temperature–transformation (TTT) diagrams and an additivity principle, in a Cartesian bidimensional

Copyright 2002 by Marcel Dekker. All Rights Reserved.

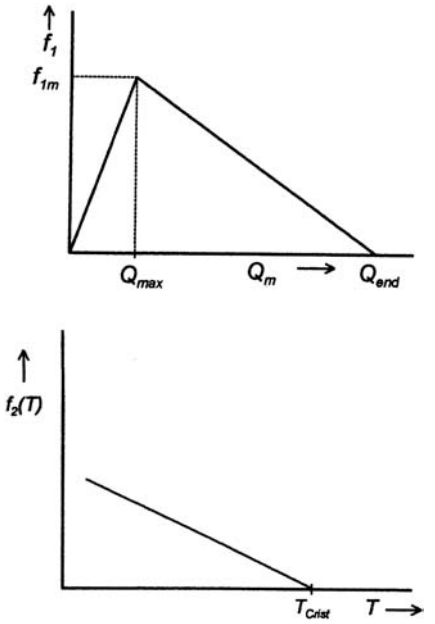

Figure 12 Functions $f_1(Q_m)$ and $f_2(T)$ used for the empirical description of the release of latent heat due to crystallization. (Reprinted from Ref. 44 with permission.)

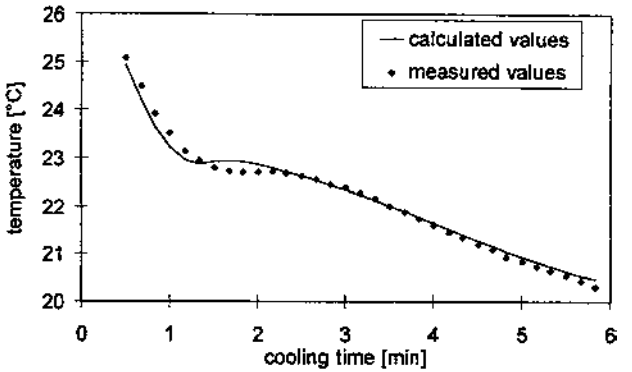

Figure 13 Measured and calculated temperature evolution of the chocolate coating during cooling. (Reprinted from Ref. 44 with permission.)

Copyright 2002 by Marcel Dekker. All Rights Reserved.

geometry or axisymmetrical tridimensional geometry. This aspect is very interesting, because the use of simple isothermal experimental data allows the modeling of more realistic anisothermal situations. The first module of the software solves the heat conservation equation with a formulation in enthalpy with a finite element method (FEM) [45], and the second module calculates the evolution of the volume fraction of the different phases at each node of the FEM mesh. The two modules are coupled to solve the complete set of variables.

A TTT diagram represents the phase transformation kinetics of a material observed in a time–temperature coordinate system. It is constructed isothermally; i.e., for each temperature considered, times of onset and finish of each phase transformation are reported on the diagram, so they should be read isothermally (Fig. 14a). It is an easy way to represent isothermal kinetics in a single diagram. Two models are used in the simulation, both based on the additivity principle. The first one allows the estimation of the induction time [47]. The second enables the calculation of the evolution of the fractions of each solid phase using an additivity principle with fictive times, after the induction time has elapsed [48]. The additivity principle consists in decomposing the thermal path followed by

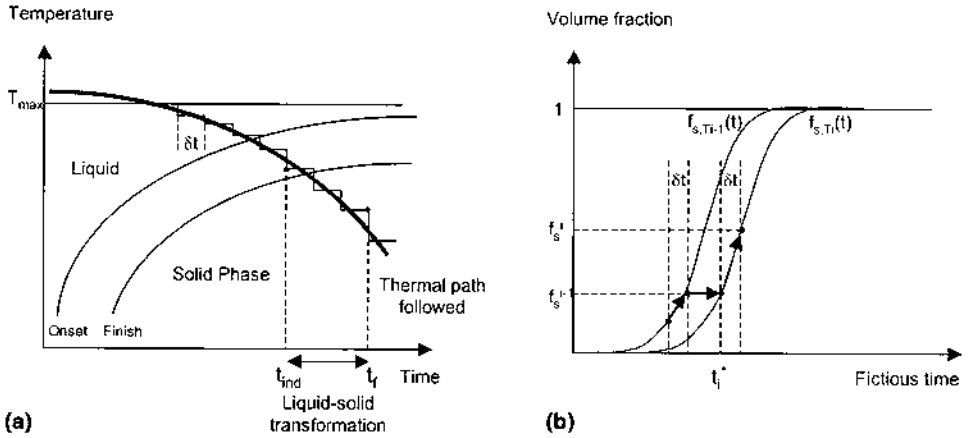

Figure 14 Schematics of the additivity principles used for a model liquid–solid transformation. (a) The thermal path followed by the sample is cut into small isothermal plateaus of duration δt, where the isothermal data of the TTT diagram can be applied. t_{ind} is the induction time, estimated for the transformation using an additivity principle. Once t_{ind} has elapsed, phase transformation begins. Estimation of its progress is presented in (b). (b) Calculation of the evolution of f_s. f_s is known at time step $i - 1$. The fictitious time t_i^* corresponding to this solid fraction on the curve $f_{s,T_i}(t)$ is calculated, where $f_{s,T_i}(t)$ is the isothermal evolution of the solid fraction at the temperature T_i of the sample at timestep i. The increment of solid fraction at time step i is then given by $f_{s,T_i}(t_i^* + \delta t) - f_{s,T_i}(t_i^*)$.

Copyright 2002 by Marcel Dekker. All Rights Reserved.

the sample in a series of small isothermal steps during which the isothermal data can be applied (Fig. 14). This supposes that the reactions of phase transformations are independent of the thermal path followed and that they are a function of only the phase fraction values already reached and the actual temperature. These hypotheses are valid in the case of an isokinetic reaction [35], i.e., when the ratio of the growth rate to the nucleation rate, v/I, is constant throughout the transformation. In spite of these limitations, the use of this principle usually provides quite a satisfactory estimate of the phase fractions formed.

For additional detail, the first part consists of estimating the induction time. For each considered phase transformation j (there may be several simultaneous phase transformations), the reaction may happen only if the temperature is in a given range $[T_{\min,j}, T_{\max,j}]$. When this criterion is fulfilled, the additivity principle described by Scheil [47] is applied to determine the induction time (or incubation time). For each isothermal plateau, an induction fraction is defined; it is the time spent on this plateau divided by the isothermal induction time at this temperature. After m_j isothermal steps are completed in the temperature domain $[T, T_{\max,j}]$, the cumulated induction fraction of transformation j, S_j, is

$$S_j = \sum_{i=1}^{m_j} \frac{\Delta t_i}{t_{\text{ind},j}(T_i)} \tag{43}$$

where Δt_i is the time spent on plateau i where the induction time is $t_{\text{ind},j}(T_i)$.

Phase transformation j starts when the induction fraction, S_j, is equal to 1. This means that in the case of an isothermal transformation, transformation starts when the elapsed time is equal to the induction time at this temperature.

When the induction time has elapsed, phase transformation starts, and the increment of solid fraction is calculated at each time step. The experimental curves of the evolution of the volume fraction of the present phases obtained with DSC are approximated with an Avrami-type expression, which provides the evolution of the volume fraction of the solid at temperature T, $f_{s,T}(t)$:

$$f_{s,T}(t) = f_{s,T,\max}\{1 - \exp[-b(T)t^{n(T)}]\} \tag{44}$$

where $f_{s,T,\max}$ is the maximum volume fraction reachable at temperature T. Time zero is taken as the end of the induction period. Parameters b and n are calculated so as to obtain the best fit with the experimental isothermal curves. This curve fit is simply used as a mathematical expression to describe the experimental curve with a simple expression.

Values of the parameters b and n are known for a whole set of temperatures in the desired domain. The evolution of the solid fraction during cooling is estimated with an additivity principle. As for the estimation of t_{ind}, this principle is based on division of the cooling curve into small isothermal plateaus at each time step (Fig. 14a). The advance of the transformation in each of these considered

Copyright 2002 by Marcel Dekker. All Rights Reserved.

plateaus i is estimated using the expression of $f_{s,T_i}(t)$ with the parameters corresponding to the temperature of this plateau, T_i, $f_{s,T_i,\max}$, $b(T_i)$, and $n(T_i)$. The fictive time at the plateau i, t_i^*, is the time corresponding on the curve $f_{s,T_i}(t)$ to the solid fraction calculated at the previous time step, f_s^{i-1}. It is given by the equation

$$t_i^* = \left(\frac{-1}{b(T_i)} \ln[1 - f_s^{i-1}] \right)^{1/n(T_i)} \tag{45}$$

The solid fraction at time i is calculated as the value of $f_{s,T_i}(t)$ at time $t_i^* + \delta t_i$:

$$f_s^i = 1 - \exp[-b(T_i)(t_i^* + \delta t_i)^{n(T_i)}] \tag{46}$$

Figure 14b shows the schematics of this calculation of the solid fraction at time step i.

Several examples are presented below that were simulated with this model and show its potential use.

1. Crystallization of Pure SOS

For this simulation, the model used isothermal crystallization of glycerol-1,3-distearate-2-oleate (SOS) presented in Ref. 39. The samples were submitted to the following thermal path in the DSC pan. Prior to cooling, SOS was held at 100°C for a few minutes to ensure a fully liquid state. It was quenched at 50°C/min to 30°C and subsequently allowed to solidify at various cooling rates, down to a minimum temperature of 24°C. Figure 15 presents the results. Times of

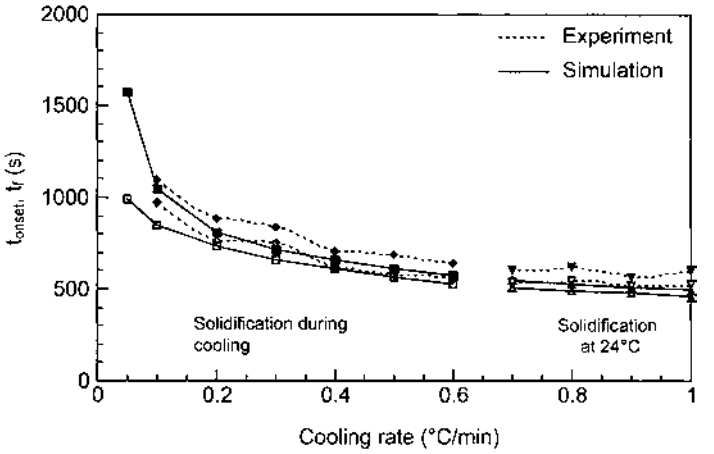

Figure 15 Influence of the cooling rate between 30°C and 24°C on solidification time of SOS. Comparison between experimental data and modeling. Open and filled symbols correspond to time of onset and finish of crystallization, respectively. (From Ref. 39.)

Copyright 2002 by Marcel Dekker. All Rights Reserved.

onset, t_s, and finish, t_f, of crystallization are plotted as a function of the cooling rate and are compared with the measurements made at cooling rates ranging from -0.05 to -1°C/min. The triangles correspond to the simulations and experiments in which this minimum temperature was reached before solidification could start. Calculated and measured start and finish times are in fairly good agreement. In particular, the slowest crystallization kinetics measured at a low cooling rate is correctly reproduced by the additivity principle.

2. Crystallization of a Binary Mixture

The FEM-TTT model was also used on the POS–SOS system based on isothermal data presented in Ref. 49. Here changes in composition between the liquid and the solid were neglected. This means that the authors assumed that no segregation between POS and SOS occurred during crystallization. Owing to the similarity of the two molecules and by observing the phase diagram [49], this assumption is reasonable. A sample of POS-SOS 25:75 w/w was cooled at a constant rate between 0.5 and 5°C/min, starting from a completely liquid state at 35°C in the DSC apparatus. Depending on the cooling conditions, the liquid can solidify in several solid phases. From the model, it appears that even at 5°C/min the temperature was almost uniform in the DSC pan. This implies that the phase fractions were also almost uniform throughout the sample. Therefore, the results are presented by considering a single value of the solid fractions for the whole sample, because all the variables are uniform. Experimental and simulated results are compared in two graphs as a function of the cooling rate. The onset and finish times of crystallization are reported in Figure 16, and the final proportions of the various solid phases formed are presented in Figure 17. Times of onset and finish of crystallization, t_{onset} and t_f, decrease with an increase in cooling rate. This is due to the undercooling; i.e., the driving force for phase nucleation and growth increases more rapidly when the cooling rate is higher. This phenomenon is well reproduced by the modeling, even though the calculated kinetics is slightly too rapid.

An increase in the cooling rate also induces the formation of more metastable phases, which crystallize more rapidly. In fact, even if a stable phase can nucleate at higher temperatures, because its crystallization kinetics is very slow the liquid is not always completely transformed in this phase before metastable phases appear that have higher nucleation and growth rates. At 0.5°C/min, β′ has sufficient time to nucleate and grow before more metastable phases appear. At 1°C/min, this is no longer the case; almost no β′ has formed, at the expense of α and sub-α. Above 2°C/min, liquid transforms almost exclusively to the sub-α phase, which later transforms to the α phase in the solid state. Globally, the model predicts the experimental results quite well. In particular, the high sensitivity of the formation of the different phases is well reproduced.

Copyright 2002 by Marcel Dekker. All Rights Reserved.

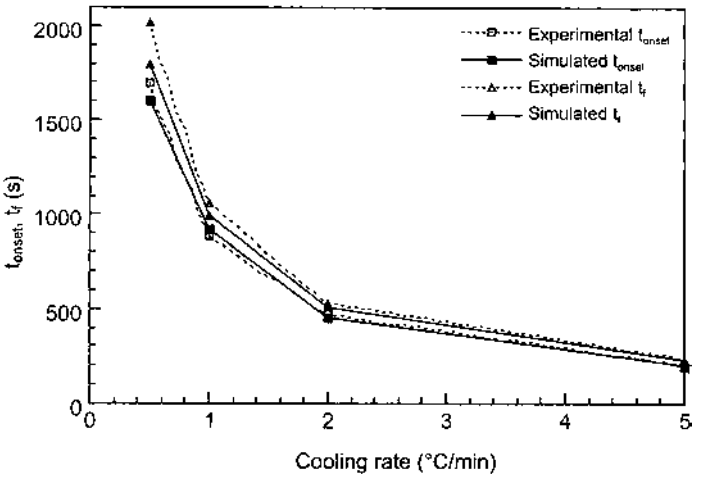

Figure 16 Experimental and simulated t_{onset} and t_f of crystallization at different cooling rates of the binary mixture POS–SOS 25:75 w/w. (From Ref. 49.)

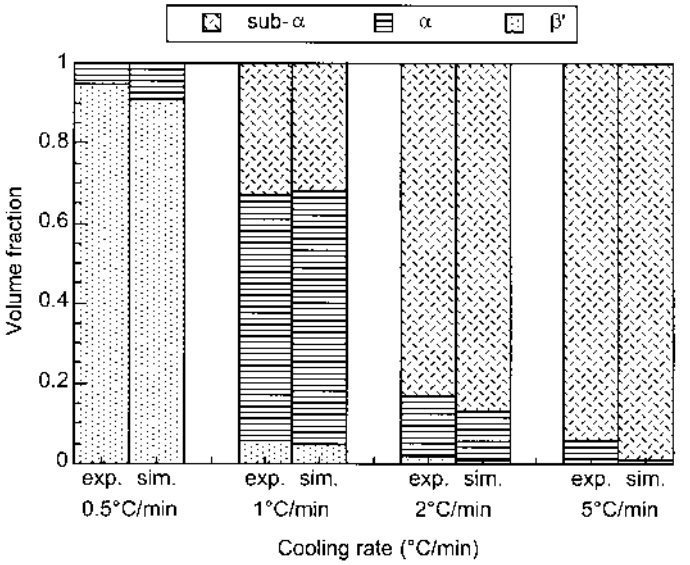

Figure 17 Experimental and simulated volume fractions of the different solid phases formed during solidification at different cooling rates of the binary mixture POS–SOS 25:75 w/w. (From Ref. 49.)

Copyright 2002 by Marcel Dekker. All Rights Reserved.

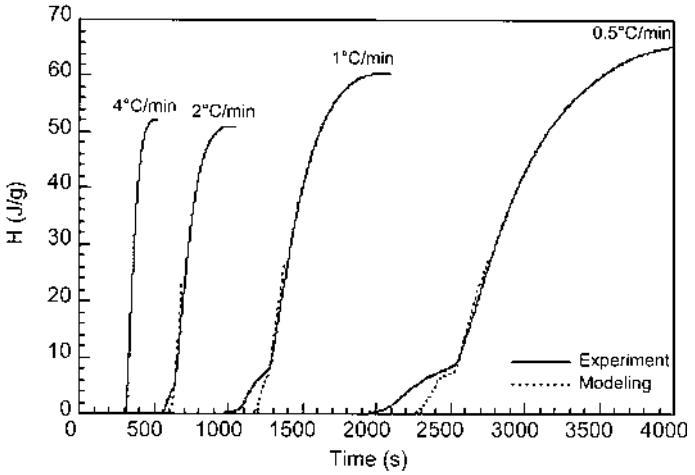

Figure 18 Comparison between the experimental and simulated evolutions of the latent heat released in the DSC pan of a cocoa butter sample cooled at a constant cooling rate. (From Ref. 50.)

3. Static Solidification of Cocoa Butter

The authors' aim was to validate the FEM-TTT model on an example of cocoa butter crystallization, even if the assumptions valid for a pure TAG component are more approximate in the case of cocoa butter.

A cocoa butter sample was cooled at a constant rate in a DSC pan. A simulation was carried out based on the TTT diagram obtained from static isothermal experiments [30].

The sample was initially in a completely liquid state at 37°C. A cooling rate between 0.5 and 4°C/min was chosen. Figure 18 presents the experimental and simulated evolution of the latent heat released by the sample for the four different cooling rates studied. As forecasted, a mixture of phases II and III was formed. Simulated results were similar to the experimental ones. Simulated curves were interrupted before the end of the crystallization, because calculation stopped when the sample reached 14°C. As a matter of fact, below this temperature, experimental measurements could not be obtained because crystallization kinetics was too fast and crystallization started before the isothermal temperature was reached. The slight bump in the experimental curves at slow cooling rates, which is also reproduced in the simulated curves, corresponds to a stop in crystallization between 17 and 16°C, because the maximal fraction of solid that can form does not change between these two temperatures.

Copyright 2002 by Marcel Dekker. All Rights Reserved.

4. Dynamic-Static Crystallization of Cocoa Butter

The model was also applied to crystallization under shear [50]. Cocoa butter, initially at 42°C, was sheared at 600 rpm and cooled at three different cooling rates. Just before the dynamic t_{onset} was reached for the chosen conditions (first t_{onset} was determined for each of the cases), a sample was taken and placed in a DSC pan, where it was submitted to an isothermal plateau at the temperature at which it was taken from the dynamic experiment. This procedure is a rough model for the tempering and cooling of chocolate. Thermal paths followed for the three experiments are presented in Figure 19. For all cases, a mixture of phases IV and V was formed, with a morphology similar to static isothermal solidification. Based on these experimental cooling conditions, solidification of a DSC pan of cocoa butter was simulated with the FEM-TTT software, using the data of the dynamic-static TTT diagram [30]. Figure 20 presents simulated and experimental times of onset and finish of crystallization. The model provides a good estimate of the kinetics of crystallization. In the case of complex crystallization kinetics, the macroscopic approach allows a satisfactory prediction of the crystallization kinetics, insofar as the TTT diagrams are known in the experimental conditions used, even if the hypotheses made in the model are not verified.

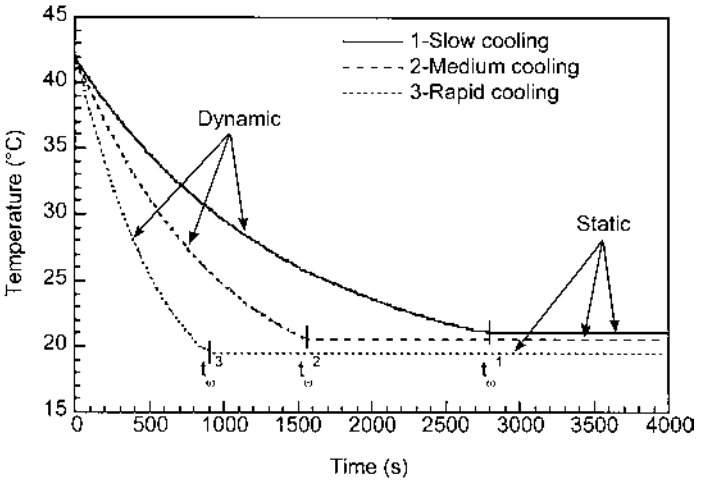

Figure 19 Cooling curves of the cocoa butter sample in the three cases of nonisothermal dynamic-static crystallization considered. The anisothermal part was operated under shear at 600 rpm; the isothermal part was static. (From Ref. 50.)

Copyright 2002 by Marcel Dekker. All Rights Reserved.

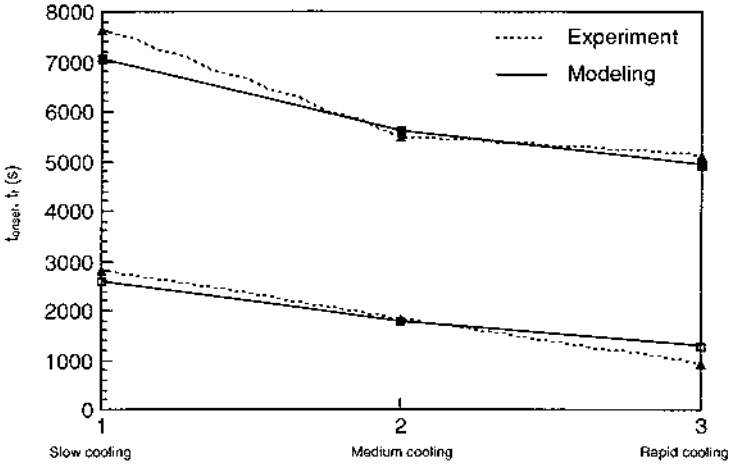

Figure 20 Times of onset and finish of the dynamic-static crystallization of cocoa butter for the three cooling paths considered and presented in Figure 19, measured experimentally and calculated with the FEM-TTT model. (From Ref. 50.)

V. CONCLUSION

Two approaches can be used to model crystallization kinetics of triglycerides and fat. If the microscopic parameters can be determined, the use of microscopic models is the most appropriate, because it applies directly the theory of nucleation and growth. For example, in the case of spherulitic crystallization, kinetic parameters can be determined experimentally. Solidification can then be modeled in a detailed way with a numerical or stochastic model for the nucleation and growth of crystals. The latter kind of microscopic model is very interesting because it also gives the stereological parameters of the microstructure. Probabilistic or numerical models are easier to use, but they provide only the evolution of the latent heat or the evolution of the solid fraction in the sample.

In the case of complex crystallization conditions, macroscopic models can provide quite a good idea of what crystallization to expect. The only difficulty consists in having a macroscopic description of the heat released due to crystallization.

Prediction of solidification times and volume fractions of phases formed showed quite good agreement with the experiments. These approaches are very promising for tackling the crystallization of systems such as fat or even food products, where microscopic parameters are not obtainable. Yet there are still

Copyright 2002 by Marcel Dekker. All Rights Reserved.

quite a number of assumptions for each model, and many experimental data must be acquired on the system to provide the necessary parameters for the models. For example, for the last model presented, isothermal crystallization kinetics data must be acquired before the model can quantitatively predict crystallization during any cooling.

In conclusion, modeling of the crystallization kinetics of TAGs and fats such as cocoa butter is limited by the lack of understanding and lack of experimental data, but it shows interesting applications, allowing better visualization of the phenomena occurring during the solidification of fat or triacylglycerols.

REFERENCES

1. R Strickland-Constable. Kinetics and Mechanisms of Crystallization. London: Academic Press, 1968.
2. R Boistelle. In: N Garti, K Sato, eds. Crystallization and Polymorphism of Fats and Fatty Acids. New York: Marcel Dekker, 1988, pp 189–226.
3. B Chalmers. Principles of Solidification. New York: Wiley, 1964.
4. M Flemings. Solidification Processing. New York: McGraw-Hill, 1974.
5. W Kurz, D Fischer. Fundamentals of Solidification. Adermannsdorf (Switzerland): Trans Tech Pub, 1989.
6. Y Long, R Shanks, Z Stachurski. Prog Polym Sci 20:651–701, 1995.
7. B Wunderlich. Macromolecular Physics, Vol. 2, Crystal Nucleation, Growth, Annealing. New York: Academic Press, 1976.
8. M Volmer, A Weber. Z Phys Chem 119:227, 1926.
9. R Becker, W Doering. Ann Chem Phys 8:212, 1940.
10. D Turnbull, J Fischer. J Chem Phys 17:71–73, 1949.
11. L Phipps. Trans Faraday Soc 60:1873–1883, 1964.
12. D Turnbull. J Chem Phys 18(2):198–202, 1950.
13. JD Hoffman, G Davis, J Lauritzen. In: NB Hanney, ed. Treatise on Solid State Chemistry. New York: Plenum Press, 1976.
14. H Frisch. J Chem Phys 27(1):90–94, 1957.
15. J Kenny, A Maffezzoli, L Nicolais. Thermochim Acta 227:83–95, 1993.
16. E Buckle. Proc Roy Soc Lond A 261:189–196, 1961.
17. M Muchova, F Lednicky. J Macromol Sci Phys B 34(1&2):55–73, 1995.
18. D Ovsienko, G Alfintsev. In: HC Freyhardt, ed. Crystals. Growth and Properties. Berlin: Springer Verlag, 1980, pp 118–169.
19. JD Hoffman, L Frolen, G Ross, J Lauritzen. J Res NBS A Phys Chem 79A(6):671–699, 1975.
20. D Bassett. CRC Crit Rev Solid State Mater Sci 12(2):97–163, 1982.
21. H Keith, F Padden. J Appl Phys 34(8):2409–2421, 1962.
22. B Wunderlich. Macromolecular Physics, Vol. 1, Crystal Structure, Morphology, Defects. New York: Academic Press, 1973.

Copyright 2002 by Marcel Dekker. All Rights Reserved.

23. M Kellens, W Meeussen, H Reynaers. J Am Oil Chem Soc 69(9):906–911, 1992.
24. DM Manning, PS Dimick. Food Microstruct 4:249–265, 1985.
25. N Garti, K Sato. Crystallization and Polymorphism of Fats and Fatty Acids. New York: Marcel Dekker, 1988.
26. G Eder, H Janeschitz-Kriegl, S Liedauer. Prog Polym Sci 15:629–714, 1990.
27. H Janeschitz-Kriegl, S Liedauer, H Wippel, G Eder. Int J Polym Mater 20:213–221, 1993.
28. G Ziegleder. Int Z Lebensm Technol Verfahrenstech 36(6):412–416, 1985.
29. G Ziegleder. Suesswaren 32:487–493, 1988.
30. P Rousset. Etude expérimentale et modélisation de la cristallisation de triacylglycérols et du beurre de cacao. PhD Dissertation 1718. Ecole Polytechniques Fédérale, Lausanne, Switzerland, 1997.
31. G Eder, H Janeschitz-Kriegl. Colloid Polym Sci 266:1087–1094, 1988.
32. W Kloek, P Walstra, T van Vliet. J Am Oil Chem Soc 77(4):389–398, 2000.
33. K van Putte, BH Bakker. J Am Oil Chem Soc 64:1138–1143, 1987.
34. M Avrami. J Chem Phys 7:1103–1112, 1939.
35. M Avrami. J Chem Phys 8:212–224, 1940.
36. W Kloek. Mechanical properties of fats in relation to their crystallization. PhD Dissertation. Wageningen Agric Univ, Wageningen, The Netherlands, 1998.
37. Ch Charbon. Modélisation stochastique de la solidification eutectique équiaxe. PhD dissertation 1347. Ecole Polytechniques Fédérale, Lausanne, Switzerland, 1995.
38. Ch Charbon, A Jacot, M Rappaz. Acta Met Mater 42(12):3953–3966, 1994.
39. P Rousset, M Rappaz. J Am Oil Chem Soc 73:1051–1057, 1996.
40. J Meijering. Philips Res Rep 8:270, 1953.
41. CJG Plummer, HH Kausch. Colloid Polym Sci 273:719–732, 1995.
42. H Tewkesbury, AGF Stapley, PJ Fryer. The use of computational models: Heat transfer in chocolate manufacture. Proc 7th Int Congr Eng Food, Part 1, Sheffield, 1997, pp 61–64.
43. W Rudnicki, M Niezgodka. Phase transitions in cocoa butter. Proc Int Conf Free Boundary Problems—Theory and Applications, Tokyo, Japan, 2000, pp 409–417.
44. K Franke. Modeling the cooling kinetics. J Food Eng 36(4):371–384, 1998.
45. P Thevoz, M Rappaz, J Desbiolles. 3-MOS: A general FEM code for the prediction of microstructures in castings. Light Metals, 1990, pp 975–984.
46. A Jacot. Modélisation des transformations de phase à l'état solide et application au traitement thermique par induction. PhD Dissertation 679. EPFL, Lausanne, Switzerland, 1997.
47. E Scheil. Arch Eisenhütt 8:565–567, 1935.
48. S Denis, D Farias, A Simon. ISIJ Int 32(3):316–325, 1992.
49. P Rousset, M Rappaz, E Minner. J Am Oil Chem Soc 75(7):857–864, 1998.
50. P Rousset, M Rappaz. In: N Widlak, R Hartel, S Narine, eds. Crystallization and Solidification Properties of Lipids, Champaign, AOCS Press, 2001, pp 96–109.

Copyright 2002 by Marcel Dekker. All Rights Reserved.

2

Fat Crystallization in O/W Emulsions Controlled by Hydrophobic Emulsifier Additives

Tarek Samir Awad and Kiyotaka Sato
Hiroshima University, Higashi-Hiroshima, Japan

I. INTRODUCTION

Crystallization of edible fats and oils in oil-in-water (O/W) emulsions is an important process in many industrial fields such as foods [1–4], cosmetics [5], and pharmaceuticals [6]. In the food industry, crystallization in the O/W emulsion phase contributes to the de-emulsifying process in whipped creams, the freezing of ice creams, and coagulation of the O/W emulsions at chilled states. Therefore, the production, quality, and stability of fat products in the emulsion state are highly influenced by crystallization of the oil phase [7], so much recent research has been aimed at the exploration of fat crystallization in O/W emulsions [8–13]. Fat crystallization results in complex phenomena in O/W emulsions and affects such parameters as the rate and extent of crystallization, influences of emulsion droplet sizes, effects of emulsifiers, droplet–droplet interactions, polymorphism, and effects of cooling rate and subsequent temperature history.

Emulsifiers have long been used to stabilize O/W and water-in-oil (W/O) emulsions, because they play the role of decreasing the interfacial tension between the phases, which facilitates the separation of one phase in the form of small droplets [14]. To stabilize the emulsion, an emulsifier forms a thin film (interface) between the internal and external phases. The nature of the thin films formed at the interface of the emulsion droplets is controlled by the type of emulsifier and affects the stability of the emulsion interface [15–17]. For example, the addition of Tween 20 or Tween 60 results in thin interfaces around the oil

Copyright 2002 by Marcel Dekker. All Rights Reserved.

droplets in the O/W emulsions, whereas a thicker layer is formed when protein-type emulsifiers (e.g., Na-caseinate) are added for emulsification. Food emulsions such as margarine (W/O) are often prepared by mixing ingredients at high temperatures followed by cooling at certain temperatures and suitable rates during the homogenization process. Among the different ingredients, emulsifiers play a role in controlling desired properties. Most baked products, such as biscuits and cookies, are oil-in-water emulsions [18]. Bakery products require suitable emulsifiers to facilitate the mixing of oil and water by reducing the interfacial tension. For shortening processes, emulsifiers are chosen according to their efficiency, which provides improved cake volume and symmetry [19–21].

The major emulsifiers are used in sufficient amounts to distribute and stabilize many droplets of the dispersed phase (separating them from the continuous phase). Other types of emulsifiers are also used as minor components, often called additives. Such additives have been proven to affect the physical properties of many emulsion-based food products [22]. By controlling crystallization and polymorphic behavior with emulsifier additives, it is possible to change the size of fat crystals in the emulsion, which is directly related to the total number of crystals. For instance, crystallizing in a certain polymorph, say the α form, results in the formation of quite tiny crystal particles, which provide a homogeneous texture. However, with β or β' polymorphs, the crystal size increases, and both the morphology and orientation of fat crystals become quite influential. Much effort has been exerted by academic and industrial researchers to understand the influence of additives on fat crystallization, enabling many manufacturers to improve the physical properties of food products such as the spreadability of butter [23,24], chocolate bloom resistance [25], and storage life of salad oils [26].

The main objectives of this chapter are to clarify the roles of the hydrophobic emulsifier additives added in the oil phase of O/W emulsions: how they modify fat crystallization and where they interact within the emulsion droplets. One may ask why the hydrophobic emulsifiers accelerate the nucleation process. The answer may not be straightforward, because their influences on fat crystallization are controlled by their physical and chemical properties and the nature of the interactions with the fat molecules occurring in the oil phase and at the oil/water interfaces. However, the results we have obtained so far indicate that the addition of hydrophobic emulsifiers in the oil phase has remarkable effects on crystallization. Fat crystals typically form a number of polymorphs, whose crystallization properties are influenced by many factors, such as temperature, rate of crystallization, time evolution for transformation, and impurity effects, as is commonly revealed in various examples [27,28]. It is reasonable to expect that these polymorphic properties of fats may interfere with the clarification of the essential properties of the interface heterogeneous nucleation that occurs in O/W emulsions.

To realize our purpose, we report results of two-step strategies employed in the last several years. First nucleation mechanisms enhanced by additives of

Copyright 2002 by Marcel Dekker. All Rights Reserved.

hydrophobic emulsifiers were studied using a model fat material, *n*-hexadecane, which does not exhibit polymorphism. Second, similar studies were performed on more complicated systems using fats that demonstrate polymorphism: palm oil, palm midfraction (PMF), and palm kernel oil (PKO). In these studies, we examined the effects of the acyl chain structures of the different hydrophobic emulsifiers with different acid moieties on the rate of crystallization of *n*-hexadecane and edible oils in O/W emulsions, using multiple techniques. It was confirmed that the rate of crystal growth, as measured by using direct microscopic observations of *n*-hexadecane and PMF (seed crystals were added to PMF), were retarded. X-ray diffraction observations have aided in the understanding of the polymorphic behavior of the crystallized fats in the O/W emulsions. It was clear that the emulsifier additives accelerated heterogeneous nucleation of fat crystals in the emulsions.

We believe that the fundamental understanding obtained in the present work sheds new light on polymorph-dependent crystallization accelerated by additives in O/W emulsions.

II. CRYSTALLIZATION KINETICS IN FAT SYSTEMS

A. Bulk Systems

Natural fats and oils are mainly composed of triacylglycerols (TAGs) (esters of glycerol and three fatty acid molecules) together with diacylglycerols, monoacylglycerols, phospholipids, and free fatty acids. Cooling rate and crystallization temperature are the main factors controlling the structure and physical properties of the crystallized TAGs. For example, with a high rate of cooling, many TAG components are crystallized simultaneously, forming solid solution or compound-forming phases [7]. In contrast, slow cooling leads to crystallization of those TAGs with higher melting points, forming the structure of separable eutectic phases. The rate of cooling of fats thereby affects their physicochemical properties such as compressibility, density, and melting behavior. Moreover, chain packing, branching, and the unsaturation of the fatty acids contained in a TAG molecule control its melting temperature (T_m) [7,29–31]. For instance, a TAG having well-packed, straight chains and saturated fatty acids reveals a higher T_m than those having loose packing, branched chains, and unsaturated fatty acids.

In natural fat crystallization systems, nucleation is initiated by some catalytic impurities such as dust particles and foreign substrates (for example, the inner surface of the container). The presence of such impurities initiates nucleation at lower levels of supercooling [32]. As crystallization progresses, nucleation begins to exist at many locations; secondary nucleation would be started due to the presence of solid crystals, which are chemically similar to the components of the melt [33].

Copyright 2002 by Marcel Dekker. All Rights Reserved.

As briefly mentioned above, TAGs exhibit polymorphism, which is defined as the ability of the chemical compound to form different crystalline structures with various states of molecular conformation and molecular packing [34,35]. There are three major polymorphic forms demonstrated by fat systems: α, β, and β′. α is unstable with hexagonal packing (H), β′ is metastable with orthorhombic perpendicular packing ($O_{\perp}$), and β is the most stable form with triclinic parallel packing ($T_{\perp}$) [36,37]. TAGs often crystallize in α or β′ although β is the most stable form. This can be explained by the fact that the β form requires a higher activation energy for crystallization than the other two forms [38]. The polymorphic transformation is an irreversible process from the least to the most stable form [39], depending on temperature and time [40,41]. At fixed temperatures α and β′ forms transform to the β form through solid–solid or solid–liquid–solid transformation mechanisms [42].

The polymorphic crystallization of fats described here must therefore be demonstrated in the fats crystallizing in the O/W emulsions when the oil phase crystallizes in polymorphic systems.

B. Nucleation of Fats in O/W Emulsions

As a general concept of nucleation of crystals, there are two types of nucleation: homogeneous and heterogeneous. Both are critically important for fat crystallization in O/W emulsions [7]. It is considered that heterogeneous nucleation contributes more to crystallization in O/W emulsions; however, some workers in a recent study [43] assumed that homogeneous nucleation contributes more.

In an emulsion system, the dispersed phase is divided into a number of droplets that vary in size (polydisperse). Catalytic impurities are therefore distributed unequally through some of the droplets (Fig. 1). This leads to isolation of the impurities that catalyze heterogeneous nucleation in the bulk system, and in this manner the value of supercooling is increased. For nucleation to be initiated, nuclei must reach a critical radius (size). When a pure fat is emulsified into many droplets, each droplet having a minute size of several micrometers, it becomes difficult to assume that the nucleation process can be homogeneous, because the scattered oil mass has no ability to spontaneously assemble into an ordered domain greater than the critical nucleus size [44]. Therefore, nucleation in emulsions is assumed to be heterogeneous and to occur by reducing the surface energy of droplets.

Heterogeneous nucleation in O/W emulsions is subdivided into three types, depending on the location of the catalytic reactions (Fig. 2):

1. Volume or bulk nucleation initiated by catalytic impurities scattered randomly in the oil phase [45].
2. Interfacial heterogeneous nucleation, which is induced by emulsifier

Copyright 2002 by Marcel Dekker. All Rights Reserved.

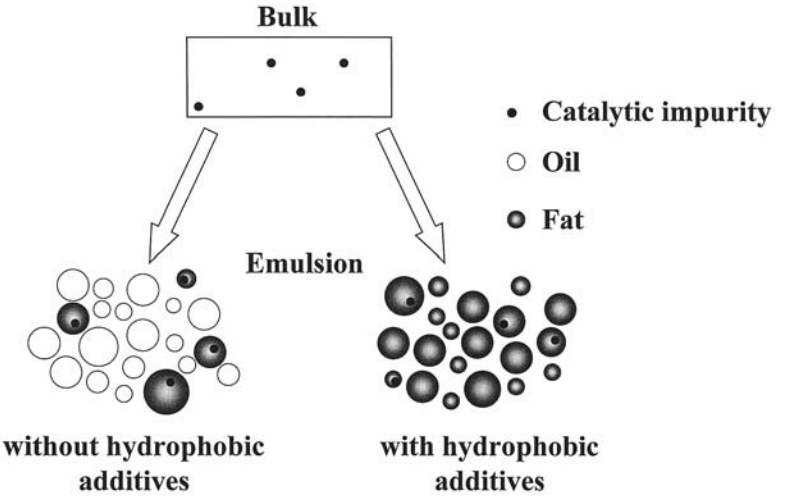

Figure 1 Crystallization of fats in O/W emulsions.

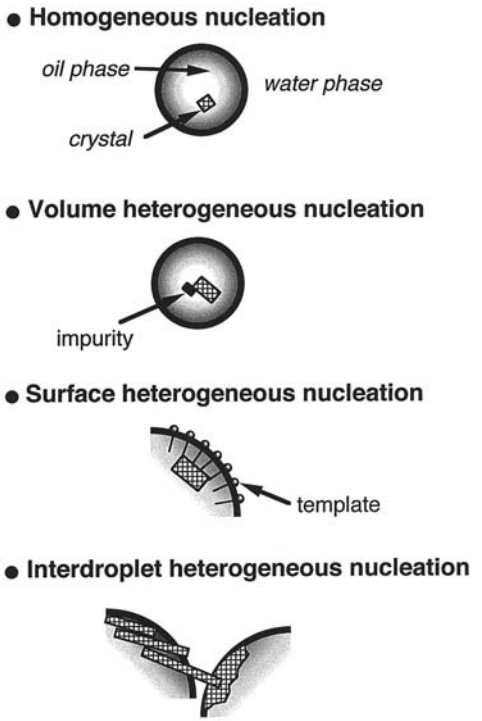

Figure 2 Major types of nucleation of crystals in O/W emulsions.

Copyright 2002 by Marcel Dekker. All Rights Reserved.

molecules providing templates at the O/W interface [1,8,46,47]. These templates assist the fat crystallization.

3. Interdroplet nucleation due to the interaction between solid droplets and liquid droplets [10,48,49].

When the O/W emulsion is heated, it melts far from its crystallization temperature and close to the bulk melting temperature. The difference in the supercooling values between the bulk and emulsion states has been studied [50]. Figure 3 shows the differential scanning calorimetric (DSC) exothermic (crystallization) and endothermic (melting) peaks of *n*-hexadecane in bulk and emulsion states. Although the melting points in the bulk and emulsion states are 18.5°C and 17.4°C, respectively, crystallization of the emulsion droplets is around 3.4°C, whereas it is 16.9°C for the bulk. This variation in the crystallization kinetics may be ascribed to the interaction with the continuous phase (water) and scattering of

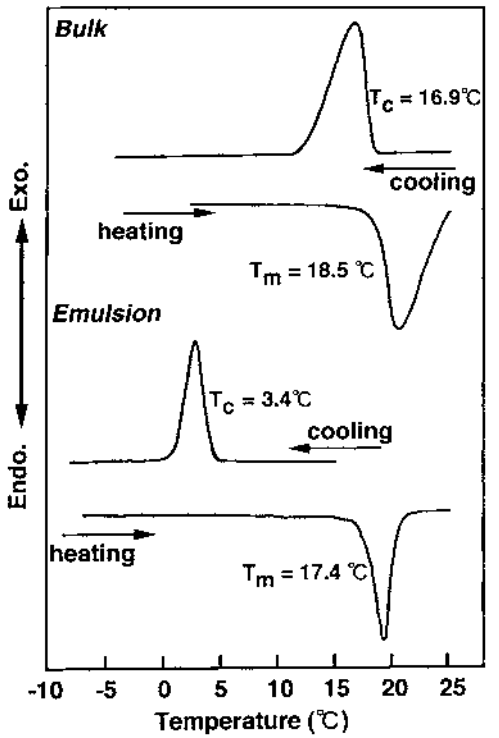

Figure 3 Crystallization and melting behaviors of *n*-hexadecane in bulk and O/W emulsion. (From Ref. 50.)

Copyright 2002 by Marcel Dekker. All Rights Reserved.

Table 1 Major Factors Affecting Fat Crystallization

Bulk	Emulsion
Temperature	Temperature
Cooling rate	Cooling rate
Impurity	Impurity
Polymorphism	Polymorphism
	Droplet size
	Droplet–droplet interaction
	Emulsifiers

the catalytic impurities into narrower areas controlled by the droplet size. Therefore, the catalytic effects of impurities are minimized in the emulsion compared with the bulk. This suggests that crystallization occurs in some droplets, then the other droplets are crystallized owing to contact with or protuberances from the crystallized droplets, which promotes crystallization in the neighboring droplets [33]. The major factors that influence fat crystallization are listed in Table 1.

III. EFFECTS OF HYDROPHOBIC EMULSIFIER ADDITIVES ON FAT CRYSTALLIZATION

A. Bulk Systems

In bulk media without impurities or template thin films, no crystallization occurs over a long time when supercooling or supersaturation is minimized. However, when template thin films are added, the induction time is dramatically minimized, as experimentally evidenced for *n*-alcohol crystallization in solution [51,52]. In such studies, the template effect was varied according to the type of host templates and the relationship between the chain lengths of the host and guest molecules (numbers of carbon atoms).

The additives affect the crystallization of many fat blends in different ways. For example, the addition of diglycerides retarded crystal growth in cocoa butter [53,54], whereas the crystal growth of trilaurin was either retarded or enhanced by additions of lauric-based molecules, depending on the shape of the molecules [55]. In a similar study the chain length of partial glycerides was the effective factor in controlling the rate of crystal growth of crystallized trilaurin [56]. In addition, the effects of some phospholipids on the crystallization of triglycerides have been shown to change the crystal habit of the resultant fat crystals [57]. Moreover, emulsifiers have been reported to play a role in polymorphic transitions [58–60].

Copyright 2002 by Marcel Dekker. All Rights Reserved.

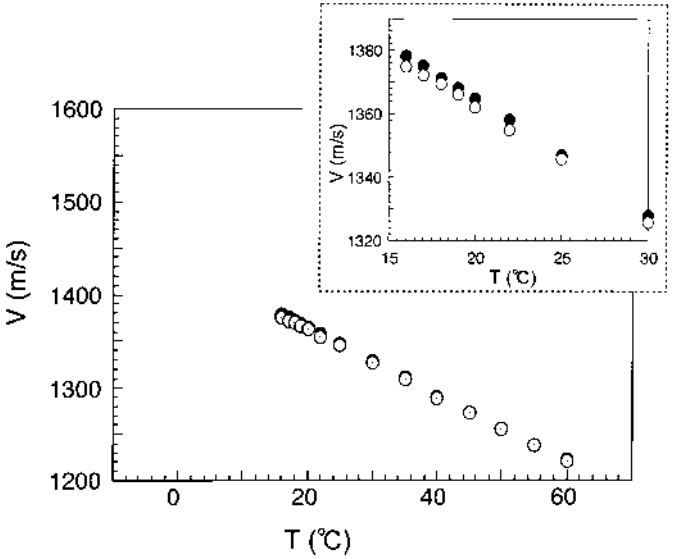

Figure 4 Temperature variation of ultrasonic velocity V of bulk n-hexadecane. (⊙) Pure; (●) with the addition of 1.0 wt% sucrose oligoesters. (From Ref. 61.)

As for the addition of hydrophobic emulsifiers to n-hexadecane, however, the additive did not demonstrate template (or seeding) effects in the bulk state [61]. Figure 4 shows the temperature variation of the ultrasonic velocity of bulk n-hexadecane systems on cooling with and without the addition of three sucrose oligoesters (SOEs). The ultrasonic velocity value increased with cooling in a linear manner and then disappeared below 16°C owing to the sudden rise in the rate of crystallization of n-hexadecane, which randomly scattered the ultrasonic wave. No visible effects were detectable on the rates of crystallization of bulk n-hexadecane from the addition of 1.0 wt% of three SOEs within experimental errors of ±1°C. This can be explained by the incapability of SOEs to arrange as catalytic template impurities in the bulk liquid, which may accelerate the heterogeneous nucleation mentioned above.

B. O/W Emulsions

Let us now consider what happens when the emulsion is homogenized with a hydrophobic emulsifier. As illustrated in Figure 1, hydrophobic emulsifier molecules are adsorbed preferentially at the O/W interface and, as will be shown later, the supercooling decreases and the extent of crystallization is enhanced. McClements et al. [47] performed a comparative study on the effects of palmitoyl

Copyright 2002 by Marcel Dekker. All Rights Reserved.

(Tween 40), stearoyl (Tween 60), and lauroyl (Tween 20) chains, indicating that Tween 40 and 60 accelerate the crystallization compared with Tween 20 because of the effects of the template films of the interface layers of the emulsifiers employed for the emulsification itself. Thus, it is reasonable to consider the effects of the absorbed layer on the formation of templates that were formed by the additives put into the oil phase.

In this section, we describe the effects of the hydrophobic emulsifier additives on fat crystallization using *n*-hexadecane as the simple model fat and palm oil, palm midfraction, and palm kernel oil as the real fat systems.

1. *n*-Hexadecane

In a series of experiments we employed sucrose oligoesters (SOEs), diacylglycerols (DAGs), and polyglycerol esters (PGEs) as nucleation-accelerating additives for *n*-hexadecane dispersed in oil-in-water emulsions [61–64]. Ultrasonic velocity and DSC measurements provided much important information about the fat crystallization in both bulk and emulsion systems. In particular, the ultrasonic velocity measurement was quite useful, because it increases and decreases during crystallization and melting, respectively [8,10–12,47,65–74]. It has been shown that the ultrasonic methods could be used to obtain information about the oil phase dispersed in an emulsion such as volume fraction, droplet size, and creaming profiles [7].

(a) Sucrose Oligoesters. The acceleration effects of sucrose oligoesters (SOEs) on crystallization temperature (T_c) have been observed during cooling processes from 20 to −5°C, in which different concentrations of an SOE having a stearic acid moiety (S-170) was added to the oil phase [61]. From the variation in the ultrasonic velocity values *V* exhibited in Figure 5, we can observe the following:

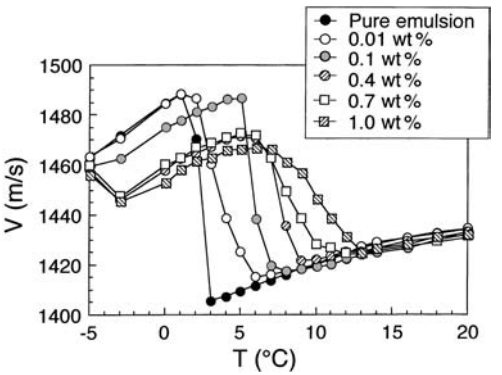

Figure 5 Temperature variation of ultrasonic velocity *V* of *n*-hexadecane–water emulsion with the addition of S-170 during the cooling process. (From Ref. 61.)

Copyright 2002 by Marcel Dekker. All Rights Reserved.

1. On cooling, V abruptly increased from around 2°C (pure emulsion) and to around 12°C (with S-170 of 1.0 wt%), owing to the crystallization of the *n*-hexadecane phases in the emulsion. The temperature at which the abrupt increase of the V value was detectable was defined as the crystallization temperature of *n*-hexadecane (T_c).
2. The rate of increase in the V values after the onset of crystallization decreased with increases in the amount of S-170. To extend our observations to a more demonstrative system, a DSC study was carried out as shown in Figure 6. T_c of the pure sample was calculated as 3.4°C as shown in the top of Figure 6a; the addition of 1 wt% of P-170 increased T_c to 13°C. As can be also seen, the exothermic peaks are shifted toward the high temperature side by increasing the amount of

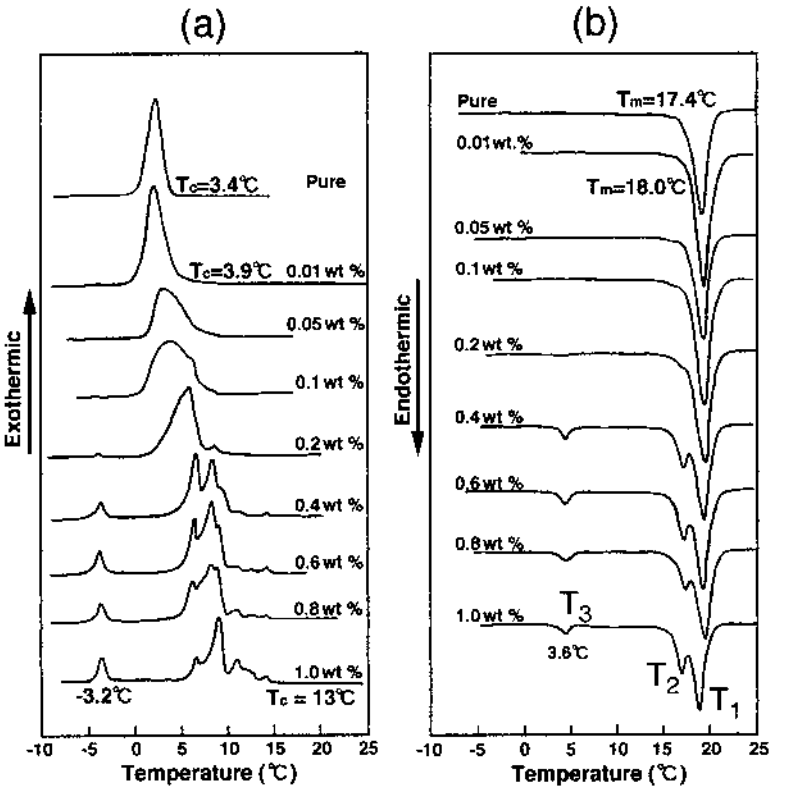

Figure 6 (a) Cooling and (b) heating DSC thermopeaks of *n*-hexadecane–water emulsion with the addition of S-170. (From Ref. 50.)

Copyright 2002 by Marcel Dekker. All Rights Reserved.

P-170. Above 0.1 wt% additive, a small exothermic peak clearly appeared around −3.2°C, and its height increased as the additive concentration was increased. This peak, which might correspond to the template formation at the interface, was not observed for the pure emulsion. The small downward peak shown in Figure 6b on heating may correspond to the structure transformation of template that appeared in the cooling process shown in Figure 6b. In addition, the two peaks T1 and T2 in Figure 6b may correspond to the melting of *n*-hexadecane and template, respectively. The effects of the addition of P-170 or other SOEs on the T_c of *n*-hexadecane are controlled by many factors related to the template structure. The total mechanism of template formation and the actual role of the additives at the interface are discussed in the final section.

To obtain information about the effects of fatty acid moieties on interfacial heterogeneous nucleation, different SOEs were examined. Figure 7 shows the effects of four SOEs having palmitic, stearic, lauric, and oleic acid moieties. The figure clearly shows the following:

1. The addition of S-170 and P-170 increased the T_c of *n*-hexadecane through two stages, depending on the concentration.
2. The addition of the SOE with lauric acid moieties (L-195) slightly increased T_c, but the effect was less manifest than with S-170 and P-170.

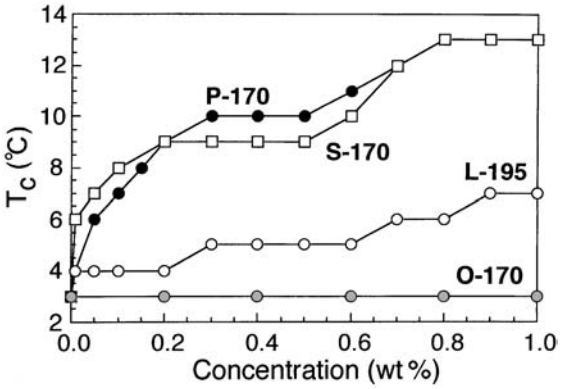

Figure 7 Variations in crystallization temperature T_c of *n*-hexadecane–water emulsions at different concentrations of sucrose oligoesters (P-170, S-170, L-195, O-170). (From Ref. 61.)

Copyright 2002 by Marcel Dekker. All Rights Reserved.

3. The SOE additives with oleic acid moieties (O-170) showed no detectable effects on the T_c of *n*-hexadecane.

The effects of SOEs were explained in terms of the physical properties of their acid moieties: The higher the melting points of the SOEs due to their chain moieties, the more accelerated was the observed nucleation. Table 2 shows the melting points of the four SOEs.

(b) Polyglycerine Esters. The addition of a polyglycerine ester (PGE) with a stearic acid moiety (DAS-750) was found to accelerate the nucleation of *n*-hexadecane in O/W emulsions [63], yet its behavior was somewhat different from that of SOEs with stearic acid moieties discussed above. Figure 8 shows the results without (pure) and with the addition of DAS-750 in small amounts (0.005 wt%) and in large amounts (1 wt%). The ultrasonic velocity measurements (Fig. 8a) show that T_c increased from 3°C (pure) to 8°C in the same manner for the two additions of DAS-750. Figure 8b shows schematic DSC thermograms of the same samples. T_c values were obtained for the pure emulsion (3.3°C) and for the emulsion with additives (8.1°C). As revealed from the exothermal peaks, the results were the same as those of the ultrasonic velocity measurements.

(c) Diacylglycerols. Five diacylglycerols (DAGs) with fatty acid moieties of behenic (DB), stearic (DS), palmitic (DP), lauric (DL), and oleic acid (DO) were added to the *n*-hexadecane [64]. Figure 9a shows the *V* values obtained by adding

Table 2 Melting and Crystallization Temperatures of Selected SOEs and DAGs

	T_c(°C)	T_m(°C)
SOE		
L-195	17.9	28.0
P-170	52.6	61.5
S-170	58.2	68.0
O-170	n.d.	n.d.
PGE		
DAS-750	46.9	53.0
DAG		
Dibehenic (DB)	72.7	77.7
Distearic (DS)	66.6	74.7
Dipalmitic (DP)	58.7	69.0
Dilauric (DL)	48.1	56.6
Dioleic (DO)	6.4	20.5

SOE = sucrose oligoester; DAG = diacylglycerol; PGE = polyglycerine ester.
n.d. = not detected.
Source: Refs. 61 and 64.

Copyright 2002 by Marcel Dekker. All Rights Reserved.

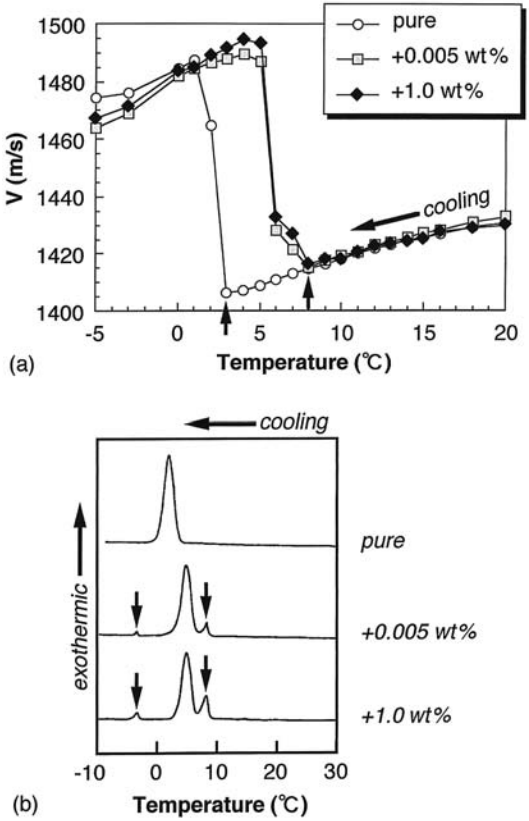

Figure 8 Variations in crystallization temperature T_c of *n*-hexadecane–water emulsions at different concentrations of polyglycerine ester (DAS-750) using (a) ultrasonic velocity technique and (b) DSC. (From Ref. 63.)

different concentrations of DB to the emulsion. At low concentrations of DB (0.01–0.05 wt%), a gradual increase in the V value was observed soon after the crystallization was initiated. When the DB concentrations were 0.1 and 0.2 wt%, two-step increases in V were observed; V increased at 8°C and again at 6°C after a gentle slope. Above these concentrations (data not shown) and up to 1 wt%, no further increase in the T_c value above 8°C was observed. Although also not shown here, the effects of DS and DP were similar to those of DB. However, the concentrations of DS and DP at which T_c reached to 8°C were 0.2 and 0.3 wt%, respectively. In contrast, DL and DO had no effect. Similar results were obtained from the DSC study.

To compare the modification ability of the different DAGs, T_c is shown as a function of the DAG concentration in Figure 9b. The figure shows that T_c

Copyright 2002 by Marcel Dekker. All Rights Reserved.

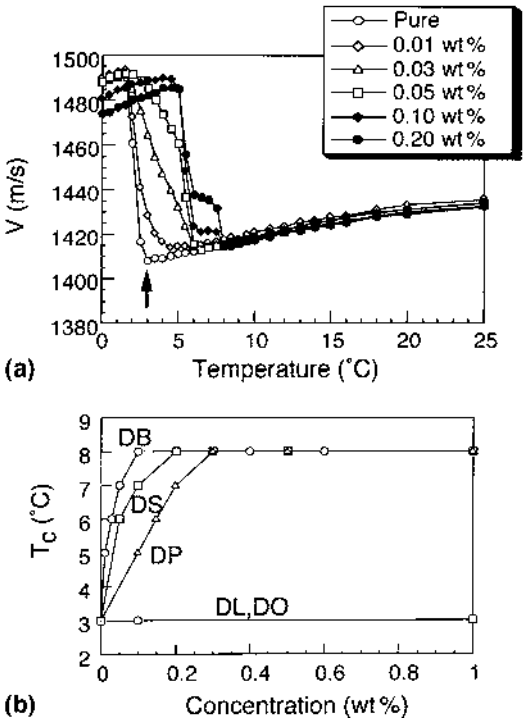

Figure 9 Variations in (a) ultrasonic velocity V values and (b) crystallization temperature T_c of *n*-hexadecane–water emulsions at different concentrations of DAGs.

dramatically increased from 3°C to 8°C with the additions of DB, DS, and DP at lower concentrations (below 0.3 wt%), whereas no increase in T_c was observed for DL and DO. In addition, the degree of T_c increase was in the order DB > DS > DP, indicating the effectiveness of acceleration of crystallization dependent on the fatty acid chains. The carbon numbers of behenic, stearic, palmitic, and lauric acid are 22, 18, 16, and 12, respectively. The melting points of the five DAGs were measured by DSC and are given in Table 2 together with the melting points of SOEs and PGE. Combining the above results with the data in the table, we can say that the acceleration of nucleation of the five DAGs clearly depends on the melting points of the DAGs, which are dominated by their fatty acid structures.

(d) Effect of Polar Headgroup. Our studies have proved that, in addition to effect of the fatty acid moiety, the polar headgroup intensely affects the fat crystallization in the framework of heterogeneous nucleation. In the case of SOEs,

Copyright 2002 by Marcel Dekker. All Rights Reserved.

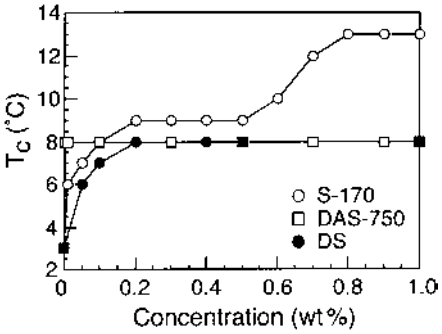

Figure 10 Variations in crystallization temperature T_c of *n*-hexadecane–water emulsions at different concentrations of sucrose oligoester (S-170), polyglycerine ester (DAS-750), and diacylglycerol (DS).

the increase in T_c showed two stages with increasing concentration (Fig. 10). It is considered that the first-stage increase in T_c at the lower additive concentrations is due to the aggregates formed at the interface, whereas the second-stage increase is caused by the formation of reversed micelles from the inside of the oil phase, as will be discussed later. In the cases of PGE and DAGs, T_c increased with increasing concentration by as much as 8°C within one stage. This indicates that PGE and DAGs have no ability to form reversed micelles at the high concentrations that accelerate the nucleation in the oil phase at the supercooling range shown in Figure 10.

(e) Crystal Growth of n*-Hexadecane Crystals.* The growth rates of bulk *n*-hexadecane crystals with the addition of SOEs and PGEs were measured in bulk liquid by using an optical microscope. The rate of displacement of the growing lateral surface of platelike crystals of *n*-hexadecane was monitored in situ at 17.1°C. The basal surfaces were not observed, because the lateral surfaces grew much faster than the basal surfaces.

The addition of S-170 [61], L-195 [61], or P-170 [62] retarded the rate of crystal growth (Fig. 11). This result proves that crystal growth does not account for the increase in T_c in the O/W emulsion; instead, the additives retard the rate of crystal growth. The addition of O-170, which showed no detectable effects on the T_c of *n*-hexadecane in the O/W emulsion system, scarcely retarded the rate of crystal growth. The retardation effects of PGEs on the rate of crystal growth of *n*-hexadecane were also observed [63]. From this, it is obvious that the acceleration effect by the additives of the hydrophobic emulsifiers must be interpreted by the nucleation process.

Copyright 2002 by Marcel Dekker. All Rights Reserved.

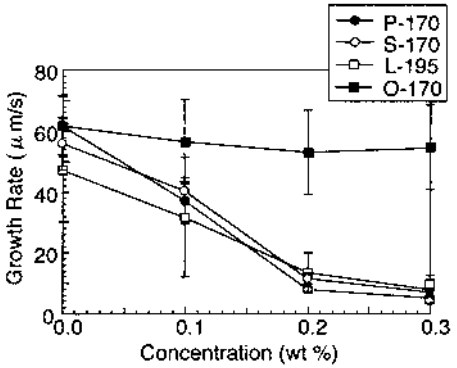

Figure 11 Variations in crystal growth rate of *n*-hexadecane from bulk liquid at 17.1°C with increasing concentrations of P-170, S-170, L-195, and O-170. (From Ref. 61.)

2. Palm Oil

Palm oil represents about 23% of the world output of vegetable oils and is employed as a food fat in its bulk state, for example in shortening or in emulsions such as margarine and cream [75,76]. The effects of the addition of the SOEs (S-170, P-170, and O-170) on palm oil in the O/W emulsion were studied by ultrasonic measurements [12]. It was shown that S-170 and P-170 reduced the degree of supercooling and hence accelerated the nucleation, yet the effect of O-170 was negligible. Table 3 shows the T_c of palm oil in bulk and in O/W emulsion, in which the T_c was defined in the same manner as for *n*-hexadecane. In the bulk without impurities, T_c was 34°C. With the addition of 1 wt% P-170

Table 3 Melting and Crystallization Temperatures of Palm Oil in Bulk State and in O/W Emulsion

	T_c(°C)	
	Bulk	Emulsion
Pure palm oil	34	11
Palm oil + S-170	30	20
Palm oil + P-170	30	18
Palm oil + O-170	34	12

Source: Ref. 12.

Copyright 2002 by Marcel Dekker. All Rights Reserved.

or S-170, T_c decreased to 30°C, and no effect was observed with the addition of O-170 in the same amount.

In the emulsion system (Fig. 12), T_c increased from 11°C (pure) to 20°C, 18°C, and 12°C with the additions of 1 wt% S-170, P-170, and O-170, respectively. The polymorphic behavior of the palm oil emulsion during crystallization at 10°C was examined by X-ray diffraction short spacing spectra, which showed that β′ was formed in the O/W emulsion [12]. However, no polymorphic transformation was indicated during the isothermal crystallization.

From the above results, it can be concluded that the crystallization of palm oil in the emulsion occurs quite slowly, exhibiting severe irreversible hysteresis properties. These properties were not observed in *n*-hexadecane experiments, where the ultrasonic velocities on cooling and heating in both the crystalline

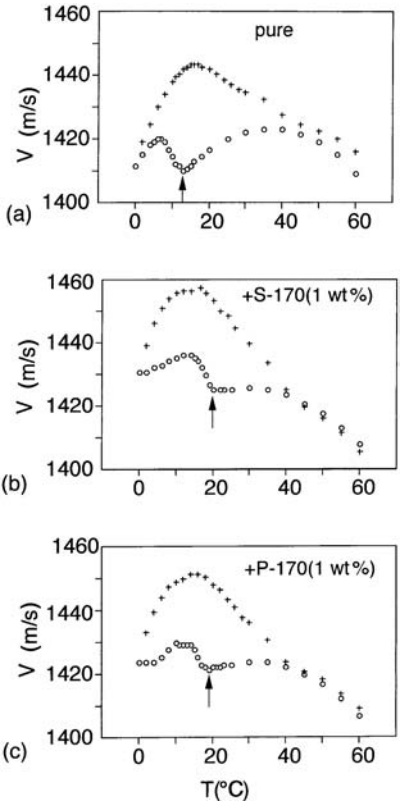

Figure 12 Time variation of ultrasonic velocity V of palm oil in O/W emulsion. (a) Pure emulsion; (b) with 1 wt% S-170; (c) with 1 wt% P-170. (○) cooling, (+) heating. The arrows point to T_c. (From Ref. 12.)

Copyright 2002 by Marcel Dekker. All Rights Reserved.

and liquid phases were the same. The difference in the thermal hysteresis in hexadecane–water emulsions was observed in supercooling.

3. Palm Midfraction

Palm midfraction (PMF), a fraction of palm oil whose melting points are between those of palm stearin and palm olein [77], has been employed for vegetable-fat-based creams as well in the production of cocoa butter equivalent fats (CBEs) used in chocolate [78]. The effects of additions of SOEs and PGEs on the crystallization of PMF in O/W emulsions were studied recently [79]. Figure 13a shows the isothermal crystallization behavior of PMF in oil-in-water emulsion at 10°C without (pure) and with the addition of 1 wt% S-170. It is obvious that the *V* values of the pure emulsion are always smaller than in emulsions with S-170

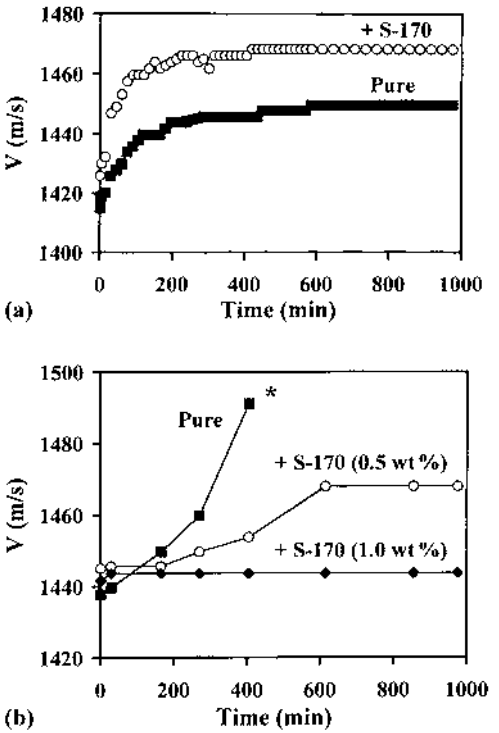

Figure 13 Time variation of (a) ultrasonic velocity *V* of PMF–water emulsions without (pure) and with the addition of S-170 during isothermal crystallization at 10°C and of (b) isothermal crystallization of bulk PMF at 25°C. *: Signal disappeared.

Copyright 2002 by Marcel Dekker. All Rights Reserved.

added. In addition, the rate of increase in V at early stages of the isothermal crystallization and the maximum V values reached at the final stage were both greater in the emulsion with S-170 added than in the pure emulsion. To prove the effects of SOEs on the acceleration of heterogeneous nucleation of PMF in an O/W emulsion, it is necessary to separate nucleation and crystal growth processes by supplying the melt with seed crystals [80]. Seed crystals of PMF (10%) were added at 25°C to the bulk PMF melt, which was cooled at the same temperature in the cell employed for the ultrasonic measurement before addition of the seed crystal [79]. As shown in Figure 13b, the V value of the bulk increased as a function of time when 0.5 wt% S-170 was added to the PMF, but the extent of increase was smaller than with the pure PMF. The addition of 1 wt% S-170 did not increase the V values. Because no nucleation was expected to occur at this crystallization temperature, the results of Figure 13b indicate that S-170 retarded the crystal growth rate, quite similarly to its effects on *n*-hexadecane.

The effects of an SOE (S-170) and a PGE (DAS-750) on the polymorphic transformation of PMF in O/W emulsion were monitored in situ by X-ray diffraction [79]. Figure 14a clearly shows that the crystallization of the pure emulsion occurred at 13°C in the α form that is shown by the single diffraction peak appeared at 0.42 nm, the β′ form appeared at 9°C as represented by the two peaks at 0.43 and 0.38 nm, and finally, at 7°C, the amount of α was greater than that of β′. With the addition of S-170 (1 wt%), as shown in Figure 14b, PMF crystallized at 17°C in the β′ form. On further cooling, the amount of β′ increased, and very little evidence of α crystallization was observed. Eventually, the amount of β′ was predominant at 7°C. However, with the addition of DAS-750 (1 wt%) as shown in Figure 14c, the sample started to crystallize in the β′ form at 17°C, but α started to crystallize and grew fast at 13°C. At 7°C, there was more α than β′. The results clearly indicate that the behavior of the polymorphic occurrence of PMF was modified by the addition of two hydrophobic emulsifiers in a different manner: S-170 preferably crystallized β′; DAS also crystallized β′, yet the rate of growth of β′ was minimized. In both cases, the α form crystallized below its melting point (13°C).

4. Palm Kernel Oil

Palm kernel oil (PKO) is extracted from the seed of the palm fruit. It is characterized by a high content of lauric and myristic acids, which are present in amounts of less than 2% in palm oil [78]. PKO is used in many foods such as chocolate and bakery products. Figure 15 shows the effects of different types of hydrophobic emulsifier additives on the crystallization temperature of PKO in O/W emulsions during cooling from 60 to −10°C. The addition of maximum amounts of S-170 and P-170 increased T_c from 0°C (pure emulsion) to 15 and 12°C, respectively. In contrast, the addition of L-195 had no effect.

Copyright 2002 by Marcel Dekker. All Rights Reserved.

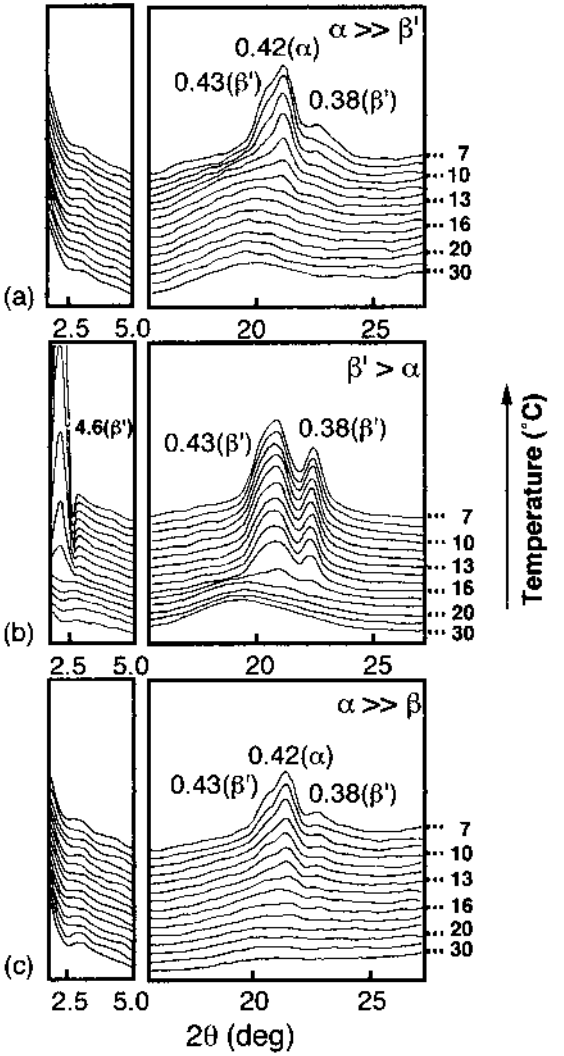

Figure 14 X-ray diffraction short and long spacing spectra of PMF–water emulsions during cooling from 30 to 7°C. (a) Pure emulsion; (b) with 1 wt% S-170; (c) with 1 wt% DAS-750.

Copyright 2002 by Marcel Dekker. All Rights Reserved.

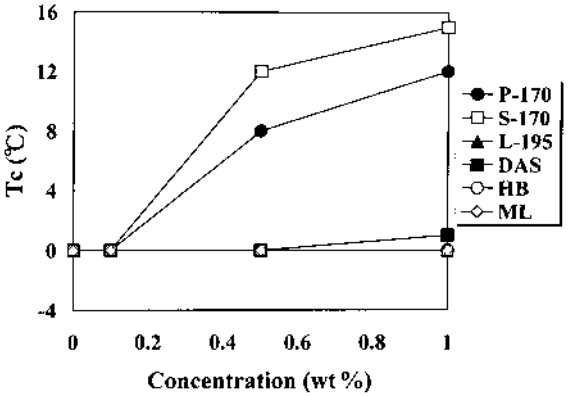

Figure 15 Variation in crystallization temperature T_c of palm kernel oil–water emulsions with different emulsifier additives.

The addition of three polyglycerine esters with behenic acid (HB-750), lauric acid (ML-750), and stearic acid (DAS-750) moieties showed that HB-750 and ML-750 had no effects up to a concentration of 1 wt%, whereas the same amount of DAS increased T_c to a lesser extent, i.e., 1°C.

IV. INTERFACIAL HETEROGENEOUS NUCLEATION

The effects of the addition of the hydrophobic emulsifiers on the rate and extent of crystallization of *n*-hexadecane and natural fats described in this chapter can be summarized as follows.

1. The addition of SOEs accelerated the nucleation process in the emulsion system through two stages as shown in the results for *n*-hexadecane (Fig. 7) and PMF. The acceleration effects were more enhanced with SOEs that have long saturated fatty acid chains.
2. The addition of PGEs and DAGs increased the T_c values through one stage as shown in Figure 10. This indicates that the ability of PGE or DAG to enhance heterogeneous nucleation is limited compared with that of SOEs.
3. Although the nucleation process was accelerated by the additives, the rate of crystal growth was retarded. Nevertheless, the total extent of crystallization was increased by the addition of the emulsifiers because of the accelerated nucleation.

Copyright 2002 by Marcel Dekker. All Rights Reserved.

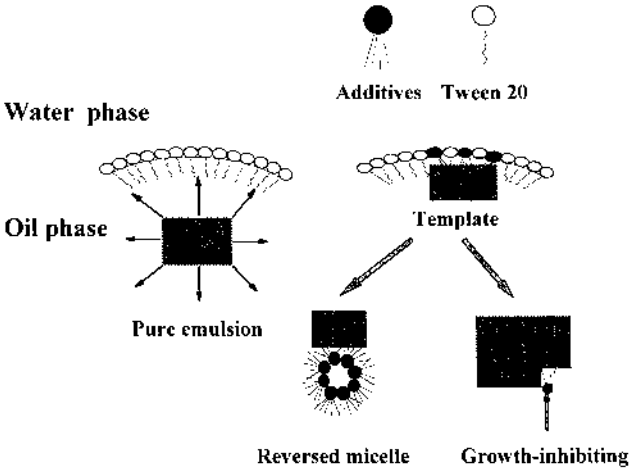

Figure 16 Schematic molecular model of interface heterogeneous nucleation.

Combining the above experimental results, the mechanism of heterogeneous nucleation at the interface (Fig. 16) can be summarized by the following discussion.

1. Additive molecules are preferentially adsorbed at the O/W interface, forming thin films. Prior to the crystallization of the oil phase, these films are crystallized, forming templates that accelerate the heterogeneous nucleation of the fat crystals at higher temperatures compared with the pure emulsion. At lower concentrations, the total amount of impurities is incorporated to the O/W interface, providing interfacial heterogeneous nucleation.
2. Reversed micelles are formed in the oil mass for the SOEs with increasing concentration of additives. The micelles promote heterogeneous nucleation in the oil droplets. Although the SOEs used in the present work are highly hydrophobic, they are scarcely solubilized in the oil phase as monomers owing to the repulsive interaction between oils and their sucrose units [81]. The SOEs tend to form molecular aggregates such as inverse micelles at high concentrations [82,83]. The acceleration of fat crystallization by the reversed micelles was indicated in cocoa butter [84,85] and triglycerides [1]. Thus, when the concentration of the SOEs was increased, the increase of T_c due to templates at the interface was followed by the effects of the reversed micelles.
3. PGEs and DAGs may accelerate heterogeneous nucleation by adsorp-

Copyright 2002 by Marcel Dekker. All Rights Reserved.

tion of their molecules at the oil/water interface. They may not have the ability to form reversed micelles in the oil mass.

4. The effects of emulsifier additives on crystal growth can be explained if we imagine the crystal surface during growth as being perturbed by impurity particles. This results in blocking of the growth at the growing crystal surfaces: The more impurity particles, the more areas are affected, which results in greater retardation of crystal growth.

V. SUMMARY

The rates of crystallization of *n*-hexadecane and other fats in the O/W emulsions were modified by the addition of different categories of hydrophobic emulsifiers, indicating two conflicting influences: acceleration of nucleation and retardation of crystal growth. It was suggested that the additives may accelerate interfacial heterogeneous nucleation, which occurs through template films formed at the oil/water interface. With higher concentrations of SOEs, heterogeneous nucleation may be accelerated at the surfaces of reversed micelles in the oil phase.

As an application to real food fats, the acceleration effects of the additives on the heterogeneous nucleation of palm oil, PMF, and PKO droplets may be used to control fat crystallization in food emulsions. As for PMF, the results clearly indicated that polymorphism was modified by the addition of hydrophobic emulsifiers. The preferential crystallization of β′ was explained by assuming that the nature of the acyl chain packing of templates and the shape of their polar headgroup influence the degree of β′ nucleation. The preferred crystallization of β′ by the additives may be applied to food fats.

Molecular level observation of template-assisted heterogeneous nucleation in O/W emulsions and the relation of fat crystallization behavior and emulsion stability to additives may be of high relevance to further research.

REFERENCES

1. W Skoda, M Van den Tempel. J Colloid Sci 18:568–584, 1963.
2. V Boekel, P Walstra. Colloid Surf 3:109–118, 1981.
3. K Boode, C Bisperink, P Walstra. Colloid Surf 61:55–74, 1991.
4. P Walstra. In: PF Fox, ed. Advanced Dairy Chemistry. London: Chapman and Hall, 1995, pp 179–211.
5. J Wang, GHJ Lee. Soc Cosmetic Chem 48:41–50, 1997.
6. F Espitalier, B Biscans, JR Authelin, C Laguerie. Chem Eng Res Design 75:257–267, 1997.

Copyright 2002 by Marcel Dekker. All Rights Reserved.

7. E Dickinson, DJ McClements. In: E Dickinson, DJ McClements, eds. Advances in Food Colloids. London: Blackie A&P, 1996, pp 211–246.
8. E Dickinson, DJ McClement, MJW Povey. J Colloid Interface Sci 142:103–110, 1991.
9. J Coupland, E Dickinson, DJ McClements, MJW Povey, CR Mimmerand. In: E Dickinson, P Walstra, eds. Food Colloids and Polymers: Stability and Mechanical Properties. Cambridge, UK: Roy Soc Chem, 1993, pp 243–249.
10. DJ McClements, E Dickinson, SR Dungan, JE Kinsella, JG Ma, MW Povey. J Colloid Interface Sci 160:293–297, 1993.
11. DJ McClements, SW Han, SR Dungan. J Am Oil Chem Soc 71:1385–1389, 1994.
12. Y Hodate, S Ueno, J Yano, T Katsuragi, Y Tezuka, T Tagawa, N Yoshimoto, K Sato. Colloid Surfaces A 128:217–224, 1997.
13. S Özilgen, C Simoneau, JB German, MJ McCarthy, DS Reid. J Sci Food Agric 61: 101–108, 1993.
14. T Katsuragi. In: N Widlak, ed. Physical Properties of Fats, Oils and Emulsifiers. Champaign, IL: AOCS Press, 1999, pp 209–217.
15. HD Goff, WK Jordan. J Dairy Sci 72:18–29, 1989.
16. DG Dalgleish, M Srinivasan, H Singh. J Agric Food Chem 43:2351–2355, 1995.
17. T Harada, K Yokomizu. J Am Oil Chem Soc 77:859–863, 2000.
18. WH Knightly. In: N Widlak, ed. Physical Properties of Fats, Oils and Emulsifiers. Champaign, IL: AOCS Press, 1999, pp 164–185.
19. E Flack. In: FD Gunstone, FB Padely, eds. Lipid Technologies and Applications. New York: Marcel Dekker, 1997, pp 305–327.
20. AC Eliasson, K Larsson. In: AC Eliasson, K Larsson, eds. Cereals in Breadmaking: A Molecular Colloidal Approach. New York: Marcel Dekker, 1993, pp 161–210.
21. IS Shepherd, RW Yoell. Cake emulsions. In: S Friberg, ed. Food Emulsions. New York: Marcel Dekker, 1976, pp 217–275.
22. N Krog. In: FD Gunstone, FB Padely, eds. Lipid Technologies and Applications. New York: Marcel Dekker, 1997, pp 521–534.
23. JG Kapsalis, JJ Betscher, T Kristoffersen, IA Gould. J Dairy Sci 43:1560–1564, 1960.
24. JG Kapsalis, T Kristoffersen, IA Gould, JJ Betscher. J Dairy Sci 46:107–113, 1963.
25. JW Duross, WH Knightly. Manuf Confect July: 50–56, 1965.
26. M Van den Tempel. In: Surface-Active Lipids in Foods. SCI Monograph No. 32. London: Soc Chem Ind 1968, pp 22–33.
27. AS Myerson, R Ginde. In: Crystals, Crystal Growth, and Nucleation. Handbook of Industrial Crystallization. Stoneham, MA: Butterworth-Heineman, 1993, pp 33–63.
28. RJ Davey, LA Polywka, SJ Maginn. In: J Garside, RJ Davey, AG Jones, eds. Advances in Industrial Crystallization. Oxford, 1991, pp 150–165.
29. P Waltra, TJ Geurts, A Noomen, A Jellema, AJS van Boekel. Dairy Technology. New York: Marcel Dekker, 1999, pp 77–105.
30. L Hernqvist. In: N Garti, K Sato, eds. Crystallization and Polymorphism of Fats and Fatty Acids. New York: Marcel Dekker, 1988, pp 97–137.
31. JM de Man. In: N Widlak, ed. Physical Properties of Fats, Oils, and Emulsifiers. Champaign, IL: AOCS Press, 1999, pp 79–95.

Copyright 2002 by Marcel Dekker. All Rights Reserved.

32. JW Mullin. Crystallization. 3rd ed. Oxford: Butterworth-Heineman, 1993, pp 172–201.
33. P Walstra, ECH van Beresteyn. Neth Milk Dairy J 29:35–65, 1975.
34. DM Small. The Physical Chemistry of Lipids. 2nd ed. New York: Plenum, 1986, pp 345–394.
35. K Sato, N Garti. In: N Garti, K Sato, eds. Crystallization and Polymorphism of Fats and Fatty Acids. New York: Marcel Dekker, 1988, pp 3–7.
36. K Larsson. Acta Chem Scand 20:2255–2260, 1966.
37. K Sato. In: N Widlak, ed. Physical Properties of Fats, Oils, and Emulsifiers. Champaign, IL: AOCS Press, 1999, pp 33–48.
38. K Sato. In: N Garti, K Sato, eds. Crystallization and Polymorphism of Fats and Fatty Acids. New York: Marcel Dekker, 1988, pp 227–263.
39. K Sato. In: FB Padely, ed. Advances in Lipid Research. London, England: JAL Press, 1996, pp 213–268.
40. K Sato, S Ueno. In: N Garti, K Sato, eds. Crystallization Phenomena in Fats and Lipid Systems. New York: Marcel Dekker, 2001, pp 177–209.
41. AE Blaurock. In: N Widlak, ed. Physical Properties of Fats, Oils, and Emulsions. Champaign, IL: AOCS Press, 1999, pp 1–32.
42. S Ueno, J Yano, H Seto, Y Amemiya, K Sato. In: N Widlak, ed. Physical Properties of Fats, Oils, and Emulsifiers. Champaign, IL: AOCS Press, 1999, pp 64–78.
43. W Kloeck, P Walstra, TV Vliet. J Am Oil Chem Soc 77:643–652, 2000.
44. MJW Povey. In: N Garti, K Sato, eds. Crystallization Phenomena in Fats and Lipid Systems. New York: Marcel Dekker, 2001, pp 251–288.
45. D Turnbull, RL Cormia. J Chem Phys 34:820–827, 1961.
46. G Grange, A Lewis, B Mutaftshiev. Palatinit Br J Nutr 54:389–394, 1986.
47. DJ McClements, SR Dungan, JB German, C Simoneau, JE Kinsella. J Food Sci 58: 1148–1151, 1994.
48. DJ McClements, E Dickinson, MJW Povey. Chem Phys Lett 172:449–456, 1990.
49. S Hindle, MJW Povey, K Smith. J Colloid Interface Sci 232:370–380, 2000.
50. T Katsuragi, N Kaneko, K Sato. J Jpn Oil Chem Soc (Yukagaku) 49:255–262, 2000.
51. H Takiguchi, K Iida, S Ueno, J Yano, K Sato. J Crystal Growth 193:641–647, 1998.
52. K Fujiwara, S Nagahisa, J Yano, S Ueno, K Sato. J Phys Chem B 104:8116–8123, 2000.
53. S Wahnelt, D Teusel, M Tulsner. Fat Sci Technol 93:117–121, 1991.
54. S Wahnelt, D Teusel, M Tulsner. Fat Sci Technol 93:174–180, 1991.
55. PR Smith, DJ Cebula, MJW Povey. J Am Oil Chem Soc 71:1367–1372, 1994.
56. PR Smith, MJW Povey. J Am Oil Chem Soc 74(2):169–171, 1997.
57. PR Smith. Eur J Lipid Sci Technol 122–127, 2000.
58. N Garti, E Wellner, S Sarig. J Cryst Growth 57:577–584, 1982.
59. N Garti, J Schlicher, S Sarig. J Am Oil Chem Soc 63:230–236, 1986.
60. K Sato, T Kuroda. J Am Oil Chem Soc 64:124–127, 1987.
61. T Katsuragi, N Kaneko, K Sato. Colloid Surf B 20:229–237, 2001.
62. N Kaneko, T Horie, S Ueno, J Yano, T Katsuragi, K Sato. J Cryst Growth 197: 263–270, 1999.
63. T Aoyama, S Ueno, K Sato. J Jpn Oil Chem Soc (Yukagaku) 49:809–816, 2000.

Copyright 2002 by Marcel Dekker. All Rights Reserved.

64. T Awad, Y Hamada, K Sato. Eur J Lipid Sci Technol (in press).
65. MJW Povey, TJ Mason. Ultrasound in Food Chemistry. London: Blackie, 1998, pp 30–65.
66. E Dickinson, MI Goller, DJ McClements, MJW Povey. In: E Dickinson, ed. Food Polymers, Gels and Colloids. London: Roy Soc Chem, 1991, pp 171–178.
67. E Dickinson, F-J Kruizenga, MJW Povey, M van der Molen. Colloid Surf A 81: 273–279, 1993.
68. DJ McClements, E Dickinson, MJW Povey, Chem Phys Lett 172:449–453, 1990.
69. W Kloek. Mechanical properties of fats in relation to their crystallization. PhD Thesis. Wageningen Univ, 1998.
70. E Dickinson, MI Goller, DJ McClements, S Peasgood, MJW Povey. J Chem Soc Faraday Trans 86:11478–11485, 1990.
71. D Kashchiev, N Kaneko, K Sato. J Colloid Interface Sci 208:167–177, 1998.
72. MJW Povey. In: E Dickinson, ed. New Physico-Chemical Techniques for the Characterization of Complex Food Systems. London: Chapman and Hall, 1995, pp 196–219.
73. E Dickinson, DJ McClements, MJW Povey. J Colloid Interface Sci 142:103–110, 1991.
74. C Garbolino, GR Ziegler, JN Coupland. J Am Oil Chem Soc 77:157–162, 2000.
75. Y Basiron. In: YH Hui, ed. Bailey's Industrial Oil and Fat Products. New York: Wiley, 1996, pp 271–375.
76. FD Gunstone. In: FD Gunstone, FB Padely, eds. Lipid Technologies and Applications. New York: Marcel Dekker, 1997, pp 19–50.
77. Economic Research Service, US Dep of Agriculture Market and Trade Economics Division. Oil Crops Year Book. Available electronically via *www.econ.org.gov*.
78. RE Timms. In: FD Gunstone, FB Padely, eds. Lipid Technologies and Applications. New York: Marcel Dekker, 1997, pp 199–222.
79. T Awad, K Sato. J Am Oil Chem Soc (in press).
80. R Boistelle. In: N Garti, K Sato, eds. Crystallization and Polymorphism of Fats and Fatty Acids. New York: Marcel Dekker, 1988, pp 189–226.
81. MA Pes, K Aramaki, N Nakamura, H Kunieda. J Colloid Interface Sci 178:666–672, 1996.
82. H Kunieda, N Kanei, I Tobita, K Kihara, A Yuki. Colloid Polym Sci 273:584–589, 1995.
83. H Kunieda, E Ogawa, K Kihara, T Tagawa. Prog Colloid Polym Sci 105:237–243, 1997.
84. S Chaiseri, PS Dimick. J Am Oil Chem Soc 72:1491–1496, 1995.
85. S Chaiseri, PS Dimick. J Am Oil Chem Soc 72:1497–1504, 1995.

Copyright 2002 by Marcel Dekker. All Rights Reserved.

3

Structure and Mechanical Properties of Fat Crystal Networks

Suresh S. Narine
University of Alberta, Edmonton, Alberta, Canada

Alejandro G. Marangoni
University of Guelph, Guelph, Ontario, Canada

I. INTRODUCTION

Fats form plasticlike networks that demonstrate a yield value and viscoelastic behavior. Fat-containing food products such as chocolate, margarine, butter, spreads, and peanut butter derive most of their macroscopic texture from such networks formed by the fat contained. The texture-providing attributes of the fat network are usually quantified by rheologically obtained indicators such as the shear elastic modulus and the hardness index as measured by cone penetrometry. The prediction of the value of these rheological indicators from processing, compositional, and structural perspectives is therefore of immense importance to the industry if processes are to be optimized and quality improved and/or maintained. This area has been the focus of academic endeavor for some 50 years, with varying degrees of success.

In this chapter we define the structural hierarchy of the network formed by a crystallizing fat (after Ref. 1), highlights the major developments in quantification of the various levels of structure, and summarizes the application of fractal geometry to the quantification of the microstructural level of structure. Furthermore, we make the case that the microstructure, by virtue of its proximity to the macroscopic world, provides important predictive information on the value of the elastic modulus of the network. Models we have developed to relate the struc-

Copyright 2002 by Marcel Dekker. All Rights Reserved.

ture at the microstructural level to the shear elastic modulus are discussed. The manipulation of the microstructure via changes in processing conditions, leading to concomitant changes in the elastic modulus of the network, is also discussed. It must be mentioned that all of the work presented here has been previously published [1–8], and therefore this chapter represents a summary of our research over the past few years rather than new, unpublished material.

II. STRUCTURAL HIERARCHY OF FAT CRYSTAL NETWORKS

Distinct structural levels are established as melted fat crystallizes. The growth of a fat crystal network can be visualized thus: The triglyceride molecules (~40 Å) present in the sample crystallize from the melt into particular polymorphic/polytypic states, forming crystallites that are sized at the submicrometer level. These crystallites then aggregate via a mass and heat transfer–limited process into larger microstructural elements (~1–10 μm). The aggregation process continues, with the microstructural elements forming ever larger clusters, until a continuous three-dimensional network is formed by the collection of microstructures (~50–140 μm). At the microstructural level, the solid network is an orthodox amorphous solid, whereas the intramicrostructural level demonstrates disordered, aperiodic, colloid-like packing. As will be discussed, this level of structure is fractal [1]. Figure 1a shows examples of the submicrometer crystallites formed during the crystallization of a melted fat, Figure 1b shows examples of micro-

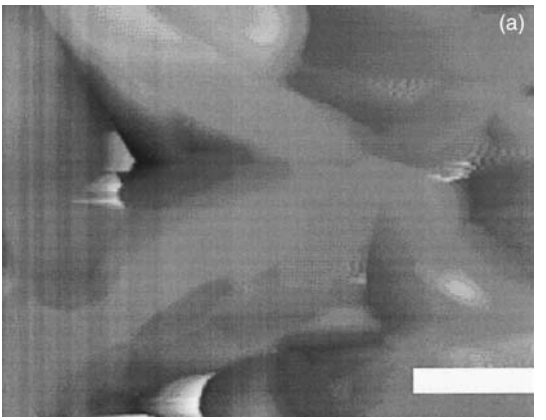

Figure 1a Submicrometer crystallites (bar = 0.5 μm).

Copyright 2002 by Marcel Dekker. All Rights Reserved.

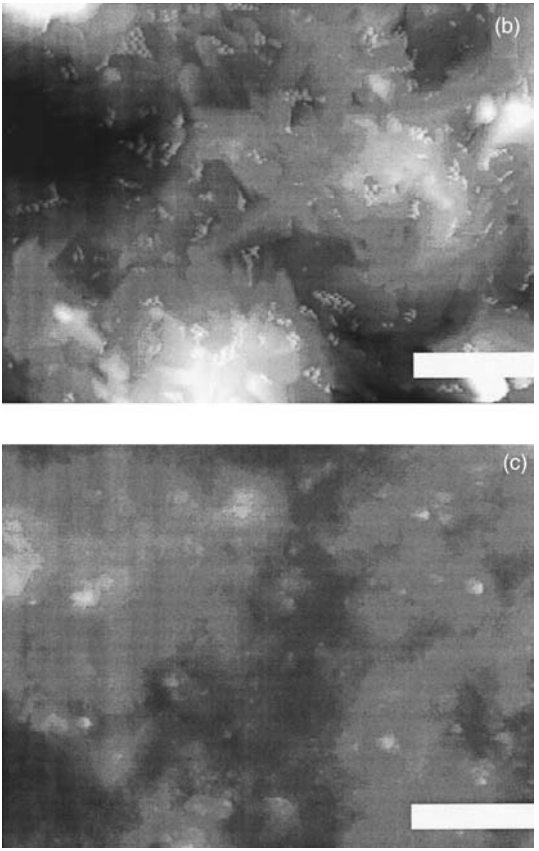

Figure 1b and 1c (b) Microstructural elements at the 1–10 μm scale (bar = 2.5 μm), and (c) microstructures at the 50–120 μm scale (bar = 12.5 μm) of cocoa butter. All images taken with an atomic force microscope operated in tapping mode.

structural elements at the 1–10 μm level, and Figure 1c shows examples of microstructures at the 50–120 μm level. These micrographs were all obtained from an atomic force microscope operated in tapping mode.

The macroscopic rheological properties of the fat network are influenced by all the levels of structure that are identified as well as by the relationships between the levels of structure and the processing conditions, which define the nature of the relationships. Figure 2 represents a schematic of this structural organization.

Copyright 2002 by Marcel Dekker. All Rights Reserved.

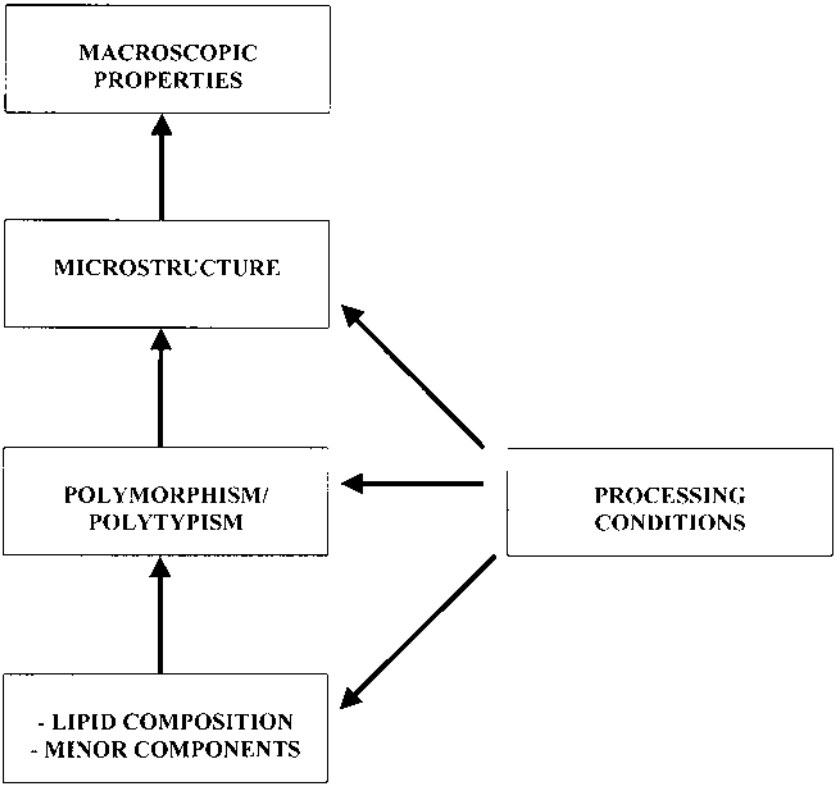

Figure 2 Schematic organization of the levels of structure in a fat crystal network, showing the influence on macroscopic properties.

III. QUANTIFYING THE LEVELS OF STRUCTURE

A. Triglyceride Composition and Structure

For the smallest scale of structure present, the triglyceride molecules, methods to determine triglyceride and fatty acid composition in fat crystal networks are well established and well reviewed in the book by Christie [9]. In addition, methods to determine fatty acid positional distribution in triglycerides have been established by two separate groups [10,11]. Triglycerides are well-known organic molecules, and therefore the bond angles and bond lengths of the various atoms within each triglyceride molecule are easily established on the basis of standard structural organic chemistry. What is nontrivial is the prediction of a particular crystal structure formed by an ensemble of triglyceride molecules of known com-

Copyright 2002 by Marcel Dekker. All Rights Reserved.

position and structure. The complexity and flexibility of the triglyceride molecules also allow different crystalline packings of the same ensemble of molecules, leading, of course, to the existence of different polymorphs.

B. Quantification of Polymorphism

By far the most popular method of quantifying the polymorphism of the crystallites formed during network formation is the determination of subcell and layered structures by X-ray diffraction. In addition to the standard methods of X-ray diffraction, a number of other techniques, such as vibrational spectroscopy, are employed in the identification of the different polymorphic forms [12–19]. Nuclear magnetic resonance (NMR) measurements have also been used to study the molecular mobility in polymorphs [20–27]. Atomic force microscopy has recently also been used to study the crystal structure of triglycerides [28].

The type(s) of polymorph(s) present in the network decidedly affects the macroscopic properties of the fat crystal network. Certainly, the type of polymorph present will dictate the melting point of the network. The shapes and sizes of the crystals and crystal aggregates found in the network are affected by the polymorphic form of the crystals, but to varying extents in different fats [29–32]. The shapes and sizes of crystals and aggregates of crystals (microstructural elements) do affect the macroscopic elastic constant of the network. However, the measurements needed to establish the different polymorphic types do not yield additional information about the nature of the molecular structure other than the subcellular and layered structures [6]. Therefore, the understanding of the link between polymorphism and morphology and size of crystals is still phenomenological in nature. Additionally, in a model created by Narine and Marangoni [2], the macroscopic elastic constant of the network is dependent on the Hamaker's constant (a constant depending on the polarizabilities of the triglyceride molecules) of the microstructural elements within the network, which in turn depends on the molecular packing in the crystals, but again, this is not yet a quantifiable link. There have been observations that show changes in macroscopic viscoelastic properties due to a polymorphic transformation in fat products; see, for example, Cornily and leMeste [33]. The β'-type polymorph is usually the most functional in fat products, because of its small crystal size ($\sim$1 μm) and thin needle-shaped morphology.

C. Quantification of Microstructure

The microstructural level of the fat crystal network may be defined as those structures in the length range between 1 and 120 μm. At the lower range of the microstructural level, one may encounter crystallites, whereas at the upper ranges, one

Copyright 2002 by Marcel Dekker. All Rights Reserved.

decidedly is observing aggregates of microstructural elements (clusters of crystallites). The upper level of structure has an enormous influence on the macroscopic rheological properties of the network, noted as early as 1987 by deMan and Beers [34]. Other researchers have also noted the importance of the microstructural level on the rheological properties of the network and the fact that the microstructure is easily changed with processing conditions of crystallization [35–37] as well as with interesterification [38].

With the advent of confocal laser scanning fluorescence microscopy (CLSFM) [39], multiple photon microscopy (MPM) [40,41], and atomic force microscopy (AFM) [5], three new tools have been added to the standard tools of light microscopy (LM) [42–45] and electron microscopy (EM) [35,46–50] that were most widely used in the past to study the microstructure of fats and foods in general. The work of Heertje et al. [35,36,39,51] on visualization of the microstructure in fats remains one of the most important contributions to the field. In their method, a cold solvent mixture (butanol–methanol) was used to remove the liquid oil form the solid fat in a sample mounted on a special holder. After removal of the liquid oil, the structure of the solid fat network could be visualized.

The nomenclature introduced earlier for the different levels of structure in fat crystal networks was developed by Narine and Marangoni in a series of publications [1–8], building upon the work of Heertje and coworkers.

The manner in which the microstructural elements aggregate to form microstructures results in them being organized in space in an aperiodic, irregular, colloidal-like pattern. Figure 3a shows the spatial organization of microstructural elements in tallow, and Figure 3b shows the spatial organization of microstructural elements in cocoa butter. Both micrographs were obtained using polarized light microscopy. Quantifying the spatial organization of this level of structure is not possible with classical geometrical tools; therefore we applied fractal geometrical tools [1].

Before describing the method of quantifying the microstructural level using fractal analysis, it is first necessary to provide readers with a short introduction to fractals. This is not intended as an exhaustive review of the topic but merely to introduce the concepts necessary for an understanding of the application of fractal geometry as it is used in the method to follow.

Fractal geometry was proposed by Benoit Mandelbrot [52] as a way of quantifying natural objects with a complex geometrical structure that defied quantification by regular geometrical methods (Eucliden geometry). We recommend the reviews by Jullien and Botet [53] and Meakin [54] on the subject of fractal aggregation. In classical Euclidean geometry, objects have integer dimensions: A line is a one-dimensional object, a plane a two-dimensional object, and a volume a three-dimensional object. In this way, Euclidean geometry is suitable for quantifying objects that are ideal, man-made, or regular.

Copyright 2002 by Marcel Dekker. All Rights Reserved.

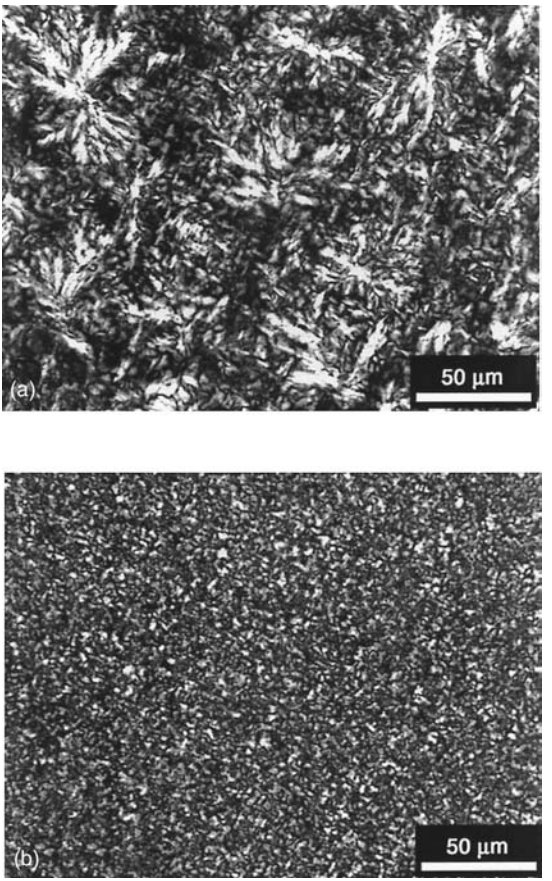

Figure 3 (a) Microstructural elements in tallow; (b) microstructural elements in cocoa butter. Both micrographs are polarized light microscopic images.

One may imagine that if enough kinks are placed in a line or a plane, the result is an object that may be classified as being intermediate between a line and a plane or a plane and a cube. The dimension of such an object is fractional (i.e., between 1 and 2 or between 2 and 3), and the object may be classified as a fractal object, from the fact that instead of having a Euclidean dimension (integer) it has a fractional dimension.

One of the most important features of fractal objects is that they are self-similar; i.e., there is a repetition of patterns in the object at many different scales. For natural objects such as trees, clouds, and coastlines, Euclidean geometry fails

Copyright 2002 by Marcel Dekker. All Rights Reserved.

to provide an adequate quantification, but many of these natural objects are self-similar at different scales. For example, a tree has branches, these branches have smaller branches, and so on, and if one changes the scale of observation of the tree, the same pattern is observed, at least in a statistical sense if not in a deterministic sense. Therefore, fractal geometry provides a good measure of such objects with nonintegral dimensions.

Fractal geometry is also useful for a disordered distribution of mass, such as in a clustering of stars in the Milky Way or the clustering of particles in a colloid. A short example is useful. For a solid two-dimensional disk, the relationship of the mass of the disk to its radius is given by

$$M(r) \propto R^2 \tag{1}$$

so that in this case the dimension is an integer and the object is a Euclidean object.

However, for a disordered distribution of mass, if at different scales of observation the patterns are statistically self-similar, then the relationship of radius to mass may be given by [53,55,56]

$$M(R) \sim R^D \tag{2}$$

where D is a fractional or *fractal* dimension. Here, the symbol $\sim$ is taken to mean ''approximately proportional to.''

Therefore, if one considers an object that is composed of a disordered collection of particles that are self-similar at different length scales, then the dimension of such an object could be fractional and should lie between two and three. Figure 4 shows a schematic of such an object. If all the particles in the object are of the same diameter, then Eq. (2) becomes

$$N(R) = c(R)^D \tag{3}$$

where $N(R)$ is the number of particles in the system at some size R. Therefore, one can plot $\log_{10}[N(R)]$ vs. $\log_{10} R$ for such an object, and the resulting slope should yield the fractal dimension of the object. This is the method that is exploited to calculate the fractal dimension of fat crystal networks.

Figure 5 shows a schematic of microstructural elements seen under a polarized light microscope. When one looks at a polarized light microscopic image of a fat crystal network under crossed polarizers, then one is able to see the sections of the microstructural elements that are oriented in a particular crystallographic manner. For elements in the focal plane of the microscope, these sections will appear as bright, focused particles, whereas for microstructural elements in the depth of the sample, the sections seen under the microscope that belong to one particular microstructural element will appear as smaller, indistinct particles (because their images are projected into the focal plane, as shown in Figure 5).

Copyright 2002 by Marcel Dekker. All Rights Reserved.

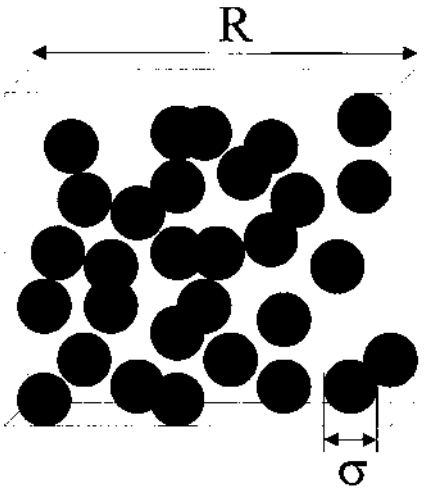

Figure 4 Schematic of a disordered object, composed of a disordered collection of particles, which may demonstrate statistical self-similarity at different magnifications.

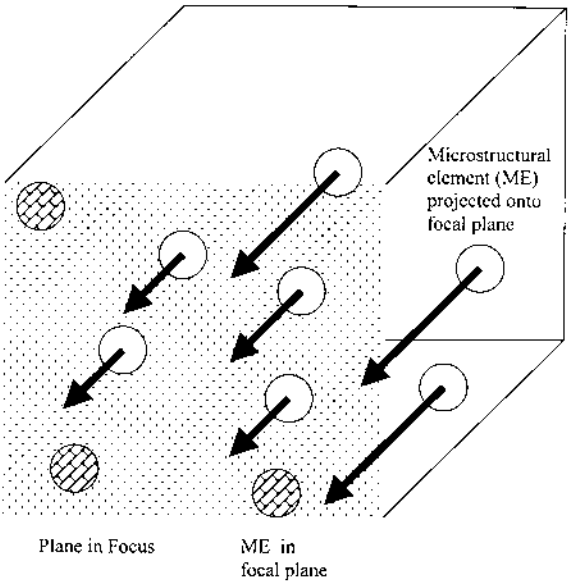

Figure 5 Schematic of microstructural elements seen under a polarized light microscope, when a sufficiently thin sample of the fat is viewed.

Copyright 2002 by Marcel Dekker. All Rights Reserved.

However, if the depth of the sample is kept sufficiently small, then it is possible to represent all of the microstructural elements within the sample in the field of view, albeit some of them will appear small and out of focus. If the sample is sufficiently thin, then not many microstructural elements are lost due to direct geometrical shadowing. In our method, one then thresholds this grayscale image of the microstructural element, ensuring that each element is represented as an individual particle (more details of this process are provided in Ref. 1). Figure 6a shows a grayscale image of the microstructural elements in lard, and Figure 6b shows this image thresholded to ensure that each microstructural element is represented. In such images, therefore, the entire mass of the sample is represented. The method for calculating the fractal dimension then consists of counting

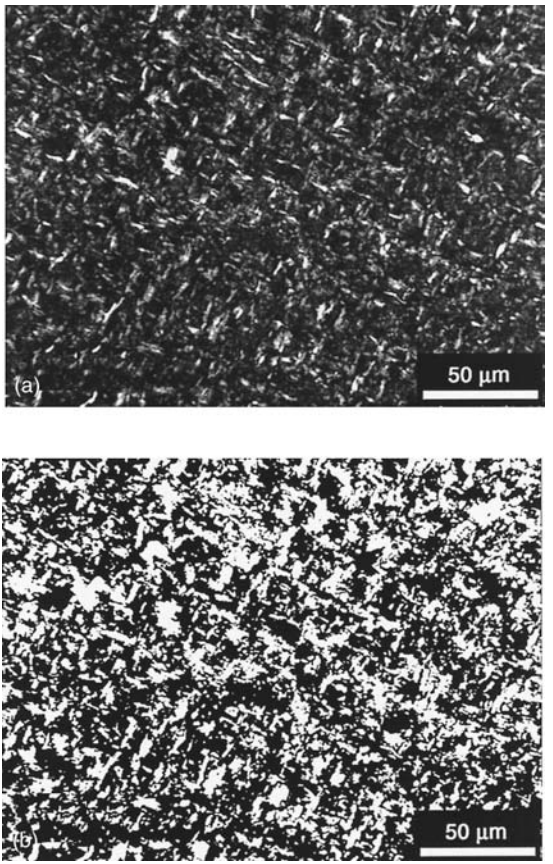

Figure 6 (a) Microstructural elements in lard; (b) thresholded image of (a).

Copyright 2002 by Marcel Dekker. All Rights Reserved.

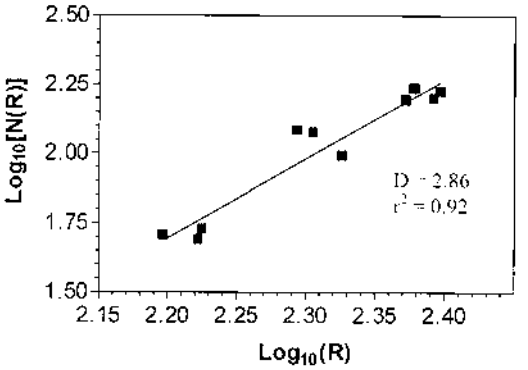

Figure 7 Plot of $\log_{10}[N(R)]$ vs. $\log_{10}R$ for lard. Slope is equivalent to fractal dimension D.

the number of particles there are in boxes of different lengths R laid over the image. One then plots $\log_{10}[N(R)]$ vs. $\log_{10}R$, the slope of the resulting line being equivalent to the fractal dimension. Figure 7 shows a typical plot of $\log_{10}[N(R)]$ vs. $\log_{10}R$ for lard. This type of plot was achieved for five different fat systems: lard, milkfat, tallow, cocoa butter, and palm oil (summarized in Ref. 1). Therefore, in addition to the traditional ways of quantifying the microstructural level (by particle size, for example), there is now a way of quantifying the spatial distribution of the packing of the microstructural elements.

IV. MECHANICAL MODEL

A. Weak-Link Theory

Now that all levels of the structural hierarchy within a fat crystal network are quantifiable (to various extents), as well as the amounts of solid fat within the network (by use mainly of pulsed nuclear magnetic resonance), it is important to relate these quantifiable parameters to rheological indicators such as the shear elastic modulus. One model to relate the microstructure to the shear elastic modulus was developed in colloidal physics by Shih et al. [57]. A brief chronology of the adaptation of this theory to the study of fat networks follows.

Interest in the microstructure of fat crystal networks in our laboratory arose during studies of factors affecting the hardness and spreadability of chemically interesterified (CIE) and enzymatically interesterified (EIE) milkfat [38,58–62]. The hardness of CIE milkfat at equivalent solid fat contents was lower than that

Copyright 2002 by Marcel Dekker. All Rights Reserved.

of their noninteresterified (NIE) counterparts [60]. Palm oil, lard, cocoa butter, Salatrim, and tallow [1,4,63,64] were also studied. The polymorphic nature and the solid fat content of interesterified and noninteresterified fat system–canola oil blends were essentially the same, but their rheological properties were very different. This provided motivation to search for a new ''structural indicator'' of the mechanical strength of fat crystal networks that was somehow related to the next logical structural level, the microstructural level of the network. A rheological approach was adopted in the references cited above, the motivation for which stemmed from work done in colloidal gels and adapted to fat crystal networks.

In 1992, Vreeker et al. [56] presented an interpretation of rheological data for aggregate fat networks in the framework of fractal theories. They showed that the elastic modulus of the network (G') varied with the particle concentration of solid fat (Φ), or solid fat content, according to a power law, similar to models for the elasticity of colloidal gels. The formation of a fat crystal network is mathematically very similar to that of a flocculating colloid, the similarity having been noted as early as 1989 by Edwards and Oakeshott [65]. Therefore, the article by Vreeker et al. exploits this similarity in providing an interpretation of rheological data for low Φ fats in terms of an elastic network model developed for colloidal gels at low particle concentrations. From this rheological investigation of the fat network, a fractal dimension could be calculated, but at this point it was unclear what this dimension meant in terms of the structure of the network.

An exciting period in the analysis of polymer and colloidal networks ensued after the introduction of the fractal concept in 1982 [52]. Since then, scaling theory has been used to explain the elastic properties of protein gels [66–69]. Much progress was made in the analysis of the microstructure of colloidal aggregates, the verdict being that they are fractal structures that are quantifiable from rheological and optical measurements [55,57,70–75]. A scaling theory to explain the elastic properties of colloidal gels was put forth by Brown and Ball [70–72]. Brown and Ball suggested that colloidal aggregates should behave as stochastic mass fractals on a scale that is large compared to the primary particle size, and they formulated a power law relationship of the elastic modulus to the solid volume fraction. This formulation was experimentally verified by various others, including Sonntag and Russel [74] and Buscall et al. [73]. In 1990, Shih et al. [57] outlined the development of a scaling theory to explain the elastic properties of colloidal gels by again considering the structure of a colloidal network as a collection of fractal flocs, except that their paper defined two separate regimes depending on the concentration of the colloidal gel. At low concentrations, the strong-link regime was appropriate; its formulation is identical to Brown's [71]. At high concentrations, the weak-link regime is appropriate; its formulation differ from both that of the strong-link regime and that suggested by Brown and Ball [70–72].

Copyright 2002 by Marcel Dekker. All Rights Reserved.

The analysis of Vreeker et al. was interesting enough for Marangoni and Rousseau [38] to apply the model developed by Shih et al. [57] for high concentration colloidal gels (weak-link theory) to fat crystal networks of high solid fat concentration. This model offered the ability to relate small-deformation rheological measurements (shear elastic modulus) to the fractal dimension of the network. Small-deformation rheological measurements provide a direct link to the microstructure of the fat network as explained in what follows. The microstructures form the level of structure closest to the macroscopic network; no other structural building block larger than the microstructures have been identified in fat crystal networks. Consequently, the level of structure that is immediately stressed when the network is stressed (such as when rheological measurements are performed) is the microstructural level. Heertje [51] showed that parallel-plate compression of a fat crystal network results in a breakage of the links between microstructures, while the microstructures themselves remain intact. Of course, catastrophic breakage of the entire structure would result in complete breakage of levels of structure below the microstructures (such as the links between microstructural elements) as well as the crunching of the microstructural elements. However, for compression and shear measurements that involve only small deformations within the elastic limit of the network, it seems likely that only the links between microstructures are stressed when the network is stressed. It follows, therefore, that the rheological behavior of the network at small deformations (small strain levels) is a reflection of the microstructural level of structure more than any other structural level in the network. It must be realized, however, that the microstructural organization is due to the manner in which the other levels of structure are arranged, therefore implicating all levels of structure in the determination of the mechanical strength of the network. However, it is essential to assign more importance to consideration of the microstructural level than has been the case in the past. As may be appreciated from the above argument, a consideration of the polymorphic nature and lipid composition of the network in isolation ignores the crucial role of the microstructural level in influencing mechanical strength of the network. The assumptions made above are essential to the weak-link model of Shih et al. [57].

It was shown experimentally by Vreeker et al. [56] and by Rousseau and coworkers [38,58–64,76] that the elastic properties of fat crystal networks at low and high solid fat contents, respectively, are highly dependent on the fractal nature of the microstructure. For the shear elastic modulus G',

$$G' = \gamma\Phi''' \tag{4}$$

where Φ is the particle volume fraction of solid fat, γ is a constant the nature of which will be explained later in this chapter, and m depends on the fractal dimen-

Copyright 2002 by Marcel Dekker. All Rights Reserved.

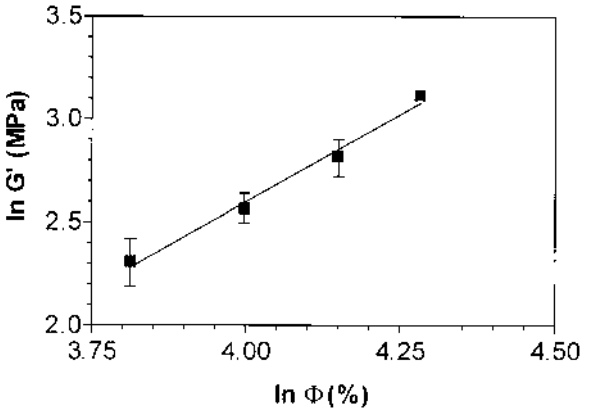

Figure 8 Plot of $\log_{10} G'$ vs. $\log_{10} \Phi$ for tallow.

sion of the network in the following manner (according to the weak-link model of Shih et al.):

$$m = \frac{1}{3 - D} \tag{5}$$

In brief, the rheological analysis consists of measuring G' for various values of Φ and plotting $\log_{10} G'$ vs. $\log_{10} \Phi$, the slope of the resulting straight line yielding $1/(3 - D)$, and the y-intercept yielding the value of the constant γ. A typical plot of $\log_{10} G'$ vs. $\log_{10} \Phi$ for tallow is shown in Figure 8.

To test whether the model of Shih et al. (the weak-link model) is applicable to fat crystal networks, it is fortunate that the method for quantifying fractal dimensions via image analysis of the in situ fat network was developed by Narine and Marangoni [1]. Table 1 shows the rheologically calculated fractal dimensions for four fat systems as well as the fractal dimensions calculated from image analysis. As is obvious from the table, the agreement between the values is excellent. This seems to strongly suggest that the weak-link model of Shih et al. applies well to fat crystal networks.

B. Modeling the Constant γ

As described in a recently published article in *Physical Review E* [2], we constructed a mechanical and structural model of fat crystal networks. In this model, the microstructural elements were assumed to be spherical, and the forces between the microstructures were attributed to the forces of interaction between neighboring microstructural elements at the interface between two microstruc-

Copyright 2002 by Marcel Dekker. All Rights Reserved.

Table 1 Fractal Dimension Calculated Via Image Analysis Compared to Fractal Dimension Calculated Via Rheology Using the Weak-Link Theory[a]

Fat system	Fractal dimension from image analysis	Fractal dimension from rheology (weak-link regime)	Percent deviation	Fractal backbone dimension x
Cocoa butter (5°C) #1	2.31 ± 1.7%	2.37 ± 4.0%	2.5	1.10
NIE milkfat #4[b] (5°C)	2.02 ± 1.2%	2.01 ± 15.7%	1.5	1.00
Palm oil (5°C)	2.82 ± 0.6%	2.82 ± 0.6%	0.0	1.10
Lard (5°C)	2.86 ± 0.6%	2.88 ± 0.5%	1.0	1.15

[a] Errors in D are standard errors of three replicates.
[b] Analyzed using DMA.

tures. These forces were formulated by first solving the Lennard-Jones potential energy between two microstructural elements considered spherical and then differentiating the resulting expression with respect to the intermicrostructural element distance. The fractal structure at the intramicrostructural level was taken into account when constructing the system of forces. It was assumed that the hydrodynamic forces and inertial forces were negligible. The final equation that emerged out of this model was

$$G' \sim \frac{mA}{6c\pi\sigma\xi d_0^3}\Phi^{1/(3-D)} \tag{6}$$

where m is the number of neighboring microstructural elements at an interface between two microstructures, A is the Hamaker's constant, c is the constant of proportionality in Eq. (3), σ is the diameter of a microstructural element, ξ is the diameter of one microstructure, and d_0 is the average equilibrium distance between microstructural elements. Therefore, from this model, compared to the scaling power law model provided by the weak-link model, the constant γ is given by

$$\gamma \sim \frac{mA}{6c\pi\sigma\xi d_0^3} \tag{7}$$

This model identifies key network parameters important in determining the value of γ. Furthermore, the model agrees well with experimental observations and with the scaling power law model of the weak-link theory, which has been shown both rheologically and by image analysis to be valid for fat crystal networks. Equation (7) provides impetus for the development of phenomenological investigations of relationships between triglyceride composition and polymorphism and

Copyright 2002 by Marcel Dekker. All Rights Reserved.

values of the Hamaker's constant and sizes of microstructural elements, as well as the effects of processing conditions on these network characteristics. Values of d_0, σ, and D can be manipulated by changes in processing conditions, and some of this potential for changes in the elastic properties of fat crystal networks due to processing conditions is discussed in the next section. By defining the network characteristics responsible for the mechanical strength of the network, the model provides an array of indicators that can be monitored during the developmental stages of tailored fat crystal networks as well as key parameters to be monitored as indicators of quality control.

V. IMPLICATIONS FOR PROCESSING-INDUCED CHANGES IN ELASTIC PROPERTIES

Fractal dimension as a measure of spatial distribution certainly seems to describe the spatial distribution of the microstructural elements within the microstructures, given the foregoing discussion, and the large amount of supporting evidence that has been published, much of which is contained either in our publications in this area [1–8] or in references cited in those publications. Additionally, it seems that it is important that we know not only how much solid mass is actually in the network (of course, the use of solid fat content as an indicator of hardness has been used extensively), but also the way in which that solid mass is distributed in space, the sizes of the individual entities formed by this solid mass, and the shape and molecular packing within these entities. It is important, therefore, to have a fundamental physical link to the information that the fractal dimension of the network imparts. For example, if someone were to ask whether the dimension has changed, what would this mean physically? And how could one tell? From an empirical examination of the microstructure of a number of fats, we have come to the conclusion that a higher fractal dimension means a higher order in the packing of the microstructural elements. For an illustration of this, Figure 9 shows milkfat and palm oil, with fractal dimensions of 2.02 and 2.82, respectively. As can be seen in the micrographs, the ordering of packing of the microstructural elements is higher in palm oil. Reference 1 shows data on five different fat systems that further support this conclusion.

Given that fractal dimension obviously affects the elastic properties of the fat, the important question to ask is, Can processing conditions be used to change the fractal dimension of a particular fat and therefore its elastic properties? If we deviate from experimental evidence for a moment and consider Figure 10, which shows two idealized heat release curves during crystallization of a hypothetical fat, it is possible to explain one way in which the order in the microstructural elemental packing can be increased. When a crystallization event occurs, there is the concomitant release of the heat of crystallization. If this heat is released

Copyright 2002 by Marcel Dekker. All Rights Reserved.

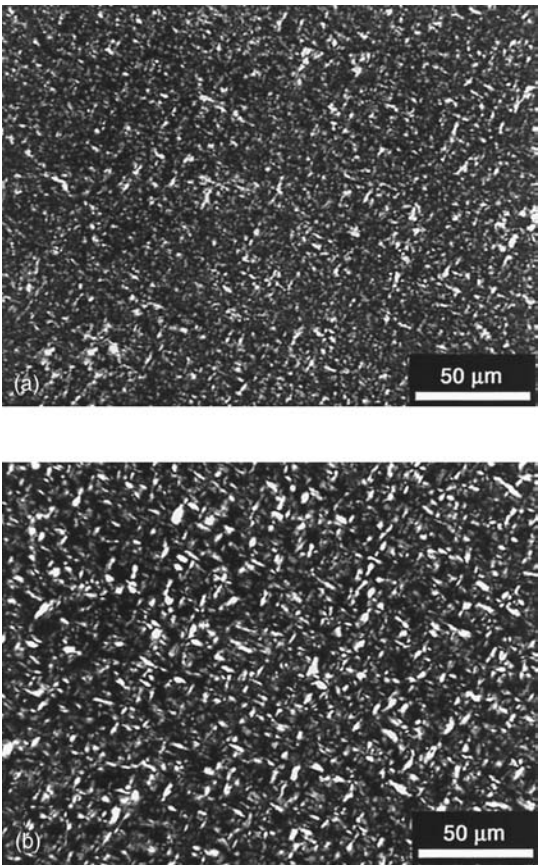

Figure 9 (a) Microstructural elements of palm oil; (b) microstructural elements of milkfat. Both micrographs were obtained by polarized light microscopy.

over a fairly long time, then the packing of the fat will be determined by the nature of its thermodynamically preferred spatial distribution. However, if we force the fat to crystallize over a shorter time period, then the structure has to accommodate the release of the heat of crystallization over a short time. The geometry that will best suit efficient dissipation of this heat is an ordered array of crystallization centers, because this will ensure that there is a significant body of liquid oil around each center of crystallization or heat release. This idea is depicted schematically in Figure 10, with the crystallization curve for the fat forced to crystallize quickly demonstrating the same area under the curve (or the same amount of heat released) but with a smaller full width at half-maximum.

Copyright 2002 by Marcel Dekker. All Rights Reserved.

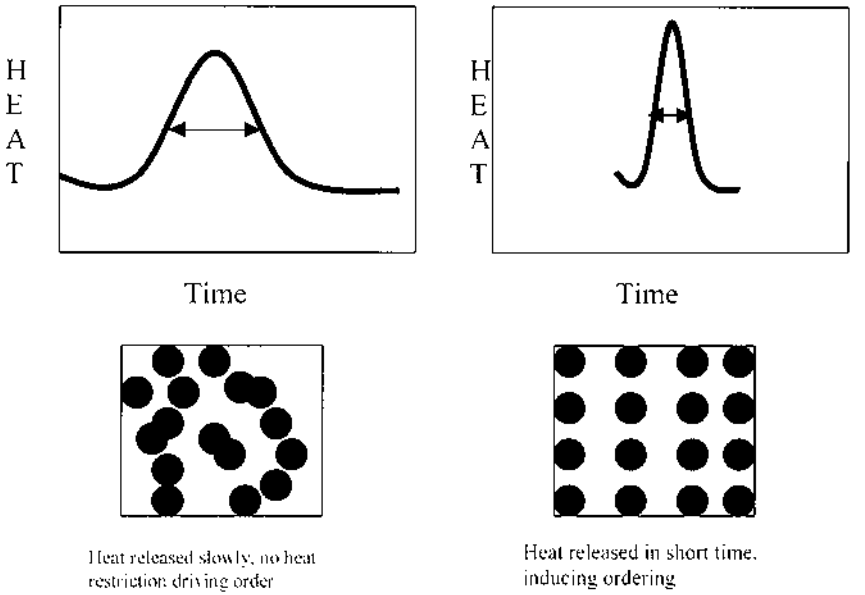

Figure 10 Schematic of crystallization curves for a hypothetical fat when the fat is allowed to crystallize slowly and when it is forced to crystallize in a short time. The schematic also shows idealized examples of what the resulting distribution of microstructural elements will be under the different rates of crystallization.

Idealized examples of the microstructure of the fat are shown below the crystallization curves. It is assumed here, of course, that the character of crystallization remains the same if the fat is processed differently. In addition, the potential to order driven by the need to dissipate heat can be negated by the actual formation of the network: As the solid network is formed, the system becomes more and more limiting in terms of mass transfer, owing to the increase in viscosity and the entrapment of those structural entities that would normally tend to align in a more ordered fashion. In some cases the shape of the crystallization curve may actually change, owing to slight polytypic changes, or a different polymorph may be formed under the new processing conditions. However, this change, if any, may also be exploited if it results in the development of order-setting characteristics (such as narrowing of peaks) or in destruction of order, such as the broadening of existing peaks. In addition, polymorphic changes affect the value of the constant γ, because the Hamaker's constant will be different for different polymorphs, and other parameters such as the intermicrostructural element distance

Copyright 2002 by Marcel Dekker. All Rights Reserved.

at the interface between two microstructures and the size and shape of the microstructural elements will change with changing polymorphic forms.

Given that the order of packing of the microstructure used as an indicator cannot always be linked in a straightforward manner to processing conditions, fats that demonstrate more ordering in the spatial distribution of their microstructural elements demonstrate sharp crystallization peaks if their crystallization is monitored by differential scanning calorimetry, the fats being crystallized at the same rate [1]. Recent work on altering processing conditions of milkfat and lard to alter their hardness, however, demonstrates that other phenomena such as fractionation, polymorphic changes, and viscosity increases also affect the mechanism of ordering. Nevertheless, regardless of the physical processes involved in the determination of the degree of ordering due to processing changes, the increase of order does result in the decrease of the elastic modulus of the system, because an increase in the order of packing of the microstructure results in an increase in the fractal dimension of the system. Narine [7] provides mathematical arguments for the increase of fractal dimension with increasing order. Therefore, microscopic observations of a particular fat system can lead to important predictions of changes in hardness due to changes in processing conditions, regardless of the complex mechanisms responsible.

VI. CONCLUSIONS

In conclusions, we must reiterate that fat crystal networks demonstrate distinct structural hierarchies. A consideration of the microstructural level and construction of models based on elastic rheological measurements implicate all levels of structure in the determination of the macroscopic elastic moduli. Consideration of the fractal arrangement of the microstructural elements is integral to the construction of models that fit well with experimental data. Furthermore, it is seen that the fractal dimension and other network characteristics such as microstructural element size and microstructural size are indicators of macroscopic hardness, and that these factors can be manipulated by processing conditions to achieve tailored elastic characteristics of fat crystal networks.

ACKNOWLEDGMENTS

We thank Rekha Narine for proofreading the manuscript. We also thank AVAC Ltd. and the Natural Sciences and Engineering Research Council (NSERC) of Canada for financial support.

Copyright 2002 by Marcel Dekker. All Rights Reserved.

REFERENCES

1. SS Narine, AG Marangoni. Phys Rev E 59(2):1908–1920, 1999.
2. SS Narine, AG Marangoni. Phys Rev E 60(6):6991–7000, 1999.
3. SS Narine, AG Marangoni. Inform 10(6):565–570, 1999.
4. SS Narine, AG Marangoni. J Am Oil Chem Soc 7–13, 1999.
5. SS Narine, AG Marangoni. J Cryst Growth 198/199:1315–1319, 1999.
6. SS Narine, AG Marangoni. Food Res Int 32:227–248, 1999.
7. SS Narine. Structure and mechanical properties of fat crystal networks. Dept Food Sci, University of Guelph, Guelph, ON, 2000.
8. SS Narine, AG Marangoni. Lebensmittelwiss Technol 2000. In press.
9. WW Christie. Lipid Analysis: Isolation, Separation, Identification and Structural Analysis of Lipids. 2nd ed. Oxford: Pergamon Press, 1982.
10. H Brockerhoff. J Lipid Res 6:10–15, 1965.
11. WEM Lands, et al. Lipids J 1:444–448, 1966.
12. RL Amey D Chapman. In: D Chapman ed. Biomembrane Structure and Function: Topics in Molecular and Structural Biology. Weinheim: 1984, pp 199–256.
13. D Chapman. J Am Oil Chem Soc 37:73–77, 1960.
14. D Chapman. J Am Oil Chem Soc 42:353–371, 1964.
15. NK Freeman, J Am Oil Chem Soc 45:798–809, 1968.
16. RT O'Connor, EF DuPre, RO Feuge J Am Oil Chem Soc. 33:88–93, 1955.
17. J Yano. Vibrational spectroscopic study on structures and polymorphic transformations of triacylglycerols. Osaka University, Osaka, Japan, 1998.
18. J Yano, et al. J Phys Chem B 101(41):8120–8128, 1997.
19. J Yano, et al. J Phys Chem B 101(41):8112–8119, 1997.
20. T Arishima et al. J Am Oil Chem Soc 73:1231–1236, 1996.
21. SM Boceik, S Ablett, IT Norton. J Am Oil Chem Soc 62:1261–1266, 1985.
22. PT Calaghan, KW Jolly. J Chem Phys Lipids 19:56–73, 1977.
23. D Chapman. J Chem Soc 1960:436–444.
24. TM Eads et al. J Am Oil Chem Soc 74:1213–1220, 1992.
25. V Gibon, F Durant, C Deroanne. J Am Oil Chem Soc 63:1047–1055, 1986.
26. JW Hagemann, JA Rothfus. J Am Oil Chem Soc 60:1123–1131, 1983.
27. IT Norton, et al. J Am Oil Chem Soc 62:1237–1244, 1985.
28. PJWL Birker, JCG Blonk. J Am Oil Chem Soc 70:319–321, 1993.
29. CW Hoerr. J Am Oil Chem Soc 37:539–546, 1960.
30. CW Hoerr, DF Waugh. J Am Oil Chem Soc 32:37–41, 1955.
31. KG Berger, GG Jewel, RJM Pollitt, In: JG Vaughan, ed. Food Microscopy. New York: Academic Press; 1979.
32. M Kellens, W Meeussen, H Reynaers. J Am Oil Chem Soc 69:906–911, 1992.
33. G Cornily, M leMeste. J Text Stud 16:383–402, 1985.
34. JM deMan, AM Beers. J Text Stud 18:303–318, 1987.
35. I Heertje et al. Food Microstruct 6:1–8, 1987.
36. I Heertje et al. Food Microstruct 7:189–193, 1988.
37. A Shukla, SSH Rizvi. Milchwissenschaft 51(3):144–148, 1996.
38. AG Marangoni, D Rousseau. J Am Oil Chem Soc 73:991–993, 1996.

Copyright 2002 by Marcel Dekker. All Rights Reserved.

39. I Heertje, et al. Food Microstruct. 6:115–120, 1987.
40. AG Marangoni, RW Hartel. Food Technol 52(9):46–52, 1998.
41. C Xu et al. Proc Natl Acad Sci USA 1996.
42. O Flint. Microscope 32:133–140, 1984.
43. O Flint. Eur Microsc Anal 10:21–23, 1991.
44. S Inoe. Video Microscopy. New York: Plenum Press, 1987.
45. SH Yiu. Food Microstruct 4:99–106, 1985.
46. BE Brooker. Trends Food Sci Technol 1:100–103, 1990.
47. W Buchheim. Food Microstruct 1:189–208, 1982.
48. JM deMan. Food Microstruct 1:209–222, 1982.
49. M Kalab. In: M Peleg, EB Bagley, eds. Physical Properties of Foods. Westport, CT: AVI, 1983, pp 43–104.
50. JA Sargeant. Food Microstruct 7:123–135, 1988.
51. I Heertje. Food Struct 12:77–94, 1993.
52. BB Mandelbrot. The Fractal Geometry of Nature. New York: Freeman, 1982.
53. R Jullien, R Botet. Aggregation and Fractal Aggregates. Singapore: World Scientific, 1987.
54. P Meakin, Phys Rev Lett 51:1119, 1983.
55. NB Uriev, IY Ladyzhinsky. Colloids Surf A 108:1–11, 1996.
56. R Vreeker, et al Colloids Surf 65:185–189, 1992.
57. WH Shih, et al. Phys Rev A 42:4772–4779, 1990.
58. D Rousseau, et al. J Am Oil Chem Soc 73:963–972, 1996.
59. D Rousseau, AR Hill, AG Marangoni. J Am Oil Chem Soc 73:973–981, 1996.
60. D Rousseau, AR Hill, AG Marangoni. J Am Oil Chem Soc 73:983–989, 1996.
61. D Rousseau, AG Marangoni. J Agric Food Chem 46:2368–2374, 1998.
62. D Rousseau, AG Marangoni. J Agric Food Chem 46:2375–2381, 1998.
63. AG Marangoni, D Rousseau. J Am Oil Chem Soc 75:1265–1271, 1998.
64. AG Marangoni, D Rousseau. J Am Oil Chem Soc 75:1633–1636, 1998.
65. SF Edwards, RBS Oakeshott. Physica D 38:88–92, 1989.
66. LGB Bremer, T van Vliet, P Walstra. J Chem Soc Faraday Trans 85:3359–3372, 1989.
67. PG de Gennes. Scaling Concepts in Polymer Physics. Ithaca, NY: Cornell Univ Press, 1979.
68. M Stading, M Langton, AM Hermansson. Food Hydrocolloids 7:195–212, 1993.
69. R Vreeker et al. Food Hydrocolloids 6:423–435, 1992.
70. RC Ball, Physica D 38:13–15, 1989.
71. WD Brown. The structure and physical properties of flocculating colloids. University of Cambridge, 1987.
72. WD Brown, RC Ball. J Phys A 18:L517, 1985.
73. R Buscall, et al. J Chem Soc Faraday Trans 84:4249–4260, 1988.
74. RC Sonntag, WB Russel. J Colloid Interface Sci 116:485–489, 1987.
75. DA Weitz, M Oliveria. Phys Rev Lett 52:1433, 1984.
76. D Rousseau, AG Marangoni, KR Jeffrey. J Am Oil Chem Soc 75:1833–1839, 1998.

Copyright 2002 by Marcel Dekker. All Rights Reserved.

4

Static Crystallization Behavior of Cocoa Butter and Its Relationship to Network Microstructure

Sara E. McGauley and Alejandro G. Marangoni
University of Guelph, Guelph, Ontario, Canada

I. INTRODUCTION

Both chemical and physical properties of cocoa butter have been shown to influence the quality and acceptability of confectionary products. Processing conditions affect the crystallization of the cocoa butter triglycerides into a particular polymorphic state, which in turn influences the microstructure and macroscopic properties of the network. The macroscopic properties determine final attributes such as viscosity, demolding, snap, surface gloss, and desired melting characteristics of the confectionary product. The levels of structure found in cocoa butter and their influence on the macroscopic rheological properties are illustrated in Figure 1.

Many researchers have studied the effect of lipid composition and polymorphism on macroscopic rheological properties but have not sufficiently considered the importance of the microstructure of the network. Depending on the source and the refining process, the chemical composition of cocoa butter may vary (Dimick, 1999). This has been shown to influence crystallization rates and hardness characteristics. Within the microstructural level, the polymorphic form of cocoa butter has been shown to affect the shape and size of the crystals (Vaeck, 1960). In terms of final product quality the polymorphic form of the crystals will determine melting characteristics. However, lipid composition and polymorphism alone cannot be used to predict the macroscopic properties of a fat crystal network.

Copyright 2002 by Marcel Dekker. All Rights Reserved.

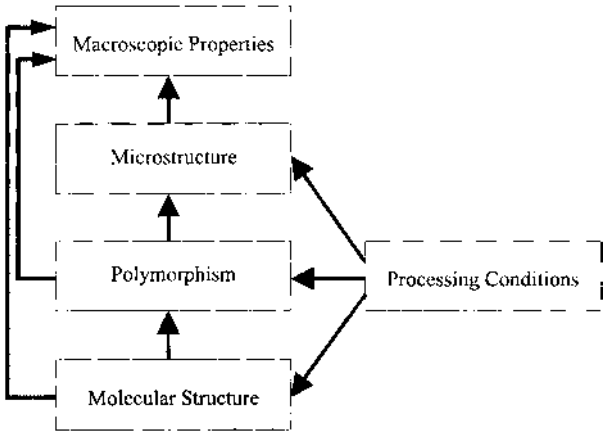

Figure 1 The influence of the various levels of structure in a fat network on the fat's macroscopic rheological properties.

Until recently, cocoa butter microstructure was studied only qualitatively. The microstructure of the unstable polymorphic form of cocoa butter has been described as a bright crystalline mass (Vaeck, 1960), whereas the more stable forms have been associated with various microstructures as described by Manning and Dimick (1985). The importance of the microstructural level of the network in the determination of macroscopic properties has led to the development of a theory that allows for quantification of this level of structure (Marangoni and Rousseau, 1996; Narine and Marangoni, 1999a).

The aim of this work is to establish a relationship between lipid composition, polymorphism, crystallization kinetics, and microstructure of statically crystallized cocoa butter.

II. CHEMICAL COMPOSITION

The smallest characteristic structure present in fat crystal networks is at the molecular level. The major constituents of fats, including cocoa butter, are triglycerides (TAGs). TAGs are composed of a variety of fatty acids esterified to a glycerol backbone. The fatty acid chains may be saturated or unsaturated, branched or linear, short or long, and contain either odd or even numbers of carbons (Small, 1986). The physical properties of triglyceride molecules are dependent on fatty acid chain composition and distribution. The composition and distribution influence the polymorphic behavior of the various solid phases, which in turn influences various macroscopic properties of the material including melting behavior and hardness (deMan, 1982).

Copyright 2002 by Marcel Dekker. All Rights Reserved.

Table 1 Lipid Composition of Cocoa Butter from Six Different Countries of Origin

Lipid class	Range (wt%)	Mean (wt%)
Triglycerides	96.21–97.30	96.97
Diglycerides	0.80–1.79	1.30
Monoglycerides	0.02–0.04	0.03
Free fatty acids	0.88–1.46	1.17
Sterols	0.10–0.14	0.12

Source: Dimick, 1999.

The major fatty acids present in cocoa butter triglycerides are palmitic acid (P), oleic acid (O), and stearic acid (S). Cocoa butter is composed mainly of symmetrical triglycerides (>75%) with oleic acid in the *sn*-2 position (POP, POS, SOS) and with trace amounts of asymmetrical triglycerides (PPO, PSO, and SSO) (Shukla, 1995; van Malssen et al., 1996). This natural fat is relatively simple insofar as it is composed of a small number of TAG components and melts over a narrow temperature range, which is important in terms of textural quality (Shukla, 1995). The typical composition of cocoa butter is shown in Table 1.

Most fats used in industry are refined before they are used as food ingredients. However, cocoa butter is obtained by hydraulic pressing of the cocoa bean cotyledons, which results in an unrefined product. Pure pressed cocoa butter contains many lipid species other than the triglyceride component, and these minor components, including diglycerides, monoglycerides, free fatty acids, and sterols, have been shown to affect crystallization behavior and final product quality (Dimick, 1999). For some products such as white chocolate, the flavor associated with unrefined cocoa butter is regarded as unpleasant, and in this case refined cocoa butter is used (Beckett, 2000). The refining process may include bleaching, degumming, neutralization, deodorization, or fractionation. These treatments generally reduce the free fatty acid content and remove more polar components, including glycolipids and phosphatides (Dimick, 1999). The cocoa butter used in our work was refined, and analysis indicated that no phospholipids were present. It has been speculated that polar components play a significant role in the formation of crystal seed nuclei (Dimick, 1999). Therefore, refined fat systems will most likely crystallize in a different manner than unrefined ones.

III. POLYMORPHISM

The structure of the solid state is the next level of structure known to affect the macroscopic properties of fats. This level of structure is particularly important

Copyright 2002 by Marcel Dekker. All Rights Reserved.

for cocoa butter. The polymorphism of the solid state can be characterized by using powder X-ray diffraction (XRD) (deMan, 1992; Larsson, 1994). In pure triglycerides, three major polymorphic forms have been noted. These are referred to in order of increasing stability as alpha (α), beta prime (β'), and beta (β). These polymorphic forms differ in several physical properties, including melting points. The method of choice for the study of fat polymorphism is powder X-ray diffraction (XRD), but other methods such as differential thermal analysis (DTA), differential scanning calorimetry (DSC), low temperature infrared spectroscopy, and microscopy may also yield useful information (deMan, 1992). When fats are analyzed by powder XRD, two types of spacings are observed; long spacings and short spacings. Long spacings correspond to reflections originating from planes formed by the methyl endgroups of the triglycerides and are dependent on the chain length and the angle of tilt of the component fatty acids. Short spacings, on the other hand, are sensitive to the cross-sectional packing of the hydrocarbon chains and are independent of chain length (deMan, 1992). The most stable form, the β polymorph, has a triclinic subcell with a characteristic short spacing at 4.6 Å. The β' form has an orthorhombic subcell structure with characteristic short spacings at 3.8 and 4.2 Å. Finally, the least stable polymorph, the α form, has a hexagonal subcell with a characteristic short spacing at 4.15 Å (Hagemann, 1988). In mixed triglyceride systems, other metastable polymorphs, called the γ and δ, and several β' polymorphs have been observed (Sato, 1996). The γ form, like the β' form, is orthorhombic perpendicular with characteristic short spacings at 3.8 and 4.2 Å (Larsson, 1994).

Polymorphism is much more complicated in natural fats, especially those with a relatively homogeneous TAG composition. This is the case of cocoa butter, in which six polymorphic forms are generally observed (Schlichter-Aronhime and Garti, 1988). However, the nomenclature of these forms is inconsistent. The chocolate industry tends to refer to the polymorphic forms as I–VI, in order of increasing stability as described by Wille and Lutton (1966). The margarine and shortening industry prefers the nomenclature γ (or sub-α), α, β'_2, β'_1, β_2, and β_1, once again in order of increasing stability as described by Larsson (1966). Early studies on cocoa butter polymorphism established a specific melting temperature for each polymorphic form (Chapman et al., 1971; Riiner, 1970; Wille and Lutton, 1966). Recently, each polymorphic form was shown to have a characteristic melting range (Table 2) (van Malssen et al., 1999). Characteristic short spacings of the six polymorphic forms of cocoa butter have also been identified (Table 3) (Larsson, 1994). In the chocolate industry, it is important that cocoa butter crystallizes in the β_1 form to prevent undesirable physical characteristics and recrystallization during storage (Beckett, 2000; Larsson, 1994).

In this study, the polymorphic forms of cocoa butter were determined from the peak melting temperature obtained by differential scanning calorimetry (DSC) and confirmed by powder XRD. After melting cocoa butter samples at 80°C and

Copyright 2002 by Marcel Dekker. All Rights Reserved.

Table 2 Melting Ranges of the Different Solid Phases (Polymorphic Forms) Found in Cocoa Butter

Polymorphic form	Melting range (°C)
γ (sub-α)	−5–+5
α	17–22
β_2'	20–27
β_1'	20–27
β_2	29–34
β_1	29–34

Source: van Malssen et al., 1999.

upon crystallization at specific temperatures for determined lengths of time, DSC melting profiles were obtained (Fig. 2). A heating rate of 5°C/min from the crystallization temperature to 50°C was used in all of the DSC experiments. The predominant polymorphic form was determined from the peak melting temperatures (Fig. 2a) based on published melting ranges (Table 2) (van Malssen et al., 1999). During crystallization, polymorphic transformations from a less stable form to a more stable polymorph may take place. In these transition regions, two peak melting temperatures were observed.

Cocoa butter crystallized at 0°C for 3 days had a melting profile displaying two peak temperatures (Fig. 2b). The first peak, at 19.7°C, is characteristic of the α form, whereas the second peak, at 24.4°C, indicates that the more stable β′ form is also present. A polymorphic transition is not always indicated by the

Table 3 Characteristic Short Spacings as Determined by XRD for the Various Polymorphic Forms of Cocoa Butter

Polymorphic form	Short spacings (Å)
γ (sub-α)	3.87(m), 4.17(s)
α	4.20(vs)
β_2'	3.87(vw), 4.20(vs)
β_1'	3.75(m), 3.88(w), 4.13(s), 4.32(s)
β_2	3.65(s), 3.73(s), 3.87(w), 3.98(s), 4.22(w), 4.58(vs), 5.13(w). 5.38(m)
β_1	3.67(s), 3.84(m), 4.01(w), 4.21(vw), 4.53(vs), 5.09(vw), 5.37(m)

The relative intensity is noted as very strong (vs), strong (s), medium (m), weak (w), or very weak (vw).
Source: Larsson, 1994.

Copyright 2002 by Marcel Dekker. All Rights Reserved.

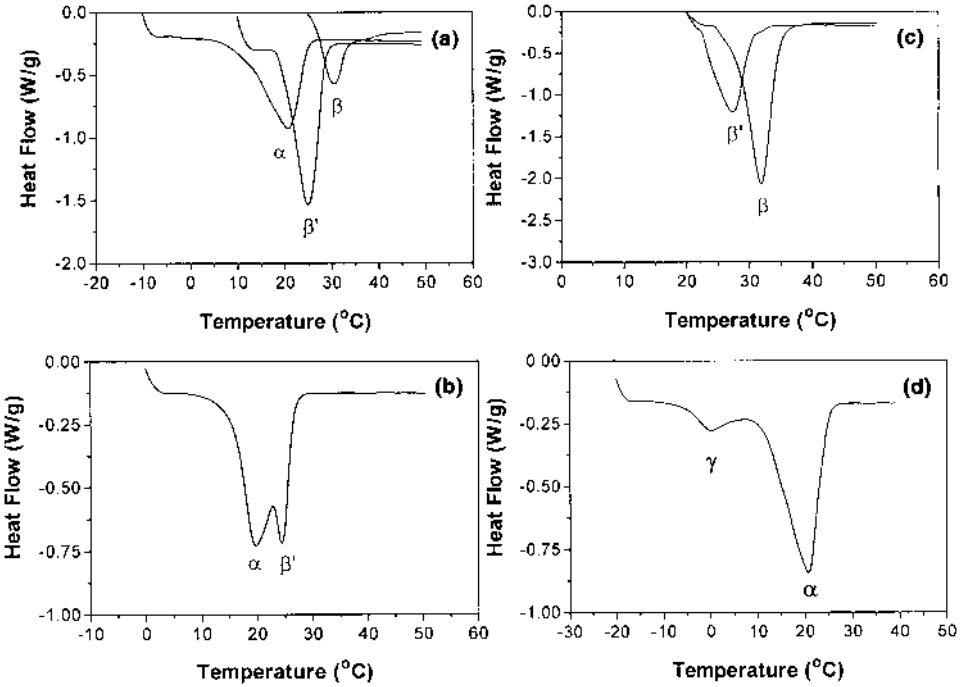

Figure 2 Overlay of three characteristic melting profiles obtained by DSC (a) of the different polymorphic forms of cocoa butter. Melting curves of cocoa butter statically crystallized at (b) 0°C, (c) 20°C for 6 days and (d) −20°C for 2 days are also shown.

presence of two peak temperatures in one melting profile. Often, some of the replicates measured at the same time–temperature combination had a single peak temperature characteristic of one polymorph, whereas the other replicates indicated the presence of another polymorphic form. Two samples measured after a 6-day incubation at 20°C displayed different melting profiles (Fig. 2c). The first had a peak temperature at 27.3°C, and the other showed a peak temperature of 31.8°C. Under these particular conditions a polymorphic transition is likely taking place from the β′ form to the more stable β polymorph.

The metastable γ polymorph has been shown to form directly from the melt at low crystallization temperatures (van Malssen et al., 1999). In our DSC experiments, the existence of a pure γ phase was not observed. However, a peak temperature of 1.6°C, which is within the reported melting range for the γ polymorph, was shown to exist concurrently with a peak temperature of 20.6°C characteristic of the α form at low temperatures (Fig. 2d). The γ form, with a peak

Copyright 2002 by Marcel Dekker. All Rights Reserved.

melting temperature between −5°C and 5°C, was not observed after 10 min, nor after 1 day as would be expected from an unstable polymorph. Rather, the DSC melting profiles indicated that the α polymorph formed after 4 min, and only following 2 days of crystallization at either −15°C or −20°C did the presence of the γ polymorph become evident. It is known that polymorphic transitions take place from a less stable to a more stable polymorph and are irreversible. Because the γ polymorph is less stable than the α form, the occurrence of a polymorphic transition is unlikely. We speculate that fractionation has taken place, resulting in the separation of different triglyceride species. Some of the lower melting triglycerides could have then crystallized into the γ form and coexisted with the α phase even after 7 days at −15°C and −20°C. DSC did not allow for measurements until 3 or 4 min into the crystallization process. Because the γ polymorph is very unstable, it is possible that there had already been a polymorphic transition to the more stable α form before the peak melting temperature could be determined.

To determine changes in polymorphism from DSC melting profiles, peak melting temperatures were plotted as a function of crystallization temperature at various times. Changes in peak melting temperature plotted as a function of time after 7 days of crystallization are shown in Figure 3. In this figure there are six statistically different regions ($P < 0.001$). The first region included crystallization temperatures from −20°C to −5°C, where peak melting temperatures ranged between 18.4 and 20.7°C, characteristic of the α polymorph. The next region included crystallization temperatures between 0°C and 10°C, with peak melting temperatures ranging from 19.7 to 25.9°C. In this region, some of the peak tem-

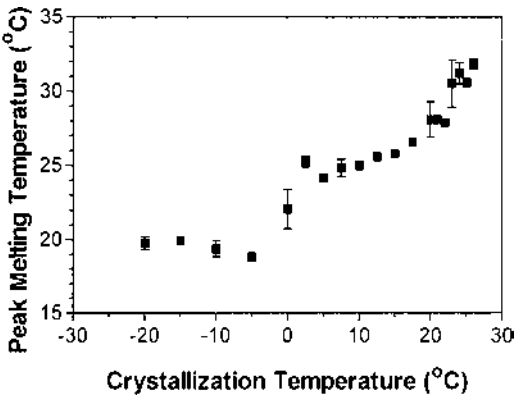

Figure 3 Peak melting temperature as a function of crystallization temperature obtained from DSC melting profiles of cocoa butter statically crystallized for 7 days. Symbols represent the average ± standard error of four replicates.

Copyright 2002 by Marcel Dekker. All Rights Reserved.

peratures were characteristic of the α form whereas others indicated the coexistence of the α and β′ polymorphs. The third statistically significant region included crystallization temperatures between 2.5 and 20°C. The peak melting temperatures found in this region ranged from 23.1 to 27.2°C characteristic of the β′ polymorph. Crystallization temperatures overlap with those in the previous region (0–10°C) because of the transition from the α polymorph to the β′ polymorph. Many of the peak temperatures in these two regions are similar, and both indicate the existence of the β′ form. The fourth region included crystallization temperatures between 10 and 22°C, with peak melting temperatures ranging from 24.9 to 28.3°C. These peak temperatures were higher than those in the third region but are also characteristic of the β′ polymorph. Therefore, this analysis indicated that at least two different β′ forms were present, with slightly different peak melting temperatures. It is difficult to distinguish between these two forms because their peak melting temperatures are so close. The fifth statistically significant region included crystallization temperatures between 20 and 25°C. Peak melting temperatures in this region ranged from 26.7 to 33.7°C, which is characteristic of the polymorphic transition region from the β′ form to the β polymorph. The final region including crystallization temperatures ranging from 23 to 26°C, with peak melting temperatures ranging from 29.0 to 33.7°C, characteristic of the β polymorph.

Similar results were found for cocoa butter crystallized statically at temperatures ranging from −20 to +26°C for all times. Our work suggests that peak melting temperatures provide a good indication of the different polymorphic forms. The various polymorphic regions discussed in this work as α, α to β′, β′, β′ to β, and β were all found to be statistically different ($P < 0.001$), as judged by their peak melting temperatures. Throughout the analysis at various times, two forms of the β′ polymorph were detected, perhaps suggesting that both the β'_2 and the β'_1 forms could be obtained by static crystallization of refined cocoa butter.

Some of the polymorphic forms determined from peak melting temperatures obtained by DSC were confirmed by using powder XRD. Using DSC, a pure γ form was not observed, even at low temperatures. XRD allowed for the determination of a polymorphic form after 2 min of crystallization at a particular temperature. Static crystallization for 2 min at −20°C gave an XRD pattern with short spacings at 3.79 and 4.19 Å (Fig. 4a) characteristic of the γ polymorphic form. These short spacings are also characteristic of the β′ form, but in this case we know that the γ polymorph was present because the next polymorph to form was the α form. Polymorphic transitions occur only from less stable polymorphs to more stable forms and are irreversible.

X-ray diffraction spacings were obtained for the α, β′, and β polymorphs identified by DSC. After crystallization for 2 min at 5°C, a short spacing was

Copyright 2002 by Marcel Dekker. All Rights Reserved.

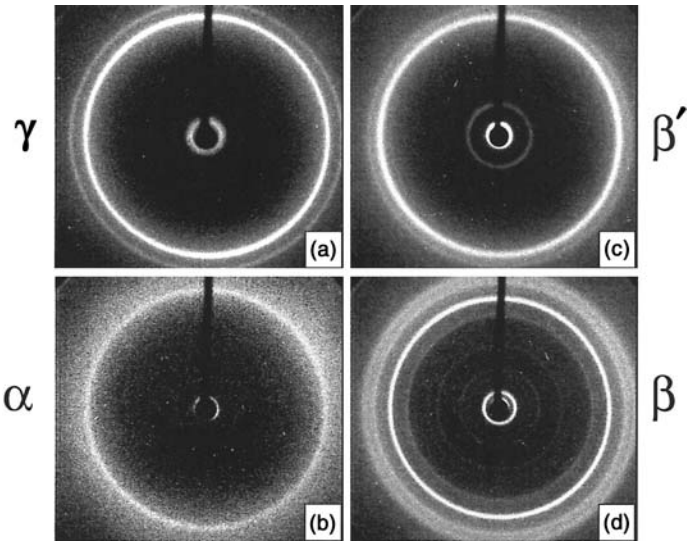

Figure 4 Characteristic X-ray diffraction patterns of the various polymorphic forms of cocoa butter crystallized at (a) −20°C for 2 min, (b) 5°C for 2 min, (c) 5°C for 5 days, and (d) 22°C for 28 days.

observed from the XRD patterns at 4.21 Å (Fig. 4b). This value is characteristic of the α form and confirms the polymorphic form determined by DSC. After 5 days of incubation at 5°C the β′ form was determined by DSC and confirmed by using XRD by the observation of short spacings at 3.81 and 4.18 Å (Fig. 4c). After crystallization at 22°C for 28 days, the diffraction pattern displayed short spacings at 3.70, 3.94, 4.58, and 5.42 Å (Fig. 4d), characteristic of the β form. Cocoa butter crystallized statically at 22°C for 28 days had a peak melting temperature of 32.7°C, which is also characteristic of the β polymorph. From the peak melting temperatures, two β′ polymorphs were found to exist. However, this was not confirmed by XRD. Only the β_2' form, with short spacings at 3.87 and 4.20 Å, was observed (Larsson, 1994). In many instances where the β_1' was determined by DSC the β polymorph was also present. It appears that in regions where both of these polymorphic forms are present, the short spacings have values that more closely resemble those of the β form.

Differential scanning calorimetric melting profiles were determined for cocoa butter that was statically crystallized from an 80°C melt to temperatures ranging from −20 to +26°C. Incubation times ranged anywhere from 1 h to 35 days depending on the crystallization temperature. Results from these DSC

Copyright 2002 by Marcel Dekker. All Rights Reserved.

experiments were confirmed by powder XRD. These data were used to construct a time–temperature state diagram for the polymorphism of statically crystallized cocoa butter (Fig. 5).

At crystallization temperatures between −15 and −20°C, both the γ and α polymorphs were observed for a 7-day period. After 2 min at −20°C, the γ form was observed by XRD but not by DSC. This was likely due to the limitations of the DSC equipment, as previously discussed in this section. The melting profiles obtained by DSC indicated that only the α polymorph was present at −15 and −20°C after 4 min of crystallization. Subsequently, we detected the existence of the γ form concurrently with the dominant α polymorph; both remained stable for 7 days. This does not indicate that cocoa butter crystallized into a more stable state and then rearranged into a less stable state. Rather, as previously discussed, we speculated that fractionation had occurred in which some of the triglycerides remained in the more stable α conformation whereas others crystallized into the unstable γ polymorph.

At crystallization temperatures ranging from −10 to +20°C, the α polymorph was initially observed, as determined by DSC. The γ polymorph has been observed by XRD to form initially at crystallization temperatures from −10 to +3°C and remain stable for 3 min (van Malssen et al., 1999). Once again, we did not obtain this result, probably because of the limitations of the DSC equipment. However, the initial formation of the α polymorph at 5 and 20°C was confirmed by XRD in our study. The α polymorphic form was found to be quite stable at

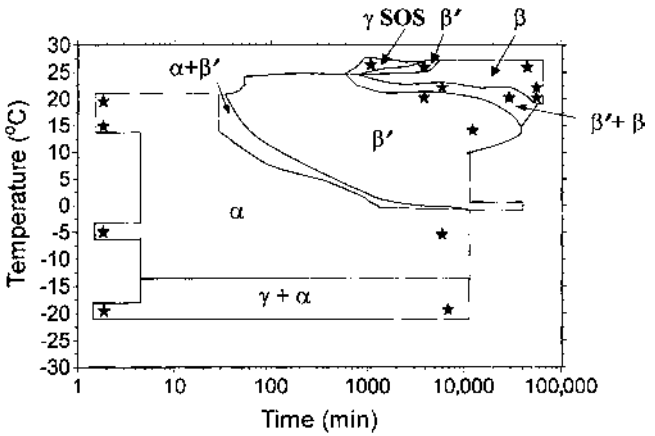

Figure 5 Time–temperature state diagram for the polymorphism of statically crystallized cocoa butter. The star symbol represents the polymorphic forms that have been determined by XRD.

Copyright 2002 by Marcel Dekker. All Rights Reserved.

low crystallization temperatures. At −10 and −5°C the α polymorph remained stable even after 7 days of incubation. At crystallization temperatures higher than −5°C, the α polymorph was found to remain stable for incubation times ranging from 10 min (17.5 and 20°C) to 2 days (0°C) depending on the crystallization temperature.

At crystallization temperatures ranging from 0 to 20°C, a polymorphic transition region from the α polymorph to the β′ form was observed. At low crystallization temperatures, the complete transformation of the less stable α polymorph to the more stable β′ polymorph can require up to 8 days of incubation, whereas at higher temperatures the transformation requires only 40 min.

The state diagram (Fig. 5) clearly shows that the β′ polymorph can be formed directly from the melt or from the melt via the α polymorph. At temperatures from 21 to 26°C, crystallization of the β′ polymorph can take from 1 h to 3 days. The stability of the β′ polymorph is dependent on the crystallization temperature. At 15°C, the β′ form remained stable for 28 days, whereas at the higher temperatures a transformation to the more stable β form occurred after a few hours.

The second polymorphic transition region, from the β′ polymorph to the β form, occurred at crystallization temperatures in the range of 20–26°C. At 20°C this transition occurred over a 3-week period, whereas at 25 and 26°C the transition was completed within hours. Finally, the β form was observed to crystallize from the melt either from the α form via the β′ polymorph or directly from the β′ polymorph. This stable polymorphic form was observed only at higher crystallization temperatures (20–26°C) and in some cases only after incubation times of 35 days. The β polymorph was found to remain stable for several weeks of storage at crystallization temperatures ranging from 22 to 26°C.

An anomalous region, termed γ-SOS, was detected at 25 and 26°C. After crystallization at 25°C for 20 h or at 26°C for 1 day, the first crystal structure formed displayed a melting range of 35.2–37.3°C. Initially we thought that this particular crystal form could be the β_1 polymorph. However, after crystallization at 25°C for 1 day and at 26°C for 3 days, results from both DSC and XRD indicated the existence of the β′ form. It is very unlikely that the stable β_1 would transform to the more unstable β′, indicating that the initial crystal form at these temperatures was not the β_1 polymorph. The XRD pattern of this anomalous crystal form obtained by crystallization at 26°C, displayed a broad short spacing at 4.45 Å (Fig. 6). This also confirmed that this particular crystal was not the β_1 polymorph found in cocoa butter. Much work involving the determination of the various polymorphic forms of POP, POS, and SOS, the main triglycerides in cocoa butter, has been carried out (Arishima et al., 1991; Sato et al., 1989). The γ polymorphic form of SOS was found to form directly from the melt at a crystallization temperature between 24 and 28°C (Sato et al., 1989). The γ form of SOS was also determined by DSC to have a melting temperature of 35.4°C, and XRD patterns illustrated two sharp

Copyright 2002 by Marcel Dekker. All Rights Reserved.

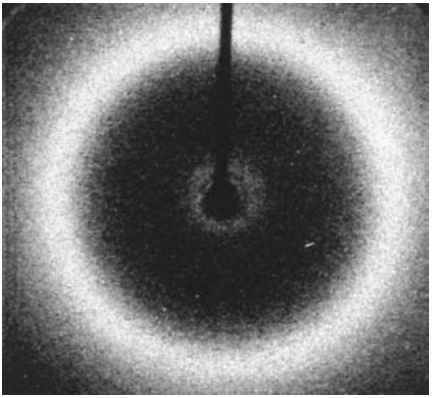

Figure 6 X-ray diffraction pattern of cocoa butter statically crystallized at 26°C for 1 day with a broad short spacing at 4.45 Å.

short spacings at 3.88 and 4.72 Å and a broad short spacing at 4.5 Å (Sato et al., 1989). In this work we observed a polymorphic form with a similar melting point and a broad short spacing at 4.45 Å. It was hypothesized that the SOS fraction of cocoa butter crystallized initially, with the remainder of the triglycerides remaining in the melt. Thereafter, the SOS rearranged and cocrystallized with POP, POS, and the minor triglycerides into the β′ crystal form.

Van Malssen et al. (1999) had previously constructed a state diagram for the polymorphism of statically crystallized cocoa butter. Even though their and our state diagrams displayed similar trends, polymorphic transitions occurred more rapidly in their study. This may be due to the fact that the cocoa butter used by van Malssen et al. (1999) was not refined. The cocoa butter used in our experiments was refined and did not contain phospholipids. Degummed cocoa butter has been found to show a significantly slower crystallization rate than unrefined cocoa butter (Dimick, 1999). When crude degummed material, which had a melting point very close to that of lecithin, and a pure *sn*-1,2 distearoyl phosphatidylcholine were added back to the refined cocoa butter, the nucleation induction time was reduced and the crystallization growth rate was increased (Dimick, 1999). The refined cocoa butter used in our research would therefore be expected to have lower crystallization rates than unrefined cocoa butter.

It must be stressed that this state diagram is specific to the cocoa butter used in this study. This particular cocoa butter has been degummed, deodorized, and bleached and therefore lacks phospholipids and other minor components, which most likely slows down its crystallization. In addition, the absence of phospholipids may also slow down polymorphic transformations.

Copyright 2002 by Marcel Dekker. All Rights Reserved.

IV. CRYSTALLIZATION KINETICS

When a fat is in the liquid state, triglyceride molecules are in random motion. Supercooling of the fat causes molecules to cluster and pack together, which eventually leads to the formation of a crystal nucleus. At high degrees of supercooling, this nucleation process is very rapid. In this instance, molecules have little time to rearrange and are not able to adopt their most thermodynamically favorable conformation. This leads to the formation of a less ordered solid. At high degrees of supercooling, however, there is also a rapid increase in viscosity, which limits heat and mass transfer. The rearrangement of triglyceride molecules into a more stable form is thus hindered. The rate of nucleation and the increased viscosity limit crystal growth, leading to a system with a large number of small crystals. When liquid fat is subjected to a lower degree of supercooling, triglyceride molecules have a greater tendency to arrange themselves into a more thermodynamically favorable conformation, resulting in a more ordered system. In addition, viscosity does not increase to the same extent, and the system thus has a decreased propensity to become limited by heat and mass transfer. At higher temperatures, nucleation is slower and crystal growth is more extensive than for systems at high degrees of supercooling. The particular crystal form of a fat system is not determined solely by chemical composition. Chemical composition and heat and mass transfer all play an important role in the final crystal structure and cannot be considered independently for fat crystallization. For example, it is difficult to determine whether an unstable crystal form was created as a result of the unfavorable conformation of the triglyceride molecules due to rapid nucleation or whether a rapid increase in viscosity limits the mass and heat transfer, making rearrangements of the molecules very difficult. Both of these factors are responsible for the resultant crystal form.

Crystallization involves nucleation and growth. The mechanism by which structure develops is best determined by considering these two steps separately. However, in most fat systems it is quite difficult to distinguish between nucleation and growth. The Avrami model has been used in the study of fat crystallization (Dibildox-Alvarado and Toro-Vazquez, 1997; Herrera and Marques Rocha, 1996; Herrera et al., 1998; Kawamura, 1979; Metin and Hartel, 1998; Wright et al., 2000; Ziegleder, 1990). The Avrami model can be used to quantify crystallization kinetics and describes the overall crystallization process, taking into account both nucleation and crystal growth (Avrami, 1939, 1940, 1941):

$$\frac{\mathrm{SFC}(t)}{\mathrm{SFC}(\infty)} = 1 - e^{-kt^n} \tag{1}$$

where SFC(t) describes the solid fat content as a function of time, SFC(∞) is the limiting SFC as time approaches infinity, k is the Avrami constant, and n is the

Copyright 2002 by Marcel Dekker. All Rights Reserved.

Avrami exponent. The Avrami constant k is a measure of the velocity of reaction and shows an Arrhenius-type dependence on the crystallization temperature (Christian, 1965; Graydon et al., 1994). The Avrami exponent n is sensitive to the mechanism of crystallization. This parameter is also sensitive to both the time dependence of nucleation and the dimensionality of growth. Nucleation can be either sporadic or instantaneous, and crystal growth may occur in one, two, or three dimensions to give rods, disks, or spherulites, respectively (Sharples, 1966). The different combinations of nucleation and growth mechanisms for different values of the Avrami exponent are shown in Table 4 (Sharples, 1966). A value of n can describe many types of nucleation and subsequent crystal growth as well as different combinations of these two processes.

The crystallization behavior of cocoa butter was examined in our work by measuring the increase in SFC as a function of time by pulsed nuclear magnetic resonance (pNMR). Crystallization curves for cocoa butter crystallized statically at −20, 10, and 15°C (Fig. 7a) and at 17.5, 20, and 22.5°C (Fig. 7b) were determined. These curves are characterized by an initial lag period followed by a rapid increase in crystal mass, which levels off at a particular SFC depending on the crystallization temperature. A high degree of supercooling (−20 to 15°C) leads to a short lag period, and the SFC increase in almost instantaneous. These curves usually tend to level off within the first 10 min of crystallization at very high SFC values (>90%). At lower degrees of supercooling (20–26°C), the initial lag period is much longer, as is the subsequent increase in crystal mass. Crystallization curves obtained at 25 and 26°C may take up to 10 days to level off and reach an SFC value of only 60%.

The crystallization curves were fitted to the Avrami equation by nonlinear regression (Marangoni, 1998) in order to quantify the crystallization kinetics and to gain insight into the nature of the crystal growth process. The Avrami exponent was then determined and plotted as a function of crystallization temperature (Fig. 8). Statistically, two different regions were determined from this graph ($P <$

Table 4 Avrami Exponent Values for the Different Types of Growth and Nucleation

Avrami exponent	Type of growth and nucleation
3 + 1 = 4	Spherulitic growth from sporadic nuclei
3 + 0 = 3	Spherulitic growth from instantaneous nuclei
2 + 1 = 3	Disklike growth from sporadic nuclei
2 + 0 = 2	Disklike growth from instantaneous nuclei
1 + 1 = 2	Rodlike growth from sporadic nuclei
1 + 0 = 1	Rodlike growth from instantaneous nuclei

Source: Sharples, 1966.

Copyright 2002 by Marcel Dekker. All Rights Reserved.

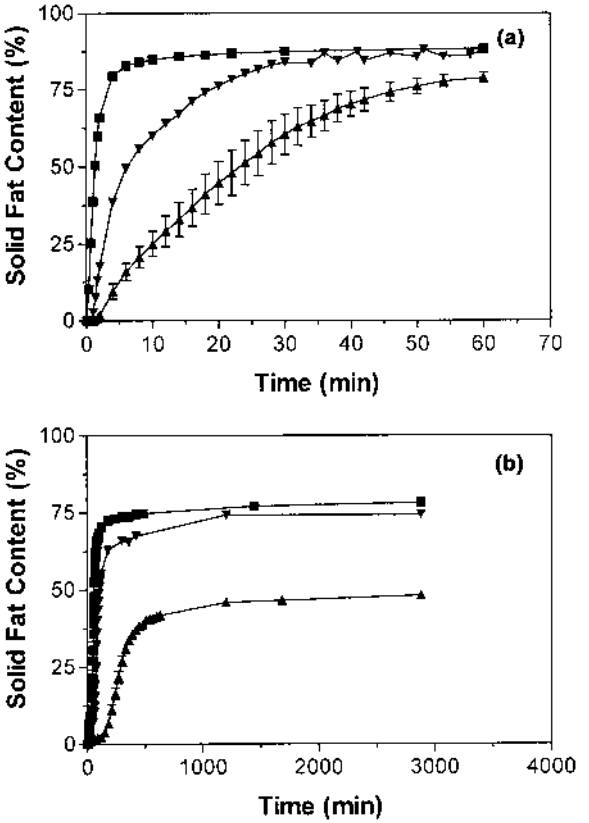

Figure 7 Crystallization curves of cocoa butter crystallized at (a) (■) −20°C, (▼) 10°C, (▲) 15°C and (b) (■) 17.5°C, (▼) 20°C and (▲) 22.5°C. Symbols represent average ± standard error of three replicates.

0.001). The first region was determined at crystallization temperatures ranging from −20 to +15°C, and the second ranged from 20 to 26°C. No statistical differences were observed within these two regions ($P > 0.05$). The value of n in the first region was less than 1.0, whereas in the second region a value of about 3.0 was obtained. The Avrami exponent was constant at low crystallization temperatures, followed by a drastic increase at 20°C. A gradual increase in n was observed above 20°C with increasing temperature. Similar results were observed for statically crystallized milkfat (Wright et al., 2000). The change in the Avrami exponent at 20°C also corresponds to changes in microstructure. Polarized light micrographs (Fig. 12; see Section V) show a granular morphology for

Copyright 2002 by Marcel Dekker. All Rights Reserved.

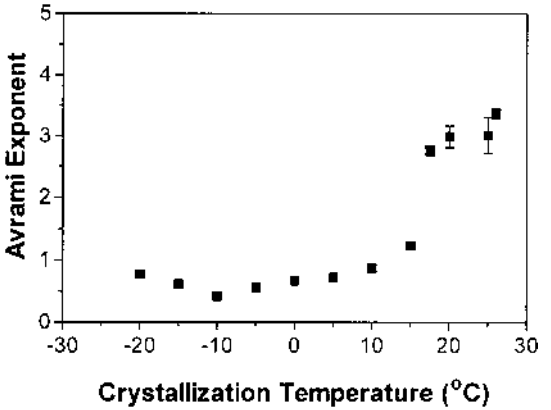

Figure 8 Changes in the Avrami exponent as a function of crystallization temperature. Symbols represent the average ± standard error of the mean of three replicates.

crystallization temperatures below 20°C. At temperatures of 20°C and above, both spherulite clusters and needle-like morphologies were observed. These microstructures indicate differences in the crystal growth geometry above and below 20°C. Therefore, the Avrami exponent could be used to distinguish between different mechanisms of crystallization.

At crystallization temperatures ranging from −20 to 0°C, the α polymorph is predominant. The β′ polymorph is the main form at crystallization temperatures between 5 and 22.5°C, whereas the major form at 25 and 26°C is the β polymorph. The Avrami exponent was found to change dramatically at crystallization temperatures above and below 20°C, suggesting that it is not a good predictor of the predominant polymorphic form. However, at low crystallization temperatures, the less stable α and β′ polymorphs are present, whereas at higher crystallization temperatures the stable β polymorph is predominant. The Avrami exponent can be used to distinguish between the unstable polymorphic forms (α and β′) and the stable β polymorph.

The induction time is defined as the point where the amount of solid fat is significantly different from zero (Sharples, 1966). Induction times were calculated in our work from the crystallization curves by extrapolating from the linearly increasing region back to the time axis (Wright et al., 2000). The logarithms of the induction times were then plotted as a function of crystallization temperature (Fig. 9). At low crystallization temperatures (−20 to 0°C), we observed a positive linear relationship between the logarithm of induction time and crystallization temperature, which then leveled off from 5 to 15°C. A discontinuity between crystallization temperatures of 15 and 17.5°C was followed by a positive

Copyright 2002 by Marcel Dekker. All Rights Reserved.

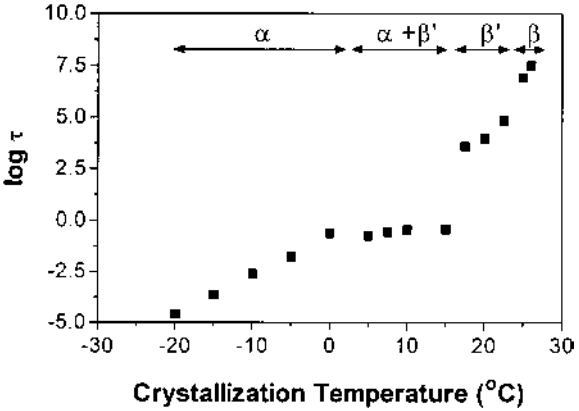

Figure 9 Induction times for statically crystallized cocoa butter as a function of crystallization temperature. The polymorphic designation indicates the dominant polymorphic form present at a particular crystallization temperature as determined from melting points and XRD patterns. Symbols represent the average ± standard error of three replicates.

linear relationship from 17.5 to 22.5°C. From 22.5 to 25°C, another discontinuity was observed. An increase was also observed between 25 and 26°C.

It has been suggested that discontinuities in the relationship between log induction time and crystallization temperature may be associated with different polymorphic forms (Dibildox-Alvarado and Toro-Vazquez, 1997). For tripalmitin, the nucleation rate has been shown to be inversely associated with the induction time, and a discontinuity was observed at temperatures where the β′ form transforms to β form (Kellens et al., 1992). Discontinuities found in the relationship between log induction time and crystallization temperature in our work are also associated with polymorphic transformations. At low crystallization temperatures (−20 to 0°C), cocoa butter crystallizes mainly in the α form. However, we also observed the coexistence of the γ and α forms at crystallization temperatures in the range −20 to −15°C. The α polymorph is initially present at crystallization temperatures ranging from 5 to 15°C, but it converts to the β′ polymorphic form after 6 h at 5°C and 40 min at 15°C. At crystallization temperatures ranging from 17.5 to 22.5°C the major form is the β′ polymorph. At 25 and 26°C, we suspected that the initial crystallization was of the SOS fraction of the cocoa butter followed by the formation of the β′ polymorph, which quickly transformed to the β polymorphic form.

Relationships between crystallization kinetics and polymorphism were sought by comparing results obtained by pNMR and DSC at the early stages of crystallization (Fig. 10). At a crystallization temperature of 17.5°C, the α poly-

Copyright 2002 by Marcel Dekker. All Rights Reserved.

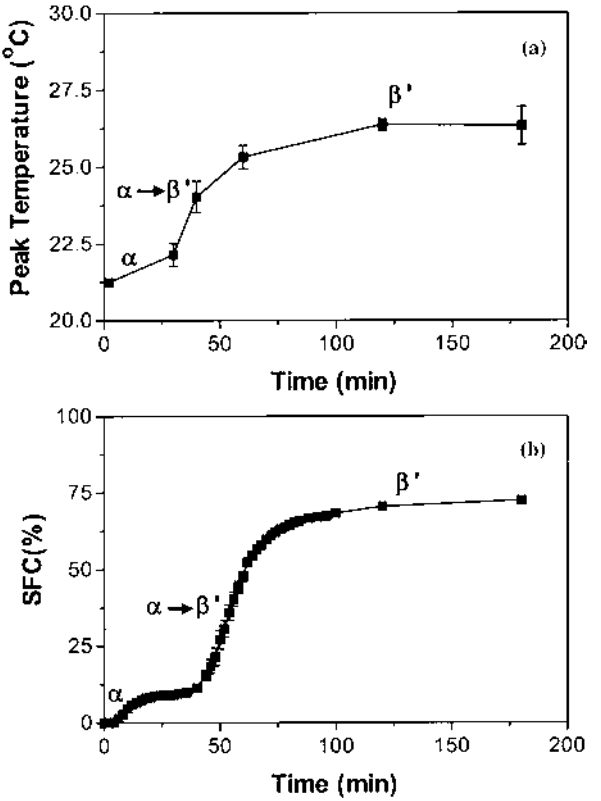

Figure 10 Comparison of the polymorphic forms as determined from peak temperatures obtained (a) from DSC melting profiles and (b) from crystallization curves of statically crystallized cocoa butter. Symbols represent the average ± standard error of three replicates.

morph formed after 4 min and remained stable for 10 min, as determined by DSC (Fig. 10a). For the next 30 min, a polymorphic transition to the more stable β′ form occurred. Finally, after 1 h, the β′ polymorph was the only crystal form present. A similar pattern could be observed from the crystallization kinetic data obtained at 17.5°C (Fig. 10b). An initial increase in SFC during the first 10 min was followed by a leveling off of the curve until 40 min. This was followed by a dramatic increase in the SFC until 60 min, when the SFC plateaued again. The initial linear increase in the crystallization curve indicates the formation of the α polymorph, whereas the second increase is associated with the formation of the β′ polymorph. The plateau observed from 10 to 40 min corresponds to the

Copyright 2002 by Marcel Dekker. All Rights Reserved.

region of α-to-β′ polymorphic transformation, as determined by DSC. Figure 10 demonstrates that in some cases measuring SFC as a function of time provides a good indication of both the formation and the transformation of the various polymorphic forms.

V. MICROSTRUCTURE

The microstructural level has a significant impact on the macroscopic rheological properties of a fat system (deMan and Beers, 1987; Heertje et al., 1987; Narine and Marangoni, 1999a). This microstructure is dependent on the molecular composition as well as its crystallization behavior, including polymorphism. Crystallization kinetics and polymorphism are dependent on processing conditions, which in turn influence the resultant microstructure (Narine and Marangoni, 1999a). Polarized light microscopy (PLM) has been used to study cocoa butter morphology since the 1930s (as reported by Vaeck, 1960). This technique distinguishes between the solid and liquid phases because the crystals of the solid phase are anisotropic whereas the liquid phase is isotropic (Chawla and deMan, 1990). PLM has been used to visually define the crystalline forms of cocoa butter during crystallization (Manning and Dimick, 1985; Vaeck, 1960). In this study, PLM was used to investigate the microstructures of the various polymorphic forms of statically crystallized cocoa butter as determined from the time–temperature state diagram (Fig. 5).

Images of the α polymorph of cocoa butter displayed a granular appearance (Fig. 11). We observed the coexistence of the γ polymorph and the α form at −20 and −15°C. However, the γ polymorph was not the dominant form. Although these images were obtained using different processing conditions, their morphologies are quite similar. Similar images of the unstable α form were observed by Vaeck (1960) and were described as a very bright crystalline mass. Polarized light micrographs of the β′ polymorph were strikingly different and dependent on processing conditions (Fig. 12). Images of the β′ polymorph obtained via the α form at low crystallization temperatures (0–10°C) were similar to the α crystal form in that they possessed a granular morphology (Figs. 12a and 12b). The β′ polymorph also crystallized via the α form, observed at 15°C, had a granular texture, but there was some evidence that the crystals were beginning to cluster (Fig. 12c). At 20°C, the α form is very unstable and the transition to the β′ polymorph is quite rapid. At this crystallization temperature the clustering of spherulites was very evident (Fig. 12d). These clusters of spherulites were found to measure approximately 600 μm. Other research groups have observed clustering of spherulites at 20°C (Vaeck, 1960). The morphology of the β′ polymorph formed directly from the melt was also observed to produce varying microstructures. Incubation of cocoa butter for 1 day at 22°C resulted in a microstruc-

Copyright 2002 by Marcel Dekker. All Rights Reserved.

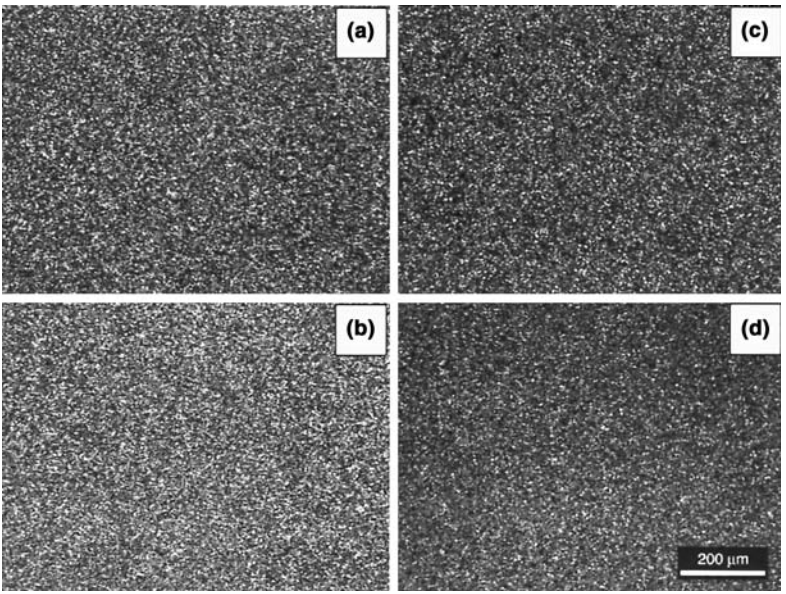

Figure 11 Images obtained by PLM of the α form of cocoa butter crystallized at (a) −20°C for 1 day, (b) −20°C for 7 days, (c) −15°C for 7 days, and (d) 0°C for 1 day.

ture (Fig. 12e) similar to that observed at 20°C, even though the β′ polymorph was crystallized directly from the melt. At 24°C, the β′ polymorph was also formed directly from the melt, but the crystallites, which measured approximately 25 μm, had a needle-like appearance (Fig. 12f). The microstructure of the β′ polymorph seems to have a greater dependence on the crystallization temperature than on the path by which it was formed.

The β polymorph can also display different microstructures (Fig. 13). At crystallization temperatures of 20 and 22°C, long incubation times of 4 or 5 weeks were required to obtain a β polymorph. After these extended incubation times, the morphology within the same sample was no longer uniform at crystallization temperatures of 20 and 22°C. A continuous phase was observed with a morphology similar to that seen in the earlier stages of crystallization. Also, large microstructures (600 μm to 2 mm) were observed at later stages of crystallization. After 4 weeks at 20°C (Fig. 13a) clusters of spherulites were observed as the continuous microstructure, but the clustering was less distinct than that observed early on in the crystallization process. The large microstructres (Fig. 13b) had a feather-like appearance and were often large enough to be seen by the naked eye. A similar structure was observed for cocoa butter crystallized at 22°C for 28

Copyright 2002 by Marcel Dekker. All Rights Reserved.

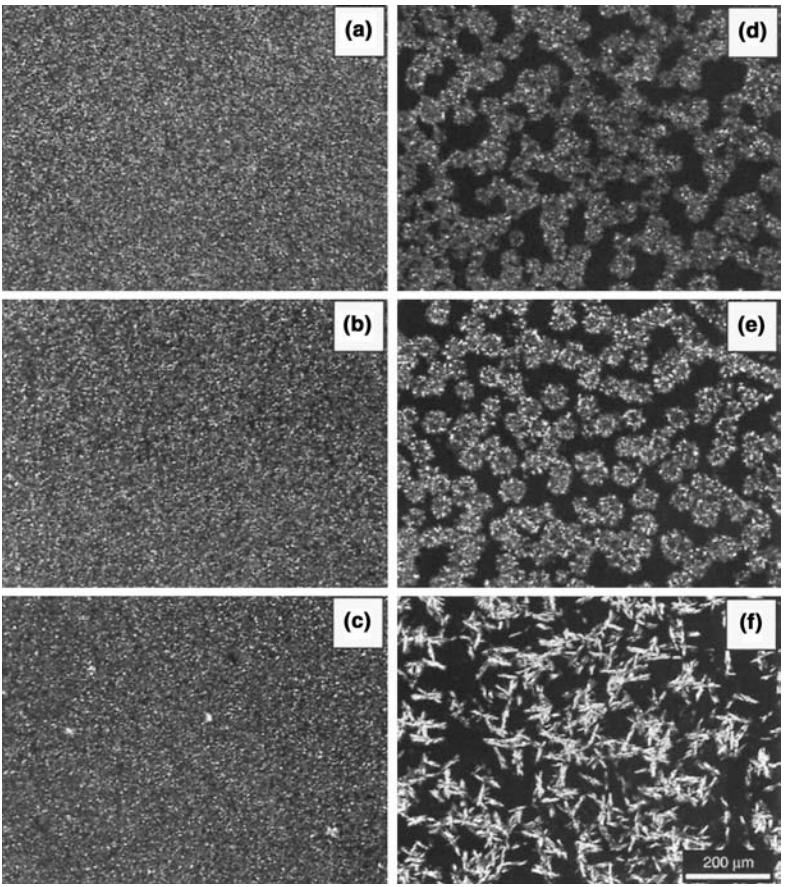

Figure 12 Micrographs of the β′ form obtained by static crystallization at (a) 0°C for 14 days, (b) 10°C for 5 days, (c) 15°C for 14 days, (d) 20°C for 1 day, (e) 22°C for 1 day, and (f) 24°C for 3 days.

days (Figs. 13c and 13d). At crystallization temperatures of 24 and 26°C, images of the β polymorph displayed a needle-like appearance, and after 7 days of incubation a second microstructure was observed. In this case, large microstructures (200–500 μm) with a granular center surrounded by feather-like crystallites were observed (Figs. 13e and 13f).

The appearance of two different microstructures after a long incubation period was speculated to be a result of phase separation, fractionation, or a combination of both. A phase separation occurs when a material exhibits different states

Copyright 2002 by Marcel Dekker. All Rights Reserved.

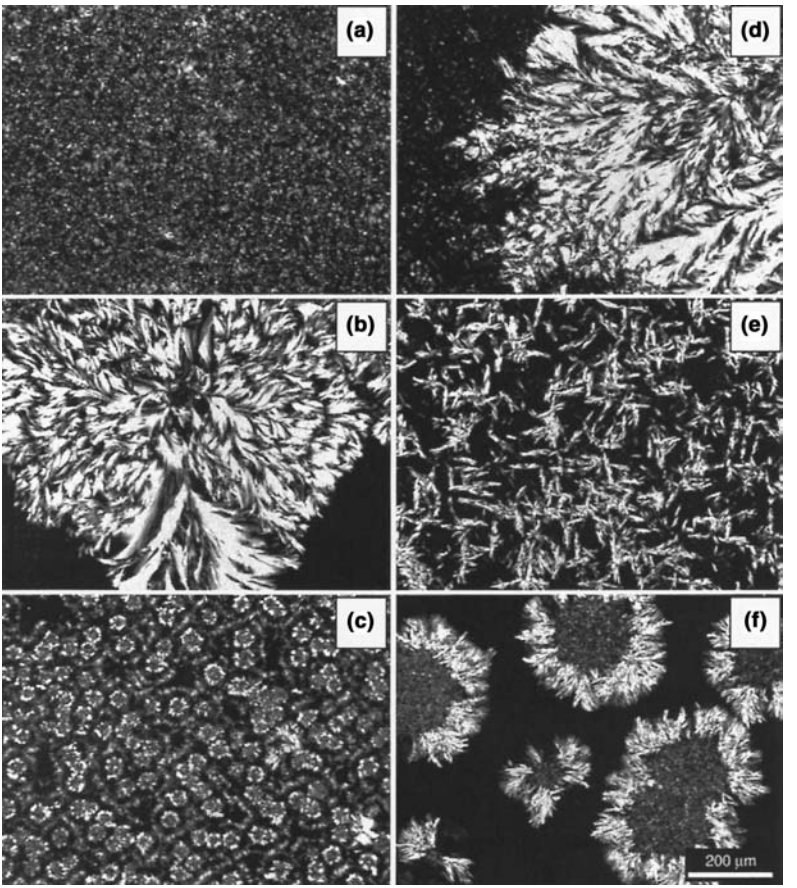

Figure 13 Images of the stable β form of cocoa butter statically crystallized at (a,b) 20°C for 28 days, (c,d) 22°C for 28 days, and (e,f) 26°C for 28 days.

of matter but the same molecular composition, as in the case of polymorphism. Fractionation as defined in Section III takes place upon separation of different molecular species. The observed differences in microstructure as a function of time in our work may have been due to phase separation, because they were observed in the β phase. The β polymorph was not found to crystallize directly from the melt at any of the crystallization temperatures used in this research. During the phase transition from the β′ form to the β polymorph, larger microstructures may have formed. The continuous microstructure, being that of the β′ polymorph, may have remained stable during the polymorphic transition, re-

Copyright 2002 by Marcel Dekker. All Rights Reserved.

sulting in the presence of two different microstructures within the same sample. Further evidence of phase separation stems from the fact that at 20 and 22°C the existence of two microstructures was observed after a longer incubation time than for 24 or 26°C. The polymorphic transition from the β′ form to the β polymorph occurs after a few days at 24 and 26°C but takes several weeks at 20 and 22°C. The existence of two microstructures was not observed until 28 days at 22°C but was seen after 7 days at 24 and 26°C. It is also possible that after a month of incubation at high temperatures a fractionation of the various triglycerides may have occurred. Studies conducted to relate morphology and compositional characteristics in cocoa butter show that the different microstructures formed over time have different molecular compositions (Manning and Dimick, 1985). At 26°C both ''feather crystals'' and ''individual'' crystals were observed within the same sample (Manning and Dimick, 1985). We described these as large microstructures with a granular center surrounded by feather-like crystallites (''feather crystals'') and needle-like crystals (''individual'' crystals). Triglyceride analysis of the two microstructures identified by Manning and Dimick (1985) indicated that the feather crystals and the individual crystals exhibited significant increases in SOS and significant decreases in POP compared to the pure sample. The triglyceride compositions of these two microstructures were similar, perhaps suggesting the occurrence of phase separation. However, this work did not examine the composition of the minor triglycerides (PPP, PPO, etc.). A difference in the composition of these molecular species may also suggest that fractionation was responsible for the different microstructures. Due to the complex behavior of natural fats such as cocoa butter it is likely that the presence of two microstructures within the same sample is a result of both phase separation and fractionation.

All of the observed microstructures of the α polymorph of cocoa butter had a granular appearance. However, the β′ polymorph and the β form can be associated with different microstructures depending on the degree of supercooling. Optical micrographs of tripalmitin also suggest that a wide range of morphologies can exist for one polymorphic form (Kellens et al., 1992). When microscopy is used to study cocoa butter polymorphism, either melting point determination or XRD patterns should be used to confirm the results.

So far, this discussion has addressed the appearance of the various polymorphic forms of cocoa butter obtained by crystallization at different temperatures. However, different polymorphic forms are observed not only at different temperatures but also at different times at the same temperature. The previous discussion of morphology concentrated on the differences observed when moving vertically along the time–temperature state diagram, but differences in polymorphism are also evident when moving horizontally along the state diagram (Fig. 5). At low temperatures, differences in morphology were not observed even after 28 days of storage. Following crystallization of cocoa butter at 0°C for 1 day (Fig. 14a),

Copyright 2002 by Marcel Dekker. All Rights Reserved.

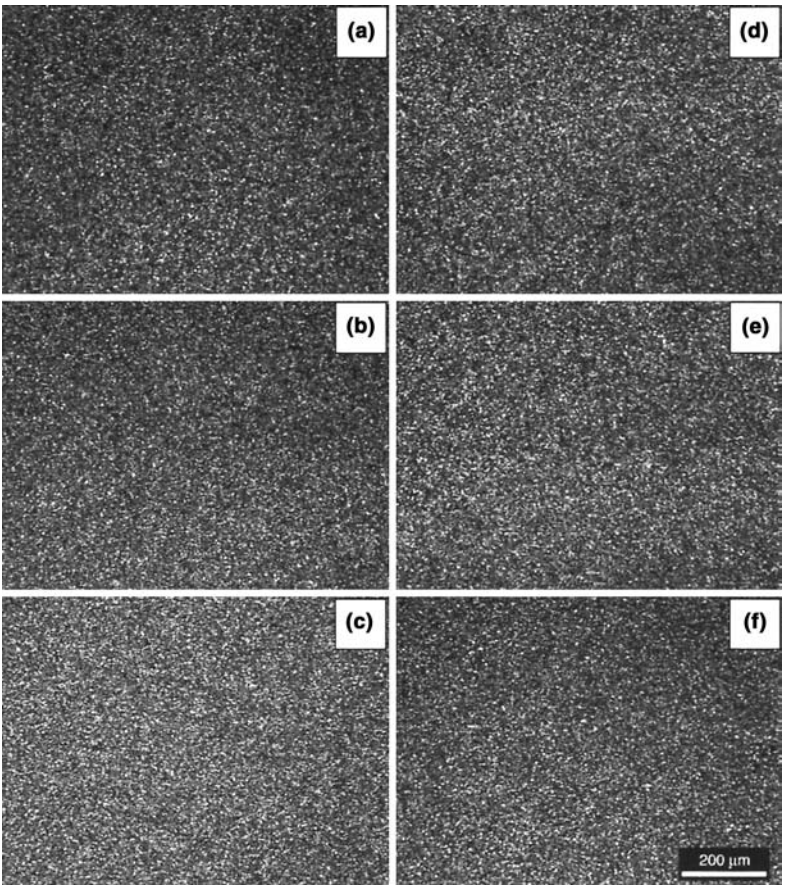

Figure 14 Polarized light microscopic images of cocoa butter statically crystallized at 0°C for (a) 1 day, (b) 5 days, (c) 7 days, (d) 14 days, (e) 21 days, and (f) 28 days.

crystals are in the α polymorph and show a granular morphology. During an incubation of 4–10 days, a polymorphic transition occurred from the α form to the more stable β′ polymorph, and the morphology observed during this transition was again granular and uniform (Figs. 14b and 14c). Finally, the β′ form was found to remain stable from 10 to 28 days, and a granular morphology was observed although a complete polymorphic transition had taken place (Figs. 14d–14f). At low crystallization temperature there is a very high solid fat content, which greatly limits mass transfer. Once the crystals form a particular microstructure, rearrangement is very difficult because of the high viscosity of the medium.

Copyright 2002 by Marcel Dekker. All Rights Reserved.

At low crystallization temperatures (0–10°C) the microstructure did not change upon changes in polymorphism.

At a crystallization temperature of 15°C, the α polymorph is stable for only the first 20 min, so images were not obtained, because only 8% of the cocoa butter was solid. All images shown in Figure 15 correspond to the β′ polymorph obtained via the α form at 15°C. From 1 day to 28 days, the microstructure was found to have a granular texture, but some clustering of the crystallites was evi-

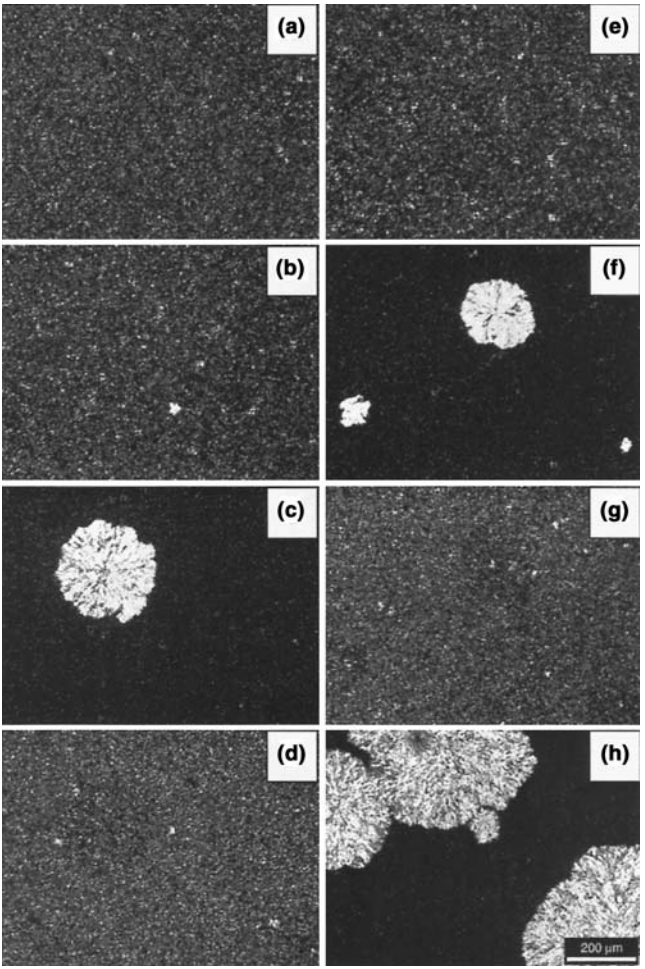

Figure 15 Polarized light microscopic images of cocoa butter crystallized at 15°C for (a) 1 day, (b,c) 7 days, (d) 14 days, (e,f) 21 days, and (g,h) 28 days.

Copyright 2002 by Marcel Dekker. All Rights Reserved.

dent (Figs. 15a, b, d, e, and g). At all times after 7 days of storage, two different microstructures were observed, the continuous granular morphology and large spherulitic microstructures (Figs. 15c, f, and h). The large microstructures (~100–600 μm) were observed in only a few of the samples incubated at 15°C for 7 days. After 28 days, these large microstructures were present in all of the samples along with the granular microstructure (Figs. 15g and h). The β′ polymorph was found to remain stable for 28 days at 15°C, so we speculate that the presence of two different microstructures within the sample is a result of cocoa butter fractionation.

Static crystallization of cocoa butter at 20°C revealed some changes in microstructure during 35 days of storage (Fig. 16). PLM images of the β′ polymorph formed after 1 day of crystallization at 20°C showed that the spherulites were clustered into an organized crystal network (Fig. 16a). These clusters started growing into each other during incubation (Figs. 16b and c), which coincided with the β′-to-β polymorphic transition, as determined from the state diagram. By the end of the polymorphic transition, the individual clusters were difficult to distinguish because of the significant increase in size (Figs. 16d and f). Also, at this point extremely large microstructures were observed in the same sample (Figs. 16e and g). As mentioned earlier we speculated that this was a result of phase separation or fractionation or a combination of both. After 35 days of incubation the polymorphic transformation is complete and the crystals are in the β polymorphic form. The two different microstructures observed at 21 and 28 days were still present. The clusters had grown into one another and were no longer distinct, resulting in a granular morphology (Fig. 16h). The large microstructures have a center with a granular morphology similar to that of the α polymorph, but the individual crystallites are much larger (Fig. 16i). On the periphery of this granular center there appears to be a distinct feather crystal growth (Fig. 16j). Although there are changes in the microstructures as a function of time, they are fairly minor. The spherulite clusters are evident throughout the 35 days of incubation but become less distinct over time. We also observed the existence of two microstructures after 21 days, but this does not necessarily indicate a phase separation, although there was a polymorphic transition from the β′ polymorph to the β polymorph at this time.

The initial microstructure observed following 1 day of incubation at 26°C was characterized by small crystallites and some larger needle-like crystals (~25 μm) (Fig. 17a). Although we were unsure which polymorphic form was present under these conditions, results obtained through DSC and XRD analysis implied that this was the γ polymorph of an SOS-rich fraction. The β′ polymorph crystallized at 26°C had crystallites (~50 μm) with a needle-like appearance (Fig. 17b). The needle-like morphology was observed at all stages of the 28-day incubation at 26°C (Figs. 17c, e, g). Manning and Dimick (1985) also observed a needle-like microstructure at 26°C. Three days after the β′-to-β polymorphic transition,

Copyright 2002 by Marcel Dekker. All Rights Reserved.

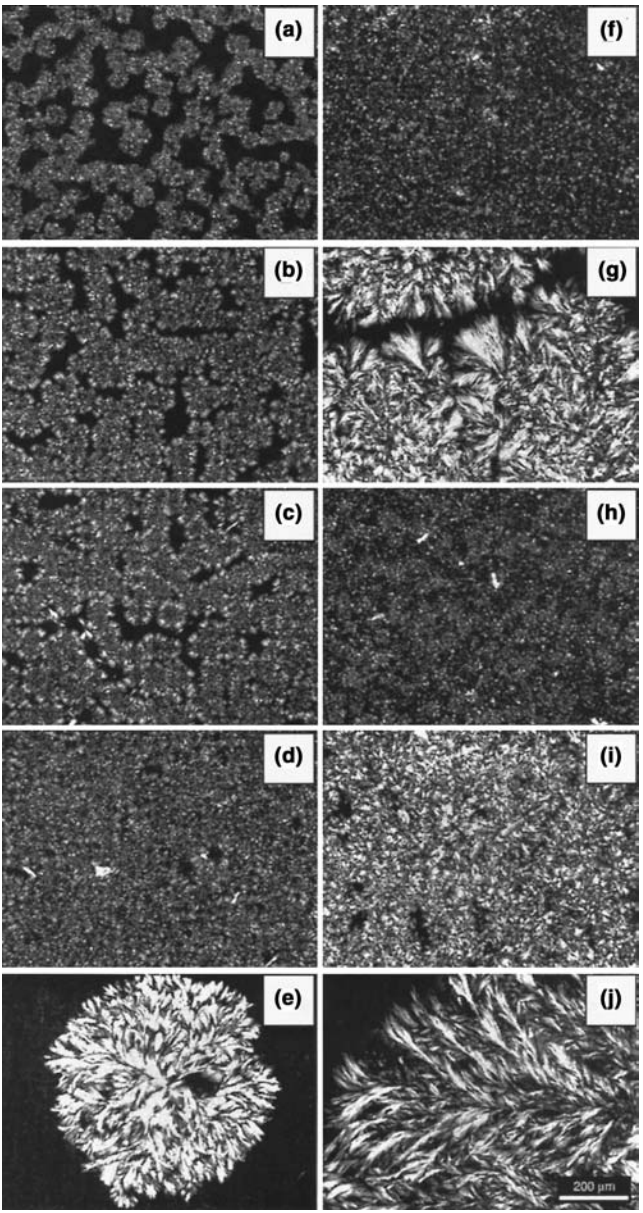

Figure 16 Polarized light microscopic images of cocoa butter statically crystallized at 20°C for (a) 1 day, (b) 5 days, (c) 7 days, (d,e) 21 days, (f,g) 28 days, and (h,i,j) 35 days.

Copyright 2002 by Marcel Dekker. All Rights Reserved.

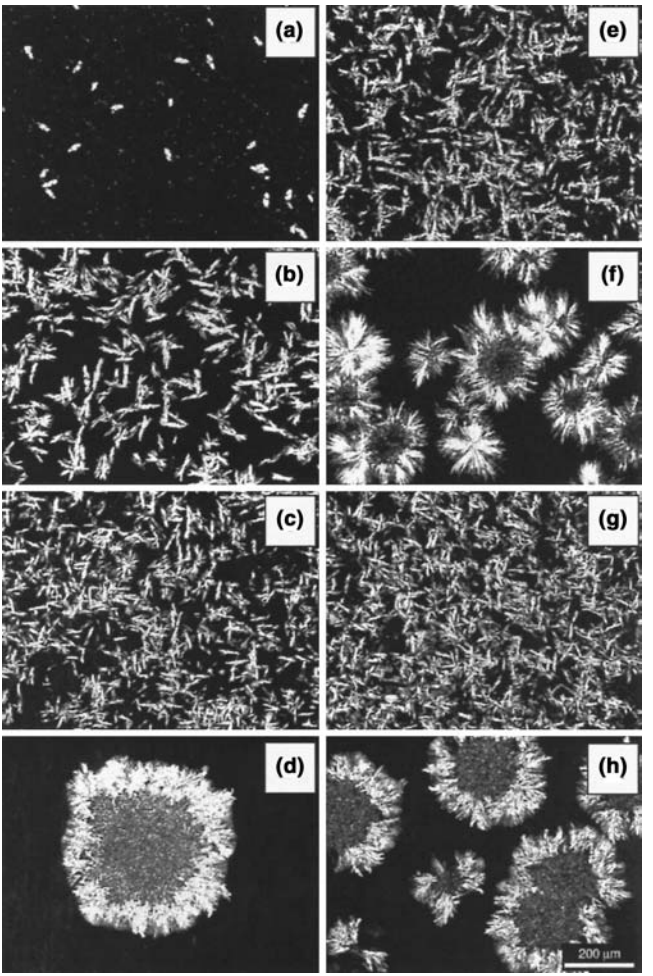

Figure 17 Images obtained by PLM of cocoa butter crystallized at 26°C for (a) 1 day, (b) 3 days, (c,d) 7 days, (e,f) 14 days, and (g,h) 28 days.

large spherulitic microstructures (~100–600 µm) were observed (Figs. 17d, f, and h). Similar to the large microstructures seen at 20°C, a granular center was observed, but this time the periphery had a needle-like appearance. Once again the existence of these two microstructures within the same sample may be the result of phase separation, fractionation, or a combination of both. Very similar microstructures were observed at 24°C, except that after 1 day the crystallites

Copyright 2002 by Marcel Dekker. All Rights Reserved.

had a needle-like appearance unlike the microstructure observed after 1 day at 26°C.

The microstructure of the various polymorphic forms is a function of both temperature and time. Cocoa butter crystallized at different temperatures may have the same polymorphic form, but the microstructure can be quite different. At low crystallization temperatures there is very little change in the microstructure during incubation because of heat and mass transfer limitations. At higher incubation temperatures only one microstructure remains stable over time, but a different microstructure forms, most likely as a result of phase separation, fractionation, or a combination of both. From these PLM images we are able to assign a set of particular microstructures to a particular polymorphic form. Until recently, microstructure was used only as a qualitative tool, but a theory has been developed in which the spatial distribution of mass can be quantified from PLM images.

Most of the research on the physical properties of cocoa butter has been focused on establishing relationships between lipid composition or polymorphism and macroscopic properties (Manning and Dimick, 1985; Vaeck, 1960). However, the microstructure of the fat crystal network is also known to influence its physical properties. Macroscopic properties of the fat crystal network are believed to depend on the nature of the microstructures, because they form the level of structure closest to the macroscopic world (Narine and Marangoni, 1999a). The concept of fractal geometry has been used to characterize the structure of the fat crystal network in various fat systems (Narine and Marangoni, 1999a). Fractal geometry was proposed in order to quantify natural objects with a complex geometrical structure that could not be explained by classical Euclidean geometry (Mandlebrot, 1983). Fractal geometry is concerned with the geometric scaling relationships and symmetries associated with fractal objects. An important characteristic of perfect fractal objects is that they are self-similar at all levels of magnification. A fractal system can display statistical self-similarity rather than exact self-similarity, where the microstructure is similar within a certain range of magnification (Meakin, 1988).

For fat crystal networks, the fractal dimension can be thought of in terms of the scaling relationship between the mass (M) and the radius of a particle or microstructure (r):

$$M \sim r^D \tag{2}$$

where D is the fractal dimension (Marangoni and Rousseau, 1996; Narine and Marangoni, 1999a). If this equation were used to define a two-dimensional disk, the value of D would be 2—an integer because the shape can be described by Euclidean geometry. However, when the distribution of mass is fractal in nature, the value of D is fractional (Narine and Marangoni, 1999b).

In our work the fractal dimension was determined from in situ PLM images

Copyright 2002 by Marcel Dekker. All Rights Reserved.

by a method developed by Narine and Marangoni (1999a). This method uses the theory of mass fractals and the equation

$$N = cR^D \tag{3}$$

where N is the number of reflections (as determined from PLM) in a cube of side R, c is a proportionality constant, and D is the fractal dimension. The determination of the fractal dimension by this method is carried out by first obtaining a PLM image that has been inverted and thresholded. A series of boxes of increasing size are then layered over the image, and the number of reflections (N) in a cube of length R is determined for various values of R. Then log N may be plotted as a function of log R, where the slope gives the fractal dimension and c is the intercept (Narine and Marangoni, 1999a). In our research, reflections of less than 10 pixels and greater than 10,000 pixels were not counted.

Fractal dimensions were determined for cocoa butter crystallized at temperatures ranging from −20 to +26°C incubated 1–35 days. Figure 18 shows the fractal dimension as a function of crystallization temperature after 7 days of crystallization. When the fractal dimension was determined as a function of crystallization temperature, two statistically different regions ($P < 0.001$) were found at all crystallization times. In the first region crystallization temperatures ranged from −20 to +15°C and the fractal dimension was about 2.12. This region was found to be statistically different from crystallization temperatures ranging from 20 to 26°C. This second region had a fractal dimension of about 2.28. The fractal dimension determined at high crystallization temperatures is very close to the

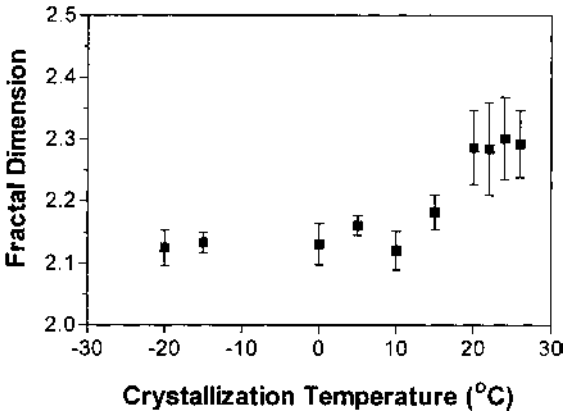

Figure 18 Fractal dimension vs. crystallization temperatures of cocoa butter statically crystallized for 7 days. Symbols represent the average ± standard error of at least eight replicates.

Copyright 2002 by Marcel Dekker. All Rights Reserved.

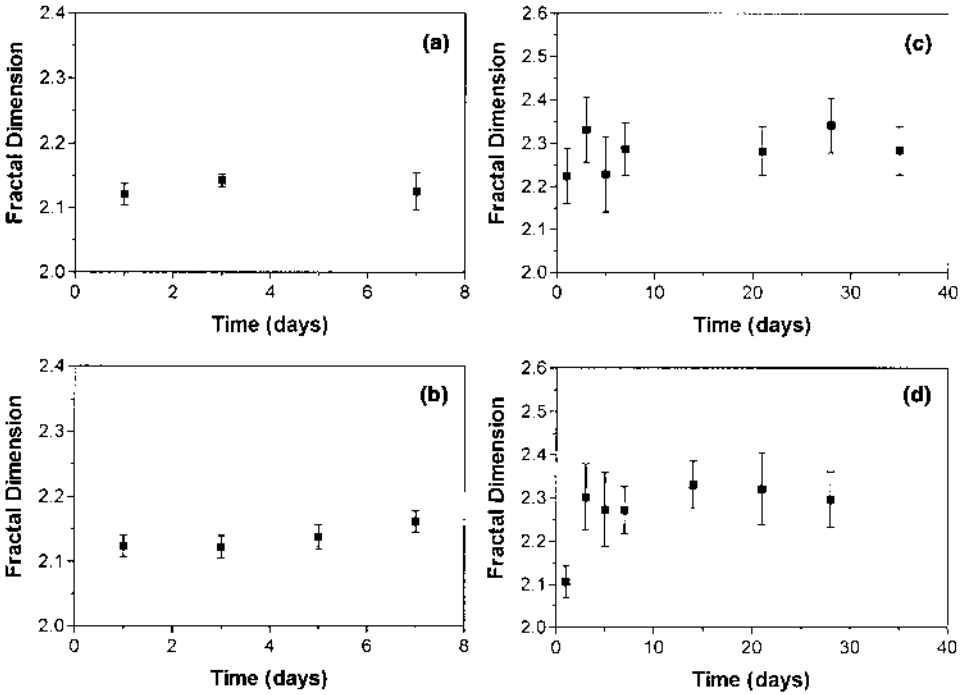

Figure 19 Fractal dimension as a function of time of cocoa butter statically crystallized at (a) −20°C, (b) 5°C, (c) 20°C, and (d) 26°C. Symbols represent the average ± standard error of at least seven replicates.

value of 2.31 obtained for cocoa butter stored at room temperature as determined by Narine and Marangoni (1999a). It has been suggested that a higher fractal dimension indicates a higher order of packing (Narine and Marangoni, 1999a). Therefore, at lower degrees of supercooling we observed a more ordered distribution of mass obtained via different crystallization mechanisms. The fractal nature of the microstructure can be related to the mechanical properties of the network, namely the elastic modulus G', by

$$G' = \lambda\phi^m \tag{4}$$

where Φ is the particle volume fraction of solid fat, m depends on the fractal dimension of the network, and λ is a constant dependent on particle properties (Narine and Marangoni, 1999a). Therefore, according to this equation, the fractal dimension and G' are inversely related as long as the volume fraction of solid

Copyright 2002 by Marcel Dekker. All Rights Reserved.

fat and the particle properties remain constant. At lower degrees of supercooling, we determined a higher fractal dimension, suggesting a lower value of G'.

The fractal dimension at a particular temperature was also determined as a function of time (Fig. 19). There were no statistical differences in the fractal dimension over time at any of the crystallization temperatures ($P > 0.05$). In most cases the microstructure at each crystallization temperature did not change drastically as a function of time (Figs. 14–17). At the higher temperatures we did observe the existence of two microstructures after long periods of incubation (Figs. 16 and 17). At crystallization temperatures of 0°C and above there were significant changes in polymorphism as a function of time. In this case, the fractal dimension was not sensitive to changes in polymorphism. It appears that once the initial microstructure is set there is very little rearrangement with time even though there are significant changes in polymorphism.

Because there were no significant changes at each crystallization temperature as a function of time, the fractal dimensions were averaged over time and plotted as a function of crystallization temperature (Fig. 20). The relationship between the fractal dimension and the crystallization temperature is very similar to that found between the Avrami exponent and crystallization temperature (Fig. 8). In both of these figures we observe two distinct regions above and below 20°C. The Avrami exponent is sensitive to the mechanism of growth, whereas the fractal dimension describes the spatial distribution of solid mass within the network. These results suggest that at lower degrees of supercooling the growth mechanism of the system leads to a more ordered fat crystal network.

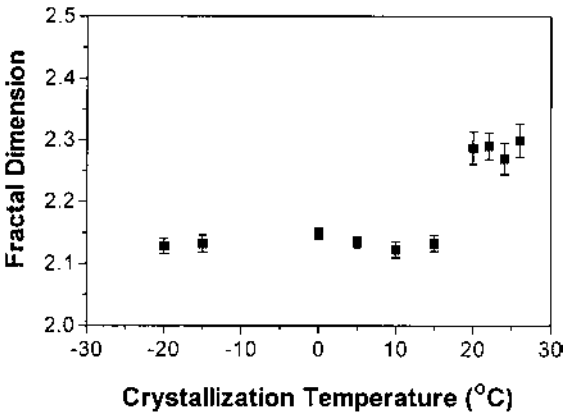

Figure 20 Fractal dimension determined microscopically vs. crystallization temperature. The fractal dimension is an average of all the time points measured at each crystallization temperature. Symbols represent the average ± standard error of at least 40 replicates.

Copyright 2002 by Marcel Dekker. All Rights Reserved.

VI. OTHER PROCESSING CONDITIONS

The work discussed in this chapter examined cocoa butter melted at 80°C for 30 min and then placed at a constant temperature for a predetermined incubation time. We thought that it might be interesting to study the effect of cold tempering on the SFC, polymorphism, microstructure, and rheological properties of statically crystallized cocoa butter. Cold tempering was achieved by melting cocoa butter samples at 80°C for 30 min, then placing them at either −15°C or 5°C for 2 days. The samples from each temperature were then transferred to incubators set to 20, 24, and 26°C and analyzed at 7 and 28 days. Polymorphism was determined from the peak melting temperature obtained from DSC melting profiles, SFC was determined by pNMR, and PLM was used to observe the microstructure.

The SFCs of the cold-tempered samples and the directly crystallized samples (Table 5) were not significantly different ($P > 0.05$). Also, the peak melting temperatures obtained by cold tempering were not statistically different from those obtained by direct crystallization ($P > 0.05$). These cold-tempered samples incubated at 20, 24, and 26°C for 28 days and the samples directly crystallized at 20, 24, and 26°C for 28 days were all found be in the β crystal form. Holding cocoa butter at −15 or +5°C before crystallizing the samples at higher temperatures does not seem to have an effect on polymorphism. However, these samples were much too soft to be analyzed rheologically. The samples at 24 and 26°C were partially liquid, and those at 20°C were brittle and crumbled when removed from the molds. Samples crystallized directly at 20 and 24°C were solid, and samples crystallized at 26°C were partially liquid even after 28 days, so G' values could not be obtained.

The microstructure of the cold-tempered cocoa butter and that of directly crystallized cocoa butter are strikingly different. Incubation at −15°C for 2 days and then at 20°C for 28 days gave a continuous network of large clusters (~350 μm) with a granular center and feather-like crystals around the perimeter (Fig.

Table 5 Solid Fat Content (SFC) for Cold-Tempered and Directly Crystallized Cocoa Butter Held at 20, 24, and 26°C for 28 Days

Cold tempered	SFC (%)	Directly crystallized	SFC (%)
20°C	78.6 ± 0.80[a]	20°C	82.3 ± 0.70[a]
24°C	63.0 ± 0.40[a]	24°C	60.6 ± 0.20[a]
26°C	52.0 ± 1.1[a]	26°C	59.3 ± 3.9[a]

[a] Average value of three replicates ± standard error of the mean.

Copyright 2002 by Marcel Dekker. All Rights Reserved.

21a). Microstructures as large as 2 mm were obtained by crystallization of cocoa butter at 5°C for 2 days followed by a 28-day incubation at 20°C (Fig. 21b). These large microstructures have a relatively small granular center (~450 μm) with a very long network of feather-like crystals extending outward. These images are similar to the large microstructures observed by direct crystallization at 20°C after 28 days (Figs. 21c and d), but in the cold-tempered samples there is no evidence of a secondary microstructure.

Crystallization at −15°C followed by incubation at 24°C gave a continuous network of large clusters (~300 μm) with a granular center surrounded by needle-like crystals (Fig. 21e). An initial temperature of 5°C followed by incubation at 24°C gave very large microstructures with relatively small granular centers (~200 μm) surrounded by many feather-like crystals (Fig. 21f). Once again these microstructures were very large (2 mm) and could be observed without the aid of the microscope. The microstructures observed after direct crystallization at 24°C gave two microstructures, one with a needle-like appearance (Fig. 21g) and the other with large microstructures with a granular center surrounded by needle-like crystallites (Fig. 21h).

The microstructural level of the cold-tempered samples was quantified by using microscopic fractal analysis. The fractal dimensions of the samples crystallized initially at −15°C and placed at 20, 24, and 26°C were found to be statistically different from those crystallized directly at 20, 24, and 26°C ($P < 0.001$). Extremely large microstructures were obtained by an initial crystallization at 5°C followed by an incubation time of 28 days (Figs. 21b and f). The fractal dimension of these samples was not determined owing to the size of the microstructures. Even using 4× magnification, only part of a single crystal could be observed. Not only does this make thresholding very difficult, but quantifying the spatial distribution of mass when only part of a crystal can be observed is not representative of the organization of the entire fat network. The cold-tempered samples held at 20°C for 28 days had a fractal dimension of 2.35 compared to a value of 2.28 determined for cocoa butter directly crystallized at 20°C. Cold-tempered samples held at 24°C for 28 days had a fractal dimension of 2.34, which is statistically different from the fractal dimension of 2.27 observed by direct crystallization. After a 28-day incubation, direct crystallization at 26°C gave a fractal dimension of 2.27, whereas a significantly higher value of 2.35 was determined for the cold-tempered samples held at 26°C. The fractal dimension values of the cold-tempered samples were significantly higher, suggesting a more ordered distribution and a lower G'.

The elastic properties of the network have been stated to be more dependent on the spatial distribution of solid mass within the network than on the total amount of solid in the network (Narine and Marangoni, 1999a). This provides a possible explanation as to why samples with a similar SFC and the same polymorphic form have different hardnesses. In previous work it was established that

Copyright 2002 by Marcel Dekker. All Rights Reserved.

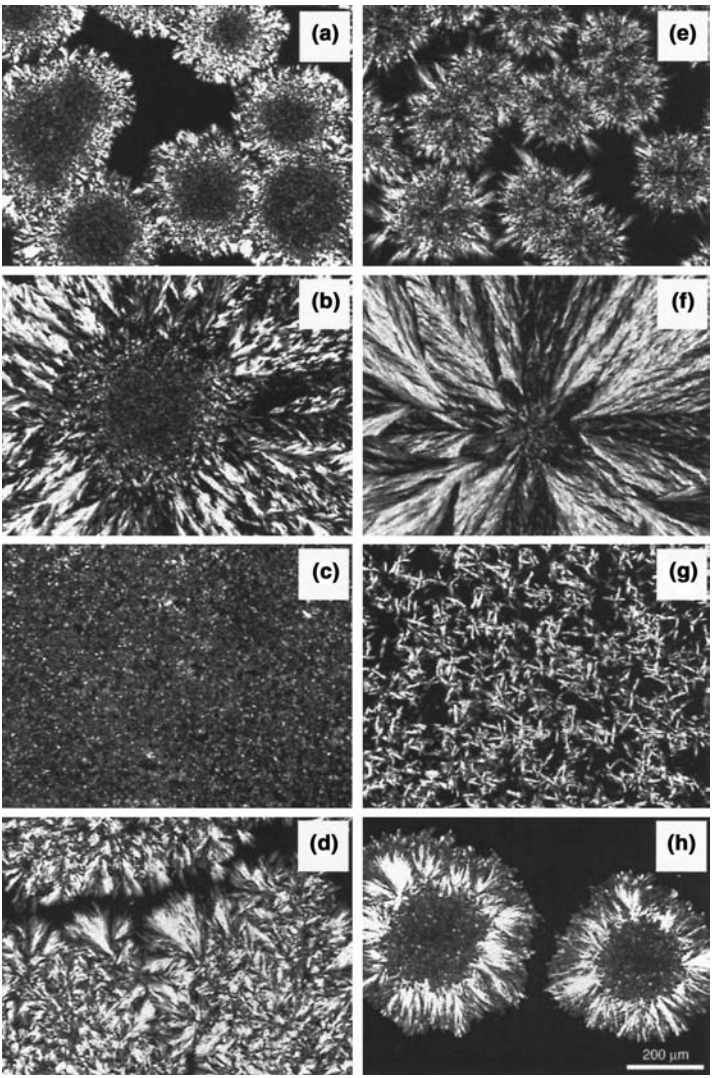

Figure 21 Polarized light microscopic images of cocoa butter crystallized at −15°C for 2 days and then held at (a) 20°C and (e) 24°C for 28 days and of cocoa butter crystallized at 5°C for 2 days and then held at (b) 20°C and (f) 24°C for 28 days. Images of direct crystallization at (c,d) 20°C and (g,h) 24°C are also shown.

Copyright 2002 by Marcel Dekker. All Rights Reserved.

the fractal dimension can be manipulated by changing the processing conditions (Narine and Marangoni, 1999a). The results we obtained by cold tempering compared to direct crystallization confirm this finding. Because the rheological properties of the cold-tempered samples could not be determined, we were unable to compare the elastic modulus (G') with that of the directly crystallized samples. However, a higher fractal dimension has been shown to result in a lower value of G' as long as the other parameters, including lipid composition, SFC, and polymorphism, remain constant (Narine and Marangoni, 1999a). This suggests that the cold-tempered samples would have a lower elastic modulus than the directly crystallized samples.

VII. CONCLUSIONS

The aim of this work was to establish a relationship between polymorphism, crystallization kinetics, microstructure, and rheological properties of statically crystallized cocoa butter. Induction time τ and the Avrami exponent n were used to quantify the crystallization kinetics of this fat system. In this study, the fractal dimension D, a mathematical indicator of structure, was used to quantify the microstructure. Correlation coefficients were determined for these three parameters (Table 6). A weak but significant correlation was determined between the induction time and the Avrami exponent ($P = 0.0126$). The induction time appears to be more sensitive to changes in polymorphism, whereas the Avrami exponent seems to depend on a more macroscopic mode of growth. No significant correlation was found between the induction time and the fractal dimension ($P = 0.0502$) in this work. Induction time and peak melting temperature describe changes in structure at the molecular level. Even though the molecular level of structure, including lipid composition and polymorphism, is important, it does not appear to be a good indicator of network microstructure.

On the other hand, a strong correlation was found between the Avrami exponent and the fractal dimension ($P < 0.001$). Distinctly different regions above and below 20°C were determined by both n and D. Also, the microstructures of these two regions observed by PLM were very different. The Avrami

Table 6 Relationship Between n and τ, D and τ, and D and n for Statically Crystallized Cocoa Butter

	n and τ	D and τ	D and n
Correlation coefficient	0.48	0.50	0.95
P value	0.0126	0.0502	<0.001

Copyright 2002 by Marcel Dekker. All Rights Reserved.

exponents, microstructures, and fractal dimensions of these two regions suggest different macroscopic network growth mechanisms. Moreover, the macroscopic rheological properties of a fat network have been observed to be closely related to its microstructural characteristics. The strong correlation between D and n is not surprising because they both describe events at the microstructural rather than the molecular level. In addition, the elastic modulus of a fat crystal network is an indicator of the macroscopic consistency of the fat network (Narine and Marangoni, 1999c). This suggests that in our work the Avrami exponent and the fractal dimension may be used, in some cases, to predict the mechanical strength or hardness of a network.

ACKNOWLEDGMENTS

We thank Dr. Michael Jennings of the University of Western Ontario for his assistance with the XRD analysis and gratefully acknowledge the financial assistance of the Natural Sciences and Engineering Research Council of Canada (NSERC).

REFERENCES

Arishima, T, N Sagi, H Mori, K Sato. (1991). Polymorphism of POS. I. Occurrence and polymorphic transformation. J Am Oil Chem Soc 68:710–715.

Avrami, M (1939). Kinetics of phase change I. General theory. J Chem Phys 7:1103–1112.

Avrami, M. (1940) Kinetics of phase change II. Transformation-time relations for random distribution of nuclei. J Chem Phys 8:212–224.

Avrami, M. (1941). Kinetics of phase change III. Granulation, phase change and microstructure. J Chem Phys 9:177–184.

Beckett, ST. (2000). The Science of Chocolate. Cambridge, UK: Royl Soc Chem, pp 31–48, 85–103.

Chapman, GM, EE Akehurst, WB Wright, (1971). Cocoa butter and confectionery fats. Studies using programmed temperature X-ray diffraction and differential scanning calorimetry. J Am Oil Chem Soc 48:824–830.

Chawla, P, JM deMan. (1990). Crystal morphology of shortenings and margarines. Food Struct 9:329–336.

Christian, JW. (1965). The Theory of Transformations in Metals and Alloys: An Advanced Textbook in Physical Metallurgy. Oxford UK: Permagon Press, pp 16–22, 471–495.

deMan, JM. (1982). Microscopy in the study of fats and emulsions. Food Microstruct 1: 209–222.

deMan, JM. (1992). X-ray diffraction spectroscopy in the study of fat polymorphism. Food Res Int 25:471–476.

Copyright 2002 by Marcel Dekker. All Rights Reserved.

deMan, JM, AM Beers. (1987). Fat crystal networks: Structure and rheological properties. J Texture Stud 18:303–318.
Dibildox-Alvarado, E, J Toro-Vazquez. (1997). Isothermal crystallization of tripalmitin in sesame oil. J Am Oil Chem Soc 74:69–76.
Dimick, PS. (1999). Compositional effect on crystallization of cocoa butter. In: N Widlat, ed. Physical Properties of Fats, Oils, and Emulsifiers. Champaign, IL: AOCS Press, pp 140–163.
Graydon, JW, SJ Thorpe, DW Kirk. (1994). Determination of the Avrami exponent for solid state transformations from non-isothermal differential scanning calorimetry. J Non-Cryst Solids 175:31–43.
Hagemann, JW. (1988). Thermal behavior and polymorphism of acylglycerides. In: N Garti, K Sato, eds. Crystallization and Polymorphism of Fats and Fatty Acids. New York: Marcel Dekker, pp 9–96.
Heertje, I, M Leunis, WJM van Zeyl, E Berends. (1987). Product microscopy of fatty products. Food Microstruct 6:1–8.
Herrera, JD, FJ Marquez Rocha. (1996). Effects of surcrose ester on the kinetics of polymorphic transition in hydrogenated sunflower oil. J Am Oil Chem Soc 73:321–326.
Herrera, ML, C Falabella, M Melgarejo, MC Anon. (1998). Isothermal crystallization of hydrogenated sunflower oil. II. Growth and solid fat content. J Am Oil Chem Soc 76:1–6.
Kawamura, K. (1979). The DSC thermal analysis of crystallization behavior in palm oil. J Am Oil Chem Soc 56:753–758.
Kellens, M, W Meeussen, H Reynaers. (1992). Study of the polymorphism and the crystallization kinetics of tripalmitin: A microscopic approach. J Am Oil Chem Soc 69: 906–911.
Larsson, K. (1966). Classification of glyceride crystal forms. Acta Chem Scand 20:2255–2260.
Larsson, K. (1994). Molecular Organization, Physical Functions and Technical Applications. Dundee, Scotland: Oily Press, pp 7–47.
Mandelbrot, B. (1983). The Fractal Geometry of Nature. New York: WH Freeman, pp 1–20, 109–131.
Manning, DM, PS Dimick. (1985). Crystal morphology of cocoa butter, Food Microstruct 4:249–265.
Marangoni, AG. (1998). On the use and misuse of the Avrami equation in characterization of the kinetics of fat crystallization. J Am Oil Chem Soc 75:1465–1467.
Marangoni, AG, D Rousseau. (1996). Is plastic fat rheology governed by the fractal nature of the fat crystal network. J Am Oil Chem Soc 73:991–994.
Meakin, P. (1988). Fractal aggregates. Adv Colloidal Interface Sci 28:249–331.
Metin, S, RW Hartel. (1998). Thermal analysis of isothermal crystallization kinetics in blends of cocoa butter with milk fat or milk fat fractions. J Am Oil Chem Soc 75: 1617–1624.
Narine, SS, AG Marangoni. (1999a). Fractal nature of fat crystal networks. Phys Rev E 59:1908–1920.
Narine, SS, AG Marangoni. (1999b). Factors affecting the texture of plastic fats. Food Technol 10:565–570.

Copyright 2002 by Marcel Dekker. All Rights Reserved.

Narine, SS, AG, Marangoni. (1999c). Relating structure of fat crystal networks to mechanical properties: A review. Food Res Int 32:227–248.
Riiner, U. (1970). Investigation of the polymorphism of fats and oils by temperature programmed X-ray diffraction. Lebens Wiss Technol 3:101–106.
Sato, K, T Arishima, ZH Wang, K Ojima, N Sagi, H Mori. (1989). Polymorphism of POP and SOS. I. Occurrence and polymorphic transformation. J Am Oil Chem Soc 66: 664–674.
Sato, K. (1996). Polymorphism of pure triacylglycerols and natural fats. In: FB Padley, ed. Advances in Applied Lipid Research, Vol 2. London: JAI Press, pp 213–268.
Schlichter-Aronhime, J, N Carti. (1988). Solidification and polymorphism in cocoa butter and the blooming problems. In: N Garti, K Sato, eds. Crystallization and Polymorphism of Fats and Fatty Acids. New York: Marcel Dekker, pp 363–394.
Sharples, A. (1966). Overall kinetics of crystallization. In: A Sharples, ed. Introduction to Polymer Crystallization. London: Arnold, pp 44–59.
Shukla, VKS. (1995). Confectionery fats. In: RJ Hamilton, ed. Developments in Oils and Fats. London: Blackie pp 66–94.
Small, DM. (1986). Glycerides. In: DJ Hanahan, ed. The Physical Chemistry of Lipids, from Alkanes to Phospholipids, Vol 4. New York: Plenum Press, pp 475–522.
Vaeck, VS. (1960). Cacao butter and fat bloom. Manuf Confect 15:35–74.
Van Malssen, K, R Peschar, H Schenk. (1996). Real-time X-ray powder diffraction investigations on cocoa butter II. The relationship between melting behaviour and composition of B-cocoa butter. J Am Oil Chem Soc 73:1217–1223.
Van Malssen, K, AV Langevelde, R Peschar, H Schenk. (1999). Phase behavior and extended phase scheme of static cocoa butter investigated with real-time X-ray powder diffraction. J Am Oil Chem Soc 76:669–676.
Wille, RL, ES Lutton. (1966). Polymorphism of cocoa butter. J Am Oil Chem Soc 43: 491–496.
Wright, AJ, RW Hartel, SS Narine, AG Marangoni. (2000). The effect of minor components on milk fat crystallization. J Am Oil Chem Soc 77:463–475.
Ziegleder, VG. (1990). DSC thermal analysis and kinetics of cocoa butter crystallization. Fat Sci Technol 92:481–485.

Copyright 2002 by Marcel Dekker. All Rights Reserved.

5

The Effect of Minor Components on Milkfat Crystallization, Microstructure, and Rheological Properties

Amanda J. Wright and Alejandro G. Marangoni
University of Guelph, Guelph, Ontario, Canada

I. INTRODUCTION

Triacylglycerols account for 93–98% of the total lipid mass in fats and oils. The balance is composed mainly of polar lipid species. These include partial glycerides, free fatty acids, and phospholipids, among others. The influence of these minor lipids on fat behavior has intrigued researchers in the related fat industries for decades. Historically, polar lipids and other surface-active compounds have been used to manipulate fat crystallization. Butter manufacturers have long considered the possibility of using additives, including monoacylglycerols (MAGs), to improve spreadability and decrease hardness (King, 1966; Morrison, 1968; Kapsalis et al., 1960; Kapsalis et al., 1963). Similarly, oil processors have added partial glycerides to salad oils to prevent the formation of crystal sediments and cloudiness during cold storage (van den Tempel, 1968), and the chocolate industry has used emulsifiers to stabilize the preferred crystal polymorphs in cocoa butter (DuRoss and Knightly, 1965). The stabilizing influence of minor components on less stable polymorphic crystal forms has been especially well documented (Aronhime et al., 1990). For example, Hernqvist and Anjou (1983) showed that diacylglycerols (DAGs) cocrystallize with rapeseed triacylglycerols (TAGs) in margarines and stabilize the β' polymorph. They serve to delay the transformation to the less desirable but thermodynamically more stable β form.

Loncin (1958) published one of the earliest studies in this area. He investigated the effect of partial glycerides on palm oil plasticity and concluded that

Copyright 2002 by Marcel Dekker. All Rights Reserved.

palm oils high in free fatty acids tended to have lower melting points. This was attributed to the formation of eutectics between the DAGs and TAGs that are present (Loncin, 1958). DAGs have been shown to influence TAG crystallization, by either accelerating or delaying the process. In trilaurin, for example, the presence of dilaurin isomers significantly reduced the growth rate (Smith et al., 1994). The effect of DAGs on TAG crystallization is related to the chemical composition of the fats. In palm olein, dipalmitoylglycerol caused rapid crystallization, palmitoyloleoylglycerol retarded crystallization, and dioleoylglycerol had no effect (Siew and Ng, 1996). Similarly, in coconut oil TAG, dilauroylglycerol retarded nucleation whereas dioleoylglycerol did not (Gordon and Rahman, 1991). Research into the influence of minor components on fat crystallization has been conducted on a number of different fats and oils by several researchers. Niiya et al. (1973a, 1973b), Reddy and Prabhakar (1987), and Riiner (1971) are some who have made significant contributions.

Minor components in milkfat have an effect on the physical properties of the fat. The addition of 1% milkfat MAGs to milkfat TAGs improved the fat's spreadability (Gerson and Escher, 1966). Unfortunately, although MAGs temporarily decreased the hardness of butter, the effect disappeared with extended storage (Kapsalis et al., 1963). King (1966) was unable to find a consistent relationship between the chemical structure of different minor lipids added to milkfat TAGs and their resulting effects on the physical properties.

II. SEPARATION OF MINOR COMPONENTS FROM MILKFAT TAGS

The effects of minor components on TAG crystallization are complex. To study the effects of milkfat minor lipids on TAG crystallization behavior, the minor components in anhydrous milkfat (AMF) from 1998 were removed from the TAGs as described by Wright et al. (2000). The separation using a packed Florisil (activated magnesium silicate) column yielded two fractions: the milkfat triacylglycerols (MF-TAGs) and minor lipid components. Milkfat DAGs were isolated from the minor lipids fraction by thin layer chromatography and added back to the MF-TAGs at the 0.1 wt% level. The samples of MF-TAGs with 0.1 wt% DAGs will be referred to as MF-DAGs.

The lipid composition of milkfat is given in Table 1. MF-TAGs represented 97.1 wt% of the total AMF mass. The minor components accounted for nearly 3 wt%. This agrees well with reports that milkfat generally contains 96–98 wt% TAGs (Christie, 1988; Bitman and Wood, 1990; National Dairy Council, 1993). Table 1 also shows that the minor components typically found in milkfat were detected in the more polar fraction.

Copyright 2002 by Marcel Dekker. All Rights Reserved.

Table 1 Reported and Experimentally Determined Composition of Milkfat (wt%)

	Reported results			
	Christie, 1988	Bitman and Wood, 1990	Natl Dairy Council, 1993	Exptl results
Triacylglycerols (MF-TAGs)	97.50	95.8	97–98	97.10
Minor polar lipids	2.50	4.20	2–3	2.90
Diacylglycerols	0.360	2.25[a]	0.28–0.59[a]	Detected
Monoacylglycerols	0.027	0.08	0.16–0.38	Detected
Cholesterol esters	trace	0.02	NR	Detected
Cholesterol	0.310	0.46	0.419	Detected
Phospholipids	0.596	1.11	0.2–1.00	Detected
Glycolipids	trace	NR	NR	Detected
Free fatty acids	NR	0.28	0.10–0.44	Detected

NR, not reported.
[a] 1,2-Diacylglycerol.

Figure 1 shows micrographs of AMF and MF-TAGs taken using multiple-photon excitation fluorescence microscopy. The AMF contains an autofluorescent compound cocrystallized within the solid TAG network (Fig. 1a). Removal of the minor components resulted in a lack of this autofluorescent compound in the MF-TAGs (Fig. 1b). The MF-TAGs were colorless, whereas the minor compo-

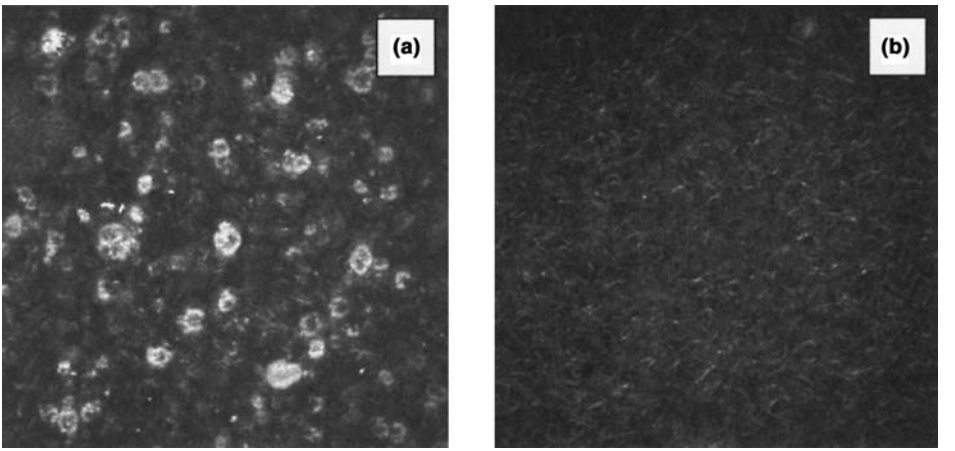

Figure 1 Three-photon excitation fluorescence micrographs of (a) anhydrous milkfat (AMF) and (b) milkfat triacylglycerols (MF-TAGs) after crystallization at 20°C for 24 h.

Copyright 2002 by Marcel Dekker. All Rights Reserved.

Table 2 Fatty Acid Composition of Anhydrous Milkfat (AMF) and Milkfat Triacylglycerols (MF-TAGs)[a]

Fatty acid	AMF (wt%)	MF-TAGs (wt%)
4:0	4.0 ± 0.26	3.6 ± 0.39
6:0	2.7 ± 0.05	2.4 ± 0.03
8:0	1.3 ± 0.03	1.2 ± 0.01
10:0	3.0 ± 0.01	2.9 ± 0.06
12:0	3.6 ± 0.02	3.5 ± 0.13
14:0	11.0 ± 0.10	11.2 ± 0.30
14:1	1.8 ± 0.01	2.0 ± 0.16
15:0	1.3 ± 0.02	1.4 ± 0.16
16:0	29.4 ± 0.35	29.4 ± 0.11
16:1	2.9 ± 0.02	3.0 ± 0.14
17:0	0.8 ± 0.02	0.8 ± 0.08
18:0	10.7 ± 0.03	10.6 ± 0.16
18:1	23.9 ± 0.18	24.2 ± 0.46
18:2	3.0 ± 0.06	3.0 ± 0.04
18:3, 20:0	0.8 ± 0.06	0.7 ± 0.03

[a] Average of two replicates and standard deviation.

Table 3 Triacylglycerol Composition (Carbon Number) of Anhydrous Milkfat (AMF) and Milkfat Triacylglycerols (MF-TAGs)[a]

TAG carbon number	AMF (wt%)	MF-TAGs (wt%)
24	0.3 ± 0.04	0.2 ± 0.01
26	0.2 ± 0.01	0.2 ± 0.01
28	0.4 ± 0.02	0.4 ± 0.01
30	1.1 ± 0.10	0.9 ± 0.05
32	2.3 ± 0.01	2.3 ± 0.07
34	5.8 ± 0.09	6.0 ± 0.11
36	12.8 ± 0.22	13.4 ± 0.13
38	14.5 ± 0.14	15.3 ± 0.15
40	11.8 ± 0.19	12.3 ± 0.01
42	8.3 ± 0.04	8.7 ± 0.06
44	7.6 ± 0.01	7.8 ± 0.05
46	8.3 ± 0.04	8.2 ± 0.04
48	9.4 ± 0.11	9.0 ± 0.01
50	9.7 ± 0.18	8.4 ± 0.24
52	7.9 ± 0.52	7.3 ± 0.79

[a] Average of two replicates and standard deviation.

Copyright 2002 by Marcel Dekker. All Rights Reserved.

nents fraction seemed to be enriched in the yellow color of the native AMF. A carotenoid-type compound was tentatively identified by gas chromatography coupled with mass spectrometry (GC-MS) in the minor components fraction (results not shown). This suggests that this autofluorescent compound may be a carotenoid, possibly annatto, the β-carotene pigment added to milkfat during butter manufacture.

Although the minor components were removed from AMF, separation did not alter either the fatty acid (FA) or TAG compositions of the bulk TAGs (MF-TAGs). The FA and TAG compositions of AMF and MF-TAGs are shown in Tables 2 and 3, respectively. The similar chemical compositions of AMF and MF-TAGs confirm that the TAGs were not fractionated during the separation. Having established this, the crystallization behaviors, microstructures, and rheological properties of the AMF, MF-TAGs, and MF-DAGs were compared.

III. EFFECT OF MINOR COMPONENTS ON MILKFAT CRYSTALLIZATION

A. Minor Components and Thermodynamic Properties

The effects of minor components on milkfat's equilibrium melting temperature and solid fat content were first investigated. Mettler dropping point (MDP) temperatures and differential scanning calorimetric (DSC) peak melting temperatures were compared for AMF, MF-TAGs, and MF-DAGs. The MDPs for AMF, MF-TAGs, and MF-DAGs, were 34.0 ± 0.2°C, 33.8 ± 0.2°C, and 34.2 ± 0.2°C, respectively. Removal of the minor components and addition of DAGs back to MF-TAGs did not significantly affect the fat's dropping point ($P > 0.05$). The peak melting temperatures of AMF, MF-TAGs, and MF-DAGs (~20°C) by DSC were also unaffected by the minor components (see Fig. 9b, Section IV). Because the melting temperatures are unaffected, AMF, MF-TAGs, and MF-DAGs will experience the same degree of supercooling; the thermodynamic driving force toward crystallization will be the same for all three fats.

Equilibrium solid fat contents (SFCs) were determined using pulsed nuclear magnetic resonance (pNMR) according to the American Oil Chemists' Society (AOCS) Official Method Cd 16-81 (AOCS, 1993). Figure 2 shows the SFC versus temperature profiles of AMF, MF-TAGs, and MF-DAGs. The curves are very similar; the fats have the same amount of solid fat present at each temperature. These results agree with those of van den Tempel (1968), who found that minor, surface-active lipids did not change a fat's equilibrium SFCs. The fact that MDP and equilibrium SFCs remain unchanged with the removal of minor components suggests that minor components have little effect on the thermodynamics of TAG crystallization. Crystallization kinetics, however, may be affected.

Copyright 2002 by Marcel Dekker. All Rights Reserved.

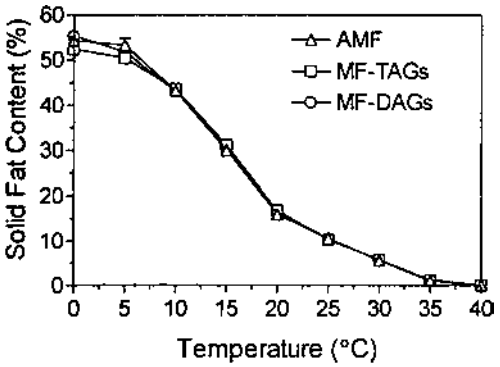

Figure 2 Solid fat content (%) versus temperature (°C) for (△) anhydrous milkfat (AMF), (□) milkfat triacylglycerols (MF-TAGs), and (○) MF-DAGs (MF-TAGs with 0.1% DAG added). Symbols represent the average and standard error of three replicates.

B. Minor Components and Crystallization Behavior

Differences in the crystallization kinetics of AMF, MF-TAGs, and MF-DAGs between 5.0 and 27.5°C were investigated. This was done by following the increases in SFC with time. The effect of minor components on the development of solid fat during crystallization is shown in Figures 3 (5.0, 10.0, 15.0°C) and 4 (20.0, 22.5, 25.0, and 27.5°C). Minor components have an inhibitory effect on crystallization, although this effect depends on the degree of supercooling. At low temperatures, AMF, MF-TAGs, and MF-DAGs displayed similar crystallization profiles. All three fats crystallized very rapidly and reached similar SFCs at 5.0, 10.0, and 15.0°C (Fig. 3). King (1966) also found that minor lipids did not influence the crystallization patterns of rapidly cooled milkfat. At higher temperatures (Fig. 4), the crystallization curves are more sigmoidal and the effect of the minor components is more obvious. Between 20.0 and 27.5°C, AMF, MF-TAGs, and MF-DAGs crystallize differently. MF-TAGs consistently crystallize before AMF (Fig. 4), and addition of the DAGs to MF-TAGs (MF-DAGs) results in a shift in the crystallization profile to one that more closely resembles AMF. At 25.0 and 27.5°C, MF-DAGs crystallization is particularly delayed. Therefore, at low degrees of supercooling, milkfat minor components delay the onset of crystallization.

Induction times for crystallization (τ_{SFC}) were determined by extrapolating the initial linearly increasing portion of the SFC versus time curve to the time axis. τ_{SFC} values are listed in Table 4. Between 5.0 and 20.0°C, the induction times for AMF, MF-TAGs, and MF-DAGs were statistically similar ($P > 0.05$). However, at higher temperatures MF-TAGs crystallized before AMF and MF-DAGs had the longest induction times ($P < 0.001$).

Copyright 2002 by Marcel Dekker. All Rights Reserved.

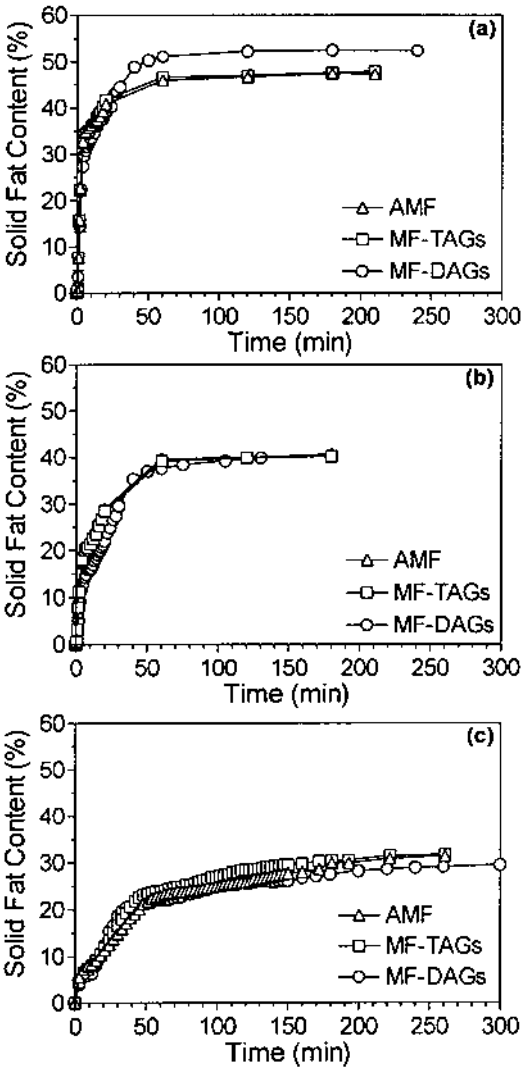

Figure 3 Solid fat content (%) versus time during static crystallization of (△) anhydrous milkfat (AMF), (□) milkfat triacylglycerols (MF-TAGs), and (○) MF-DAGs (MF-TAGs with 0.1% DAG added) at (a) 5.0, (b) 10.0, and (c) 15.0°C. Symbols represent the average and standard error of three replicates.

Copyright 2002 by Marcel Dekker. All Rights Reserved.

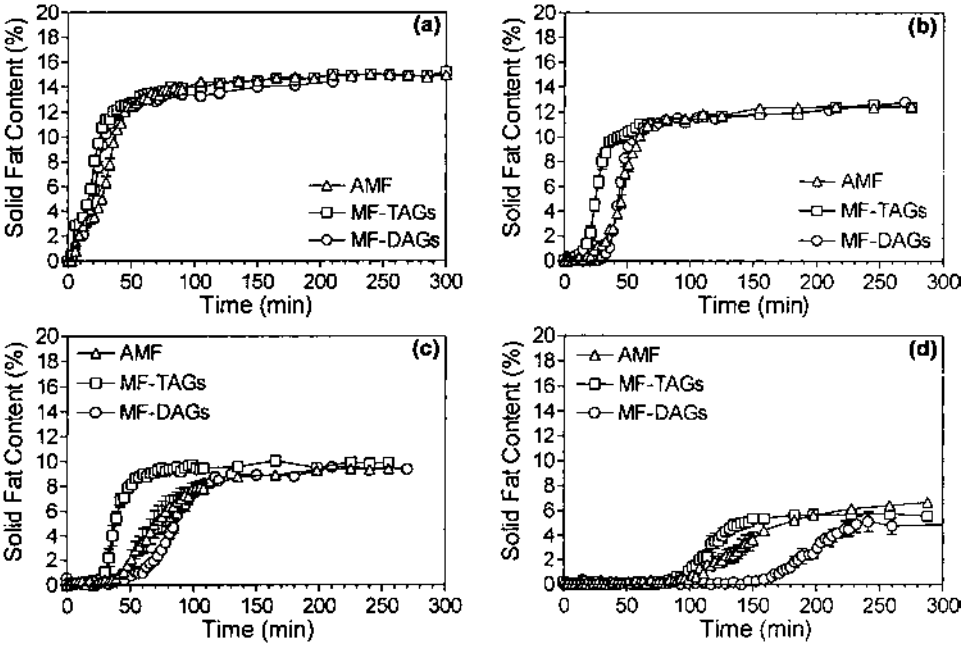

Figure 4 Solid fat content (%) versus time during static crystallization of (△) anhydrous milkfat (AMF), (□) milkfat triacylglycerols (MF-TAGs), and (○) MF-DAGs (MF-TAGs with 0.1% DAG added) at (a) 20.0, (b) 22.5, (c) 25.0 and (d) 27.5°C. Symbols represent the average and standard error of three replicates.

Table 4 Crystallization Induction Times (τ_{SFC}) for AMF, MF-TAGs, and MF-DAGs at 5.0, 10.0, 15.0, 20.0, 22.5, 25.0, and 27.5°C[a]

Temperature (°C)	τ_{SFC} (min)		
	AMF	MF-TAGs	MF-DAGs
5	0.05 ± 0^{A}	0.05 ± 0^{A}	0.05 ± 0^{A}
10	0.5 ± 0^{A}	0.5 ± 0^{A}	0.5 ± 0^{A}
15	2.0 ± 0^{A}	1.8 ± 0.29^{A}	2.0 ± 0^{A}
20	5.3 ± 0.58^{B}	4.3 ± 0.58^{B}	5.3 ± 0.58^{B}
22.5	23.3 ± 1.16^{D}	14.8 ± 0.29^{C}	35.3 ± 1.53^{F}
25	45.3 ± 0.29^{G}	29.8 ± 0.29^{E}	57.0 ± 1.00^{H}
27.5	107.8 ± 0.29^{J}	95.7 ± 0.29^{I}	163.7 ± 1.53^{K}

[a] Mean value of three replicates with standard deviation of the mean. Different superscript letters (A–K) indicate significant differences ($P < 0.05$).

Copyright 2002 by Marcel Dekker. All Rights Reserved.

Crystallization kinetics were further quantified by fitting the crystallization curves to the Avrami equation. The Avrami equation (Avrami, 1939, 1940, 1941) can be used to quantify crystallization kinetics and gives an indication of the nature of the crystal growth process. The form of the equation used in these studies was

$$\frac{\mathrm{SFC}(t)}{\mathrm{SFC}(\infty)} = 1 - e^{-kt^n} \tag{1}$$

where SFC(t) describes the SFC as a function of time, SFC(∞) is the limiting SFC as time approaches infinity, k is the Avrami constant, and n is the Avrami exponent. This equation was developed to describe the kinetics of liquid–solid phase transitions in metals, and its principles were first applied to polymer crystallization in the 1950s. Researchers have used the Avrami model in the study of fat crystallization (Dibildox-Alvarado and Toro-Vazquez, 1997; Herrera et al., 1998; Kawamura, 1979; Metin and Hartel, 1998; Ziegleder, 1990). The equation describes an event in which there is an initial lag period where crystallization occurs very slowly and a subsequent rapid increase in crystal mass (Avrami, 1939). This model takes into account that crystallization occurs by both nucleation and crystal growth (Christian, 1965) and is based on the assumptions of isothermal transformation conditions, spatially random nucleation, and linear growth kinetics in which the growth rate of the new phase depends only on temperature and not on time (Henderson, 1979).

The Avrami parameters provide information on the nature of the crystallization process. The constant k represents a crystallization rate constant. It depends primarily on the crystallization temperature (Kawamura, 1979) and generally follows an Arrhenius-type temperature dependence (Graydon et al., 1994). k takes both the nucleation and crystal growth rates into account (Sharples, 1966). Halftimes of crystallization, $t_{1/2}$, reflect the magnitudes of the rate constants according to the relationship

$$t_{1/2} = \left(\frac{0.693}{k}\right)^{1/n} \tag{2}$$

The Avrami exponent, n, sometimes referred to as an index of crystallization, indicates the crystal growth mechanism. This parameter is a combined function of the time dependence of nucleation and the number of dimensions in which growth takes place (Sharples, 1966). Nucleation is either instantaneous, with nuclei appearing all at once early on in the process, or sporadic, with the number of nuclei increasing linearly with time (Sharples, 1966). Growth occurs as rods, disks, or spherulites in one, two, or three dimensions, respectively (Kawamura,

Copyright 2002 by Marcel Dekker. All Rights Reserved.

Table 5 Values for the Avrami Exponent, n, for Different Types of Nucleation and Growth

n	Type of crystal growth and nucleation expected
3 + 1 = 4	Spherulitic growth from sporadic nuclei
3 + 0 = 3	Spherulitic growth from instantaneous nuclei
2 + 1 = 3	Disk-like growth from sporadic nuclei
2 + 0 = 2	Disk-like growth from instantaneous nuclei
1 + 1 = 2	Rod-like growth from sporadic nuclei
1 + 0 = 1	Rod-like growth from instantaneous nuclei

Source: Sharples, 1966.

1979). Table 5 lists the values of the Avrami exponent, n, expected for various types of nucleation and growth.

The SFC crystallization curves for AMF, MF-TAGs, and MF-DAGs (Figs. 3 and 4) were fitted to the Avrami equation by least squares nonlinear regression. The equation fit the data very well over the entire range of fractional crystallization; correlation coefficients were always greater than 0.96. Table 6 lists the Avrami rate constants (k), half-times of crystallization ($t_{1/2}$), and exponents (n).

As expected, k decreased with increasing crystallization temperature. Below 20.0°C, temperature had a very strong influence on k ($P < 0.001$). Between 22.5 and 27.5°C, however, k was not correlated with temperature ($P > 0.05$). The largest decrease in k occurred between 20.0 and 22.5°C. Here, over only a couple of degrees, the Avrami constants dropped by a factor of roughly 1000. Over the entire 5.0–20°C range, k for AMF, MF-TAGs, and MF-DAGs decreased by only a factor of 10. The increase in $t_{1/2}$ for the three fats as a function of increasing temperature reflects the decrease in k at higher temperatures (Table 6).

Changes in k and n as a function of crystallization temperature are shown in Figure 5. These graphs highlight two distinct regions of crystallization behavior, one above and the other below 20°C. The division between these two regions is very pronounced. Figure 5b shows that the Avrami exponent remains constant and low (around 0.60) below 20°C. Between 5.0 and 15.0°C, there was no significant effect of temperature on n ($P > 0.05$). This is not surprising, because n generally tends to remain constant over an appreciable temperature range and is independent of the degree of supercooling (Christian, 1965; Graydon et al., 1994). Around 20°C, n began to increase. This is the same point at which the greatest change in the Avrami constant occurred. Above 20.0°C, n continued to increase as the temperature was increased.

No significant differences were observed between k values for AMF and MF-TAGs ($P > 0.05$). MF-DAGs did have significantly lower values of k than

Copyright 2002 by Marcel Dekker. All Rights Reserved.

Table 6 Avrami Constants, k, Half-Times of Crystallization, $t_{1/2}$, and Avrami Exponents, n, for AMF, MF-TAGs, and MF-DAGs at 5.0, 10.0, 15.0, 20.0, 22.5, 25.0, and 27.5°C[a]

Temp (°C)	k (t^{-n})	$t_{1/2}$ (min)	n
AMF			
5.0	0.3 ± 0.02^{A}	3.5 ± 0.2^{K}	0.6 ± 0.01^{F}
10.0	0.2 ± 0.04^{B}	10.3 ± 1.7^{K}	0.6 ± 0.03^{F}
15.0	$0.1 \pm 0.02 \times 10^{-1C}$	36.3 ± 0.8^{K}	0.6 ± 0.01^{F}
20.0	$1.0 \times 10^{-2} \pm 0.1 \times 10^{-2D}$	32.3 ± 3.5^{J}	1.5 ± 0.04^{E}
22.5	$1.6 \times 10^{-7} \pm 4.8 \times 10^{-8D}$	61.4 ± 14.7^{H}	4.0 ± 0.03^{C}
25.0	$2.5 \times 10^{-6} \pm 2.5 \times 10^{-6D}$	74.1 ± 12.2^{E}	3.0 ± 0.2^{D}
27.5	$6.7 \times 10^{-10} \pm 8.2 \times 10^{-10D}$	165.7 ± 51.3^{B}	$4.4 \pm 0.2^{B,C}$
MF-TAGs			
5.0	0.3 ± 0.03^{A}	3.6 ± 0.3^{K}	0.7 ± 0.02^{F}
10.0	0.2 ± 0.01^{B}	10.1 ± 0.6^{K}	0.7 ± 0.01^{F}
15.0	0.1 ± 0.01^{C}	33.6 ± 4.1^{K}	0.7 ± 0.02^{F}
20.0	$0.1 \pm 0.04 \times 10^{-1C}$	23.9 ± 0.9^{J}	0.7 ± 0.01^{F}
22.5	$2.2 \times 10^{-5} \pm 4.4 \times 10^{-5D}$	27.5 ± 1.4^{I}	2.4 ± 0.05^{F}
25.0	$1.6 \times 10^{-7} \pm 1.2 \times 10^{-7D}$	54.5 ± 9.2^{G}	$3.9 \pm 0.2^{B,C}$
27.5	$3.0 \times 10^{-11} \pm 2.5 \times 10^{-11D}$	126.9 ± 11.3^{C}	$5.0 \pm 0.1^{A,B}$
MF-DAGs			
5.0	0.3 ± 0.04^{A}	5.3 ± 0.6^{K}	0.6 ± 0.03^{F}
10.0	$0.1 \pm 0.03 \times 10^{-1A}$	16.5 ± 0.4^{K}	$0.8 \pm 0.01^{E,F}$
15.0	$0.1 \pm 0.01 \times 10^{-1A}$	27.9 ± 0.4^{K}	0.6 ± 0.01^{F}
20.0	$0.01 \pm 0.04 \times 10^{-1C}$	25.8 ± 3.9^{J}	$1.3 \pm 0.06^{E,F}$
22.5	$2.4 \times 10^{-8} \pm 2.7 \times 10^{-8D}$	50.0 ± 13.2^{F}	$4.7 \pm 0.3^{A,B,C}$
25.0	$2.6 \times 10^{-9} \pm 1.8 \times 10^{-9D}$	87.2 ± 15.9^{D}	$4.5 \pm 0.2^{B,C}$
27.5	$4.9 \times 10^{-12} \pm 8.5 \times 10^{-12D}$	234.9 ± 80.1^{A}	5.5 ± 0.4^{A}

[a] Mean value of three replicates with standard error of the mean. Different superscript letters (A–K) indicate significant differences ($P < 0.05$) within either k, $t_{1/2}$, or n columns.

either AMF or MF-TAGs above 20°C ($P < 0.001$). Although the native mixture of milkfat minor components did not seem to affect the rate of crystallization, DAGs alone did seem to slow down the rate. Similarly, there were no significant differences observed between n for AMF and those for MF-TAGs either above or below 20°C ($P > 0.05$). Whereas below 20°C the exponent values for MF-DAGs were the same as for AMF and MF-TAGs, above 20°C n for MF-DAGs were slightly higher than for the other fats ($P < 0.001$). This reflects the more sigmoidal nature of its crystallization curves at 25.0 and 27.5°C (Fig. 4).

The similarities in n for AMF and MF-TAGs suggest that these fats crystallize in a similar fashion. The differences observed for MF-DAGs may be indicative of slightly different crystal growth modes related to the presence of the

Copyright 2002 by Marcel Dekker. All Rights Reserved.

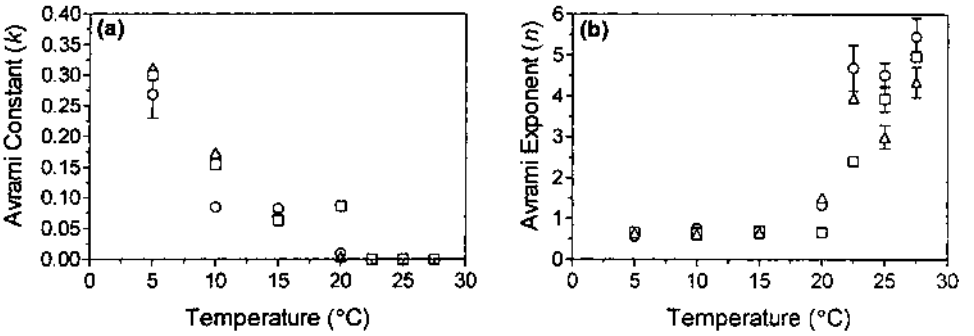

Figure 5 Avrami rate constants k (a) and (b) Avrami exponents n for (△) anhydrous milkfat (AMF), (□) milkfat triacylglycerols (MF-TAGs), and (○) MF-DAGs (MF-TAGs with 0.1% DAG added) as a function of crystallization temperature. Symbols represent the average and standard error of three replicates.

DAGs. In all three—AMF, MF-TAGs, and MF-DAGs—the sharp change in n around 20.0°C suggests the existence of different crystallization mechanisms depending on the degree of supercooling. The change in n at about this point should indicate differences in crystal growth geometry (Christian, 1965).

An increase in the induction time and a more sigmoidal crystallization curve are generally indicated by a higher Avrami exponent (Avrami, 1940; Sharples, 1966). This was found to be true; at higher temperatures, values of τ and n were significantly higher, and crystallization curves appeared more sigmoidal. According to Sharples (1966), the experimental n of roughly 0.6 below 20°C may suggest rod-like growth in only one dimension from instantaneous nuclei. Generally, as the rate of crystallization increases, the growth mechanism changes from lineal to polyhedral in nature, as indicated by an increase in the Avrami exponent (Avrami, 1940). The experimental increase in n suggests that crystal growth above 20.0°C changes from a one-dimensional to a multidimensional event.

Beyond this it is impossible to draw unambiguous conclusions about the growth mechanism on the basis of the determined Avrami exponent unless the type of growth can be verified microscopically. The situation is further complicated by the fact that although n should be an integer, fractional values are obtained in some analyses, even in cases where the Avrami equation is very accurately obeyed (Sharples, 1966). Fractional values for n were consistently obtained from the AMF, MF-TAGs, and MF-DAGs crystallization curves despite correlation coefficients of at least 0.96. Christian (1965) reported that for some cases of metals and alloys in which growth is diffusion-controlled, fractional exponents correlate with specific growth mechanisms. In such cases an exponent of roughly

Copyright 2002 by Marcel Dekker. All Rights Reserved.

0.5 may indicate precipitation on crystal dislocations. Similarly, values greater than 2.5 reflect growth of all shapes with increasing nucleation rate (Christian, 1965).

Although the Avrami equation is being used increasingly in fat research, it has limitations when the nature of the growth process cannot be visualized. The resolution of crystal nuclei during the initial stages of growth is beyond the resolving power of a light microscope; thus it is difficult to make definite conclusions about the modes of crystal growth observed at different temperatures. Having said this, the Avrami exponent does provide a phenomenological index of crystallization. Accordingly, the similarities in n between AMF and MF-TAGs point to the fact that removal of the minor components does not change the growth mode, and the distinct change in exponent around 20°C suggests a change in the crystal growth mechanism in both fats.

C. Minor Components and Nucleation

Anhydrous milkfat, MF-TAGs, and MF-DAGs crystallization behavior was also compared by using an optical scattering approach using a phase transition analyzer (Phase Technology, Richmond, BC, Canada). In this setup, a beam of light is directed onto the sample from above. A matrix of optical sensors, in tandem with a lens system, is also placed perpendicularly above the sample. As crystals begin to appear in the sample, the incident light beam is scattered by the solid–liquid phase boundaries, and scattered light impinges via the lens onto the detectors. As more and more crystal mass develops, the signal output increases and is automatically recorded. This technique was found to be very sensitive to early crystallization events, possibly in the vicinity of nucleation (Wright et al., 2001). Therefore, induction times from this method are referred to as $\tau_{nucleation}$. Induction times were defined as the time when two consecutive signal readings of 1.0 were observed. This point represents a significant deviation from the baseline noise. It also proved to be reproducible and more sensitive than linear extrapolation. Table 7 lists $\tau_{nucleation}$ values determined for AMF and MF-TAGs between 15.0 and 27.5°C.

Temperature had a significant effect on $\tau_{nucleation}$ ($P < 0.001$). At higher degrees of supercooling, no significant differences ($P > 0.05$) were found between AMF and MF-TAGs. However, at 25.0 and 27.5°C, the induction times for AMF were significantly greater than those for MF-TAGs ($P < 0.05$). The same trend was observed for τ_{SFC} ; differences between AMF and MF-TAGs emerged at higher temperatures. The presence of the minor components delayed the onset of crystallization including nucleation and growth.

Values of $\tau_{nucleation}$ were used to calculate free energies of nucleation (ΔG_c) above 20°C according to the Fisher–Turnbull equation (Strickland-Constable, 1968):

Copyright 2002 by Marcel Dekker. All Rights Reserved.

Table 7 Induction Times ($\tau_{nucleation}$) Determined with a Phase Transition Analyzer for AMF and MF-TAGs at 15.0, 20.0, 22.5, 25.0, and 27.5°C[a]

Temperature (°C)	$\tau_{nucleation}$ (s)	
	AMF	MF-TAGs
15	4.0 ± 0[A]	6.0 ± 0[A]
20	70.7 ± 22.3[A]	136.0 ± 5.9[A]
22.5	409.3 ± 52.8[B]	342.0 ± 29.5[B]
25	1027.3 ± 66.1[C]	602.7 ± 61.3[D]
27.5	1986.0 ± 138.4[E]	776.7 ± 52.3[F]

[a] Mean value of three replicates with standard deviation. Different superscript letters (A–F) indicate significant differences ($P < 0.05$) between values.

$$J = \frac{NkT}{h} \exp\left[-\frac{\Delta G_d}{\mathrm{kT}}\right] \exp\left[-\frac{\Delta G_c}{\mathrm{kT}}\right] \tag{3}$$

where J is the rate of nucleation and is inversely proportional to the induction time of nucleation ($\tau_{nucleation}$), N is the number of molecules per cubic centimeter in the liquid phase, k is the gas constant per molecule, T is the crystallization temperature, h is Planck's constant, and ΔG_d is the activation free energy of diffusion. ΔG_c is the activation free energy of nucleation and, for a spherical nucleus, is related to the surface free energy of the crystal/liquid melt interface (σ) and the degree of supercooling (ΔT) according to the relationship (Strickland-Constable, 1968):

$$\Delta G_c = \frac{16}{3}\left(\frac{\pi\sigma^3 T_m^2}{(\Delta H)^2(\Delta T)^2}\right) \tag{4}$$

where ΔH is the enthalpy of nucleation and T_m is the melting temperature of the fat. The calculation involves plotting ln τT vs. $1/T(\Delta T)^2$ over the temperature range of interest. The slope of this curve (m) then permits calculation of the activation free energies of nucleation (ΔG_c) at each temperature within that range, according to the equation

$$\Delta G_c = \frac{mK}{(T_m - T)^2} \tag{5}$$

Copyright 2002 by Marcel Dekker. All Rights Reserved.

Table 8 Free Energies of Nucleation (ΔG_c) Calculated for AMF and MF-TAGs at 22.5, 25.0, and 27.5°C According to the Fisher–Turnbull Equation[a]

Temperature (°C)	ΔG_c (kJ/mol)	
	AMF	MF-TAGs
22.5	$2.0 \pm 0.3^{C,B,D}$	1.1 ± 0.2^{D}
25	3.3 ± 0.4^{B}	$1.7 \pm 0.3^{C,D}$
27.5	5.9 ± 0.6^{A}	$3.1 \pm 0.6^{B,C}$

[a] Mean value of three replicates with standard deviation. Different superscript letters (A–D) indicate significant differences ($P < 0.05$) between values.

Values of ΔG_c calculated for AMF and MF-TAGs at 22.5, 25.0, and 27.5°C are listed in Table 8. Higher values of ΔG_c reflect the fact that at higher temperatures (low degrees of supercooling) the energy barrier to nucleation is higher. Comparing ΔG_c values for AMF and MF-TAGs above 20°C, the presence of the minor components increases the energy barrier to nucleation. A delay in the overall crystallization process in the presence of the minor components is reflected in τ_{SFC} (Table 4) and the crystallization curves (Fig. 4). Longer $\tau_{nucleation}$ times (corresponding to higher ΔG_c) for AMF compared to MF-TAGs above 20°C suggest that minor components do this by inhibiting nucleation. Possibly minor components interfere with nucleation, extending the time until enough suitable nuclei are present for significant growth (marked by an increase in SFC) to occur. Once solid fat begins to develop (after τ_{SFC}), the growth modes and crystallization rates are the same for AMF and MF-TAGs (Table 6).

Value of ΔG_c were calculated for AMF and MF-TAGs below 20°C as well. ΔG_c values were determined separately between 15.0 and 18.0°C and between 22.5 and 27.5°C because of the clear change in the mode of crystallization above and below 20°C (see Fig. 5). Values of ΔG_c calculated between 15.0 and 18.0°C are listed in Table 9. The lower values of ΔG_c at 15.0°C compared to those at 18.0°C reflect the fact that nucleation will occur more readily at higher degrees of supercooling. Also, ΔG_c for MF-TAGs is lower than for AMF. Although the SFC crystallization curves for AMF and MF-TAGs are identical below 20°C, Table 9 suggests that minor components do affect the propensity of the TAGs to nucleate below 20°C.

Comparing Tables 8 and 9, we observe that the ΔG_c values calculated for the fats below 20°C are much higher than those above 20°C, although the energy

Copyright 2002 by Marcel Dekker. All Rights Reserved.

Table 9 Free Energies of Nucleation (ΔG_c) Determined for AMF and MF-TAGs at 15.0, 16.5, and 18.0°C[a]

Temperature (°C)	ΔG_c (kJ/mol)	
	AMF	MF-TAGs
15	$14.9 \pm 0.3^{C,D}$	11.6 ± 0.5^{E}
16.5	17.4 ± 0.4^{B}	13.6 ± 0.6^{D}
18	20.6 ± 0.4^{A}	$16.1 \pm 0.7^{B,C}$

[a] Mean value of three replicates with standard deviation. Different superscript letters (A–E) indicate significant differences ($P < 0.05$) between values.

barrier to nucleation should be lower at lower temperatures. Within both temperature ranges (15.0–18.0°C and 22.5–27.5°C) this holds true; ΔG_c increases with temperature. However, between the two regions the results are contrary to what we would expect. Figure 6 shows that the slope of ln τT vs. $1/T(\Delta T)^2$ is much steeper below 20°C than between 22.5 and 27.5°C. This results in significantly higher values of ΔG_c below 20°C. The discrepancy we observed reminds us that the Fisher–Turnbull equation is valid only under certain conditions. ΔG_c is determined by assuming that ΔG_d is negligible or constant. However, this is not a valid assumption in all cases. At high degrees of supercooling, when the melt

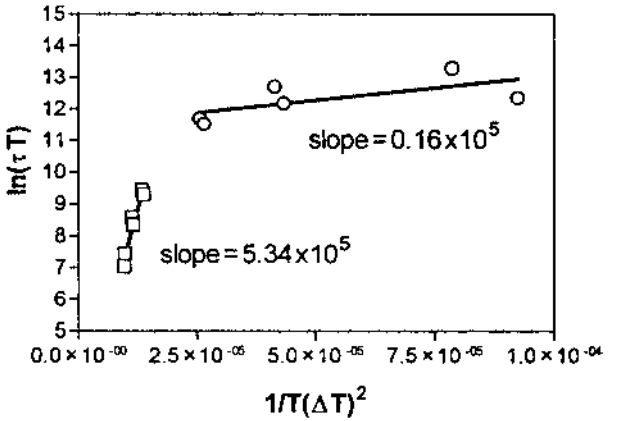

Figure 6 Determination of ΔG_c according to the Fisher–Turnbull equation. Plot of ln τT versus $1/T(\Delta T)^2$ showing regions of differing slopes above and below 20°C.

Copyright 2002 by Marcel Dekker. All Rights Reserved.

viscosity is high, nucleation will be highly dependent on molecular diffusion. ΔG_d will then be an important contributor to the overall change in free energy of the system.

D. Differences in Effect of DAG Addition on MF-TAGs Crystallization Behavior Between 1998 and 2000

Minor components were also removed from AMF in 2000. Again, the FA and TAG compositions of AMF and MF-TAGs were similar, and there were no differences in the dropping temperatures or equilibrium SFC values. Also, the crystallization behavior of AMF and MF-TAGs from 1998 and 2000 were identical (data not shown). However, the effects of adding native milkfat DAGs back to the MF-TAGs differed from 1998. Again, the thermodynamics of the MF-TAGs were unchanged by the addition of DAGs. The crystallization kinetics, however, were affected differently than in 1998. The pronounced delay in crystallization observed for the 1998 MF-DAGs was not evident in the 2000 MF-DAGs. Figure 7 shows the crystallization curves for AMF, MF-TAGs, and MF-DAGs from both 1998 and 2000 (MF-DAG-1998 and MF-DAG-2000) at 25.0°C.

Figure 7 shows that although in 1998 0.1 wt% DAGs significantly increased the MF-TAGs induction time, in 2000, DAG addition had only a small effect on the TAG crystallization. $\tau_{nucleation}$ for AMF, MF-TAGs, MF-DAGs-1998, and MF-

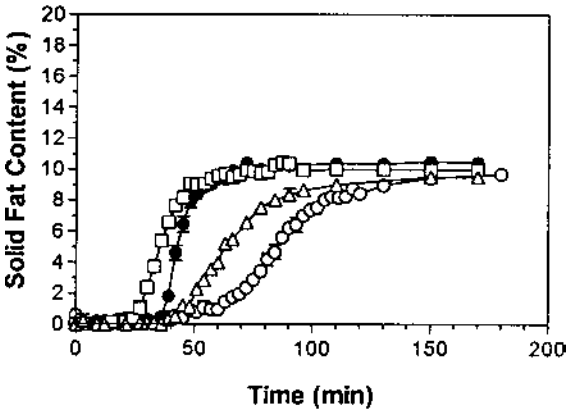

Figure 7 Solid fat content (%) versus time during static crystallization of (△) anhydrous milkfat (AMF), (□) milkfat triacylglycerols (MF-TAGs), (○) MF-DAGs-1998 (MF-TAGs with 0.1% DAG added), and (●) MF-DAGs-2000 (MF-TAGs with 0.1% DAG added) at 25.0°C. Symbols represent the average and standard error of three replicates.

Copyright 2002 by Marcel Dekker. All Rights Reserved.

Table 10 Nucleation Induction Times ($\tau_{nucleation}$) for AMF, MF-TAGs, MF-DAGs-1998, and MF-DAGs-2000 at 25.0°C[a]

	$\tau_{nucleation}$ (min)
AMF	17.1 ± 1.1[A]
MF-TAGs	10.0 ± 1.0[B]
MF-DAGs-1998	16.8 ± 1.9[A]
MF-DAGs-2000	9.6 ± 0.9[B]

[a] Mean value of three replicates with standard derivation: Similar superscript letters (A and B) indicate statistical similarity ($P > 0.05$).

DAGs-2000 are compared in Table 10. In 1998, addition of the milkfat DAGs to MF-TAGs delayed nucleation, whereas, in 2000 this had no effect. Stereospecific analysis of the 1998 and 2000 DAGs revealed differences in the fatty acid (FA) positional distribution between the two years, which may explain their differing effects on crystallization. Table 11 shows the FA composition of the *sn*-1, 3 DAGs in the 1998 and 2000 milkfat DAGs and in milkfat's high melting fraction (HMF).

The *sn*-1, 3 positions of the 1998 DAGs were enriched in palmitic acid (C16), whereas the primary positions of the 2000 DAGs were enriched in oleic

Table 11 Fatty Acid Composition (wt%) of 1998 and 2000 Milkfat *sn*-1,3 Diacylglycerols (DAG) and Milkfat's High Melting Fraction (HMF)[a]

Fatty acid	1998 *sn*-1,3 DAG	2000 *sn*-1,3 DAG	HMF[b]
6:0	0.2 ± 0.3	2.1 ± 0.1	0.2 ± 0.2
8:0	0.1 ± 0.2	1.3 ± 0.1	0.3 ± 0.2
10:0	1.5 ± 0.0	3.0 ± 0.2	1.8 ± 0.8
12:0	3.8 ± 0.3	4.0 ± 0.4	3.8 ± 1.0
14:0	15.0 ± 0.1	10.8 ± 0.7	16.5 ± 1.7
16:0	48.2 ± 0.1	29.5 ± 2.5	45.4 ± 1.0
18:0	13.5 ± 0.0	7.3 ± 0.5	22.0 ± 2.8
18:1	17.7 ± 0.1	42.1 ± 3.2	9.9 ± 1.6

[a] Mean value of three replicates with standard deviation.
[b] Adapted from Wright et al. (1999).

Copyright 2002 by Marcel Dekker. All Rights Reserved.

acid (C18:1). Palmitic acid is the most prominent FA in HMF. Molecular complementarity between the 1998 DAGs and HMF molecules may allow the DAGs to cocrystallize within early HMF seed crystals and retard subsequent crystallization. We can speculate that in the 2000 DAGs, the oleic acid–enriched *sn*-1 and *sn*-3 positions led to incompatibilities with the HMF molecules. As a result, these DAGs are prevented from cocrystallizing with the HMF and subsequently delaying crystallization.

E. Effect of Standard DAG Isomer Addition on Crystallization Behavior of MF-TAGs

To further investigate the effect of DAG composition on MF-TAGs crystallization, racemic and *sn*-1,2-specific DAGs of palmitic and oleic acid were added to the 2000 MF-TAG at the 0.1 wt% level. These included racemic mixtures of dipalmitin and diolein (PP and OO), *sn*-1,2 dipalmitin (1,2PP), *sn*-1,2 diolein (1,2OO), and *sn*-1 palmitic, 2 oleic (1P, 2O). Addition of the DAG standards did not significantly affect the Mettler dropping temperature ($P > 0.05$) (Table 12).

Figure 8 shows that addition of the *sn*-1,2 DAG standards (1,2PP, 1,2OO, and 1P, 2O) did delay the crystallization of MF-TAGs at 25.0°C. In contrast, the racemic mixtures of DAGs (PP and OO) slightly enhanced MF-TAGs crystallization. Induction times and free energies of nucleation ($\tau_{nucleation}$ and ΔG_c, respectively) for MF-TAGs and MF-TAGs with 0.1 wt% addition of the standard DAGs

Table 12 Mettler Dropping Temperature for MF-TAGs and MF-TAGs with 0.1 wt% Addition of DAG Standards (PP, 1,2PP, OO, 1,2OO, and 1P,2O)[a]

Sample	Dropping temperature (°C)
MF-TAGs	34.8 ± 0.1^{A}
PP	34.9 ± 0.1^{A}
1,2PP	34.7 ± 0.2^{A}
OO	34.7 ± 0.1^{A}
1,2OO	34.8 ± 0.1^{A}
1P,2O	34.8 ± 0.1^{A}

[a] Mean value of three replicates with standard deviation. Similar superscript letter (A) indicates statistical similarity ($P > 0.05$) of values.

Copyright 2002 by Marcel Dekker. All Rights Reserved.

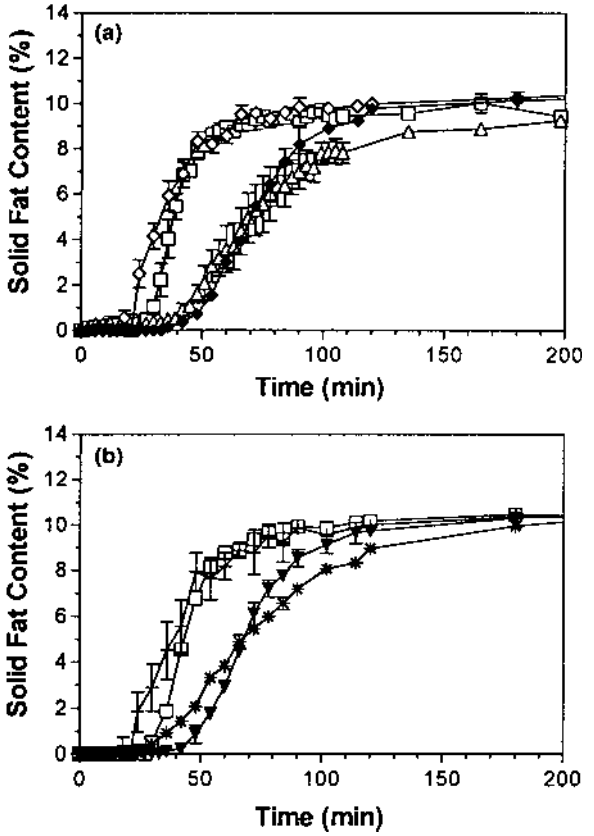

Figure 8 (a) Solid fat content (%) versus time during static crystallization of (△) anhydrous milkfat (AMF), (□) milkfat triacylglycerols (MF-TAGs), and MF-TAGs with 0.1% standard DAG added (◇) OO and (◆) 1,200 at 25.0°C. (b) Solid fat content (%) versus time during static crystallization of milkfat triacylglycerols (MF-TAGs) and MF-TAGs with 0.1% standard DAG added [(+) PP, (∗) 1,2PP, and (▼) 1P,2O] at 25.0°C. Symbols represent the average and standard error of three replicates.

are shown in Table 13. The monoacid 1,2-specific isomers (1,2PP and 1,2OO) increased ΔG_c, suggesting that they inhibited TAG nucleation. Although 1P, 2O delayed the development of solid fat (Fig. 8), it did not significantly affect ΔG_c for MF-TAGs (Table 13). Therefore, 1P, 2O delayed crystal growth, but not by exerting an effect on nucleation.

Differences observed in the crystallization behaviors of the DAGTAG

Copyright 2002 by Marcel Dekker. All Rights Reserved.

Table 13 Induction Time and Free Energy of Nucleation for MF-TAGs and MF-TAGs with 0.1 wt% DAG Standards (PP, OO, 1,2PP, 1,2OO, 1P,2O) at 25.0°C[a]

	Induction time (min)	Nucleation free energy (kJ/mol)
MF-TAGs	10.04 ± 1.02[A]	1.67 ± 0.33[B,C]
PP	9.47 ± 0.91[A]	1.89 ± 0.35[B,C]
OO	9.80 ± 0.17[A]	1.33 ± 0.18[C]
1,2PP	9.23 ± 1.22[A]	2.45 ± 0.23[A,B]
1,2OO	8.37 ± 0.38[B]	2.88 ± 0.23[A]
1P,2O	7.84 ± 1.68[B]	1.40 ± 0.37[C]

[a] Mean value of three replicates with standard deviation. Different superscript letters (A–C) indicate significant differences ($P < 0.05$).

blends cannot be attributed to differences in melting temperatures of the DAG. Table 14 shows that both PP and 1,2PP, for example, have peak melting temperatures of approximately 50 and 65°C, although they affected the MF-TAGs crystallization very differently. From their high melting temperatures, we might expect the dipalmitin standards to both act as seeds in the crystallization of MF-TAGs. Only the racemic mixture (PP) had this effect. 1,2PP had the same effect of delaying crystallization as 1,2OO, despite the fact that at the crystallization temperature (25.0°C) we would expect 1,2PP to be in the solid state and 1,2OO to be in the liquid state.

The racemic purity of the standard DAGs does seem to be related to their

Table 14 Peak Melting Temperatures (°C) by Differential Scanning Calorimetry for Standard DAG (PP, 1,2PP, OO, 1,2OO, and 1P,2O)

	Peak 1 (°C)	Peak 2 (°C)
PP	50	65
1,2PP	50	68
OO	24	—
1,2OO	7	—
PO	7	15

Copyright 2002 by Marcel Dekker. All Rights Reserved.

ability to delay milkfat crystallization. Only the *sn*-1,2 DAGs delayed crystallization. This effect may be related to known differences between *sn*-1,2 and *sn*-1,3 DAGs. For example, the ability of DAGs to stabilize the β′ crystal in TAGs depends on the DAGs' racemic from (Hernqvist et al., 1981). 1, 2 and 2, 3 DAG isomers are generally more effective than 1,3 DAG at delaying the velocity of phase transformations in fats (Wähnelt et al., 1991). For example, 1,2-dilaurin is a stronger α and β′ stabilizer in trilaurin than 1, 3-dilaurin (Smith et al., 1994). Shannon et al. (1992) confirmed that 1,2 and 1,3 DAGs have different crystal structures and polymorphism. The α polymorph has been identified in *sn*-1,2 DAG but not in *sn*-1,3 DAG (Howe and Malkin, 1951). Also, the directionality of the fatty acid chains in the crystalline state is different for the DAGs. In *sn*-1,3 DAG, the fatty acid chains extend in opposite directions, and these molecules tend to pack in monolayers. In contrast, the fatty acid chains in *sn*-1,2 DAG extend in the same direction (Larsson, 1994). The shape of these molecules is more reminiscent of the tuning fork arrangement that describes TAG conformation. Different polymorphic behaviors between the racemic and *sn*-1,2 DAGs then may account for the differing effects on crystallization. There were, however, no obvious differences in the polymorphism of the pure DAG standards or the DAGMF-TAG blends as monitored by DSC. The melting profiles of pure PP and 1,2PP, for example, are similar after crystallization at 25°C for 5 and 20 min (data not shown), indicating the formation of the same polymorphs upon crystallization.

The reported effects of DAG isomerism on TAG crystallization rate is somewhat variable. In palm olein, the 1, 3 isomer of dipalmitin caused rapid crystallization (Siew and Ng, 1996), whereas 1, 3-DAGs were especially effective at reducing the TAG growth rate in trilaurin (Smith and Povey, 1997). Therefore, although DAG stereospecificity may be a factor, the effect of DAGs on TAG crystallization is also related to composition (Gordon and Rahman, 1991; Siew and Ng, 1996; Smith et al., 1994). In trilaurin, for example, the maximum growth rate inhibition was observed when glycerides with the same chain length as the TAGs were added (Smith and Povey, 1997).

The differences in crystallization behaviors observed between MF-DAG-1998 and MF-DAGs-2000 are still unexplained. Possibly the differences are related to different interactions between the DAGs and MF-TAGs molecules and to varying degrees of complementarity between the glycerides in 1998 and 2000. Unfortunately, the complex FA composition of milkfat makes it difficult to speculate on molecular interactions and packing arrangements. Studies with the DAG standards showed that racemic purity of the DAGs was more important to the effect on MF-TAGs crystallization than was the DAGs' FA composition. The milkfat DAGs added to the MF-TAGs were a mixture of 1,3 and 1,2 or 2,3 isomers. Unfortunately we don't know the relative proportion of each isomer in 1998 and 2000.

Copyright 2002 by Marcel Dekker. All Rights Reserved.

IV. EFFECT OF MILKFAT MINOR COMPONENTS ON POLYMORPHIC BEHAVIOR

The possible influence of minor components on milkfat's polymorphic behavior was investigated using DSC and X-ray diffraction spectroscopy (XRD). The heat flow properties in the crystallization and melting modes were monitored by DSC for AMF, MF-TAGs, and MF-DAGs-1998. Figure 9 shows that no differences were observed between the three samples. At heating and cooling rates of 5°C/min, the crystallization onset temperature was roughly 18°C, and the peak melting temperature for samples held at 5°C for 24 h was approximately 20°C.

The polymorphic state of the crystals after 24 h at 5.0 and 25.0°C was determined by XRD as previously described (Wright et al., 2000). In all cases, the XRD patterns were identical and the β'_{-2} crystal was observed. Figure 10 shows a typical XRD pattern obtained for AMF, MF-TAGs, and MF-DAGs after 24 h at 5.0 and 25.0°C. Reflections at 3.8, 4.2, and 39 Å were detected in all three fats. The reflections nearest the center of each image represents the long spacing, and the outer two reflection rings are the short spacings. The XRD patterns indicate that the absence of minor components and the presence of only the milkfat DAGs did not alter the formation of milkfat's typical β'_{-2} polymorphic form at 5.0 or 25.0°C.

Values for log τ_{SFC} and log $\tau_{nucleation}$ are plotted as a function of crystallization temperature in Figures 11a and 11b, respectively. This type of plot indicates whether different polymorphic forms are present in the temperature range studied. A continuous curve indicates that at all temperatures the same crystal polymorph

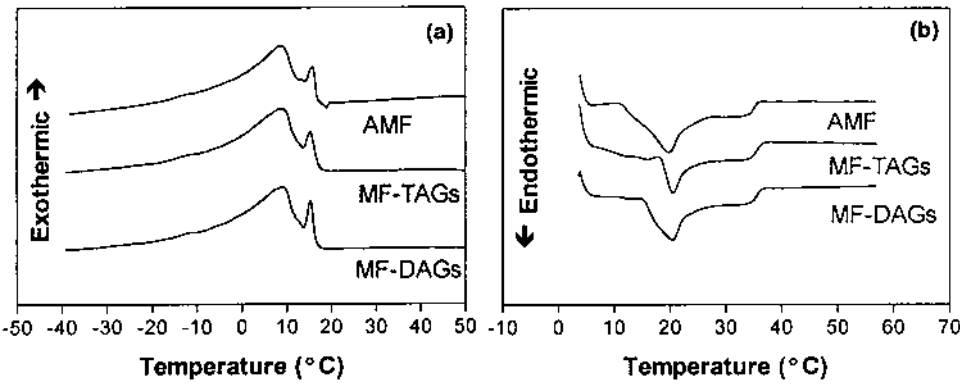

Figure 9 Differential scanning calorimetric curves of AMF, MF-TAGs, and MF-DAGs in (a) the crystallization mode and (b) the melting mode at 5.0°C/min.

Copyright 2002 by Marcel Dekker. All Rights Reserved.

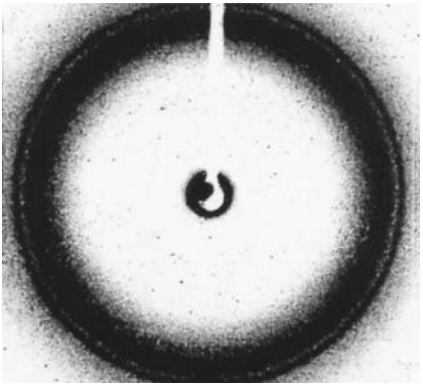

Figure 10 Powder X-ray diffraction pattern characteristic of AMF, MF-TAGs, and MF-DAGs after 24 h at 5.0 and 25.0°C.

is formed. A discontinuous curve indicates the existence of different polymorphs above and below the discontinuity (Ng, 1990; Dibildox-Alvrado and Toro-Vazquez, 1997; Herrera et al., 1998). At approximately 20°C the curves in Figures 11a and 11b show a change in slope. Accordingly, these discontinuities may indicate that AMF and MF-TAGs crystallize in different polymorphic forms above and below 20°C.

Recall that prominent changes in the Avrami parameters were also observed around 20°C (Fig. 5). These changes in crystallization mode and the discontinuities in Figure 11 are perhaps related to the formation of the α crystal at lower temperatures. Milkfat crystallizes predominantly in the β′ crystal form, although at high rates of cooling (≥ 1°C/min) and at high degrees of supercooling, the α crystal will form below 20.0°C. The clear point of the α crystal is approximately 20°C, at which point the α crystals transform to the more stable β′ polymorph (Grotenhuis et al., 1999). Evidence that the changes observed in crystallization behavior were related to α-crystal formation was sought by DSC. AMF was rapidly cooled at 10°C/min to 15.0°C, held for 2 min, and subsequently melted at 5°C/min. AMF was also cooled at 10°C/min to 15.0, 20.0, and 22.5°C, held for 30 min, and then melted at 5°C/min. Figure 12a shows that there is a sharp melting peak below 20°C that is not present when the sample is held at 15°C for 30 min (Fig. 12b). When the sample is held for 30 min, only one broad melting endotherm is present around 20°C. Figure 12b shows the presence of a lower melting form in the milkfat below 20°C that is not evident at 20°C or above. This could be related to formation of the α crystal or to the crystallization of different TAG fractions.

Copyright 2002 by Marcel Dekker. All Rights Reserved.

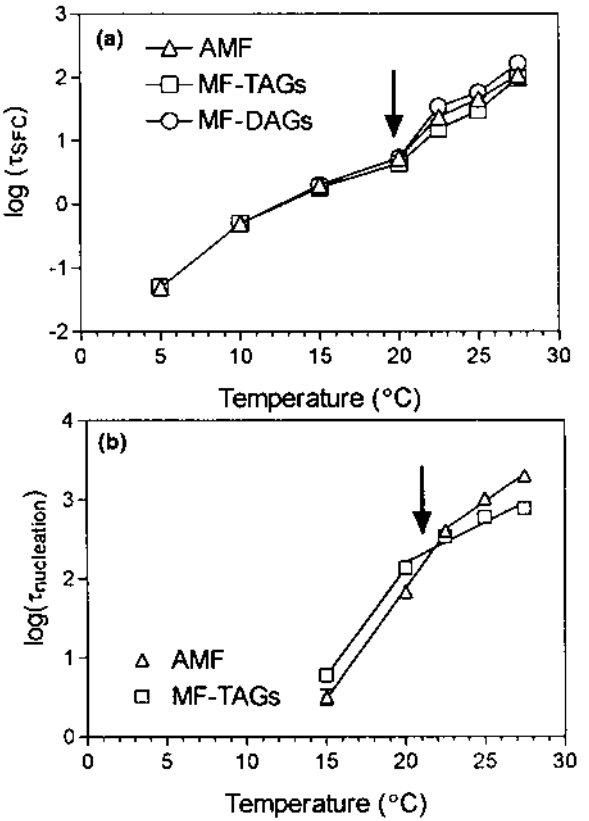

Figure 11 (a) log τ_{SFC} versus crystallization temperature and (b) log $\tau_{nucleation}$ versus crystallization temperature. The discontinuity of the curves suggests the formation of different polymorphic forms upon crystallization above and below 20.0°C.

V. EFFECT OF MINOR COMPONENTS ON MILKFAT MICROSTRUCTURE AND RHEOLOGICAL PROPERTIES

The microstructures of AMF, MF-TAGs, and MF-DAGs-1998 after 24 h at 5.0, 10.0, 15.0, 20.0, 22.5, 25.0, and 27.5°C were visualized using polarized light microscopy (PLM). Images representative of the three fats at 5.0, 10.0, 15.0, and 20.0°C are shown in Figure 13. Minor components did not affect the appearance of the microstructures over this temperature range. The influence of temperature on crystal network structure, however, is very obvious. With a high degree of

Copyright 2002 by Marcel Dekker. All Rights Reserved.

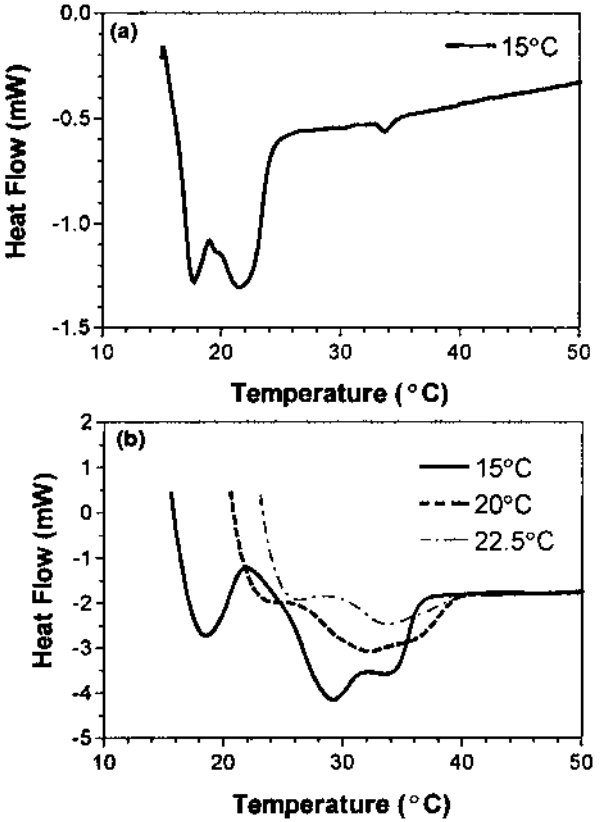

Figure 12 (a) Differential scanning calorimetric (DSC) melting curves of AMF cooled from 80°C at 10°C/min to 15°C, held for 2 min, and melted at 5°C/min. (b) DSC melting curves of AMF cooled from 80°C at 10°C/min to 15, 20, and 22.5°C, held for 30 min, and melted at 5°C/min.

supercooling (ΔT = 28°C at 5.0°C), nucleation proceeds very rapidly, and the resulting pattern of crystal structures resembles a starry night. By 20.0°C, a combination of sharper reflections and larger crystal clusters is observed. At even higher temperatures (22.5, 25.0, and 27.5°C), only the larger microstructures are observed. Micrographs of AMF, MF-TAGs, and MF-DAGs at 22.5°C are shown in Figure 14. Images representative of the fats at 25.0 and 27.5°C are shown in Figures 15a and 15b, respectively. The change in microstructure around 20°C is related to a decrease in the degree of supercooling during crystallization and

Copyright 2002 by Marcel Dekker. All Rights Reserved.

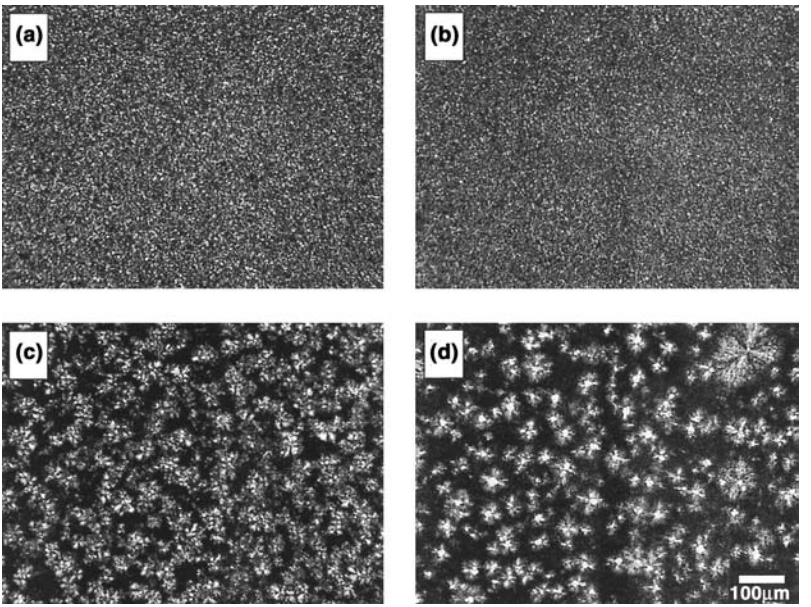

Figure 13 Polarized light micrographs representative of AMF, MF-TAGs, and MF-DAGs after 24 h at (a) 5.0°C, (b) 10.0°C, (c) 15.0°C, and (d) 20.0°C.

possibly the formation of α crystals below 20°C. Above 20°C the initial number of nuclei present will therefore be lower and crystal growth will predominate.

Although the microstructures of AMF, MF-TAGs, and MF-DAGs are very similar at these temperatures, it appears that, particularly at 22.5°C, there are fewer microstructures (crystal clusters) present in the MF-TAGs and MF-DAGs than in AMF. At 22.5°C, the average size of the crystal clusters in AMF appeared to be smaller than in the MF-TAGs and MF-DAGs. To quantify any differences between the fats, the number of microstructures (cluster centers) in the micrographs of AMF, MF-TAGs, and MF-DAGs at 10× magnification above 20°C were counted. The only significant difference was observed at 22.5°C ($P < 0.0001$). At this temperature, the average number of microstructures present in the AMF micrographs was significantly higher than in MF-TAGs ($P < 0.05$). Also, MF-DAGs contained significantly fewer microstructures than the other two fats at 22.5°C ($P < 0.05$). The average numbers of cluster centers for AMF, MF-TAGs, and MF-DAGs at 22.5°C were 95.4 ± 11.0, 71.7 ± 18.0, and 47.5 ± 16.4, respectively.

The fact that fewer microstructures are observed in the micrographs of MF-

Copyright 2002 by Marcel Dekker. All Rights Reserved.

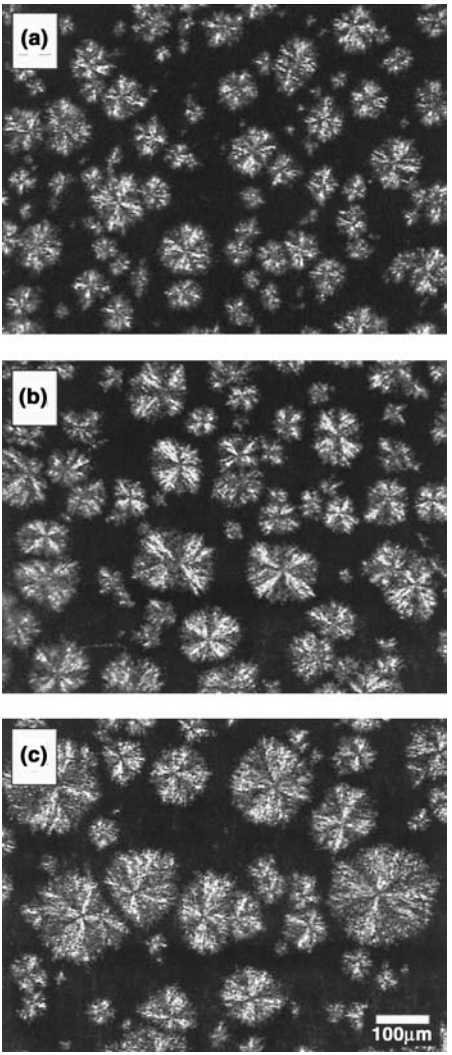

Figure 14 Polarized light micrographs of (a) AMF, (b) MF-TAGs, and (c) MF-DAGs after 24 h at 22.5°C.

Copyright 2002 by Marcel Dekker. All Rights Reserved.

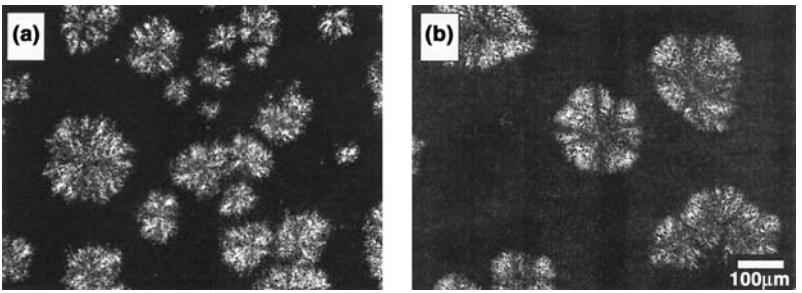

Figure 15 Polarized light micrographs representative of AMF, MF-TAGs, and MF-DAGs after 24 h at (a) 25.0°C and (b) 27.5°C.

TAGs and MF-DAGs at 22.5°C suggests that the microstructures of these fats are, on average, smaller than that of AMF. Figure 14 shows that AMF does seem to contain more small microstructures than the other two fats. It is tempting to speculate on the effect of minor components on crystallization on the basis of this difference. For example, the fact that AMF contains more and smaller microstructures than MF-TAGs or MF-DAGs could point to increased nucleation events and limited crystal growth. We must remember, though, that the microstructures that were counted are not crystals. They are clusters of reflections that are made up of crystal aggregates. A microstructure does not originate from a single nucleation event.

To further quantify the microstructures of AMF, MF-TAGs, and MF-DAGs, the concept of fractal dimensions was used. Fractal dimensions (D) have been used extensively by our group to characterize the spatial distribution of mass in fat crystal networks (Marangoni and Rousseau, 1996; Narine and Marangoni, 1999a). Equation (6) shows that the storage modulus (G') of a fat scales with the volume fraction of solids (Φ = SFC/100) in a power law fashion.

$$G' = \lambda\phi^m \tag{6}$$

where m is a scaling factor related to D and for the weak-link regime in a three-dimensional system is equivalent to $1/(3 - D)$. m is determined rheologically by determining G' in the linear viscoelastic region (LVR) for a fat and dilutions of the fat with oil. The dilutions allow for the determination of G' over a range of Φ values for the fat. The volume fraction of solids (Φ) is equivalent to the mass fraction of solids determined by pNMR. LVR G' values were determined for AMF and MF-TAGs and for the fats diluted with canola oil (95/5, 90/10, 85/15, 80/20, and 75/25 fat/oil). This was done as previously described using small-deformation oscillatory stress sweeps with a CarriMed CSL^2 500 Rheometer (TA Instruments). When ln G' is plotted as a function of ln Φ for the dilutions

Copyright 2002 by Marcel Dekker. All Rights Reserved.

of a fat as in Figure 16, D can be calculated from the slope of the line (Marangoni and Rousseau, 1996; Narine and Marangoni, 1999a).

Fractal dimensions can also be determined by image analysis using a particle counting procedure developed in our laboratory (Narine and Marangoni, 1999a). The theory behind this approach and details of the analysis are discussed extensively by Narine and Marangoni (1999a). Polarized light micrographs captured with a CCD camera were first inverted and then thresholded to represent each reflection of light in the micrograph as a black ''particle'' in a binary image. A series of increasingly larger squares were then laid over the image, and the ''particles'' in each box were counted. All objects greater than 1 pixel in size were counted as particles. When the number of particles per box is plotted as a function of the length of each box on a log-log graph, the slope of this line is D (Narine and Marangoni, 1999a). Fractal dimensions determined from the particle counting analysis (D_{PLM}) for AMF, MF-TAGs, and MF-DAGs between 5.0 and 25.0°C are listed in Table 15.

Although there were no significant differences in D_{PLM} among the three fats ($P > 0.05$), D was significantly affected by temperature ($P < 0.0001$). Table 15 and Figure 17 show that higher values of D were obtained at higher temperatures. Narine and Marangoni (1999a) proposed that higher values of the fractal dimension are associated with more ordered systems. At higher temperatures, crystallization proceeds more slowly than at lower temperatures. As a result, crystals will have more time to arrange themselves in more ordered networks.

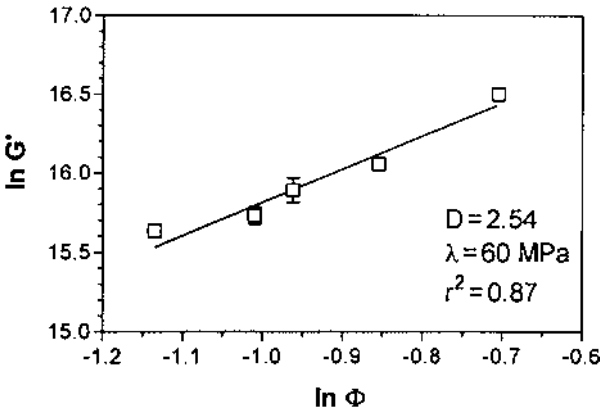

Figure 16 Plot of ln G' versus ln Φ for AMF. The fractal dimension (D) can be determined from the slope of the plot.

Copyright 2002 by Marcel Dekker. All Rights Reserved.

Table 15 Fractal Dimension Determined by Particle Counting (D_{PLM}) for AMF, MF-TAGs, and MF-DAGs after 24 h Crystallization at 5.0, 10.0, 15.0, 20.0, 22.5, 25.0, and 27.5°C[a]

Temperature (°C)	AMF	MF-TAGs	MF-DAGs
5	1.97 ± 0.03 (n = 17)	1.99 ± 0.04 (n = 16)	2.00 ± 0.03 (n = 18)
10	2.00 ± 0.04 (n = 17)	1.99 ± 0.05 (n = 18)	1.99 ± 0.05 (n = 19)
15	2.07 ± 0.12 (n = 22)	2.06 ± 0.16 (n = 18)	2.08 ± 0.11 (n = 19)
20	2.10 ± 0.20 (n = 19)	2.15 ± 0.26 (n = 19)	2.15 ± 0.23 (n = 18)
22.5	2.13 ± 0.29 (n = 16)	2.23 ± 0.32 (n = 16)	2.25 ± 0.43 (n = 17)
25	2.24 ± 0.40 (n = 19)	2.28 ± 0.46 (n = 19)	2.19 ± 0.48 (n = 19)

[a] Mean value of three replicates with standard deviation.
n = number of samples.

In an attempt to quantify the relationship between crystallization behavior and microstructure, D_{PLM} was plotted as a function of τ_{SFC} (Fig. 18a), Avrami k (Fig. 18b), and Avrami n (Fig. 18c). It was thought that because n gives an indication of the mode of crystal growth, it might correlate more strongly with structure (and hence D) than τ_{SFC} and k, which are indicators of the crystallization kinetics. Figure 18 shows that all three parameters of crystallization (τ_{SFC}, k, and

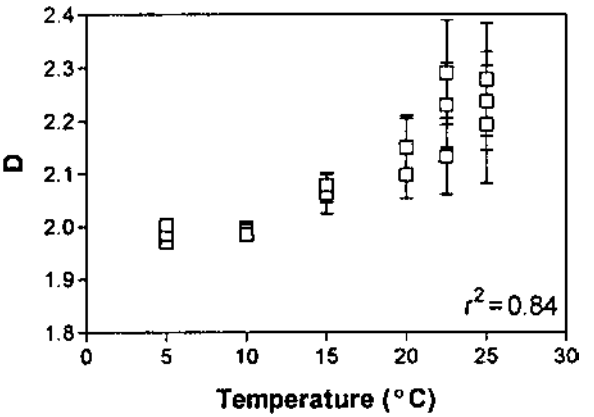

Figure 17 D_{PLM} versus temperature (°C). Symbols represent the average and standard error of three replicates.

Copyright 2002 by Marcel Dekker. All Rights Reserved.

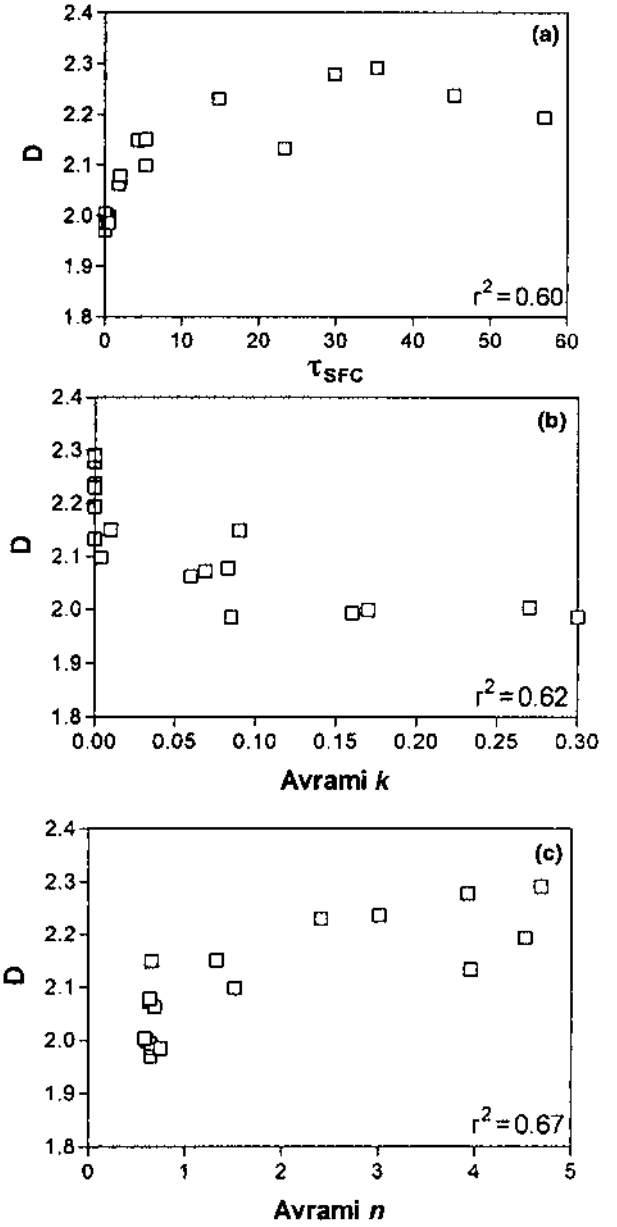

Figure 18 Correlation between crystallization and structure; D versus (a) τ_{SFC}, (b) Avrami constant k (c) and Avrami exponent n.

Copyright 2002 by Marcel Dekker. All Rights Reserved.

n) were significantly correlated with D_{PLM}($P < 0.05$). Some of the correlation observed must be related to the fact that τ_{SFC}, k, and n are all highly dependent on temperature ($P < 0.001$). It would seem, therefore, that supercooling is the biggest determinant of structure in milkfat.

Values of D were also determined for AMF and MF-TAGs after 24 h at 5.0°C using the rheological approach. Because of the very soft nature of milkfat and the difficulties in obtaining an accurate G' value at a low solids content, D was determined rheologically only at 5.0°C. Table 16 compares the fractional solids content (Φ), storage moduli (LVR G'), values of fractal dimension ($D_{rheology}$), and the pre-exponential term (λ) determined for AMF and MF-TAGs in the rheological analysis. The fractal dimension determined by image analysis (D_{PLM}) and an average particle diameter for the three fats at 5.0°C are also shown, as are indicators of the fats' macroscopic hardness. Where these parameters were determined for MF-DAGs, their values are also included in Table 16.

Table 16 shows that values of D determined rheologically did not agree with the values determined by image analysis. There were, however, no significant differences observed between D values for AMF and MF-TAGs determined by either method. Therefore, the spatial distribution of mass would seem to be unaffected by the presence or absence of minor components. λ [the pre-exponential term in Eq. (6)] is a constant independent of the volume fraction of solids but dependent on the size of the particles in the fractal network and on the interactions

Table 16 Microstructural Analysis of AMF, MF-TAGs, and MF-DAGs at 5.0°C after 24 h[a,b]

	AMF	MF-TAGs	MF-DAGs
Φ	0.49 ± 0.01^{A}	0.49 ± 0.01^{A}	0.52 ± 0.01^{B}
LVR G' (MPa)	11.7 ± 1.7^{A}	10.2 ± 2.2^{A}	—
$D_{rheology}$	2.62 ± 0.04^{A}	2.71 ± 0.05^{A}	—
λ (MPa)	95.1 ± 19.3^{A}	135.5 ± 22.1^{A}	—
D_{PLM}	1.97 ± 0.03^{A}	1.99 ± 0.04^{A}	2.00 ± 0.03^{A}
Equivalent particle diameter (μm)	1.25 ± 0.04^{A}	1.31 ± 0.09^{A}	1.33 ± 0.02^{A}
Cone penetrometry force at 4 mm deformation (N)	17.92 ± 2.09^{A}	19.35 ± 4.92^{A}	17.34 ± 3.89^{A}
Parallel plate compression yield value (N)	48.94 ± 4.75^{A}	52.46 ± 4.15^{A}	46.16 ± 7.73^{A}

[a] Different superscript letters (A and B) indicate significant differences ($P < 0.05$) within each row.
[b] Includes small-deformation testing (fractional solids content (Φ), storage moduli in the LVR (LVR G'), $D_{rheology}$, and λ), image analysis results (D_{PLM} and equivalent particle diameter), and large-deformation rheological testing (cone penetrometry force at 4 mm deformation and parallel-plate compression yield value).
LVR = linear viscoelastic region.

Copyright 2002 by Marcel Dekker. All Rights Reserved.

between them (Marangoni, 2000; Narine and Marangoni, 1999a). A model has been proposed by our group for λ (Marangoni, 2000; Narine and Marangoni, 1999b):

$$\lambda \sim \frac{A}{\pi a \gamma d_0^2} \tag{7}$$

where A is Hamacker's constant, a is the diameter of a microstructural element (primary particle within a cluster), γ is the strain, and d_0 is the average equilibrium distance between clusters. Two systems with the same D value could potentially have different λ values because of differences in their particle properties. In this case, values of λ determined for AMF and MF-TAGs at 5.0°C were statistically similar ($P > 0.05$). Table 16 shows that the equivalent particle diameter was also similar for the three fats at 5.0°C ($P > 0.05$).

Minor components did not affect the TAG microstructure at 5.0°C. Neither did they significantly affect the samples' hardness at 5.0°C. Large-deformation mechanical testing was performed using an SMS materials tester (Stable Micro Systems, Surrey, England) at 5.0°C using both a 45° cone and a parallel-plate attachment. A constant deformation rate of 10 mm/s was used in the tests. The force at a cone penetration depth of 4 mm and the yield force values detected using the parallel-plate geometry were compared for the three fats. Table 16 shows that there were no significant differences in these hardness indicators for the three fats ($P > 0.05$). Minor components, therefore, did not affect the mechanical properties of the TAG crystal networks at 5°C.

Minor components in milkfat represent a diverse group of lipid species with variable composition. Removal of these minor components in 1998 and 2000 did not affect the thermodynamic properties of the AMF TAGs. Minor components, however, do exert an inhibitory influence on the TAG crystallization behavior. Primarily, they serve to increase τ_{SFC} and $\tau_{nucleation}$ above 20°C. The ability of minor components to delay crystallization at lower degrees of supercooling may be related to the fact that milkfat has different modes of growth above and below 20°C. Although τ_{AMF} values were greater than $\tau_{MF\text{-}TAGs}$ values, minor components did not significantly affect the rate (Avrami k) or mode (Avrami n) of crystallization once crystallization began. Neither did they affect the fat's microstructure or rheological properties at 5°C. Between 5.0 and 27.5°C, the microstructures of AMF and MF-TAGs were similar. At 22.5°C, however, significantly fewer microstructures were observed in the MF-TAGs micrographs than in those for AMF.

The system thermodynamics were not affected by the addition of milkfat DAGs to the MF-TAGs. However, the effect on crystallization behavior differed between 1998 and 2000. In 1998, the DAGs altered the crystallization behavior of the MF-TAGs above 20°C. They significantly increased τ_{SFC} and $\tau_{nucleation}$, de-

Copyright 2002 by Marcel Dekker. All Rights Reserved.

creased the crystallization rate (k), and also changed the index of crystallization (significantly higher values of n). Although they did not affect the microstructure or rheological properties at 5.0°C, the microstructures observed in MF-DAGs-1998 at 22.5 °C were smaller and less numerous than those of either AMF or MF-TAGs. The marked delay in crystallization exerted by the 1998 DAG was not observed by the 2000 DAG. τ_{SFC} was only slightly increased by the DAG addition, whereas $\tau_{nucleation}$ for MF-DAGs-2000 was statistically similar to $\tau_{nucleation}$ for MF-TAGs. The differences observed between the 1998 and 2000 MF-DAGs may be related to fatty acid compositional differences or differences in the racemic purity of the DAGs.

REFERENCES

American Oil Chemists' Society. (1993). Official Methods and Recommended Practices of the American Oil Chemists Society. 4th ed. Champaign, IL: AOCS Press.

Aronhime, J, S Sarig, N Garti. (1990). Emulsifiers as additives in fats: Effect on polymorphic transformations and crystal properties of fatty acids and triglycerides. Food Struct 9:337–352.

Avrami, M. (1939). Kinetics of phase change I. General theory. J Chem Phys 7:1103–1112.

Avrami, M. (1940). Kinetics of phase change II. Transformation-time relations for random distribution of nuclei. J Chem Phys 8:212–224.

Avrami, M. (1941). Kinetics of phase change III. Granulation, phase change, and microstructure. J Chem Phys 9:177–184.

Bitman, J, DL Wood. (1990). Changes in milk phospholipids during lactation. J Dairy Sci 73:1208–1216.

Christian, JW. (1965). The Theory of Transformations in Metals and Alloys: An Advanced Textbook in Physical Metallurgy. London: Pergamon Press, pp 16–22, 471–495.

Christie, WW. (1988). Lipid Analysis: Isolation, Separation, Identification, and Structural Analysis of Lipids. 2nd ed. New York: Pergamon Press, pp 93–96, 115–119.

Dibildox-Alvarado, E, J Toro-Vazquez. (1997). Isothermal crystallization of tripalmitin in sesame oil. J Am Oil Chem Soc 74(2): 69–76.

DuRoss, JW, WH Knightly. (1965). Relationship of sorbitan monostearate and Polysorbate 60 to bloom resistance in properly tempered chocolate. Manuf Confect July: 50–56.

Gerson, T, WL Escher. (1966). The effect of monoglycerides on the spreadability of butter. NZ J Sci 9:528–533.

Gordon, MH, IA Rahman. (1991). Effects of minor components on the crystallization of coconut oil. J Am Oil Chem Soc 68(8): 577–579.

Graydon, JW, SJ Thorpe, DW Kirk. (1994). Determination of the Avrami exponent for solid state transformations from non-isothermal differential scanning calorimetry. J Non-Cryst Solids 175:31–43.

Grotenhuis, TE, GA van Aken, KF van Malssen, H Schenk. (1999). Polymorphism of

Copyright 2002 by Marcel Dekker. All Rights Reserved.

milk fat studied by differential scanning calorimetry and real-time X-ray powder diffraction. J Am Oil Chem Soc 76(9):1031–1039.
Henderson, DW. (1979). Thermal analysis of non-isothermal crystallization kinetics in glass forming liquids. J Non-Cryst Solids 30:301–315.
Hernqvist, L, K Anjou. (1983). Diglycerides as a stabilizer of the beta prime crystal form in margarines and fats. Fette Seifen Anstrichm 85(2):64–66.
Hernqvist, L, B Herslöf, K Larsson, O Podlaha. (1981). Polymorphism of rapeseed oil with a low content of erucic acid and possibilities to stabilise the β′-crystal form in fats. J Sci Food Agric 32:1197–1202.
Herrera, ML, C Falabella, M Melgarejo, MC Añon. (1998). Isothermal crystallization of hydrogenated sunflower oil: II. Growth and solid fat content. J Am Oil Chem Soc 76(1):1–6.
Howe, RJ, T Malkin. (1951). An X-ray and thermal examination of glycerides. Part XI. The 1,2-diglycerides and further observations on 1,3-diglycerides. J Chem Soc 1951:2663–2667.
Kapsalis, JG, JJ Betscher, T Kristoffersen, IA Gould. (1960). Effect of chemical additives on the spreading quality of butter. I. The consistency of butter as determined by mechanical and consumer panel evaluation methods. J Dairy Sci 43:1560–1564.
Kapsalis, JG, T Kristoffersen, IA Gould, JJ Betscher. (1963). Effect of chemical additives on the spreading quality of butter. II. Laboratory and plant churnings. J Dairy Sci 46(2):107–113.
Kawamura, K. (1979). The DSC thermal analysis of crystallization behaviour in palm oil. J Am Oil Chem Soc 56(8):753–758.
King, N. (1966). The effect of some surface active substances on the physical forms of milk fat. Proc 17th Int Dairy Congress Munich C:2:289–294.
Larsson, K. (1994). Lipids in the solid state. In: K Larsson, ed. Lipids: Molecular Organization, Physical Functions and Technical Applications. Dundee, Scotland: Oily Press, pp 7–44.
Loncin, M. (1958). Influence des glycerides partiels sur la plasticite des matieres grasses. Oleagineux 13(1):33–37.
Marangoni, AG (2000). Elasticity of high-volume-fraction fractal aggregate networks: A thermodynamic approach. Phys Rev B 62:13950–13955.
Marangoni, AG, D Rousseau. (1996). Is plastic fat rheology governed by the fractal nature of the fat crystal network? J Am Oil Chem Soc 73(8):991–994.
Metin, S, RW Hartel. (1998). Thermal analysis of isothermal crystallization kinetics in blends of cocoa butter with milk fat or milk fat fractions. J Am Oil Chem Soc 75(11):1617–1624.
Morrison, WR. (1968). Surface-active lipids in milk and milk products, Surface-Active Lipids in Foods. SCI Monograph No. 32. London. Soc Chem Ind, pp 75–91.
Narine, SS, AG Marangoni. (1999a). Fractal nature of fat crystal networks. Phys Rev E 59(2):1908–1920.
Narine, SS, AG Marangoni. (1999b). Mechanical and structural model of fractal networks of fat crystals at low deformations. Phys Rev E 60(6):6991–7000.
National Dairy Council (NDC). (1993). Newer Knowledge of Milk and Other Fluid Dairy Products. Rosemont, IL: NDC.

Copyright 2002 by Marcel Dekker. All Rights Reserved.

Ng, WL. (1990). A study of the kinetics of nucleation in a palm oil melt. J Am Oil Chem Soc 67(11):879–881.
Niiya, I, T Maruyama, M Imamura, M Okada, T Matsumoto. (1973a). Effect of emulsifiers on the crystal growth of edible solid fats. Part III. Effect of saturated fatty acid monoglyceride. Jpn J Food Sci Technol 20(5):182–189.
Niiya, I, T Maruyama, M Imamura, M Okada, T Matsumoto. (1973b). Effect of emulsifiers on the crystal growth of edible solid fats. Part IV. Effect of propylene glycol ester of fatty acid and unsaturated fatty acid monoglycerides. Jpn J Food Sci Technol 20(5):191–198.
Reddy, SY, JV Prabhakar. (1987). Effect of diglycerides on the solidification properties of sal (Shorea robusta) fat. Fat Sci Technol 10:394–397.
Riiner, U. (1971). The effect of hydrolysis on the solidification of fats. Lebensm-Wiss U-Technol 4(3):76–80.
Shannon, RJ, Fenerty, RJ Hamilton. (1992). The polymorphism of diglycerides. J Sci Food Agric 60:405–417.
Sharples, A. (1966). Overall kinetics of crystallization, In: A Sharples, ed. Introduction to Polymer Crystallization. London; Edward Arnold, pp 44–59.
Siew, WL, WL Ng. (1996). Effect of diglycerides on the crystallisation of palm oleins. J Sci Food Agric 71:496–500.
Smith, PR, MJW Povey. (1997). Short communication: The effect of partial glycerides on trilaurin crystallization. J Am Oil Chem Soc 74(2):169–171.
Smith, PR, DJ Cebula, MJW Povey. (1994). The effect of lauric-based molecules on trilaurin crystallization. J Am Oil Chem Soc 71(12):1367–1372.
Strickland-Constable, RF. (1968). Nucleation of solids. In: RF Strickland-Constable, ed. Kinetics and Mechanism of Crystallization. London: Academic Press, pp 74–129.
Van den Tempel, M. (1968). Effects of emulsifiers on the crystallization of triglycerides. Surface-Active Lipids in Foods. SCI Monograph No. 32. London. Soc Chem Ind, pp 22–33.
Wähnelt, S, D Meusel, M Tülsner. (1991). Influence of diglycerides on the phase behaviour of edible fats. Fat Sci Technol 93(4):117–121.
Wright, AJ, SE McGauley, SS Narine, WM Willis, RW Lencki, AG Marangoni. (1999). Solvent effects on the crystallization behaviour of milk fat fractions. J Agric Food Chem 48(4):1033–1040.
Wright, AJ, RW Hartel, SS Narine, AG Marangoni. (2000). The effect of minor components on milk fat crystallization. J Am Oil Chem Soc 77(5):463–475.
Wright, AJ, SS Narine, AG Marangoni. (2001). Comparison of experimental techniques used in lipid crystallization studies. In: N Widlak, RW Hartel, SS Narine, eds. Crystallization and Solidification Properties of Lipids. Champaign, IL: AOCS Press, pp 120–131.
Ziegleder, G. (1990). DSC thermal analysis and kinetics of cocoa butter crystallization. Fat Sci Technol 92(12):481–485.

Copyright 2002 by Marcel Dekker. All Rights Reserved.

6

Steady-State Fluorescence Polarization Spectroscopy as a Tool to Determine Microviscosity and Structural Order in Lipid Systems

Alejandro G. Marangoni
University of Guelph, Guelph, Ontario, Canada

I. INTRODUCTION

The kinetic interactions between solvent and solute molecules in free solution determine their rotational and translational diffusion characteristics. Fluorescence polarization is a spectroscopic technique that allows the determination of motional preferences of reporter molecules in fluids with respect to both the rate of motion and the orientational restriction of that motion [1,2]. For spherical molecules in isotropic fluids at low concentrations, these motions can be described by the Stokes–Einstein and Perrin relationships, and if these motions have an equal probability of occurring in any dimension they are referred to as isotropic. However, when a fluid displays structure, or anisotropy, the motion of diffusing molecules may be restricted, generally to different extents in different dimensions, and these motions are said to be anisotropic. New approaches must then be taken in order to describe the probe's hydrodynamic behavior. By measuring the hydrodynamic properties of a fluorescent probe in solution, it is possible to extract valuable information on the physical structure and properties of a fluid. Knowledge of the physical structure and properties of food fluids and matrices is essential for solving practical problems in food research.

Copyright 2002 by Marcel Dekker. All Rights Reserved.

II. THEORY

A fluorescent molecule (fluorophore) embedded or dissolved in a rigid matrix or fluid is excited with a short pulse (for decay measurements) or a continuous beam (for steady-state measurements) of polarized monochromatic light. There are three ways by which this plane of polarized light can be depolarized by the fluorophore [1]:

1. The photoselection principle states that the probability of absorption of the incoming polarized light by a fluorophore is proportional to $\cos^2 \theta$, θ being the angle between the fluorophore's absorption dipole moment and the plane of polarization (electronic vector) of the incoming light (Fig. 1). The photoselection process is not an all-or-none process; therefore, for a population of randomly oriented fluorescent molecules, there will be a symmetrical distribution of excited molecules about the $\theta = 0$ axis (Z axis in Fig. 2). Molecules with transition dipoles not exactly aligned with the incoming plane of polarized light ($\theta > 0$) will then emit light with components both parallel and perpendicular to the plane of polarization of the incident light, leading to a depolarization of the incoming beam or pulse [3].
2. The angle between the absorption and emission transition dipole moments (α) of the fluorophore will cause a certain amount of depolarization [4], which will be proportional to the magnitude of α (Fig. 1).

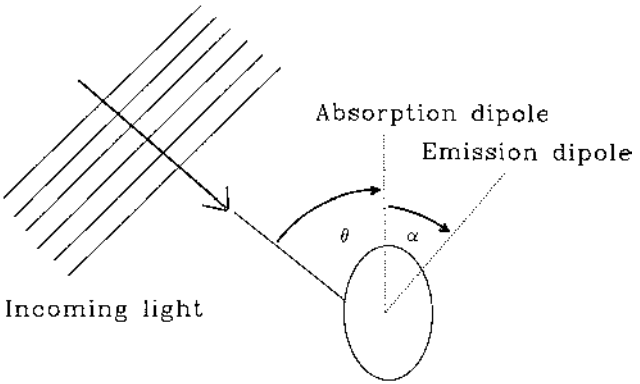

Figure 1 Schematic of the interaction of polarized light with a fluorophore. The angle θ represents the angle between the plane of incoming polarized light (electronic vector) and the absorption dipole moment, and the angle α represents the angle between the absorption and emission dipoles in the absence of molecular rotation.

Copyright 2002 by Marcel Dekker. All Rights Reserved.

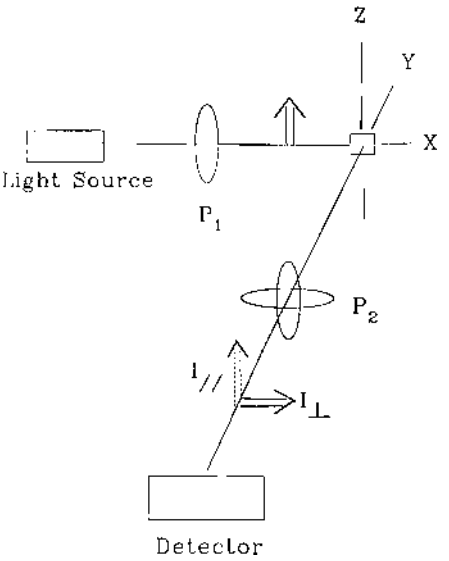

Figure 2 A typical L-format layout for the measurement of fluorescence anisotropy. A monochromatic pulse or continuous beam of light is polarized through P_1 along the *Z* axis and interacts with the sample. This interaction may cause the depolarization of the incoming plane of polarized light, which will be quantified by measuring the intensities of fluorescent light parallel and perpendicular to the incoming plane of polarization by rotating polarizer P_2.

However, for most fluorescence measurements, the absorption and emission dipoles are parallel ($\alpha = 0$), as excitation occurs at the last absorption band [5].

3. The fluorophore will absorb the incoming light, rotate, and emit light that will therefore be depolarized relative to the incoming plane of polarized light. It is this process of motional depolarization that we will be most concerned about, as it will allow us to determine the hydrodynamic properties of the fluorophore by monitoring depolarization.

A fluorophore that absorbs incoming electromagnetic radiation will undergo rotational diffusion. This rotational diffusion is best described by a ''wobbling'' rotation model (Fig. 3) [6]. The fluorophore will rotate and trace a cone that can be described by the angle between the absorption dipole and the axis of rotation (θ_a) and the angle between the emission dipole and the axis of rotation (θ_e) [3]. If the rate of rotational motion of a fluorophore in a matrix or fluid is

Copyright 2002 by Marcel Dekker. All Rights Reserved.

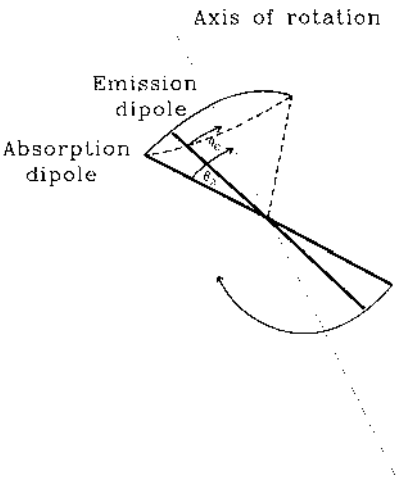

Figure 3 Typical ''wobbling'' rotation of a fluorophore tracing a cone. This rotation is characterized by the angles between the absorption dipole and the axis of rotation (θ_a), and between the emission dipole and the axis of rotation (θ_e).

on the order of the fluorescence lifetime of its excited state (the lifetime or relaxation time is the time required for the fluorescence process to fall to $1/e$ of its initial value, which on a time scale occurs in the nanosecond range) and the molecule is free to undergo rotation, then the emitted light will be depolarized relative to the plane of polarization of the exciting pulse or beam. Long fluorescence lifetimes relative to the rate of molecular rotation will lead to large depolarizations, whereas short lifetimes will lead to small depolarizations. Both are undesirable for measurement purposes. Hence, the rotational motion of the molecule will be characterized by a rotational correlation time (Φ), a time constant that characterizes the molecule's rate of rotation (ν). The rotational correlation time is the time required by the fluorophore to rotate through an arc of 1 radian [$\Phi = (2\pi\nu)^{-1}$]. From the rotational correlation time of the fluorophore it is possible to determine the submicroscopic ''viscosity'' (microviscosity) of an isotropic fluid, which is simply the intermolecular frictional force that opposes the molecule's rotational diffusion [4].

To derive a relationship between microviscosity and the fluorophore's hydrodynamic properties, it is necessary to quantify the extent of depolarization caused by the molecule's rotation. There are two ways of performing these measurements: under steady-state conditions (continuous illumination) or under time-resolved conditions (picosecond pulse excitation followed by nanosecond fluorescence emission decay). Steady-state instrumentation is relatively easy to

Copyright 2002 by Marcel Dekker. All Rights Reserved.

operate and inexpensive, and it can be used on a routine basis. However, valuable information can also be obtained from time-resolved measurements that cannot be obtained from steady-state measurements. Fortunately, much of the information that can be derived only from time-resolved experiments has been theoretically and empirically related to measurable parameters under steady-state conditions.

The extent of depolarization can be expressed as a polarization value p or an anisotropy value r, which are defined as

$$r = \frac{I_{\parallel} - I_{\perp}}{I_{\parallel} - 2I_{\perp}} \tag{1}$$

$$p = \frac{I_{\parallel} - I_{\perp}}{I_{\parallel} - I_{\perp}} \tag{2}$$

where $I_{\parallel}$ and $I_{\perp}$ are the fluorescence intensities observed through a polarizer oriented parallel and perpendicular, respectively, to the plane of polarization of the excitation pulse or beam. The geometry of such an experiment (L-format) is depicted in Figure 2. Nowadays, T-format instruments are becoming more widely used. In such an arrangement, detectors with emission polarizers (P_2) oriented parallel and perpendicular to the excitation polarizer (P_1) are placed at 90° to the sample holder, one on each side, hence a T arrangement. T-format instruments allow for the simultaneous determination of $I_{\parallel}$ and $I_{\perp}$ rather than having to rotate the emission polarizer for every measurement as in the L-format arrangement. The total intensity of the emitted light (F) is given by

$$F = I_{\parallel} + 2I_{\perp} \tag{3}$$

The greater the extent of the fluorophore's rotation, as in low-viscosity isotropic media, the greater the rotational correlation time for the probe's motion, and the greater the perpendicular fluorescence intensity component will be, resulting in a low anisotropy or polarization value.

Excitation of the fluorescent molecule in an isotropic fluid with a picosecond pulse of polarized light (generally from a laser) [7] will result in double exponential decay curves for $I_{\parallel}$ and $I_{\perp}$ and a single exponential decay curve for F, having the form (adapted from Refs. 3, 4, and 8)

$$I_{\parallel}(t) = \frac{1}{3}F_0 e^{-t/\tau} + \frac{2}{3}F_0 r_0 \exp\left[-\left(\frac{1}{\tau} + \frac{1}{\Phi}\right)t\right] \tag{4}$$

$$I_{\perp}(t) = \frac{1}{3}F_0 e^{-t/\tau} - \frac{1}{3}F_0 r_0 \exp\left[-\left(\frac{1}{\tau} + \frac{1}{\Phi}\right)t\right] \tag{5}$$

Copyright 2002 by Marcel Dekker. All Rights Reserved.

$$F(t) = I_{\parallel}(t) + 2\, I_{\perp}(t) = F_0 e^{-t/\tau} \tag{6}$$

It is evident from these decay curves that the decrease in the intensity of the emitted parallel and perpendicular fluorescence components as a function of time will depend on the initial total peak intensity of the emitted fluorescent light (F_0), on the limiting fluorescence anisotropy (r_0), and on the lifetime of the excited state (τ) as well as on the rotational correlation time of the molecule (Φ).

The value r_0 is the limiting fluorescence anisotropy, that is, the anisotropy of a fluorophore in the absence of rotational diffusion. Usually, this parameter is determined by measuring the anisotropy of a probe dissolved in ethylene–propylene glycol or propylene glycol–glycerol (or appropriate fluid) at low temperatures (−50 to −70°C). A quantitative relationship therefore exists between the angle α (the angle between the absorption and emission dipoles) and the limiting fluorescence anisotropy [3]:

$$r_0 = \frac{3\cos^2 \alpha - 1}{5} \tag{7}$$

Maximum values for r_0 are observed when the absorption and emission dipoles are collinear ($\alpha = 0$, $r_0 = 0.4$).

It is possible, then, to monitor the decay of the anisotropy value as a function of time by simply incorporating the time-dependent decays in perpendicular and parallel fluorescence intensities into Eq. (1):

$$r(t) = \frac{I_{\parallel}(t) - I_{\perp}(t)}{I_{\parallel}T) - 2I_{\perp}(t)} = r_0 e^{-t/\Phi} \tag{8}$$

From Eq. (8) it can be seen that the decay in anisotropy is solely dependent on the limiting fluorescence anisotropy r_0 and the rotational correlation time Φ of the fluorophore. The time-resolved decay in anisotropy for a fluorophore in an isotropic medium is shown in Figure 4 (curve *b*).

Steady-state measurements correspond to the summation of the time–response function over times from zero to infinity for the fluorescence intensities [8], whereas for the anisotropy it is the summation of $r(t)$ over $F(t)$ from zero to infinity. Therefore, the steady-state values for $I_{\parallel}(t)$, $I_{\perp}(t)$, and $r(t)$, Which are designated by $I_{\parallel}$, $I_{\perp}$, and r_s, respectively, are given by

$$I_{\parallel} = \frac{1}{\tau}\int_0^{\infty} I_{\parallel}(t)\, dt \tag{9}$$

Copyright 2002 by Marcel Dekker. All Rights Reserved.

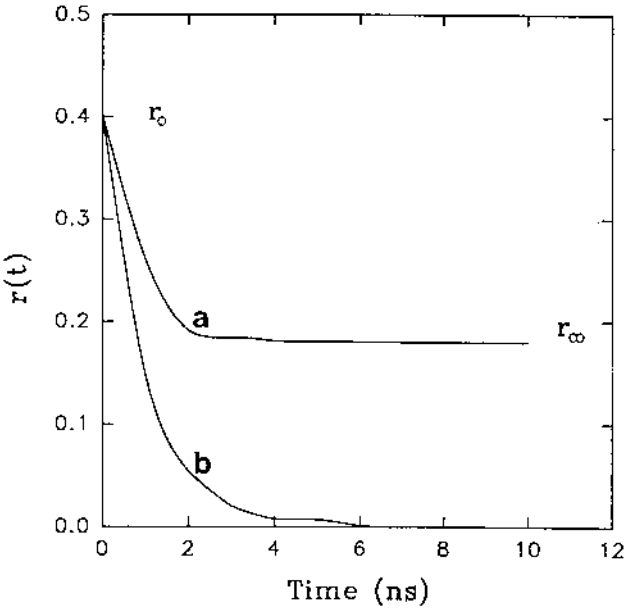

Figure 4 Exponential decay curves for the time-resolved anisotropy of a fluorophore excited with a picosecond pulse of monochromatic light. The molecule is rotating with a rotational correlation time of 1 ns. Curve *a* represents a typical decay curve in an anisotropic medium, and curve *b* represents a typical decay curve in an isotropic medium. The limiting anisotropy r_0 and infinite time anisotropy r_∞ are shown in the figure.

$$I_\perp = \frac{1}{\tau}\int_0^\infty I_\perp(t)\, dt \tag{10}$$

and

$$r_s = \frac{\int_0^\infty r(t)F(t)\, dt}{\int_0^\infty F(t)\, dt} \tag{11}$$

If this approach is followed, the general form of the Perrin equation can be obtained, which relates the steady-state fluorescence anisotropy (r_s) of a spherical fluorophore rotating in an isotropic medium to its rotational correlation time (Φ):

Copyright 2002 by Marcel Dekker. All Rights Reserved.

$$\frac{r_0}{r_s} = 1 + \frac{\tau}{\Phi} \tag{12}$$

The rotational correlation time Φ is related to the viscosity of the isotropic medium (η) and the hydrodynamic volume of the rotating unit (V) by

$$\Phi = \frac{\eta V}{RT} \tag{13}$$

Hence,

$$\frac{r_0}{r_s} = 1 + \frac{RT\tau}{\eta V} \tag{14}$$

$$\frac{1}{r_s} = \frac{1}{r_0} + \frac{R}{r_0}\left(\frac{T\tau}{\eta}\right) \tag{15}$$

where r_0 is the limiting fluorescence anisotropy, r_s is the steady-state fluorescence anisotropy, R is the universal gas constant, T is the absolute temperature, τ is the fluorescence lifetime of the fluorophore, V is the hydrodynamic volume of the rotating unit, and η is the solvent viscosity. Generally, R and V are grouped into a single constant C, which should be expressed as $C(r)$, because it shows a slight dependence on the value or r_s:

$$\frac{1}{r_s} = \frac{1}{r_0} + \frac{C(r)}{r_0}\left(\frac{T\tau}{\eta}\right) \tag{16}$$

Alternatively, the fluorescence lifetime (τ) and limiting fluorescence anisotropy (r_0) can also be incorporated into the constant, resulting in a new constant that takes into account the contributions of the fluorescence lifetime and limiting anisotropy, yielding

$$\frac{1}{r_s} = \frac{1}{r_0} + K(r)\frac{T\tau}{\eta} \tag{17}$$

Hence, it is possible to construct a standard curve relating viscometric measurements to steady-state anisotropy measurements for a particular fluid and use the quantitative relationship to determine the viscosity of the fluid by fluorescence polarization [4,9–11]. A standard curve in a reference ''calibration'' oil such as white paraffin oil can be used to determine the viscosity of another fluid as long as the calibration fluid is similar in dielectric constant and viscosity to the fluid being analyzed. It is important to keep in mind that the same fluorescent probe may display different behavior even in different hydrocarbon calibration oils, hence one must exercise caution when determining absolute values for microvis-

Copyright 2002 by Marcel Dekker. All Rights Reserved.

cosity. Historically, American White Oil USP35 has been used as the calibration fluid for the study of hydrocarbon-like fluids. Regardless of these limitations, the microviscosity values derived from the Perrin equation, even when they are only ''apparent'' values, are the best approximation to the value of the ''true'' microviscosity of the system. On the other hand, if the calibration and test fluids are of similar viscosities and dielectric constants, a true, absolute value for viscosity can be obtained.

The relationships derived with the Perrin equation apply only to spherical fluorophores, which generally does not include fluorescent dyes [9]. If a fluorescent molecule has a planar structure, serious deviations from the Perrin equation can occur. It is therefore essential to determine which molecular motions result in the observed depolarizations and how the latter relate to the structure of the fluorescent probe. The rate of rotation of the fluorophore is an average of the in-plane (ν_{ip}) and out-of-plane (ν_{op}) rates of rotation [9]. The in-plane rotation is about an axis normal to the ring plane, whereas the out-of-plane rotation is about an axis contained in the ring plane at right angles to the absorption oscillator. There are three cases of interest in relation to the Perrin equation:

1. When $r_0 = 0.4$, $\alpha = 0$, that is, when the absorption and emission dipoles are collinear, generally when the dye is excited at the last absorption band, ν (or Φ) corresponds to the average of the in-plane and out-of-plane rates of rotation of the molecule.
2. When $r_0 = 0.1$, $\alpha = 45°$, ν corresponds to the out-of-plane rate of rotation only.
3. When $r_0 = -0.25$, $\alpha = 90°$, ν corresponds to the in-plane rate of rotation only.

It is only in the first case that the Perrin equation can be applied reasonably accurately. Under those conditions where the measured rate of rotation corresponds to the average of the in-plane and out-of-plane rates of rotation, the corresponding microviscosity is the harmonic mean of the effective viscosities opposing the in-plane and out-of-plane rotation and should be referred to as η, the ''effective'' microviscosity of an equivalent spherical rotating unit. The hydrodynamic volume of the rotating fluorophore, V [see Eq. (14)], would then correspond to the effective volume of a rotating sphere and should be referred to as V_0. Hence, in addition to being able to determine the microviscosity from the values of the rotational correlation time or the rate of rotation, it is possible to evaluate the structural order or degree of anisotropy of a fluid by monitoring the changes in the rate of rotation (ν) with changes in the maximal anisotropy (r_0). This is achieved by determining the rate of rotation or rotational correlation time by the Perrin equation [11] as a function of r_0:

$$\nu = \frac{r_0/r_s - 1}{2\pi\tau} \tag{18}$$

Copyright 2002 by Marcel Dekker. All Rights Reserved.

Different values for r_0 are obtained by exciting the fluorophore at different wavelengths (an excitation spectrum) in a dense medium at low temperatures, that is, in the absence of molecular rotation. This procedure allows us to ''map'' the transition dipoles of the molecule embedded in the fluid [4,9]. If the motions of the molecule are isotropic, and if the medium is isotropic, then the plot of ν vs. r_0 should be a straight line. However, if the plot shows that there the rate of rotation has a strong dependence on the limiting anisotropy, this means that the depolarizing rotations are anisotropic and/or that the medium is anisotropic. By determining the rate of rotation of the fluorophore at r_0 values of 0.1 and -0.25, it is possible to calculate ν_{op} and ν_{ip}, respectively, using Eq. (18). From the determined rates of rotation, the respective rotational correlation times can be calculated and subsequently used to determine the ratio of in-plane to out-of-plane microviscosities:

$$\frac{\nu_{op}}{\nu_{ip}} = \frac{\Phi_{ip}}{\Phi_{op}} = \frac{\eta_{ip}}{\eta_{op}} \tag{19}$$

This ratio is an indication of the ''structural order'' of the fluid matrix, and for an isotropic fluid it should be close to unity [4]. In order to differentiate between anisotropy of the medium and that of the molecular rotations, one should compare the ν vs. r_0 plots (determined from the steady-state anisotropy measurements at low temperatures in high density fluids at different excitation wavelengths) for a particular fluorophore embedded in an isotropic medium to a similar plot for the probe embedded in the test fluid. If, for example, a strong dependence of ν on the value of r_0 is evident for both media and the ratio of in-plane to out-of-plane rotational rates is very high (>10), one can conclude that the rotations are anisotropic but the medium is isotropic. The technique of differential polarized phase fluorometry [8,12], which is beyond the scope of this chapter, has been successfully applied to study the types of rotations displayed by fluorophores embedded in different media.

If the medium is highly ordered or anisotropic, the Perrin equation does not hold and microviscosity can be used only qualitatively. In this case, a fluorophore is restricted to certain motions that will occur to different extents in different dimensions. An example of such a phenomenon would be a fluorescent molecule that would align itself along the fatty acid chains of phospholipids in the phospholipid bilayer of a liposome. For fluorophores in an anisotropic medium, the time-resolved fluorescence anisotropy does not fall to zero (see Fig. 4, curve a), that is, the depolarizing rotations of the fluorophore will not attain an isotropic distribution at infinite time. The anisotropy will decay to an ''infinite-time'' anisotropy (r_∞) rather than to zero and will have the form

$$r(t) = (r_0 - r)e^{-t/\Phi} + r_\infty \tag{20}$$

Copyright 2002 by Marcel Dekker. All Rights Reserved.

By deriving a modified Perrin equation for anisotropic motion in anisotropic media, similarly to the isotropic case, one obtains

$$r_f = \frac{r_0 - r_\infty}{1 + \tau/\Phi} + r_\infty = r_s + r_\infty \tag{21}$$

where r_f is the kinetic component of the decay, determined by the time constants of the decay, and r_∞ corresponds to the infinite-time, static, ''structural order'' component of the decay [6,13,14]. The value of r_∞ is determined by the degree to which the emission dipoles are prevented from attaining an isotropic distribution at infinite time [3]. Equations (20) and (21) pertain to situations where the anisotropic decay can be described by a single rotational correlation time (Φ).

Owing to the enormous differences between the rotational motions of a fluorophore in an isotropic medium and those of a fluorophore in an anisotropic medium, it is not possible to use a standard Perrin calibration curve generated from an isotropic calibration fluid [Eq. (16)] to determine the microviscosity of a highly ordered system from anisotropy measurements [using Eq. (21)]. A phospholipid–triglyceride micelle in an aqueous medium, for example, will display gradients in microviscosity from the water/phospholipid interface to the interior core of the micelle. Fluorophores that partition into the core of the emulsion can be used to monitor the microviscosity of the interior of the micelle, whereas fluorophores that align themselves along the fatty acid chains of the phospholipid monolayer coating the oil droplet can be used only to monitor the structural order of the monolayer. A microviscosity value for the phospholipid monolayer would be neither accurate nor useful in describing the physical properties of this region. In the case of a liposome phospholipid bilayer, with an even higher level of structure, the concept of microviscosity becomes even less useful. Fluorescent probes are not spherical and are generally the same size as the surrounding molecules; hence, the Einstein–Stokes hydrodynamic theory does not apply. The bulky fluorophore will also perturb the packing of the fatty acid chains [15]. Microviscosity gradients from the surface to the core of the membrane represent an additional problem because of the large volume element of the probe relative to the surrounding molecules. The probe itself will experience different microviscosities along its molecular backbone [3]. Another approach must be taken for the study of membranes, monolayers, and phospholipid bilayers. The determination of the structural order of such an ordered system can prove to be very useful [6,13,16].

A model independent form for the structural order parameter S has been derived [17] that has the form

$$S = \left(\frac{r_\infty}{r_0}\right)^{1/2} \tag{22}$$

Copyright 2002 by Marcel Dekker. All Rights Reserved.

Van Blitterswijk et al. [6] used time-resolved fluorescence anisotropy to measure the infinite-time anisotropy (r_∞) (refer to Fig. 4) and the limiting anisotropy (r_0) for a series of biological and artificial membranes, plotted the infinite-time anisotropy (r_∞) versus the measured steady-state anisotropy (r_s), and obtained a linear relationship for the probe 1,6-diphenylhexatriene (DPH):

$$r_\infty = \frac{4}{3} r_s - 0.1 \tag{23}$$

for $0.13 < r_s < 0.28$.

Van der Meer et al. [16] extended this equation to a general case having the form

$$r_\infty = \frac{r_0 r_s^2}{r_0 r_s + (r_0 - r_s)^2/m} \tag{24}$$

where m is a constant that expresses the difference between the rotational diffusion of the probe in the membrane (or anisotropic matrix) and that in the isotropic reference oil. Values of m for different probes embedded in a series of membranes are listed in the paper by van der Meer et al. [16]. The power of this technique in the determination of the ''structural order'' of a system is tremendous, as will be appreciated in Section III.

Presently, there are a myriad of fluorophores that can be used in fluorescence polarization experiments. An ideal hydrocarbon employed as a fluorescence probe should have the following characteristics [9]:

1. Rigid structure to avoid depolarization due to rotations of side groups.
2. High and constant r_0 values when excited in the last electronic absorption band. These properties provide a depolarization that is unaffected by small shifts in the absorption spectrum;.
3. Regions in the absorption spectrum for which $r_0 = 0.1$ and -0.25, for the evaluations of in-plane and out-of-plane rotations of the fluorophore.
4. A lifetime of the excited state in the range of 1–8 ns. For such lifetimes, values of r_0/r_s are such that microviscosities in the range of 1–100 mPa/s can be measured with reasonable accuracy.
5. High values for the extinction coefficients and quantum yield, because these will increase the fluorescence signal.
6. Minimum overlap between absorption and emission spectra, to eliminate depolarization due to energy transfer in the case of high local concentration of the probe.
7. Inexpensive, readily available, and nontoxic.

Copyright 2002 by Marcel Dekker. All Rights Reserved.

Certain precautions must be taken when measuring fluorescence anisotropy. Scattering of the polarized light from slightly turbid samples may cause an artificial increase in the measured anisotropy of light, whereas scattering of the emitted fluorescent light may reduce the measured anisotropy [9]. Hence, a correction for light scattering must be included in all measurements, using the equation [18]

$$r_s = \frac{(I_{\parallel} - I^s_{\parallel}) - (I_{\perp} - I^s_{\perp})G}{(I_{\parallel} - I^s_{\parallel}) + 2(I_{\perp} - I^s_{\perp})G} \tag{25}$$

where $I^s_{\parallel}$ and $I^s_{\perp}$ are the intensities of the measured light emitted from the unlabeled sample, i.e., in the absence of the fluorophore (a ''blank''), through polarizers arranged parallel and perpendicular to the excitation polarizer (see Fig. 2).

However, if the contribution of the scattered light to the total intensity of the fluorescent components is smaller than 5%, this contribution can be safely neglected. Stray light can be filtered out by using interference (bandpass) filters on the excitation side, and scattered light on the emission side can be filtered out with cutoff filters. The factor G is an instrumental factor that is usually close to unity. G is the ratio of the intensity of emitted fluorescent light with the excitation and emission polarizers both aligned horizontally ($I_{\perp\perp}$) to the intensity of the emitted fluorescent light with the excitation and emission polarizers aligned horizontally and vertically, respectively ($I_{\perp\parallel}$).

Figure 5 shows the structures of three of the most common types of probes presently used: 1,6-diphenyl-1,3,5-hexatriene (DPH), *trans*-parinaric acid (*t*-PA), and the *n*-(9-anthroyloxy) fatty acids (9-AS), DPH is by far the best studied probe. It has excellent properties—an r_0 of 0.4 (emission and excitation dipoles are collinear), a maximal fluorescence lifetime of the excited state of 11.4 ns—the resulting depolarizations are mainly due to out-of-plane rotations, and it is readily available and inexpensive. DPH will partition deep into a phospholipid bilayer and would partition into the core of a micelle. *trans*-Parinaric acid also proves to be a very useful probe in the study of emulsions and phospholipid bilayers, because the carboxyl group will partition into the aqueous phase while the fatty acid chain aligns itself with the fatty acid chains of the phospholipids or surfactants, probing that particular region of the structure. The anthroyloxy fatty acids work in the same fashion as *t*-PA; however, it is also possible to monitor gradients in the structural order of a bilayer or emulsion monolayer by using probes with the anthroyloxy group attached to different carbons along the fatty acid chain. This makes it possible to obtain a transverse section of order along the bilayer/monolayer. Other probes include the trimethylamine (TMA) derivative of DPH (which can be used as a ''surface'' probe); perylene, a large four-membered aromatic planar molecule that has useful properties [9]; and 4-heptadecyl-7-hydroxycoumarin, which has been used as a probe for the headgroup region of lipid

Copyright 2002 by Marcel Dekker. All Rights Reserved.

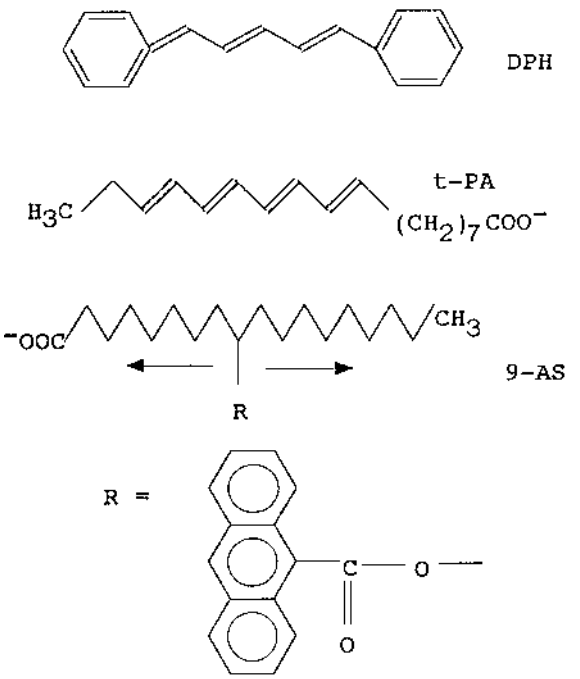

Figure 5 Structural formulas for some commonly used fluorophores in fluorescence anisotropy experiments: 1,6-diphenyl-1,3,5-hexatriene (DPH), *trans*-parinaric acid (*t*-PA), and the *n*-(9-anthroyloxy) fatty acid series (9-AS).

phospholipid bilayers [19]. A point to keep in mind is that when using a fluorescent probe that is covalently attached to a larger structure (*e.g.*, phospholipid-DPH), the rate of rotation observed is that of the complex and not the fluorophore alone. Several companies produce common and more specialized probes for any particular application.

The next section presents examples of the many applications of fluorescence polarization spectroscopy in food research, some of which are presently being developed in my laboratory.

III. APPLICATIONS

Some practical applications of steady-state fluorescence polarization spectroscopy in food-related research are presented in this section. The nature of the

Copyright 2002 by Marcel Dekker. All Rights Reserved.

technique makes it ideal for the study of the viscosity of oil and oil products, the structure and properties of emulsions and liposomes, and the structure and function of biological membranes. From the theory presented it is possible to gain insight into the structure of lipid fluids and matrices relevant to food research. By developing a better understanding of the structural parameters and physical properties of foods and food components, it is possible to better predict the performance and stability of a food product. For a complete and thorough outline of the experimental technique of fluorescence polarization, the reader is referred to the paper by Nealon et al. [18].

A. Viscosity and Structure of Vegetable Oils

The viscosity of edible oils can be accurately determined with the aid of fluorescence anisotropy, because they behave as isotropic fluids. In order to investigate this potential application, canola oil, canola margarine fat, and heavy white paraffin oil were labeled with DPH (Sigma, St. Louis, MO) at a concentration of 2 mM. Labeling with DPH was performed by adding 2 μL of a 1 mM solution of DPH in tetrahydrofuran to 1 mL of the oils and fat with constant stirring. A Shimadzu RF540 recording spectrofluorophotometer (TekScience, Mississauga, ON) was used for these experiments. Canola oil and margarine were purchased from a local supermarket. Canola margarine fat was extracted by melting the margarine, separating the aqueous and fat layers, drying the fat layer over Na_2SO_4, and filtering it through a Whatman No. 1 filter. Canola oil was dried over Na_2SO_4 and filtered through a Whatman No. 1 filter. Purified heavy white paraffin oil USP/FCC (Fisher, St. Louis, MO) of a Saybolt viscosity of 335/350 was used without further purification. The incorporation of DPH into the oils and melted fat was immediate, and no lag time was observed. Generally, fluorescent probes partition slowly into a hydrophobic phase (as in the case of an emulsion or an aqueous dispersion of liposomes), where their fluorescent yield increases dramatically. This can be monitored by measuring increases in fluorescence intensity as a function of time. Anisotropy measurements should not be performed until the measured fluorescence intensity has reached a plateau value, which corresponds to complete partition of the probe into the hydrophobic phase. The emission spectrum of DPH in the paraffin oil is shown in Figure 6. DPH shows an emission maximum at 435 nm. The contribution of unlabeled paraffin oil to the fluorescence intensities was less than 5%. The contributions to the measured fluorescence intensities of unlabeled canola oil and margarine fat were 46% and 73%, respectively, which are outside the range of usefulness for fluorescence anisotropy measurements. However, as will be evident later, these contributions were not from scattering components but rather from other fluorescent molecules present in the oil and margarine, which proved to be useful in our anisotropic measurements.

Copyright 2002 by Marcel Dekker. All Rights Reserved.

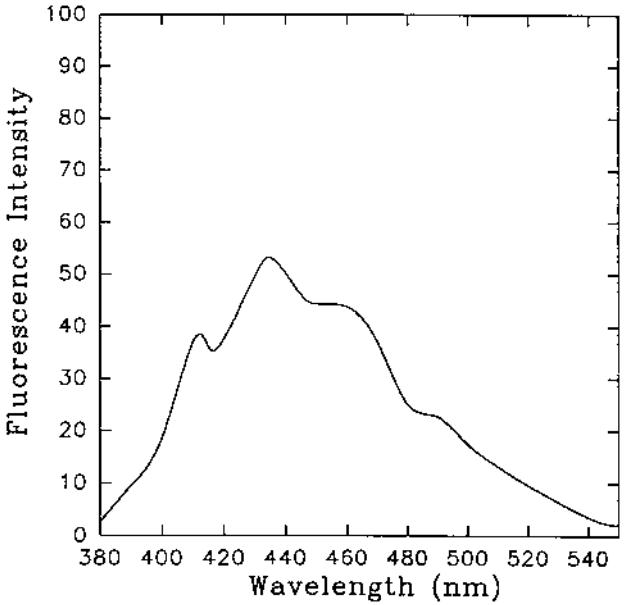

Figure 6 Fluorescence emission spectrum of 2 mM DPH dissolved in heavy white paraffin oil at 50°C, excited at 360 nm.

The temperature dependence of the DPH anisotropy in canola oil and paraffin oil is presented as curves *a* and *b*, respectively, in Figure 7. Canola margarine was not included because it crystallized at 40°C, the matrix became opaque, and no fluorescence signal was detectable. To correlate viscosity to fluorescence anisotropy, the viscosity of the two oils and the fat were measured by rotational viscometry (Fig. 8) at temperatures above 50°C to ensure that all fat was melted. Samples were equilibrated at 50°C for 6 h prior to measurements to destroy any thermal history of the system. All samples displayed Newtonian rheological behavior.

In order to apply the Perrin equation [Eq. (16)] the value for the fluorescence lifetime of the excited state at different temperatures has to be determined. In the absence of a fluorometer with time-resolved measurement capabilities, this is performed by measuring the total fluorescence intensity [Eq. (3)] as a function of temperature. This was performed only for paraffin oil, because the other samples showed high interference. The fluorescence intensity reaches a plateau at 0–10°C. The value for the lifetime of DPH in the absence of dynamic quenching processes (at low temperatures) is 11.4 ns (τ_0) and is proportional to the plateau

Copyright 2002 by Marcel Dekker. All Rights Reserved.

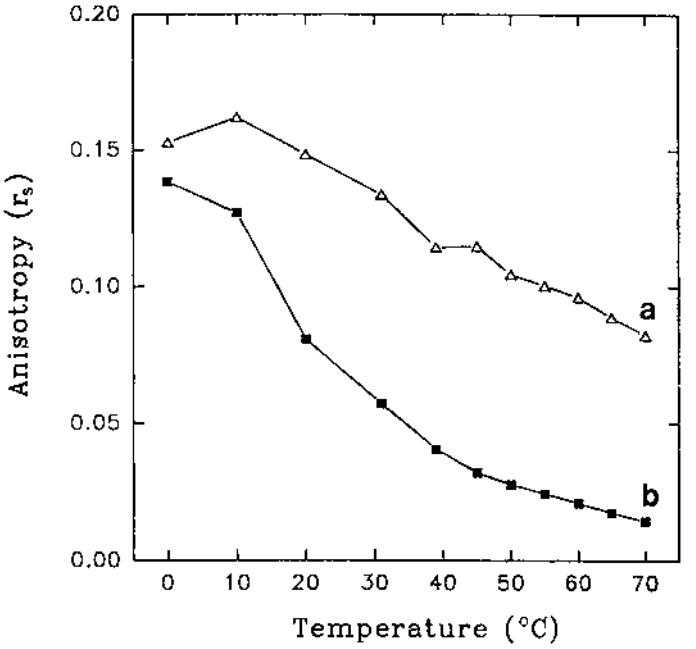

Figure 7 Temperature dependence of the measured steady-state anisotropy in DPH-labeled canola oil (a) and heavy white paraffin oil (b). Samples were excited at 360 nm, and emission was measured at 435 nm; excitation and emission slits were set at 2 nm and 5 nm, respectively.

value of the total fluorescence intensity. The lifetime of the excited state (τ) can therefore be calculated as

$$\tau = \frac{F}{F_0}\tau_0 \tag{26}$$

where F is the measured total intensity of fluorescent emission at temperature T, F_0 is the measured ''plateau'' total intensity of fluorescent emission at low temperatures, and τ_0 is the lifetime of the excited state in the absence of dynamic quenching processes. It is best to use the quantum yield (the fraction of excited molecules that become de-excited by fluorescence or ''fluorescence efficiency'') rather than the fluorescence intensity in the determination of the lifetime of the excited state. Using quantum yields minimizes potential interferences from other fluorescent molecules and compensates for instrumental factors. This is achieved

Copyright 2002 by Marcel Dekker. All Rights Reserved.

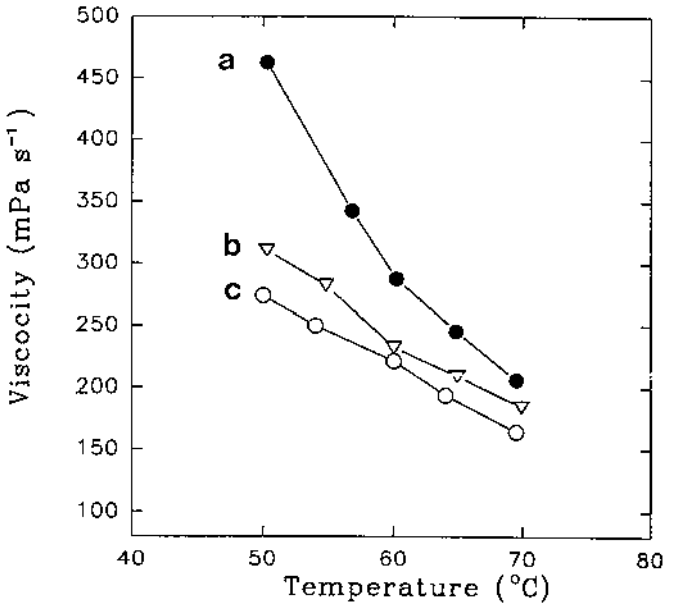

Figure 8 Temperature dependence of the measured macroscopic viscosity of heavy white paraffin oil (a), canola margarine (b), and canola oil (c). Viscometric measurements were performed with a Haake RV3 rotary viscometer using an MVIIP probe (r = 18.4 mm, height 60 mm) and a 21 mm radius cup. Temperature was controlled with a Haake F3 circulating water bath, and sample temperature was monitored with a YSI Model 42SC Tele-thermometer. Viscosity was calculated from the slope of the shear stress vs. shear strain plots taking six points in the shear strain rate region between 3.52 and 79.64 s^{-1}.

by measuring the fluorescence intensity of a standard fluorescent solution for which the quantum yield has been determined. One such solution is 0.5 M quinine sulfate in sulfuric acid, which has a quantum yield of 0.7 and can be used to calibrate the intensity values obtained from the spectrofluorophotometer [1].

The temperature dependence of the DPH fluorescence lifetime in paraffin oil is shown in Figure 9. The lifetime values derived from this experiment were used in the derivation of Perrin equations for all systems [Eq. (16)]. Perrin plots for canola oil, canola margarine fat, and heavy white paraffin oil are shown in Figure 10. These curves can be used for the determination of viscosities at different temperatures by measuring steady-state anisotropies. The correlations obtained are presented in Table 1.

The viscosities of the fats and oils in the temperature range chosen can be determined by steady-state fluorescence polarization by measuring the anisotropy

Copyright 2002 by Marcel Dekker. All Rights Reserved.

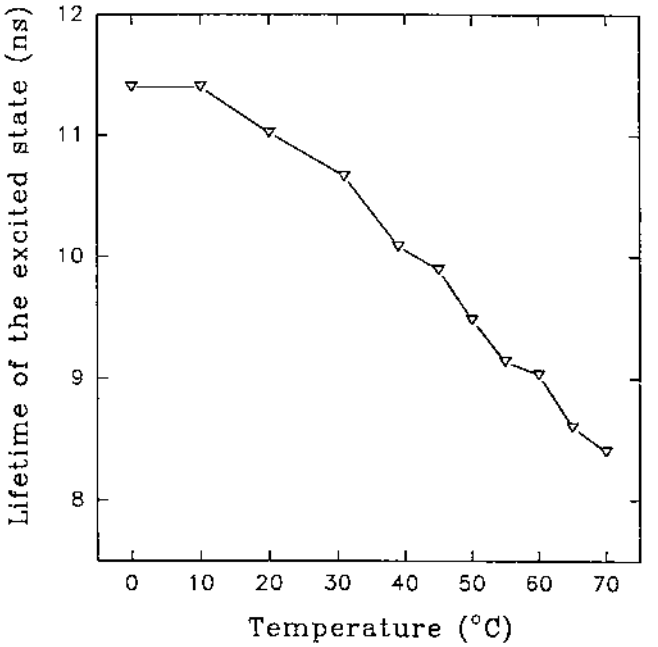

Figure 9 Temperature dependence of the lifetime of the excited state (τ) of DPH in heavy white paraffin oil. Lifetime of the excited state was calculated as the ratio of the total fluorescence intensity at 0°C to the total intensity at a particular temperature multiplied by 11.4 ns, which is the lifetime of DPH in the absence of dynamic quenching processes. At low temperatures the quantum yield approaches 1 in the absence of static quenching processes. The value of τ is used in the Perrin equation.

value at a specified temperature and deriving a viscosity value from the Perrin plots. It was not possible to use the white paraffin oil as a standard for the determination of viscosities for canola oil and margarine because of the high level of endogenous fluorescence of the latter. The anisotropy values measured for canola oil and canola margarine fat, in the absence and presence of DPH, followed the same trends (Fig. 11). It was therefore hypothesized that the antioxidants present in the oil and margarine were contributing to the motional depolarization and hence to the measured anisotropy. Scattering effects were disregarded because the samples were clear. It was therefore possible to construct a Perrin plot with the anisotropy values determined for unlabeled oil and margarine fat (this effect was not observed in paraffin oil) according to Eq. (17), because the fluorescence lifetimes of the fluorescent species were not known. This finding could prove to be quite useful in quality control operations. If no antioxidants had been present

Copyright 2002 by Marcel Dekker. All Rights Reserved.

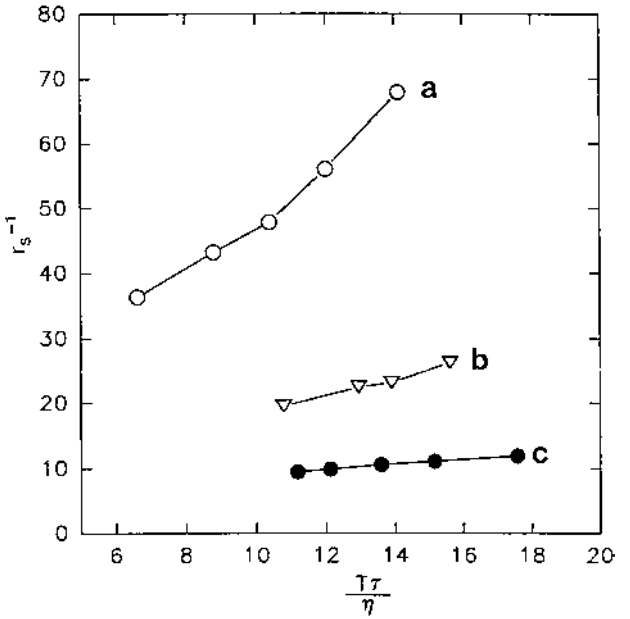

Figure 10 Perrin plot for heavy white paraffin oil (a), canola margarine fat (b), and canola oil (c).

in the oil, more reliable values for the microviscosity could have been obtained and the r_s–viscosity relationships derived for paraffin oil could have been applied to the canola oil and canola margarine fat systems. This technique could be used to monitor increases in oil viscosity during hydrogenation or interesterification, or analytically in product development and research applications.

Table 1 Slope, Intercept, and Correlation Coefficient for the Perrin Equations Derived for Canola Oil, Canola Margarine Fat, and Heavy White Paraffin Oil[a]

Sample	Intercept	Slope	Correlation coefficient
Paraffin oil	6.96185	4.16960	0.987
Canola oil	5.26837	0.38282	0.996
Canola margarine	4.64320	1.36544	0.992

[a] $\frac{1}{r_s} = \frac{1}{r_0} + K(r)\frac{T\tau}{\eta}$.

Copyright 2002 by Marcel Dekker. All Rights Reserved.

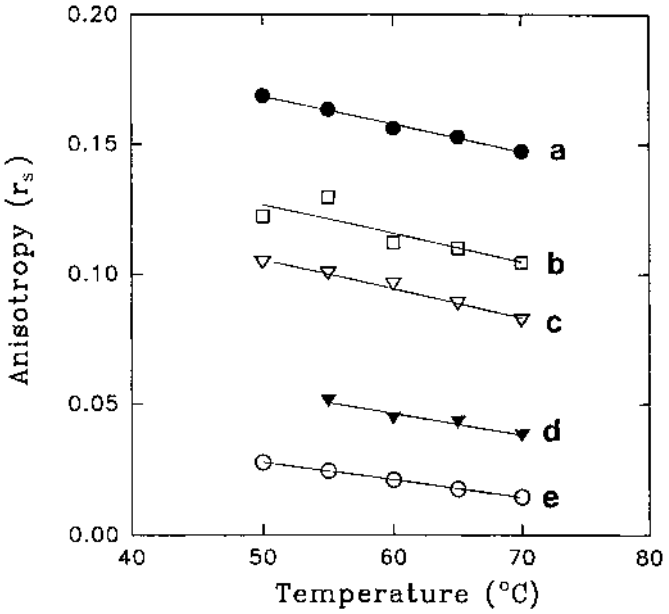

Figure 11 Temperature dependence of the measured steady-state anisotropy for (a) unlabeled canola oil, (b) unlabeled canola margarine fat, (c) DPH-labeled canola oil, (d) DPH-labeled canola margarine fat, and (e) DPH-labeled heavy white paraffin oil.

The power of this technique in studying the structure of food systems is exemplified by monitoring the changes in the rotational correlation time Φ of DPH in canola oil [as determined by Eq. (12)] as a function of temperature (Fig. 12). The rotational correlation time versus temperature plot changes slope at 40°C, suggesting that some microenvironment or the whole system is undergoing a structural change. Such behavior was not observed in the paraffin oil. The increases in Φ would suggest that the probe has become more immobilized. At temperatures below 10°C, the decreases in Φ are due to the crystallization of the oil and subsequent increase in turbidity. The effects of these structural changes could aid us in developing an understanding of the functionality of canola oil as a food ingredient and help to predict its performance in a food product.

B. Effects of Cholesterol on Cellular Membranes

In order to study the effects of cholesterol on biological membranes, it is necessary to study these effects in artificial membranes. Dipalmitoylphosphatidylcholine vesicles labeled with DPH show a phase transition at 41–42°C (Fig. 13, curve

Copyright 2002 by Marcel Dekker. All Rights Reserved.

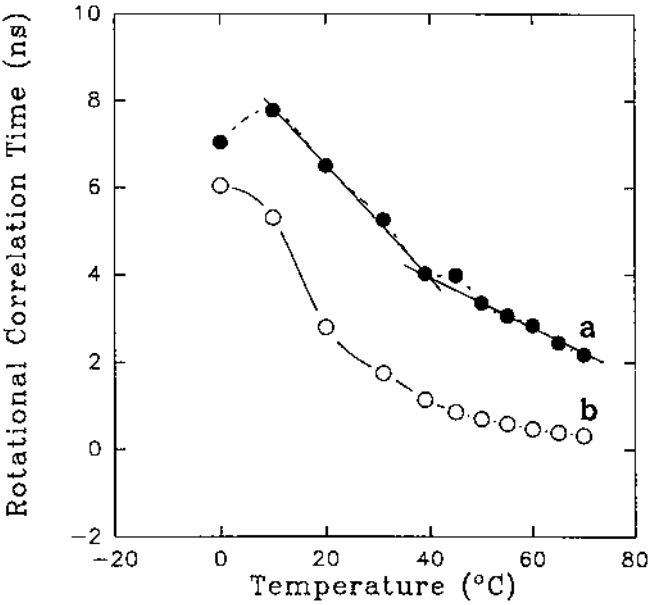

Figure 12 Temperature dependence of the rotational correlation time Φ of DPH in canola oil (a) and in heavy white paraffin oil (b). Notice an abrupt change in Φ at 40°C for DPH rotating in canola oil, suggesting a possible change in the structural characteristics of the oil.

b), as determined by measuring the polarization value *p* [Eq. (2)] at different temperatures across the phase transition temperature. In this transition, the bilayer phospholipids undergo a transition from a solid gel, in which the fatty acid chains are arranged in an all-trans configuration and trans–gauche isomerizations about the C—C bonds are restricted, to a liquid crystalline phase, in which the phospholipid fatty acid chains are less ordered, the average thickness of the bilayer decreases, and trans–gauche isomerizations about the C—C bonds are not restricted. DPH is known to partition equally into solid gel and liquid crystalline phases [20]. Cholesterol, when incorporated into the bilayer at a 45 mol% basis, will prevent this transition from occurring by incorporating into the membrane and increasing the order of the system in the liquid crystalline state and decreasing the order of the system in the solid gel state, thus preventing the formation of the solid gel phase at temperatures below the phase transition temperature (Fig. 13, curve a). Fluorescence polarization has proven to be an invaluable technique in the development of the understanding of the effects of cholesterol, fatty acid unsaturation, divalent cations, fatty acid chain length, and phospholipid head-

Copyright 2002 by Marcel Dekker. All Rights Reserved.

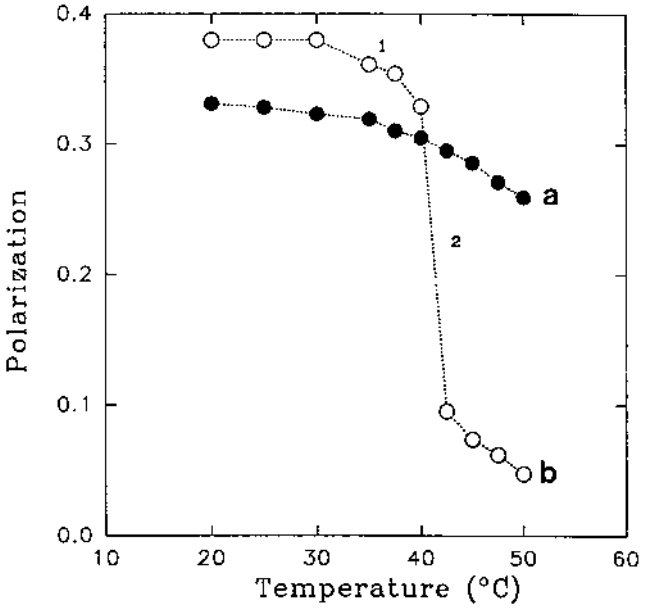

Figure 13 Dipalmitoylphosphatidylcholine liposomes undergo a phase transition at 41–42°C (curve *b*). This transition is characterized by a pretransition (region 1 in curve *b*) and a main transition (region 2 in curve *b*) and has been shown to be a solid gel-to-liquid crystalline transition of the membrane phospholipids. This phase transition is abolished when cholesterol is incorporated in the membranes at 45 mol% (curve *a*). Cholesterol increases the order of membranes in the liquid crystalline phase and decrease the order of membranes in the solid gel phase. (Adapted from Ref. 3.)

group type on the physical properties and hence biological function of membranes.

C. Microviscosity and Structure of Emulsions

The viscosity of the interior of micelles and the effects of surfactants on the structure and physical properties of the micelle can be determined by fluorescence polarization. Shinitzky et al. [9] studied the effects of introducing uncharged hydrophilic groups into the surface of a micelle on the fluidity of the micelle interior. Cetyl alcohol (CA) and cetyltrimethylammonium bromide (CTAB) were mixed in different ratios, and the microviscosity of the interior of the micelle was determined by measuring the polarization value of perylene embedded in

Copyright 2002 by Marcel Dekker. All Rights Reserved.

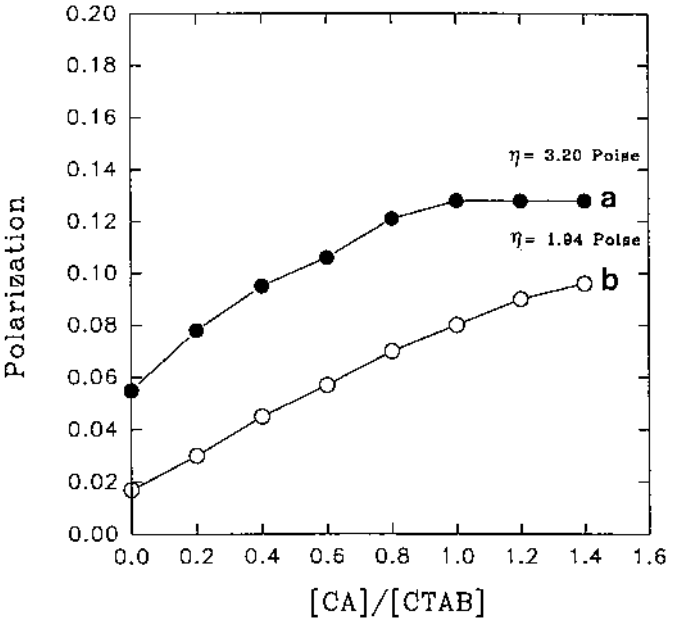

Figure 14 Fluorescence polarization (p) of perylene-labeled cetyl alcohol (CA)–cetyltrimethylammonium bromide (CTAB) mixed micelles at different molar ratios at 2.5°C (a) and 27.0°C (b). (Adapted from Ref. 9.)

the core of the micelle. Figure 14 shows the changes in the measured polarization value as a function of the molar ratio of CA to CTAB at 2.5 and 27.0°C. As the proportion of CA is increased, the microviscosity of the micelle interior increases, especially at small proportions of CA, and reaches a plateau value at 2.5°C. The temperature dependence of the calculated microviscosity [from Eq. (16)] can be described by

$$\eta = Ae^{\Delta E/RT} \tag{27}$$

where ΔE is the flow activation energy for the fluorophore in the core of the micelle, A is a characteristic pre-exponential factor, T is the absolute temperature

Figure 15 Dependence of the structural order parameter of DPH in microsomal membranes derived from chilling-resistant tomato fruit (a) and chilling-sensitive tomato fruit (b). The phase transition temperature of these biological membranes is an indication of the susceptibility of the fruit to cold temperature damage. (Data reanalyzed from Ref. 22.)

Copyright 2002 by Marcel Dekker. All Rights Reserved.

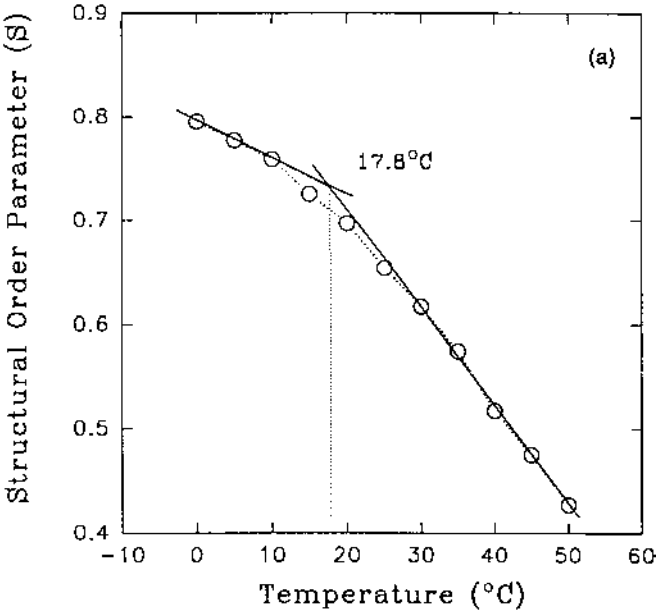

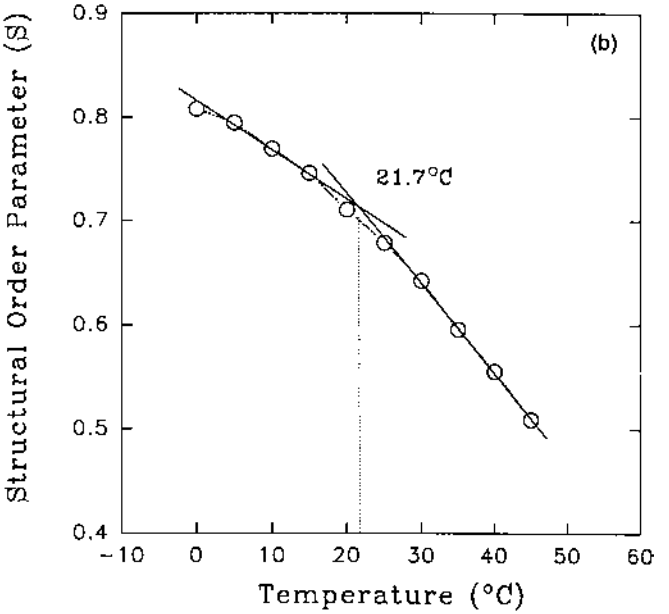

Copyright 2002 by Marcel Dekker. All Rights Reserved.

in kelvin, and R is the universal gas constant. The flow activation energy (ΔE) can be calculated from two temperatures as

$$\Delta E = R\frac{T_1T_2}{T_1 - T_2}\ln\frac{\eta_1}{\eta_2} \tag{28}$$

where T_1 and T_2 correspond to the chosen experimental absolute temperatures in kelvins, and η_1 and η_2 correspond to the determined microviscosities at the chosen temperatures, derived from fluorescence anisotropy measurements using a Perrin equation [16].

By plotting the flow activation energy as a function of the molar ratio of CA to CTAB, one can determine that ΔE approaches a limiting value of 2.5 kcal/mol at 0% CTAB, which corresponds to hypothetical 100% cetyl alcohol micelles. This value for ΔE is very similar to that of *n*-dodecane (ΔE = 2.8kcal/mol), suggesting that the interior of the micelle becomes more *n*-dodecane-like as the proportion of CA is increased. This type of information could prove very useful in the design and performance evaluation of surfactants and in the design, assessment, and study of emulsions.

Care must be exercised when choosing a fluorescent probe for the study of emulsions. If the fluorescence lifetime of the excited state for the fluorophore is too long, the effect of the micelle rotation will influence the value of the anisotropy. Fluorescence lifetimes below 12 ns should not pose a problem in this respect.

D. Chilling Resistance and Chilling Sensitivity of Tomato Fruit

Chilling injury is the physiological damage that occurs in many tropical and subtropical plants and plant products at cold but nonfreezing temperatures in the range 0–15°C. The biochemical mechanism by which chilling injury is induced is the formation of lateral phase separations in biological membranes due to phase transitions in the membrane lipids. These transitions from a liquid crystalline phase (''normal'') to a solid gel phase (''injured'') are believed to initiate a cascade of events that leads to membrane structural damage and eventually to cellular death [21]. Our work on chilling-sensitive and chilling-resistant tomato fruit has shown that phase transitions in chilling-resistant fruit microsomal membranes occur at lower temperatures than in chilling-sensitive fruit membranes [22]. Tomato fruit microsomal membranes labeled with DPH show a phase transition at 17.8°C for resistant tomato fruit (Fig. 15a) and at 21.7°C for sensitive fruit (Fig. 15b) as determined by plotting the structural order parameter [Eq. (21)] of the membranes as a function of temperature. By using phase transition temperatures as an index of susceptibility to cold temperatures, it would be possible to discriminate between resistant and sensitive tomato varieties, with enormous implications for the storage and commercial transportation of fresh tomato fruit.

Copyright 2002 by Marcel Dekker. All Rights Reserved.

IV. CONCLUSIONS

In this chapter, a general introduction to the theory and application of fluorescence polarization spectroscopy has been presented. This technique opens up the interesting possibility of studying the hydrodynamic properties of a fluid at the molecular level. With the growing importance of knowledge of the structure of lipid liquid phases (e.g., liquid crystalline phases), this technique may find more widespread application in fats and oils research.

REFERENCES

1. ID Campbell, RA Dwek. Biological Spectroscopy. Redwood City, CA: Benjamin/Cummings, 1984.
2. RF De Grell. Fluorescence polarization: A review of laboratory applications. Am Biotechnol Lab August:29–33, 1988.
3. WH Sawyer. In: Advances in Membrane Fluidity, Vol 1 Methods for Studying Membrane Fluidity. RC Aloia, CC Curtain and M Gordon (Editors) New York: Alan R. Liss, 1988, pp 161–191.
4. M Shinitzky, Y Barenholz. Biochim Biophys Acta 515:367–394, 1978.
5. JR Lakowicz. Principles of Fluorescence Spectroscopy. New York: Plenum Press, 1983.
6. WJ van Blitterswijk, RP van Hoeven, BW van der Meer. Biochim Biophys Acta 644:323–332, 1981.
7. K Hildebrand, C Nicolau. Biochim Biophys Acta 553:365–377, 1979.
8. JR Lakowicz, FG Prendergast. Science 200:1399–1401, 1978.
9. M Shinitzky, AC Dianoux, C Gitler, G Weber. Biochemistry 10: 2106–2113, 1971.
10. M Shinitzky, Y Barenholz. J Biol Chem 249:2652–2657, 1974.
11. M Shinitzky, I Yuli. Chem Phys Lipids 30:261–282, 1982.
12. JR Lakowicz, FG Prendergast, D Hogen. Biochemistry 18:508–519, 1979.
13. F Jähnig. Proc Natl Acad Sci USA 76:6361–6365, 1979.
14. G van Ginkel, H van Langen, YK Levine. Biochimie 71:23–32, 1989.
15. V Ben Yashar, M Menashe, RL Biltonen, ML Johnson, Y Barenholz. Biochim Biophys Acta 904:117–124, 1987.
16. BW van der Meer, RP van Hoeven, WJ van Blitterswijk. Biochim Biophys Acta 854:38–44, 1986.
17. G Lipari, A Szabo. Biophys J 30:489–506, 1980.
18. DG Nealon, EMB Sorensen, D Acosta. J Tissue Culture Methods 9:11–17, 1984.
19. R Pal, WA Petri, V Ben-Yashar, RR Wagner, Y Barenholz, Biochemistry 24:573–581, 1985.
20. K Florine-Casteel, GW Feigenson. Biochim Biophys Acta 941:102–106, 1988.
21. KL Parkin, AG Marangoni, RL Jackman, RY Yada, DW Stanley. J Food Biochem 13:127–153, 1989.
22. AG Marangoni, DW Stanley. Phytochemistry 28:2293–2301, 1989.

Copyright 2002 by Marcel Dekker. All Rights Reserved.

7
Texture of Fats

John M. deMan
University of Guelph, Guelph, Ontario, Canada

Leny deMan
deMan Food Technology Services, Inc., Guelph, Ontario, Canada

I. INTRODUCTION

Texture has been defined as the way in which various constituents and structural elements are arranged and combined into a micro- and macrostructure and this structure is externally manifested in terms of flow and deformation [1]. The structural elements of fats consist of solid fat crystals. They are suspended in liquid oil and when present in sufficient quantity form a three-dimensional network that imparts plastic properties to the fat. The external manifestations of this network structure include a number of physical and mechanical properties such as hardness, softness, spreadability, brittleness, shortening power, and aeration properties.

The texture of fats is influenced by a number of factors, including the solids content, the fatty acid and triacylglycerol composition of the solids, the polymorphic behavior of the fat crystals, the size and shape of the crystals, the nature of the crystal network, mechanical treatment, and temperature history [2]. Many of these factors are interrelated, making it difficult to establish the effect of each independently. Our work on texture has been mainly concerned with natural fats, margarines, and shortenings. The ingredients of these plastic fats may include a blend of partially hydrogenated oils, a blend of partially hydrogenated and unhydrogenated oils, a blend of interesterified fats to provide the solids and an unhydrogenated oil, interesterified fats only, a blend of unmodified fats, unmodified fat only, unmodified fat with liquid or hydrogenated fat, or some combinations of these. Unmodified fats are lard, tallow, butter, palm oil, and palm kernel

Copyright 2002 by Marcel Dekker. All Rights Reserved.

oil. All of the unmodified fats can be fractionated into a soft fraction and a hard fraction or into several fractions.

Margarines can be divided into soft (or tub) margarines and stick margarines. The stick margarines can be subdivided into soft stick and hard stick. The soft stick is mainly used as a sandwich spread like the soft margarines, and the hard stick is used for baking. The trend nowadays is to incorporate as much liquid oil as possible into the soft and soft stick margarines in order to claim the highest possible amount of polyunsaturated or monounsaturated fatty acids, following current nutritional recommendations. Incorporation of high levels of liquid oil has an economic advantage, because only a small portion of the fat has to be modified either by hydrogenation or by interesterification. High levels of polyunsaturated fatty acids in shortenings are undesirable, especially for commercial baking, because polyunsaturated fatty acids are prone to oxidize, especially in baked goods, reducing the product's shelf life. There are shortenings for different uses: all-purpose shortenings and puff pastry, cookie, cake, and pastry shortenings. Good physical properties are essential for good quality margarines. These properties include emulsion stability with no oil separation, a shiny surface, smooth texture with no graininess, no brittleness, good spreadability, and, in the case of retail margarines, a clean and complete meltdown in the mouth. Texture is equally important in shortenings.

II. SOLID FAT CONTENT

The fat in margarines and shortenings consists of liquid and solid components. The solids consist of fat crystals that incorporate the liquid oil in a crystal network. The amount of crystals present or, in other words, the amount of solids, the crystal size, and the strength of the network are important in determining the texture. The solid fat content (SFC) is determined by either nuclear magnetic resonance spectroscopy (NMR) or dilatometry. The dilatometry method is old and cumbersome but is still in use. NMR can also be used to estimate the SFC in the finished product by transferring a tube of the finished product into the NMR tube by means of a stainless steel open probe [3]. The manner in which the solid fat content is determined is very important. There are two official methods, the American Oil Chemists' Society (AOCS) method, which is used in the Americas, and the IUPAC method, which is used mainly in the rest of the world. In the AOCS method the fat is cooled at 0°C for 15 min, tempered at 26.7°C for 30 min, and cooled again to 0°C for 15 min, and then measurements are taken at the various temperatures after the samples have been left for 30 min at those temperatures. In the IUPAC method samples are not tempered; instead, the fat is cooled at 0°C for 30 min and then measurements are taken as in the AOCS method. There is quite a difference in the SFC values obtained at temperatures

Copyright 2002 by Marcel Dekker. All Rights Reserved.

Table 1 Mean Solid Fat Content (%) as Determined by the AOCS and IUPAC Methods

Study	Ref.	Number of samples	Temperature (°C)	Mean SFC (%) AOCS	Mean SFC (%) IUPAC
N. American stick margarines	4	27	10	31.1	40.4
			21	15.0	19.6
Malaysian soft margarines	5	7	10	20.7	27.2
			20	10.1	13.7
Malaysian plastic fats	6	9	10	38.4	50.9
			20	16.4	23.2

below that of the tempering temperature of 26.7°C. Table 1 shows some of these differences. The data in Table 1 were collected from several studies [4–6]. The AOCS method is more representative of the solids content of the finished products than the IUPAC method [4,5]. The reason is that in the scraped surface heat exchanger used in the manufacture of margarines and shortenings the fat solidifies on the cold surface of the heat exchanger, is then scraped off, is partially melted when mixed with the remaining fat, solidifies again on the surface, and so on [7]. At no time is the fat cooled entirely to 0°C. When the fat is cooled in the SFC method to 0°C, mixed crystals of various melting points will be formed, and these will partially melt at 26.7°C. Subsequent cooling to 0°C will solidify only the higher melting fat crystals.

The range and mean of solid fat content of North American soft and stick margarines as determined by the AOCS method are displayed in Table 2. The dropping points of these fats are normally below body temperature.

Table 2 Range and Mean of SFC (AOCS Method) at 10°C and Dropping Point of Commercial North American Soft and Stick Margarines

	Soft (N = 27)	Stick (N = 32)
SFC (%) at 10°C		
Range	7.1–18.8	23.0–38.1
Mean	13.7	30.2
Dropping point (°C)		
Range	27.3–34.2	31.5–35.8
Mean	31.3	33.4

N = Number of samples.

Copyright 2002 by Marcel Dekker. All Rights Reserved.

III. POLYMORPHISM

The fat crystals in margarines and shortenings can exist in two polymorphic forms, β′ and β. The α form in margarines and shortenings is very short-lived and does not exist in the finished product. β′ crystals are the most desirable. They are relatively small and can incorporate a large amount of liquid oil in the crystal network. β′ crystals result in a glossy surface and smooth texture. β crystals are initially also small, but they have a tendency to grow together into large needle-like agglomerates (Fig. 1), which result in a sensation of sandiness in the mouth. β crystals are less able to incorporate liquid oil than β′ crystals. The surface sheen of margarine becomes dull, and when the crystals become very large the surface may appear mottled and the texture becomes brittle. When β′ crystals change into the β form, the melting point of the product can increase by several degrees Celsius. This is undesirable for proper meltdown in the mouth. The transformation from β′ to β may proceed via the solid state or via the liquid form as indicated in Figure 2. Because of the increase in melting point the solid fat content may increase. The presence of β crystals in shortenings results in poor aeration in cakes and loss of creaming power.

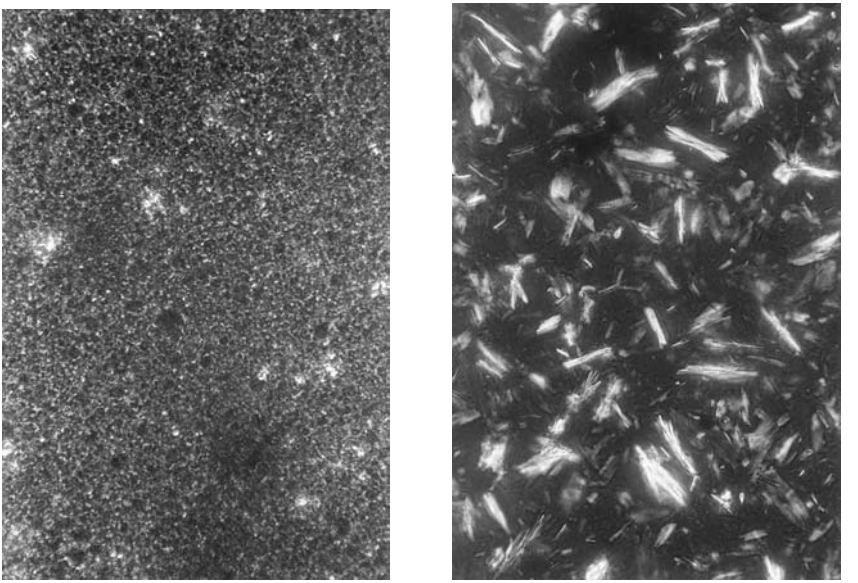

(a) (b)

Figure 1 Fat crystals. (a) β′ crystals in a margarine. (b) β crystals in a shortening.

Copyright 2002 by Marcel Dekker. All Rights Reserved.

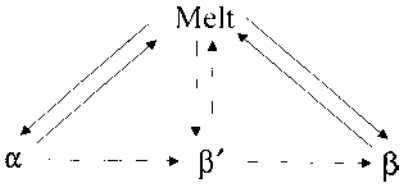

Figure 2 Pathways of polymorphic transitions.

IV. CRYSTAL NETWORK

The hypothesis that the crystals inside a plastic fat form a three-dimensional network originated with the work of Haighton [7] and has since been generally accepted. The network hypothesis, reviewed by deMan and Beers [8], involves the formation of a three-dimensional interlocking structure held together with weak forces between crystal particles. Postulated are two types of interparticle bonds; weak bonds that are easily disturbed and re-formed and stronger bonds that cannot easily be broken. The weak bonds account for the decrease in hardness when mechanical treatment is applied to the fat (work softening) and its subsequent recovery of hardness when the fat is left undisturbed (setting).

The formation of the network was proposed to happen as crystal particles aligned themselves under the influence of van der Waals attractive forces. The adoption of this hypothesis is based on the idea that the crystal particles are loosely suspended in liquid oil. It appears that this scenario is similar to the gel formation of protein and carbohydrate particles. Such rigid gels can be formed with very low concentrations of solids. In plastic fats, conditions are different. Plasticity in fats is attained only at solids concentrations of 10–15%. Below this level the fat is pourable. At higher solids concentrations, 25–35%, the fat becomes brittle. Plasticity is dependent not only on solid fat concentration but also on crystal size. Plastic fats have crystal sizes ranging from 0.5 to 5 μm. When crystal size increases to 25–50 μm the fat will also be brittle, and this most often happens when β′ crystals are transformed to β crystals.

The major objection to the network hypothesis is that crystals in a plastic fat are tightly packed and not in a loose arrangement as suggested by the protein gel model. In experiments where the crystals of a plastic fat were suspended in isobutanol [9,10] it could be shown that the sedimented crystals occupied a tenfold greater volume than they did in the original fat. Under the tightly packed conditions in a fat there is no room for these crystals to move freely to form a network. It has been suggested [2] that this situation is better described by the term ‘‘entanglement.’’ As the fat is deformed by mechanical action, crystals can

Copyright 2002 by Marcel Dekker. All Rights Reserved.

slide along one another, but because of the close packing this temporary softening effect is limited.

Recently, the increase in the hardness of fats during postcrystallization processes has been described as sintering [11,12]. A schematic representation of this process was given by Johansson and Bergenstahl [12]. The choice of the term ''sintering'' is unfortunate. The dictionary definition of sintering is ''formation of a solid from small particles by application of heat.'' Postcrystallization hardness is not achieved by application of heat, nor does the plastic fat become a solid. It has been suggested that this sintering is better described by the term ''entanglement.''

V. COMPOSITION OF THE SOLIDS OF FATS

The solid fat crystals are responsible for the plastic properties of fats. It is therefore not surprising that separating the solids cleanly from the liquid oil has been a desirable objective for studying the composition of the solids. Early attempts involved washing away the liquid oil with detergent solutions, but the method proved unsatisfactory. More recently it was demonstrated that solvents can be found that dissolve the liquid oil but not the fat crystals [10,13]. This makes it possible to isolate the solids of a fat with isobutanol. Further information on the solid fat can be obtained from a fractionation procedure that involves dissolving the fat in acetone and separating crystal fractions obtained at successively lower temperatures [13,14].

A. Fatty Acid Composition

Most of the solids of North American margarines are made from hydrogenated liquid oils such as soybean and canola. The fatty acid composition of some common vegetable oils is displayed in Table 3. Marine oils are sometimes used in plastic fat formulations, but they have to be hydrogenated because of their extreme susceptibility to oxidation, which results in a distinct odor and taste in the product if used in unmodified form. Most of the oils in Table 3 contain low levels of saturated fatty acids; the exceptions are cottonseed and palm oil. Stearic acid content (18:0) varies from 2% to 4% in these oils, but the palmitic acid (16:0) content is exceptionally high in cottonseed and palm oil. D'Sousa et al. [13,14] examined the solids of margarines by acetone fractionation at 15, 10, 5, and 0°C. They found that the high melting point triacylglycerols (HMGs) obtained at 15°C consisted mainly of saturated and trans fatty acids. Subsequent fractions contained more trans and less saturated fatty acids. The 16:0 content of the 15°C HMG fraction of North American soft and stick margarines was low (less than 12%) in products that show β crystallinity. When the 16:0 content was higher

Copyright 2002 by Marcel Dekker. All Rights Reserved.

Table 3 Fatty Acid Composition (%) of Common Vegetable Oils

Oil	16:0	18:0	18:1	18:2	18:3
Canola	4	2	59	21	11
Soybean	11	4	24	54	7
Sunflower	6	4	14	76	—
Sunflower, high oleic	4	4	78	12	—
Corn	11	2	25	57	1
Olive	12	2	72	8	1
Peanut	10	3	50	30	—
Cottonseed	25	2	18	50	—
Palm	44	4	39	10	—

(17% and more) in the 15°C HMG, the products were in the β′ form. Canola and sunflower oil contain low levels of 16:0 fatty acids (Table 3), and this is reflected in the HMG when it is hydrogenated. In the HMG the 16:0 content is higher than in the original oil. In order to stabilize the β′ crystals of canola and sunflower margarines, a hydrogenated palm oil or palm oil fraction should be incorporated to increase the chain length diversity of the solid triacylglycerol.

B. Triacylglycerol Composition

D'Souza et al. [13,14] also analyzed the HMG of margarines for triacylglycerol (TAG) composition and found that the 15°C fraction contained high levels of

Table 4 Triacylglycerol Composition (%) by Carbon Number of Common Vegetable Oils

	Carbon number				
Oil	48	50	52	54	56
Canola	—	1.1	13.0	76.8	5.6
Soybean	—	3.3	27.6	66.7	1.7
Sunflower	—	2.8	20.2	75.1	0.7
Sunflower, high oleic	—	2.0	15.0	80.6	1.0
Corn	—	4.6	30.4	64.2	0.8
Olive	—	4.7	27.7	66.7	0.9
Peanut	—	5.5	30.9	54.2	5.3
Cottonseed	0.9	13.6	43.5	40.5	1.3
Palm	8.0	42.5	40.5	9.0	—

Copyright 2002 by Marcel Dekker. All Rights Reserved.

Table 5 Melting Point (°C) of Triacylglycerols (TAGs)

TAG	β′	β
Trisaturated–long-chain		
SSS	64.2	73.5
SPS	64.2	68.7
PSS	63.2	65.2
PSP	68.8	—[a]
PPS	59.9	62.9
PPP	56.7	66.2
Trisaturated–long-medium-chain		
SCS	58.7	60.7
PSM	47.3	58.3
PCP	46.5	51.5
PCyP	42.9	47.9
Trisaturated–medium-chain		
MMM	46.2	58.2
MMLa	42.2	47.8
Disaturated–monounsaturated		
SSO	34.8	39.8
SPO	35.2	40.2
SOS	36.7	41.2
PSO	35.4	40.4
PPO	35.4	40.4
POP	30.5	35.3
Disaturated–monopolyunsaturated		
PLS	20.1	24.9
PPL	13.6	18.6
Monosaturated–dimonounsaturated		
SOO	18.8	23.7
POO	14.2	19.2
Trimonounsaturated		
OOO	−11.8	5.1

S = 18:0, P = 16:0, O = 18:1, L = 18:2, M = 14:0, La = 12:0, C = 10:0, Cy = 8:0.

[a] Difficult to obtain in the β form.

Source: Ref. 27.

Copyright 2002 by Marcel Dekker. All Rights Reserved.

54-carbon TAG (C54) in the margarines that were in the β form (>65%) The C54 TAG in vegetable oils consists mainly of 18-carbon fatty acids. TAGs containing saturated and/or trans fatty acids of the same chain length are strong β formers. Table 4 shows the TAG composition by carbon number of some vegetable oils. Canola and sunflower oils have high levels of C54 TAG, and palm oil has very low levels of C54. When these fats are hydrogenated, the TAG composition in the solids and in the HMG shifts to lower levels of C54 and higher levels of C50 and C52. The C50 TAG contains two 16-carbon fatty acids and one 18-carbon, the C52 TAG contains one 16:0 carbon fatty acid and two 18-carbon. Because the 16-carbon fatty acids consist mainly of 16:0 and are therefore already saturated, they will constitute a greater part of the solids as TAG C50 and C52 than as TAG C54. Incorporation of palm oil, especially hydrogenated palm oil, into a margarine or shortening formulation will greatly stabilize the β′ structure. *Trans* fatty acids have melting points in between those of their monounsaturated and saturated forms. For instance, the melting point of oleic acid (18:1) is 13°C, that of stearic acid (18:0) is 70°C, and that of elaidic acid (18:1 *trans*) is 44°C. *Trans* fatty acids in TAG behave like saturated fatty acids. Table 5 shows a series of TAGs with their β and β′ melting points. No β melting point is shown for the TAG PSP. This TAG is unique in that it is extremely difficult to obtain in the β form. Therefore, it is desirable to incorporate high levels of this TAG in margarines and shortenings. The TAG PEP (E stands for elaidic) behaves like PSP [15] but has a lower melting point than PSP. PEP is produced when POP is selectively hydrogenated. Palm oil is rich in POP. Table 6 lists the main TAGs in palm oil. Palm oil can be fractionated into palm olein, palm superolein, and palm midfraction. Palm midfraction has the highest content of POP.

Table 6 Major Triacylglycerols of Palm Oil

TAG	Carbon no.	Percent
PPP[a]	48	6.0
PPS[a]	50	1.0
PSP[a]	50	0.5
POP	50	26.0
PPO[a]	50	6.0
PLP	50	7.0
POO	52	19.0
POS[a]	52	3.0
PLO	52	4.0
OOO	54	3.0

[a] Likely to be in the palm stearin fraction.

Copyright 2002 by Marcel Dekker. All Rights Reserved.

Fatty acids are not randomly distributed in the three positions of the TAG in oils and fats. In vegetable oils the saturated and long-chain mono fatty acids have a tendency to occupy the 1 and 3 positions. This is favorable for the formation of β′ stable TAGs PEP or PEE (also a stable β′ TAG) upon hydrogenation. Lard is an exceptional fat in that most of the palmitic acid is located in the 2-position. This makes lard a fat that crystallizes in the β form [17].

VI. MELTING AND CRYSTALLIZATION CHARACTERISTICS OF THE SOLIDS

D'Sousa et al. [13,14] investigated the melting and crystallization behavior of the HMGs by differential scanning calorimetric (DSC) analysis. Figure 3 shows the melting temperature of the HMG fractions of stick margarines obtained at 0, 5, 10, and 15°C. Melting temperatures varied from 54 to 37°C; crystallization temperatures were about 20°C lower. This illustrates that a hardstock must crystallize at a relatively high temperature to get fast and proper crystallization in the scraped surface heat exchanger [7]. The 15°C acetone fractions of a number ($N = 10$) of soft margarines were investigated, and they behaved similarly to those of the stick margarines [13]. The solids of the soft margarines at 5°C were isolated by dissolving the liquid part with isobutanol, and their mean DSC melting temperature was 47°C. The mean SFC at 5°C of the soft margarines was 14%, which was in close agreement with the mean yield of the solids separated with isobutanol at 5°C. Separation of the solids with isobutanol is illustrated in

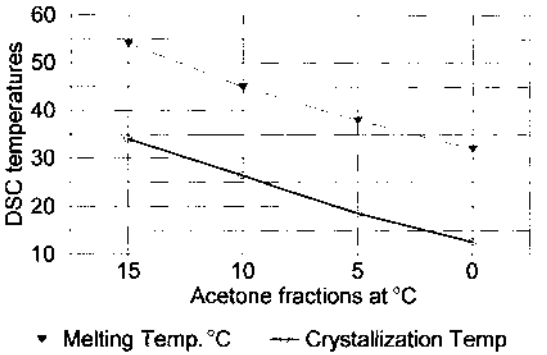

Figure 3 Differential scanning calorimetric (▼) melting and (○) crystallization temperatures of high melting point triglycerols (HMGs) of stick margarines obtained by acetone crystallization at 15, 10, 5, and 0°C.

Copyright 2002 by Marcel Dekker. All Rights Reserved.

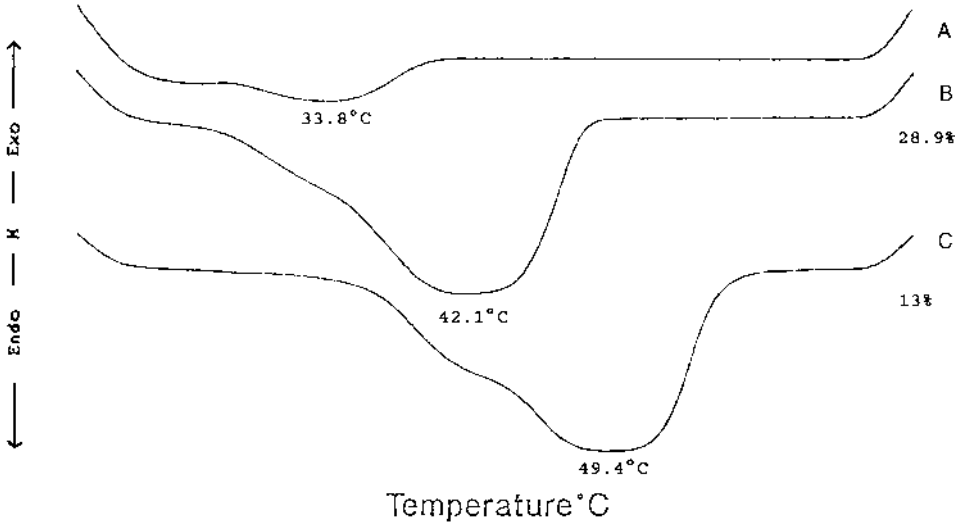

Figure 4 DSC melting curves of (A) a stick margarine and its butanol-isolated fractions (B) at 4°C and (C) at 20°C. SFC of fat (AOCS method): at 4°C 31.6% and at 20°C 11.1%.

Figure 4 for DSC of one margarine [18]. In this figure the solids were isolated at 4 and 20°C. The original melting point of the margarine was 33.8°C. The solids obtained at 4°C melted at 42.1°C, and those obtained at 20°C melted at 49.4°C. The yields of the solids at 4°C and 20°C were 28.9% and 13%, respectively; the SFCs at those temperatures were 31.6% and 11.1%, respectively, as determined by the AOCS method.

VII. HARDSTOCK AND LIQUID OIL

As mentioned earlier, the trend in soft margarine production today is to incorporate as much liquid oil as possible in order to claim the highest possible level of mono- or polyunsaturates. This should be achieved without unfavorable effects on the structure when the margarine is left at room temperature for a short time. Incorporation of liquid oil, especially at high levels, can change the β′ form rapidly into the β form This is demonstrated in the case of palm oil, palm stearin, and a commercially hydrogenated palm olein of dropping point 41.7°C in Table 7 [16]. This table illustrates that palm oil diluted with 20% liquid oil will show more β′ than β crystals; when diluted with 40% liquid oil it will show more β than β′ crystals. Hydrogenated palm oil is more stable in the β′ form

Copyright 2002 by Marcel Dekker. All Rights Reserved.

Table 7 Characteristics of Palm Oil Products in Dilution with Liquid Oil and Polymorphic Forms After Temperature Cycling Between 4 and 20°C

Sample	Liquid oil (%)	Dropping point (°C)	SFC at 10°C	Polymorphic form	Number of temp. cycles
Palm oil					
80%	20	38.6	31.7	$\beta' \gg \beta$	1
60%	40	37.3	19.4	$\beta > \beta'$	1
Palm stearin					
60%	40	50.3	35.7	β	1
Hydrogenated palm oil					
30%	70	36.5	13.5	β'	4
25%	25	34.9	12.9	$\beta' = \beta$	4
Hydrogenated palm olein					
40%	60	35.8	26.4	β'	4
20%	80	30.2	12.8	β'	4

than nonhydrogenated palm oil when it is diluted with liquid oil. It will remain in the β' form when up to 70% liquid oil is added. A commercially hydrogenated palm olein stayed in the β' form even when diluted with 80% liquid oil. This is exceptional because all soft margarines that we have analyzed showed β crystal levels ranging up to 100%. A formulation for soft margarines containing a hardstock of hydrogenated palm olein at a level of 20% or perhaps even less would be suitable for a soft margarine. For the data in Table 7 a cycling temperature between 4 and 20°C was employed. Temperature history is another important item that plays a role in polymorphic transition in margarines and shortenings.

VIII. TEMPERATURE CYCLING

Margarine and shortening must be able to withstand some abuse during transport and storage. Temperature fluctuation and improper refrigeration are the most common forms of abuse. In the evaluation of new formulations, suitable cycling temperatures are between 15 and 4°C for soft margarines and between 20 and 4°C for stick margarines [19]. Shortenings are stored at room temperature, and cycling temperatures are best between 20 and 30°C. After a series of temperature-cycling procedures, changes in appearance and texture should be noted. In addition, sensory meltdown in margarines and creaming power in shortening should

Copyright 2002 by Marcel Dekker. All Rights Reserved.

be determined. X-ray diffraction analysis is used after each cycle to determine the polymorphic forms present.

IX. INTERESTERIFICATION

So far we have examined hardstock from hydrogenated sources. Hydrogenation leads to the formation of *trans* fatty acids unless the oil is fully hydrogenated. *Trans* fatty acids are thought to be nutritionally undesirable, and for this reason interesterification can be used to replace hydrogenation. In both hydrogenation and interesterification a hardstock is required to maintain a high level of polyunsaturated fatty acids or monounsaturated fatty acids. Hardstock promotes rapid crystallization. The various hardstocks must have similar melting characteristics, as shown in Figure 3. This indicates the need to find TAGs with similar melting and crystallization behaviors. Table 5 shows the β′ and β melting points of trisaturated TAGs. It is very important to avoid producing β crystals; therefore the focus should be on the behavior of β′ crystals. The β′ melting points of the TAGs of the long-chain trisaturates range from 56.7 to 68.8°C. The mean melting point of the HMGs of the margarines obtained in the 15°C acetone fraction was 55°C. Therefore part of the IE solids of soft margarines should consist of long-chain trisaturates. The triacylglycerols PPP and SSS should be avoided, because these are β-tending. Incorporation of palmitic acid lowers the melting point of the trisaturated TAG. Combining triglycerides containing long chain saturated fatty acids with those containing medium and short chain saturated fatty acids (e.g. palm oil and palm kernel oil) will result in a eutectic, which will also lower the melting point. It would seem that a hardstock for IE soft margarines should consist of 25% HMG with a melting point of 55°C. Substitution of a medium-chain fatty acid into a long-chain saturated TAG lowers the melting point by 10–15°C (Table 5).

The melting points of disaturated-monounsaturated TAG are almost half of those of their trisaturated equivalents (Table 5) and fall within the narrow range of 30–36°C. Interesterification of long-chain saturated fatty acids with medium-chain ones is a very attractive option and will result in a steeper SFC curve than interesterfication to produce monounsaturated TAG. TAG consisting of two saturated long chain fatty acids and a saturated medium chain fatty acid could provide the solid fat at lower temperatures, e.g., at temperatures of 10–20°C. The melting points of disaturated-polyunsaturated and monosaturated-dimonounsaturated TAG are close together. TAG with melting points of 5–10°C may cause postcrystallization. Exit temperatures of margarines from the scraped surface heat exchanger are around 15°C. When stored at refrigeration temperatures, TAG with melting points of 5–10°C that have not crystallized as mixed crystals will very slowly crystallize, causing postcrystallization. Erickson and

Copyright 2002 by Marcel Dekker. All Rights Reserved.

Table 8 Saturated Fatty Acids (%) in Fats and Oils

Fatty acid	14:0	16:0	18:0	Total
Palm oil	1	44	4	49
Palm stearin	2	50–68	4–6	54–74
Fully hydrogenated palm oil	1	44	55	100
Tallow	6	27	14	47
Lard	2	22	9	33
Mutton	5	25	30	60
Palm kernel[a]	16	8	2	82
Highly sat soybean[b]		23	20	43

[a] Includes 12:0 = 48%, 10:0 = 4%, 8:0 = 5%.
[b] From Ref. 28.

Erickson [20] recommend that a β′ hard fat be added at a level of 5–10% in margarines formulated from hydrogenated soybean oil. This recommendation also applies to interesterified formulations. As mentioned earlier, hydrogenated palm olein or palm midfraction is a very good β′-tending fat. Added at a level of 1% in the soft margarine formulation it would make up about 10% of the solids. This would result in a *trans* content of 0.3%, because only one-third of PEP is a trans acid. In the chemical interesterification process the only variable is the fatty acid composition, whereas in the hydrogenation process hydrogen pressure, temperature, catalyst concentration, and type of catalyst can influence the formation of solids. Therefore, close attention should be paid to the fatty acid composition of the blend to be interesterified. Sources of saturated fatty acids, especially palmitic, can be supplied by fractionated palm stearin. Other sources are listed in Table 8. Fully hydrogenated liquid oils such as soybean and canola result in very high levels of stearic acid, which increase the melting point and will decrease chain length diversity. When the fatty acid composition of a blend is known it is possible to calculate which TAG will be formed by the randomization process [21,22]. Knowledge of the TAG levels and their melting points may make it possible to estimate the solids that will be formed.

The chemical interesterification process results in the fatty acids being distributed randomly, unlike those of natural oils and fats. The advantage of having the 16:0 fatty acids in the 1- and/or 3-position is eliminated. It will therefore be more difficult to keep interesterified fats in the β′ form.

X. TEXTURE

The texture of plastic fats can be determined in several ways. In this chapter, three main methods are discussed:

Copyright 2002 by Marcel Dekker. All Rights Reserved.

1. Cone penetrometry
2. Penetration by a probe
3. Compression between parallel plates

Items 2 and 3 are discussed under the heading ''Force Measurements.''

A. Cone Penetrometry

Cone penetrometry is a form of distance measurement. The cone penetrometer consists of a cone and vertical shaft assembly that is allowed to sink into a plastic fat under the force of gravity for a specific time, after which the depth of penetration is measured in tenths of a millimeter. The cone comes to rest when its load is in equilibrium with the strength of the plastic body. According to the AOCS method, the results of the cone penetrometer measurements are reported as depth of penetration in units of 0.1 mm. This is a measure of softness, with increasing penetration values indicating greater deformation. Haighton [7] suggested converting the penetration depth to yield value according to the formula

$$C = KW/p^{1.6}$$

where K is a constant that depends on the cone angle, W is the weight of the assembly, and p is the depth of penetration in units of 0.1 mm that is indicated on the scale of the instrument. The exponent 1.6 is not a constant value for all products, and to eliminate this uncertainty Vasic and deMan [23] suggested converting penetration readings to hardness, defined as force divided by area of deformation and calculated as

$$H = 10W(0.5625\ p^2 + 25.25\ p + 50.265)$$

In the AOCS Method Cc 16–60, the cone angle is specified as 20°.

B. Force Measurements

1. Penetration with a Probe

In the penetration test, force is measured when a probe is pushed at a constant speed into a food or plastic fat that is contained in a small container. The probe can be round, rectangular, or conical. Usually the maximum force is recorded at a specified depth. Force is usually expressed as newtons per square centimeter. The shape of the penetration curve can reveal characteristics about the sample

2. Compression Between Parallel Plates

In the parallel-plate test, force is measured in uniaxial compression and is unrestrained in the other direction. In this case a cylindrical sample of fat of, e.g., 2 cm height is compressed to 1 cm at a certain speed. This kind of test can reveal

Copyright 2002 by Marcel Dekker. All Rights Reserved.

more information about the sample than the penetration test. The force is expressed as newtons per square centimeter.

XI. TEXTURE MEASUREMENTS OF COMMERCIAL PRODUCTS

In texture measurements of plastic fats it is important not to disturb the integrity of the sample. This is not a problem with the cone penetrometer, although the sample should be held in a container. In probe penetration a small cup with a small hole in the bottom to let out the air is pushed into the product and left for at least one day at the temperature of measurement before the test [4,24]. In the compression test a stainless steel borer is pushed into the sample, which is then

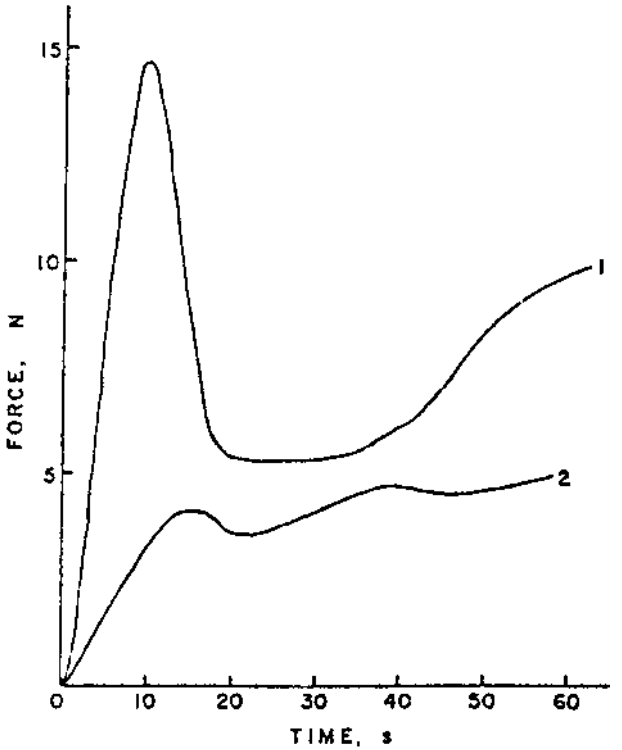

Figure 5 Texture measurements of a canola stick margarine. Curve 1: Compression of a cylindrical sample. Curve 2: Penetration by a probe.

Copyright 2002 by Marcel Dekker. All Rights Reserved.

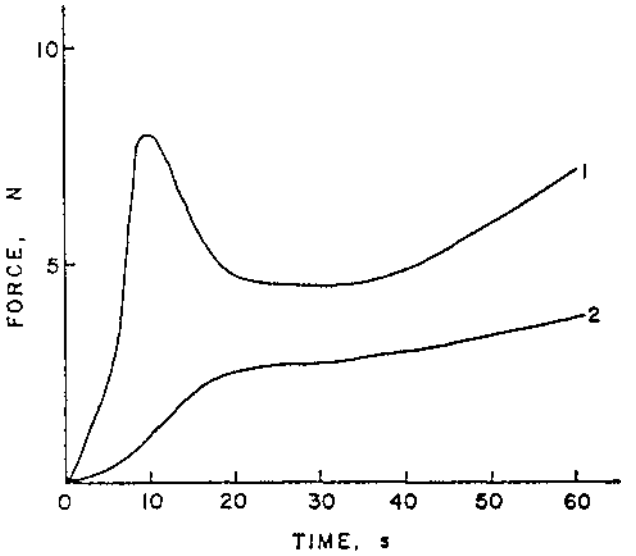

Figure 6 Texture measurements of a soybean stick margarine. Curve 1: Compression of a cylindrical sample. Curve 2: Penetration by a probe.

extruded as a fat cylinder sized to a certain length by two parallel wires mounted on a special cutting device. The test is not suitable for soft margarines but is very useful in the evaluation of shortening and stick and puff pastry margarines, because it can reveal information about the structure of the fats [24]. Measurements by cone penetrometry are convenient and accurate.

A comparison of the two methods that measure force as a function of deformation of two margarines are displayed in Figure 5 and 6, which show a probe penetration and the compression of a cylindrical sample between parallel plates. In Figure 5 the sample is a canola margarine. Curve 1 is the result of compression of a cylinder of 2 cm height and 2 cm diameter to 1 cm at a speed of 1 cm/min. There is a breaking force or peak force at 15 N, with a steep downward curve that reaches a plateau force followed by another increase. Curve 2 is the penetration curve of a round probe of an area of 0.332 cm^2 that is forced into margarine that was contained in a cup with a diameter of 1.6 cm at a speed of 1 cm/min. In Figure 6 the sample was a soybean margarine. When the two figures are compared it appears that the compression curve in the canola margarine (Fig. 5) is steep going up and coming down and the plateau force is about one-third of the breaking force. During compression the fat cylinder broke into pieces, indicating that the sample was brittle. This is confirmed by the unevenness of the penetration curve. In the soybean margarine (Fig. 6) the breaking force (peak force) was

Copyright 2002 by Marcel Dekker. All Rights Reserved.

much lower (7.5 N) and the plateau force was two-thirds of the peak force. The penetration curve was smooth. During compression the soybean margarine cylinder showed a diagonal break, but the sample did not crumble.

A series of shortenings were evaluated, and they showed different force curves [24]. Figure 7 presents examples of results of penetration tests. Curve 1 represents an all-purpose soy–palm shortening that had a smooth texture and was in the β′ form. Curve 2 represents an all-purpose soy shortening that was in the β form and had the same solid fat level as the shortening of curve 1. It is obviously brittle. Curve 3 represents a mixture of tallow and lard; it was in the β form and was not as brittle as the product of curve 2. Curve 4 represents lard. Lard is almost always in the β form. Curve 5 is for a blend of tallow and hydrogenated vegetable oil in the β′ form and appears smooth. Curve 6, for a palm–palm kernel product in the β′ form, indicates a smooth texture.

The same shortenings were analyzed with the compression test, and the results are shown in Figure 8. Curves 1, 2, and 3 represent those of all-purpose shortenings. Curves 1 and 2 are for soy–palm and 3 for soy–canola–palm. All

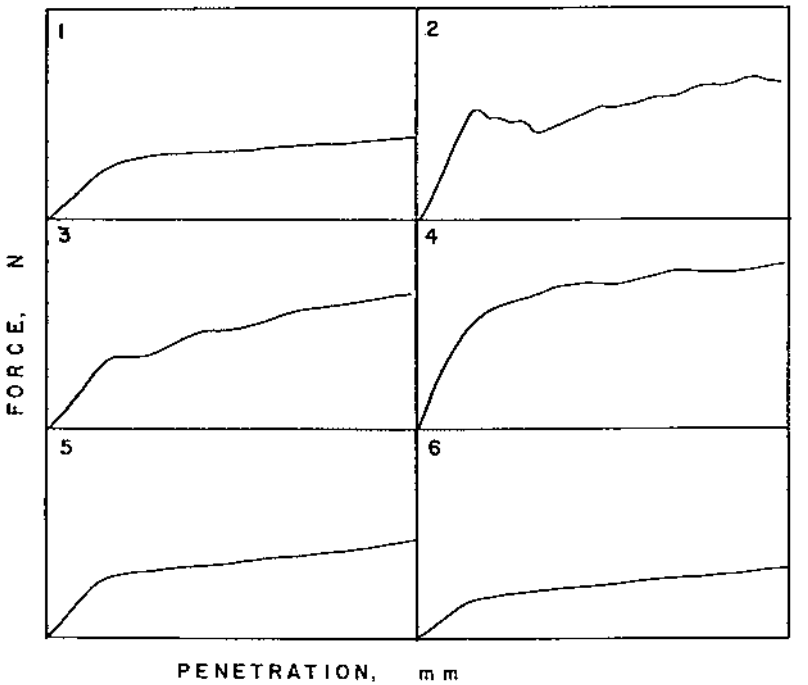

Figure 7 Texture measurements by means of penetration by a probe. See text for details.

Copyright 2002 by Marcel Dekker. All Rights Reserved.

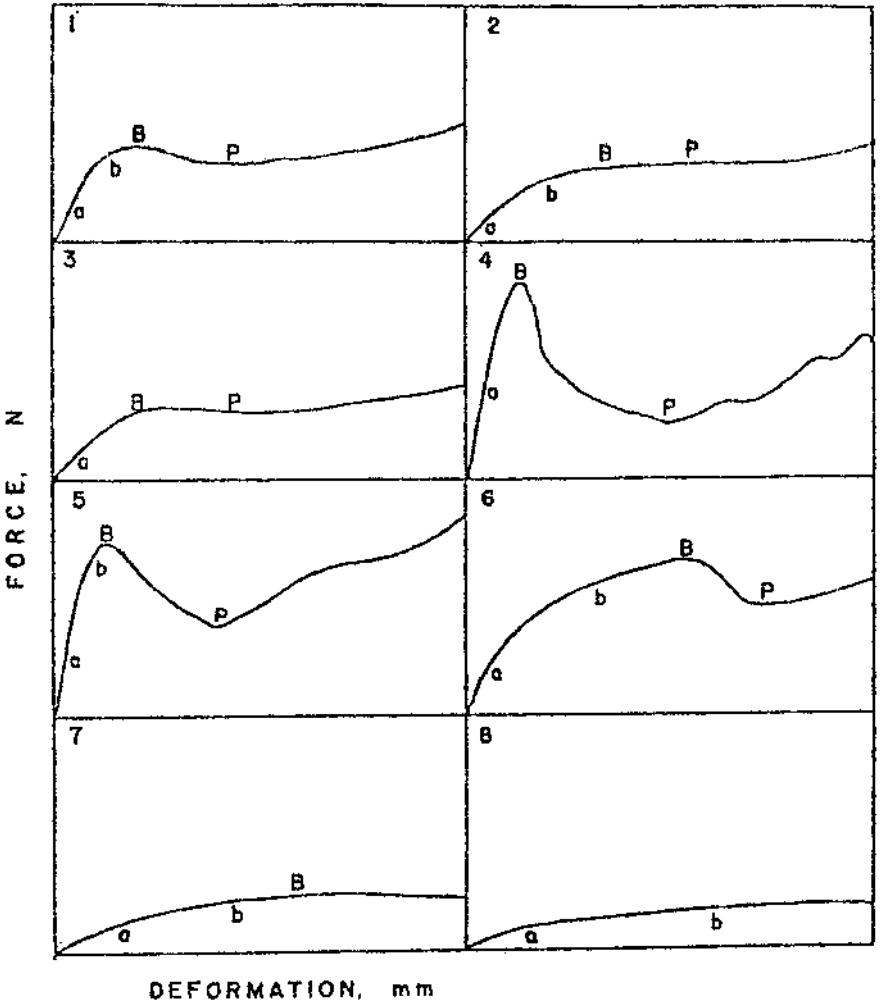

Figure 8 Texture measurements by means of compression of cylindrical sample between parallel plate. See text for details.

are in the β′ form and of smooth texture. Curve 1 shows a slight brittleness. Curve 4, for the soy-only all-purpose shortening, confirms the brittleness observed in the penetration test. In this curve it is possible to put a value to the brittleness when peak force minus plateau force is divided by the peak force, giving 0.63, or 63%. Curve 5 is for the blend of tallow and lard and shows this product to

Copyright 2002 by Marcel Dekker. All Rights Reserved.

be less brittle than the product of curve 4. Curve 6 is typical for lard. Curves 7 and 8 are for palm products, curve 7 for palm–hydrogenated vegetable oil and 8 for palm–palm kernel oil. The latter did not have a breaking force. The cylindrical fat sample did not show any crack when compressed to half its size; it just bulged at the sides, indicating an unusual smoothness or plasticity. Table 9 shows the SFC levels in the above products together with the penetration and compression values. According to Dixon [25], the initial slope of the compression curves represents the elastic nonrecoverable deformation. On the curves this is indicated as *a*. After the initial straight part, the curves show a different, more rounded and less steep, slope, which according to Dixon is an indication of viscous flow. This portion of the curve is indicated by *b*. Some of the shortening curves do not exhibit this viscous part *b* during compression (curve 4, Fig. 8) or show only a small portion of *b* (curve 5) Other samples show a very large *b* section (curves 6 and 7). The viscous flow will continue until a break appears in the sample, which is indicated as *B*, the breaking force. The breaking force *B* can appear early during compression at small deformation, or the sample can tolerate a large deformation before a crack appears, as shown by curves 6 and 7.

The accuracy of the various textural evaluation tests expressed as the mean coefficients of variance of the replicates for stick margarines ($N = 27$) and for shortenings ($N = 22$) in the cone penetrometer is 6.6% and 4.2%, respectively, constant-speed penetration 5.3% and 4.2%, and constant-speed compression 10.7% and 9.7%, respectively. The accuracy of the compression test was not as good as that of the other tests, because the compression test requires more handling of the sample.

The correlation coefficients *within* the three textural methods was very good for both margarines and shortenings ($r > 0.9$), but the correlation coefficient *between* the three textural tests and the SFC of the fat or the solids content of

Table 9 SFC (%) and Textural Characteristics (N/cm^2) of Shortenings at 20°C

Sample	SFC (%) of sample	Penetration force (N/cm^2)	Compression force (N/cm^2)
Soy–palm	15.5	4.2	0.9
Soy–palm	12.5	2.6	0.6
Soy–canola–palm	13.5	3.0	0.6
Soy	13.6	5.4	2.0
Tallow–lard	34.0	13.4	4.3
Lard	23.0	4.6	1.5
Palm–vegetable	25.1	4.9	0.6
Palm–palm kernel	11.4	2.9	None

Copyright 2002 by Marcel Dekker. All Rights Reserved.

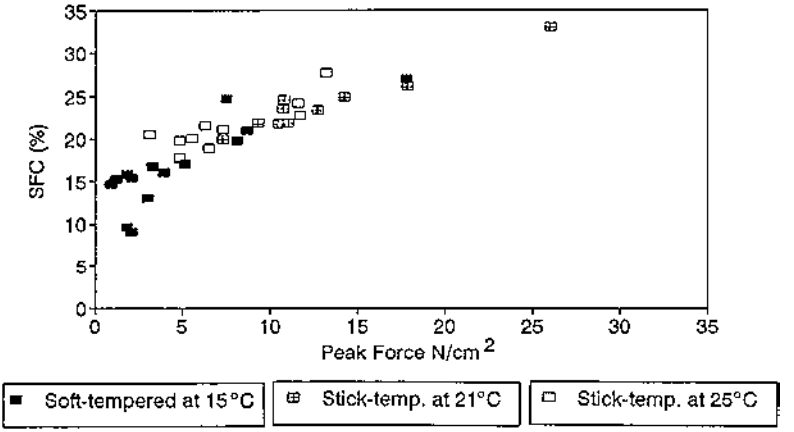

Figure 9 Relationship between SFC (%) and texture by probe penetration (N) of soft and stick margarines. Samples were crystallized and tempered under controlled conditions.

the product at the same temperature as that of the texture test was much lower and in most cases not significant. This proves that forces other than the solid fat content play an important role in the textural characteristics of margarines and shortenings.

XII. TEXTURE OF FATS CRYSTALLIZED AND TEMPERED UNDER CONTROLLED CONDITIONS

A. By Penetration

A number of fats separated from soft and stick margarines were transferred into small cups [19], heated to 60°C to destroy crystal memory, and then placed in a bath that was placed in the freezer at −15°C to obtain quick crystallization. The following day the soft margarine fats were tempered at 15°C and the stick margarine fat at 21 and 25°C for one day. Thereafter the samples were placed in the refrigerator. The texture of the soft margarine fats was evaluated at 4°C, and that of the stick margarine fats at 15°C. Texture evaluation was performed by penetration of a stainless steel probe as described previously. NMR tubes filled with the same fats were given the same temperature treatment as the fat in the cups in order to estimate the SFC in the cups. Figure 9 shows the relationship between the SFC and the texture of the fats as peak force in newtons per square centimeter. The linear correlation coefficient (r) was 0.8926 and was significant ($P < 0.01$). All but two of the samples contained hydrogenated hardstock.

Copyright 2002 by Marcel Dekker. All Rights Reserved.

The hardstock of the other two samples was interesterified and showed the lowest SFC but not the lowest peak force. This experiment indicates that correlation between SFC and texture can be significant when crystallization takes place under the same circumstances and when hardstocks are hydrogenated.

B. By Compression

In another experiment, fats of a hydrogenated shortening and a puff pastry margarine, a nonhydrogenated palm oil, and lard were examined for their textural behavior using the compression test [26]. The reason for using the compression test was that it gives better information for shortening, especially puff pastry margarines and lard that are used in doughs that require rolling and folding. They need plasticity that can withstand force without breakage. Luer-Lok syringes were used (inside diameter 31 mm). The end of the syringe was cut off, and a plastic cap covered one end. They were filled with the fats and heated and cooled as follows: 60°C (2 h) → 45°C (20 min) → 5°C (2 h) → tempering temperature (1 day) → 20°C (4 weeks). Texture was measured at 20°C. Fats in NMR tubes were temperature treated in the same way as the fats in the syringes. The fat cylinders in the syringes were pushed out by the plunger and sized to 2 cm in length. In the texture test they were compressed to 1 cm as described earlier.

Table 10 shows the effect of tempering on the SFC content and the texture of the fats. At higher tempering temperature and upon cooling to 20°C the SFC was lower; the higher the temperature, the lower the SFC at 20°C. Texture at 20°C was equally affected by the tempering temperature. Palm oil had an SFC

Table 10 Effect of Tempering Temperature on the Texture of Fats as Measured by Compression of Cylindrical Samples at 20°C

Sample	Tempering temp. (°C)	SFC at 20°C (%)	Breaking force at 20°C (N)
All-purpose shortening A	20	17.6	7.9
	24	16.8	6.0
	28	14.3	3.3
Palm oil	20	31.2	12.4
	24	27.3	8.8
	28	25.6	8.9
Puff pastry	25	28.3	30.9
	30	24.9	16.6
	35	23.8	11.3

Temperature treatment: 60°C for 2 h → 45°C for 20 min → 5°C for 2 h → 20°C for 1 day → tempering temp for 1 day → 20°C for 4 weeks.

Copyright 2002 by Marcel Dekker. All Rights Reserved.

Table 11 Effect of Crystallization Temperature on the Texture of Fats as Measured by Compression of Cylindrical Samples at 20°C

Sample	Crystallization temp (°C)	SFC at 20°C	Breaking force at 20°C (N)
All-purpose B	10	15.6	4.8
	0	15.3	3.3
	−10	15.6	3.0
Palm oil	10	31.4	13.6
	0	31.2	11.5
	−10	31.7	9.0
Puff pastry	10	31.9	41.6
	0	31.6	35.3
	−10	31.1	31.1

Temperature treatment: 60°C for 2 h → 45°C for 20 min → crystallization temp for 2 h → 20°C for 5 weeks.

of 27.3%, and the all-purpose shortening an SFC of 17.6%, and texture values were 7.9 and 8.8 N, respectively. A similar texture was associated with a large difference in SFC. Similarly, the SFC of palm oil at 31.2% and of puff pastry margarine at 28.3% had very different textures—12.4 and 30.9 N, respectively. The solids in palm oil are unlike those in the other two fats, which were hydrogenated.

In another experiment the effect of crystallization temperature on the texture of the same fats was examined. Temperature treatment was as follows: 60°C (2 h) → 45°C (20 min) → crystallization temperature (2 h) → 20°C (5 weeks). Results are shown in Table 11. Crystallization temperature had no effect on the

Table 12 Effect of Processing Conditions on the SFC and Texture of Lard at 10°C

Product	Time (wk)	SFC (%)	Breaking force (N)
1	1	30.9	15.5
	12	30.9	16.7
2	1	30.6	9.0
	12	30.6	9.4
3	1	31.1	17.2
	12	31.1	16.9

Copyright 2002 by Marcel Dekker. All Rights Reserved.

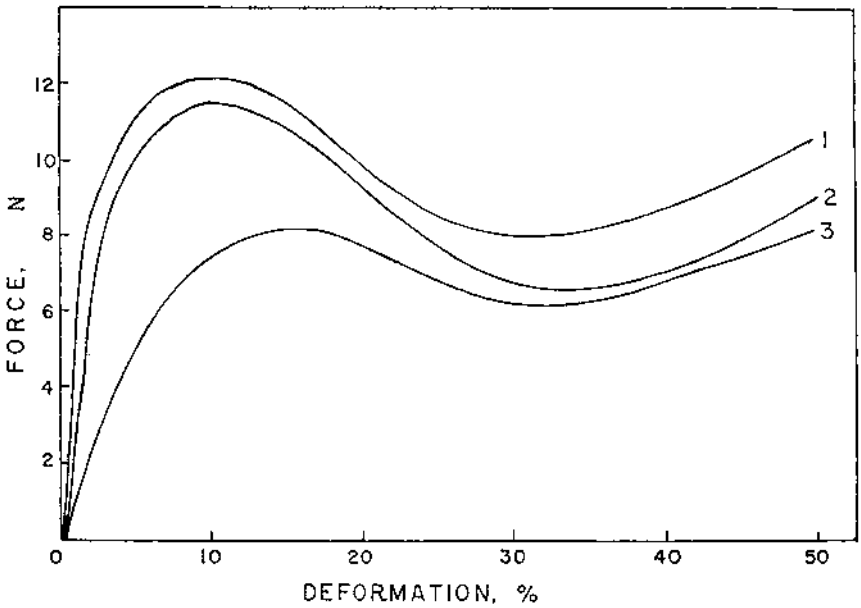

Figure 10 Texture of a commercial puff pastry margarine measured by compression of cylindrical samples at 20°C. Curve 1: As received from the manufacturer. Curve 2: Tempered at 25°C for 1 day and stored for 3 weeks at 20°C. Curve 3: Tempered for 1 day at 30°C and stored for 3 weeks at 20°C.

level of SFC in all cases, but it had an effect on texture. The lower the temperature of crystallization, the softer the texture. Lower crystallization temperature results in smaller crystals and a more plastic network structure. Palm oil and the puff pastry fat with similar SFC had very different textures. This is another indication that composition of the solids has a large influence on texture.

In another experiment lard was processed commercially on different scraped surface heat exchangers The products were stored under the same conditions and examined over a 12-week period. Table 12 shows the effect of processing condition on SFC and texture. The SFCs of the lards were practically the same, indicating no difference in tempering or storage temperature, but the texture of product 2 was much softer as a result of different processing conditions. The SFCs of palm oil, puff pastry fat, and lard in Tables 11 and 12 were similar; the texture of lard was slightly firmer than that of palm oil, but the puff pastry fat was much harder than the others. This may indicate that the solid TAGs in these products are of different compositions. The SFCs of palm and lard are

Copyright 2002 by Marcel Dekker. All Rights Reserved.

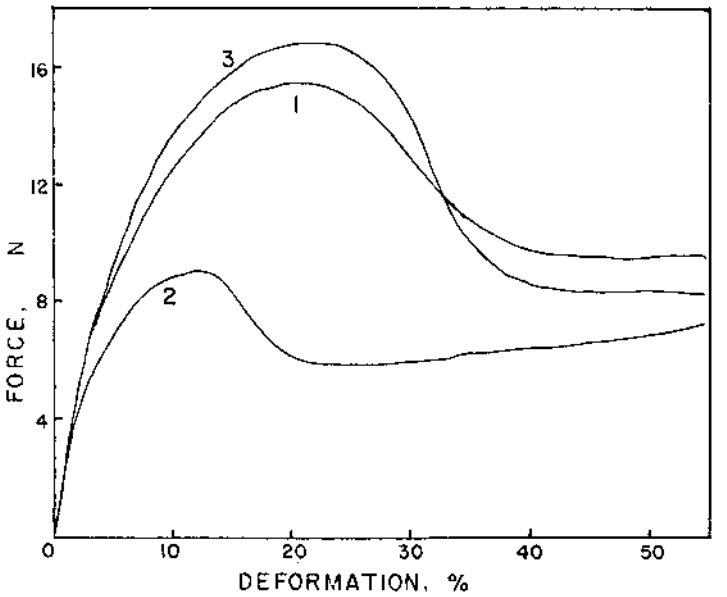

Figure 11 Texture of commercial lard processed under three different conditions.

unhydrogenated and must include solid TAG with oleic acid, whereas those of the puff pastry fat contained probably more trans acid than oleic acid.

Processing conditions can be manipulated in such a way that the crystal network can be either weak or strong. After processing, texture can also be changed by tempering conditions, and that is illustrated in the case of the original puff pastry margarine (Fig. 10). Hardness at 20°C was reduced after tempering at 25 and 30°C for one day. The compression curves of the puff pastry margarine also illustrate a plasticity similar to that of lard in Figure 11. Both products are used in dough that requires rolling.

XIII. CONCLUSION

Texture of fats depends on the chemical composition of the solids, crystallization temperatures, storage conditions, and mechanical treatment. Making a hydrogenated product on the basis of SFC using natural oils or interesterified oils can result in very different properties. The use of compression between parallel plates

Copyright 2002 by Marcel Dekker. All Rights Reserved.

to evaluate texture reveals more about the plasticity of a product than penetration tests.

REFERENCES

1. JM deMan. Principles of Food Chemistry. Gaithersburg, MD: Aspen Pub 1999, pp 33–110.
2. JM deMan. In: N Widlak, ed. Physical Properties of Fats, Oils and Emulsifiers. Champaign, IL: AOCS Press, 2000, pp 79–95.
3. L deMan, JM deMan, B Blackman. Physical and textural evaluation of some shortenings and margarines. J Am Oil Chem Soc 66:128–132, 1989.
4. L deMan, E Postmus, JM deMan. Textural and physical properties of North American stick margarines. J Am Oil Chem Soc 67:323–328, 1990.
5. NA Idris, L deMan, TS Tang, CL Chong. Chemical composition and physical properties of soft (tub) margarines sold in Malaysia. J Am Oil Chem Soc 73:995–1001, 1996.
6. NA Idris, L deMan, TS Tang, CL Chong. Chemical and physical properties of plastic fat products sold in Malaysia. J Food Lipids 4:145–164, 1997.
7. AJ Haighton. Blending, chilling and tempering of margarines and shortenings. J Am Oil Chem Soc 53:397–399, 1976.
8. JM deMan, AM Beers. Fat crystal networks: Structure and rheological properties. J Text Stud 18:303–318, 1988.
9. P Chawla, JM deMan. Measurements of size distribution of fat crystals using laser particle counter. J Am Oil Chem Soc 67:329–332, 1990.
10. P Chawla, JM deMan. Crystal morphology of shortening and margarines. Food Struct 9:329–336, 1990.
11. IM Heertje, WJM Lennis, van Zeyl, E Berendse. Product morphology of fat products. Food Microstruct 6:1–8, 1987.
12. D Johansson, B Bergenstahl. Sintering of fat crystal networks in oil during post-crystallization processes. J Am Oil Chem Soc 72:911–920, 1995.
13. V D'Souza, JM deMan, L deMan. Chemical and physical properties of the solid fat in commercial soft margarines J Am Oil Chem Soc 69:1198–1206, 1992.
14. V D'Souza, L deMan, JM deMan. Chemical and physical properties of the high melting glyceride fraction of commercial margarines. J Am Oil Chem Soc 68:153–162, 1991.
15. PG Elisabettini, A Lognay, N deSmedt, E Istasse, E Deffense, F Durant. Synthesis and physicochemical characteristics of mixed diacid triglycerides that contain elaidic acid. J Am Oil Chem Soc 75:285–291, 1998.
16. L deMan, YL Xu, HS Chen, JM deMan. Polymorphic stability of hydrogenated palm oleins in dilutions with unhydrogenated liquid oils. J Am Oil Chem Soc 70:431–433, 1993.
17. L Wiedermann, TJ Weiss, GA Jacobson, KF Mattil. A comparison of sodium methoxide treated lards. J Am Oil Chem Soc 38:389–395, 1961.

Copyright 2002 by Marcel Dekker. All Rights Reserved.

18. L deMan, JM deMan. DSC: A tool in the evaluation of fats and fat products. Malaysian Oil Sci Technol 7(2):17–26, 1998.
19. L deMan, JM deMan, B Blackman. Effect of tempering on the texture and polymorphic behaviour of margarine fats. Fat Sci Technol 97:55–60, 1995.
20. DR Erickson, MD Erickson. Hydrogenation and base stock formulation. In: Practical Hand Book of Soybean Processing and Utilization, Champaign, IL: AOCS Press and United Soybean Board, 1995, pp 218–238.
21. A Roozenaal. Interesterification of oils and fats. INFORM 3: 1232–1237, 1992.
22. B Sreeninasan. Interesterification of fats. J Am Oil Chem Soc 55:796–805, 1978.
23. I Vasic, JM deMan. Rheology and Texture of Foodstuffs. London: Soc Chem Ind 1968.
24. L deMan, JM deMan, B Blackman. Physical and textural characteristics of some North American shortenings. J Am Oil Chem Soc 68:63–69, 1991.
25. BD Dixon. Spreadability of butter: A new approach. Aust J Dairy Technol September: 87–93, 1966.
26. L deMan, JM deMan. Texture measurements of some plastic fats. Oils-Fats-Lipids. Proc 21st World Congress Int Soc Fat Res. (ISF) The Hague. Bridgwater, UK: PJ Barnes & Assoc, 1995, Vol 3, pp. 543–546.
27. J Fabien. PhD Thesis. Univ New South Wales. Australia, 1992.
28. LL Kok, EG Hammond, PJ White. *Trans*-free margarines from highly saturated soybean oil. J Am Oil Chem Soc 76:1175–1181, 1999.

Copyright 2002 by Marcel Dekker. All Rights Reserved.

8
Fat Crystal Behavior in Food Emulsions

Dérick Rousseau
Ryerson University, Toronto, Ontario, Canada

I. INTRODUCTION

Many natural and manufactured substances exist or have been processed as emulsions, including some foods, pharmaceuticals and cosmetics, coal, insecticides, and crude oil [1–4]. Food emulsions are broadly defined as any system where there are at least two immiscible phases consisting of solids, liquids, gases, and/or liquid crystals. Oil-in-water (O/W) emulsions (cream, dressings, etc.) are typically fluid and may contain a (partially) crystalline oil phase, whereas food-related water-in-oil (W/O) emulsions (butter, margarine, etc.) are typically solid-like [5].

Outside of foods, the presence of colloidal particles significantly influences many processes. For example, during bitumen extraction from oilsands, oil droplets in a continuous water phase are stabilized by hydrophobic mineral particles. Removal of oil droplets is important to increase oil yield and protect the environment, yet the capital and operating costs are high [6]. In pharmaceuticals, partially solid emulsions can used for topical delivery [7]. And, as will be discussed, colloidal particles substantially influence the formation and stability of many food emulsions. Although it describes generalities on how colloids can affect emulsion properties, this chapter is primarily concerned with the application of fat crystals and their effects on emulsion stability.

II. EMULSION FORMATION AND STABILITY

In its simplest form, an emulsion consists of an oil phase, an aqueous phase, and an interface. The formation of a food emulsion is a dynamic process that results

Copyright 2002 by Marcel Dekker. All Rights Reserved.

in the formation of droplets, generally in the range of 0.1–30 μm in size. The increase in interfacial area following emulsification is typically on the order of 10^6 m^2 per cubic meter of dispersed liquid [8]. Contact between oil and water molecules is energetically unfavorable, given their respective hydrophobicity and hydrophilicity [9]. In order to remain appealing for consumers, food emulsions must remain stable over long periods of storage. Being thermodynamically unstable systems, they must be stabilized by improvement of their kinetic stability [10,11], where ''stability'' may be defined as the resistance to physical changes [12].

After enough time, any emulsion will collapse as the aqueous and apolar phases attempt to minimize contact area. There are five main mechanisms that can contribute to emulsion instability: (1) creaming; (2) flocculation; (3) Ostwald ripening; (4) (partial) coalescence; and (5) phase inversion [13]. Creaming (or settling) is due to differences in density between the two phases under the influence of gravity and leads to phase separation [14]. Flocculation is best described as the aggregation of particles due to weak attractive forces between colloids, as typically well described by the Derjaguin–Landau–Verwey–Overbeek (DLVO) theory [15]. Flocculation depends on the energy of interaction between two particles as a function of interparticle distance. The interaction energy is a combination of attractive and repulsive forces. In emulsions, attraction is dependent on London–van der Waals forces whereas repulsion is due to surfactants present at the interface [16]. During flocculation, particles retain their structural integrity [9]; during coalescence, however, two colliding droplets will form a single larger entity as the thin film separating two neighboring droplets ruptures. The Laplace pressure difference causes the droplet to form a single larger droplet [17]. If droplets contain crystalline matter, partial coalescence may take place [18]. Intraglobular fat crystals may pierce droplet membranes and coalesce with other partially crystalline droplets to form an irregularly shaped aggregate, particularly in a flow field. Partial coalescence can lead to phase inversion in which an oil-in-water (O/W) emulsion becomes a water-in-oil (W/O) emulsion, such as during the churning of butter [19]. Lastly, Ostwald ripening is the growth of larger droplets at the expense of smaller ones and is related to the solubility gradient found between small and large droplets [20]. In food emulsions, it is usually of little importance, because there is typically limited solubility between the aqueous and oil phases [21].

The rate at which an emulsion breaks down will be strongly influenced by composition, storage conditions (e.g., temperature fluctuations), and processing (e.g., shear) conditions. Much research dealing with emulsion stabilization has examined the improvement of kinetic stability and the use of emulsifying agents and thickeners. Stabilization is usually achieved by adding small surfactant molecules (e.g., polysorbates, phospholipids) and/or proteins (e.g., milk proteins) and/or thickening agents (gums, gelatin) to the emulsion [22].

Emulsifiers play two roles in emulsion kinetic stability. They lower interfa-

Copyright 2002 by Marcel Dekker. All Rights Reserved.

cial tension between the oil and water phases [23], and they form a mechanically cohesive interfacial film around the droplets, thereby preventing coalescence [24]. Surfactants can impart dynamic properties to the interface that allow it to resist tangential stresses [25]. Some thickening agents (e.g., gum arabic and gum tragacanth) are also surface-active [26]. These agents can influence interfacial phenomena such as surface tension, surface viscosity, and elasticity (or viscoelasticity) [12,27]. Typically, these surface-active agents accumulate at the interface when their free energy in the adsorbed state is lower than that in the unadsorbed state [16]. Depending on conditions, emulsions may be more stable at lower temperature owing to increased phase viscosity. As will be discussed, however, lower temperatures can also destabilize emulsions. Stability against coalescence can also be achieved by mechanical means, such as by reducing the average droplet size an emulsion contains via homogenization (e.g., milk) [28].

III. THE ROLE OF FAT CRYSTALS IN EMULSION STABILITY

The presence of fat crystals can either stabilize or destabilize emulsion droplets, strongly depending on whether they are intraglobular or present in the continuous phase [29].

A. Fat Crystals as Emulsion Stabilizers

It is known that in many emulsified foods solid particles are necessary for emulsion stabilization (e.g., ice crystals in ice cream, egg yolk particles in mayonnaise, and fat particles in whipping cream) [30]. For these particles (such as fat crystals) to assist in the stabilization of emulsions, they must collect at the emulsion droplet interface and adsorb on the surface on the droplet [31], providing a physical barrier to coalescence [32]. The first study on the colloidal stabilization of emulsions was conducted by Pickering [33], who investigated the influence of different metal sulfates on the kinetic stability of emulsions. The study of colloidal particles in food emulsions, in particular the role of fat crystals, is a much more recent phenomenon, being first examined in the 1960s [34]. Stabilizing crystals may originate by way of surfactant solidification at the interface [predominantly monoacylglycerols (MAGs)] and/or the migration of previously formed crystals toward the droplet interface [2].

B. Fat Crystals as Emulsion Destabilizers

As part of the dispersed phase, lipids in a state of incipient or advanced crystallization may substantially increase emulsion destabilization. During processing and/or storage, intraglobular fat (e.g., in cream, margarines) may solidify, form-

Copyright 2002 by Marcel Dekker. All Rights Reserved.

ing crystals that can protrude through and disrupt the interface, leading to droplet coalescence and eventual phase inversion, if necessary [35].

IV. PARAMETERS DICTATING THE ROLE OF FAT CRYSTALS IN EMULSION

The key factors that will determine the influence of fat crystals on emulsion stabilization are

1. The wettability of the crystals at the interface [2]
2. Interfacial film rheology [25]
3. Particle microstructure (polymorphism, morphology, etc.) [36]
4. Location of fat crystals in the dispersed phase (O/W emulsion) or continuous phase (W/O emulsion) [37]

All of these factors are intimately related via interparticle interactions [38]. These will now be discussed in detail.

A. Wettability and Contact Angles

Contact angles see many uses in the food area. For example, they have been used to examine the adhesion of edible oil to food contact surfaces [39]. In a food system where both hydrophilic (aqueous) and hydrophobic (oil) phases are present, there is a constant struggle by both phases to minimize their contact area. Similarly, if a drop of water is placed on a hydrophobic surface, such as a fat crystal, the water will not want to spread on it and instead will bead. The primary use of contact angles is to help characterize a surface with respect to its surface free energy and critical surface tension, as an aid to understanding wetting behavior and surface morphology, for example. The surface free energy (γ_s) of a solid surface can be defined by

$$\gamma_s = \left(\frac{\Delta G^c}{2}\right) = \left(\frac{\partial G}{\partial A}\right)_{T,P,n_i} \tag{1}$$

where ΔG^c = free energy of cohesion, G = Gibbs free energy, and A = area. Therefore, wetting is a thermodynamic process. The free energy change involved will determine the rate at which wetting proceeds and how far it can progress against external forces [40].

Fat crystals influence emulsion (in)stability, depending primarily on how they are wetted by the continuous or dispersed phases [37], based on a concept

Copyright 2002 by Marcel Dekker. All Rights Reserved.

introduced by Finkle et al. [41]. During or after emulsification, particles may adsorb to the interface if it is energetically favorable (Figs. 1a and 1b). Depending on the type of emulsion (O/W or W/O), the composition of the aqueous and oil phase, and the composition and surface properties of the particles, adsorbed particles will preferentially wet the aqueous or oil phase (Fig. 1c). The behavior of a particle at the interface will be described by the contact angle [29], which is the angle formed at the boundary between three phases (Fig. 1d). In this particular case, water acts as the continuous phase and oil as the dispersed phase, and the colloidal particle is partially embedded within the interface at an equilibrium distance dictated by the interparticle forces. With a contact angle at the solid/water/oil interface across the water phase smaller than 90°, the particle will stabilize O/W emulsions. With contact angles greater than 90°, the particles stabilize a W/O emulsion [42]. If the particles used are completely wetted by either the oil or water phase (and therefore the contact angle is 180°), they become fully dispersed in that phase and any emulsion-stabilizing effect is negated. A 90° contact angle means that a crystal is equally wetted by the oil and aqueous phases. In practice, for O/W emulsions, the contact angle should be 60–70° for optimal stability [43].

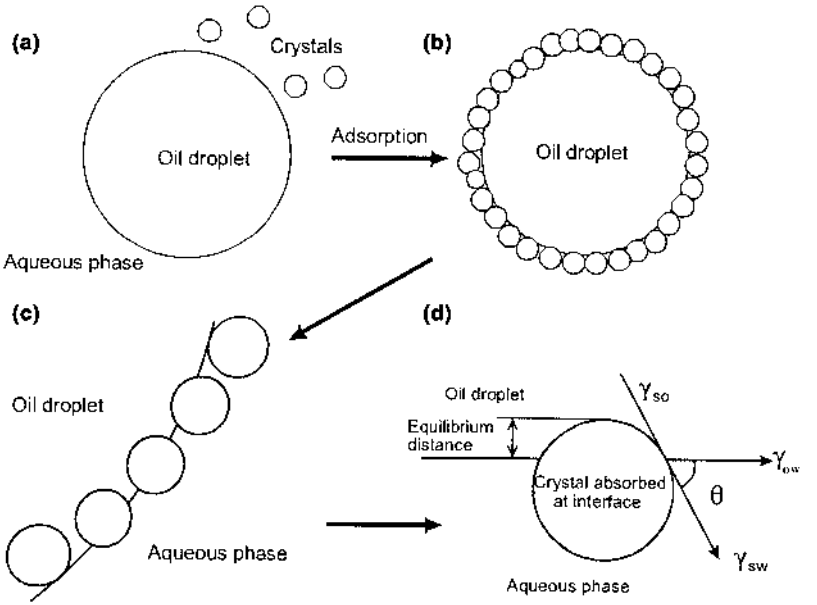

Figure 1 Adsorption and contact angles of fat crystals at the interface of an oil-in-water. (Adapted from Ref. 30.)

Copyright 2002 by Marcel Dekker. All Rights Reserved.

The important parameters in an emulsified system consisting of solid particles and two immiscible liquid phases are γ_{ow}, γ_{so}, and γ_{sw}, which are the surface tensions of the oil/water, solid/oil, and solid/water interfaces, respectively. Reinders [44] stated that three possibilities exist.

If the crystal is completely wetted by water, then

$$\gamma_{sw} > \gamma_{ow} - \gamma_{so} \tag{2}$$

If the crystal is completely wetted by oil, then

$$\gamma_{os} > \gamma_{ow} - \gamma_{sw} \tag{3}$$

Finally, if the crystal is wetted by both the water and oil phases, then

$$\gamma_{ow} > \gamma_{os} - \gamma_{sw} \tag{4}$$

It is only in this third situation that a fat crystal would locate itself at the oil/water interface. The ''resolution'' of forces at the junction point between these three tensions is described by using Young's equation [45],

$$\gamma_{ow} \cos \theta = -\gamma_{ow} \cos(180 - \theta) = \gamma_{sw} - \gamma_{so} \tag{5a}$$

where θ is the Young's contact angle measured through the oil phase,

$$\gamma_{ow} \cos \theta = -\gamma_{ow} \cos(180 - \theta) = \gamma_{so} - \gamma_{sw} \tag{5b}$$

where θ is the Young's contact angle measured through the water phase.

The angle in any system will depend on the various surface and/or interfacial properties of the phases. Thermodynamically, the surface and interfacial tensions, hydrophobic and hydrophilic properties, and the presence of impurities and particle properties such as roughness determine these properties. Viewed in general terms, the contact angle can indicate the relative surface properties of solids or interfacial properties of liquids and may be used to gauge the amount of interaction between various phases [46]. In foods, depending on the final application, it is possible to modify the contact between aqueous and oil phases.

Equilibrium will occur when the presence of a surface-active agent does not lower γ any further. This concentration is typically at the critical micelle concentration [47]. Modification of the contact angle (and therefore emulsion stability) can be achieved by a modification of the aqueous, oil, or solid phase so as to alter γ_{ow}, γ_{os}, or γ_{sw}. As described later, this can be achieved with the use of surfactants. The interfacial tension and surface tension are measurements of droplet deformation. Neither γ_{sw} nor γ_{so} can be directly measured, because the solid cannot be ''deformed.'' To solve Young's equation and to determine the solid/water and solid/oil interfacial surface tensions, the equation-of-state approach for interfacial surface tensions is required [48]:

Copyright 2002 by Marcel Dekker. All Rights Reserved.

$$\gamma_{sw} = \frac{(\gamma_{ow})^{1/2} - (\gamma_{sw})^{1/2}}{1 - 0.015(\gamma_{ow} \times \gamma_{sw})^{1/2}} \tag{6}$$

With Eq. (5a) or (5b) and Eq. (6), the unknown variables can be calculated. Combining the appropriate equations results in:

$$\cos\theta = \frac{(0.015\gamma_{sw} - 2.00)(\gamma_{ow}\,\gamma_{sw})^{1/2} + \gamma_{ow}}{\gamma_{ow}[0.015(\gamma_{ow}\gamma_{sw})^{1/2} - 1]} \tag{7}$$

This semiempirical equation of state was proposed by Good [46] and allows the calculation of γ_{sw} once the contact angle and oil/water interfacial tension are known.

The hydrophobic or hydrophilic nature of the solid and the liquid can dictate the shape and contact angle of the droplet. In practice, hydrophobic solids will have high interfacial surface tensions with aqueous droplets and smaller contact angles, resulting in droplets with a more spherical shape. Conversely, droplets formed on hydrophilic surfaces will be flatter, with a larger contact angle, due to the low interfacial tension between hydrophilic surfaces and the droplet. Gelot et al. [49] found that carbon black, which is hydrophobic, promoted formation of W/O (water-in-toluene) emulsions.

Zettlemoyer [50] developed a unifying theory for interactions at interfaces, based on dispersion forces. This was later modified by Johansson and Bergenstaohl [51], who included an interaction term (I). At the interface between two immiscible liquids (e.g., water and oil), the interfacial tension can be expressed as

$$\gamma_{12} = \gamma_1 + \gamma_2 - 2(\gamma_1^d\gamma_2^d)^{1/2} - I_{12} \tag{8}$$

where $\gamma_1 = \gamma_1^d + \gamma_1^p$, $\gamma_2 = \gamma_2^d + \gamma_2^p$, d represents the dispersion forces, and p represents the polar forces. One $(\gamma_1^d\gamma_2^d)^{1/2}$ is the force of attraction of phase 1 for phase 2, and the second is the force of attraction of phase 2 for phase 1. I_{12} is the attraction of the polar phase for the nonpolar phase due to polar interaction and opposes γ_1 and γ_2.

The interfacial tension is the sum of the contributions of tension between two adjacent monolayers in direct contact (Fig. 2). Components 1 and 2 in Eq. (8) can be replaced by a fat crystal (or solid) and oil (SO), a fat crystal and water (SW), or oil and water (OW). Because fat crystals and oil are essentially apolar, $I_{SO} \cong 0$, and γ_o consists of dispersion forces only, we obtain

$$-\gamma_{ow}\cos\theta = -\gamma_{ow} + 2(\sqrt{\gamma_o^d} - \sqrt{\gamma_w^d}) \times (\sqrt{\gamma_o^d} - \sqrt{\gamma_s^d}) + I_{sw} - I_{ow} \tag{9}$$

Treating $2(\sqrt{\gamma_o^d} - \sqrt{\gamma_w^d}) \times (\sqrt{\gamma_o^d} - \sqrt{\gamma_s^d})$ as a constant C, we obtain

$$-\gamma_{ow}\cos\theta = -\gamma_{ow} + C + I_{sw} - I_{ow} \tag{10}$$

Copyright 2002 by Marcel Dekker. All Rights Reserved.

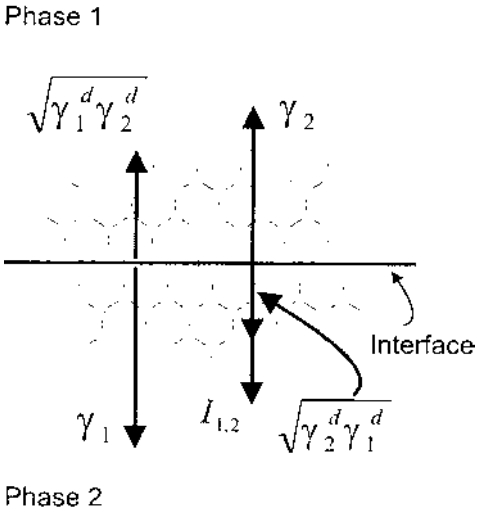

Figure 2 Interface between two adjacent phases. (Adapted from Refs. 51 and 52.)

Derivations of equations similar to Eq. (10) are shown in Campbell [53]. The importance of C can be estimated in this way. The term γ_w^d is ~22 mN/m, and γ_o^d is dependent on the type of oil but typically ranges from 32 to 36 mN/m; for example, for cottonseed oil $\gamma_o^d = 35.4$ mN/m, and for oleic acid $\gamma_o^d = 32.5$ mN/m. The term γ_s^d has never been calculated and is not available in the literature. However, the density difference between crystals (ρ_s) and oil (ρ_o) is ~1.1. The term γ_s^d originates from van der Waals interactions; it can be assumed that it is proportional to the Hamaker constant ($\gamma_s^d \propto A_H$). The Hamaker constant is dependent on density as follows:

$$A_H \propto \rho^2 \tag{11}$$

We therefore obtain

$$\gamma_s^d \approx \left(\frac{\rho_s}{\rho_o}\right)^2 \gamma_o^d \approx 1.21\gamma_o^d \tag{12}$$

Using the previously given γ_o^d values for oleic acid and cottonseed oil, γ_s^d is equal to 39.3 and 42.8 mN/m, respectively. Hence the corresponding values for C are -1.1 and -1.5, with an average value of -1.3 mN/m. Equation (10) can therefore be written as

$$1 - \cos\theta = \frac{I_{sw} - I_{ow} - 1.3}{\gamma_{ow}} \tag{13}$$

Copyright 2002 by Marcel Dekker. All Rights Reserved.

When viewed through the oil phase, Eq. (13) shows than an increase in polar interactions for fat crystal and water (I_{sw}) results in an increase in contact angle. Therefore, a high (I_{sw}) value drives a fat crystal toward the water phase. This would occur with polar crystals. Likewise, a high (I_{ow}) value drives a fat crystal toward the oil phase and lowers the contact angle. This would occur with nonpolar crystals.

Johansson and Bergenståhl [51] mentioned that a high I_{ow} force as well as a high value for γ_{ow} represented a resistance to fat crystal penetration at the interface. It follows that, using Eq. (11), for interfacial crystal penetration, high polar interaction excess ($I_{sw} - I_{ow}$) would be necessary to increase the contact angle, assuming a high γ_{ow}. Figure 3 shows the effect of three emulsifiers on polar excess energy of an oil–water–palm stearin crystal system. Shown are the polar excess energies for crystals approaching the oil/water interface from the water side and from the oil side (advancing and receding contact angles, respectively).

There are limitations to this model, however. Notably, these equations assume that the colloid surfaces are ideal—absolutely smooth and flat, completely homogeneous, and isotropic. In reality, surfaces are rather rough and chemically heterogeneous [54]. Such surfaces are difficult to achieve; the only representative surfaces are carefully cleaved mica and perfect crystals. The role of surface roughness is discussed later.

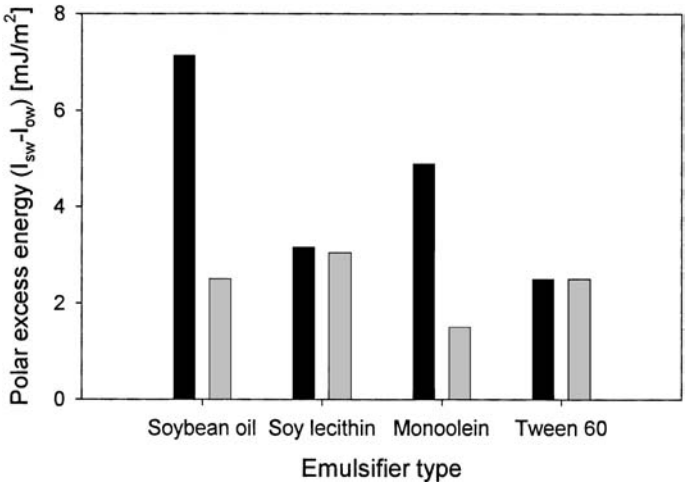

Figure 3 The influence of emulsifiers (1–2% in oil phase) on the polar excess energy for a water–oil–fat crystal system. Shown are the polar excess energies for crystals approaching the oil/water interface from the water side (advancing contact angle) and from the oil side (receding contact angle). (Adapted from Ref. 51.)

Copyright 2002 by Marcel Dekker. All Rights Reserved.

1. Energy Considerations for Crystals at an Interface

The formation of an emulsion stabilized by interfacial fat crystals depends on the free energy change associated with the transfer of a crystal from the continuous phase to the droplet surface. If we consider a fat crystal of radius r immersed to its equilibrium distance within an interface, this depth will be $1 - \cos\theta$ (Fig. 1d) [3]. The interfacial tension attributed to this crystal will be

$$\pi r^2[2\gamma_{os}(1 - \cos\theta) + 2\gamma_{ws}(1 - \cos\theta) - \gamma_{ws}\sin^2\theta] \tag{14}$$

The third term in brackets represents the energy lost because an area $\pi r^2 \sin^2\theta$ of the O/W interface has been removed to accommodate the particle. Substituting in Young's equation [Eq. (5)], the energy in Eq. (14) becomes

$$\pi r^2 \gamma_{ws} - \pi r^2 4\gamma_{ow}(1 - \cos\theta)^2 \tag{15}$$

The first term in Eq. (15) is the interfacial energy of the particle fully immersed in the aqueous phase, whereas the second term represents the change in interfacial energy when the particle is transferred from the bulk to the interface. For example, if we assume that $\gamma_{ow} = 30$ mN/m and $r \sim 0.29$ μm, then at room temperature $\pi r^2 \gamma_{ow} \approx 2 \times 10^6\, kT$. Therefore, a particle embedded in the interface between the oil and water phases is trapped in a deep energy well. It was Pieranski [55], during a microscopic study of polystyrene spheres, who proposed that such particles were trapped at an interface in an energy well deeper than kT. The stability of the system was surmised to depend on the depth of the well. In this system, he calculated that the energy was larger than kT by a factor of 10^6, thereby indicating that the repulsion potential was much larger than the attraction potential. In any given case, the resistance energy will be highest with a contact angle of 90° [16]. Theoretical studies of the energetics of interfacial particles can be found in Tambe and Sharma [32], Levine and Bowen [56,57], Levine et al. [3,58], Chan et al. [59], Jacques et al. [60], and Rapachietta and Neumann [61].

2. Dependence of Contact Angles on Surfactants

Contact angles will be modified by surfactant composition, which may influence many properties of the interface such as surface charge, surface tension, and surface viscosity [62,63]. In an elegant study on the effects of fat crystals in emulsion stability, Campbell [53] examined the role of different emulsifiers (three MAGs with different iodine values, Span 80, and lecithin) on the contact angles of a hardened palm oil–soybean oil–water (PO/SBO/H_2O) system. In Table 1, the effect of 0.3% emulsifier on the contact angle of oil droplets in water is shown. There was no effect of the different types of emulsifiers on the contact angle, which stayed constant at ~150°. With the addition of sodium caseinate (1% w/w) to the aqueous phase, however, smaller contact angles were obtained.

Copyright 2002 by Marcel Dekker. All Rights Reserved.

Table 1 Effect of Sodium Caseinate (1% w/w) and/or Emulsifier (0.3% w/w) in the Oil Phase on the Contact Angle in a Hardened Palm Oil–Soybean Oil–Water System

Emulsifier	Contact angle with 0.3% emulsifier (w/w) in oil phase	Contact angle with emulsifier and 1% (w/w) sodium caseinate in aqueous phase
No emulsifier	150°	—
Saturated MAG	150°	148°
Partly saturated MAG	151°	142°
Unsaturated MAG	150°	130°
Span 80	151°	130°
Lecithin	149°	82°

Source: Ref. 53.

The results of the emulsions containing added sodium caseinate, when plotted as $\gamma_{ow} \cos \theta$ versus γ_{ow}, did not fall on a straight line, as with the PO/SBO/H_2O system (Fig. 4). This can be explained as the protein affecting the I_{sw} (polar interactions, discussed earlier), which then led to decreases in contact angles. The surfactants used will preferentially adsorb to one interface, depending on their polarity [53]. Van Boekel [18] found that certain emulsifiers enhanced the wettability of the crystals by the aqueous phase, thereby promoting emulsion instability. Darling [37] found a good relationship between contact angles and emulsion instability. In a study on the churning of butterfat, it was found that as the milkfat crystals became preferentially wetted by the aqueous phase, the emulsion droplets became increasingly unstable. This was likely a function of the wetting properties. As the contact angle increased, the crystals protruded more from the oil droplet [64]. Tambe and Sharma [65] examined the role of stearic acid as emulsifier on the contact angle of calcite crystals in a water–*n*-decane emulsion (Fig. 5). As the stearic acid concentration increased, the calcite crystals became more hydrophobic, with the contact angle value increasing from 40° at 10^{-4}% (w/w) to 130° at 0.5% (w/w).

3. Fat Crystal Surface Heterogeneity and Contact Angle Hysteresis

Surfaces may be broadly subdivided into high energy and low energy surfaces. High energy surfaces are generally hard solids such as diamond, silica, and most metals, these being characterized on the basis that liquids having high surface

Copyright 2002 by Marcel Dekker. All Rights Reserved.

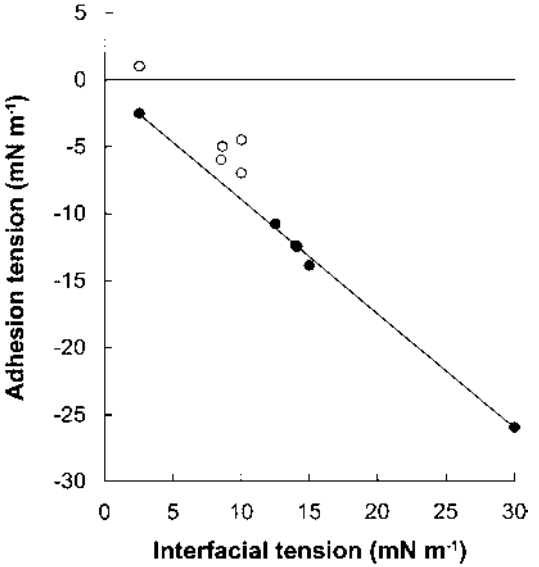

Figure 4 Adhesion tension versus interfacial tension for a hardened palm oil–soybean oil–water system (○) with and (●) without 1% (w/w) sodium caseinate in the aqueous phase. (Results from Ref. 53.)

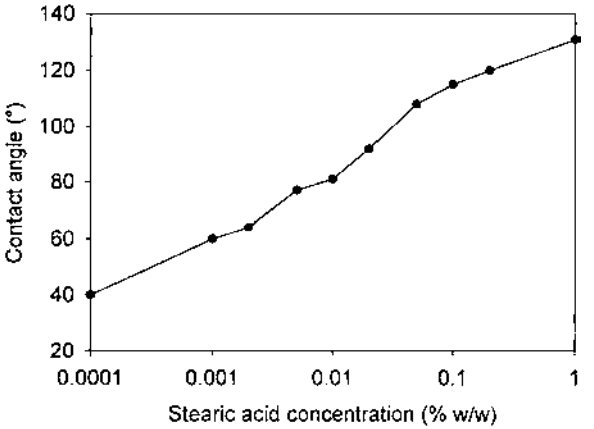

Figure 5 Dependence of calcite crystal contact angles in water–*n*-decane–calcite crystal system on stearic acid concentration. (Results from Ref. 65.)

Copyright 2002 by Marcel Dekker. All Rights Reserved.

tension (i.e., water) will spread with a zero contact angle. High energy solids have surface free energies that range from several hundred to several thousand ergs per square centimeter. Low energy surfaces include most liquids and low melting solids such as fats, oils, and organic polymers and have surface free energies of less than 1000 erg/cm^2. The surface energy characteristics do not necessarily correspond to the mechanical properties of the substance forming the surface, because the latter are determined primarily by the structure underlying the surface.

The majority of surfaces are heterogeneous and have a certain degree of roughness associated with them. Deviations from a perfectly smooth topography, both microscopically and macroscopically, have many causes, including variations in chemical composition; both primary material components and impurities present either as an adsorbed film or as molecules or even atoms. Other causes include stress on the system such as deformation of the surface, swelling of the solid surface, and possible molecular reorientation or reorganization of surface molecules. Other less important causes of surface heterogeneity include variation in crystallographic faces on a homogeneous solid and/or the existence of crystal edges and corners, steps or ledges, and dislocations.

An important fact to consider when dealing with surface roughness is that it is time-dependent, even during the time scale of observation. Therefore, it can affect macroscopically observable properties such as contact angles. The most commonly used parameter for the estimation of surface roughness is the roughness factor [40],

$$r = A/a \tag{16}$$

where A is the true surface and a is the surface measured in the plane of the interface.

For ideal surfaces $r = 1$, and for all other surfaces $r > 1$, because the true surface of any solid will be rougher than the geometric surface. The effect of a roughened surface will be to magnify the existing wetting properties of a solid. Hence, a surface that has a positive wetting tendency will wet more readily if its surface becomes wetter.

Wenzel [40] modified Young's contact angle equation to incorporate the roughness factor such that

$$r(\gamma_{sw} - \gamma_{so}) = \gamma_{ow} \cos \theta' \tag{17}$$

where θ' is the contact angle on the rough surface (the apparent contact angle).

Busscher et al. [66] studied the surface roughness of polymers and found that for a surface roughness of <0.1 μm there was no effect on contact angle. However, contrary to Wenzel [40], they found that surface roughness did not affect contact angles between 60° and 86°. As mentioned earlier, the Wenzel equation essentially indicates that roughness amplifies the wetting behavior on

Copyright 2002 by Marcel Dekker. All Rights Reserved.

a flat surface. Hence, according to Wenzel [40], for any equilibrium contact angle greater than 90° the contact angle increases for rough surfaces, whereas for any equilibrium contact angle less than 90° the contact angle decreases.

For any system, contact angles are typically measured after a droplet has come to rest. However, in dynamic systems the contact angle is rate-dependent, and it thus becomes necessary to include information detailing the rate at which the three-phase line is moving. In this context, roughness can play an important role.

The difference between the receding and advancing contact angles is called hysteresis and is simply defined as

$$H = \theta_a - \theta_r \tag{18}$$

where θ_a is the advancing contact angle, and θ_r is the receding contact angle.

It has been shown that the receding angle is more sensitive to roughness effects than the advancing angle, including roughness on the scale of surface defects. Hysteresis has also been found to increase with decreasing droplet size, though this effect appears to be linked to the larger anomaly of the effect of curvature of the three-phase line [46].

With respect to fat crystals in food applications, the literature is very scant. Although crystal roughness has been studied for some time [67], the question of how the roughness of fat crystals affects contact angles remains virtually unanswered. Substantial progress in the area of surface roughness was made by Neumann [68], who examined contact angle dependence on heterogeneous surfaces.

B. Interfacial Rheology

Most food emulsions are highly complex systems in terms of both composition and structure and also kinetically and thermodynamically speaking [69]. To control the formation, stability, and rheology of food emulsions requires an understanding of the interactions between the various elements present in the system [70]. Recently, progress has been made in understanding the interaction behavior at the O/W interface between some of the components found in food emulsions, particularly between different proteins and surfactants and, to a lesser extent, between proteins and fat crystals.

As with bulk emulsion properties, the interface can exhibit viscous, elastic, and viscoelastic properties [10]. In the presence of an interfacial particle film, an interface will begin to demonstrate viscoelastic behavior. The ability of an emulsion to resist coalescence will depend largely on the properties of the interface. A highly viscous and rigid interfacial film laden with particles will retard the rate of film drainage and resist rupture, thereby promoting stability [71,72]. Hence, by controlling interface rheology, one can control the drainage of thin

Copyright 2002 by Marcel Dekker. All Rights Reserved.

liquid films trapped between coalescing droplets, which may also affect the displacement of crystals away from the interface during droplet coalescence [65,73]. This increases emulsion stability by retarding the rate of film drainage between coalescing droplets and increasing the displacement energy of interfacial particles (discussed earlier) present between two coalescing droplets [74].

Beyond the simple presence of fat crystals at interfaces, it is important to evaluate fat crystal interactions at the interface with protein and surfactants. These interactions can largely dictate the stability of an emulsion stabilized by fat crystals.

For example, Kiosseoglou [75] discussed the role of surface-active lipids at the O/W interface on the viscoelastic parameters of bovine serum albumin (BSA), sodium caseinate, and egg yolk films during adsorption at the olive oil/protein solution interface. It was postulated that film viscoelasticity was the result of the interaction of surface-active lipids with folded and unfolded proteins at the interface. Benjamins et al. [76] were the first to report on the development of interfacial viscoelasticity at the O/W interface. They found that the proteins with the least conformational flexibility increased the interfacial viscoelastic modulus the most (ovalbumin $>$ BSA $>$ sodium caseinate).

The composition of the stabilizing layer around droplets will be affected by the strength of the interactions between the surface-active species, the ratio between emulsifiers and droplet surface area, and the presence of any interfacial competitive behavior. During the emulsification process, it has been shown that competitive adsorption between different proteins and between surfactants and proteins occurs at the O/W interface [77–80] and at the air/water interface [81], where they compete for attachment, thereby affecting emulsion stability [82,83]. Because of their smaller size, surfactants have a propensity to displace proteins from the interface. This phenomenon has been observed microscopically using confocal microscopy [84]. Dickinson et al. [85] observed sudden changes in interfacial shear during displacement of one milk protein by another (e.g., α-lactalbumin by β-casein). Gaonkar and Borwankar [86] examined the interfacial competitive adsorption of MAGs and lecithin and found the latter to be more surface-active than the former. The competitive adsorption behavior of proteins and surfactants at the interface will influence the role of crystals at the interface, because interactions between proteins and fat crystals in the interfacial region may affect the mechanical strength of the interfacial film [87]. Mackie et al. [88] observed that valve homogenization provoked shear-induced structural changes in Tween 20 and β-casein, resulting in altered interfacial adsorption. This may have important implications for emulsion formation, because shearing may alter emulsifier behavior in a manner not predicted from initial emulsifier properties.

Modification of the interface will also occur as a result of fat crystal–emulsifier interactions. Many food emulsions (e.g., ice cream, margarine) are prepared

Copyright 2002 by Marcel Dekker. All Rights Reserved.

by mixing the ingredients at elevated temperatures (above the melting point of all crystallizing components) and cooling the product as it is homogenized. Phase transitions occur during this process. Emulsifiers, commonly used in many foods, can significantly alter the crystallization behavior of fat crystals, which ultimately influences the final properties of the finished emulsion, including its organoleptic properties as well as its stability.

Emulsifiers have the ability to adsorb onto surfaces or interfaces. In particular, emulsifiers can interact with fat crystals. For example, lecithin has been shown to adsorb to fat crystals, making their surface more polar [89]. Adsorption has been shown to be rapid (<5 min) for polar lecithins and slow (hours) for less polar lecithins. Xu et al. [90] found that sodium caseinate stabilized emulsions by forming a layer of caseinate submicelles around the fat particles at the interface. They also observed that xanthan gum caused the fat structure inside food emulsions to be less ordered, thereby increasing emulsion instability. Brooker [91,92] proposed that fat crystals act as transporters for the transfer of interfacial material to the surface of expanding bubbles during the rising of bread dough. Observations showed that a larger number of smaller crystals provided greater interfacial material to expanding bubbles than larger crystals or crystal aggregates, because of the greater surface area of the former. Excellent work on fat crystal–emulsifier interactions was performed by Johansson and Bergenståhl [93], who examined adsorption isotherms of emulsifiers to fat crystals and the resulting effect on sedimentation behavior. They found that at high concentrations, most of the emulsifiers examined adsorbed weakly to fat crystals and formed tight monolayers, leading to increased adhesion. At low concentrations, loosely packed layers formed and decreased adhesion was observed. In agreement with work by Campbell [53] and Darling [37], MAGs, their esters, and fatty acid esters provided fat crystals with increased polarity, thereby giving surface activity to these crystals.

C. Role of Morphology

Particle shape is of some importance in food emulsion stability, but the extent to which it plays a role remains largely unknown. Schudel et al. [94] studied the role of surface morphology of spheroidal hematite particles on aggregation behavior in aqueous solutions. They found that surface roughness on a length scale of 5–10 nm was not an important factor because differences in surface roughness did not appreciably affect aggregation rate constants. They also found that the DLVO theory underestimated aggregation by many orders of magnitude and attributed this to the surface heterogeneity or particle roughness. However, Fuji et al. [62] found that surface modification of silica with alkoxy groups substantially influenced wettability. Microscopic contact angles were dependent on nanoscopic (molecular and atomic) properties, which dictated contact angle measurements.

Copyright 2002 by Marcel Dekker. All Rights Reserved.

Campbell [53] mentioned that crystal morphology could affect emulsion stability, because the equilibrium position of crystals at the O/W interface could be dependent on particle microstructure. Dippenaar [95] examined the role of crystal morphology with respect to froth stability. Crystals examined included quartz, galena, sulfur, and glass beads. Rough particles of quartz or sulfur would float with more than half of their crystal volume in the air phase with a contact angle smaller than 90° and less than half of their volume in the air phase if the contact angle was greater than 90°. Rods and platelets tangentially oriented themselves at the interface. Film destabilization (rupture) was observed when the liquid film thinned down to approximately half of the particle diameter. Overall, the orientation of smooth, spherical particles at an air/water interface was governed by the contact angle of the liquid on the solid. With nonspherical particles, the orientation in the interface was also a function of particle shape. The applicability of such research to food systems is limited. However, it does provide insight into possible mechanisms of stabilization and disruption.

Lipid morphology at interfaces will also be dependent on the composition of the aqueous phase. For example, in a study examining the stability of MAGs at oil/water interfaces, Domínguez and Patino [96] found that the structure of monopalmitin films spread on aqueous solutions of sugars was dependent on the type of sugar added (sucrose, fructose, or glucose). Schulman and Leja [42] noted that polar groups of emulsifiers adsorbed at an oil/water interface are oriented toward the water phase whereas the hydrocarbon chains are oriented toward the oil phase. Funasaki et al. [21] discussed the orientation states of TAG molecules at air/water interfaces and postulated different conformations based on fatty acid chain length (Fig. 6). In triacetin, two of three chains exist in the air and the other in water. Tributyrin, tricaproin, and tristearin have all three of their chains oriented toward the air; however, only the latter has parallel chains.

Such observations raise the importance of interfacial conformation and the role this conformation plays in fat crystal microstructure, particularly in emul-

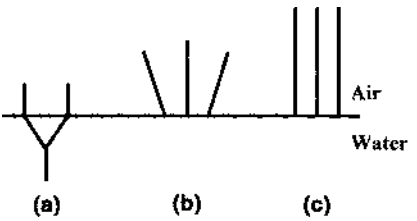

Figure 6 Representation of the orientation state of TAGs at the air/water interface. (a) Triacetin; (b) tributyrin; (c) tristearin. (Adapted from Ref. 21.)

Copyright 2002 by Marcel Dekker. All Rights Reserved.

sions. It can be postulated that the microstructure of a fat that crystallizes at an O/W interface will depend on interfacial tension between the phases, with a greater interfacial tension leading to aliphatic chains being less exposed to the aqueous environment than in an environment with a lower interfacial tension. The interfacial conformation that a fat crystal adopts at an interface will dictate the morphology of the crystal, which may dictate its role in emulsion stability and hence potentially the rheological properties of the interface.

As shown by Johannson and Bergenståhl [89,93]. MAGs, MAG esters, and fatty acid esters adsorb to fat crystals with the aliphatic chains directed toward the crystals owing to chemical complementarity. This is in agreement with the results presented by Campbell [53], who demonstrated, using contact angle measurements, that food emulsifiers (monoglycerides, lecithins) render fat crystals more polar. At low concentrations, loosely packed layers were formed by these emulsifiers, causing a weak steric stabilization of the fat crystals. This has important implications for certain foods. For instance, when sorbitan esters of fatty acids are added to margarine to stabilize the β′ form of the fat crystals, the strength of the crystal network thereby decreases as a result of the weak stabilization effect of sorbitan esters. This results in oiling out.

For emulsifiers whose headgroup is large and highly polar, a destabilization can occur, due to an increase in polar interaction between crystals even at low emulsifier concentration. Generally, when emulsifier concentrations increase, tight layers are formed and adhesion between the crystals increases. The increase in adhesion may be interpreted as an increase in the polarity of the surface. Pure phosphatidylcholine stabilizes fat crystals weakly at low concentrations. At slightly higher concentrations, a small region of weak destabilization occurs, which changes to strong stabilization at intermediate and high concentrations. Hence, adsorption is complicated and difficult to understand, at least at low concentrations. At high concentrations, double layers (or aggregates) are formed on the fat surface, with the hydrocarbon chains directed toward the oil in the outermost layer.

Lucassen-Reynders and van den Tempel [97] found that the presence of water- and oil-soluble surfactants reduced the interaction between tristearin crystals, allowing the crystals to reach the interface of W/O emulsion droplets. Ogden and Rosenthal [87,98] found that lysozyme and tristearin crystals increased interfacial shear viscosity synergistically in various systems. They found that crystals were flocculating at the interface. Results were obtained at a planar interface using a torsion-wire shear viscometer. Therefore, determination of the rate of protein–fat crystal interactions was impossible because the surface in an emulsion is many orders of magnitude greater than a planar interface. Ogden and Rosenthal [36] cleverly examined interactions between sodium caseinate and stable β′ and β crystals at the O/W interface. They found that interactions between β′ crystals and sodium caseinate at the interface increased interfacial shear viscosity more

Copyright 2002 by Marcel Dekker. All Rights Reserved.

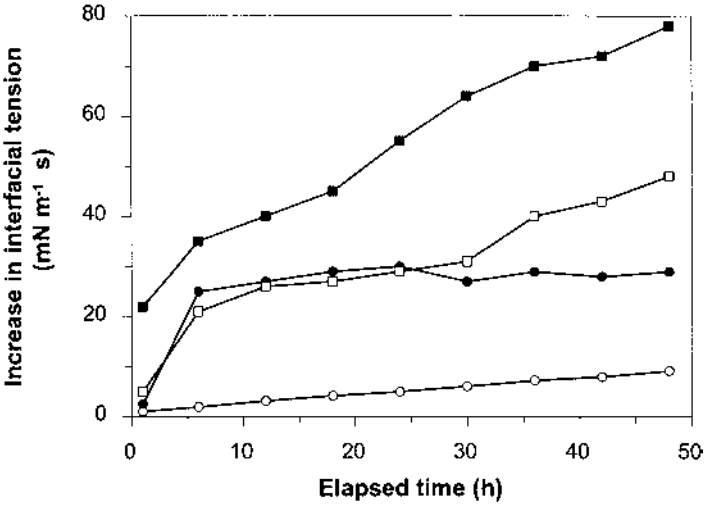

Figure 7 Interfacial shear viscosity as affected by the interaction of sodium caseinate and different polymorphic form of fat crystals located at the interface. (○), β-polymorph hydrogenated palm oil mid fraction (HPMF) crystallized in hexane; (●), β-polymorph tristearin crystallized in oil; (□), β′-polymorph HPMF crystallized in hexane; (■), β′-polymorph HPMF crystallized in oil. (Results from Ref. 36.)

than β crystals, as depicted in Figure 7. Generally, β′ crystals should lead to higher viscosity than β crystals, given their smaller size and higher surface area, and should also lead to more particle interactions and potentially to greater interfacial viscosity. Interestingly, the β crystals used in their study were smaller than β′ crystals, contrary to many literature findings.

Discontinuities in interfacial tension versus temperature have been reported by Lutton et al. [99] and Krog and Larsson [100]. Lutton et al. [99] surmised that a break in γ versus temperature was the result of the melting of an interfacial surfactant monolayer. The abrupt change in slope resulting from the melting could be interpreted from

$$\left(\frac{\partial H}{\partial A}\right)_{P,T} = \gamma - T\left(\frac{\partial \gamma}{\partial T}\right)_{P,A} \tag{19}$$

where H is the enthalpy of the interface, A the area of the interface, T the temperature, P the pressure, and γ the interfacial tension.

The change in $\partial H/\partial A$ at the break corresponded to the surfactant monolayer's α-form heat of fusion. Estimated areas for the surfactant molecules below

Copyright 2002 by Marcel Dekker. All Rights Reserved.

the inflection point were ~20 Å^2, indicating that the emulsifiers were closely packed as in a crystal. Surfactant areas above the inflection point were ~60 Å^2/molecule, compatible with the picture of chains in a liquid state and interacting less strongly.

Krog and Larsson [100] found that monopalmitin ''squeezed out'' milk protein from the interface at its critical crystallization temperature (Fig. 8). With only milk protein in the aqueous phase and no monopalmitin (MP) in the oil phase, the interfacial tension remained at ~10 mN/m irrespective of temperature (from 40 to 5°C). With MP in the oil phase and no milk protein in the aqueous phase, an interfacial tension of ~17 mN/m was obtained at 40°C, which then dropped sharply at ~18°C when the MP began to crystallize. In a combined system containing both the MP and milk proteins, the initial interfacial tension was ~10 mN/m. Upon decreasing the temperature slowly to 5°C, a sharp decrease in interfacial tension took place at 18°C, indicating the ''squeezing out'' of the milk protein by the MP. This effect of MAGs is commonly reported in the formation of ice cream structure. In a study of contact angles in a system containing oil, water, and fat crystals, Campbell [53] found that the addition of sodium caseinate to the aqueous phase lowered contact angles. It was postulated that the presence of emulsifier in the oil phase influenced the degree of protein adsorption to the fat crystal surface.

All of these results clearly indicate that interactions between crystals and

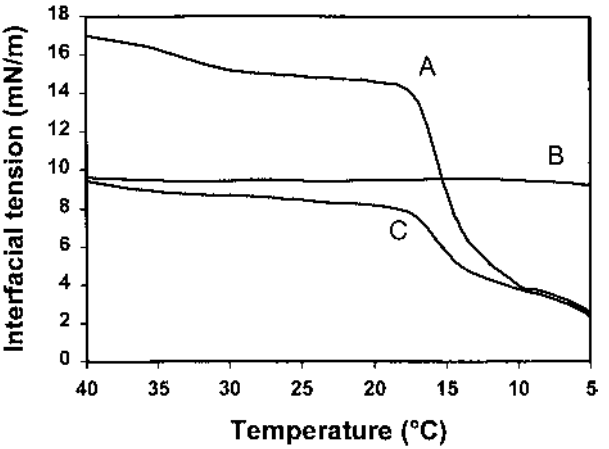

Figure 8 Interfacial tension versus temperature at the oil/water interface. Curve A: 0.2% monopalmitin (MP) in the oil phase against distilled water. Curve B: Oil with no emulsifier against a solution of 0.01% milk protein in distilled water. Curve C: 0.2% MP in oil against a solution of 0.01% milk protein in distilled water. (Adapted from Ref. 100.)

Copyright 2002 by Marcel Dekker. All Rights Reserved.

proteins do exist. Fat crystals can be expected to have little or no surface charge; therefore most of the interactions involving fat crystals would be adhesive in nature [93]. Most likely, in a mixed protein–fat crystal system, where there appears to be a synergistic effect, the hydrophobic moieties of the proteins orient themselves toward the fat crystals and oil phase and interact. Given the environmental conditions in emulsions (i.e., water + oil + surface-active agent), this leads to a net association between the protein and fat crystals due to hydrophobic interactions [101] in which the associated molecules have a more negative Gibbs energy than the sum of the hydrophobic effects of the individual molecules [102]. The importance of these interactions is sufficient to alter the rheological properties of the emulsion.

D. Location of Fat Crystals

The location of the crystals within the emulsion is also of importance. The next two subsections discuss how emulsion stabilization is achieved by droplet coverage and how interglobular fat can destabilize oil droplets.

1. Interfacial Particles

Interfacial fat crystals will stabilize an emulsion by providing steric hindrance to droplet–droplet coalescence and by reducing the rate of film thinning between droplets. The microstructure of the interfacial particles will partially dictate the efficiency of stabilization. Microstructure is a complex and poorly understood phenomenon that is dictated by polymorphism and morphology, which in turn is dictated by processing conditions and composition. A key concept of fat crystallization is its stochasticity [103], whereby identical fats will not transform at identical temperatures during cooling or heating. However, as has been shown by many, the polymorphic form of a fat does not necessarily dictate morphology [104,105], and the role of interfacial crystal morphology remains poorly understood. Few researchers have examined the importance of crystal morphology.

Microstructure will influence droplet coverage by particles. In O/W emulsions, full droplet coverage is deemed essential in food emulsions for proper stabilization [13]. The changes in microstructure will influence droplet coverage, fat crystal contact angles, and aggregation behavior.

Five factors are deemed necessary for the stabilization of emulsions via solid particles:

1. The crystals must be located at the interface before any stabilization can take place.
2. They must remain at the interface, which will be a function of their size, shape, composition, and hence wetting behavior.
3. The crystals must form a monolayer film covering the entirety of the

Copyright 2002 by Marcel Dekker. All Rights Reserved.

droplet. Partial droplet coverage will not effectively sterically stabilize the droplet.

4. Hydrophobic crystals will tend to stabilize W/O emulsions, whereas more hydrophilic crystals will tend to stabilize O/W emulsions.
5. Some interaction between particles appears to be necessary for effective stabilization.

It is widely acknowledged that the formation of a sufficiently dense layer of solid particles at the interface is necessary to stabilize an emulsion. Interfacial particle concentration will depend on the number of droplets and their size distribution. For example, Figure 9 shows an asymptotic relationship between the proportion of adsorbed particles and particle concentration for submicrometer silica particles between the bulk and dispersed phases [3,58]. The proportion of particles that adsorb to the interface during emulsification falls quickly from an initial value of ~0.8 at low particle concentrations to ~0.1 at higher particle concentrations. As described in this study, emulsion stability increased as particle concentration increased toward its asymptotic value. Figure 10 illustrates the effect of particle concentration on the drainage of thin films bounded by films covered by colloidal particles. These results were obtained based on a model developed by Tambe and Sharma [73]. It is shown that at a high concentration of interfacial colloidal particles, the rate of film drainage between emulsion droplets is substantially decreased.

An understanding of such phenomena is of crucial importance in many fields. For example, a study of crude oil demulsification revealed that a critical

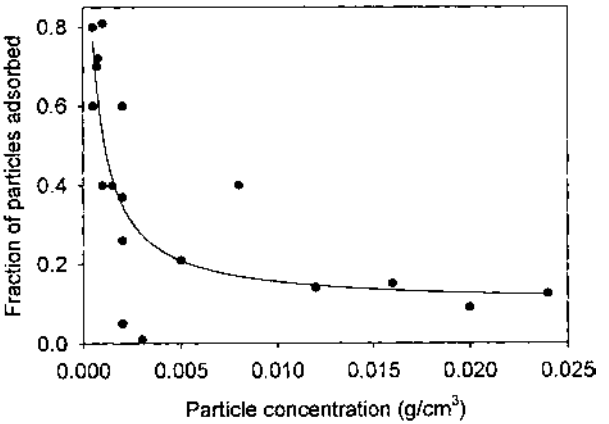

Figure 9 Effect of initial particle concentration on the fraction of particles used in emulsion stabilization. (Adapted from Ref. 58.)

Copyright 2002 by Marcel Dekker. All Rights Reserved.

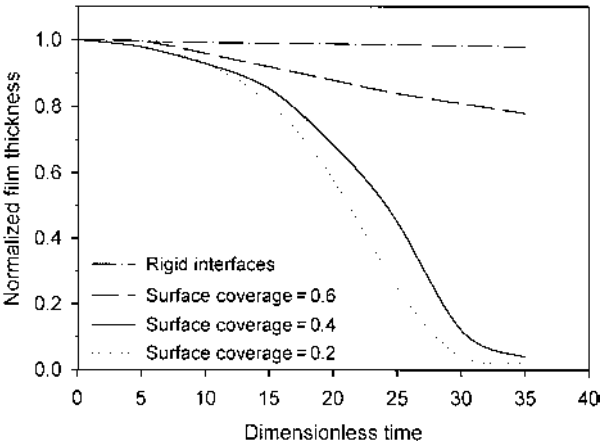

Figure 10 The influence of droplet surface particle concentration on the drainage of thin liquid films between droplets. (Adapted from Ref. 106.)

particle size existed above which a particle could not be supported at the interface [107]. Full coverage will be best achieved with small particles [108]. As described by Schulman and Leja [42] in a study of O/W emulsions stabilized by $BaSO_4$, the particles used during emulsion stabilization should be substantially smaller than the droplet size. In their study, Schulman and Leja reported that ''very good'' emulsions were obtained with powder particles measuring less than 1 μm and that ''poor'' emulsions resulted from particles larger than 10 μm. Similarly, Thompson et al. [109] found that North Sea crude oil emulsion ($d \sim 10$ μm) was stabilized only by wax crystals in the (sub)micrometer range. Dissolution of the wax crystals immediately destabilized the emulsion. Gelot et al. [99] extensively investigated the role of various solids with many surfactants. They observed that hydrophilic particles (kaolinite and bentonite) formed stable O/W emulsions whereas hydrophobic particles (carbon black) formed stable W/O emulsions. They noticed that the size of the emulsion droplets was inversely proportional to the amount of solids used. In the food area, Garti et al. [110] examined W/O/W emulsions stabilized by α crystals (the α form was maintained by an α-tending emulsifier). Crystals had to be submicrometer in size to stabilize emulsions with droplets ranging from 6 to 18 μm in size. Larger crystals could not effectively adsorb to the interface and flocculated as free crystals in the continuous phase. As shown in Figure 11, smaller crystals are likely to provide better coverage than larger crystals (Figs. 11a vs. 11b). The best will be obtained by fat that crystallizes directly at the interface, as depicted in Figure 11c. This phenomenon has been viewed by Buchheim and Dejmek [111] and Juriaanse and

Copyright 2002 by Marcel Dekker. All Rights Reserved.

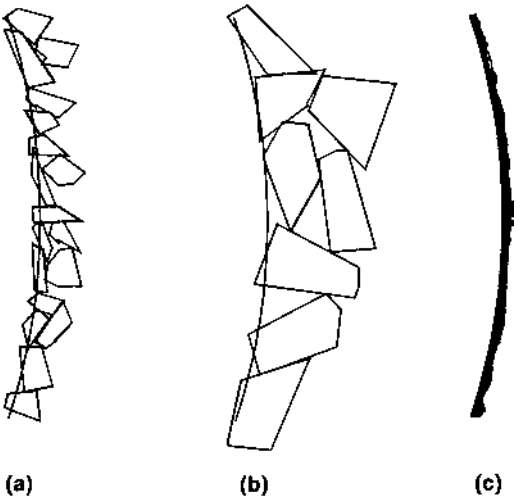

Figure 11 Effect of fat crystal size on droplet coverage. (a) ~1 μm crystals; (b) ~5 μm crystals; (c) submicrometer crystals.

Heertje [112], who found that water droplets in butter emulsions were covered by a thin layer of platelike crystals.

In evaluating emulsion stability, the amount of complete emulsion droplet coverage by particles can be evaluated using the equation

$$F_p = \frac{3.6F_d r_p}{r_d(1 + \delta)^2} \tag{20}$$

where F_p is the volume fraction of the total volume of particles, F_d is the volume fraction of the dispersed phase, r_p is the particle radius, r_d is the droplet radius, and δ is the fractional area of coverage.

Equation (20) assumes spherical particles with identical densities packed hexagonally with contact angles close to 90° and a particle-to-particle surface-to-surface distance of $2\delta r_p$. For example, if we assume that $F_d = 0.2$, $r_p = 0.1$ μm, $r_d = 2$ μm, and $\delta = 0.5$, we would require 1.6% particles in the emulsion. Levine et al. [3,58] observed that when emulsion droplets were incompletely covered by silica particles, the particles aggregated and densely packed only part of the emulsion droplet surface while leaving uncovered (''bald'') patches on the surface. The covered areas and exposed areas possessed different interfacial tensions. Levine et al. attributed the close association of these particles to van der Waals forces.

The migration of fat crystals toward the O/W interface occurs at a rate

Copyright 2002 by Marcel Dekker. All Rights Reserved.

given by Von Smoluchowski's theory [113]. During emulsion preparation, there is a random distribution of droplets and solid particles present. Given the lack of repulsive forces, rapid flocculation occurs, as given by

$$t_{1/2} = \frac{3\eta}{4kT_0} \tag{21}$$

where η is the viscosity of the medium and N_0 is the number of particles per cubic centimeter.

According to W/O emulsion work by Lucassen-Reynders [34] droplet coverage is achieved only if the number of particles is much higher than the number of droplets. In her study, the number of tristearate crystals was ~1000 times the number of droplets, indicating that half of the fat crystals flocculated in ~1 s compared with ~1000 s for the water droplets. Hence, the fat crystals were able to cover the droplets and form a network before any real droplet coalescence could occur, thereby stabilizing the emulsion. The network formation, however, also hindered the free diffusion of crystals to the interface. Without the presence of surfactants in the initial emulsion mix, no stabilization was observed. With added surfactant, however, crystal flocculation was reduced as the interparticle bond energy was lowered. Results showed that partial flocculation was best for W/O emulsion stabilization by tristearin. Lagaly et al. [114] also observed that surfactants aided the colloidal stabilization of emulsions.

2. Role of Temperature

For most emulsions, an increase in temperature accelerates emulsion breakdown. This is often due to a decrease in the continuous phase viscosity, which will favor droplet aggregation. It is a well-known fact that temperature strongly influences the physical properties of fat crystals. Fats can reversibly undergo solid–liquid phase transitions [115]. In an emulsion, fat crystallization can exert a strong influence on emulsion stability, rheology, and appearance [35,116]. Xu et al. [90] found that increased temperature (5°C vs. 22°C) lowered the bulk viscosity of O/W emulsions, resulting in emulsion destabilization. Boode et al. [35] showed that temperature cycling that did not lead to complete melting of the fat induced substantial partial coalescence. In a study on the interfacial competitive adsorption of MAGs and lecithin, Gaonkar and Borwankar [86] found no influence of temperature.

Thompson et al. [109] studied emulsification and demulsification related to crude oil production, in particular the role of temperature. The stability of crude oil emulsions was strongly temperature-dependent and in fact demanded the presence of wax crystals. Fat crystals ranged in size from submicrometer to ~50 μm needles. In the temperature range 30–50°C, emulsion instability substan-

Copyright 2002 by Marcel Dekker. All Rights Reserved.

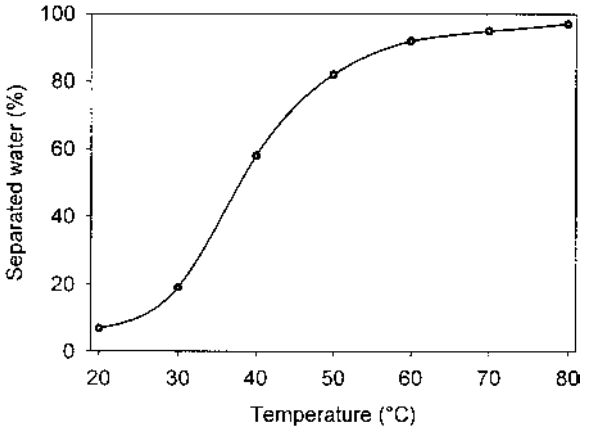

Figure 12 Effect of temperature on the stability of crude oil emulsions stabilized by wax crystals. (Adapted from Ref. 109.)

tially increased as interfacial wax crystals melted (Fig. 12). Thompson et al. hypothesized that between 20 and 30°C the larger crystals partially melted, thereby decreasing in size and maintaining surface coverage of the emulsion droplets. Above 30°C, however, the majority of the crystals dissolved.

In addition to their role in reducing surface tension, the physical state of polar lipids can also play an important role in food emulsions. Like TAGs, MAGs and diacylglycerols (DAGs) are polymorphic, yet they have higher melting points than the corresponding TAGs [117]. Saturated MAGs (e.g., stearic or palmitic acid) have melting points 10–12°C above those of the corresponding TAGs (e.g., tristearin or tripalmitin), whereas with unsaturated MAGs (e.g., monoolein), the melting difference is ~30°C [118]. Hence it is not surprising that MAGs and DAGs can be present as crystals in an emulsion. Temperature is particularly important with respect to the physical properties of MAGs. At low temperatures, MAGs form crystals at the interface, which can be dubbed surface-active crystals because they expose their methyl ends toward the oil phase and their polar moieties toward the aqueous phase [100].

Emulsifiers also influence TAG crystallization behavior, which influences droplet coverage. In particular, emulsifiers can slow down the $\beta' \rightarrow \beta$ transition and prevent oiling-out in crystal networks [119]. Given their polar nature, MAGs can also form liquid crystals in a suspension of water and oil [120]. This suspension, heated to the so-called Krafft point (where the melting point of the MAG is reached), leads to a mesophase structure with alternating water layers and lipid bilayers as the water penetrates through the planes of the polar groups [118]. In

Copyright 2002 by Marcel Dekker. All Rights Reserved.

the late 1960s, Friberg proposed that the lamellar liquid crystalline phase could stabilize O/W emulsions by forming an interfacial film (see Ref. 2). Hernqvist [121] reviewed findings on liquid crystals and their influence on the crystallization of TAGs. He reported that the liquid crystals (L_2 phase) increased the $\beta' \rightarrow \beta$ transition rate of trimyristin–triolein and soy–canola oil systems, thereby affecting emulsion properties.

3. Intraglobular Fat Crystallization

The controlled destabilization of emulsified fats by intraglobular fat crystals is integral to the proper processing of many foods (e.g., butter, spreads, and ice cream). During a cooling regime, intraglobular fat may crystallize, and under perikinetic or orthokinetic conditions ensuing collisions between droplets may lead to flocculation. With fat crystals present at the interface, oil droplets may become disrupted. Protruding crystals, being preferentially wetted by the available liquid oil, form between the two droplets [116]. Due to the structural rigidity of the crystals, the droplets are prevented from fully coalescing—a process known as partial coalescence (Fig. 13).

The induction of crystallization in other droplets can be caused by crystals protruding into neighboring droplets and acting as nucleation sites for subsequent growth [122,123]. A prerequisite for partial coalescence to occur is that crystals must be present at the interface. Other factors influencing partial coalescence are a small enough distance between globules and a sufficient amount of solid fat [19]. The fat phase then forms a continuous fat crystal network that physically hinders the dispersed phase from migrating and eventually coalescing [35]. The resulting spatial distribution of solid mass within the fat crystal network can be described as fractal. Substantial progress in the characterization of fat crystal

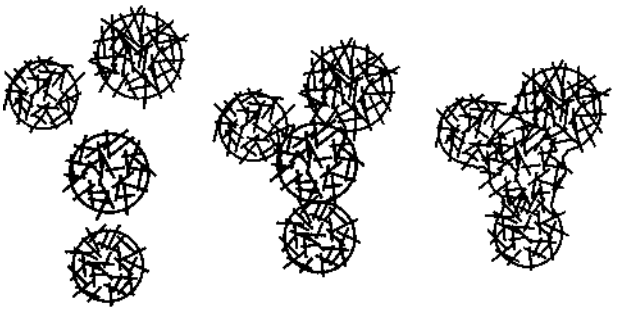

Figure 13 Partial coalescence of partially crystallized oil droplets. (Adapted from Ref. 18.)

Copyright 2002 by Marcel Dekker. All Rights Reserved.

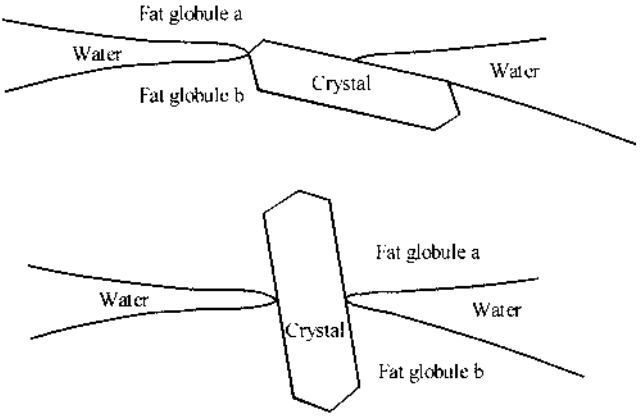

Figure 14 Importance of crystal orientation on droplet coalescence and phase inversion. (Adapted from Ref. 18.)

networks using the fractal geometry approach has been made by Narine and Marangoni [124].

Darling and Birkett [30] studied the role of fat crystallization in the reduction of emulsion stability in O/W emulsions. With freeze-fracture transmission electron microscopy, they showed the mechanism by which fat crystals penetrated the interfacial membrane, causing the breakdown of the emulsion. One of the main factors causing emulsion breakdown was crystal size, as described previously. Van Boekel [18] found that the presence of fat crystals in the dispersed phase led to shear sensitivity. He postulated that the crystals adsorbed to the interface and that these crystals pierced the film between approaching droplets. To minimize this, attempts were made to cool milkfat quickly to decrease crystal size, but they were unsuccessful. Another factor potentially affecting interdroplet piercing is the orientation of the crystals at the interface. As shown in Figure 14, fat crystals are much more likely to pierce emulsion droplets when their sharp ends protrude toward the interface. Boode et al. [35] pointed out that for crystals to pierce approaching droplets, they had to be within reach of the droplet interface. Crystals ''preferentially'' oriented toward other droplets will be more likely to pierce the droplet interface. As previously discussed, this is partly dependent on particle microstructure.

Based on work by Einstein [125], Boode et al. [35] determined the average time required for crystals to migrate from the center of droplets to the interface, using the equation

$$t = \frac{6\pi\eta_0 r_c r_d^2}{kT} \tag{22}$$

Copyright 2002 by Marcel Dekker. All Rights Reserved.

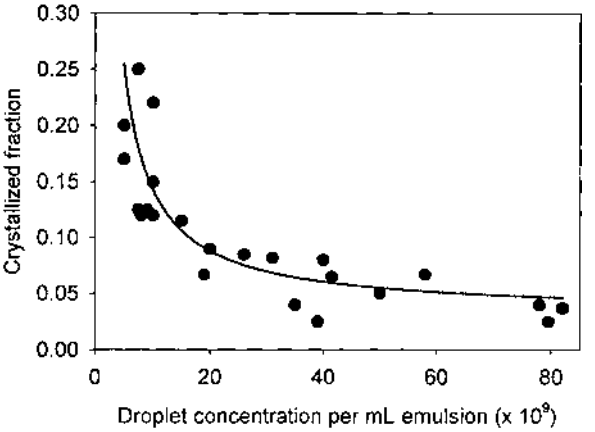

Figure 15 Crystallization of tristearin in emulsion (20% w/w) at 38°C, as a function of droplet concentration. (Adapted from Ref. 127.)

where r_c is the crystal diameter, r_d is the droplet diameter, T is the average time required for a crystal to diffuse from the center of an oil droplet to the interface, and η_0 is the oil droplet viscosity.

For example, if we assume that $r_c = 0.1$ μm, $r_d = 1$ μm, and $\eta_0 = 0.04$ Pa·s, then at 35°C crystals would reach the interface in ~20 s. This is, of course, an ideal situation. However, even if we assume crystal nonsphericity and crystal sizes different from 0.1 μm, then crystals would encounter the interface every few seconds.

Partial coalescence will strongly dependent on the crystals formed within the droplet. Many factors will influence the final properties of a fat crystal. Thus far, we have mentioned the role of morphology and polymorphism. Other factors that will determine the rate of partial coalescence include the volume fraction of droplets, the total solid fat present within the emulsion, and if the emulsion is placed in a shear field.

(a) Volume Droplet Size. It is now known that the greater the number of droplets, the greater the likelihood of partial coalescence occurring. Intradroplet crystallization will increase with an increase in droplet size [126] (Fig. 15). This can be explained by postulating that the impurities and droplets are in similar concentrations [127]. If we assume that the impurities are randomly distributed within the volume of each droplet, the probability of finding a given number of emulsified impurities per volume v can be determined by a Poisson distribution, and the probability of finding no impurities in a droplet at all is

$$P(0) = \exp[-\nu N] = \exp\left[-\frac{\pi}{6} D^3 N\right] \tag{23}$$

Copyright 2002 by Marcel Dekker. All Rights Reserved.

where D is the droplet diameter and N is the total number of catalytic impurities acting as nucleation sites per cubic centimeter.

(b) Solid Fat. The proportion of intradroplet fat will have a strong influence on the overall stability of the emulsion. If very little or no solid fat is found within a droplet, it is unlikely that droplet disruption would occur. The rate of partial coalescence will be strongly dependent on the amount of solid fat present within droplets [19,128]. With a higher SFC, the number of fat crystals that can stick out of an oil droplet increases and hence the probability of interdroplet bridging increases. For example, Harada and Yokomizo [129] diminished the SFC of O/W emulsions stored at <0°C by using emulsifiers. In so doing, emulsions remained stable for a longer time.

(c) Shear Field. The influence of a shear field on the crystallization of emulsions is of great interest as it relates to the crystallization behavior observed during processing and distribution. Emulsions can be destabilized in a controlled manner under shear to deliver desirable properties; uncontrolled or unintentional destabilization may lead to poor product performance. Van Boekel [18] found that emulsions not containing fat crystals were insensitive to shear whereas emulsions containing crystals were very sensitive to shear. Under the influence of shear, droplets will encounter each other much more readily than under quiescent conditions. If droplets contain fat crystals adsorbed to the interface, they can pierce the film between approaching droplets.

The enhanced destabilization of a shear field on crystal-containing droplets is due to the closer distance of approach between droplets under shear and the increased contact time as they roll around each other during an event. In a flow field, it is much more likely that an interface will be pierced than that a collision will occur due to Brownian motion.

Darling [37] examined the effect of shear rates on the emulsion stability for a model butterfat emulsion (Table 2). The model involved the following aggregation process:

Table 2 Effect of Shear Rate on the Flocculation and Coalescence Kinetics of a Model Butterfat Emulsion

Shear rate (s^{-1})	Rate of flocculation k_1 ($\times 10^{-4}$)	Rate of deflocculation k_{-1} ($\times 10^{-2}$)	Rate of coalescence k_2 ($\times 10^{-2}$)
879	5.14	1.35	0.66
1049	4.05	1.36	2.48
1188	4.08	0.1	57.35
1340	4.37	0.1	54.98

Source: Ref. 37.

Copyright 2002 by Marcel Dekker. All Rights Reserved.

$$A + B \underset{k_{-1}}{\overset{k_1}{\leftrightarrow}} AB_{\text{floc}} \overset{k_2}{\rightarrow} AG_{\text{coalesced}}$$

where A and B are either unreacted: $(A + B)$, flocculated: (AB_{floc}), and coalesced: $(AB_{\text{coalesced}})$ and k_1, k_{-1}, and k_2 are rate constants. Results revealed that as shear rate is increased, so is coalescence.

4. Homogeneous and Heterogeneous Nucleation and Growth

In many emulsions of practical interest, the dispersed phase may be partially crystalline. Crystallization can occur as a result of two types of fat nucleation: homogeneous and heterogeneous. In either case, nucleation is the rate-determining step [130]. During homogeneous nucleation, there are no impurities present to act as nucleation catalysts [131]. Such conditions will occur only if the total number of droplets in a system exceeds the total number of catalytic impurities. Heterogeneous nucleation involves the presence of impurities that serve as nucleation sites for intradroplet crystallization. Trace impurities generally provide the initial nucleation sites that induce orientation and order [132]. After initiation of nucleation, the crystals may behave as secondary nucleation sites and promote further crystallization. Crystallization can then proceed unhindered throughout the fat mass. This is typical of the crystallization of W/O emulsions. In an O/W emulsion, however, heterogeneous nucleation does not necessarily occur, because nuclei formed in any one unit of the dispersed phase will not influence crystallization in another unless droplet collision occurs [133]. Hence, it is quite possible that fat crystallization within emulsions will be different than in bulk fats [127,134]. For example, Söderberg et al. [135] performed a milk fat crystallization study and found that intraglobular milk fat crystallized in the β'_2 form, whereas milk fat in the continuous fat phase crystallized in the β'_1 form. Walstra [136] distinguished four types of globules in milkfat and butter globules, using polarized light microscopy (Fig. 16). His observations indicated that the distribution of the fat crystals within droplets varied substantially. Type O globules did not contain any crystals. Type N globules contained intraglobular needles of varying number and shape. In type L globules, the droplet interface was birefringent, indicating the presence of crystals oriented at the interface. Finally, type M was

Figure 16 Intradroplet crystal type in milkfat as viewed with a polarized light microscope. (Adapted from Ref. 136.)

Copyright 2002 by Marcel Dekker. All Rights Reserved.

essentially a combination of type L and N globules, consisting of interfacial crystals and needle-like crystals.

5. Nucleation Kinetics

In the liquid state, lipids are disordered [137]. Collections of a few TAG molecules associated and disassociate dynamically. However, as the temperature is lowered, a stable nucleus will form. A nucleus arises through the stepwise addition of molecules to an embryo, accompanied by an increase in free energy [126].

Following work by Kloek et al. [131], the nucleation rate (J_N) per unit volume and unit time is

$$J_N = N\frac{k_b T}{h}\exp\left[\frac{-\alpha\,\Delta S}{R_g}\right]\exp\left[\frac{-\Delta G^*_{3D}}{k_b T}\right] \tag{24}$$

The term $N(k_bT/h)$ represents the maximum collision frequency in a system of N molecules where k_b is the Boltzmann constant, T is the temperature, and h is the Planck constant. The term that describes the conformation of molecules for inclusion into a nucleus is

$$\exp\left[\frac{-\alpha\,\Delta S}{R_g}\right] \tag{25}$$

where α is the fraction of TAG molecules in the proper conformation for incorporation into a nucleus, R_g is the universal gas constant, and ΔS is the molar loss of entropy upon incorporation into a nucleus.

ΔS is given by

$$\Delta S = \frac{\Delta H_{f,i}}{T_{m,i}} \tag{26}$$

where ΔH_f is the molar enthalpy of fusion in polymorph i and T_m is the absolute melting temperature of polymorph i.

The term $\exp\,[-\Delta G^*_{3D}/k_bT]$ in Eq. (24) is related to the Gibbs activation energy (ΔG^*_{3D}) of a nucleus of a critical size, given by

$$\Delta G^*_{3D} = \frac{16\pi v_c^2 \gamma^3 N_{av}^2}{3\Delta\mu^2} \tag{27}$$

where v_c is the molecular volume in a crystal γ is the Gibbs surface energy, N_{av} is Avogadro's number, and $\Delta\mu$ is the difference in chemical potential.

The difference in chemical potential in solution is given by

$$\Delta\mu_{solution} = R_g T \ln \beta \tag{28}$$

Copyright 2002 by Marcel Dekker. All Rights Reserved.

where β is the supersaturation ratio dictating the ratio of solubilities of the crystallizing component in saturated and supersaturated conditions.

The difference in chemical potential of the crystallizing component at its melting temperature is by

$$\Delta\mu_{\text{melt}} = \Delta H_{f,i} \frac{T_{\text{m},i} - T}{T_{\text{m},i}} \tag{29}$$

It can be assumed that the potential barrier will be lower in the case of heterogeneous nucleation, and if heterogeneous nucleation is possible it will occur at a higher temperature than homogeneous nucleation [103]. Discussion and modeling of heterogeneous and homogeneous nucleation has been provided by Kloek et al. [131], Kashchiev et al. [154], Walstra and van Beresteyn [155], and Kaneko et al. [156], among others.

6. Modeling Crystallization Kinetics in Emulsions

Crystallization of fats in emulsions is largely kinetically driven, although thermodynamics necessarily come into play. As has been mentioned, crystallization kinetics are largely dictated by the type of nucleation encountered in a system.

(a) Crystallization Kinetics of Partial Coalescence. Boode and Walstra [138] developed a simulation model to describe the crystallization kinetics of partial coalescence. It included coalescence kinetics for single droplets containing fat crystals, droplets without crystals, and clusters of droplets based on Smoluchowski's equation for orthokinetic aggregation, which describes the frequency of encounters (b_{ij}) between globules i and j in a polydisperse environment:

$$b_{ij} = \frac{G}{6}(d_i + d_j)^3 N_i N_j \tag{30}$$

where G is the velocity gradient, N_i is the number of globules of i, and d_i is the diameter of globules i. This model differentiates between single droplets enclosing crystals (S_i), single droplets without crystals (S_i), and clumps containing crystals (C_i). Single droplets without crystals become part of clumps by colliding with a crystal-containing droplet.

The partial coalescence efficiency of collision factor J_e is

$$J_e = P(d_i^*)^m \tag{31}$$

where m is the globule size factor and P is a factor independent of globule size.

In Eq. (31), $d_i^* = d_i^*/d_{\min}$, where $d_{\min}$ is the diameter of smallest globule, if $m < 0$, where the smallest globules are more efficient and $d_i^* = d_i/d_{\max}$, where $d_{\max}$ is the diameter of the largest globule, if $m > 0$, where the largest globules are more efficient.

Copyright 2002 by Marcel Dekker. All Rights Reserved.

The partial coalescence rate of single globules (J_s) is modeled with the fitting parameters P_s and m_s, whereas aggregation of clumps containing crystals (J_c) is modeled with P_c and m_c. Therefore, the coalescence frequency for single globules (b_{ij}^S) is

$$b_{ij}^S = J_s \frac{G}{6}(d_i + d_j)^3[N_{S,i}(N_j - N_{C,j}) + N_{S,j}(N_i - N_{C,i}) + N_{S,i}N_{S,j}] \quad (32)$$

And if clumps are implicated in partial coalescence, then their coalescence frequency b_{ij}^C is

$$b_{ij}^C = J_c \frac{G}{6}(d_i + d_j)^3[N_{C,i}N_j + N_{C,j}N_i - N_{C,i}N_{C,j}] \quad (33)$$

And the overall coalescence frequency b_{ij} is

$$b_{ij} = b_{ij}^S + b_{ij}^C \quad (34)$$

The rate of change of globules per size class i equals

$$\frac{dN_i}{dt} = \frac{1}{2}\sum_{j=1}^{j=i-1} b_{ik} - \sum_{j=1}^{\infty} b_{ij} \quad (35)$$

The ability of oil droplets to aggregate, expressed as the initial coalescence efficiency (α_{init}), describes the initial fraction of encounters between oil droplets necessary to set off partial coalescence,

$$\alpha_{init} = t^*/t \quad (36)$$

where t^* is the time required to reach the same change in droplet size distribution equivalent to that observed in time t if all collisions led to partial coalescence.

Coalescence progress is represented by the evolution of droplet size m and P_c/P_s, assuming $m_s = m_c$. A bigger m indicates a greater tendency for larger droplets to aggregate compared to smaller droplets, thereby leading to a bimodal droplet size distribution. The model predicts that the droplets least prone to partial coalescence will be the smallest droplets that contain the smallest crystals and as little solid fat as possible.

V. THE NEED FOR FAT CRYSTALS IN FOODS

The need to characterize fat crystallization in real foods is paramount to deciphering the mechanisms that explain the functional properties of fats in emulsified foods. This section briefly examines how common emulsions depend on the presence of fat crystals.

Copyright 2002 by Marcel Dekker. All Rights Reserved.

A. Whipped Cream

Whipped cream is produced by the incorporation of air into cream at a temperature below the crystallization temperature of some of the TAGs in cream. The development of a stable structure in whipped cream depends on interactions between fat globules and between globules and air bubbles. The initial stabilization process does not involve fat. Air stabilization is a two-step process involving the selective adsorption of whey proteins to the bubble surface, leading to the formation of a protein air/water interface [139]. In the final product, fat globules primarily stabilize bubbles, but remnants of the initial protein interface persist between globules [140].

Whipped cream structure is strongly dependent on partial coalescence, during which it evolves from a viscous fluid to a viscoelastic solid [82]. In the interfacial structure of air bubbles in normal whipped cream, sparsely distributed fat crystals measuring ~1 μm essentially lie in the plane of the air/water interface. For adsorption of fat to occur, the cream must be stored at the correct temperature, which allows an ideal SFC to be reached [91]. In defective whipped cream, large crystals penetrate the air/water interface of most bubbles (Brooker, 1990).

B. Doughs and Batters

Cake batters are complex colloidal systems of fat (or oil) in an aqueous continuous phase containing flour, sugar, eggs, and baking powder [141]. In such a system, fat crystals can adsorb at the air/oil interface of cake batters [139]. During mixing, fat crystals become coated with an interfacial layer of egg protein. Incorporated air is covered entirely with oil and an underlying layer of fat crystals. During heating of the batter, the fat crystals melt and profoundly affect its colloidal structure. Air bubbles initially covered by fat crystals move from the lipid to the aqueous phase, where they become stabilized by (colloidal) egg protein [91].

The role of fat crystals in bread dough is similar to their role in cake batter. They are responsible for good volume and expansion without collapse [92]. As in cake batter, in bread dough it is also essential that the initial dough contain some solid fat, not only oil. It is now well known that adding shortening to bread dough leads to a more uniform, finer crumb structure. In a study by Baldwin et al. [142], the use of lard or fat systems that were completely liquid in a dough at ~40°C produced low volume loaves with poor cell development compared to a dough devoid of any solid fat.

Crystal polymorphic form strongly influences final dough properties. For example, according to Knightly [143] and Baldwin et al. [142], the β′ form is best for fats used in bread and cakes whereas the β form is best for pie crusts. Where air incorporation is important, β′ crystals in dough provide for many small bubbles and greater loaf volume whereas β crystals allow the incorporation of

Copyright 2002 by Marcel Dekker. All Rights Reserved.

relatively little air and result in an open grain structure [91]. This has been explained as β′ crystals forming tighter lattices because of their smaller size.

In the creaming method used in cake baking, β′ crystals (in the form of 1–2 μm needles) are best at improving volume and texture [141].

C. Ice Cream

Ice cream is a physically complex, partially frozen foam mixture of water, cream, and sugar that consists of about 50% air by volume. Ice crystals and air bubbles typically measure 20–50 μm and 50–100 μm, respectively.

Ice cream structure development occurs at each step of the manufacturing process—mixing, pasteurization, homogenization, aging, freezing, and hardening. Pasteurization melts all of the ice cream ingredients, including the cream lipids. During homogenization, amphiphiles in solution adsorb to the surface of newly formed fat globules initially devoid of interfacial material. Milk protein will be displaced from the droplet interface via competitive adsorption with small molecule surfactants, rendering the globules more vulnerable to partial coalescence [78].

Air is incorporated during concurrent whipping and freezing, and partial coalescence occurs. Colliding fat globules coalesce and eventually surround and stabilize the air cells, thereby creating a semicontinuous network throughout the product. The ice cream foam is thermodynamically unstable, yet it can be stabilized by partially coalesced fat droplets to air cells [82]. Adsorption of de-emulsified fat particles at the air/water interface can stabilize the foam structure by reducing drainage and hence coalescence [144].

Interactions between the homogenized fat globules in the ice cream emulsion and the air cells in the finished product depend on the presence of surfactants such as crystallized MAGs at the interface [100].

D. Butter and Margarine

During the churning of butter, the formation of fat crystals is essential for emulsion *de*stabilization. As cream is cooled, fat crystals grow and puncture the interface between two colliding globules, leading to aggregation and eventually to phase inversion [37] (Fig. 6). This leads to the formation of aggregated, irregularly shaped clumps rather than energetically favored droplets [12]. According to Walstra [17], this system can no longer be considered an emulsion because it consists of three phases.

E. Low Calorie Spreads

In the 1980s, there was a huge shift in the eating habits of the inhabitants of the United States, Canada, and many European countries with respect to the fat con-

Copyright 2002 by Marcel Dekker. All Rights Reserved.

tent of foods. To acknowledge the desire of consumers who wanted to decrease their dietary intake of fat, spreads with 60%, 40%, 20%, and even 0% fat appeared on the market. With very low amounts of fat (<20%), it was virtually impossible to keep the fat in the continuous phase.

Research led to the development of very low fat spreads stabilized with liquid crystals. When emulsifiers such as MAGs and phospholipids are heated above their melting point in the presence of water, they take up the available water and swell into a continuous swollen lamellar liquid crystal phase. When this phase is cooled below its transition temperature, the lamellar phase structure is retained and a highly viscous phase, called the α-gel phase, is formed. By crystallization, this phase may be transformed into an even stiffer gel known as a coagel. Research efforts thus far indicate that it appears to be composed of a network of MAG crystals enclosing water droplets [145]. In the mid-1990s, Unilever developed a ''fat''-free margarine containing 3% MAGs in the lamellar mesomorph, the crystal network's building block [146]. Using a thermal analysis and microscopy approach, Heertje et al. [147] showed that the three-dimensional network formed by the liquid crystals was surprisingly similar to that normally observed with ''traditional'' TAG fat crystal networks. Although it is evident that liquid crystals can play an important role in food emulsions, few results have been published in this area.

VI. SOME PARTING THOUGHTS

This chapter has endeavored to draw attention to some of the factors affecting the role of fat crystals in emulsion stability. The importance of wetting and contact angles, interfacial viscosity, location of the intervening fat crystals, and the (micro)structure of these fat crystals has been discussed. A review of the literature reveals that more and more research is being performed in both applied and basic systems that involve fat crystals. However, the behavior of fat crystals in truly multicomponent, multiphasic emulsified systems that incorporate not only fat crystals but also surfactants, proteins, thickeners, and all other components capable of influencing physicochemical properties remains to be fully explored. Xu et al. [90] made some progress in this area. Using an ingenious nondestructive light backscattering technique, they examined the role of fat crystals in situ in food emulsions. They found that the presence of sodium caseinate in emulsions facilitated the formation of fat crystal structure, presumably because the submicelles form a layered structure around the fat particles [148]. For the same emulsion, they reported that xanthan gum disordered the fat particle packing structure. Unfortunately, they were vague as to the meaning of ''fat structure formation'' in both their theory and observed results. Koczo et al. [149] examined flocculation

Copyright 2002 by Marcel Dekker. All Rights Reserved.

of food emulsions in the presence of guar gum and xanthan gum and showed that dispersion separation by xanthan gum was due to the geometrical incompatibility between xanthan gum and the fat particles.

An area where there will be substantial progress in the near future is the elucidation of crystal surface and interface nanostructure. For example, innovative work by Vollhardt [150] examined the nucleation and growth of three-dimensional nuclei of methyl stearate from two-dimensional monolayers.

It should be evident that simply predicting the behavior of single components in a complex system is no easy task. Perhaps the best way to envision a complex emulsion structure is to identify the phase equilibria of the final microstructure. As mentioned, the many forces between the various phases govern emulsion microstructure. Hence, it is important to understand the intermolecular interactions at the molecular, microscopic, and macroscopic levels [151].

For example, Razumovsky and Damodaran [152] examined the potential thermodynamic incompatibility of various proteins at the air/water interface. In such systems, what would the role of intervening fat crystals be? Part of the solution lies in determining phase continuity and the interplay of phase behavior and kinetics along with potential thermodynamic incompatibility of the various components [153]. In so doing, one could predict the behavior of particle systems in which individual particles have different properties (size, shape, and interactions) [145]. Therefore, the long-term challenge of determining the true extent of the role of fat crystals in emulsions is to combine the thermodynamics and physics of structure formation processes and the influence of individual components.

REFERENCES

1. H Huai, CD Flint, AF Gaines, ThF Tadros. The stabilisation of aqueous suspension of coal particles. Fuel 77:1851–1860, 1998.
2. SE Friberg. Emulsion stability. In: SE Friberg, K Larsson, eds. Food Emulsions. 3rd ed. New York: Marcel Dekker, 1997, pp 1–55.
3. S Levine, BD Bowen, SJ Partridge. Stabilization of emulsions by fine particles. II. Capillary and van der Waals forces between particles. Colloids Surf 38:345–364, 1989.
4. VB Menon, DT Wasan. Characterization of oil-water interfaces containing finely divided solids with applications to the coalescence of water-in-oil emulsions: A review. Colloids Surf 29:7–27, 1988.
5. DG Dalgleish. Food emulsions. In: J Sjöblom, ed. Emulsions and Emulsion Stability. New York: Marcel Dekker, 1996, pp 287–325.
6. N Yan, JH Masliyah. Demulsification of solids-stabilized oil-in-water emulsions. Colloids Surf A 117:15–25, 1996.

Copyright 2002 by Marcel Dekker. All Rights Reserved.

7. UT Lashmar, JP Richardson, A Erbod. Correlation of physical parameters of an oil in water emulsion with manufacturing procedures and stability. Int J Pharm 125: 315–325, 1995.
8. EH Lucassen-Reynders. Dynamic interfacial properties in emulsification. In: P Becher, ed. Encyclopedia of Emulsion Technology, Vol 4. New York: Marcel Dekker, 1996.
9. DJ McClements, K Demetriades. An integrated approach to the development of reduced-fat food emulsions. Crit Rev Food Sci Technol 38:511–536, 1998.
10. DJ McClements. Food Emulsions: Principles, Practice and Techniques. New York: CRC Press, 1999.
11. BA Bergenståhl, PM Claesson. Surface forces in emulsions. In: SE Friberg, K Larsson, eds. Food Emulsions 3rd ed. New York: Marcel Dekker, 1997, pp 57–107.
12. H Mulder, P Walstra. The Milk Fat Globule: Emulsion Science as Applied to Milk Products and Comparable Foods. Wageningen, The Netherlands: Pudoc, 1974.
13. P Walstra. Overview of emulsion and foam stability. In: E Dickinson, ed. Food Emulsions and Foams. London: Roy Soc Chem, 1987.
14. D Beydoun, D Guang, RP Chabra, JA Raper. Particle settling in oil-in-water emulsions. Powder Technol 97:72–76, 1998.
15. EJW Verwey, JThG Overbeek. Theory of the Stability of Lyophobic Colloids. New York: Elsevier, 1948.
16. P Becher. Emulsions: Theory and Practice. ACS Monograph Ser No. 162. New York: Reinhold, 1965.
17. P Walstra. Emulsion stability. In: P Becher, ed. Encyclopedia of Emulsion Technology, Vol 4. New York: Marcel Dekker, 1996.
18. MAJS van Boekel. Influence of fat crystals in the oil phase on stability of oil-in-water emulsions. PhD Thesis. Wageningen Agric Univ, The Netherlands, 1980.
19. K Boode, P Walstra, AEA de Groot-Mostert. Partial coalescence of oil-in-water emulsions. 2. Influence of the properties of the fat. Colloids Surf A: Physicochem Eng Aspects 81:139–151, 1993.
20. E Dickinson, C Ritzoulis, Y Yamamoto, H Logan. Ostwald ripening of protein-stabilized emulsions: Effect of transglutaminase crosslinking. Colloids Surf B Interfaces 12:139–146, 1999.
21. N Funasaki, S Hada, K Suzuki. The dissolution state of a triglyceride molecule in water and its orientation state at the air-water interface. Chem Pharm Bull 24:731–735, 1976.
22. E Dickinson, CC Woskett. Competitive adsorption between proteins and small-molecule surfactants in food emulsions. In: RD Bee, P Richmond, J Mingins, eds. Food Colloids. London: Roy Soc Chem, 1989.
23. CC Ho, MC Chow. The effect of the refining process on the interfacial properties of palm oil. J Am Oil Chem Soc 77:191–199, 2000.
24. E Dickinson. Structure and composition of adsorbed protein layers and the relationship to emulsion stability. J Chem Soc Faraday Trans 88:2973–2983, 1992.
25. EH Lucassen-Reynders. Interfacial viscoelasticity in emulsions and foams. Food Struct 12:1–12, 1993.
26. E Dickinson. The role of hydrocolloids in stabilising particular dispersions and

Copyright 2002 by Marcel Dekker. All Rights Reserved.

emulsions. In: GO Phillipis, DJ Wedlock, PA Williams, eds. Gums and Stabilisers for the Food Industry, Vol 4. Oxford, UK: IRL Press, 1988.
27. RF Lee. Agents which promote and stabilize water-in-oil emulsions. Spill Sci Technol Bull 5:117–126, 1999.
28. HE Swaisgood. Characteristics of milk. In: OR Fennema, ed. Food Chemistry. 3rd ed. New York: Marcel Dekker, 1996, pp 841–876.
29. D Johansson, B Bergenståhl, E Lundgren. Wetting of fat crystals by triglyceride oil and water. 1. The effect of additives. J Am Oil Chem Soc 72:921–931, 1995.
30. DF Darling, RJ Birkett. Food colloids in practice. In: E Dickinson, ed. Food Emulsions and Foams. London: Roy Soc Chem, 1987.
31. MP Aronson. Flocculation of emulsions by free surfactant in purified systems. Colloids Surf 58:195–202, 1991.
32. DE Tambe, MM Sharma. Factors controlling the stability of colloid-stabilized emulsions. II. A model for the rheological properties of colloid-laden interfaces. J Colloid Interface Sci 162:1–10, 1994.
33. SU Pickering. Emulsions. J Chem Soc 91:2001–2021, 1907.
34. EH Lucassen-Reynders. Stabilization of water in oil emulsions by solid particles. PhD Thesis. Wageningen Agric Univ, The Netherlands, 1962.
35. K Boode, C Bisperink, P Walstra. Destabilization of O/W emulsions containing fat crystals by temperature cycling. Colloids Surf 61:55–74, 1991.
36. LG Ogden, AJ Rosenthal. Interactions between fat crystal networks and sodium caseinate at the sunflower oil-water interface. J Am Oil Chem Soc 75:1841–1847, 1998.
37. DF Darling. Recent advances in the destabilization of dairy emulsions. J Dairy Res 49:695–712, 1982.
38. LH Wesdorp, HJ Human, S Bruin. Modelling and control of the product structure of food emulsions. In: RP Singh, MA Wirakartakusumah, eds. Advances in Food Engineering. Boca Raton, FL: CRC Press, 1992.
39. M-C Michalski, S Desobry, M-N Pons, J Hardy. Adhesion of edible oils to food contact surfaces. J Am Oil Chem Soc 75:447–454, 1998.
40. RN Wenzel. Resistance of solid surfaces to wetting by water. Ind Eng Chem 28: 988–994, 1936.
41. P Finkle, HD Draper, JH Hildebrand. J Am Chem Soc 45:2780. (Cited in Ref.42.)
42. JH Schulman, J Leja. Control of contact angles at the oil-water-solid interfaces. Emulsions stabilized by solid particles ($BaSO_4$). Trans Faraday Soc 18:598–605, 1954.
43. LD Ford, R Borwankar, RW Martin Jr, DN Holcomb. Dressings and sauces. In: SE Friberg, K Larsson, eds. Food Emulsions. 3rd ed. New York: Marcel Dekker, 1997, pp 361–412.
44. W Reinders. Die verteilung eines suspendieiten pulvers oder eines kolloid gelösten Stoffes Zwischen Zwei: Lösungsmitteln, 1913.
45. T Young. In: G Peacock, ed. Miscellaneous Works. London: Murray. (Cited in Ref. 4.)
46. RJ Good. Contact angles and the surface free energy of solids. In: RJ Good, RR Stromberg, eds. Surface and Colloid Science, Vol. 2. New York: Plenum Press, 1979, pp 1–30.

Copyright 2002 by Marcel Dekker. All Rights Reserved.

47. D Exerowa, R Seder, R Ivanova, T Kolanov, ThF Tadros. Transition from electrostatic to steric stabilization in films from ABS triblock copolymers of poly(ethylene oxide) and poly(polypropylene oxide). Colloids Surf A 123–124:277–282, 1997.
48. D Li, AW Neumann. Contact angles on hydrophobic solid surfaces and their interpretation. J Colloid Interface Sci 148:190–200, 1992.
49. A Gelot, W Friesen, HA Hamza. Emulsification of oil and water in the presence of finely divided solids and surface-active agents. Colloids Surf 12:271–303, 1984.
50. AC Zettlemoyer. Hydrophobic surfaces. In: FM Fowkes, ed. Hydrophobic surfaces. New York: Academic Press, 1964, pp 1–27.
51. D Johansson, B Bergenstaohl. Wetting of fat crystals by triglyceride oil and water 2. Adhesion to the oil/water interface. J Am Oil Chem Soc 72:933–938, 1995.
52. Zettlemoyer. 1969.
53. IJ Campbell. The role of fat crystals in emulsion stability. In: RD Bee, P Richmond, J Mingins, eds. Food Colloids. Cambridge, UK: Roy Soc Chemistry, 1989, pp 272–282.
54. DY Kwok, CNC Lam, A Li, A Leung, R Wu, E Mok, AW Neumann. Measuring and interpreting contact angles: A complex issue. Colloids Surf A 142:219–235, 1999.
55. P Pieranski. Two-dimensional interfacial colloidal crystals. Phys Rev Lett 45:569–572, 1980.
56. S Levine, BD Bowen. Capillary interactions of spherical particles adsorbed on the surface of an oil/water droplet stabilized by the particles. Part I. Colloids Surf 59: 379–386, 1991.
57. S Levine, BD Bowen. Capillary interaction of spherical particles adsorbed on the surface of an oil/water droplet stabilized by the particles. 3. Effective interfacial tension. Colloids Surf A 70:33–45, 1993.
58. S Levine, BD Bowen, SJ Partridge. Stabilization of emulsions by fine particles. I. Partitioning of particles between continuous phase and oil/water interface. Colloids Surf 38:325–343, 1989.
59. DYC Chan, JD Henry Jr, LR White. The interaction of colloidal particles collected at fluid interfaces. J Colloids Interface Sci 79:410–418, 1981.
60. MT Jacques, AD Hovarongkura, JD Henry Jr. Feasibility of separation processes in liquid-liquid-solid systems: Free energy and stability analyses. AIChE J 25:160–170, 1979.
61. AV Rapacchietta, AW Neumann. Force and free-energy analyses of small particles at fluid interfaces. II. Spheres. J Colloid Interface Sci 59:555–567, 1977.
62. M Fuji, T Takei, T Watanabe, M Chikazawa. Wettability of fine silica powder surfaces modified with several normal alcohols. Colloids Surf A. 154:13–24, 1999.
63. MS Romero-Cano, A Martin-Rodriguez, G Chauveteau, FJ de la Nieves. Colloidal stabilization of polystyrene particles by adsorption of nonionic surfactants. J Colloid Interface Sci 198:266–272, 1998.
64. K Boode, P Walstra. Partial coalescence of oil-in-water emulsions. 1. Nature of the aggregation. Colloids Surf A: Physicochem Eng Aspects 81:121–137, 1993.
65. DE Tambe, MM Sharma. Factors controlling the stability of colloid-stabilized emulsions. I. An experimental investigation. J Colloid Interface Sci 157:244–253, 1993.

Copyright 2002 by Marcel Dekker. All Rights Reserved.

66. HJ Busscher, AWJ Van Pelt, HP De Jong, J Arends. The effect of surface roughening of polymers on measured contact angles of liquids. Colloids Surf 9:319–331, 1984.
67. WK Burton, N Cabrera, CF Frank. Trans Roy Soc Lond A 243:299, 1951.
68. AW Neumann. Contact angles and their temperature dependence: Thermodynamic status, measurement, interpretation and application. Adv Colloid Interface Sci 4: 105–191, 1974.
69. P Walstra. On the usefulness of dairy research. Int Dairy J 8:155–161, 1998.
70. HD Goff, WK Jordan. Action of emulsifiers in promoting fat destabilization during the manufacture of ice cream. J Sci Food Agric 62:283–289, 1989.
71. DA Edwards, DT Wasan. A micromechanical model of linear surface rheological behavior. Chem Eng Sci 46:1247–1257, 1991.
72. GDM MacKay, AY Mclean, OJ Betancourt, BD Johnson. The formation of water-in-oil emulsion subsequent to an oil spill. J Inst Petrol 59:164–172, 1973.
73. DE Tambe, MM Sharma. Hydrodynamics of thin liquid films bounded by viscoelastic interfaces. J Colloid Interface Sci 147:137–151, 1991.
74. DE Tambe, MM Sharma. Factors controlling the stability of colloid-stabilized emulsions. II. Measurement of the rheological properties of colloid-laden interface. J Colloid Interface Sci 162:1–10, 1995.
75. W Kiosseoglou. Minor surface-active lipids of olive oil and viscoelasticity of protein films at the olive oil-water interface. J Disp Sci Technol 13:135–144, 1992.
76. J Benjamins, A Cagna, EH Lucassen-Reynders. Viscoelastic properties of triacylglycerol/water interfaces covered by proteins. Colloids Surf A 114:245–254, 1996.
77. J-L Gelin, L Poyen, R Rizzotti, M LeMeste, J-L Courthaudon, D Lorient. Interactions between food components in ice cream. Part 1. Unfrozen emulsions. Food Hydrocolloids 10:385–393, 1996.
78. NM Barfod, N Krog, G Largsen, W Buchheim. Effect of emulsifiers on protein-fat interaction in ice cream mix during ageing. I. Quantitative analyses. Fat Sci Technol 93:24–29, 1991.
79. J-L Courthaudon, E Dickinson, DG Dalgleish. Competitive adsorption of β-casein and nonionic surfactants in oil in water emulsions. J Colloid Interface Sci 145: 390–395, 1991.
80. J-L Courthaudon, E Dickinson, Y Matsumura. Competitive adsorption of β-lactoglobulin + Tween 20 at the oil-water interface. Colloids Surf 56:293–300, 1991.
81. RCA Keller, R Orsel, RJ Hamer. Competitive adsorption behaviour of wheat flour components and emulsifiers at an air-water interface. J Cereal Sci 25:175–183, 1997.
82. HD Goff. Colloidal aspects of ice cream: A review. Int Dairy J 7:363–373, 1997.
83. JA De Feijter, J Benjamins, M Tamboer. Adsorption displacement of proteins by surfactants in oil-in-water emulsions. Colloids Surf 27:243–266, 1987.
84. I Heertje, J Nederlof, HACM Hendrickx, EH Lucassen-Reynders. The observation of the displacement of emulsifiers by confocal scanning laser microscopy. Food Sci Technol 9:305–316, 1990.
85. E Dickinson, SE Rolfe, DG Dalgleish. Surface shear viscometry as a probe of pro-

Copyright 2002 by Marcel Dekker. All Rights Reserved.

tein-protein interactions in mixed milk protein films adsorbed at the oil-water interface. Int J Biol Macromol 12:189–194, 1990.
86. AG Gaonkar, RP Borwankar. Competitive adsorption of monoglycerides and lecithin at the vegetable oil-water interface. Colloids Surf 59:331–343, 1991.
87. LG Ogden, AJ Rosenthal. Interactions between tristearin crystals and proteins at the oil-water interface. J Colloid Interface Sci 190:38–47, 1997.
88. AR Mackie, SM Nativel, DR Wilsen, S Ladha, DC Clark. Process-induced changes in molecular structure that alter adsorbed layer properties in oil-in-water emulsions stabilized by β-casein/Tween 20 mixtures. J Sci Food Agric 70:413–421, 1996.
89. D Johansson, B Bergenståhl. The influence of food emulsifiers on fat and sugar dispersion in oils. II. Rheology, colloidal forces. J Am Oil Chem Soc 69:718–727, 1992.
90. W Xu, A Nikolov, DT Wasan, A Gonsalves, RP Borwankar. Fat particle structure and stability of food emulsion. J Food Sci 63:183–188, 1998.
91. BE Brooker. The stabilization of air in foods containing air: A review. Food Struct 12:115–122, 1993.
92. BE Brooker. The role of fat in the stabilisation of gas cells in bread dough. J Cereal Chem 24:187–198, 1996.
93. D Johansson, B Bergenståhl. The influence of food emulsifiers on fat and sugar dispersion in oils. I. Adsorption, sedimentation. J Am Oil Chem Soc 69:705–717, 1992.
94. M Schudel, SH Behrens, H Holthoff, R Kretzschmar, M Borkovec. Absolute aggregation rate constants of hematite particles in aqueous suspensions: A comparison of two different surface morphologies. J Colloid Interface Sci 196:241–253, 1997.
95. A Dippenaar. The destabilization of froths by solids. I. The mechanism of film rupture. Int J Miner Process 9:1–14, 1982.
96. MR Domínguez, JMR Patino. Structural characteristics of monopalmitin monolayer spreads on aqueous sugar solutions. J Colloid Interface Sci 218:369–376, 1999.
97. EH Lucassen-Reynders, M van den Tempel. Stabilization of water-in-oil emulsions by solid particles. J Phys Chem 67:731–734, 1963.
98. LG Ogden, AJ Rosenthal. Influence of tristearin crystals on the apparent interfacial shear viscosity of aqueous lysozyme-hydrocarbon model systems. J Colloid Interface Sci 168:539–541, 1994.
99. ES Lutton, CE Stauffer, JB Martin, AJ Fehl. Solid and liquid monomolecular film at oil/H_2O interfaces. J Colloid Interface Sci 30:283–290, 1969.
100. N Krog, K Larsson. Crystallization at interfaces in food emulsions: A general phenomenon. Fat Sci Technol 94:55–57, 1992.
101. J Israelachvilii. Intermolecular and Surface Forces. 2nd ed. San Diego, CA: Academic Press, 1992.
102. J Lyklema. Fundamental of Interface and Colloid Science, Vol 1, Fundamentals. London: Academic Press, 1992.
103. D Clausse, JP Dumas, PHE Meijer, F Broto. Phase transformations in emulsions. Part I: Effects of thermal treatments on nucleation phenomena: Experiments and model. J Dispersion Sci Technol 8:1–28, 1987.
104. D Rousseau, AG Marangoni, KR Jeffreys. The influence of chemical interesterifi-

Copyright 2002 by Marcel Dekker. All Rights Reserved.

cation on the physicochemical properties of complex fat systems. 2. Morphology and polymorphism. J Am Oil Chem Soc 75:1833–1839, 1998.
105. M Kellens, W Meeussen, H Reynaers. Study of the polymorphism and the crystallization of tripalmitin: A microscopic approach. J Am Oil Chem Soc 69:906–911, 1992.
106. DE Tambe, MM Sharma. Factors controlling the stability of colloid-stabilized emulsions. II. A model for the rheological properties of colloid-laden interfaces. J Colloid Interface Sci 162:1–10, 1994.
107. M Bobra. Water-in-oil emulsification: A physicochemical study. Proc 1991 Int Oil Spill Con. Washington, DC: Am Petrol Inst, 1991.
108. TR Briggs. Emulsions with finely divided solids. J Ind Eng Chem 13:1008–1010, 1921.
109. DG Thompson, AS Taylor, DE Graham. Emulsification and demulsification related to crude oil production. Colloids Surf 15:175–189, 1985.
110. N Garti, A Aserin, I Tiunova, H Benyamin. Double emulsions of W/O/W stabilized by fat microcrystals. Part I. Selection of emulsifiers and fat microcrystalline particles. J Am Oil Chem Soc 76:383–389, 1999.
111. W Buchheim, P Dejmek. Milk and dairy-type emulsions. In: SE Friberg, K Larsson, eds. Food Emulsions. 3rd ed. New York: Marcel Dekker, 1997, pp 235–278.
112. AC Juriaansee, I Heertje. Microstructure of shortenings, margarine and butter: A review. Food Microstruct 7:181–188, 1988.
113. RJ Hunter. Introduction to Modern Colloid Science. New York: Oxford Univ Press, 1993.
114. G Lagaly, M Reese, S Abend. Smectites as colloidal stabilizers of emulsion. I. Preparation and properties of emulsions with smectites and nonionic surfactants. Appl Clay Sci 14:83–103, 1999.
115. RE Timms. Phase behavior of fats and their mixtures. Prog Lipid Res 23:1–38, 1984.
116. MAJS van Boekel, P Walstra. Stability of oil-in-water emulsions with crystals in the disperse phase. Colloids Surf 3:109–118, 1981.
117. AE Bailey. Melting and Solidification of Fats. New York: Interscience, 1950.
118. N Krog. Food emulsifiers and their chemical and physical properties. In: SE Friberg, K Larsson, eds. Food Emulsions. 3rd ed. New York: Marcel Dekker, 1997.
119. J Madsen. Emulsifiers used in margarine, low calorie spread, shortening, bakery compound and filling. Fat Sci Technol 89:165–170, 1987.
120. A-C Eliasson, K Larsson. Cereals in Breadmaking: A Molecular Colloidal Approach. New York: Marcel Dekker, 1993.
121. L Hernqvist. Polar lipids in emulsions and microemulsions. In: E Dickinson, ed. Food Emulsions and Foams. London: Roy Soc Chem, 1987.
122. DJ McClements, E Dickinson, SR Sungan, JE Kinsella, JG Ma, MJW Povey. Effect of emulsifier type on the crystallization kinetics of oil-in-water emulsions containing a mixture of solid and liquid droplets. J Colloid Interface Sci 160:293–297, 1993.
123. DJ McClements, SR Dungan, JB German, C Simoneau, JE Kinsella. Droplet size and emulsifier type affect crystallization and melting of hydrocarbon-in-oil emulsions. J Food Sci 58:1148–1151, 1178, 1993.

Copyright 2002 by Marcel Dekker. All Rights Reserved.

124. SS Narine, AG Marangoni. Fractal nature of fat crystal networks. Phys Rev E 59: 1908–1920, 1999.
125. A Einstein. Eine neue Bestimmung der Moleküldimensionen. Ann Phys 19:289–306, 1906.
126. GM Pound, WK La Mer. Kinetics of crystalline nucleation formation in supercooled liquid tin. 74:2323–2332, 1952.
127. W Skoda, M van den Tempel. Crystallization of emulsified triglycerides. J Colloid Interface Sci 18:568–584, 1963.
128. E Davies, E Dickinson RD Bee. Shear stability of sodium caseinate emulsions containing monoglyceride and triglyceride crystals. Food Hydrocolloids 14:145–153, 2000.
129. T Harada, K Yokomizo. Demulsification of oil-in-water emulsion under freezing conditions: Effect of crystal structure modifier. J Am Oil Chem Soc 77:859–863, 2000.
130. D Turnbull, RE Cech. Microscopic observation of the solidification of small metal droplets. J Appl Phys 21:804–810, 1950.
131. W Kloek, P Walstra, T Van Vliet. Nucleation kinetics of emulsified triglyceride mixtures. J Am Oil Chem Soc 77:643–652, 2000.
132. K Larsson. Lipids: Molecular Organization, Physical Functions and Technical Applications, Dundee, Scotland: The Oily Press, 1994, pp 1–41.
133. KG Berger. Ice cream. In: SE Friberg, K Larsson, eds. Food Emulsions 3rd ed. New York: Marcel Dekker, 1997.
134. C Simoneau, MJ McCarthy, DS Reid, JB German. Influence of triglyceride composition on crystallization kinetics of model emulsions. J Food Eng 19:365–387, 1993.
135. I Söderberg, L Hernqvist, W Buchhein. Milk fat crystallization in natural milk fat globules. Milchwissenschaft 44:403–406, 1989.
136. P Walstra. On the crystallization habit in fat globules. Neth Milk Dairy J 21:166–191, 1967.
137. L Hernqvist. On the structure of triglycerides in the liquid state and fat crystallization. Fette Seifen Anstrichtm 86:297–300, 1984.
138. K Boode, P Walstra. Kinetics of partial coalescence in oil-in-water emulsions. In: E Dickinson, P Walstra, eds. Food Colloids and Polymers: Stability and Mechanical Properties. Cambridge, UK: Roy Soc Chem, 1993, pp 23–30.
139. BE Brooker, M Anderson, AT Andrews. The development of structure in whipped cream. Food Microstruct 5:277–285, 1986.
140. W Buchheim, NM Barfod, N Krog. Relation between microstructure, destabilization phenomena and rheological properties of whippable emulsions. Food Microstruct 4:221–232, 1985.
141. A-C Eliasson, J Silverio. Fat in baking. In: SE Friberg, K Larsson, eds. Food Emulsions. 3rd ed. New York: Marcel Dekker, 1997.
142. RR Baldwin, RG Johansen, WJ Keough, ST Titcomb, RH Cotton. Continuous breadmaking: The role that fat plays. Cereal Sci Today 8:273–276, 284, 296, 1963.
143. WH Knightly. Shortening systems: Fats, oils, and surface-active agents—Present and future. Cereal Chem 58:171–174, 1981.
144. S Turan, M Kirkland, RD Bee. On the stability of the gas phase in ice-cream. In:

Copyright 2002 by Marcel Dekker. All Rights Reserved.

E Dickinson, Rodríguez Patino, eds. Food Emulsions and Foams. Cambridge, UK: Roy Soc Chem, 1999.
145. S Bruin. Phase equilibria for food product and process design. Fluid Phase Equilibria 158–160: 657–671, 1999.
146. H Nieuwenhuis. Putting science on the supermarket shelf. Inform 10:194–197, 1999.
147. I Heertje, E-C Roijers, HACM Hendrickx. Liquid crystalline phases in the structuring of food products. Food Sci Technol 31:387–396, 1998.
148. K Koczo, AD Nikolov, DT Wasan, RP Borwankar, A Gonsalves. Layering of sodium caseinate sub-micelles in thin liquid film. J Colloid Interface Sci 178:694–702, 1996.
149. K Koczo, DT Wasan, RP Borwankar, A Gonsalves. Flocculation of food dispersion by gums: Isotropic/anisotropic dispersion separation by xanthan gum. Food Hydrocolloids 12:43–53, 1997.
150. D Vollhardt. Nucleation and growth of three-dimensional aggregates in supersaturated monolayers at the air-water interface. Constant surface pressure relaxation of methyl stearate. Colloids Surf A 143:185–195, 1998.
151. VB Tolstoguzov. Structure-property relationships in foods. In: N Parris, A Kato, LK Creamer, J Pearce, eds. Macromolecular Interactions in Food Technology. Washington, DC: Am Chem Soc, 1996.
152. L Razumovsky, S Damodaran. Thermodynamic incompatibility of proteins at the air-water interface. Colloids Surf B 13:251–261, 1999.
153. VB Tolstoguzov. Thermodynamic incompatibility of food macromolecules. In: E Dickinson, P Walstra, eds. Food Colloids and Polymers: Stability and Mechanical Properties. London: Roy Soc Chem, 1993, pp 94–102.
154. D Kashchiev, N Kaneko, K Sato. Kinetics of crystallization in poly disperse emulsion. J Colloid Interface Sci 208:167–177, 1998.
155. P Walstra, ECH van Beresteyn. Crystallization of milk fat in the emulsified state. Neth Milk Dairy J 29:35–65, 1975.
156. N Kaneko, T Hone, S Ueno, J Yano, T Katsuragi, K Sato. Impurity effects on crystallization rates of n-hexadecane in oil-in-water emulsions. J Crystal Growth 197:263–270, 1999.

Copyright 2002 by Marcel Dekker. All Rights Reserved.

9

Food Emulsifiers: Structure–Reactivity Relationships, Design, and Applications

Nissim Garti
Casali Institute of Applied Chemistry, The Hebrew University of Jerusalem, Jerusalem, Israel

I. INTRODUCTION

Nature has provided us with various food-dispersed components; some are liquids (water-in-oil or oil-in-water emulsions), and some are semisolids or solids (dispersed fats, proteins, and carbohydrates). Some components are dissolved in continuous phases, and others are dispersed in various complex molecular and physical macro- or microstructured networks. This infinite number of structural combinations are organized and arranged in very complex types of assemblies such as dispersions, emulsions, foams, and gels. In addition, foods contain hundreds of small molecules as minor ingredients and various other added compounds termed ''food additives.'' Additives act as vitamins, antioxidants, preservatives, acidulants, enzymes, flavors, colorants, amphiphiles, and so on.

Amphiphilic molecules, when adsorbed on surfaces (or interfaces), act as surface-active molecules, or ''surfactants.'' Surfactants have the tendency to spontaneously migrate from solution and adsorb onto dispersed liquid or solid interfaces; once the surface is fully covered, they aggregate in the solution. Surfactants play a major role in determining and altering the physical properties as well as the microstructure of the final products, modifying the texture and stability of the products. Surfactants are often called dispersing agents, emulsifiers, foaming agents, stabilizers, etc., depending on their performance activities and their effect on the final product.

Copyright 2002 by Marcel Dekker. All Rights Reserved.

Technologists are not always aware of the surfactant–substrate structure–reactivity relationships and in many cases will select a surfactant on the basis of producer recommendations or a trial-and-error approach.

In addition to the monomeric amphiphiles, many macromolecular amphiphiles exist in the technologist's list of options. Some macromolecules, such as proteins, adsorb onto interfaces and act as emulsifiers, imparting short-term stability. Others, such as hydrocolloids, impart long-term stability, viscosity, or gelation and are termed stabilizers.

Proteins, polysaccharides, lipoproteins, glycolipids, polar lipids, and other functional macromolecules have been recognized as good surface-active molecules that can be used in many food applications. The surface activity of proteins and their competitive adsorption with other amphiphiles have been carefully studied. New concepts have been stated, and new rules have been set for the use of these macromolecules as emulsifiers or stabilizers.

For many of us dealing with foods, the ability to control the properties and stability of food products as well as the rheology, texture, foam, crystallization properties, etc. is a key factor in the development of designed processed products. It is therefore the goal of many scientists to disentangle the complexity of these systems and to better understand the microstructure of food colloids and food emulsions.

Because emulsions and dispersions are thermodynamically unstable systems, a search is continuously under way for new amphiphiles to serve as improved emulsifiers and stabilizers to prolong food stability.

This review concentrates on trends and progress in the exploration of new emulsifiers extracted from natural or biotechnological sources and chemically or enzymatically modified to fit the needs of new and advanced products in the food industry.

Food colloids, emulsions, and foams, in their broad definition, are systems in which the dispersed phase consists of liquid, semisolid, or even solid lipophilic components and the continuous phase is water. Solidification is achieved through crystallization or through gelation. The third component in these dispersions is, in most cases, an amphiphilic molecule (monomeric or polymeric) that tends to migrate to the oil/water interface and ''help'' during the formation of the dispersion or the emulsion; once formed, it enhances stabilization during storage or use. The emulsifier reduces the interfacial tension between the two phases and thereafter reduces the amount of work required to overcome the surface energy in order to disperse one system into the other. In the second stage the emulsifier contributes to the stabilization of the dispersed droplets, preventing them, by electrostatic or steric effects, from flocculating, coalescing, and rupturing to separate into two immiscible phases.

It is not within the scope of this chapter to discuss the detailed mechanisms

Copyright 2002 by Marcel Dekker. All Rights Reserved.

by which stabilization can take place. The only restriction valid in our concept of stabilization will be that the amphiphile will indeed absorb onto the interface and act as a true (real) emulsifier. We therefore exclude from this chapter macromolecules (such as certain polysaccharides) that stabilize emulsions (mostly in concentrated systems) by exerting a viscosity effect on the continuous phase (depletion stabilization).

II. EMULSIFIERS IN FOOD MICROSTRUCTURES

When trying to classify surfactants we always tend to correlate the hydrophilic–lipophilic balance (HLB) of the surface-active matter to its functionality and performance at the interfaces of two phases (liquid/liquid, liquid/air, liquid/solid, and solid/air). Most past scientific efforts were made in correlating HLB values (and different similar variations on the hydrophilicity–hydrophobicity relationship) of surfactants to the stability of liquid/liquid interfaces (emulsions) and liquid/air interfaces (foams) and only to some extent to solid/liquid interfaces (dispersions or suspensions). The HLB concept has proven to be difficult to calculate or evaluate in composite mixtures of surfactants—inaccurate and irrelevant in some cases and misleading in others. In most foods, especially in processed foods, a system consists of a mixture of more than one type of dispersion (baked goods, ice cream), and therefore more than one type of interaction between the surface-active matter and the two phases must be considered. The complexity of the systems prevents the use of simplistic models of HLB values to study the behavior of fractal systems, gelled systems, bicontinuous phases, and/or other viscoelastic networks entangled in each other. Therefore, our understanding of the structure–reactivity relationship of surfactants and the dispersed systems remains quite obscure, and many technologists still prefer to use a ''personal touch,'' ''long-term experience,'' or ''the art of food colloids'' to solve complex dispersion systems. Lack of reproducibility, the proprietary nature of some information, and misleading data have caused scientific confusion and delays in real progress for many years. As a result, some of the problems related to dispersed systems remain obscure and unsolved.

In 1997 Esumi and Ueno [1] edited a book on the structure–performance relationships in surfactants, in which the authors stress ''the need to understand the properties and performance of surfactants at various interfaces such as air–liquid, liquid–liquid and solid–liquid.'' The book has a few chapters on adsorption theories and some information on the microstructure of nonionic surfactants in solution, some modeling aspects of the association and adsorption of surfactants, and several chapters on the particular behavior of specific surfactants (polymeric, gemini, bile acids, and others) in solution. No significant clear guidelines

Copyright 2002 by Marcel Dekker. All Rights Reserved.

on the correlations between the structure of the surfactants and their performance are given. The authors do not deal with food systems (maybe because of the complexity of the subject) but rather concentrate on simple model systems.

In a very recent book [2], Dalgleish emphasizes the unique nature of food emulsions and dedicates special attention to proteins and emulsion activity.

Rosen and Dahanayake recently wrote a book [3] in which the key issue is an attempt to address the question, What do we want surfactants to do? The authors claim that

> Surfactants must have two major sets of properties: 1) they should adsorb at interfaces and, as a result of this adsorption, they should change the properties of interfaces, and 2) they should aggregate in the solvent in which they are dissolved and, as a result of this aggregation, should change the properties of the solution phase.

Therefore, in order to select which surfactants to use, one must first decide what performance is expected from the surfactant. To achieve the desired performance, the properties of the interface or the properties of the continuous phase must be altered by the adsorbed surfactant. Because performance is generally observable as a macroscopic property (such as emulsification or foaming) rather than as a chemical or molecular interaction (e.g., the formation of a monomolecular film at an interface), it is important to understand the relationships between these macroscopic performance properties and the molecular level changes of the interfaces or the solution phase and to correlate them to the chemical structure of the surfactant.

Rosen and Dahanayake [3] use a simplified, logical, and obvious approach for the classification of surfactants that is directly correlated to macroscopic phenomena or performance properties such as (1) wetting or waterproofing, (2) foaming or defoaming, (3) emulsification or demulsification, (4) dispersion or flocculation of solids in liquids, (5) solubilization of solvent-insoluble material in a solvent, and (6) viscosity increase or decrease.

Rosen and Dahanakake [3] explore the properties of a large number of industrial surfactants with respect to their performance in industrial processes and formulations and lead the readers to a conclusion that surfactant performance depends on measurable and tangible properties such as surface and interfacial tensions, effectiveness of adsorption, molecular surface area, efficiency of adsorption, wetting, spreading coefficients, CMC values, Krafft and cloud points, and solubilization capacity, among others. Such an approach seems to be beneficial and relevant for rather simple diluted manufactured emulsions, foams, or dispersions in which the number of components is limited and the measured parameters reflect the product's characteristics. However, when dealing with more concentrated and complex systems such as natural and processed foods in which several different types of components are present, it seems that simplification is

Copyright 2002 by Marcel Dekker. All Rights Reserved.

actually complicated and sometimes irrelevant. Measuring the classical parameters such as surface and interfacial tensions and wetting will provide only a limited understanding of the system and will not be sufficient for correlating the chemical structure of the surfactant to its performance. Much more is needed to be able to select surfactants for a certain task or to design surfactants for certain uses. It is quite understandable that Rosen and Dahanakake chose to exclude food systems from their book. In some processed food systems such as cloudy beverage emulsions or dressings, one can use the Rosen and Dahanakake approach and learn more on the guidelines for selection of emulsifiers and foaming agents. But in other systems such as baked goods, ice cream, and meat emulsions, other criteria are needed.

Moreover, from a ''quick look,'' it often seems that the amphiphiles in use have totally irrelevant properties such as adsorption at interfaces and reduction of surface or interfacial tensions and stabilization of the dispersed systems, and their real properties are not clear or derived from the surfactant-component interactions. These examples include ''emulsifiers for antistaling effects in baked goods,'' ''crystal structure modifiers of fats in ice cream or margarine,'' and ''viscosity controllers of the fat–sugar matrix in chocolate.'' However, close examination of these phenomena and many others reveals that the activities consist of several stages, including always a priori some of the major characteristics of the amphiphile, i.e., strong surface adsorption and/or a strong tendency to self-aggregate or self-associate to form nanostructures in solvent.

In the past [4–6] it was common to characterize amphiphiles according to their major performance in food systems: (1) emulsification and stabilization, (2) protein interactions, (3) polysaccharide complexation, (4) aeration, and (5) crystal structure modification of fats. Such classifications correlate the surfactant chemical structure to its interaction (chemical or physical) with substrates such as fats, polysaccharides, and proteins. It was confirmed that certain surfactants interact molecularly with macromolecules, forming complexes and/or hybrids, and alter the macromolecular behavior at the interface. Such activity is an important new contribution of cosurfactants to the surface performance of other surfactants [7]. Such interactions are sometimes a very important contribution of amphiphiles to food systems.

In order to examine the performance of food surfactants in a simplified way, we discuss separately their performance at interfaces and in solvents (mainly in water).

A. Adsorption at Interfaces

Surfactants tend to adsorb at any interface when that action will result in decreasing the interfacial tension (i.e., decreasing the dissimilarity of the groups contacting each other). Consequently the adsorbed surfactant will provide repulsive

Copyright 2002 by Marcel Dekker. All Rights Reserved.

forces (electrostatic or steric) and its lipophilic groups will cause a distortion of the structure of the solvent. This distortion of the structure of the solvent (usually water) will force some additional surfactant molecules to be expelled to the interfaces of the system, where they orient themselves so as to minimize contact between their hydrophobic groups and water molecules. The surface of the aqueous solution becomes covered with a single layer of surfactant molecules with their hydrophobic groups oriented predominantly toward the air. A decrease of surface tension is an excellent indication of the adsorption of surface-active material at the interface. In any disperse system (foam, emulsion, dispersion), adsorption of the surfactant to the two-phase interface is a prerequisite for its performance. Surfactant performance is therefore dictated in many cases by its ability to reduce surface or interfacial tension. Therefore, it is important to know that the reduction in surface tension is influenced mainly by the nature and lipophilicity of the lipophilic groups, the chain length of the surfactant (longer chains lower surface tension), the hydrophilic headgroups (larger headgroups result in higher surface tensions), and the charge density of the headgroups. Surfactants that will reduce the surface or interfacial tension of the two phases to a greater extent are called more efficient surfactants and will eventually save on the work required to break the dispersed phase into the continuous phase, forming droplets, bubbles, and solid particles [2,8,9].

Most food emulsifiers are unpurified mixtures of surfactants consisting of lipophilic tails that are mainly fatty acids derived from vegetable or animal fats. The fatty acids are composed of lauric, myristic, palmitic, and stearic acids and/or of unsaturated fatty acids such as oleic, linoleic, and linolenic fatty acids. The headgroups are often more complex structures composed of polyglycerols, lactic or polylactic acids, tartaric acid, polyethylene glycols, or polysugars (polyols) [10]. For example, Tween 60 is said to be sorbitan monostearate with an average of 20 ethylene oxide (EO) groups attached to the sorbitan moiety. However, in reality the tail consists of a variable mixture of stearic (C18:0), palmitic (C16:0), and some myristic (C14:0) or even lauric (C12:0) acids attached to the sorbitan moiety. The fatty acids are esterified with sorbitan (five- and/or six-member sorbitol ring). The sorbitan esters are mostly monoesters, but di- and tri- and even tetra- or pentaesters are also found. In addition, the sorbitan moiety is mixed with some starting materials such as sorbitol esters and some side reaction products such as isosorbide esters. The ethoxylation occurs on various sorbitan hydroxyl moieties. The designation 20 EO denotes an average of between about 12 and about 25 grafted EO groups in the mixture of sorbitans. In addition, the commercial product contains dioxans, free ethylene glycols and ethylene oxides, and significant amounts of free fatty acids, soaps, waxes, etc. Similarly, another important surfactant called diacetyltartaric acid esters of monoglycerides is a very complex mixture of free fatty acids, mono- and diglycerides, esters of tartaric

Copyright 2002 by Marcel Dekker. All Rights Reserved.

acid, esters of mono- and diacetyltartaric acid ester, and esters of esterified and nonesterified polytartaric acid.

As a result of the complexity of the internal composition of the surfactants, one cannot measure, with any accuracy, the surface tension of the water/air interfaces in the presence of these surfactants, and it is an even more complex task to estimate the interfacial tension of water and various oils (most oils are mixtures of many triglycerides) in the presence of these surfactants. Moreover, food systems also contain dissolved sugars, electrolytes, and minor components that complicate the estimation of the real interfacial values even more. These are only some of the reasons why surface or interfacial tensions are not sufficient criteria for evaluation of the surfactant capabilities for adsorption or aggregation. Similarly, as mentioned previously, HLB values, which are often assigned to simple surfactants (such as ethoxylated surfactants), are irrelevant when assigned to certain food emulsifiers. For example, the HLB of sodium stearoyl lactylate (SSL) was reported by various authors to be 5.7, 12, and 18. None of these values can help in assessing the emulsification capabilities of the surfactant. On the other hand, the HLBs of sorbitan esters (SPANs) and ethoxylated sorbitan esters (Tweens) have been tabulated and are known to any technologist, and very often they are used without anyone questioning their accuracy. HLB values therefore provide mostly qualitative information (general guidelines).

In spite of these critical remarks, the food emulsifiers can be divided into two major categories:

1. Hydrophobic. Examples include sorbitan esters, mono- and diglycerides of fatty acids, polyglycerol polyricinoleate, highly substituted sugars, polyglycerol esters, and propylene glycol esters.
2. Hydrophilic. Examples include ethoxylated sorbitan esters, monoglyceride derivatives such as lactates, tartarates, citrates, low-substituted polyglycerol esters, and monosubstituted sugar esters.

Hydrophilic surfactants adsorb best on aqueous phases, whereas hydrophobic surfactants adsorb best on lipophilic surfaces (oils). Data on adsorption at constant temperature are usually plotted as a function of the surfactant equilibrium concentration; plots for solid substrates are termed Langmuir isotherms. From such isotherms the maximum surfactant concentration at the interface (Γ_{max}) can be derived and the maximum area occupied by the surfactant at the interface (A_{max}) can be calculated. In addition, the Gibbs adsorption equation can be extracted.

If the contact angle between the surfactant solution and the solid surface can also be measured, it is possible to derive a variety of other parameters such as efficiency of adsorption, effectiveness of adsorption, and spreading coefficients. The result of such adsorption is a significant change in the interfacial

Copyright 2002 by Marcel Dekker. All Rights Reserved.

properties, which will affect several performance phenomena such as wetting and dewetting, foaming and defoaming, emulsification and demulsification, dispersion and flocculation of solids, and adhesion. Surfactants that are efficient in reducing interfacial tensions, e.g., nonionic surfactants with long-chain fatty acids and large hydrophillic groups, such as ethoxylated sorbitan esters or sucrose fatty acid monoesters, have efficient and effective adsorption isotherms. They reduce contact angles between the surface and the surfactant solution, and as a result they will be efficient emulsifiers for the formation of oil-in-water emulsions and good dispersing agents for particles in aqueous systems and/or good foaming agents (foam height) and good foam stabilizers. Similarly, hydrophobic surfactants will affect the solvent continuous phase and form good water-in-oil emulsions and stable foams or dispersions.

Some important questions are: Are these parameters sufficient to predict the stability properties of the dispersed system? Are surfactant with efficient adsorption also capable of stabilizing emulsions against creaming, flocculation, and coalescence for prolonged periods of time? Can stability be correlated to the surfactant characteristics? The answer to this last question is unequivocally negative. Emulsion stability depends on a variety of additional factors, mainly quantitative estimation of the electrostatic repulsions, evaluation of the van der Waals attractive interactions, and, if existing (for nonionic and polymeric amphiphiles), the steric interactions, which can be repulsive or attractive depending on both the nature of the dispersed phase and that of the continuous phase. Researchers have tried to use the HLB concepts in a broader way and have experimentally calculated the ''required HLB'' values for the dispersed liquid phase. Different oils were given specific values for which the emulsification would be best at given emulsification conditions. This concept is still in use by some technologists. A better concept known as ''the four major HLB-temperature requirements for stable emulsions'' was developed by Shinoda. It is somewhat more complicated but more accurate. The Shinoda parameters are used by some technologists but ignored by others [11,12,15].

It should be stressed that knowing the characteristics of the surfactant and of the dispersed and continuous phases has merit but is still not sufficient to give quick and reliable information to the technologist.

An important factor is the work that is introduced into the system during the emulsification stage. Preparation includes the method of components addition, temperature of the emulsification process, emulsification equipment and method, geometry of the homogenizers, shear rate, demulsification that may take place during the process, etc.

One must not ignore the role of minor ingredients in the emulsification process. Some additives are noninteracting whereas others coadsorb onto the interface or change the nature of the continuous or dispersed phase.

Copyright 2002 by Marcel Dekker. All Rights Reserved.

Can these general rules of adsorption and reduction of interfacial tensions be directly translated into a working system? The answer is not clear and depends, as previously said, on the complexity of the system.

Can one narrow down the number of surfactants to be used for a given emulsification job? Even if the possibility exists it still leaves the technologist with a large number of options. Attempts were made in the past to give additional guidelines. Some are more successful and others less. In my opinion there is no ''good recipe'' for guaranteed success.

Emulsions in which water is the internal dispersed phase are termed water-in-oil emulsions (W/O), whereas emulsions in which oil is the dispersed phase and water is the continuous phase are known as oil-in-water (O/W) emulsions. More complex systems, in which one emulsion is further dispersed into another continuous phase, are called double emulsions, multiple emulsions, or emulsified emulsions [13–21] (Fig. 1). Two main types of double emulsions have been carefully studied: W/O/W and O/W/O double emulsions. The average inner droplet size of the W/O emulsion in the double emulsion is usually smaller than 0.5 μm; that of the outer, external double emulsion is quite large and often exceeds 20 μm.

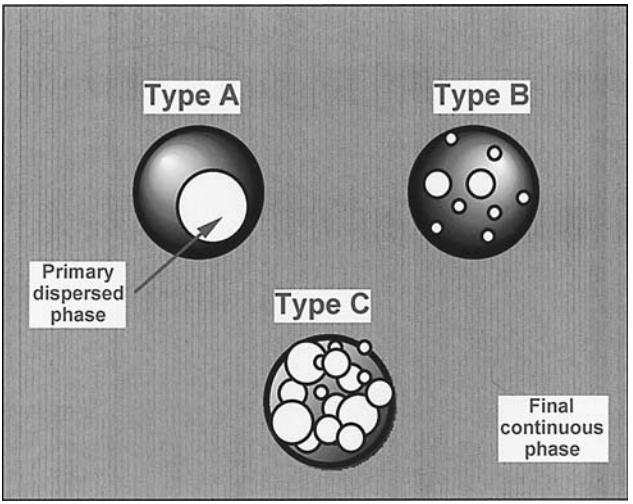

Figure 1 Droplet classification in multiple emulsions. Type A is a single-compartment double emulsion; type B is a double emulsion with a few compartments; type C is a multicompartment double emulsion.

Copyright 2002 by Marcel Dekker. All Rights Reserved.

1. Emulsification

Some of the main considerations during the preparation of any emulsion should include:

1. Selection of a surfactant with good surface properties, i.e., effective and efficient reduction of surface and interfacial tensions and effective adsorption. When adsorption of the surfactant makes the surface of the liquid or solid more hydrophilic, the interfacial tension between the aqueous solution and the second phase will be decreased and it will be easier to increase the area of that interface.
2. Selection of temperature, pH, pressure, and mode of addition of the dispersed phase into the continuous phase.
3. The application of mechanical work (shear, cavitation, etc.). If mechanical energy in the form of shear or mixing is applied to the two liquids, emulsions or dispersions with relatively small droplet sizes and narrow size distributions will be obtained.
4. Assurance that surfactants that are effective in reducing surface tension will also provide full coverage, strong adsorption, and sufficient repulsive electrostatic and steric interactions. Anionic or cationic emulsifiers with large surface charge density are effective electrostatically, whereas nonionic or polymeric amphiphilic surfactants have strong steric stabilization capabilities. The reduction in surface energy facilitates the formation of an emulsion but does not necessarily increase the stability of the emulsion or dispersion. The surfactant must provide sufficient electrostatic repulsion or steric repulsive forces to act as energy barriers against coalescence of the dispersed particles or droplets. The two main contributions to the stability of macromolecular stabilized emulsions are related to droplets approaching to a distance at which compression occurs (without interpenetration) (Fig. 2):

   (i) *Volume restriction*, G_r, which is derived from the reduction in the entropy of polymeric chains (configurational entropy) arising from the reduction in the total volume available to each chain if an interaction takes place.
   (ii) The *mixing term*, G_{mix}, which comes from a buildup in polymeric amphiphile segment concentration in the interaction zone between the droplets, which leads to an increase in the local osmotic pressure and free energy (Fig. 3).
5. Any additional interfering parameters, such as the role of minor components in relation to their reactivity and interaction with the surfactant.

Polymeric surfactants have significant advantages over monomeric surfactants because they can anchor onto the dispersed phase at several sites at the

Copyright 2002 by Marcel Dekker. All Rights Reserved.

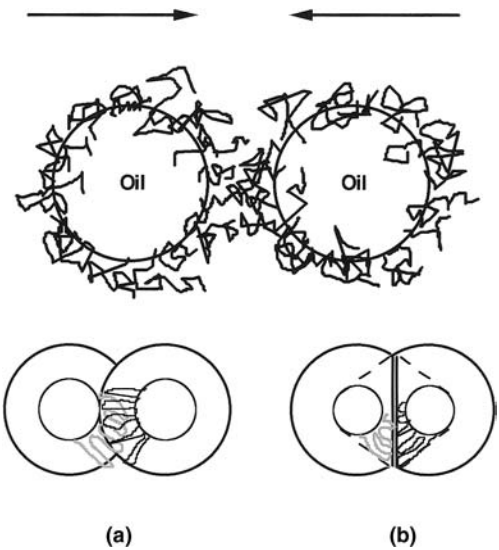

Figure 2 Two limiting models for steric stabilization. (a) Interpenetration of adsorbed layers without compression; (b) compression without interpenetration.

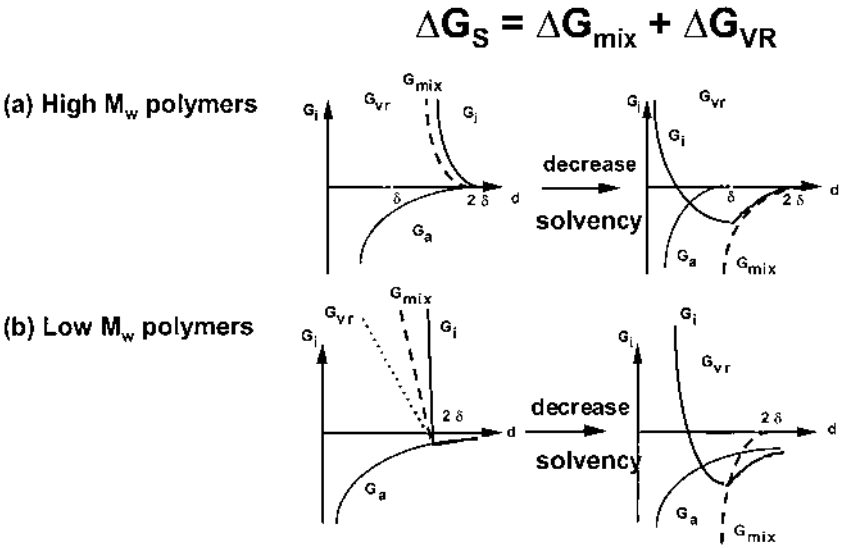

Figure 3 (a) Interaction free energy diagrams for two droplets stabilized by high molar mass polymer. (b) The interaction free energy diagrams for two droplets stabilized by low molar mass polymer.

Copyright 2002 by Marcel Dekker. All Rights Reserved.

same time and the adsorption is considered irreversible (Fig. 2). Proteins provide steric stabilization and are preferred as emulsifiers in many food systems. Selection of the the proper emulsifier is not an easy task, because many additional parameters must be considered such as surface viscosity, surface pressure, dynamic surface tension, rate of migration to the interface, relaxation time on the interface, and competitive adsorption with other surfactants (both polymeric and monomeric).

It is beyond the scope of this chapter to analyze in detail the various surface interactions and forces that proteins can provide. The number of amphiphilic proteins in the world of proteins is limited, which means that the proteins in use are mainly caseins, whey proteins, β-lactoglobulins (BLGs), egg albumin, bovine serum albumin (BSA), lysozyme, and soy proteins. All other plant proteins have very limited ability to strongly adsorb onto interfaces and reduce interfacial tension to only a minor extent. However, chemical and enzymatic modifications will improve the performance of these proteins (pea, cotton, and cereal proteins), and as a result a few modified proteins can be found in the marketplace that have relatively improved performance.

2. Adhesion

In many foods adhesion is an undesirable phenomenon, but in some food systems we need to promote adhesion between two phases. The surfactants play a key role in both the promotion and prevention of adhesion. If, upon adsorption, the selected surfactants will make the surfaces of the two phases more similar in nature and attractive to each other, the surfaces will have a chance to become colloidal and adhere to each other. If a polar solid has to be phase-adhered to a nonpolar hydrocarbon phase, a surfactant with a hydrocarbon chain should adsorb onto the polar solid, with its hydrophilic head oriented toward the polar solid and its hydrocarbon groups oriented away from it. This allows the polar solid surface to become hydrocarbon-like and thus more likely to adhere to the hydrocarbon phase.

B. Surfactants in Solution

Surfactants can self-aggregate in water by exposing their hydrophilic groups to the water and their hydrophobic groups to the aggregate core, which minimizes the free energy of the system and reduces its interfacial tension. Once they reach a critical micelle concentration (CMC), the aggregated surfactants form so-called micelles (Fig. 4) of various shapes (spherical, disklike, cylindrical, sheetlike, etc.). The micelles are termed ''direct micelles'' when the lipophilic tails of the surfactants form a hydrophobic core while the continuous phase is hydrophilic (i.e., water). The micelles are termed ''inverted micelles'' (or reverse micelles,

Copyright 2002 by Marcel Dekker. All Rights Reserved.

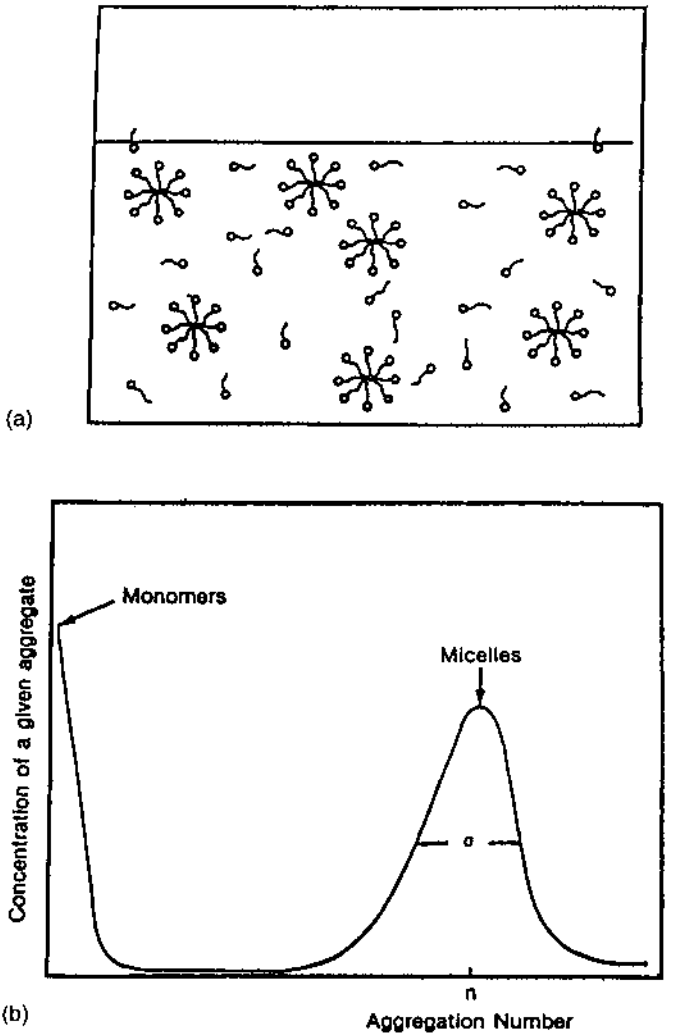

Figure 4 (a) Schematic of the equilibrium coexistence of surfactant monomers and micelles in solution. (b) A typical aggregation size distribution curve.

Copyright 2002 by Marcel Dekker. All Rights Reserved.

or indirect micelles) when the core is hydrophilic and the tails are facing a lipophilic solvent. Many micelles are composed of more than one surfactant and are termed ''mixed micelles.'' Some are nonionic (uncharged), whereas others are charged and are neutralized by counter ions (Fig. 5).

It is therefore expected that hydrophilic surfactants will tend to form direct micelles in water whereas lipophilic surfactants will aggregate spontaneously into inverted micelles. However, in reality it is possible, under certain conditions, that direct micelles will transform into inverted micelles and vice versa. This effect is achieved in the presence of cosolvents and coemulsifiers. The thermodynamic and geometrical guidelines for the formation of such systems are well documented but are beyond the scope of this chapter [22,23]. It is important to note that the micelles self-assemble and there is no need for external mechanical energy. The micelles have a strong tendency to solubilize in their core water-immiscible liquids (solvents or oils, for direct micelles) or water (for inverted micelles) that otherwise will not be soluble in the system. The solubilization capacity depends on the nature of the surfactants, the curvature of the swollen micelles, and thermodynamic considerations. From a practical point of view these nanosized structures are thermodynamically stable, spontaneously formed, transparent, and nonviscous and can solubilize large quantities of solvents, water, and ''active matter'' (vitamins, antioxidants, amino acids, flavouring agents, colorants, nutraceuticals, carriers, etc.). Nanostructures composed of swollen micelles and solubilized matter are known as microemulsions (Fig. 6).

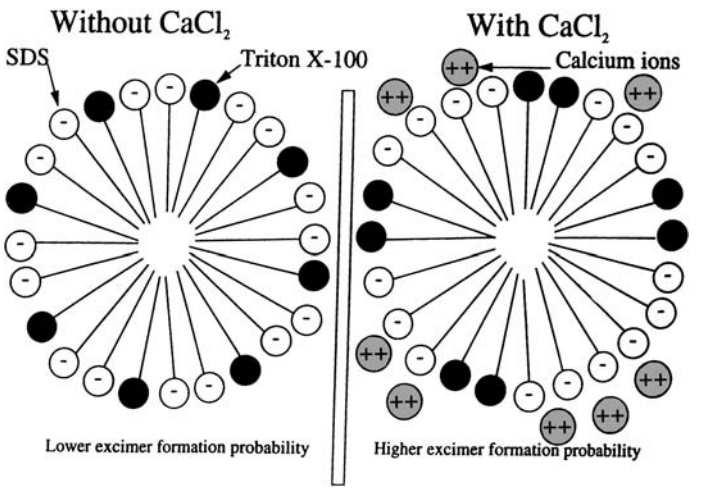

Figure 5 Schematic illustration of mixed micelles.

Copyright 2002 by Marcel Dekker. All Rights Reserved.

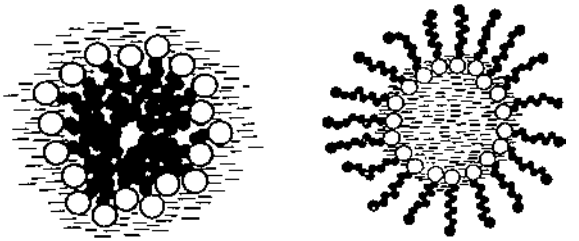

Figure 6 Schematic illustration of swollen micelles (direct and reversed microemulsions).

Many attempts have been made to characterize these nanostructures by a good general definition. The best present definition states: A microemulsion is a mixture of two immiscible liquid phases into nanosized aggregations in the presence of surfactants and sometimes with a need of cosolvents or cosurfactant. This definition does not mention the size or shape of the nanodroplets or nanostructures. The sizes are always smaller than 0.1 μm (mostly a few nanometers), and the shapes can be spherical, disklike, cylindrical, or sheetlike (termed bicontinuous phases).

The original microemulsion was first detected as a distinct entity by Hoar and Schulman in 1943 [24] and consisted of water, benzene, hexanol, and potassium oleate. Most of Schulman's work dealt with four-component systems: a hydrocarbon, an ionic surfactant, a cosurfactant (i.e., four- to eight-carbon-chain aliphatic alcohol), and an aqueous phase. The microemulsion was formed only when the surfactant–cosurfactant blend formed a mixed film at the oil/water interface, resulting in interfacial pressure exceeding the initial positive interfacial tension (so-called negative interfacial tension). The microemulsion was therefore produced spontaneously. During years of research many important geometrical and compositional parameters of microemulsions were studied.

It was established that microemulsions are not necessarily four-component systems. It is well documented, for example, that certain ternary water–oil–nonionic surfactant systems can form microemulsions [25].

The phase behavior of microemulsions can, at fixed pressure and temperature, best be represented by using a ternary diagram [26]. These diagrams provide a simple perspective of phase behavior that is difficult to understand in any other way. A ternary diagram showing a two-phase region and a single-phase region as a function of temperature is shown in Figure 7 [27]. Any system whose overall composition lies within the two-phase region will exist as two phases whose compositions are represented by the ends of the tie lines. In accordance with the

Copyright 2002 by Marcel Dekker. All Rights Reserved.

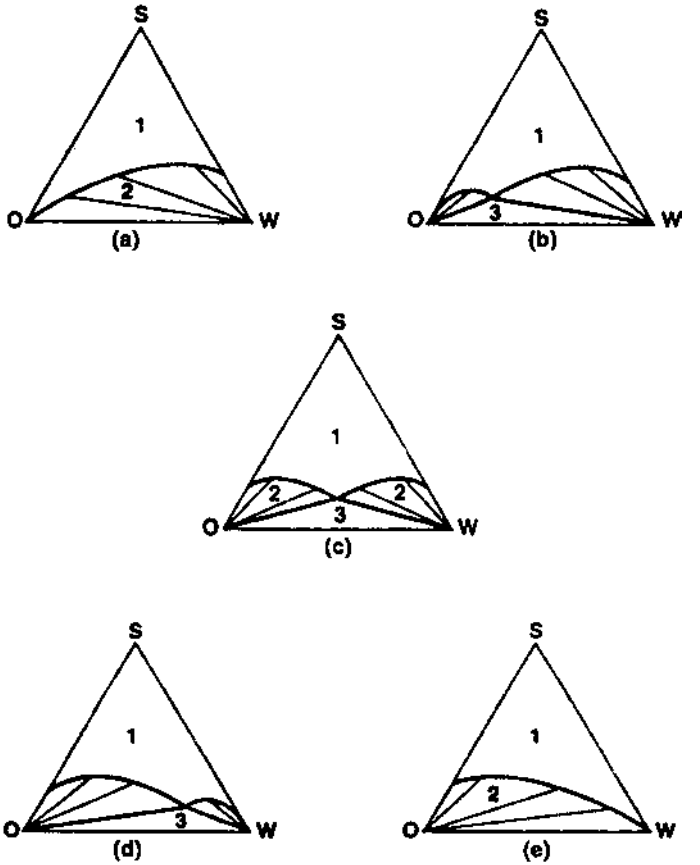

Figure 7 Evolution of phase diagram of microemulsions shown schematically. The sequence of phase diagrams is obtained experimentally by varying temperature, salinity, oil chain length, or surfactant chemistry. Theoretically, many of these changes can be lumped into changes in the spontaneous curvature.

phase rule, the surfactant concentration in the phase can be varied independently over a restricted range.

At high amphiphilic concentration two additional isotropic regions can be depicted. They represent lyotropic liquid crystalline mesophases (Figs. 8 and 9). In the phase diagram represented in Figure 8, at 25°C one can find the L_1 region and the L_2 region of direct microemulsions and the region of inverse solubilization. C_L is the channel connecting L_1 and L_2. D is the region of monophasic lamellar liquid crystals.

Copyright 2002 by Marcel Dekker. All Rights Reserved.

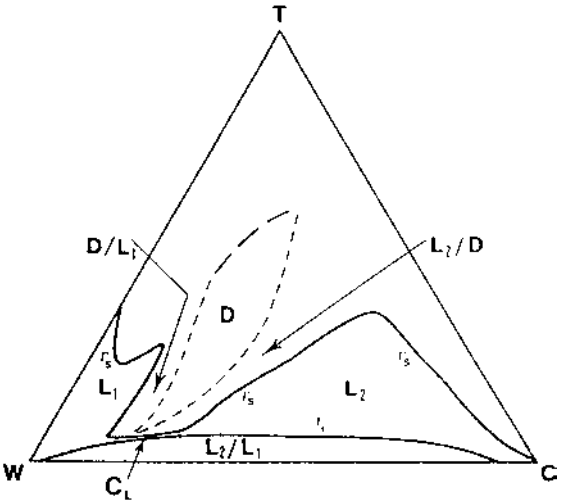

Figure 8 Ternary phase diagram of the water–sodium dodecylsulfate–1-pentanol system ($T = 25°C$). L_1 and L_2 are, respectively, the region of ''direct'' solubilization and the region of inverse solubilization. C_L is the channel connecting L_1 and L_2. D is the region of ''monophasic'' lamellar liquid crystals.

Determination of the structures of the different phases was, and in many cases still is, a difficult task. Methods such as light scattering, small-angle X-ray scattering (SAXS), small-angle neutron scattering (SANS), quasi-elastic light scattering (QELS), sedimentation, and dielectric measurements have been exercised. In spite of the great progress in developing proper techniques and microstructural models (QELS and SANS) for determining the sizes and shapes of droplets, there is a lack of detailed understanding of the systems.

Very few food applications for microemulsions exist, mostly, again, because the complexity of the foods causes the destruction of these structures and their survival in the food environment is questionable. However, the soft drinks and to some extent the alcoholic beverage industries discovered the potential of these nanosized structures in the formulation of clear drinks enriched with flavors, vitamins, and other nutraceuticals. The industry is now in a stage of testing the market for such unique applications. Technologists and scientists are already using microemulsions as vehicles and microreactors for certain food applications. It was found that the curved interfaces are excellent reaction sites for selective organic and enzymatic reactions to prepare certain flavoring agents, amino acids, peptides, sugars, sweeteners, etc., in situ. The potential is huge, and the discovery of the advantages of these systems is now only in its infancy.

Copyright 2002 by Marcel Dekker. All Rights Reserved.

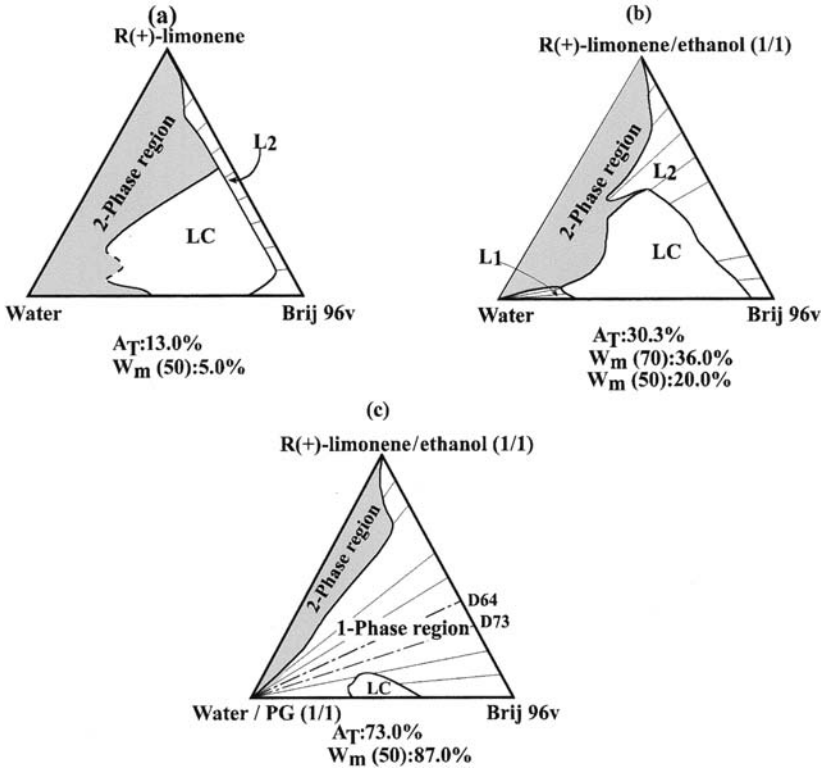

Figure 9 Effect of the addition of alcohol and cosolvent on the phase diagram (T = 25°C). (a) Three-component diagram: water, limonene, and surfactant (Brij 96). (b) Effect of ethanol addition. (c) Effect of ethanol and propylene glycol addition.

1. Structures in Concentrated Solutions: Lyotropic Liquid Crystalline Mesophases

In concentrated aqueous surfactant solutions, interaggregate forces influence the sizes and shapes of the aggregates. This leads to positionally ordered structures characterized by long-range orientational alignment and spatial periodicities that cannot be ascribed to spherical micelles (Fig. 10) [28]. Nevertheless, all three classical structural shapes—spheres, cylinders, and planes—are respectively revealed in hexagonal, discrete (globular) micellar, and lamellar mesophase microstructures [22]. These lyotropic mesophases cover all possible arrangements of repetitive surfaces in 3-D space from infinite 2-D lamellae stacked on a 1-D

Copyright 2002 by Marcel Dekker. All Rights Reserved.

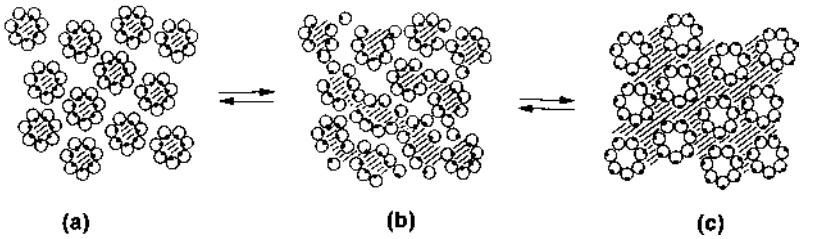

Figure 10 Local dynamic domain structure model for the bicontinuous microemulsion of NaDEHP–*n*-heptane–water. Hatched and blank regions represent water and oil, and the small black and large open circles represent the hydrophilic and hydrophobic portions, respectively, of the surfactant molecules.

lattice, via infinite cylinders stacked on a 2-D hexagonal lattice, to finite-size discontinuous inverse micelles packed on a 3-D cubic lattice as will now be described [29].

(a) The Lamellar Phase (L_α). The lamellar phase (designated L_α) consists of alternating stacks of infinite planar bilayers (also designated as membranes) separated by intervening layers of solvent, usually water, and arranged periodically parallel to one another [30,31]. The surfactants in the bilayers are organized in such a way that the hydrophobic tails of the surfactant molecules are at the center of the lamellae and the hydrophilic portions of the molecules are in contact with the solvent layer. This phase exhibits quasi-long-range positional solidlike order (even at high dilution) along the direction perpendicular to the layers. In the two other in-plane directions the system is liquidlike, i.e., the solvent and surfactant molecules are free to move in this plane (Figs. 11–13). Stable lamellar phases are almost ubiquitous in the concentrated region of the phase diagrams of binary and multicomponent systems. However, their existence in very dilute solutions has only recently been observed and studied systematically [28].

The swelling of lamellae by solvents depends on the bilayer elasticity. One may distinguish between rigid and flexible bilayers. In many binary surfactant–water systems, the well-defined interface of the surfactant bilayers is insensitive to thermal fluctuations on a length scale comparable with the lamellar spacing. For rigid bilayers the membrane is virtually rigid and thermal fluctuations have little effect on the membrane shape. For example, the system sodium laurate–water has a lamellar phase that exists only at high (>40%) surfactant concentrations, corresponding to rather small repeat distances. On the other hand, flexible bilayers exhibit high configurational entropy.

When the membranes of a multilayer system are elastic, thermally excited

Copyright 2002 by Marcel Dekker. All Rights Reserved.

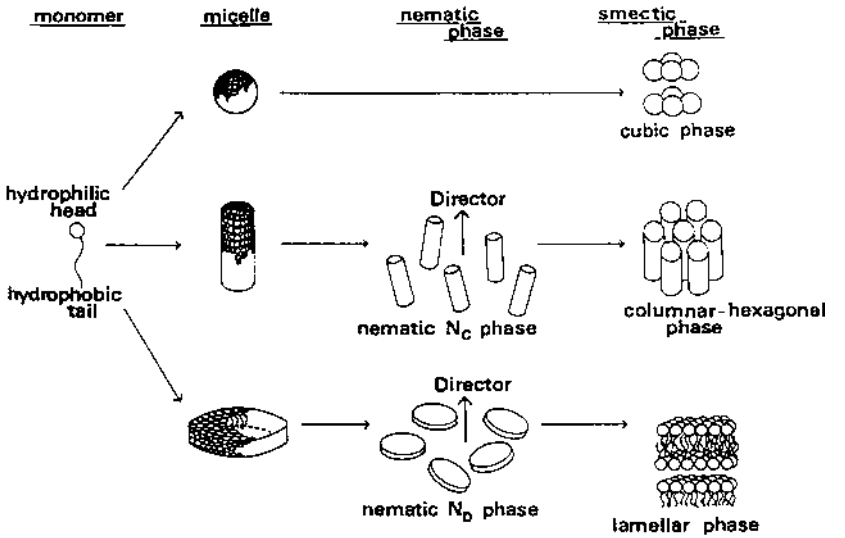

Figure 11 Schematic representation of possible structures of aggregates and their associated mesophases formed by soaplike surfactants in water. The concentration of surfactant should be read as increasing from left to right and from top to bottom.

undulations have to be included in the free energy. The undulations are confined to a smaller region of space as two such membranes approach each other to within a distance shorter than their persistence length.

In summary, electrostatic repulsion stabilizes lamellar phases in ionic systems, whereas entropy reduction stabilizes lamellar phases in nonionic systems or in ionic systems in apolar solvents or in high ionic strength water. Also, the presence of suitable cosurfactants (generally alcohols) that increase the flexibility of the membranes leads to the formation of dilute lamellar phases.

(b) The Hexagonal Phase (H_I, H_{II}). If the fluid surfactant aggregates consist of indefinitely long cylinders rather than bilayers, then 2-D fluid phases will be formed. The simplest and best established of these are the normal (H_I) and inverse (H_{II}) hexagonal phases. In the H_I phase, the surfactant molecules aggregate into circular cylindrical micelles, which pack onto the hexagonal lattice, with a continuous water region filling the volume between the cylinders. In the H_{II} phase, the cylinders contain water cores surrounded by the surfactant polar headgroups, with the remaining volume completely filled by the fluidic chains at an essentially uniform liquid alkane density [32] (Figs. 11–14). It should be noted that the H_I phase could in principle swell without a significant change in the interfacial area per molecule, whereas swelling of the H_{II} phase lattice inevitably causes the in-

Copyright 2002 by Marcel Dekker. All Rights Reserved.

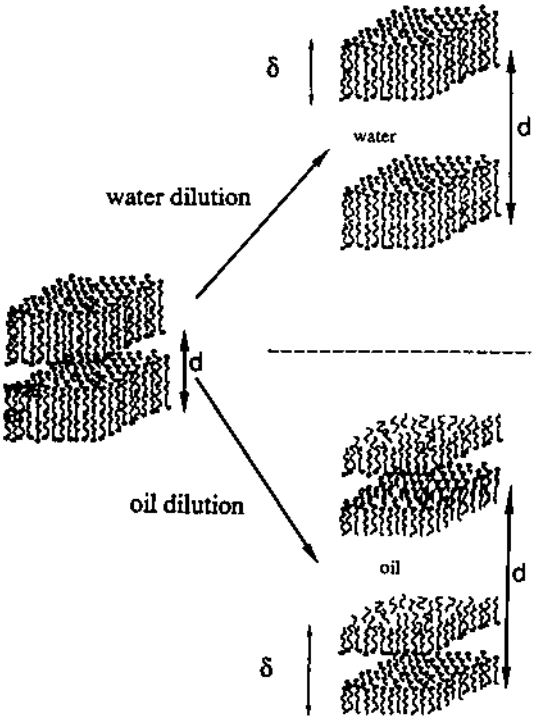

Figure 12 Schematic drawing of the membrane structure of lyotropic lamellar phases. The lamellar phase can be swollen either with water (hydrophilic solvent) or oil (hydrophobic solvent), leading to direct or inverted bilayers. The membrane thickness is δ; *d* is the smectic repeating distance.

terfacial area per molecule to increase. Also, for the H_I phase the water continuum is a true solvent, in the sense that, although a structured fluid, it is able to freely fill all the polar volume unoccupied by the surfactant headgroups. For the H_{II} phase, this situation is not necessarily the case, because the hydrocarbon chains are pinned at one end to the polar interface by the headgroups, and the conformational state of the hydrocarbon chains in part determines whether the hydrophobic region can be uniformly filled and hence the H_{II} phase allowed to form [33].

Although most of the reported hexagonal phases are based on aggregates that have a single curved surfactant layer (monolayers), a more complex type has been found in certain systems, whose structure appears to be based on a hexagonal packing of cylinders formed by curved lipid bilayers that separate an internal and an external region of the same polarity [34–38].

Copyright 2002 by Marcel Dekker. All Rights Reserved.

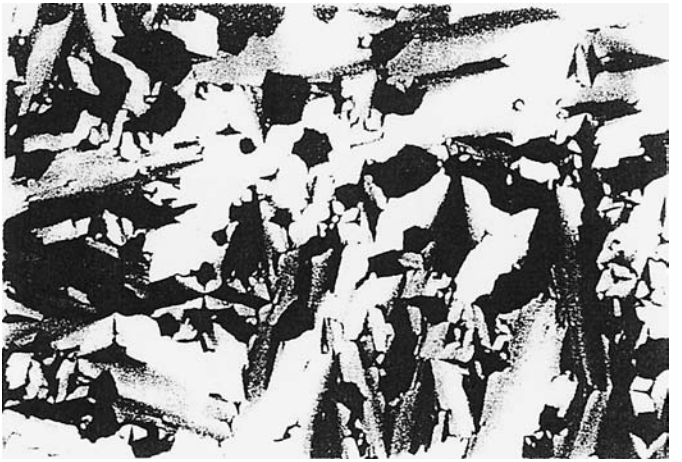

(a)

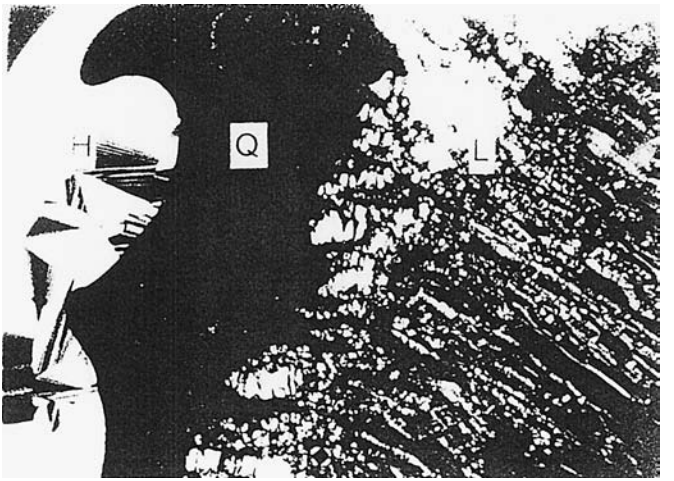

(b)

Figure 13 (a) Photograph of the focal conic fan texture of smectic A liquid crystal phase (S_{mA}) at $T = 303$ K, typical for all the dry surfactants β-C_7Gl, β-C_8Gl, β-C_9Gl, and β-C_{10}Gl. (b) Photograph of the textures of the binary system *n*-octyl–β-D-glucopyranoside–water using the penetration method, crossed polarizers, magnification 100×, temperature $T = 295$ K. The textures show the polymorphism H, Q, L. (c) Photograph showing the textures of the hexagonal phase in the systems β-C_7Gl–water, β-C_8Gl–water, and β-C_9Gl–water. Crossed polarizers, magnification 100×. (d) Photograph showing the textures of the lamellar phase in the systems β-C_7Gl–water, β-C_8Gl–water, β-C_9Gl–water, and β-C_{10}Gl–water. Crossed polarizers, magnification 100×.

Copyright 2002 by Marcel Dekker. All Rights Reserved.

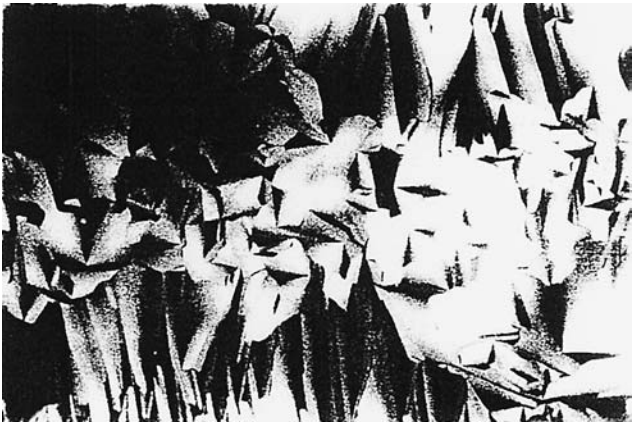

(c)

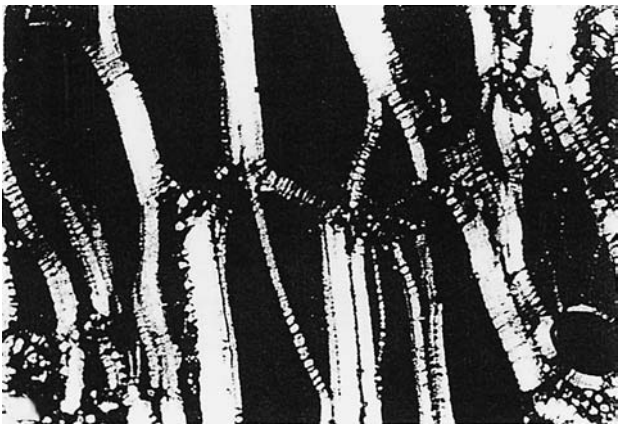

(d)

In contrast to lamellar phases, swelling of hexagonal phases may a priori proceed via two different processes; either increasing the distance between adjacent cylindrical tubes or increasing the cylindrical radius [39]. The first possibility may be rejected on both theoretical and experimental considerations. This is because the cylinders may wander through the interstices of the hexagonal phase when the lattice parameter grows too large compared to their diameter [40]. The swelling of the cylindrical tubes themselves may be accomplished by tuning the spontaneous radius of curvature via the addition of salt, as was shown for the system SDS–brine–pentanol–cyclohexane [39].

Copyright 2002 by Marcel Dekker. All Rights Reserved.

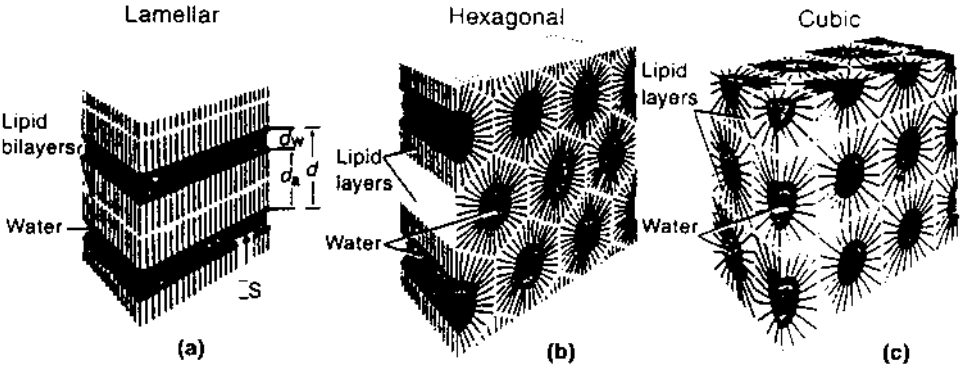

Figure 14 Perspective diagrams of the lamellar phase L, the hexagonal phase with hydrocarbon-filled cylinders H_I, and the hexagonal phase with water-filled cylinders H_{II}. Conversions from L to H_{II} can occur following the packing and shape of the molecules. Swelling of the lamellar phase to include thick interbilayer water layers depends on the presence of charged polar groups.

(c) The Cubic Phases. Lyotropic cubic phases have been the subject of many structural studies [33,41–43]. Their structure is more complicated and less readily visualized. Almost all the 3-D fluid phases observed so far are of cubic symmetry, although rhombohedral, tetragonal, and orthorhombic phases of inverse topology have been detected in a few systems (based for example, on SDS or lipids) [44]. There are two distinct classes of cubic phases:

1. Bicontinuous cubes, denoted by the symbol V, in which a single bilayer of surfactant divides space into two interwoven continuous networks of water (for oil-continuous, type II systems; whereas for type I systems the positions of the water and surfactant are reversed) and thus the phase is continuous in water and in surfactant.
2. Micellar cubes, indicated by the symbol I, consisting of discrete micellar aggregates arranged in cubic lattices (Fig. 15).

Cubic phases have also been classified by symmetry parameters. At least six or seven cubic phases have been established [45]. Two of them are bicontinuous:

1. A cubic phase of space group *Ia*3*d*, which was the first cubic structure to be solved [46] and is among the most commonly observed structures [47]. The *Ia*3*d* structure belongs to a body-centered space group of rods (essentially a surfactant bilayer with a circular cross section) connected 3 by 3 to generate two interwoven but unconnected 3-D net-

Copyright 2002 by Marcel Dekker. All Rights Reserved.

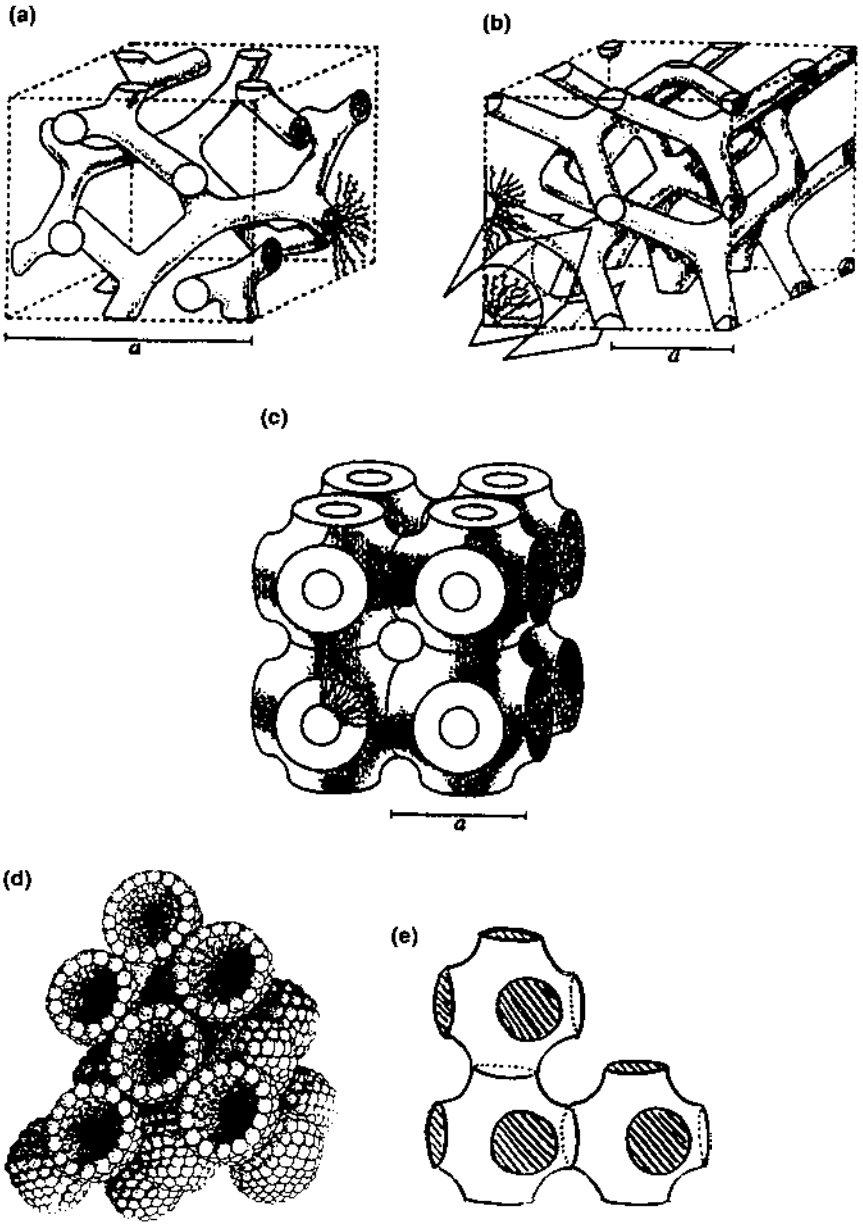

Figure 15 Different arrangements of bilayers in cubic symmetry. (a) A gyroid structure; (b) a double diamond (as in two interwoven diamond lattices); (c) ''plumber's nightmare'' with the same symmetry. (d,e) Schematic illustration of some proposed structures of the cubic phase. The most acceptable structure is at the left (d).

Copyright 2002 by Marcel Dekker. All Rights Reserved.

works. A chiral cubic phase of space group P [43] has been observed so far in only one lipid–protein–water system [48]. Its proposed structure is similar to that of $Ia3d$: It has one water–lipid network interwoven with one network of quasispherical inverse micelles that encloses the protein molecules.

2. A cubic phase of space group $Pn3m$. It has a primitive cubic lattice formed by rods connected 4 by 4 at tetrahedral angles, forming two independent but interwoven diamond lattices [47] (see Fig. 15).

Bicontinuous cubic phases can be described by periodic minimal surfaces, which are well known in differential geometry. In the case of inverted bicontinuous cubic phases, the periodic minimal surfaces lie along the middle of the bilayer. They are saddle surfaces whose mean curvature is zero everywhere (i.e., positive and negative curvatures of the bilayers forming the rods balance each other at every point [47,48]) and have negative Gaussian curvature [33,41,43].

Very few applications for the liquid crystalline structure in food systems are known at present. However, it seems that technologists are starting to discover the potential of the lamellar and cubic phases for entrapment of flavors and for release of active nutraceuticals or additives. Recently [49,50] it was stressed that some advanced nanosized new structures termed cubosomes can be derived from the cubic phases. These unique structures are excellent reservoirs and microreactors for the protection of sensitive materials against oxidation and hydrolysis and as solubilization reservoirs and microreactors for selective processes with high selectivity and specificity.

C. How Do We Select a Surfactant for Self-Organized Systems?

The key question always remains, How do we select an appropriate surfactant for a given application? The classical factors such as CMC values of surfactants are presumably relevant for certain applications in which only very minor quantities of solubilizates are introduced in the micelle core and for detergency and cleaning applications in which the solutions are very diluted with continuous phase (just above the CMCs of the surfactants). However, in food applications, in order to achieve good solubilization of one phase into the other (in many cases, equal amounts or ratios of 1:1), it is essential to use very large quantities of surfactants (in many cases equal to those of the two phases). The microemulsions consist of very large excesses of surfactants, and therefore parameters such as CMC values are not relevant to micellization. It is therefore essential to develop new tools for the selection of surfactants to form microemulsions. One of these tools is the critical packing parameter (CPP). The ratio of the surfactant molecular volume v to the surface area of the headgroup a_0 and the chain length l_0 of the tail of the surfactant is defined in a simple equation,

Copyright 2002 by Marcel Dekker. All Rights Reserved.

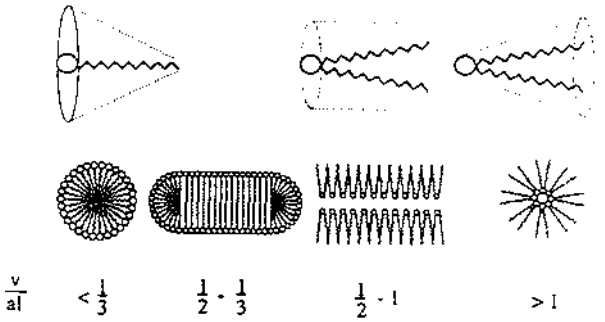

Figure 16 Schematic diagram of possible aggregate shapes expected for different geometries of the surfactant molecule according to $R = v/al$ criteria.

$$\text{CPP} = v/a_0 l_0$$

The critical packing parameter indicates that when a simple surfactant with single chains and relatively large headgroup is selected the CPP will be <0.33 and the expected aggregate structure will consist of spherical or ellipsoidal micelles. Similarly, a surfactant that has relatively small headgroups or an ionic surfactant in the presence of a large amount of electrolyte will have a critical packing parameter of 0.33–0.5 and the expected aggregate structure will consist of cylindrical or rod-shaped micelles. Surfactants with double chains with large headgroups and flexible chains will form vesicles, and those with small headgroups and very large hydrophobic groups will have a CPP > 1.0 and will form reversed micelles (Fig. 16). If CPP $< 1/3$, the surfactant will self-aggregate into spherical direct micelles, whereas if CPP > 1, reverse micelles will be formed.

D. Adsorption on Fats and Polymorphism–Crystal Structure Modification

Long-chain compounds, such as fatty acids and their esters, may occur in different crystal forms known as polymorphs. Fat polymorphism, therefore, describes phase changes and structural modifications of the solid fat phase [51] (Fig. 17-1). The polymorphic fat forms differ in melting points, solubility, crystal morphology and network, rheology, etc. In particular, it is widely acknowledged that the habit of fat crystals is related to their polymorphic state. This property significantly affects the physical properties of food products such as texture, flavor release, solid separation, rheology, and particle flow. In most cases, the physical properties of stable polymorphs—high melting point, slow crystallization, large crystal sizes, hardening kinetics, and so on—are not desirable in fat products.

Copyright 2002 by Marcel Dekker. All Rights Reserved.

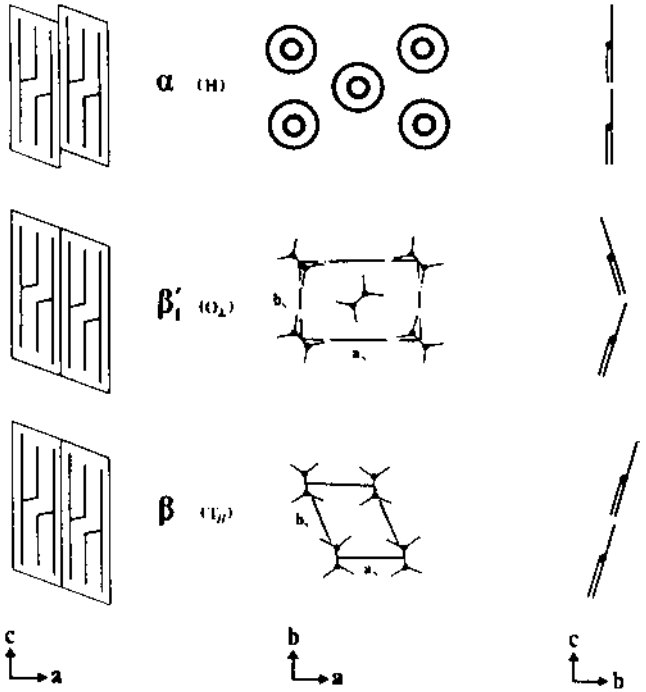

Figure 17-1 Three projections: α, β'_1, and β. Schematic orientations of the triglycerides molecules (*ca* plane), hydrocarbon close packing (*ba* plane), and the differences in chain directions (*cb* plane).

Polymorphism can be easily demonstrated by X-ray diffraction (Fig. 17-2). It is now generally accepted that the major crystal forms are the α form, or hexagonal; the β′ form, or orthorhombic; and the β form, or triclinic (Fig. 17-1). Crystals in the α form have the lowest melting points, whereas the β form have the highest. α is the least stable and β the most stable. When oil is quench-cooled, the α form will be crystallized, and when the cooling is slow, the β form will be formed.

The polymorphic forms can cause phase separations in fat products and destroy the fine-grained network between fat crystals themselves and/or between fats and other ingredients. Therefore, controlling the polymorphic transformation of triglycerides and altering the physical properties and rheological behavior of fats have been subjects of interest to technologists and scientists. An important polymorphism example is margarine. Although α-form crystals are first formed upon quench-cooling of the hot emulsion, a good margarine will have largely β′ crystals within minutes of manufacture, as shown in Figure 17-3. A faulty marga-

Copyright 2002 by Marcel Dekker. All Rights Reserved.

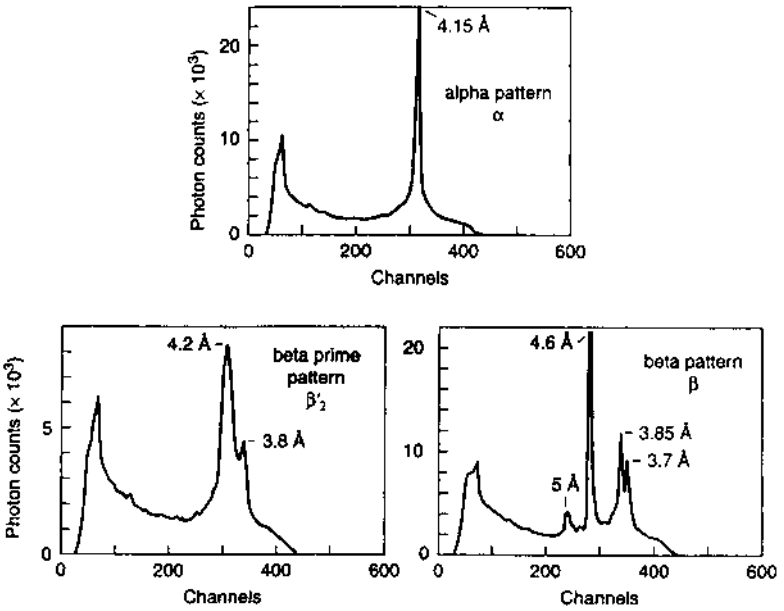

Figure 17-2 Wide-angle X-ray diffraction patterns from the three major crystal forms.

rine will exhibit an additional peak (besides those of β′ at 4.2 and 3.8 Å) at 4.6 Å that corresponds to the β form. The β-form crystals are large and melt at temperatures above body temperature, resulting in grainy mouthfeel. β-Type margarine is not a defective product. It can be used in squeeze margarine but not in spread margarines.

Many other substructures (polymorphic crystals) have been detected and characterized in fats, mono- and diglycerides, etc., from various sources. Examples include sub-α, sub-β′, γ, β_1, and β_2, as in sn-1,3-stearoyl-2-oleoyl glycerol type of fat (Fig. 17-4).

Emulsifiers are key players in polymorphic transformation studies. They alter the fat surface properties, resulting in changes in crystal size and nature. Early reviews by van den Tempel [52] and Garti [53] showed that many types of emulsifiers tend to reduce the crystal growth rate of natural fat blends. Since then, further work has been performed on the effects of different emulsifiers on fats not only in bulk but also in emulsion systems. Garti and Yano [54] discuss in great detail the progress made in this field in recent years.

Emulsifier behavior during fat crystallization can be divided into four cases depending on the mode of interaction (Fig. 18):

Copyright 2002 by Marcel Dekker. All Rights Reserved.

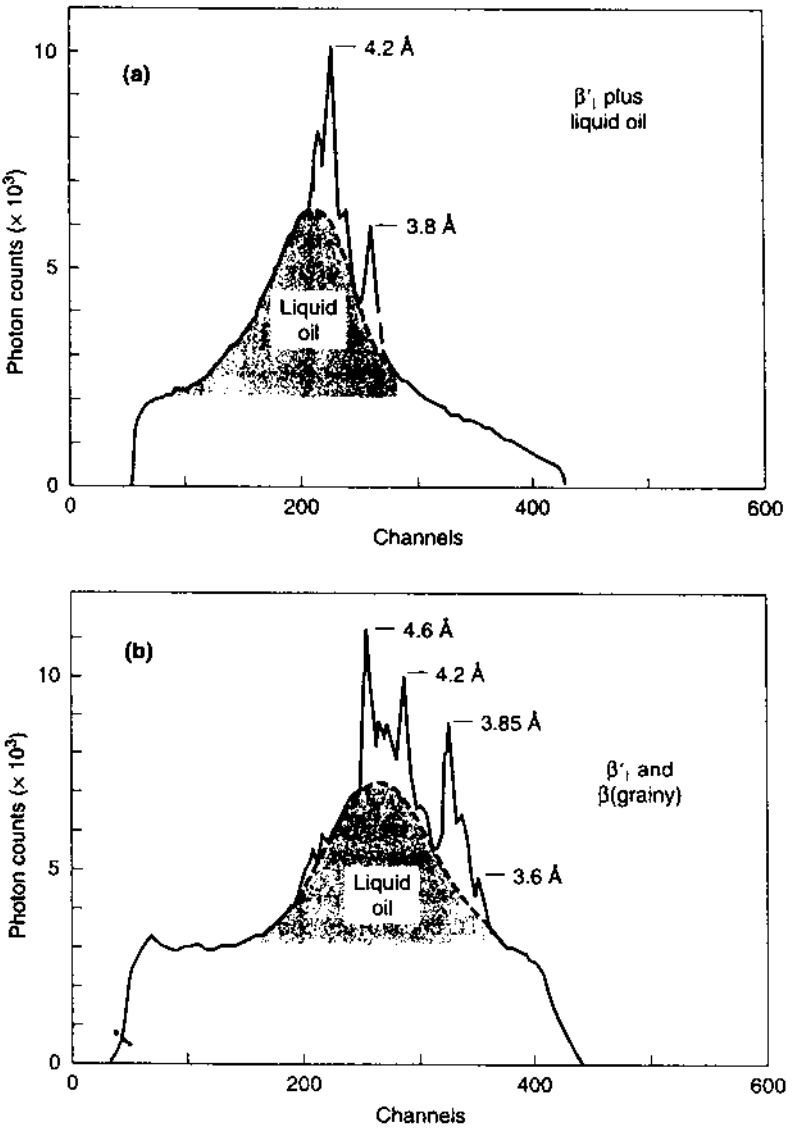

Figure 17-3 Wide-angle X-ray diffraction patterns from (a) a good margarine; and (b) a grainy margarine. A large proportion of liquid oil is indicated by the shaded areas in both patterns.

Copyright 2002 by Marcel Dekker. All Rights Reserved.

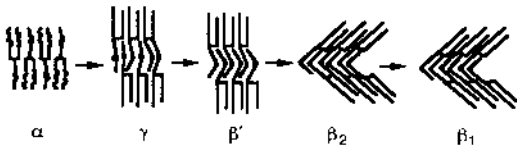

Form	Subcell		Olefinic group	Aliphatic group
	stearoyl(st.)	oleoyl(ol.)		
α	H	H	n.s.	disordered
γ	//-type	H	n.s.	disordered
β′	$O_{\perp}$	n.s.	n.s.	st. ordered ol. disordered
β_2	$T_{//}$	$T_{//}$ or $O'_{//}$	*scs′*	st. ordered ol. ordered
β_1	$T_{//}$	$T_{//}$	*scs′*	st. ordered ol. ordered

Figure 17-4 Molecular models of five polymorphs of *sn*-1,3-stearoyl-2-oleoyl glycerol (SOS).

Case 1. A limited amount of emulsifier is miscible in a fat system. The small amount of emulsifier acts as an impurity and results in imperfect fat crystals. It will promote or retard polymorphic transformation of fat crystals.

Case 2. Fats and emulsifiers are highly miscible. In this case, a fat–emulsifier binary phase shows miscible phase behavior or molecular compound formation.

Case 3. Fats and emulsifiers are totally immiscible in the solid state. In nucleation, emulsifiers may work as seeds for the formation of fat crystals under special conditions, for example, a template film. In crystal growth, the emulsifiers are adsorbed at steps or kinks of fat crystals at crystal/liquid interfaces and inhibit crystal growth, thereby modifying crystal morphology.

Case 4. In an emulsion system, emulsifiers may induce fat–emulsifier interaction. Acceleration of nucleation may occur at the interface of the emulsion, with adsorbed hydrophilic emulsifiers becoming templates for heterogeneous nucleation.

The transformation of triglycerides from unstable or metastable forms to stable polymorphs occurs spontaneously and irreversibly at the expense of the unstable forms. Figure 19 shows the Gibbs free energy–temperature relationships

Copyright 2002 by Marcel Dekker. All Rights Reserved.

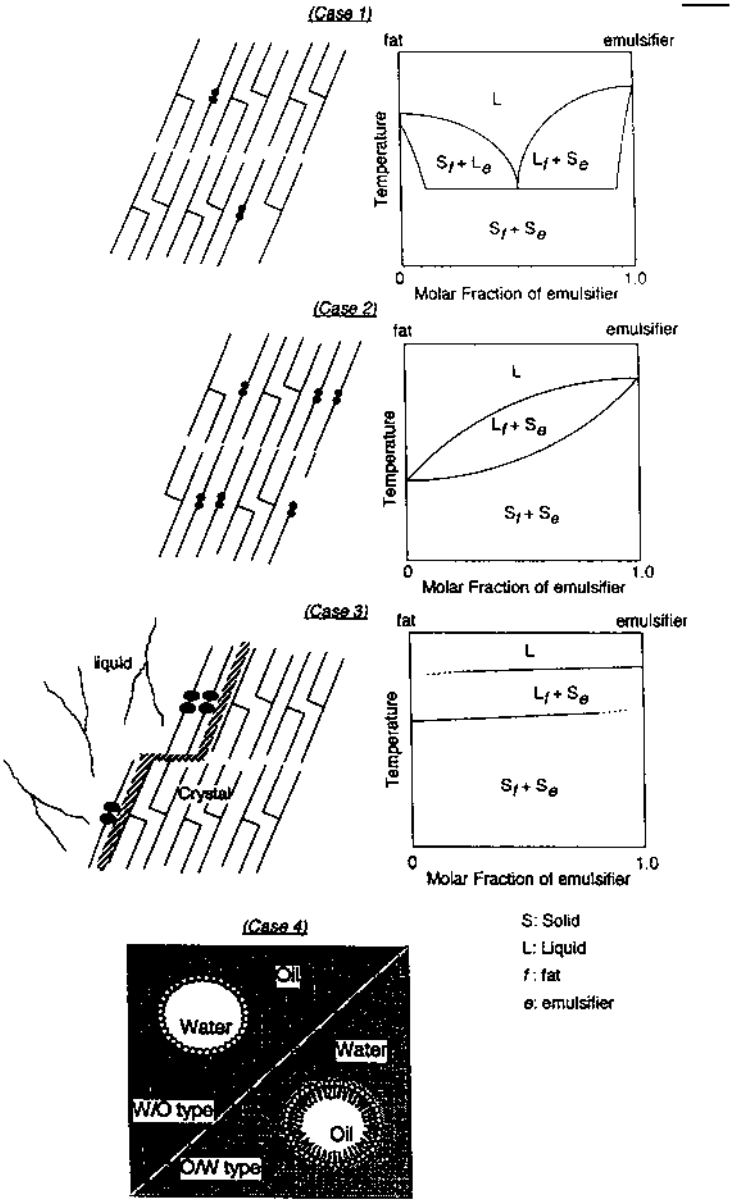

Figure 18 Classification of fat–emulsifier interactions. In cases 1–3, typical phase diagrams of the fat–emulsifier binary mixture are also shown. Case 4 shows two types of emulsions, W/O and O/W.

Copyright 2002 by Marcel Dekker. All Rights Reserved.

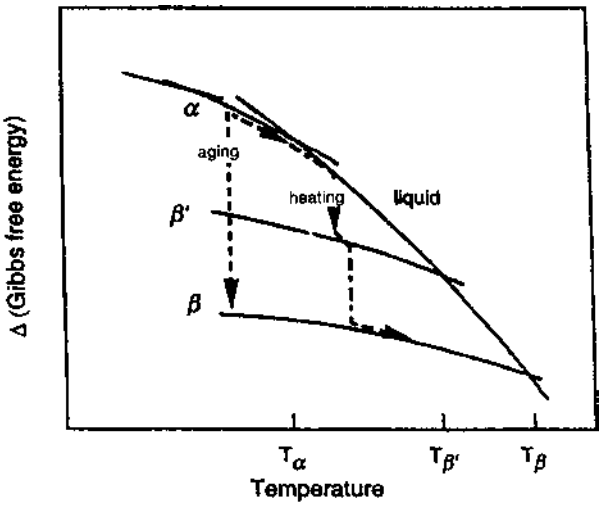

Figure 19 Gibbs free energy–temperature relationship of monoacid triglyceride polymorphs.

of three polymorphs of monoacid triglycerides. When the neat liquids are cooled below the melting point T_α, the α form crystallizes first. Then, during aging or heating, this form transforms to the most stable β form directly without melting in the case of short-chain triglycerides or after melting and recrystallization in the case of long-chain triglycerides.

Some fats have more than one crystalline form. Fats are therefore considered polymorphic crystalline compounds.

Among the polymorphs of fats, the β form is desirable in salad dressings, because its physical dimensions prevent the crystals from settling. However, in most cases, the β′ phase is the preferred structure with the proper functionality in the fat products, due to its small crystal size—it is about 1 μm long with a thin needle-shaped morphology. This relatively small crystal results in good plasticity and gives the desired softness to fat products such as margarine and shortening. In addition, β′ crystals can form complicated mixtures with other components such as liquid oils, surfactants, and water. Therefore, the β′-to-β transition of fat crystals results in deterioration of the end products.

Emulsifiers sensitively modify the rates of crystal growth and polymorphic transition of fats through the preferred adsorption at or inclusion in fat crystals [55,56]. The retardation or acceleration of the polymorphic transformation is influenced by the hydrophobic moiety structure. Figure 20 shows the effect of emulsifiers on the α-to-β transformation of tristearin during aging at room temperature

Copyright 2002 by Marcel Dekker. All Rights Reserved.

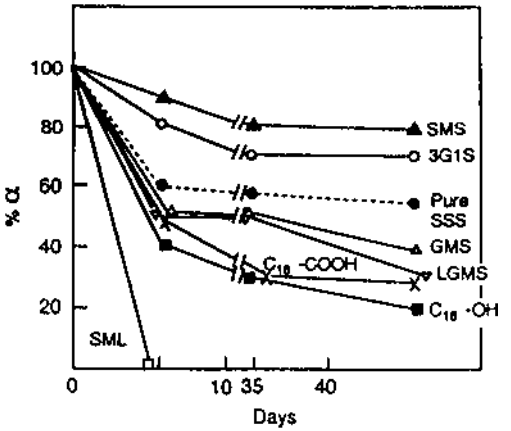

Figure 20 Aging of tristearin at room temperature in the presence of additives at 10 wt%. (●) Neat tristearin, (▲) tristearin + SMS, (○) tristearin + 3G1S, (△) tristearin + GMS, (▽) tristearin + LGMS, (×) tristearin + stearic acid, (■) tristearin + stearoyl alcohol, and (□) tristearin + SML.

[53]. Among the solid emulsifiers, sorbitan monostearate (SMS) and triglycerol-1-stearate (3G1S), which have in common a particular feature, delayed the transformation; the α form was stabilized by the presence of these emulsifiers. On the other hand, glycerol-1-stearate (GMS) and lactate glycerol-1-stearate (LGMS) enhanced it. Any liquid surfactant like sorbitan monolaurate (SML) significantly accelerates the transformation from the α to the β form. These results suggest that the retardation or acceleration of the polymorphic transformation by the additive in the solid state is also connected to the hydrophobic moiety structure.

To elucidate the effects of hydrophilic and hydrophobic moieties independently, Smith and coworkers [57–59] investigated the effects of lauric-based amphiphilic molecules on the crystallization of trilaurin. The crystallization was monitored by using temperature gradient microscopy combined with differential scanning calorimetry (DSC) and X-ray diffraction at forced cooling rates of between 10 and 100°C/h. Without additives, thin lath-like β crystals were formed. These crystals increased in size with time and had nearly perfect, large facets. The addition of lauric acid and monolaurin caused a definite morphological change in the β form. In addition, the twinning density was increased, as evidenced by the increase in imperfection of the crystals. The addition of dilaurin caused the facet and crystal sizes of β crystals to be considerably reduced. Growth distance versus time plots are illustrated in Figure 21. Both lauric acid and monolaurin (not shown) increased the growth rate of trilaurin, whereas the dilaurates decreased it. 1,3-Dilaurin is particularly effective at retarding the growth rate. In addition,

Copyright 2002 by Marcel Dekker. All Rights Reserved.

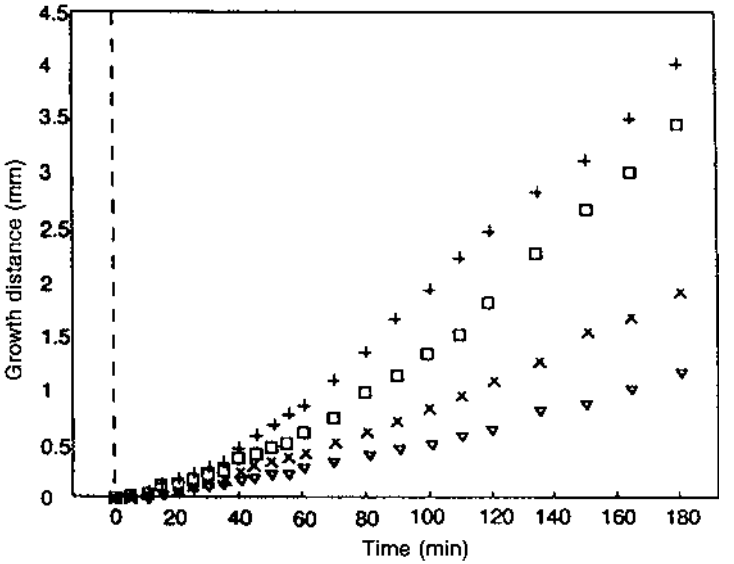

Figure 21 Growth distance plotted against time for all systems at a slide movement rate of 1 mm/h (additive level 2 wt%) (□) Trilaurin; (+) trilaurin + lauric acid; (×) trilaurin + 1,2-dilaurin; (▽) trilaurin + 1,3-dilaurin.

increasing the concentration of the additive leads to greater retardation for the dilaurin-containing sample, with limited increases in growth rates for the monolaurin- and lauric acid–containing samples. Namely, the crystallization rate is increased but facet and crystal size are reduced by the smaller molecules, because these molecules can easily fit into the trilaurin lattice. The crystal growth rate is slightly increased by these molecules. The defect density is increased by the additives. On the other hand, bulkier additives like dilaurin may block the growth sites, which leads to a reduction in growth rate. Because 1,3- and 1,2-dilaurin have different shapes and fit into the lattice in different ways, the effects of these two isomers might be different [57,58].

The effect of the hydrocarbon chain length of additives on the crystal growth of trilaurin is also observed when caprate (C_{10})- and myristate (C_{14})-based amphiphilic molecules are added [59]. All the caprate additives retarded the growth rate to some extent. The effect of the myristate additives was the same as that of laurate additives. Consequently, one can conclude that the maximal inhibition of crystal growth of trilaurin occurs when the chain length is similar to that of the host and then decreases as the difference between the host and guest chain lengths increases. Among the several additives, the 1,3-diglyceride

Copyright 2002 by Marcel Dekker. All Rights Reserved.

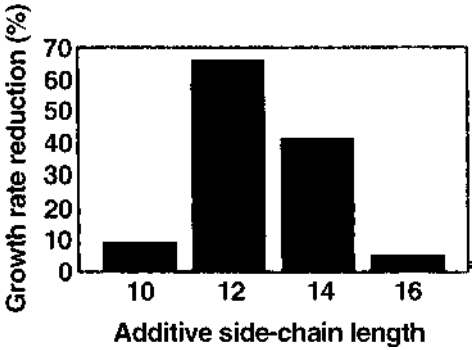

Figure 22 Effect of 1,3-diglyceride side-chain length on the crystal growth of trilaurin.

isomer reduced growth rates significantly. Figure 22 shows the effect of the side-chain length of 1,3-diglyceride on the growth rate of trilaurin β. From the growth rate dependence on undercooling, a simple incorporation mechanism was proposed for the different additives incorporated into the fat [58].

1. Cocoa Butter

Cocoa butter, the main constituent of chocolate, has six polymorphs, I–VI, that are distinguishable by melting points and X-ray diffraction patterns. Chocolate blooming was explained by two main concepts: (1) phase separation of high and low melting triglycerides in cocoa butter and (2) polymorphic transformation from the metastable V form to the most stable VI form. To retard the blooming phenomena, lecithins have been used as the most favored additives [60]. Also, Wahnelt et al. [61,62] showed that diglycerides can retard the crystal growth of cocoa butter.

Figure 23 shows the effects of added soy lecithin on the viscosity of chocolate [60]. The maximum thinning is produced by about 0.5% lecithin; above this there is a tendency for the viscosity to increase. Figure 23b shows the fat and lecithin contents of chocolate of the same viscosity and indicates the saving in cocoa butter as soy lecithin is increased [60]. These two figures show the large viscosity change and the saving in cocoa butter with the addition of lecithin. The reason for this effect is not completely understood. Figure 23c shows some information concerning the site of action. The addition of lecithin to a suspension of cocoa particles in cocoa butter gives only a slight reduction in viscosity (upper curve). However, the addition of lecithin to a suspension of ground sugar in cocoa butter has a marked effect on the viscosity (lower curve). Therefore, the major contribution to the viscosity-reducing effects of lecithin in chocolate is the action

Copyright 2002 by Marcel Dekker. All Rights Reserved.

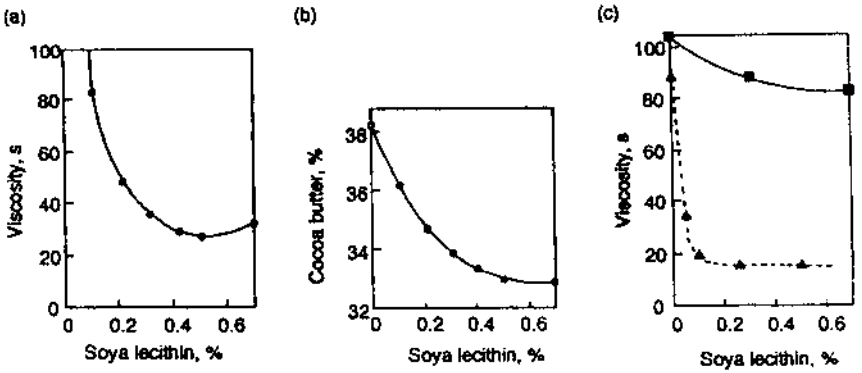

Figure 23 (a) Effect of adding soy lecithin [initial viscosity of plain chocolate (cocoa butter content, 34.8%), >200 s] on the viscosity of chocolate. (b) Fat and lecithin contents of chocolate of identical viscosity (42 s). (c) Effect of adding soy lecithin to suspensions of (■) cocoa butter and (▲) ground sugar in cocoa butter on viscosity. Viscosity was measured at 50°C on Bournville Redwood-type viscometer.

at the surface of the sugar particles. The flow characteristics of plain chocolate in the presence of the various emulsifiers are summarized in Table 1. Again it can be seen that the sugar ester was found to be inefficient in comparison to the other emulsifiers.

Early studies [63–65] demonstrated that the more hydrophilic emulsifiers such as ethoxylated sorbitan ester, diacetyltartaric acid esters, and monoglyceride lactate primarily affect polymorphic transformations and have no effect on bulk viscosity. Garti et al. [66] studied the effect of sorbitan esters and ethoxylated sorbitan esters on the transitions among the IV, V, and VI forms. Their results

Table 1 Flow Characteristics of Plain Chocolate with Added Surface-Active Lipids at 50°C

Addition	Casson plastic viscosity	Casson yield value
0.3% Soy lecithin	6.1	92
0.3% Phospholipid YN	10.3	30
0.3% Polyglyceryl polyricinoleate	32.5	25
0.3% Sucrose dipalmitate	8.6	166
0.8% Polyglyceryl polyricinoleate	20.3	(0)
Cocoa butter to similar plastic viscosity	7.3	72

Copyright 2002 by Marcel Dekker. All Rights Reserved.

suggested that some combinations of those emulsifiers accelerate the transition of form IV into form V by increasing the liquid fraction of the fat prior to its transition. Much additional work is required to reproduce the early findings and to explain (1) the selectivity in adsorption of hydrophilic emulsifiers versus hydrophobic ones on the sugar or fat particles in the bulk after they have been formed and (2) the effect of these emulsifiers on the crystalline sugar and/or fat particles.

Moran [67] tried to explore the effect of some emulsifiers on the viscosity of fat–sugar mixtures, using three systems: (1) palm kernel stearin fat (stearin I) + sugar (50 wt% sugar), (2) palm kernel stearin fat (stearin II) + sugar (50 wt% sugar), and (3) chocolate (system 1 or 2 + milk powder and cocoa powder). The viscosity of the sugar–fat systems was lowered by the incorporation of any of the emulsifiers (sorbitan esters, sucrose esters, lecithin, or polyglycerol stearate). Among the emulsifiers, polyglycerol stearate and sucrose dioleate were more effective than soy lecithin. In addition, the additives retarded the crystallization of the stearin fat at a low degree of supercooling. Therefore, the claims made in the past that emulsifiers are adsorbed selectively on sugar particles and do not affect fat particles were too early and not accurate. It also becomes clear that the emulsifiers retard crystallization, slow the polymorphic transformations, and affect the rheological properties of the chocolate network. That is, they play a significant role in the crystallization processes and during storage (solid–solid transformation). As for the reason for this effect, water and sugar binding capabilities remain to be observed and proven.

2. Hydrogenated Sunflower Oil

The effect of sucrose ester (P-170, m.p. 57°C) on the crystallization kinetics of hydrogenated sunflower oil was studied by Herrera and Marques Rocha [68] by means of an optical method. Table 2 shows the effects of the addition of sucrose ester on the induction time of crystallization by cooling to crystallization temperatures (T_c) of 30 and 33°C at two cooling rates. At a T_c of 30°C, there was only a small difference in induction time at slow and fast cooling rates. At $T_c = 33$°C, the effect of cooling rate was noticeable and the induction times were shorter at slow crystallization rates. With the addition of sugar ester, the nucleation of β was delayed; the sugar esters affected the formation of critical nuclei and prolonged induction times. Table 3 indicates the effect of the emulsifier on the β′-to-β transition when the sample was crystallized at 30°C. At all concentrations, the emulsifier delayed the transition 24 h. Moreover, long times were needed to complete the transition. The kinetic mode of the transition process was described on the basis of Avrami's equation,

$$1 - X = \exp(-Kt^n)$$

Copyright 2002 by Marcel Dekker. All Rights Reserved.

Table 2 Induction Times for Crystallization of Hydrogenated Sunflower Seed Oil

Amount of sucrose esters (%)	T_c (°C)	Cooling rate (°C/min)	Induction time (min)[a]
0	30	2	10.4 ± 0.1
		7	13.6 ± 0.3
	33	2	36.6 ± 0.4
		7	50.7 ± 0.8
0.01	30	2	12.6 ± 0.4
		7	24.1 ± 0.4
	33	2	56.9 ± 1.1
		7	144.8 ± 1.7
0.05	30	2	45.3 ± 1.2
		7	54.6 ± 1.2
	33	2	72.8 ± 1.3
		7	268.4 ± 2.6
0.1	30	2	105.8 ± 2.1
		7	115.5 ± 2.0
	33	2	456.7 ± 5.3
		7	453.5 ± 4.2

T_c = crystallization temperature.
[a] Mean ± one standard deviation.

where X, is the β fraction; n, is the mode of nucleation and/or growth of β nuclei; t, time; and K, the shape factor of β. By plotting the transformation curves (β fraction vs. time) and fitting the Avrami equation, the n value is approximately 1 in all the concentrations of additives. This result suggests that only the β′ form could be obtained from the melt. The β form could not be obtained directly from the melt. The β′-to-β transition is not liquid-mediated and probably occurs during the solid-state transformation.

Similarly, cocoa butter (CB) will develop a texture of good consistency and uniform matrix in chocolate if the fats solidify from the melt into a crystalline IV or V polymorphic modification of the cocoa butter. Severe fat migration (fat bloom) will take place after prolonged storage or temperature fluctuations if the CB modification is crystallized or transformed in situ into the VI form. Several additional products suffer from similar problems. It is well documented that the formation of crystal structure and the solution- or solid-mediated transformations can be delayed, slowed, or enhanced by small amounts of specific amphiphiles dissolved or dispersed in the fat during the crystallization stages.

Copyright 2002 by Marcel Dekker. All Rights Reserved.

Table 3 Effect of Sucrose Ester of β′-to-β Polymorphic Transition on Hydrogenated Sunflower Seed Oil at 30°C[a]

Storage time (days)	Sucrose ester content (%)			
	0	0.01	0.05	0.1
	(a) Slow crystallization			
0	β′	β′	β′	β′
1	β′	β′	β′	β′
2	β′ ≪ β	β′	β′	β′
3		β′ ≪ β	β′ ≪ β	β′ ≪ β
8	β′ = β	β′ = β		
31			β′ = β	β′ = β
60	β			
76		β		
98			β	β
	(b) Quick crystallization			
0	β′	β′	β′	β′
1	β′	β′	β′	β′
2	β′	β′	β′	β′
		β′ ≫		
3	β′ ≫ β	β′	β′	β′
4			β′ ≫ β	β′ ≫ β
18	β′ = β	β′ = β		
35			β′ = β	β′ = β
76	β			
88		β		
106			β	
120				β

[a] Storage temperature: 25°C.

3. Nucleation in Emulsion Systems

It is beyond the scope of this chapter to discuss in detail the effect of emulsifiers in emulsions. We mention only one specific case. In fat systems, some emulsifiers act as heteronuclei. Nucleation of fat crystals is accelerated through catalytic actions of such impurities. This effect is rather obvious in emulsion systems [69]. It has been indicated that nucleation is accelerated at the interface of the emulsion, on which the adsorbed hydrophobic emulsifiers become templates for heterogeneous nucleation.

As a model system of heterogeneous nucleation, the crystallization of the oil phase in O/W emulsions has been studied systematically. Figure 24 shows the variation in the ultrasonic velocity values of *n*-hexadecane in O/W emulsions

Copyright 2002 by Marcel Dekker. All Rights Reserved.

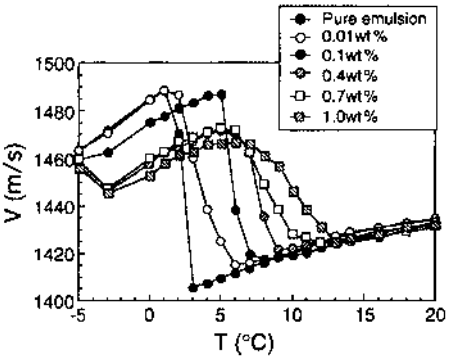

Figure 24 Temperature variation of ultrasonic velocity (V) of *n*-hexadecane–water emulsion with the addition of S-170 during cooling.

with and without the addition of sugar esters with stearic moieties (S-170). On cooling, the ultrasonic velocity values abruptly increase at 2°C in pure microemulsion, due to the crystallization of the *n*-hexadecane phases in the emulsion. The crystallization temperature, T_c, is increased with increasing amounts of S-170 (0.01–1 wt%) from 2°C to 12°C. This type of acceleration with added hydrophobic emulsifiers on nucleation was not observed in the bulk system. Therefore, it is considered that the fatty acid chains of S-170, which are adsorbed at the oil/water interface at the molecular level, are solidified on cooling and thereby play the role of a catalytic template film for the heterogeneous nucleation of *n*-hexadecane.

Figure 25 shows the T_c variations of *n*-hexadecane in the O/W emulsion systems with the addition of four sugar esters having stearic (S-170), palmitic (P-170), lauric (L-195), and oleic (O-170) acids. The addition of S-170 and P-170 showed similar profiles of increasing the T_c of *n*-hexadecane through the two stages depending on their concentrations. Although in a rather moderate manner, the increase in T_c due to L-195 showed basically the same two-stage processes [69].

The two-stage processes can be discussed by taking into account the adsorption of the sucrose oligoester molecules at the oil/water interface and the formation of a reversed micelle phase (Fig. 26). The sugar esters employed in the present study are rather lipophilic and therefore are strongly adsorbed onto the oil/water interface in the surfactant–water–oil systems. Even in the surfactant–oil systems, sugar esters are not solubilized into the oil phase and form molecular aggregates such as reversed micelles in the oil phase [68–70, 209]. Accordingly, when the concentrations of the additions of sugar esters in *n*-hexadecane in the O/W emulsion systems are low, all of them could be adsorbed at

Copyright 2002 by Marcel Dekker. All Rights Reserved.

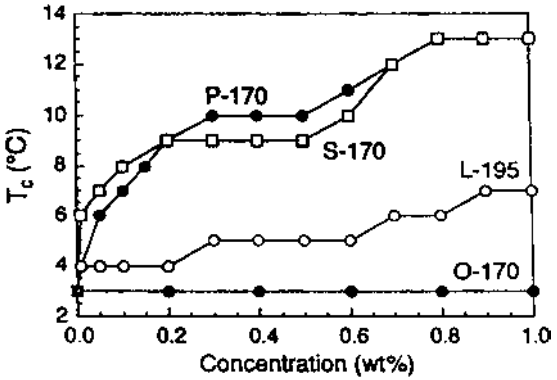

Figure 25 Variations in crystal growth rate of *n*-hexadecane from bulk liquid at T_c = 17.1°C with P-170, S-170, L-195, and O-170 (1.0 wt% added).

the water/oil interface. S-170 and P-170 are adsorbed at the interface and may accelerate the heterogeneous nucleation of the oil phase at the surface of droplets when the O/W emulsion is cooled. The DSC measurement of the crystallization behavior of *n*-hexadecane with addition of P-170 suggested the formation of molecular aggregations with Tween 20 on the oil/water interface [71]. With higher concentrations of the additives, the adsorption at the interface is saturated and excess molecules of the sugar esters may form reversed micelles. Such molecular aggregates might be solidified in the liquid oil phase in the cooling process and accelerate the nucleation in the oil phase [71,72]. Therefore, as to the two stages of the acceleration of nucleation shown in Figure 26, the first rapid increase may

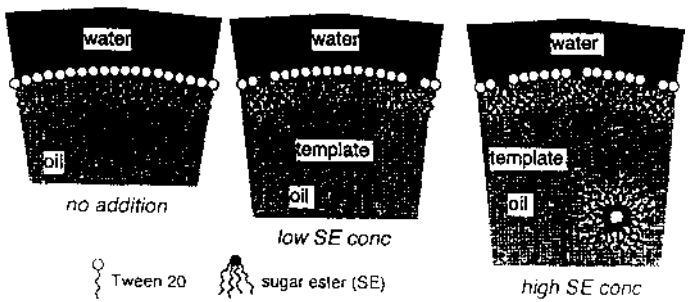

Figure 26 A model of interface heterogeneous nucleation in O/W emulsion.

Copyright 2002 by Marcel Dekker. All Rights Reserved.

correspond to the heterogeneous nucleation at the interface, and the second increase is ascribed to the formation of the reversed micelles.

E. Influence of Emulsifiers on Fat Dispersions in Oil

In his doctoral thesis, Lucassen-Reynders [73] showed that monoolein can adsorb onto tristearin. Johansson and coworkers [74–76] carried out detailed work on model fat systems dispersed in oil. They studied the adsorption of various emulsifiers to the crystals (fats and sugar) dispersed in oils. The adsorbed amount, the strength of the adsorption, and their relationship to the character of the emulsifiers, crystals, and oils were obtained.

The main conclusions drawn from the study are as follows:

1. Most of the emulsifiers studied adsorb weakly to fat crystals at high concentrations. At low concentrations, loosely packed layers are formed and a decrease in adhesion is observed. Unsaturated monoglycerides and phospholipids cause a decrease in adhesion for all concentrations examined.
2. The emulsifiers adsorb more strongly to sugar crystals than to fat crystals and form tightly packed monolayers with hydrocarbon chains directed toward the oil. The crystals are then stabilized sterically, the adhesion between them is weaker, and sediments are more compact. Phospholipids reduce the adhesion between sugar crystals, resulting in much denser sediments.
3. Saturated monoglycerides in amounts over the solubilization limit tend to precipitate as a network between fat or sugar crystals, which causes bulky sediments and results in better stability against oiling-out.

F. Adsorption of Fat Particles onto Oil Droplets

For many years it was known that emulsions can be stabilized by solid fat particles that adsorb onto the water/oil interface. Such stabilization was called Pickering or mechanical stabilization. Recently, we reported that emulsifiers can help modify the fat particles and crystallize them (prior to forming the emulsion) into the α or β' form. The modified particles will better wet the interface and will be better oriented to the interface and thus will better stabilize the emulsions. It was found that the best emulsion stability could be achieved if the fat particles that adsorb onto the oil droplets are crystallized by quench cooling so that the most hydrophilic α-form triglyceride particles will be obtained. These particles added to the W/O interface will stabilize the emulsion against coalescence. Garti and

Copyright 2002 by Marcel Dekker. All Rights Reserved.

coworkers are involved in the project, and results from W/O emulsions as well as the stabilization of W/O/W double emulsions are very encouraging [77,78].

G. Some Remarks on the Effect of Emulsifiers as Crystal Structure Modifiers

Books have been written on chocolate blooming, fat crystallization in salad dressings, crystalline fat transformations in margarines, and similar phenomena that occur in foods, but even today there is no consensus on the precise mechanistic pathways of such transformations. Even more difficult is the correlation between surfactant activities and the blooming phenomenon. Needless to say, the structure–reactivity or surfactant–fat relationship is not yet totally resolved, and the same debate still exists. However, many aspects have been clarified, and it is a consensus today that the surfactants migrate from the bulk to the interface and adsorb on the nucleating fat crystals. As expected, the surfactants, therefore, act in their classical way of migration to interfaces. However, the mode of adsorption, the thickness of the adsorbed layer, the desorption mode, and the dynamic aspects are not yet clear. Recently, it was established that the surfactants can form mono- or bilayered structures on the fat particles, can cause a sintering effect between fat particles, and can cause repulsive forces. The surfactants can slow down the nucleation and growth rate or enhance either at the expense of the other. Can we correlate the surfactant chemical structure to its surface and bulk performance? Can we predict surfactant action, or can we design surfactant activities? The answer seems again to be complicated. It is easier to experimentally examine various surfactants and measure their overall effect than to try to predict their activity and to design an ideal amphiphile to perform as a crystal structure modifier of fats.

The effects of surfactants on the crystallization patterns of other food components were also studied. Surfactants affect the crystallization of sugars (sucrose, sorbitol, glucose, fructose, etc) from aqueous solutions. Surfactants affect yields of crystallization, rates of precipitation and crystallization, mode of crystallization, crystal structures, and crystal morphologies and habits. Surfactants also affect crystal size and amounts of impurities that cocrystallize. The effects are tremendous, and an almost endless number of effects have been described. In many cases, the studies are descriptive and the mechanisms involved in these effects are still obscure.

Any matter crystallizing in solution as a result of a cooling process will be affected by amphiphilic molecules during its crystallization stages. Nucleation of ice, hydrocolloids, starch, etc. is strongly affected by the presence of amphiphiles.

Copyright 2002 by Marcel Dekker. All Rights Reserved.

The reverse phenomenon of thawing of any food system is also expected to be influenced by amphiphiles. One can slow down or enhance melting phenomena by the use of surfactants.

Frying is accompanied by the release of water vapors from the the fried substrate and penetration of oil that sometimes solidifies upon cooling within the pores of the fried matter. Surfactants have been tested for their effect on reducing fat migration and fat intake.

Waterproofing is an important issue in food products. Surfactants can be very helpful in reducing water wetting and penetration into hydrophilic substrates such as wafers. Coating or dipping a food product in surfactant solutions significantly slows water migration into the product.

Surfactants adsorb on almost any dispersed substrate, and therefore it is not surprising that they also adsorb onto minor components of food systems and affect their stability against oxidation or hydrolysis, affect their crystallization patterns, and modify their dissolution behavior.

H. Other Surfactant–Substrate Interactions

Several of the major roles that surfactants play in dispersed systems are well documented in the literature, but the amphiphiles fulfill many additional less studied functions in food colloids that are directly related to their chemical structure.

Of significant importance are the surfactant interactions with macromolecules known also as biosurfactants. Proteins and carbohydrates are the two main food components that under certain circumstances exhibit surface activities and under other conditions interact directly with amphiphilic molecules that can alter the major properties and functionalities of the macromolecules. One of the major important effects is the complexation of monoglyceride esters with amylose (a component of starch that is a major ingredient in wheat flour needed in the baking process). Another important effect that occurs during baking is related to the interaction of molecules such as diacetyltartaric acid esters (DATAEs) with the wheat protein gluten. The two interactions are key factors in forming the viscoelastic network of proteins and starch that are responsible for the volume of bread and its shelf life, respectively.

III. CHEMICAL STRUCTURES OF SURFACTANTS AND THEIR APPLICATIONS

A. Lecithins and Lysolecithins

Crude oils of any kind always contain small quantities of phospholipids in addition to the triglycerides that are their main components. These are mainly deriva-

Copyright 2002 by Marcel Dekker. All Rights Reserved.

tives of phosphonyl-3-glycerol, whose alcohol functions at positions 1 and 2 are esterified by two different or identical fatty acids, whereas the phosphoric residue can be esterified by either an amino alcohol or a polyol. About 60% of these phospholipids (PLs) are found in the cell membranes of living organisms.

As a result of their marked amphiphilic characteristics, phospholipids are becoming increasingly important in all areas related to modern dispersed media such as agriculture, food, pharmacology, and cosmetics and because of their ability to form stable structures such as planar, cylindrical, or spherical bilayers or multilayers. Figure 27 highlights the amphiphilic character of phospholipids. R1 and R2 are nonpolar side chains that exhibit a pronounced lipophilic character because of their long carbon chains.

The interfacial behavior of phospholipids is well documented. The intermolecular forces of the amphiphilic molecule such as electrostatic forces are quite weak. The van der Waals interactions, induced dipole–induced dipole interac-

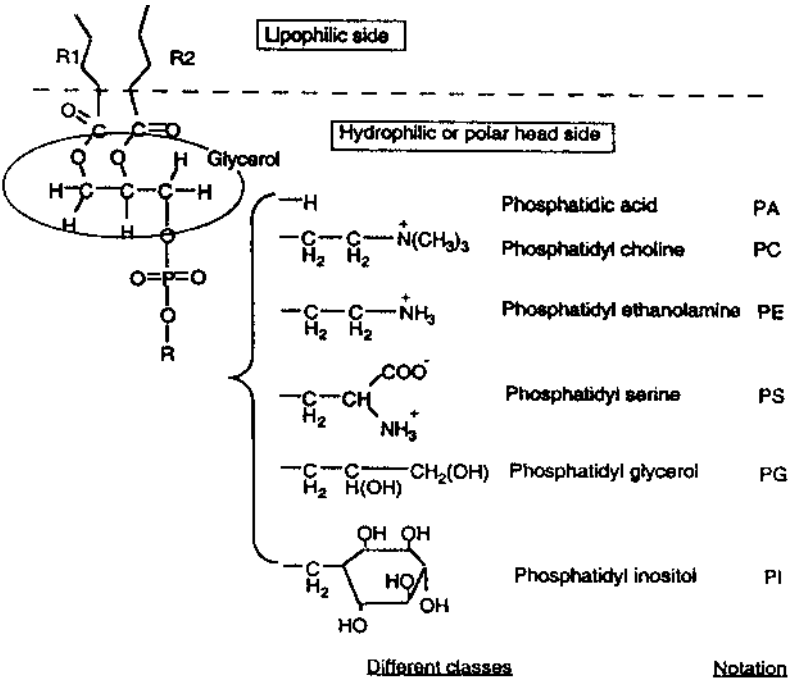

Figure 27 Six types of glycerophospholipids according to the nature of the substituent, as well as their usual abbreviated notation. The most well known (and most often used) is phosphatidylcholine (PC), also called lecithin.

Copyright 2002 by Marcel Dekker. All Rights Reserved.

tions, and hydrophobic interactions are very significant. Phospholipids are also known to be key participants as nucleators and crystal structure modifiers in the crystallization of fats and lipids. Phospholipids are present in many solid food matrices such as margarines, chocolate, and spreads, in which they control viscosity and fat microstructure, among other things. Therefore, the crystalline structures as well as liquid crystalline structures of the phospholipids are important factors in these processes and have been well documented and correlated to the cocrystallization events.

Crude lecithins consisting of phospholipids and sphingolipids (sphingosine and phytosphingosine—phospholipds that do not have the glycerol ester structure but do have the phosphoric ester of a long carbon chain hydroxyl amino base) have been extracted, for generations, from products such as soybeans, wheat, oats, and eggs. The crude mixtures are very inexpensive materials. However, to better benefit from some of the structural properties of these phospholipids (two-tailed surfactants with unique phosphated headgroups), it is essential to purify them.

Manufacturers treat the crude oily lecithin in various ways and extract products with various degrees of purity and specificity. Products such as plastic lecithins, deoiled lecithins, phosphatidyl choline–enriched lecithins, pure phosphatidylcholines (>98% PC), phosphatidylserines (PS); phosphatidylethanolamine (PE), phosphatidylinositol (PI), and phosphatidic acids (PA) mixture of fatty acids or mixtures of phospholipids with any particular fatty acid have been separated and are commercially available. Prices range from less than $1 per kilogram (crude lecithins) to thousands of U.S. dollars (pure selected fatty acid PC or PS). The inexpensive mixtures are widely used in food applications, and the purified lipids are used in very sophisticated pharmaceutical applications for drug stabilization, delivery, and targeting.

Lecithins are essentially hydrophobic molecules (mainly soluble in oil) but are widely used for more sophisticated applications in aqueous solutions or micro- and nanostructures. Phase diagrams of crude and purified lecithins in water in many combinations with other cosurfactants and cosolvents are available, but owing to the complexity of the phospholipid structure and their internal composition phase diagram structuring is always a difficult task. The crude lecithin phase diagrams show very limited abilities to solubilize water or oil components, whereas the purified phospholipids form unique microstructures with significant solubilization capacities and unique properties. In general, lecithins form mainly lamellar liquid crystalline structures in water that are good for pharmaceutical applications. However, it will be difficult to use the phospholipids as emulsifiers for stabilization of either water-in-oil or oil-in-water emulsions because of their poor stabilization capabilities. Once one of the tail fatty acids is removed (enzymatically) to form a lysolecithin, the emulsification activity improves and many new food applications can be found.

Copyright 2002 by Marcel Dekker. All Rights Reserved.

It has been known for a very long time that it is a good idea to ''hydrophilize'' lecithin by detaching one of its tail chains, replacing it with a hydrophilic functional group such as acetyl or epoxy. Hydrolyzing one of the fatty acids to form lysolecithin is an industrial process. Lysolecithin is far more hydrophilic than lecithin and can act as a good oil-in-water emulsifier. All the attempts to fully hydrolyze lecithin to lysolecithin in solvents and in emulsions led to a complex mixture of partially hydrolyzed lecithins and a relatively poorly performing emulsifier.

Attempts have been made to enzymatically hydrolyze lecithin with phospholipase A_2 to form lysolecithin. The product is a good imitation of what nature offers in very small quantities. The partially hydrolyzed lecithins, or, the fully converted lysolecithin, are the subject of recent work conducted to carry out the reactions in ''microemulsions as microreactor'' for the PLA_2 enzymatic process (Fig. 28) [79,80].

Lysolecithin exists in nature, but its quantities are very minute and no commercial processes for its direct extraction have been developed.

Industrial lecithins have only 60–65% lecithin with 30–35% soybean oil as plasticizer. Many other types of lecithins exist on the market, including clari-

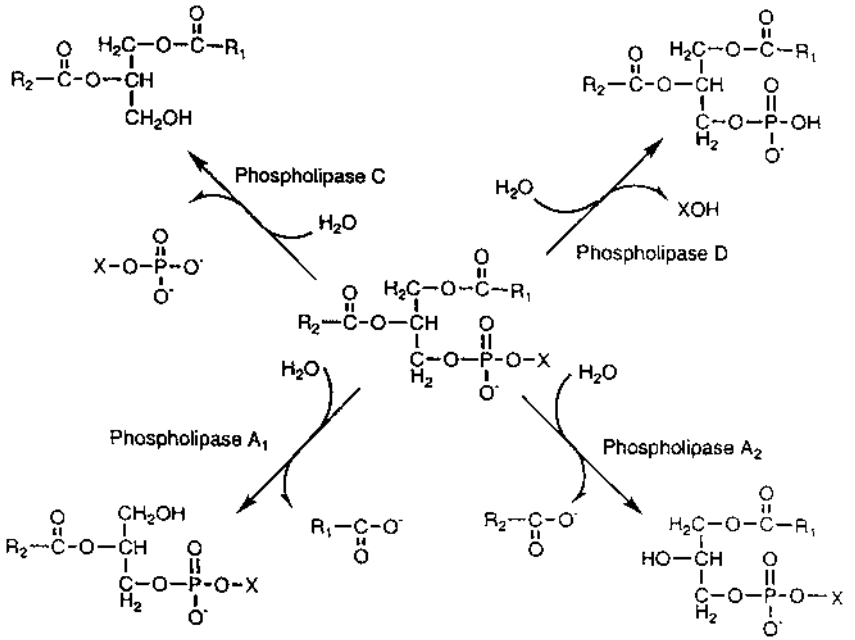

Figure 28 Cleavage of functional groups by different types of phospholipases.

Copyright 2002 by Marcel Dekker. All Rights Reserved.

fied lecithin (carefully filtered), compounded lecithin (combined with surfactants or other additives or blended with carriers to form a product with special properties), deoiled lecithin (dry or granulated powders with high phosphatide content), modified lecithins (chemically or enzymatically hydrogenated, hydroxylated, ethoxylated, halogenated, sulfonated, acylated, succinylated, ozonized, and phosphorylated—the most common being hydroxylated and acetylated), and fractionated lecithin (for cosmetic and pharmaceutical applications) [81].

Lecithins are considered a GRAS (Generally Recognized As Safe) material by the United Nations Food and Agriculture Organization (FAO).

Lecithins have many beneficial properties and are used in many commercial applications (including nutritional and health). However, the main function of the phosphatides is their emulsifying ability for fats and oils.

The long-chain fatty acid moieties contribute hydrophobic properties; those properties are counterbalanced by the polar or hydrophilic character of the phosphate moiety. In an oil–water system the phospholipid components concentrate at the oil/water interface. The polar, hydrophilic parts of the molecules are directed toward the aqueous phase, and the nonpolar, hydrophobic (or lipophilic) parts are directed toward the oil phase. Concentration of phosphatides at the oil/water interface lowers the surface tension and makes it possible for emulsions to form. Once the emulsion is formed, the phosphatide molecules at the surface of the oil or water droplets act as barriers to prevent the droplets from coalescing and thus stabilize the emulsion.

1. Major Uses of Lecithins

Some of the major functional uses of lecithin products are as (1) emulsifiers in food emulsions, (2) solubilizing agents for various compounds in aqueous systems, (3) sol dispersing agents, and (4) foaming and defoaming agents.

Examples of food emulsions include milk, butter, margarine, puddings, chocolate, bakery items, cheese, milk and cream replacers, ice cream, and processed meat products such as hamburgers and hot dogs.

Most processed food emulsions are not stabilized by emulsification alone. The particle size of the dispersed phase has to be much smaller for dynamic stability than is practically possible with foods. Emulsifier–stabilizer systems, however, are normally used to make stable food emulsions. Lecithin will break up (emulsify) the particles, and a stabilizer (water-soluble polymer, etc.) will hold the particles in a dispersed orientation, giving a stable emulsion.

Lysolecithins, which are more hydrophilic, show stronger oil-in-water emulsifying properties. Stable microemulsions have been prepared with various fractionated lecithins. These microemulsions are used in direct applications as reservoirs for certain active materials (flavors, antioxidants, nutraceuticals, etc.) or as microreactors for enzymatic reactions. Several of these applications were

Copyright 2002 by Marcel Dekker. All Rights Reserved.

developed in my laboratory, including preparation of lysolecithin in microemulsions as microreactors, solubilization of lycopene in microemulsions, and crystallization of Aspartame in a new polymorphic modification in food microemulsions.

Lecithin is one of the most effective surfactants for dispersing sols. This seems to be due to its affinity for solid/liquid surface interfaces. Phosphatides seem particularly attracted to particles that contain metals or metal salts. Examples of food sols include some liquid chocolates, instant drinks, some frosting mixes, and pigmented foods.

Upgraded lecithins have been employed as effective foam control agents. Examples of uses include whipped toppings, ice creams, and many types of candies. Upgraded lecithin products have also been employed as effective defoaming agents in foams caused by powdered proteins in water. This is an excellent example of the system specificity of lecithin products.

Commercial soybean lecithin products are commonly used in food applications that are not directly related to their emulsification activities. For example, one can find soybean lecithin as a coemulsifier and complexing agent for amylose in baked goods. A spray-dried combination of modified partial glycerol, lecithins, and milk solids is used in wheat flours to ensure uniformity in high quality breadmaking; in instant pudding mixes to enhance smoothness; in coffee whiteners, beverage mixes, and whole-milk powders to enhance their solubility, in infant formulas to promote remixing, in egg replacements as a release agent, and in ice cream to increase smoothness and prevent graininess.

Liposomes are tiny hollow bodies made of phospholipids and filled with water; their diameter is 200–500 nm (Fig. 29). They were originally made to imitate cells so that the transport of substances into and out of the cell could be studied. Liposomes form compartments without which the cell would be unable to function and that are really the basic structures of life. Together with water,

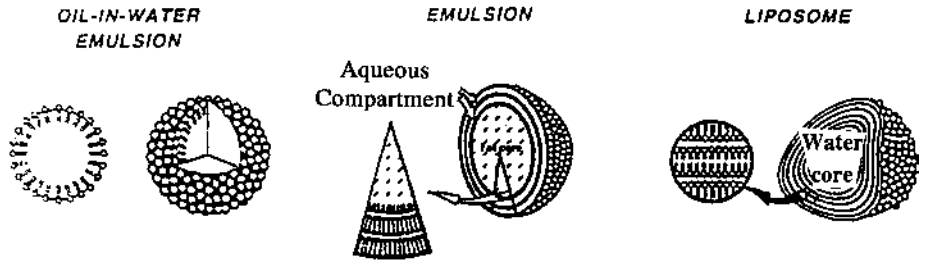

Figure 29 Schematic illustration of a liposome, an O/W submicrometer emulsion droplet, and proposed structure for an emulsion particle.

Copyright 2002 by Marcel Dekker. All Rights Reserved.

phospholipids form double layers with a structure that enables them to act as ''cell walls,'' dividing the compartments from each other. This has great technical advantage [81,82].

Liposomes can store water-soluble substances in the core of the bilayer membrane. This has two useful effects. First, distribution of the encapsulated substances in the food is far more homogeneous than is possible with classical emulsifiers. Second, the encapsulated substances are immobilized because of the liposomes stability. They do not migrate, and it takes a long time to release them from the product. This means, for example, that a lemon-flavored cake stays fresh longer and tastes of lemon for a longer time too. Nowadays it is possible to produce liposomes in most of the homogenizers used in the food industry if the right fraction of lecithin is used. It is possible to form membrane-like structures that can withstand many mechanical and thermal loads.

The use of lecithin fractions as liposome formers in food is relatively new. By fractionating the complex mixture of lecithin and removing part of the phospholipids it is possible to optimize these special functions and to form liposomes.

One can think of many food applications for liposomes. Three examples are

1. **Water retention**. Maintenance of freshness in baked goods is a very important factor. If a ''liposome cream'' is made, a large portion of the water will be firmly bound in the finished bread and it will take a considerable time to release the water, which keeps the bread fresher longer.
2. **Flavor retention**. Liposome formation can increase the surface area of the product by manyfold and the flavor will be tremendously improved. The subjective freshness of a cake is greatly enhanced by the very fine fat distribution brought about by the liposomes.
3. **Protection against inactivation**. Yeast cells in frozen dough are exposed to considerable stress. Ice crystals inactivate some of the yeast cells. In the past, attempts were made to get around the problem by just adding more yeast. Now we know that liposomes are a more effective solution. They provide the yeast with sufficient protection against the cold. The reason is that the membranes of the yeast cells have a high content of unsaturated fatty acids, so they remain fluid and are not inactivated or destroyed by crystallization. When the temperature of the dough rises again, they are ready at once. The baking yield improves significantly.

It should be noted that liposomes can also be loaded with water-insoluble (fat-soluble) matter such as vitamins or flavorings. Flavoring agents encapsulated in liposomes do not diffuse through the membrane until they are needed.

Copyright 2002 by Marcel Dekker. All Rights Reserved.

2. Lecithins from Other Sources

Phospholipids can be obtained from various sources, two of which are oilseed lecithins and egg yolk lecithins. The phospholipid composition of soybean lecithin appears to vary according to the method of extraction. PC content ranges from 29 to 46%; PE, from 21 to 34%; and PI, from 13 to 21%. Other minor constituents are phosphatidylserine, phosphatidic acid, lyso-PC, lyso-PE, and lyso-PI. In addition to soybeans, lecithin has been found in many other oilseeds, including peanuts, cottonseed, sesame, safflower, and sunflower, among others.

Only limited quantities of cottonseed lecithins are available [83]. Most of the phospholipids are contained in the non-oil materials (1–2%) separated from hydraulically pressed oil by alkali or water washing. Different extraction methods normally used in the oilseed crushing industry cause a few differences in the percentage of phospholipids or fatty acids in cottonseed oil. Limited data are available in the literature on the composition of cottonseed phospholipids. Scientists have not individually separated and quantified all of the lecithin and cephalin components.

All major cottonseed phospholipids [83] are present in the cottonseed lecithins: phosphatidylinositol (13.4 wt% total phosphorus), phosphatidylserine (2.4 wt%), phosphatidic acid (8.8 wt%), phosphatidylcholine (23.2 wt%), and phosphatidylethanolamine (13.5 wt%). Because cottonseed oil and lecithin have only trace amounts of fatty acids with more than two double bonds (linolenic acid), they are stable to oxidation and rancidity. Other sources of phospholipids (e.g., soybeans) contain linolenic acid in amounts that can affect flavor, color, and odor. With the potential for increasing revenues, decreasing waste disposal costs, and reducing emulsion problems, glandless cottonseed oil and lecithin products become economically attractive.

Patents for commercial preparations of corn phosphatides and for products containing lecithin (cosmetics, ointments, foaming agents, and rust inhibitors) were issued during the 1930–1950s [84,85]. The growth in demand for corn sweeteners may make other products of the corn refining industry, such as lecithin, more available and competitive. Similar compositions were noted for the major phospholipids of phosphatidylcholine, phosphatidylinositol, and phosphatidic acid. Glycolipids represent a higher proportion of polar lipids in corn than in soybean lecithin. The percentages of minor components, sterylglycoside ester, and other glycolipids are more than twice that of soybean lecithin. Both the glycolipids and phospholipids of corn have lower percentages of linolenic acid and are more saturated than those of soybean. Linoleic acid varies from 42% to 70% depending on the variety of corn. This genotypic effect on fatty acid composition of phospholipids introduces the possibility that lecithin with selected contents of these nutritional components can be obtained by corn breeding.

Copyright 2002 by Marcel Dekker. All Rights Reserved.

Potential sources of phospholipids include canola/rapeseed; sunflower seed; peanuts; palm kernel; cereal grains of wheat, barley, and rice; and, olive, mango, and avocado fruits.

Egg yolk solids are 65–70% fats, consisting of 65% triglycerides, 30% phospholipids, and 4% cholesterol. The natural emulsifying property of egg yolk is primarily due to lecithoproteins, i.e., lipoproteins containing lecithin. These lipoproteins can be separated by high speed centrifugation of egg yolk into the sediment, called granules, and the supernatant fraction, called plasma. Granules represent 19–23% of the yolk solids, whereas plasma represents 78% of the liquid phase. On the dry weight basis, granules contain about 34% lipid, of which 37% is phospholipids, mainly PC (82%) and PE (15%). Plasma contains a low density lipoprotein (LDL) fraction that is 84–89% lipid, of which 26% is phospholipid (71–76% PC, 16–20% PE, and 8–9% sphingomyelin and lysophospholipid) [81].

Owing to the good emulsifying properties of egg yolk lipoproteins, oil can be dispersed in other food ingredients, so the lipoproteins can contribute to the consistency of mayonnaise and salad dressing and to the structure of cream puff shells. Whereas whole eggs are used in rolls, sponge and layer cakes, and bread, yolks are used in salad dressings, mayonnaise, doughnuts, sweet goods, and cakes that require more yellow color.

Milk is one of the naturally occurring emulsions found in foods. Cow's milk contains milk fat (3–6%), protein (3–4%), lactose (5%), and ash (>1%). Of the milk fat, the phospholipid fraction generally is no greater than 1% (triglycerides compose 97–98% of the total milk fat). Other lipids found are sterols, carotenoids, and fat-soluble vitamins. All of these components of milk add to its emulsification.

B. Glycolipids

Nonphosphorus molecules always accompany plant or egg phospholipids with amphiphilic characteristics, which are termed glycolipids. The main glycolipids are diglyceride ethers of mono- or disaccharides (Danisco Co., Copenhagen, private communication) (Fig. 30).

Ceramides and phytoceramides (amides of fatty acids with sphingosine or phytosphingosine) may be linked with galactose (animals) or with glucose (plants). The compounds thus formed are cerebrosides. Close examination of the structure of these molecules reveals that their amphiphilic nature is intriguing. However, these types of molecules are not readily available and are very expensive. Therefore, their surface-active properties have not been extensively explored and none have become commercially available.

Investigators [86] have made attempts to extract from natural sources or to design and prepare new types of simplified glycolipids to imitate those found

Copyright 2002 by Marcel Dekker. All Rights Reserved.

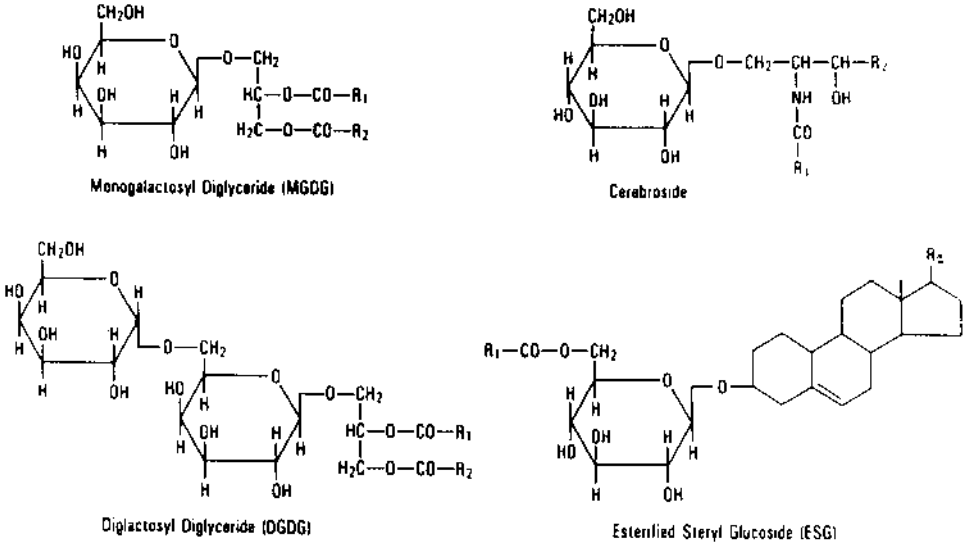

Figure 30 Schematic structures of glycolipids.

in very small percentages in nature. Esters of dimeric or trimeric glycerides such as digalactosyl diglyceride (DGDG) (Fig. 30) from cereal grains (oats, wheat, soy) have been found and identified in oats and extracted. Some studies related to the surface properties of these molecules have been published and show significant promise. It should be noted that these products are still very minor constituents in cereals and it is rare to find them in concentrations exceeding 2 wt%.

Scientists believe that eventually advanced extraction, separation, and purification methods will decrease extraction costs and that glycolipids such as DGDG and trigalactosyl diglyceride (TGDG) will become commercial products for water-in-oil and oil-in-water emulsions [86].

C. Saponins

The unsaponifiable part of most fats comprises constituents that have very low solubility in water and significant solubility in fat and lipophilic solvents. Those products include diverse hydrocarbons, terpenic compounds, fatty alcohols, and fat-soluble vitamins (Fig. 31). Those products cannot serve as emulsifiers. However, in certain vegetables and fruits, a terpenic component is attached to a saccharidic structure by an etheric or esteric link, forming a very water-soluble structure typical of compounds known under the general name saponins.

Saponins have been known for generations and have been commercially

Copyright 2002 by Marcel Dekker. All Rights Reserved.

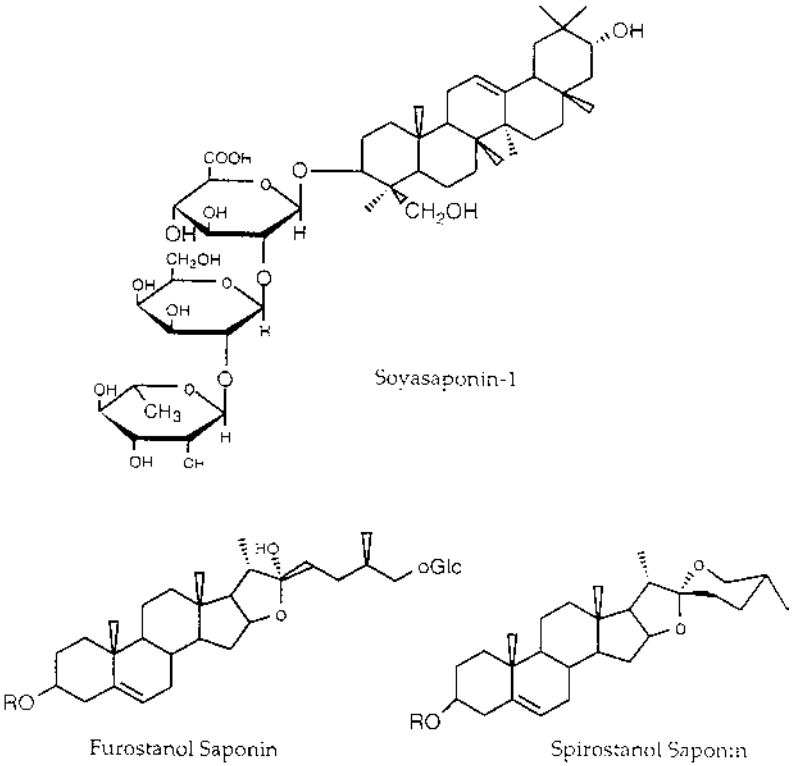

Figure 31 Schematic structures of three different types of saponins.

available for years. Their high price and high HLB values have limited their application to certain photographic emulsions and cosmetic and pharmaceutical applications. Recent studies indicate that saponins can form stable ''surface complexes'' at various oil-in-water interfaces together with other monomeric emulsifiers and stabilize the emulsions in an improved manner (Fig. 32) [86]. Saponins are also known to bind to cholesterol and reduce its levels in human beings.

It was only within the last few years that saponins were rediscovered and their presence was noted in a new category of functional foods consisting of nutraceuticals with health benefits. In many plants' seeds the major components are hydrocolloids such as fenugreek gum, locust bean gum (LBG), and guar gum with considerably high concentrations of saponins. It is therefore a trend in some labs to search for new saponin-rich plants from which the saponins can be extracted [87].

Copyright 2002 by Marcel Dekker. All Rights Reserved.

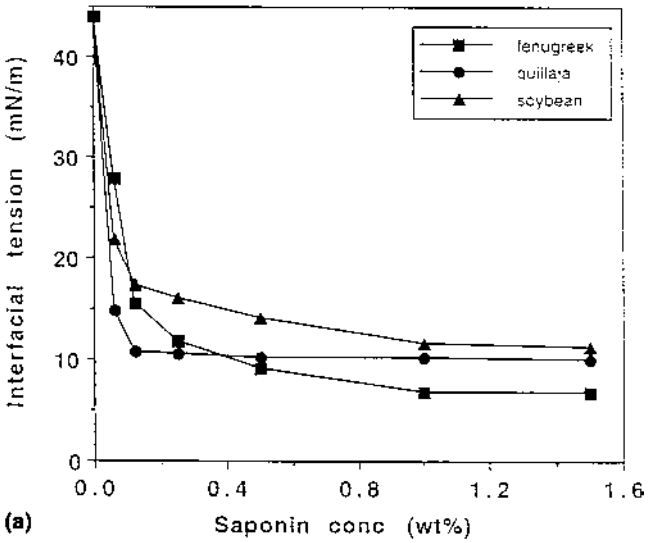

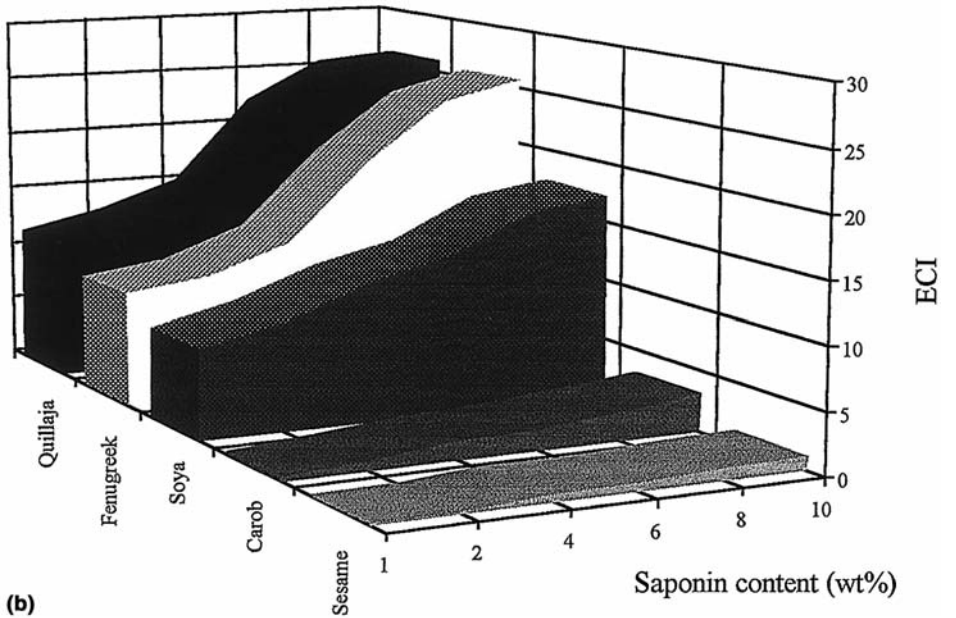

Figure 32 (a) Interfacial tension of *n*-tetradecane–water at 25°C as a function of the concentration of the crude saponin extract fraction. (b) Emulsification capacity index (ECI) as a function of saponin content (in weight percent) in oil-in-water emulsions stabilized with five types of saponins.

Copyright 2002 by Marcel Dekker. All Rights Reserved.

It is our belief that when the price drops and the availability of these products increases, saponins will be found in an increasing number of O/W emulsions.

D. Mono- and Diglycerides of Fatty Acids

Fats and oils are excellent sources for many amphiphilic molecules because they are inexpensive, easy to extract, and easy to handle. Chemical reactions and/or enzymatic processes are often carried out on certain fats and/or oils to obtain molecules with hydrophobic and hydrophilic groups attached to each other. One of the most common emulsifiers for water-in-oil emulsions are monoglycerides of fatty acids. Hydrogenated oils or natural fats, when transesterified with glycerol, yield mixtures of mono- and diesters of fatty acids.

Many chemists and enzymologists have made tremendous efforts to treat fats in situ with fatty acids to form the monoglycerides. These attempts have included the use of advanced (coated, activated, encapsulated, etc.) alkaline or acidic reagents, biotechnological methods, or enzymes (lipases from different sources treated in various manners) to form α-monoglycerides in high yields, high specificity (only α-monoglycerides without any β-mono modification), and low cost, without the need of an expensive and difficult molecular distillation process. In spite of the fact that lipases are inexpensive and well-documented enzymes, no good commercial and economical process has so far been employed in industrial-scale processes.

The amounts of mono- or diglycerides in plants, fruits, flowers, tissues, fungi, bacteria, etc. are very low, and it is not economically feasible to extract them from any of these sources.

Lipid fractions (oleoresins), in which the monoglyceride content is somewhat higher (up to 2–3 wt%), have been explored and used for some applications. Many of the oleoresins extracted from fruits, flowers, spices, leaves, etc. consist of various triglycerides, nonsaponifiable fats (waxes), and monoglyceride derivatives. These fractions are sometimes ''self-emulsifiable'' and can form in situ water-in-oil emulsions. Such oleoresins from tomato, rosemary, sage, paprika, etc. can provide other functional properties.

Mono- and diglycerides are commercially prepared from the direct esterification of edible fats or fatty acids (of vegetable or animal origin) with glycerol at elevated temperatures or from the glycerolysis of oils, i.e., the transesterification of an oil with glycerol (Fig. 33) [5,88]. In transesterification, triglycerides are heated with glycerol and a catalyst, usually sodium hydroxide, under vacuum at 200°C. As the fatty acids are cleaved from the triglycerides, some migrate to the free hydroxyls of the glycerol molecules to form the mono- and diglycerides. The yield of monoglycerides (MGs) depends on the ratio of triglyceride to glycerol. Such methods were demonstrated by reacting the oils of coconut, peanut, sesame, linseed, and sardine with glycerol and by the direct esterification of fatty

Copyright 2002 by Marcel Dekker. All Rights Reserved.

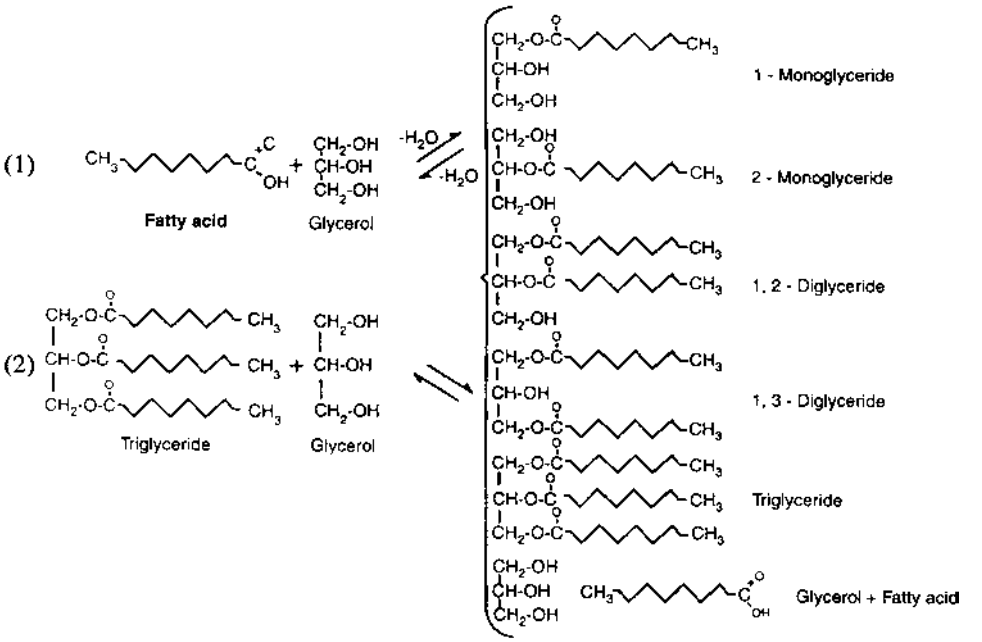

Figure 33 Preparation of monoglycerides of fatty acids by (1) transesterification of fats with glycerol and (2) direct esterification from fatty acids, at elevated temperatures and in the presence of alkaline catalyst.

acids with glycerol. Feuge and Bailey [88] demonstrated that the proportions of glycerol and mono-, di-, and triglycerides could be calculated statistically. The reaction mixtures contain small traces of free glycerol and free fatty acids, which can be removed by distillation to obtain 95–98% pure MG. Commercial MGs usually contain about 40–50% monoester, 40% diester, and 10% triglycerides.

Mono- and diglycerides of fatty acids exist in several structural modifications. In monoglycerides, if the fatty acid is attached to the middle, β (2-position), carbon, the molecule is symmetrical and the monoglyceride will be termed a β-monoglyceride. If the fatty acid is attached to carbon-1 it will be termed an α-monoglyceride. At 20°C the relative proportions of the two isomers are 95:5 in favor of attachment at the terminal α-position, but at 200°C this ratio changes to 82:18 [89]. In diglycerides the fatty acids can attach to any two of the three positions.

Mono- and diglycerides can be solid or liquid materials depending on the nature of the fatty acids composing the molecule. Monoglycerides composed of

Copyright 2002 by Marcel Dekker. All Rights Reserved.

mainly oleic acid or unsaturated fatty acids will be liquid and more sensitive to oxidation and degradation, whereas monoglycerides composed of saturated fatty acids will be solid powders or waxy materials. The melting point of the product will depend on the origin and structural composition of the fatty acids [90].

Because mono- and diglycerides are mostly lipophilic, they are soluble in oil and only to a limited extent in water. They are strongly adsorbed at the triglyceride/water interface, and they readily form a liquid crystalline phase in association with water. Hence, they are excellent emulsifiers. Similar to other emulsifiers, MGs are found in the O/W interface with the polar groups (hydroxyls) of the molecule in the aqueous phase and the nonpolar group (the fatty acid) in the lipid phase. In this manner, monoglycerides act to reduce the interfacial tension and to stabilize emulsions. Their lipophilic character causes them to be excellent W/O emulsifiers, as in margarine.

The major uses of mono- and diglycerides are in bakery products, prepared cake mixes, margarine, convenience foods, coffee whiteners, and frozen desserts. Normally they are used along with a fat system and frequently in conjunction with other emulsifiers. Monoglycerides containing oleic acid are used as emulsifiers in ice cream. Those prepared from lard, tallow, cottonseed, soybean, and peanut oils (usually partially hydrogenated) have been used as emulsifiers in cake and icing shortenings. Fully hydrogenated MGs from meat fats and vegetable oils have been used as emulsifiers in yeast-raised baked goods, cake shortenings, ice cream, confections, and many other food products [81].

Compounds that contain esters of fatty acids and free hydroxyl groups are used as emulsifiers in bakery products. Of these compounds, MGs and DGs of saturated fatty acids, mostly those composed of stearic acid (MGS and MDGS), are the most used because their functions are ideally suited for shortenings. To enhance MGS activity as an emulsifier, other compounds and/or modified MGs are added. These compounds (to be discussed later) would include sorbitan and polyoxyethylene sorbitan esters of fatty acids; propylene glycol esterified with fatty acids; and lecithin or lactylated, acetylated, and succinylated monoglycerides [81]. Basically, MGS and MDGS and their modifications greatly improve bakery products by functioning as dough conditioners and strengtheners and as bread and crumb softeners. They also increase shelf life and tenderness, ensure good fat distribution, stabilize icing, and improve slicing, volume, aeration, and moisture retention. Of these functions, in baked products and other cereal-based products, the emulsifiers function primarily to improve the emulsification of fatty components in bread, to complex starch (amylose), to strengthen protein (gluten–gluten interaction), and to improve aeration (amount of air trapped in the batter) by reducing the surface tension of the aqueous phase. Emulsification is often the secondary function [81]. The complexation of the MGS is essential in improving bread shelf life. The starch present in the wheat granule will swell upon the addition of water and stirring, release part of its amylase (the wheat starch consists

Copyright 2002 by Marcel Dekker. All Rights Reserved.

of amylase and amylopectin), and eventually gel. After baking, cooling, and mainly after prolonged storage, the amylase will tend to recrystallize and lose some of the water (the recrystallization can also occur upon loss of water). The phenomenon is called starch retrogradation and leads to bread staling. The addition of MGS to the dough will cause kinetic slowdown of the retrogradation, because the complex will interfere with the recrystallization process. The excellent fit of MGS in the helical structure of the amylase makes this emulsifier the best choice as an antistaling agent. Other emulsifiers have lower complexing ability [the amylose complexing index (ACI) of GMP-glycerol monopalmitate is 100, whereas that of SSL-sodium stearoyl lactylate is 78, and that of lecithin of 28] and are less efficient.

The interaction of emulsifiers with proteins is a more complex phenomenon and will be better explained in Section III.L.1 dealing with other emulsifiers. For additional mechanistic considerations the reader is referred to the more specific literature dealing with protein surfactant interactions.

Whereas bakery products are among the most important uses for mono- and diglycerides, there are many other products in which they also play an important role [81]. These include imitation dairy products, frozen desserts, pasta dishes, cereals, snacks, processed potatoes, chewing gum, peanut butter, jellies, puddings, cheese spreads, syrups, candies, margarine, diet margarine, shortening, salad dressings, mayonnaise, sour cream, ice cream, whipping cream, caramel, butter cream, cake mix, and cream fillings.

The use of emulsifiers has improved the structural properties of ice cream. These emulsifiers, generally containing MG and DG, help to disperse fat globules throughout the ice cream mix and prevent them from clumping together and churning out as butter granules during the freeze-mixing operations. Emulsifiers further help to improve whipping properties to reach the desired overrun, i.e., the increase in volume caused by whipping air into the mix during the freezing process [81]. Also, in ice cream, the use of emulsifiers makes the product drier and stiffer when drawn from the freezer, which allows it to be packaged without melting. Other related products that profit from these emulsifier effects are sandwiches, factory-filled cones and individual servings, tarts, éclairs, and cake rolls [81].

E. Monoglyceride Derivatives

Although monoglycerides are used quite extensively as emulsifiers in food products, many compounds have been reacted with them to form new emulsifiers with different functions. These include ethylene oxide (Fig. 34a), succinic anhydride (Fig. 34b), tartaric acid (Fig. 34c), citric acid (Fig. 34d), lactic acid (Fig. 34e), and acetic acid (Fig. 34f) [5,81,88,91].

Copyright 2002 by Marcel Dekker. All Rights Reserved.

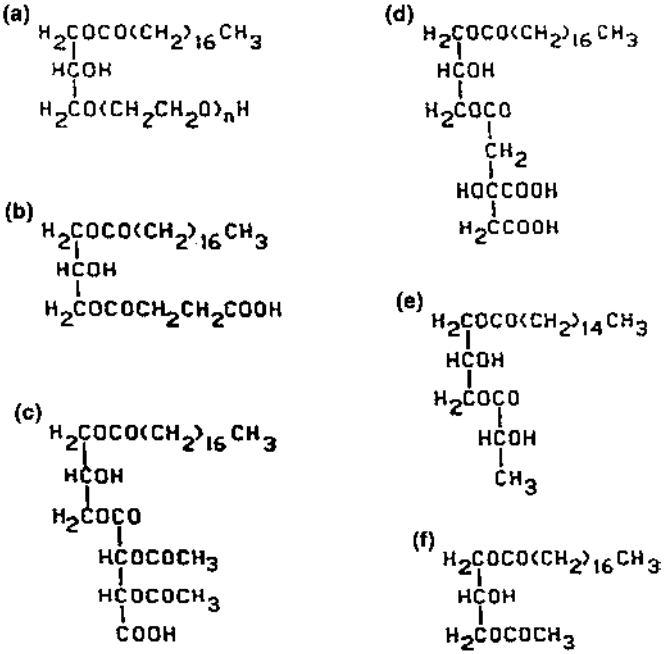

Figure 34 Monoglyceride derivatives. (a) Ethoxylated monostearate; (b) succinic acid ester of monostearate; (c) diacetyl tartaric acid of monostearate; (d) citric acid ester of monostearate; (e) lactic acid ester of monopalmitate; (f) acetic acid ester of monostearate.

1. Ethoxylated Monoglycerides

Ethoxylated monoglycerides (Fig. 34a) are made by treating MG with ethylene oxide. They are very hydrophilic compounds and are widely used as dough conditioners in breads. They are also used as emulsifiers in cakes and cake mixes, in whipped vegetable oil toppings and topping mixes, in icings and icing mixes, in frozen desserts, and in edible vegetable fat–water emulsions intended for use as substitutes for milk or cream in coffee.

2. Succinylated Monoglycerides

Succinylated monoglycerides, which are mixtures of acidic and neutral succinic acid esters of MG and DG. Fig. 34b shows some of these structures that are made by the succinylation of a product obtained by the glycerolysis of edible fats and oils or by the direct esterification of glycerol with an edible fat-forming fatty acid.

Copyright 2002 by Marcel Dekker. All Rights Reserved.

They are used as emulsifiers in liquid and plastic shortenings at a level not exceeding 3% by weight of the shortening and as dough conditioners in bread baking.

3. Diacetyl Tartaric Acid Ester of Monoglycerides

Diacetyl tartaric acid ester (DATAE) of MG (Fig. 34c) is more hydrophilic than MG itself and is therefore also an excellent emulsifier. Because of the added carboxylic group, it has the ability to bind gluten in wheat dough and thus improve the ability of the gluten to hold gas bubbles. In the mixing of the dough, after the addition of water, the proteins (gliadin and glutenin that compose the gluten) adsorb water and swell to form a viscoelastic structure capable of retaining gas. The stability and machinability of the dough depends on the number and volume of gas compartments formed by the proteins and the elasticity and strength of the network. Additional compartments will allow more gas retention and better bread volume.

The ability of an amphiphilic molecule to interact with protein is an important characteristic of a food emulsifier because it contributes to the volume of any baked product. The mechanism of such an interaction is not yet clear. Some investigators claim that the hydrophilic head, via its carboxylic groups, interacts with the free amino groups of the protein and serves as a cross-linker to another protein. Other investigators think that the emulsifier interacts with the hydrophobic sites of the protein via ''hydrophobic interaction.'' In any event, the emulsifier forms additional compartments in which the gas released from the yeast will be entrapped.

Diacetyl tartaric acid ester of monoglycerides was found to be one of the most effective emulsifiers as a volume improver and is widely used in baked goods to give additional volume.

The preparation of the DATAE is quite difficult and requires care and sophistication. The process includes the formation of acetic anhydride of tartaric acid in the presence of acetic anhydride and further esterification of the anhydride tartaric acetate with monoglycerides or monodiglycerides of fatty acids [5,88,91]. The product is a mixture of DATAE together with the raw materials and some side reaction products. Figure 35 illustrates the reaction and the products that are obtained. The complexity of the process and the sensitivity of the product to hydrolysis lead to the existence of many versions of the DATAE. Figure 36 shows the volume of rolls with varying dosages of DATAE (Panodan) in Danish flour and also the variation in fermentation time. The increase in volume with increasing emulsifier dosage is clearly seen.

4. Citric Acid Ester of Monoglycerides

Citric acid ester of MG (Fig. 34d), the amphiphile that is produced by reacting MG with citric acid, is used by the meat industry as an emulsifier in sausages.

Copyright 2002 by Marcel Dekker. All Rights Reserved.

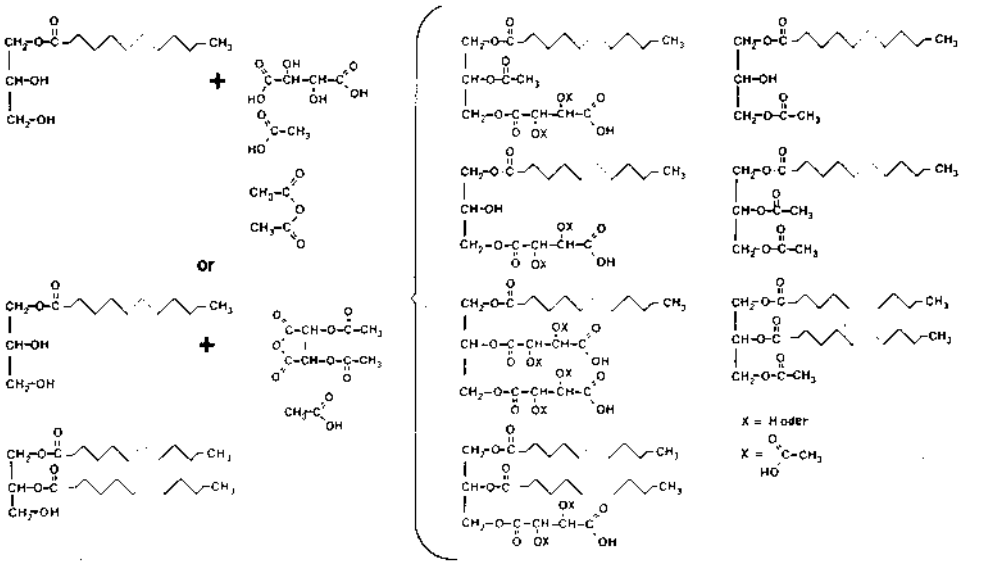

Figure 35 Preparation pathways of DATAE. (Top) From distilled monoglyceride and acetic anydride and tartaric acid and (bottom) from monoglycerides and monodiglycerides with diacetyltartaric acid and acetic acid. In both cases a complex mixture of products is obtained.

This compound is also used in margarine as an antispattering agent. Monoglyceride citrate has also been used as a synergist and solubilizer for antioxidants in oils and fats.

5. Monoglyceride Lactate

Several forms of lactylated esters are used as emulsifiers in foods. One form is the lactic acid derivative of monoglyceride (MGL) (Fig. 34e), and another is the sodium or calcium salt of lactic acid ester of fatty acids (CSL and SSL, discussed in Section III.G). The MGL can be used to improve aeration and foam stability in whipped toppings. It is also used in cake mix shortenings. Glycerol lactyl palmitate, formed from the reaction of an MG with lactic acid, is a common emulsifier for cake shortenings and cake mixes. It also serves as an agglomerating agent for toppings. Patents have been granted on methods for preparing mixed glycerol esters of fatty and lactic acid.

Copyright 2002 by Marcel Dekker. All Rights Reserved.

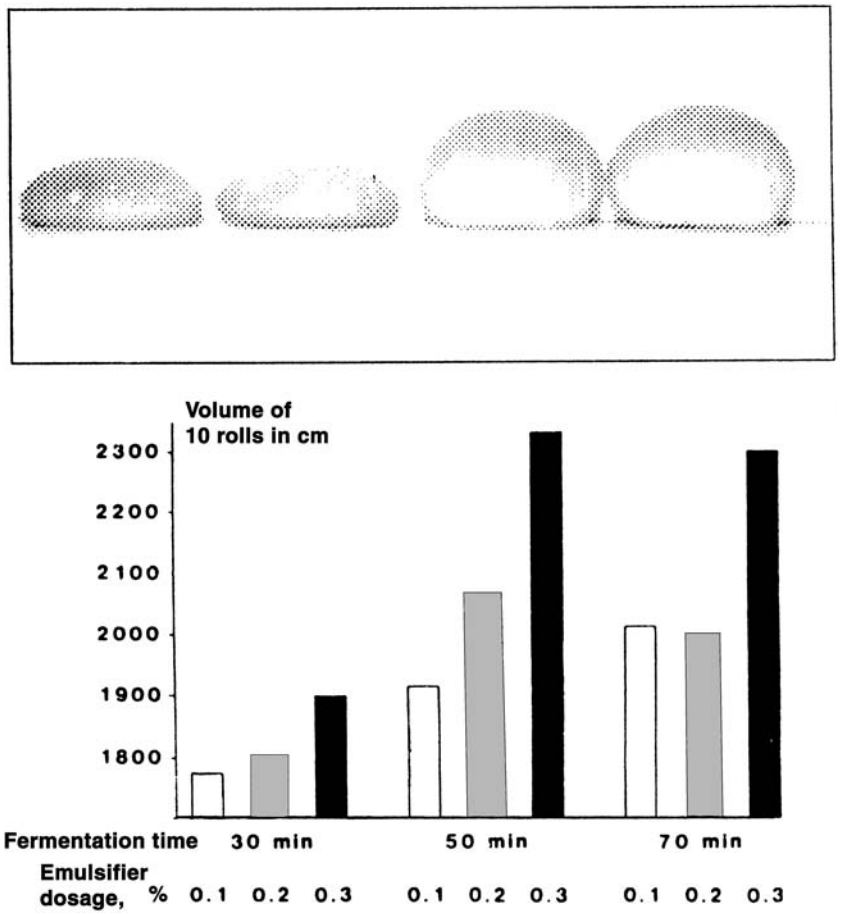

Figure 36 Volume of rolls as a function of emulsifier dosage and fermentation time with Panodan 10 (DATAE) in Danish flour.

6. Monoglyceride Acetate

Another derivative of MG that has been very useful as a food emulsifier is acetoglyceride (GMA), produced by re-esterification of MG or DG with triacetin or by acetylation of MG with acetic anhydride. The final result is a glycerol backbone containing either one or two acetic groups and one long-chain fatty acid (Fig. 34f). When fully hydrogenated these modified glycerides have the unique property of being (and remaining) highly flexible, nongreasy plastic solids at and below room temperature. They are bendable and can be stretched appreciably,

Copyright 2002 by Marcel Dekker. All Rights Reserved.

i.e., over 800%, before breaking. The flexibility of solidified acetostearin products is attributed to the shape and arrangement of their crystal formation. GMA can exist in several crystal forms or polymorphs but is unique in that the lower melting form is stable for all practical purposes. Another property of GMA is that pure products, such as 1,2-diaceto-3-stearin, prepared by reacting acetic anhydride with molecular distilled 1-monostearin, will form practically transparent films. Melting points and other properties can be tailored to a considerable extent by changing the composition of the long-chain fatty acid groups and the degree of acetylation. For food uses, GMAs may be classified according as (1) nongreasy, plastic fats of relatively sharp melting points for use in protective coating materials, (2) low melting fats having extraordinary resistance to rancidity, and (3) low melting oils that possess good resistance to rancidity and remain either liquid or plastic at temperatures far below freezing [81]. Over the past two decades, GMAs have found several uses in foods. Solid products are used as coatings for fruit, nuts, frozen baked goods, meat, and meat products, where thin films form oxygen and moisture barriers. Liquid GMAs are used as release agents in candy production and as food lubricants in nut, raisin, and other products. Spraying GMAs on the inside of ice cream sugar cones has been reported to extend their shelf life. GMAs have been used as coatings for meats, meat products, poultry, and seafood. GMAs belong to the group of alpha-tending emulsifiers, which are those that maintain their stability in the flexible α-crystal form. These types of compounds help improve agglomeration and thus the whipability and foam stabilization of various food emulsions, such as those found in whipped toppings and other dessert products. Other uses include plasticizers for chewing gum, release agents, and defoamers [81].

F. Propylene Glycol Esters

In general, propylene glycol mono- and diesters are prepared by direct esterification of propylene glycol with fatty acids. Their lipophilic quality makes them W/O emulsifiers. For example, propylene glycol monostearate (PGMS) is a strongly lipophilic emulsifier with a low hydrophilic–lipophilic balance. Compounds of this class are prepared by the esterification of propylene glycol with fatty acid and have properties similar to those of glyceryl-lactoylpalmitate and acetoglycerides. The commercial esters of propylene glycol have been confined primarily to those derived from the higher fatty acids, although pure esters of many fatty acids have been prepared. For example, the monoesters include fatty acids of laurate, palmitate, stearate, oleate, and ricinoleate, whereas the diesters include laurate, myristate, palmitate, and stearate [81]. Propylene glycol fatty acid esters are listed among emulsifiers that may be added to fats at the manufacturer's level and have been approved by the FDA for use in foods [81]. PGMS and propylene glycol monopalmitate are most often used in cakes, cake mixes,

Copyright 2002 by Marcel Dekker. All Rights Reserved.

whipped toppings, and bread. They are also used in combination with distilled monoglycerides to obtain excellent cake batter behavior resulting in increased cake volume and uniform structure and in whipped toppings (due to their aerating and foam-stabilizing properties).

G. Stearoyl Lactylates

Stearoyl lactylates (SLs) are made by the reaction of lactic acid, fatty acids, and a suitable sodium or calcium source at elevated temperatures and under controlled conditions (vacuum and nitrogen). The product is known as SSL and CSL, respectively. Figure 37 illustrates the process reaction pathway and the internal product composition of all components of the reaction mixture.

Sodium and calcium stearoyl lactylates are widely used as dough stabilizers and conditioners in yeast-raised baked products. These products combine two sets of properties: the ability to complex amylose and improve bread shelf life and the ability to strongly interact with gluten to improve dough stability and bread volume [81].

Calcium stearoyl-2-lactylate (CSL) alters the structure of wheat gluten as explained by Thompson, and further studies have indicated that the CSL cannot be removed by solvent extraction once the bread has been baked. In the complex formed by the emulsifier with the wheat gluten, as in yeast-raised doughs, a strong protein network is formed that allows the carbon dioxide produced during pro-

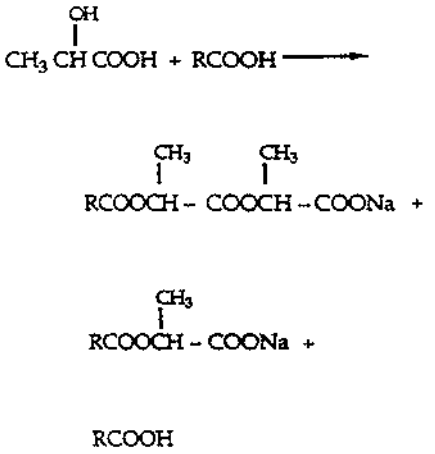

Figure 37 The reaction pathway and the product composition of SSL. R = stearic or palmitic.

Copyright 2002 by Marcel Dekker. All Rights Reserved.

cessing to be retained. This reaction results in better texture and greater volume of the baked products.

In addition to complexing with protein, CSL has also been shown to inhibit the transition temperature of dilute starch–water mixtures in the amylograph (instrument measuring activity of amylase in baked goods) and to sharply increase the maximum paste viscosity [81]. The effect of starch gelatinization is associated with the observed reduction in the rate of firming in bread containing CSL. In general, stearoyl lactylates form complexes with both protein and starch. Their ability to complex with starch allows for effective antistaling agents in bread, whereas their interaction with protein (gluten) results in a finer crumb structure, increased volume, and a better crust for the finished loaf. Furthermore, sodium stearoyl lactylates can be used, under certain conditions, in imitation sour cream to improve its heat stability and resistance to melting [81].

H. Sorbitan Esters and Ethoxylated Sorbitan Esters

Sorbitol is a sugar alcohol belonging to the group of hexahydric alcohols made by hydrogenation of glucose. When esterified, water is split off and the hydroxylated tetrahydrofuran 1,4-anhydrosorbitan is formed as the main product. The free hydroxy groups can react with fatty acids to form sorbitan esters (Fig. 38) [92]. Another product of the esterification is 1,5-anhydrohydroxypentahydropyran, which can dehydrate further to isosorbide. The synthesis of sorbitan esters was discussed by Markley [93], who described the interesterification of triglycerides and sorbitol at several temperatures, with different catalysts, and under varied conditions. He also reported on a series of fatty acid esters of sorbitan (mixed monoesters) that included lauric, palmitic, stearic, and oleic acids. These compounds are sold under the trade name SPAN.

By modifying sorbitan's pattern of esterification to different degrees with ethers of ethylene oxide, products marketed under the trade name Tween are made (Fig. 39). As is the case of most compounds of this type, their industrial use depends on the nature of the fatty acid with which the alcohols are esterified, the degree of esterification, and the formation of polyoxyalkylene derivatives [93]. When such products are ethoxylated (with 20 mol of ethylene oxide), a hydrophilic range of sorbitan esters called polysorbates is produced. Owing to these factors, sorbitan esters can exhibit a wide range of HLB values, from 1.8 to 16.7, and can be used as W/O or O/W emulsions for numerous applications [92]. Many of the polysorbates have been used in feeding studies in animals. It was concluded that the polysorbates are no more toxic than many other foodstuffs.

Sorbitan monostearate is most often used in combination with the polysorbates in cakes, cake mixes, whipped toppings, cake icings, fillings, confectionery coatings, and coffee whiteners. Polyoxyethylene (20 EO) sorbitan monostearate 60 (Polysorbate 60) can be combined with lipophilic emulsifiers such as sorbitan

Copyright 2002 by Marcel Dekker. All Rights Reserved.

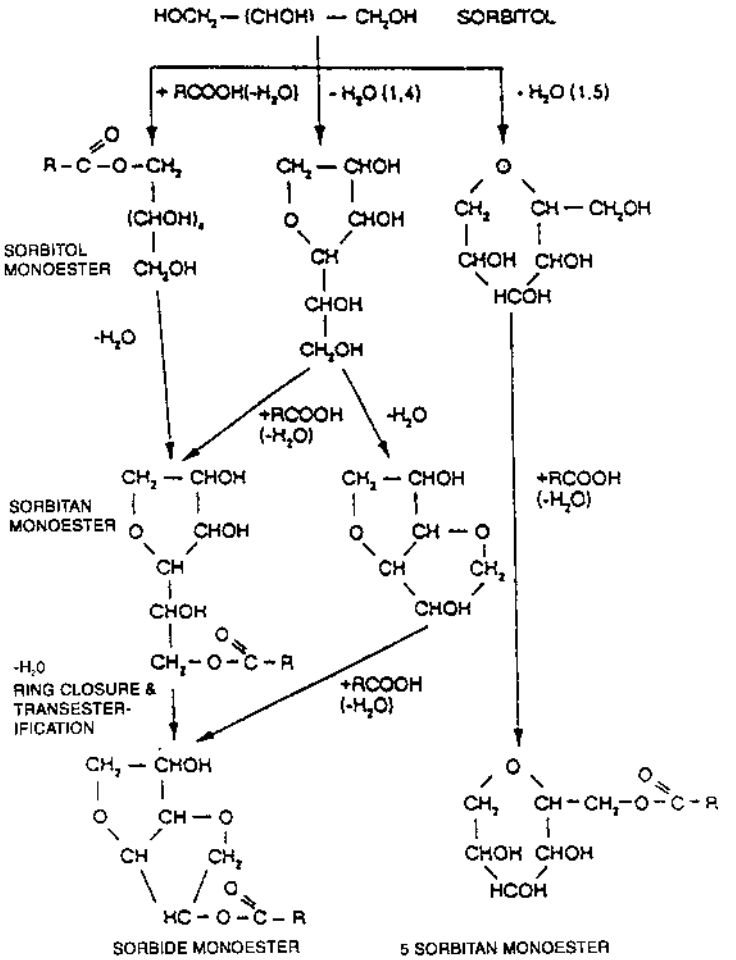

Figure 38 Schematic of chemical structure and preparation pathways of sorbitan esters.

monostearate and glycerol monostearate to give cakes greater volume and finer, more uniform grain, adding tenderness without fragility. In icings, these combined emulsifiers increase lightness by improved emulsification of the fat and the hydrocolloidal phase to prevent oiling-off or sticking to the wrapper. Polysorbate 60 is also used in prepared dry mixes, whipped toppings, bread and other yeast-raised products, and coffee whiteners. Polyoxyethylene (EO 20) sorbitan monooleate (Polysorbate 80) is used in ice cream and frozen desserts for resis-

Copyright 2002 by Marcel Dekker. All Rights Reserved.

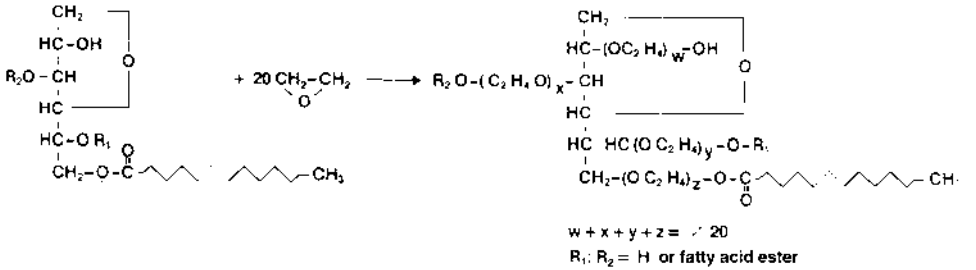

Figure 39 Schematic of chemical structure and preparation pathway of ethoxylated sorbitan esters.

tance to heat shock and to improve texture and palatability. It is also used in nonstandardized baked goods, prepared mixes, fillings, icings, toppings, and very often as a solubilizing agent for flavors. Polysorbate 65 (polyoxyethylene sorbitan tristearate) is also used in frozen desserts, whipped toppings, cakes, cake mixes, and coffee whiteners [81].

Cocoa butter is a yellow fat that shows brittleness below 20°C, begins softening at 30°C, and exhibits a sharp complete melting below body temperature. The liquid/solid ratio at different temperatures characterizes its fundamental thermal behavior. Cocoa butter is a complex mixture of several fats and oils such as POP (15%) SOS (29%), POS (40%), and others such as PPS, PSS, SOA, SOA, and SOO [94,95]. As a result of the complex composition of the fat in cocoa, the product tends to crystallize in stages characterized by a solid fat index (SFI) curve, which quantifies the percentage of the solid phase content as a function of the cocoa butter temperature. The effect of sorbitan esters and sugar esters on the blooming of chocolate was described in Section III.E.1. The organoleptics in the chocolate depend very much on the nature of the polymorphs present in the product at a given temperature and under particular storage conditions. Many efforts have been made to clarify the phase behavior of these fats and the factors affecting the polymorphic transformations in relation to the quality of the chocolate. The polymorphic transformation leads to ''instability'' in the sugar–cocoa solid matrix, resulting occasionally in migration of one of the cocoa fat polymorphs from the interior, along the cocoa fiber to the chocolate's surface. This phenomenon is known as chocolate bloom.

Sorbitan esters of fatty acids are effective antibloom agents (fat crystal modifiers) in confectionery products containing cocoa butter and cocoa butter substitute. In chocolate, the undesirable bloom is inhibited by the use of sorbitan esters of fatty acids. Chocolate has a dull gray-white appearance when it has

Copyright 2002 by Marcel Dekker. All Rights Reserved.

bloomed, but when the blooming is inhibited the chocolate is bright and shiny with a rich appearance. It is thought that these sorbitan esters modify fat crystals by retarding or inhibiting the reversion of crystalline fat to a more stable form.

I. Polyglycerol Esters

The synthesis of polyglycerols and their fatty acid esters was the subject of a very comprehensive review by Babayan and McIntyre [96,97], who stated that polyglycerols are generally prepared by the polymerization of glycerol under alkaline conditions at elevated temperatures (about 230°C). The esters are also made by direct esterification of the polyol with the free fatty acid at elevated temperatures. The esters can also be made by the interesterification of a triglyceride with a polyol in the presence of an alkaline catalyst (Fig. 40). The polyglycerols contained from 2 to 30 glycerol moieties. In Babayan and McIntyre's proposed mechanism [97] for the formation of polyglycerols, an ether linkage for every three carbon atoms is repeated as the polymer chain lengthens. During the metabolic processes in humans and animals, the ether linkage was found to be subject to cleavage, thus ensuring the utilization of polyglycerol ester products such as glycerol and fatty acids. From these experiments a series of polyglycerol esters (PGEs) were found that are very effective food emulsifiers.

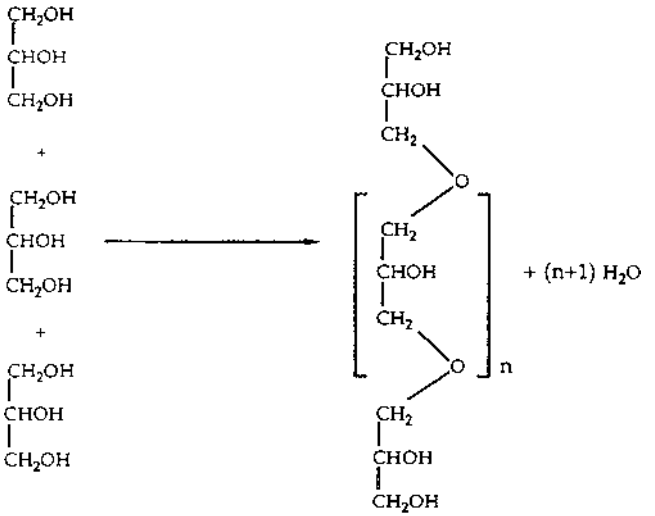

Figure 40 Schematic of chemical structure and preparation pathway of polyglycerol esters.

Copyright 2002 by Marcel Dekker. All Rights Reserved.

In general, the PGEs used in food applications are made by the polymerization of glycerol to form a molecule containing from two to 10 glycerol moieties. The polyol, or polymerized glycerol, is then esterified with selected fatty acids. To obtain the desired physical characteristics and functional properties, the polymerization and esterification reactions are carefully controlled. The final product can provide a broad range of HLB values.

Polyglycerol esters are multifunctional, a property that allows them to be used as fat substitutes as well as emulsifiers. For example, they are used as surface-active agents in whipped toppings and frozen desserts, as antibloom agents in confectioneries, as antispattering agents in cooking oils, as flavor dispersants and stabilizers in beverages, as texture enhancers in prepared cake mixes, and as binders of ingredients and lubricants in extruded snacks. When used in liquid salad dressings, PGEs can prevent the separation of oil and water, make products creamy, and aid in color and flavor dispersion. They also aid in getting oil-based flavors into solution in oil-based flavor mixes and often allow mixing of incompatible ingredients in hard-to-emulsify mixes. Polyglycerol (mainly di-, tri-, and tetraglycerol) esters of fatty acids are used in aerated foods containing fat, such as cakes and sponges. PGEs impart excellent properties to cake batter to increase the cake volume and uniform structure when used in cake margarine in combinations with distilled MGs. Triglycerol monostearate (4G1S) can be used as a whipping agent and as an aerator in nonaqueous lipid systems. In this capacity it reduces costs by eliminating the need for egg whites and vegetable protein as foaming agents and eliminates an extra processing step. It further aids in shelf stability, because no water is required for functionality. By aerating readily in either batch or continuous automatic whipping equipment, 4G1S sets rapidly after whipping, which allows product extrusion through dies of various shapes. This product is available in kosher quality and resists microbial growth. A modification of 4G1S was designed for use as an emulsifier in icing and cake shortenings to produce high quality filler-type butter cream and flat icings. This product provides smooth texture, good body, and greater moisture retention [98].

Octaglycerol monooleate (8G1O) and octaglycerol monostearate (8G1S) are also commercially available as emulsifiers. 8G1O is used as a viscosity reducer in high protein systems, as an emulsion stabilizer, and as a beverage-clouding agent. It is also used in imitation cheese products to retard oiling-off or the separation of fat and casein and to improve the meltdown characteristics of the finished cheese with a dramatic reduction in the viscosity of the product. In ice cream toppings, 8G1O can be used to provide emulsion stability and improve gloss. 8G1O can also be used to reduce the cholesterol content in casein, which would make the product useful as an ingredient in imitation meats, cheeses, and other dairy products. In food analogs such as imitation bacon, 8G1O can be used to prevent the vegetable oils from separating during storage and to improve the product texture. 8G1S is used as a whipping agent, an emulsion, and a freeze-

Copyright 2002 by Marcel Dekker. All Rights Reserved.

thaw stabilizer. In pet foods, 8G1S can be used to produce a glossy, moist appearance, which makes the product more appealing. Both products, 8G1O and 8G1S, can be used as polysorbate replacers and to disperse flavors and colors into aqueous systems. Both of them are also relatively free of any flavor character note.

These compounds range in appearance from a soft white solid (triglycerol monopalmitate) to hard white beads (hexaglycerol dipalmitate and hexaglyceryl distearate) to a pale yellow liquid (decaglycerol dioleate). When these compounds were tested as emulsifiers in dessert toppings, results showed markedly superior organoleptic qualities, improved color characteristics, and enhanced emulsifying characteristics. Furthermore, the hexaglycerol distearate outperformed all other emulsifiers tested (including sorbitan monostearate and Polysorbate 60) [98,99].

J. Sucrose Esters

Sucrose esters (SEs) (Fig. 41), particularly the mono- and diesters, are potentially very valuable as emulsifiers and as such offer a number of unique advantages. They are nontoxic, odorless, tasteless, nonirritating to the skin, and easily digested. They are biodegradable under both aerobic and anaerobic conditions, and, unlike most other nonionic surfactants, they are normally solids and may be used as powdered or spray-dried products.

Sucrose esters have a structure found in many of the typical emulsifiers, i.e., both polar and nonpolar groups in the same molecule. Because there are eight possible positions that can be esterified with fatty acids, the final product can offer a wide range of HLB values, from one extreme (lipophilic HLB value of 1) to the other (hydrophilic HLB value of 20) [100].

The SEs were first synthesized in 1956 by Osipow and coworkers [101] by the transesterification reaction between sucrose and a methyl ester of a fatty acid in the presence of a basic catalyst and dimethyl formamide (Fig. 41). However, because of the toxicity of DMF and other similar solvents, and because of the difficulty in removing DMF, from the reaction product, other methods were investigated. One of these methods, a microemulsion process, used sucrose, the methyl ester of a fatty acid, propylene glycol, sodium soap, and a potassium carbonate catalyst, all entailing time-consuming and costly steps [102,103].

The first solvent-free interesterification process for the production of SE for food use was developed in 1969 and patented in 1972 [103]. The initial article was followed by a series of other reports that described further developments of the method [102]. SE was prepared by the solvent-free interesterification of molten sucrose and fatty acid esters at temperatures of 170–180°C. The type of fatty acid ester employed markedly affected the yield of sucrose esters, which varies according to the conditions. Also, by varying the ratio of sucrose to methyl ester and type of fatty acid, a wide range of products can be obtained. This method led to the issuance of a patent in 1973 and was commercialized in Japan.

Copyright 2002 by Marcel Dekker. All Rights Reserved.

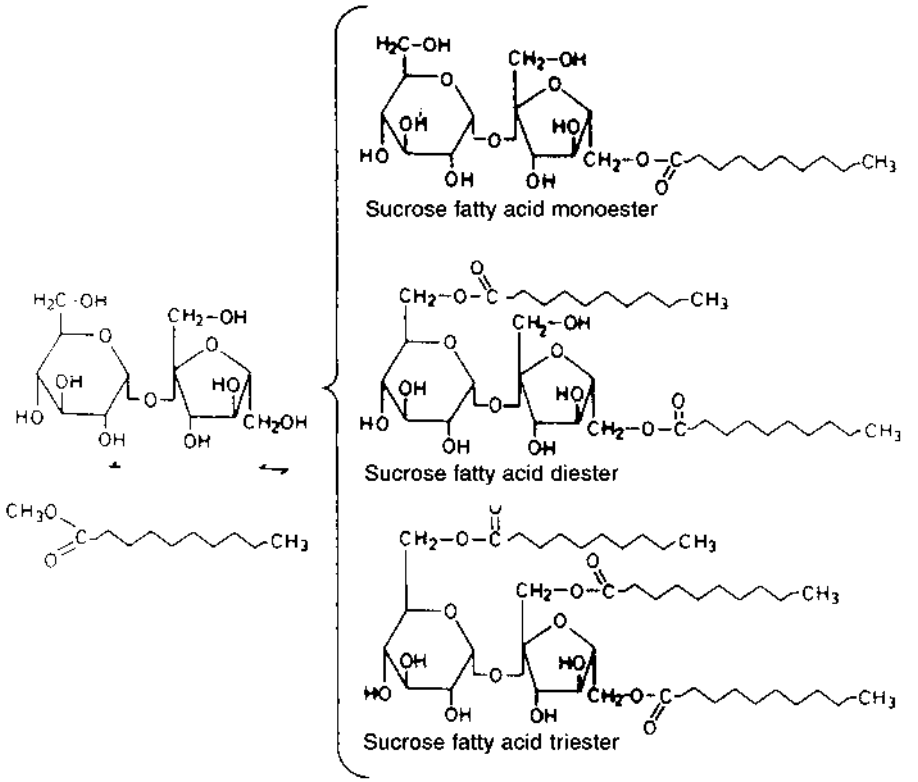

Figure 41 Synthesis of sucrose esters by transesterification of fatty acid methyl esters and sucrose.

Sucrose polyesters were also synthesized with a high degree of substitution (six to eight groups per mole) by a two-stage reaction in the presence of a catalyst generated by the addition of alkali metal hydride or Na-K alloy. In the first stage of preparation, a mixture of 3 mol of methyl esters of fatty acids and 1 mol of sucrose reacted in the presence of a potassium soap to form a one-phase melt containing lower esters of sucrose. In the second stage, more methyl esters were added to prepare the highly substituted sucrose esters in a yield that exceeded 90%. This was a solvent-free reaction system also. Unlike the method of Feuge et al. [104], this one was accomplished without the use of large amounts of soap and at somewhat lower temperatures.

In another method, the sucrose ester is prepared by reacting solid, particulate sucrose with at least one triglyceride in the presence of a basic transesterifica-

Copyright 2002 by Marcel Dekker. All Rights Reserved.

tion catalyst (potassium carbonate) in a temperature range of 110–140°C, at atmospheric pressure, and in the absence of any solvent. This process uses a heterogeneous reaction mixture wherein the sucrose is suspended in the triglyceride. The reaction product, comprising a mixture of compounds, can be used directly as a biodegradable, nontoxic surfactant without any purification, although if desired the sucrose esters in the product can be separated and purified by conventional techniques.

There are many methods for producing sucrose esters other than those presented in this chapter. The ones described herein represent some of the earlier methods developed. For additional information about this subject, other reviews and articles are recommended [e.g., 102].

Sucrose esters have manifold applications in food, including (1) cakes, cookies, and breads; (2) as emulsified oils and fats in coffee whiteners, whipped cream, recombined milk, shortening oil, ice cream, and low calorie margarine; (3) instant foods such as curry, soybean curd (tofu), cocoa, and cake mixes; (4) confectionery use in biscuits, chocolate, chewing gum, rice cakes, and tablet candy; and (5) starch retrogradation. One of the newest uses is as a low calorie, cholesterol-free fat substitute. Additionally, these sucrose polyesters are reported to have a fat content of zero calories and to lower cholesterol levels. If so, then these products may be used as a home-cooking oil as well as for making salted snacks, potato chips, etc. They could be used as cooking oils in restaurants and in the fast food industry as deep frying oils. They may be used in other items such as ice cream, margarine, mayonnaise, salad dressings, desserts, and in meats. One of their major advantages is their ability to pass through the body without being absorbed. Furthermore, they are also reported to eliminate some cholesterol already in the body. The manufacturer of these products is presently seeking FDA approval.

The ultimate application of sucrose polyesters as a food emulsifier will depend on the HLB value, which is determined by the specific fatty acid used and its quantity. For example, one such product made from stearic acid used as an emulsifier in shortening or margarine could have an HLB value of 2–3, whereas another product made from a different proportion of stearic acid and used as an emulsifier in ice cream or in other dairy products could have an HLB value of 11.

In bakery foods, SE is used in many ways. The addition of wheat glycolipids and SE to wheat flour allowed fortification of soy flour by up to 16% without loss in the bread's physical properties. These would include an increase in water absorption and maximum hot-paste viscosity and volume, crumb grain, and bread softness. In addition, sugar esters have the ability to spare shortening and strengthen dough, i.e., improve gas retention with faster proofing. It has been concluded that sucrose monoesters are very good dough strengtheners. The monomyristate, monostearate, and monooleate esters were almost as effective as the

Copyright 2002 by Marcel Dekker. All Rights Reserved.

monolaurate ester, but the monocaprylate ester was somewhat less effective. The crumb-softening ability of sucrose monostearate was significant but not as effective as that of sodium stearoyl-2-lactylate, one of the most widely used commercial bread softeners. The crumb-softening effect of sucrose monoesters is diminished as the fatty acid chain length decreases from C_{18} to C_8. Tsen et al. [105] reported that 25% of the shortening in cookies could be replaced with less than 1% sucrose esters, resulting in a lower caloric intake value. In 1974, Tsen [106] reported on the fortification of wheat flour with soy flour to which several fatty acid derivatives, including sucrose esters, fatty esters of polyalkoxylated polyolglycosides, sodium or calcium stearoyl-2-lactylate, and ethoxylated monoglycerides and glycolipids were added. Generally, adding soy flour to wheat flour can produce adverse effects such as (1) altered absorption, mixing, and machining properties; (2) changed fermentation rates; (3) poor crumb grain and color; (4) reduced loaf volume; and (5) a beany flavor. However, the addition of the surfactants tested was found to eliminate many of these negative effects caused by fortification with soy flour. Ebeler and Walker [107] reported that SE improved the volume and tenderness of white layer cakes. Also, SE was able to produce a more desirable texture. By hydrating SE prior to addition, the resulting cake volume (ca. 3400 cm^3) was on average 20–160 cm^3 greater than when SE were added in powder form. Sugar esters with HLB values of 11 and 15 (the more polar compounds) were the most effective.

K. Polyglycerol Polyricinoleate

Polyglycerol polyricinoleate (PGPR) is one of the most hydrophobic emulsifiers in use in foods. It gained much attention recently, because it was approved for use in certain confectionery applications, mainly in chocolate-based coatings. Up to 2.64 mg/kg body weight per day is permitted in the United Kingdom. The product is based on a three-step reaction [108]. In the first step, glycerol is polymerized at elevated temperatures (~250°C) to form polyclycerol (tri-, tetra-, and pentaglycerol ethers). In the second step polycondensed ricinoleic acid is formed from ricinoleic acid. An esterification between the polyricinoleic acid and polyglycerol is thereafter carried out at lower temperatures to form oligomeric polyglycerol polyricinoleate (Fig. 42).

Several manufactures have mastered the process and adjusted the internal composition to its performance in chocolate as rheology controller. The internal product composition and structure are proprietary information. PGPR has exceptionally good water-binding properties, which is of major importance for its effect in chocolate.

It is important to note that PGPR has long been known to reduce the ''yield value'' of chocolate mass whereas its effect on total viscosity is limited (Fig. 43) [108]. Up to 0.3 wt% lecithins is necessary (as demonstrated from viscosity

Copyright 2002 by Marcel Dekker. All Rights Reserved.

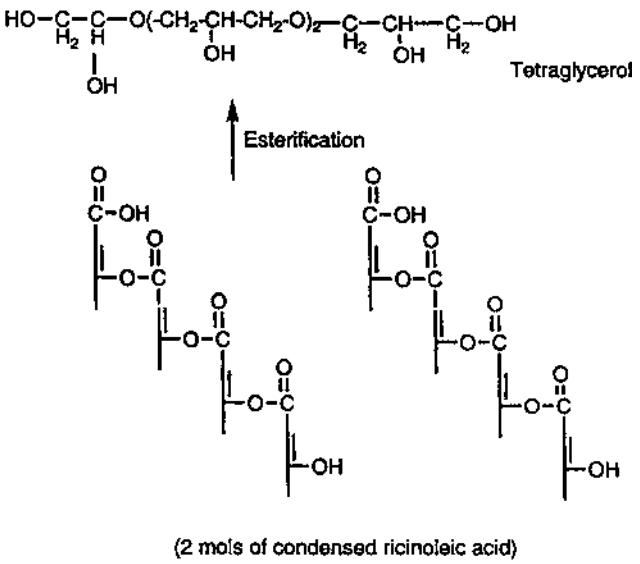

Figure 42 The principal structural formula of polyglycerol polyricinoleate (PGPR).

measurements) to obtain full coverage of the solid particles. Further increase of lecithin levels up to 0.5 wt% of chocolate mass does not add significantly to the viscosity reduction.

Figure 44 shows the flow curve for various levels of a typical combination of emulsifiers in milk chocolate [108]. The synergy between PGPR and lecithin or ammonium phosphatide is clearly shown. There is no difference in the yield obtained whether lecithin or ammonium phosphatide is used. The slope of the curve, however, shows that ammonium phosphatide is somewhat superior with respect to the reduction of viscosity. A dose of 0.3% PGPR lowers the ''yield value'' from 26 Pa to 2 Pa. An addition of 0.9% lecithin lowers the yield only to 24 Pa.

No structural or other physical evidence exists to support this claim. By increasing the addition of PGPR, low viscosity is achieved at low shear rates. Its synergistic effects with lecithins and ammonium phosphatide are known and documented. However, its mechanism of action is not yet well studied. The manufacturers claim that all three emulsifiers form a monolayer around the nonfat particles, especially around the sugar particles. The sugar particles will therefore be covered by an outer lipophilic layer that will bind to the oil (or fat). These

Copyright 2002 by Marcel Dekker. All Rights Reserved.

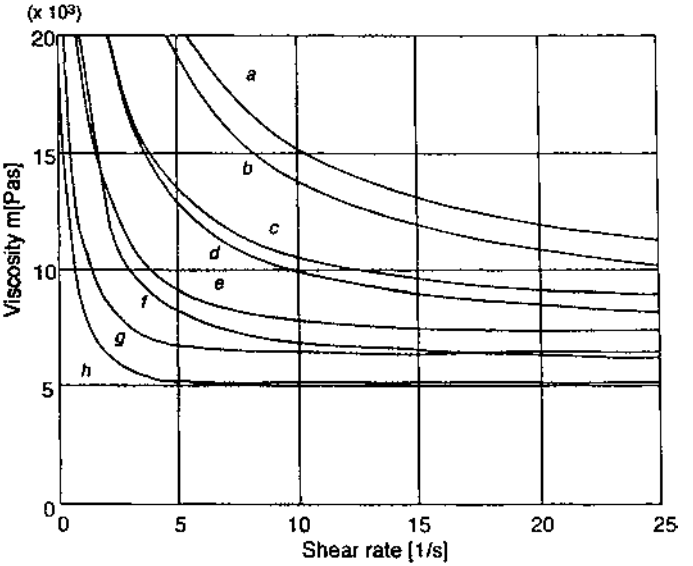

Figure 43 The viscosity reduction effect of PGPR (P-4125) when lecithin or ammonium phosphatide YN is present at 0.3%. (a) 0.3% lecithin; (b) 0.3% YN; (c) 0.3% lecithin + 0.1% P-4125; (d) 0.3% YN + 0.1% P-4125; (e) 0.3% lecithin + 0.2% P-4125; (f) 0.3% YN + 0.2% P-4125; (g) 0.3% lecithin + 0.3% P-4125; (h) 0.3% YN + 0.3% P-4125. The first two curves showing (a) addition of 0.3% lecithin and (b) addition of 0.3% ammonium phosphatide are shown only as reference. (From Ref. 108.)

surfaces will slide easily against each other compared to the surfaces of wet sugar particles, which will tend to stick to each other. This is a sort of greasing effect that will lower both the plastic viscosity and the yield value. The better ability of PGPR to bind water in comparison to lecithin is explained in terms of its molecular size and sites of binding. In spite of the fact that lecithin and PGPR are believed to bind primarily or even solely onto sugar particles, it was recently demonstrated that lecithin, monoglycerides, and other amphiphiles also adsorb on fat particles [109,110]. The competitive adsorption of the emulsifiers on fat and sugars might play an important role in controlling the rheology as well as the polymorphism of the fats. PGPR has not been extensively studied, and its adsorption isotherms on fat crystals is not known. The role that PGPR plays in bulk crystallization is also unknown. However, the attractiveness of PGPR to chocolate producers, ice cream makers, and food technologists is increasing.

Copyright 2002 by Marcel Dekker. All Rights Reserved.

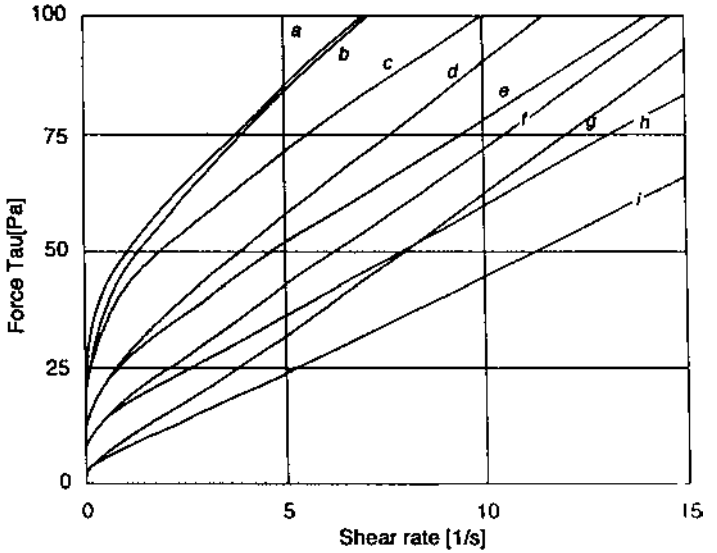

Figure 44 The flow curves for levels of a typical combination of emulsifiers in a milk chocolate. (a) 0.4% lecithin (yield value, 26); (b) 0.4% YN (22); (c) 0.9% lecithin (24); (d) 0.4% lecithin + 0.1% P-4125 (13); (e) 0.4% YN + 0.1% P-4125 (13); (f) 0.4% lecithin + 0.2% P-4125 (8); (g) 0.4% lecithin + 0.3% P-4125 (2); (h) 0.4% YN + 0.2% P-4125 (8); (i) 0.4% YN + 0.3% P-4125 (2). (From Ref. 108.)

More fundamental work is needed to better explain the reactivity of PGPR in the crystallization process and in the formation of emulsions based on fats and cocoa butter.

L. Amphiphilic Naturally Occurring Macromolecules and Biosurfactants

Special attention must be given to proteins and other biosurfactants as food emulsifiers. This is an important area of investigation that has gained the interest of many researchers in view of the tremendous potential natural biopolymers and biosurfactants might have in the food industry. Native proteins and macromolecules modified chemically or enzymatically in situ can replace synthetic emulsifiers in sophisticated applications.

1. Native Proteins

Proteins are natural polymeric surfactants. The importance of proteins in relation to food colloids and emulsions is so critical that thousands of studies have been

Copyright 2002 by Marcel Dekker. All Rights Reserved.

devoted to elucidate their action at various food interfaces [111–120]. Many proteins, such as caseins, whey proteins (lactoglobulins, lysozymes, ovalbumins), bovine and human serum albumins, and gelatins, have been known for many decades as emulsifiers, and an enormous amount of research work has been carried out to clarify the microstructures of emulsions such as milk, ice cream, and other dairy products [111–119]. In recent years studies have brought forth new microscopic techniques that enabled a direct look into the microstructure of some of these complex emulsions. Many of the key questions have been answered by cryo-TEM photomicrographs.

Many papers and review articles have been written on amphiphilic proteins, and many studies concerning their activity at oil/water interfaces have been published [111–119]. Proteins can adsorb on a fluid interface in several modes such as flexible, random coil, globular, and highly structured. In all the modes of adsorption the protein has numerous anchoring points (Fig. 45). Much progress has been made in understanding the concepts of steric stabilization and the physicochemical factors that affect emulsion structure and stability in the presence of food proteins. Emulsions are inherently unstable. The use of macromolecules, for example, can inhibit creaming but enhance flocculation. The droplets in a stable emulsion are prevented from flocculating by either electrostatic or steric stabilization. For monomeric emulsifiers the considerations are simple, but protein-stabilized emulsions can provide both types of stabilization, although full coverage of the interface is required. If the surface is poorly covered, bridging flocculation can occur. Coalescence is an irreversible process and occurs when significant interfacial thinning takes place.

Measurements of the static and dynamic properties of adsorption, amount of adsorbed protein G, surface pressure π, surface viscosity μ, and surface visco-

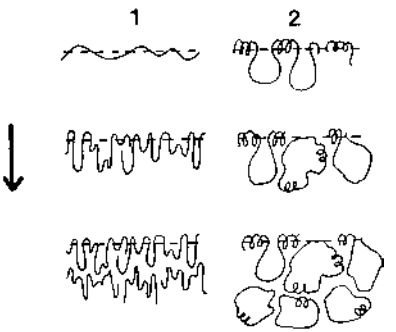

Figure 45 Schematic representation of protein structure at a fluid interface. 1 = flexible, random-coil proteins; 2 = globular, highly structured proteins. The arrow denotes increasing protein concentration.

Copyright 2002 by Marcel Dekker. All Rights Reserved.

elasticity E were carried out. Adsorption (both static and dynamic), desorption, and film properties have been proposed. Theories of liquid film drainage, droplet deformation, the critical thickness for rupture, and the viscoelastic properties of emulsions stabilized by proteins were reviewed and adapted to the specific characteristics of thick films formed on the oil interfaces. In addition, many kinetic questions of adsorption, surface pressure, and surface rheology with time have been considered.

Halling [120] claimed that proteins form a highly viscoelastic film on surfaces that will oppose the surface deformation (either in shear or dilution) that is required for the later stages of drainage and for rupture of the lamellae. This theory has faced many difficulties owing to the fact that the rheological interfacial properties also depend on other factors such as bulk protein concentration, pH, and film age, and therefore this criterion cannot be the only one to explain the role of proteins at the interface. Proteins also have a very significant effect on interdroplet forces, and while adsorbing at the oil/water interface (likely mainly on the aqueous phase side) they will affect the van der Waals forces via steric interactions between the adsorbed layers of proteins. Double-layer repulsive forces can also be expected to exist, provided that the radius of gyration of the adsorbed polymer is much less than the Debye length. As the molecular weight of the protein increases, the contribution of the steric stabilization effect (rather than that of the electrostatic forces) will dominate the repulsive forces.

The best steric stabilization will occur when the polymer covers the interface fully (sparse covering can cause build-up of attractive forces) and forms a thick unruptured film. A good solvent will dissolve the dangling chains of the polymer thoroughly. (A good solvent causes the polymer chains to stay apart in solution.)

Other important aspects are the liquid drainage between approaching emulsion droplets, droplet deformation, transport of molecules in the bulk, rate of macromolecular adsorption, competition between surfactants, and possible chemical reactions.

Many food systems are composed of a combination of monomeric and macromolecular emulsifiers. Efforts have been made to evaluate the contribution of each emulsifier at the interface. Many researchers have discussed interfacial compositions and competitive adsorption. Several key questions have been raised: What is the interfacial composition in the freshly made emulsions? How does it change with time? How does it change when the new surfactant becomes available to the system? The general answer seems to be that the more surface-active molecule will displace the less active one from the interface.

Many semiempirical studies of the emulsifying and foaming behavior of food grade proteins have been reported [121–125]. Such semiempirical information is essential for technologists but gives little insight into the key physicochemical factors involved. Many proteins have been reported to stabilize emulsions,

Copyright 2002 by Marcel Dekker. All Rights Reserved.

including lysozyme, bovine serum albumin, myosin, soy protein, α-lactoglobulin, and gelatin. Each of these proteins might have some advantages in the key factors affecting stabilization such as adsorption (kinetics of diffusion, induction period, extent of surface tension lowering, number of adsorbing sites, thickness of the film, extent of coverage, etc.), desorption (reversibility of adsorption, competitive adsorption, conditions for interfacial replacement), and film properties (thickness of adsorbed protein film, denaturation on the surface, coagulation formation of mixed film with other proteins or with low molecular weight surfactants, surface rheology).

A basic knowledge of the physicochemical properties of food proteins and an understanding of the many factors that affect food quality are required to fabricate widely accepted food products. Although soy proteins have largely been considered as economical substitutes for more expensive protein ingredients, they should be viewed as vital functional components that will enable the food technologist to fabricate new foods.

The trend toward quick-service convenience foods requiring fabrication, dehydration, rehydration, etc., brought the versatility of textured proteins to the forefront in the mid and late 1960s. Likewise, the economic performance of soy protein in chopped emulsified meats, egg white replacement in cakes, and the substitution of nonfat dry milk in baked goods all point to a lower cost per unit of performance, while at the same time maintaining the required level of consumer acceptance.

In the domestic market, all soy protein products are gaining in acceptance as useful and economical ingredients in the manufacture of conventional foods and in the design of new foods. More food package labels are listing soy protein products in their ingredient listings. We can expect this trend to continue with increasing food development efforts.

In the following, some examples of major food proteins will illustrate the major emulsification activities of proteins.

(a) Caseins. The heterogeneous milk protein casein is commonly the major macromolecular component of the adsorbed layer that surrounds dispersed fat particles or oil droplets. The exceptional emulsifying properties of casein are attributed [121] to a molecular structure that is highly disordered and substantially hydrophobic. Casein in milk exists as ''casein micelles'': polydisperse proteinaceous colloidal particles containing the four major monomeric caseins α_{s1}, β, α_{s2}, and κ (in the approximate proportions 4:4:1:1, respectively) linked by calcium ions and colloidal calcium phosphate. The caseins α_{s1}, β, and κ have fairly similar molecular masses and iso-ionic points (pH 5.2 ± 0.2) but rather different molecular charges (−20, −12, and −4) at neutral pH [121]. The commercial emulsifier sodium (or potassium) caseinate lacks calcium phosphate and is consequently less aggregated than the casein in milk, but it has roughly the same protein

Copyright 2002 by Marcel Dekker. All Rights Reserved.

composition. My intention is to compare the properties of emulsions stabilized by the individual caseins α_{s1}, β, and κ with those stabilized by sodium caseinate in order to gain insight into the competitive and cooperative aspects of protein adsorption and colloid stabilization in casein-containing systems.

Adsorption experiments at fluid interfaces have shown [121,122] that α-casein is more surface-active than α_{s1}-casein, but direct evidence for preferential adsorption of α-casein in emulsions is rather limited [123,126]. Replacement of complex real emulsion systems by a model system of monodisperse polystyrene latex particles enables adsorbed proteins to be compared in a systematic manner. Studies were carried out on various monomeric caseins that had adsorbed separately on negatively charged latex particles [124–126]. Consistent with its having a higher net charge in solution than α- or α-casein, α_{s1}-casein adsorbed on latex gives coated particles of higher electrophoretic mobility than either of the other two caseins (Fig. 46). However, in the presence of calcium ions at concentrations above ~1 mM, latex particles coated with κ-casein carry higher effective negative charge than those coated with α_{s1}- or β-casein. This is interpreted as being

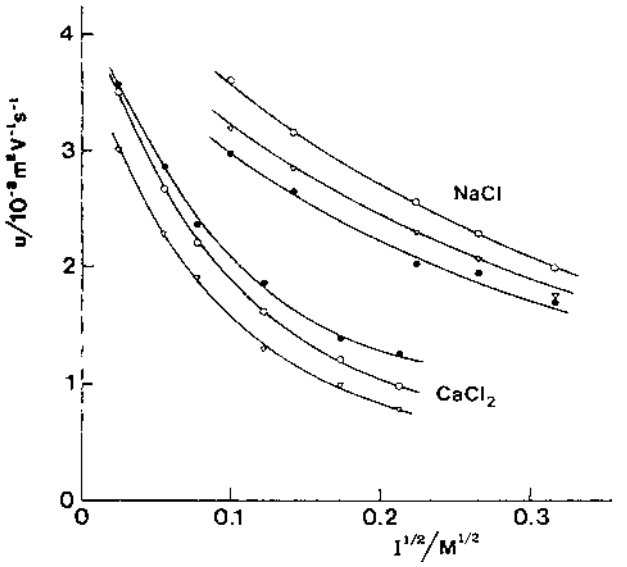

Figure 46 Electrophoretic mobilities of casein-stabilized *n*-hexadecane emulsion droplets at 25°C and pH 7.5 in the presence of sodium chloride or calcium chloride. The mobility u is plotted against the square root of the ionic strength I: (●) α_{s1}-casein; (▽) β-casein; (○) κ-casein.

Copyright 2002 by Marcel Dekker. All Rights Reserved.

due to the strong binding of calcium ions to α_{s1}- or β-casein, which reduced the net negative charge on the adsorbed protein layer. The adsorption characteristics of sodium caseinate on latices are intermediate between those for α_{s1}- and β-caseins, which suggests that, at solid surfaces at least, β-casein does not displace α_{s1}-casein over a short experimental time scale.

(b) Soy Proteins. Emulsion instability can appear visually as creaming or fat separation or a mixture of both. Emulsions stabilized by proteins seem to be very stable [112,127]. Their inherently high stability makes the measurements of coalescence in protein-stabilized emulsion a relatively difficult task. It can be tedious to follow the change in emulsion droplet-size distribution as a function of time or processing conditions, because it may take a long time to measure any change in droplet sizes. Most work has been done on low viscosity, low concentration O/W emulsions where measurements are simple. As a result the most important work has been done on whey and egg proteins. In addition it was assumed that other vegetable proteins such as soy protein, pea proteins, and cereal proteins were considered poor amphiphiles. These proteins were therefore used in high viscosity or gelled systems (baked goods, meat products, meat replacers, etc.) and their functionalities were judged and evaluated in view of the rheological properties and texture performance, and little was done on their surface characteristics and emulsification capabilities. With soy milk products, tofu, and other related products (nonviscous products) gaining worldwide attention because of the health aspects it becomes essential to learn more about the surface potential of soy proteins. Moreover, many other vegetable proteins have been examined. It seems that although native proteins might have structural drawbacks as emulsifiers, small or minor modifications can reveal significant potential. Figure 47 shows some coalescence stability characteristics of some proteins using the hexane extraction technique. Table 4 stresses the flocculation characteristics of the emulsions stabilized by various proteins. One can see that soy proteins are inferior to the classical amphiphilic proteins, but the functionality is still considerable [117].

2. Chemically Modified Proteins

Many physical and chemical properties of proteins can be modified to enhance their surface activity. Some of the most important characteristics, such as surface film strength, viscoelasticity, and colloid stability, can be changed by extrinsic changes (pH, ionic strength, temperature, etc.), and others such as hydrophobicity, flexibility of the polymer, and net charge can be altered by affecting the intrinsic properties of the protein (chemical or enzymatic modifications). The chemical modification of proteins will affect both protein–protein interactions and the interactions of protein with other surfactants.

Copyright 2002 by Marcel Dekker. All Rights Reserved.

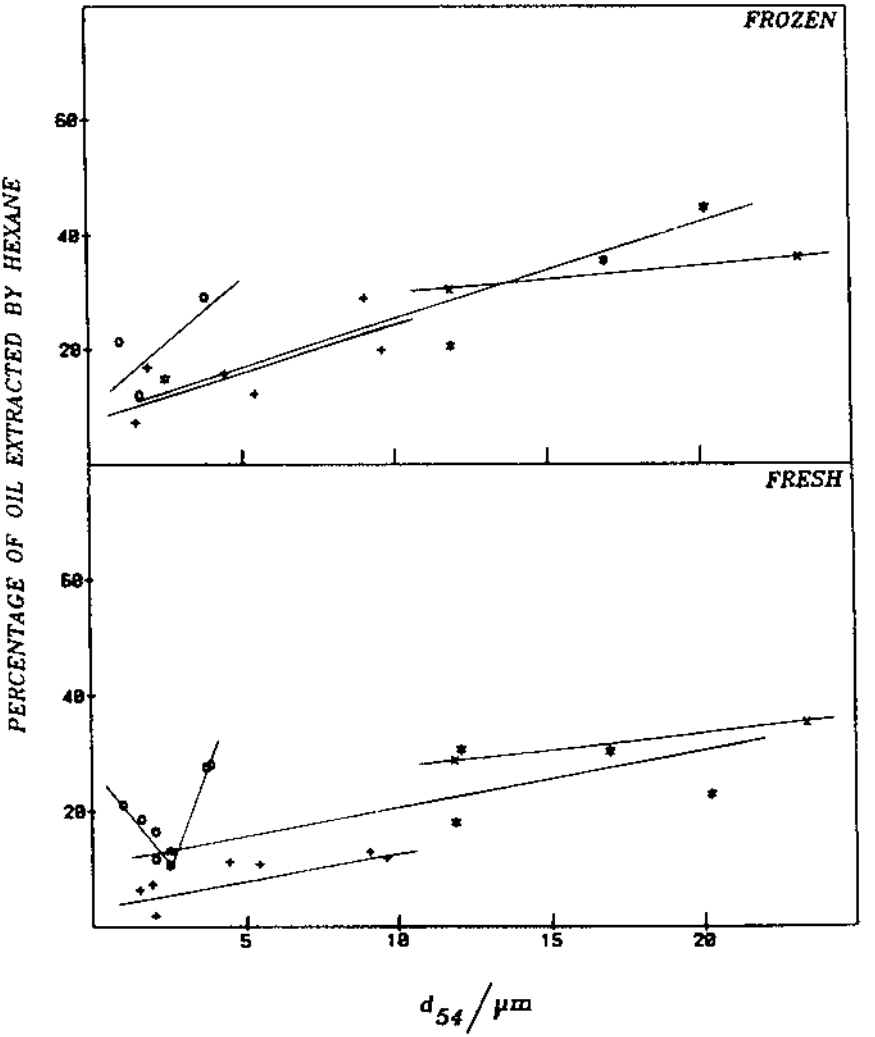

Figure 47 Comparison of coalescence stabilities of fresh and frozen emulsions in 0.2 M NaCl at pH 7. The percentage of oil extracted by hexane is plotted against mean droplet diameter d_{54}: (+) caseinate; □ WPC; (*) BP; (×) SP. WPC: Whey protein concentrate; BP: Bovine protein; SP: serum protein.

Copyright 2002 by Marcel Dekker. All Rights Reserved.

Table 4 Flocculation Stability of Selected Protein-Stabilized Emulsions

	Average degree of flocculation		
Protein[a]	0–6	0–7	0.2–7
Caseinate	0.9	0	0.3
WPC	1.3	1.2	1.2
BP	0.5	1.0	1.8
SP	2.7	1.1	5.0

[a] WPC = whey protein concentrate; BP = bovine protein; SP = serum protein.

Some of the most common extrinsic modifications are [119,128–133].

1. Change of pH (Table 5), which will affect the film-forming properties of the protein rather than lowering the degree of electrostatic repulsion or steric stabilization (for example, pH effect on BSA solution). The pH will affect the hydrophobicity of the protein (for example, BLG), which will result in improved emulsifying activity.

Table 5 Effect of pH on Some Film and Foaming Properties of Bovine Serum Albumin

	Film			
pH	Surface pressure[a] (mN/m)	Surface yield stress[b] (mN/m)	Film elasticity (mN/m)	Foam drainage half-life (min)
4.0	2.8	3.0	2.2	5.0
5.0	15.0	3.8	5.0	8.0
5.5	19.0	4.0	5.2	9.6
6.0	14.0	4.3	5.4	8.5
7.0	10.0	3.0	2.3	6.3
8.0	2.0	2.2	1.8	6.0

[a] Surface pressure of protein solutions (5×10^{-3} wt% in 10 mM citrate) was measured after 5 min at a temperature of 23°C.

[b] Surface yield stress was estimated by measuring surface viscosity using a Brookfield viscometer: protein solutions of 0.1 wt% in 10 mM citrate (pH 3–5.5) and phosphate (pH 5.7–8) buffers at 3°C after 5 min.

Copyright 2002 by Marcel Dekker. All Rights Reserved.

Table 6 Changes in Surface Hydrophobicity due to Thermal Denaturation[a]

Temperature (°C)	Hydrophobicity[b]				
	Ov[c]	7S[c]	κ-C[c]	BLG[c]	BSA[c]
20	10	260	430	2700	3200
50	10	260	480	2700	3100
60	10	270	600	2600	3000
70	15	400	750	2400	2500
80	1950	500	1050	1500	2000

[a] 0–2 wt% protein solutions in 0.1 M phosphate buffer (pH 7.4) heated at a rate of 1°C/min from 20 to 80°C, then immediately cooled to 20°C after reaching the given temperature.
[b] Determined by fluorescent probe method using *cis*-parinaric acid.
[c] Abbreviations: Ov = ovalbumin; 7S = 7S soy globulin; κ-C = κ-casein; BSA = bovine serum albumin; BLG = β-lactoglobulin.
Source: Ref. 134.

2. Use of *cis*-parinaric acid [129] to affect the flexibility of the protein and as a result to change its hydrophobicity (BSA, lysozyme, ovalbumin, R-casein, and BLG) [130].
3. Thermal denaturation, which affects the protein folding and protein association ability and alters the hydrophobicity of the protein [131,132] (Table 6).

Intrinsic chemical modifications serve as a way of enhancing many of the functional surface characteristics of the protein (Table 7).

Some of the most common chemical modifications are (Table 8)

1. ***Acylation and alkylation***. Among the chemical processes, acylation of lysine residues in certain proteins has been studied most extensively.

Table 7 Consequences of Alterations of Net Charge in the Chemical Modification of Proteins on the Surface Activity of the Protein

1. Isoelectric point changes.
2. Changes in protein associations, e.g., hydrophobic, electrostatic.
3. Randomness in protein structure due to electrostatic repulsion.
4. Stabilization against heat-induced denaturation (?).
5. Enhanced surface hydrophobicity or hydrophilicity.
6. Increased amphiphilic behavior of proteins, i.e., more surface-active (detergent-like).

Copyright 2002 by Marcel Dekker. All Rights Reserved.

Table 8 Amino Acid Side Groups in Chemically Modified Proteins

Group	Modification
Amino (lys)	Acylation; akylation
Carbonyl (asp, glu)	Esterification; amide formation
Disulfide (cystine)	Reduction
Sulfhydryl (cys)	Alkylation; oxidation
Thioether (met)	
Imidazole (his)	
Indole (trp)	
Phenolic (phe)	Acylation
Guanidino (arg)	Condensation by dicarbonyls

Similarly, acetylation and succinylation have also been the subject of a few studies. Acylation and alkylation will increase the solubility of proteins, thereby improving their functional properties in general and their emulsifying and foaming properties in particular.

2. ***Disulfide bond reduction***, which might also cause some release of structural constraints imposed by the disulfide bond and protein unfolding at the interface. Soy glycenin, which has limited film-forming properties due to its compact, stable, disulfide-linked structure [128] will be significantly more surface-active when some of its six disulfide-linked acidic and basic subunits have been reduced (Fig. 48).
3. Reduction, oxidation–reduction, or oxidation of the amino acid cysteine to form an open thiol (sulfhydryl) groups.
4. Alkylation. An important option for chemically modified proteins with effects similar to those of other reactions in which hydrophilic group is attached to the protein to improve its hydrophilicity.

3. Enzymatically Modified Proteins

Watanabe and Arai wrote an excellent review on the properties of enzymatically modified proteins and compared the chemical and enzymatic processes of various proteins [135]. Enzymatic processes can normally be carried out under milder and therefore safer experimental conditions than conventional chemical processes. Proteolytic enzymes have been used on proteins to improve their solubility: soy protein, leaf protein concentrates, fish protein concentrates, meat proteins, egg proteins, milk proteins, and blood proteins. Special attention was given to caseins, gelatins, egg proteins, and cereals. Partial hydrolysis of these proteins under well-controlled conditions can produce emulsifying and whipping agents

Copyright 2002 by Marcel Dekker. All Rights Reserved.

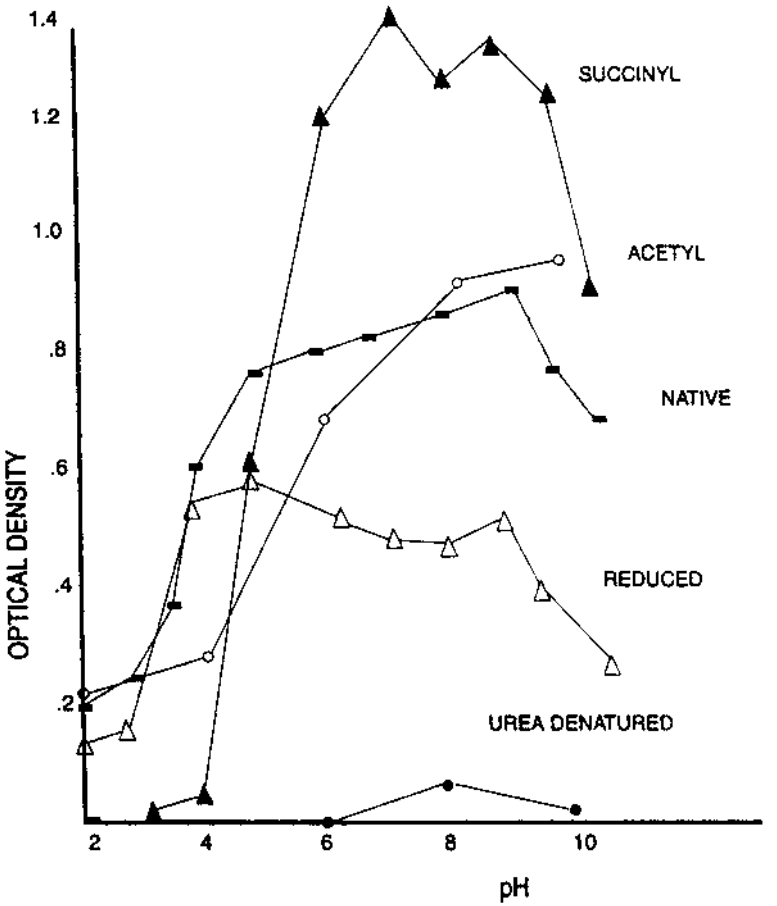

Figure 48 Effect of pH on the emulsifying activity of various types of modified BSA. Optical density at 550 nm is plotted against pH for diluted solution (pH 7.0, 0.1 M NaCl) and an oil-phase volume fraction of 0.6. The urea-denatured sample was obtained by treating BSA with 0.01 M dithiothreitol for 4 h at 40°C. Acylation was accomplished with 10:1 ratio by weight of anhydride to protein at pH 8–9 for 1 h at 25°C.

for use in food processing, and the production of such substances has even been practiced on an industrial scale. Some of these industrially produced protein hydrolysates have great emulsifying capacity. This is evaluated by gradually adding soybean oil to an aqueous solution of protein hydrolysate under conditions of controlled stirring until the resulting emulsion reverts from oil-in-water to water-in-oil.

Copyright 2002 by Marcel Dekker. All Rights Reserved.

More sophisticated processes developed by Watanabe et al. [136], include attachment of amino acid esters to improve hydrophobicity. An excellent example is the dramatic change in the enzymatically modified gelatin (EMG) [137–139] (Fig. 49).

The modified proteins EMG-12 and EMG-6 were tried in a variety of food products such as mayonnaise, baked bread, and ice cream, and were found to significantly improve the quality of the final product by changing the emulsification capacity (efficiency) of the proteins.

4. Lipid Proteins (Lipoproteins)

Proteins and polar lipids coexist in biological systems, mainly unassociated with each other but also as composite structures with specific actions [137]. They have a very important physical property in common: an inherently amphiphilic nature, which provides the driving force for the formation of associative structures of lipids as well as for stabilizing some food colloids.

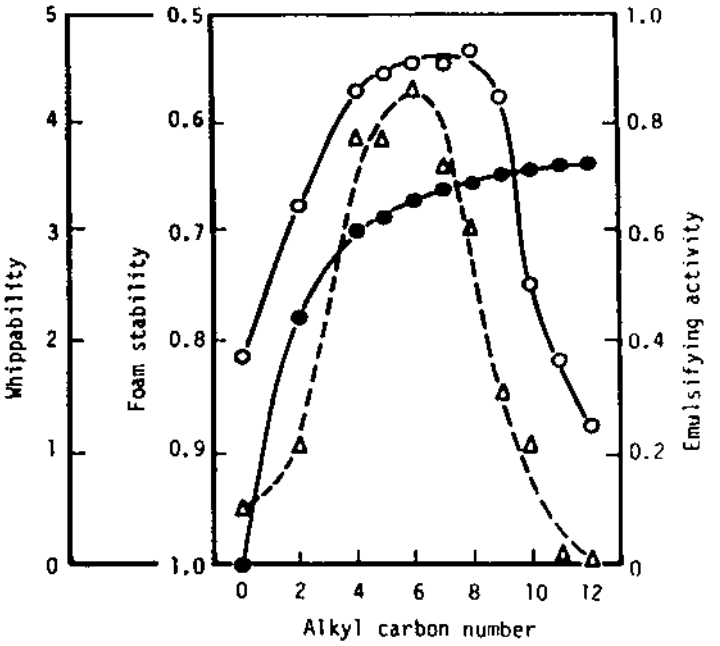

Figure 49 Functional properties of EMG products with attached L-leucine *n*-alkyl esters. Whippability (○), foam stability (△), and emulsifying activity (●) are plotted against the number of carbon atoms in the alkyl chain.

Copyright 2002 by Marcel Dekker. All Rights Reserved.

The possible interactions of proteins (globular) and water-soluble lipids with a synthetic emulsifier have been recognized and studied. Proteins have a strong affinity toward both polar lipids and aromatic surfactants. Their interactions with nonionic surfactants are very limited. Proteins also strongly interact with water-insoluble polar lipids (electrostatically dependent interaction).

The hybrid or complex nonchemical interactions are the basis for the construction of new artificial systems composed of certain proteins, such as β-lactoglobulin or serum albumin, with sodium dodecyl sulfate (SDS) to be used in systems in which electrostatic stabilization of O/W emulsions is essential.

Ovalbumin appears to undergo only unspecified interaction with ionic surfactants in solution. Serum albumin, having specific binding sites for anionic surfactants, shows a different surface tension profile when mixed with SDS, especially in the low SDS concentration range. Saturation of the high affinity binding sites for SDS does not affect the surface tension obtained by pure serum albumin, although the surfactant binding increases serum albumin stability. When the SDS concentration exceeds the concentration for the specific binding, however, the surface tension isotherm resembles the one seen for, e.g., ovalbumin and SDS.

5. Natural Hydrocolloids as Food Emulsifiers

Water-soluble polysaccharides are often termed hydrocolloids or gums. They enhance viscosity and/or form gels in aqueous systems. Technologists call them ''stabilizers'' because some food colloids consisting of gums will exhibit long-term stability. Colloid scientists claim that hydrocolloids are not ''true'' emulsifiers, because they do not ''actively'' adsorb onto liquid interfaces.

Gum arabic, locust bean gum, tragacanth, xanthan, pectins, and other naturally occurring molecules have been used for many years in foods, in part because of their surface activity. Terminology such as ''additives that retard precipitation of dispersed particles,'' ''agents that decrease creaming rates of oil droplets or foams,'' ''dispersants that prevent aggregation/disaggregation of dispersed solid or liquid particles,'' ''stabilizers that prevent syneresis of gelled systems, condition or stabilize food systems,'' and ''emulsifiers that retard coalescence of oil droplets'' are often used by food technologists to describe the role of such additives in the final food product. In general these molecules are termed stabilizers [137–145].

The use of such molecules in the food industry was known for decades but was based primarily on practical trial-and-error experience. Only during the last 15 years has more scientific work been carried out to better understand the structural association and surface activity of these molecules.

In the past, the term ''stabilizers'' was used to denote molecules that are responsible for the maintenance of bulk (the continuous phase), providing homo-

Copyright 2002 by Marcel Dekker. All Rights Reserved.

geneous structure and texture throughout the system, preventing any sedimentation or creaming or any separation of free fat or aqueous serum.

In more recent texts scientists distinguish between stabilizers and emulsifiers. It has been stated [142–145] that hydrocolloids are not emulsifiers but rather stabilizers and that

> An emulsifier is a single chemical or mixture of components having a capacity for promoting emulsion formation and a short-term stability by interfacial action. A stabilizer is a single chemical component, or a mixture of components, that can offer long-term stability of an emulsion, possibly by a mechanism involving adsorption, but not necessarily so.

See Figure 50.

Proteins, being indispensable components of an overwhelming majority of food emulsions, can, in principle, emulsify an oil phase in water and stabilize the emulsion. The increased resistance of oil drops to coalescence due to protein action is associated with the formation, at the interfacial surface, of an adsorption layer of high viscosity and mechanical strength, the so-called [142–144] structural-mechanical barrier. Other investigators hold the view that the electrostatic and steric components of the disjoining pressure play a greater role in the stabilization of emulsions. The proteins have the ability to attain a high strength of the adsorption layer in comparison to the low molecular weight surfactants as well

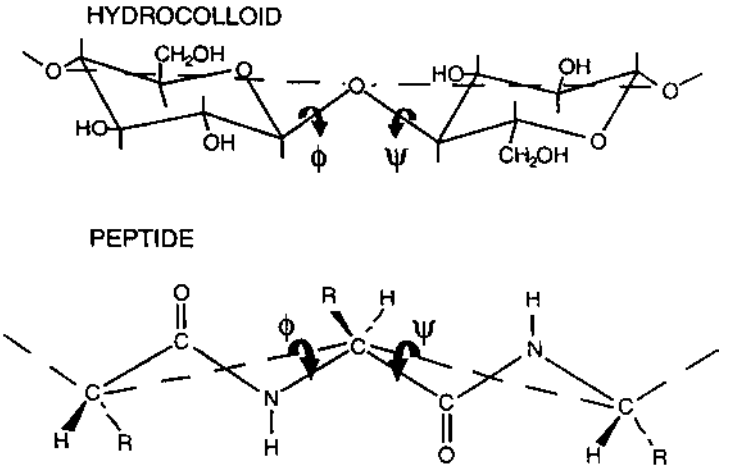

Figure 50 Structure of a typical hydrocolloid, emphasizing its rigidity in comparison to the structure of the flexible proteins with the ability to rotate.

Copyright 2002 by Marcel Dekker. All Rights Reserved.

as a considerable increase in viscosity of the dispersion medium, which results in higher kinetic stability of the emulsion.

Are some polysaccharides surface-active, and can they be used as emulsifiers? This is a cardinal question still in debate among scientists. Many patents have been filed on methods for preparation of food emulsions with polysaccharides as emulsifiers and stabilizers. However, close examination of some of theses reports reveals that the stabilization effect can be derived from one or both of two possible effects: increase in the viscosity of the dispersed phase and/or hydrocolloid surface adsorption.

The following review discusses the status of research activities carried out on various gums as emulsifiers and tries to clarify questions related to adsorption at interfaces of certain gums. It does not deal in detail with protein-polysaccharide mixtures, complexes, or the phase separation resulting from the incompatibility of certain polysaccharides and proteins.

(a) Gum Arabic. It is well documented that gum arabic, a natural polysaccharide, has excellent emulsification properties for oil-in-water emulsions. It is widely used in food, cosmetics, and pharmaceutical applications. An excellent example of its use is in cloudy emulsions, as an opacity builder for citrus beverages [146–149]. Gum arabic is added at high levels (up to 20% of the total emulsion) to an aqueous sugar solution and emulsified with an oil phase consisting of orange oil and weighting agents (i.e., brominated vegetable oil, sucrose esters, sucrose diacetate hexaisobutyrate, or ester gums). Stable oil-in-water emulsions with high opacity and low creaming are obtained. A very comprehensive review [147] with almost 90 references was published in 1997 that discusses in great detail all the substantial developments concerning the regulatory aspects of gum arabic and elucidation of its structure and functional characteristics.

Street and Anderson [147] and Anderson [149,150] predetermined the structure of the gum by submitting it to a series of Smith degradations. It was shown that the uronic acid and rhamnose are located at the periphery of the molecule, and the core was found to consist of a β-(1,3)-galactopyranose chain with branches linked through the 1- and 6-positions. Figure 51 illustrates the structure of gum arabic determined by the combined use of computer modeling [151] and chemical analysis. In other works, Churms et al. [152] and Stephen and Churms [153] proposed a more functional structure based on CMR (carbon magnetic resonance) and Smith degradation analysis.

Gum arabic was found to consist of mixed calcium, magnesium, and potassium salts of a galactopyranose backbone chain linked β-(1-6) to various branches containing arabinofuranose, arabinopyranose, rhamnopyranose, glucuronic acid, and 4-*O*-methyl glucuronic acid.

Gum arabic is always ‘‘contaminated’’ with proteineous matter. Hydroxyproline, serine, and proline are the most abundant amino acids in the protein-

Copyright 2002 by Marcel Dekker. All Rights Reserved.

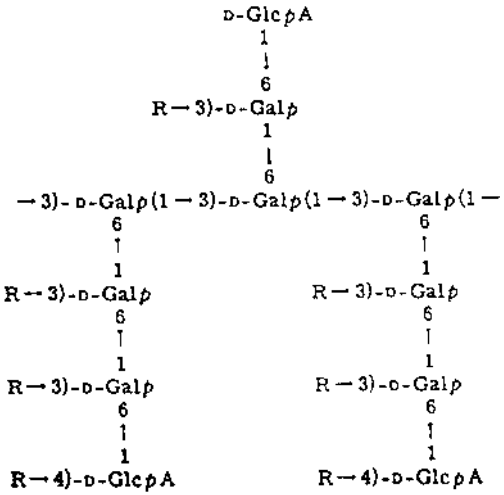

Figure 51 Schematic illustration of a possible core structure of the gum arabic. R = L-Rha*p* (1 →, L-Ara*f* (1 →, D-Gal*p* (1 → 3)-L-Ara*f* (1 →, or L-Ara*p* (1 → 3)-L-Ara *f* (1 →.

aceous residue. The role of the proteinaceous components in gum arabic was the subject of several recent studies. It was reported that acacia gum with the highest nitrogen content resulted in emulsions with the highest surface pressure (π) and surface viscosities (η) at any of the pH levels tested [154]. It was concluded that the protein-rich, high molecular weight component (the arabinogalacto–protein complex) is the fraction that provides the functionality of gum arabic as an emulsion stabilizer.

Those emulsions also exhibited high surface viscosity that did not change upon dilution [155,156]. Stable and deflocculated emulsions should be covered with adsorbed polymer that provides full coverage, firm anchoring, a thick layer, and low redesorption.

In more detailed studies investigators [157–159] recognized the significance of the molecular weight characteristics and properties of the gum. They showed that the gum consists of two distinct fractions: a high molecular mass arabinogalacto–protein complex (AGP), representing about 30% of the total, and a lower molecular mass fraction.

It was demonstrated that the emulsification capability (average droplet size diameter) of heat-treated gum arabic was reduced dramatically by the denaturation effect of the ''active'' protein (Fig. 52). A similar effect was recorded at a low pH. The effect of the protein content on the emulsifying activity was found to correlate well with measurements of the surface pressure and surface elasticity.

Copyright 2002 by Marcel Dekker. All Rights Reserved.

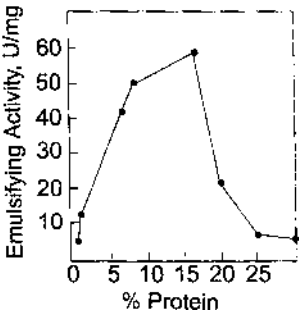

Figure 52 Emulsifying activity (U/mg) as a function of percentage of protein in gum arabic.

In more recent work by Randall et al. [158] it was shown that the gum actually consists of three distinct fractions: a high molecular mass arabinogalacto–protein complex (AGP), glycoprotein (G1), and a lower molecular mass fraction that is protein-deficient (poor in protein) (AG). It was proved that the AGP fraction is degraded by proteolytic enzymes, with its molecular mass decreasing to a value similar to that of the AG fraction [158]. It was suggested that the AGP fraction consists of about five carbohydrate blocks of molecular mass 2.8×10^5 linked together by a polypeptide chain, which may contain as many as 1600 amino acid residues. It is likely that the polypeptide chain is located at the periphery of the molecule, thus facilitating its adsorption onto hydrophobic substances. The AG fraction is not degraded by proteolytic enzyme and may simply be a fragment of the AGP fraction.

At relatively low concentrations, gum arabic yields solutions that are essentially Newtonian in behavior and have very low viscosities compared to other polysaccharides of similar molecular mass. This behavior is similar to that of globular proteins. The intrinsic viscosities at pH 5.5 of gum arabic solutions are similar to those of β-lactoglobulin. Randall et al. [158] and Williams et al. [148] concluded that the AGP fraction is responsible for the gum's emulsifying ability. Consequently, relatively high concentrations of gum arabic are required to produce stable emulsions of relatively small droplet size. At a lower gum arabic concentration, there is insufficient surface-active material to fully coat all the droplets. Therefore, it has been concluded that although gum arabic is basically a polysaccharide, its interfacial and emulsifying properties are derived from its proteinaceous nature.

A schematic illustration of the structure of the arabinogalacto–protein complex at the oil/water interface is shown in Figure 53.

Copyright 2002 by Marcel Dekker. All Rights Reserved.

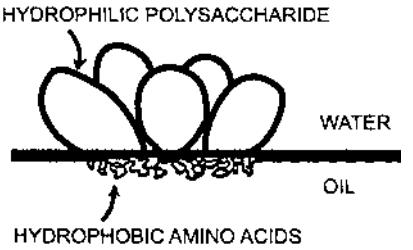

Figure 53 Schematic illustration of the structure of the arabinogalacto-protein complex at the oil/water interface.

(b) Galactomannans. Galactomannans are the most common plant food reserve polysaccharides. They belong to the legume family and consist of a β-(1,4)-linked D-mannan backbone grafted with α-(1,6)-linked D-galactose stubs for certain of the mannose residues [160] (Fig. 54).

There is great diversity in the chemical structure of the galactomannans due to the variety of plant sources. This diversity includes a wide variation in

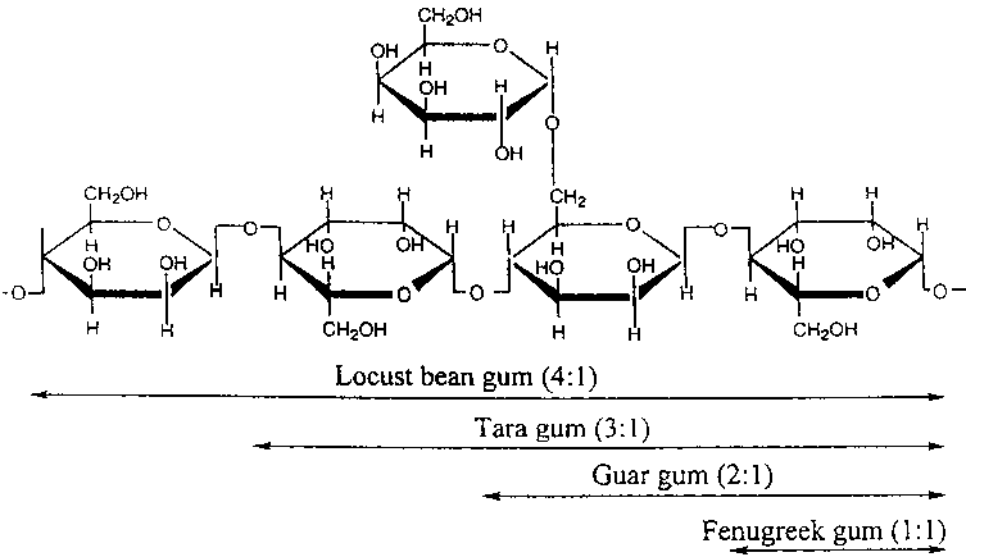

Figure 54 Schematic illustration of the structure of guar gum and locust bean gum (LBG). (From Ref. 160.)

Copyright 2002 by Marcel Dekker. All Rights Reserved.

the degree of galactose substitution (locust bean, tara, guar, and fenugreek gums, respectively,) have (galactose/mannose ratios of 1:4, 1:3, 1:2, and 1:1) and significant differences in the distribution of galactose substituents along the mannose chain.

Galactomannans exist as fluctuating random coil chains with nonspecific viscosity behavior in aqueous solutions. The thickening properties, self-gelling properties, and contribution to gel formation are usually obtained in conjunction with other gums. Differences in structure significantly affect those functionalities. Several studies have been carried out on the structural aspects of the gums and their rheological behavior in aqueous systems, but very little has been done with respect to their interfacial characteristics.

From preliminary work [150,161,162] on the competitive flocculation efficiency on latex particles it was concluded that guar (and also xanthan) gum adsorption is weak and increases with concentration without going through a maximum (minimum flocculation) in comparison to dextran, casein, or gum arabic, which adsorb very strongly and exhibit a clear maximum at low protein concentrations (Fig. 55).

However, latex surfaces are quite different than the oil/water interface in ''true'' food emulsions. The ability of a number of industrial gums to act as steric stabilizers of O/W emulsions in the presence of various low molecular weight emulsifiers has been observed [161]. The surface and interfacial properties of LBG, guar, and fenugreek have been recently studied in our lab [163–168]. The emulsification capabilities and stability of oil-in-water emulsions and their adsorption isotherms have been determined and examined [163–168]. It was found

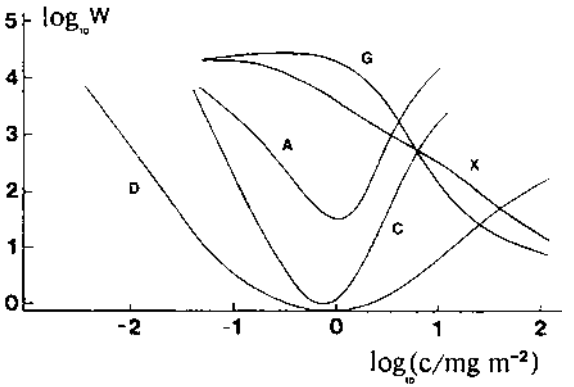

Figure 55 Comparative flocculation efficiency W of food biopolymers (latex diameter 88 nm, particle density $4.5 \times 10^{11}/cm^3$, sodium chloride concentration 6.7×10^{-2} mol/dm^3, 28°C, pH 5.9). D, dextran 7500; C, caseinate; A, gum arabic; X, xanthan; G, guar.

Copyright 2002 by Marcel Dekker. All Rights Reserved.

that both LBG and guar gum reduce the surface tension of water at low concentrations (up to 0.5 wt%) and that the surface tension of the gum solutions is time-dependent. As expected, equilibrium surface tensions decreased and adsorption rates increased significantly with increasing gum concentration. The lowest surface tensions measured for LBG, guar, and fenugreek gums were 50, 55, and 48 mN/m, respectively [163], in comparison to 42 and 43 mN/m for tragacanth and xanthan gums, respectively. This surface activity seems to be relatively pronounced in view of the chemical structure and expected hydrophilicity.

Interfacial tensions between water and various oils (Table 9) were found to be significantly lower in comparison to other hydrocolloids or well-known emulsifying proteins.

The gums do not exhibit a clear critical micellar concentration at concentrations of up to 0.7 wt%.

Relatively large oil droplets (10–50 μm) were formed when guar or LBG gum solutions were emulsified with 5 wt% vegetable oil or tetradecane in the presence of 0.5 wt% gum (Fig. 56) [163–165]. The large droplet sizes were attributed to the inefficient gum adsorption onto the interface (tails or loops) allowing coalescence to occur during the preparation stage.

Fenugreek gum, another member of the galactomannan family, was studied as a nutraceutical component by [169,170] and Madar and Shomer [171]. The galactose-stabilizing side-chain moieties are grafted, on average, onto every one of the mannose groups in the backbone (galactose/mannose ratio of 1), and the biopolymer is very hydrophilic and difficult to gel. This particular gum was se-

Table 9 Oil/Water Interfacial Tensions (γ_i) Measured With and Without the Addition of LBG (25°C, 720 min)

	LBG concentration (wt%)	Interfacial tension γ_i (mN/m)
Tetradecane	0	44
	0.7	25
Paraffinic oil	0	36
	0.7	22
Toluene	0	36
	0.7	17
Castor oil	0	16
	0.7	12
Soy oil	0	30
	0.7	16.5

Copyright 2002 by Marcel Dekker. All Rights Reserved.

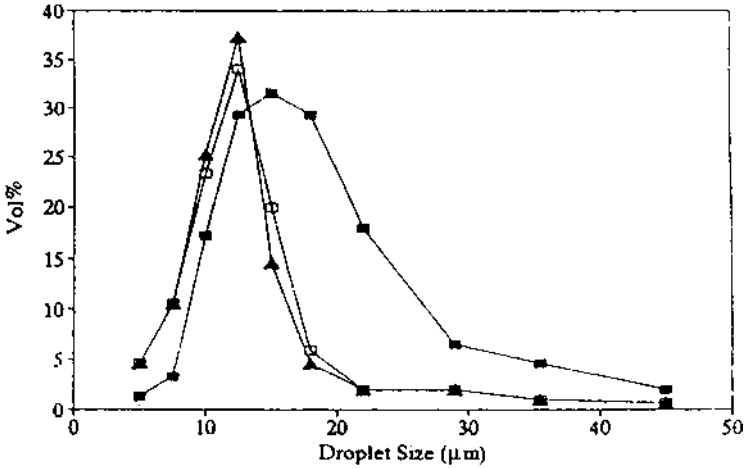

Figure 56 Droplet size distribution of 5 wt% tetradecane-in-water emulsion prepared with 0.5 wt% guar gum, (▲) immediately after preparation, (□) after 1 week, and (■) after 1 month of aging at room temperature. (From Ref. 163.)

lected because preliminary results showed that it had a strong tendency to adsorb on hydrophobic surfaces and to reduce cholesterol levels in aqueous dispersions.

Much to our surprise [166–168,172–173] it was found that (1) the fenugreek polysaccharide is always accompanied by proteinaceous matter and (2) it exhibits significant surface activity and contributes very little rheologically to the continuous phase. The chemical composition of native extracted fenugreek gum (termed FG-1) is 2.9 wt% protein and 85.9 wt% polysaccharides. Of the total carbohydrates, over 50% are surface-active, water-soluble polysaccharides. After extensive purification, protein content was reduced to 0.95 wt%, lipids to 0.4 wt%, ash to 0.5 wt%, and moisture to 8.7 wt%, and the carbohydrate content was increased to 89.7 wt% (FG-3 fraction). The surface tension of the native gum (FG-1) is similar to that of guar, and the interfacial tension is slightly higher (20 for guar vs. 28 mN/m for fenugreek). However, the emulsification capabilities of the gum fractions were very impressive. Most droplets were in the range of 2–5 μm (over 75% by volume or number) at 0.3 wt% gum levels. Most surprising was the fact that the emulsions could be aged for over 4 weeks at temperatures of 4–50°C without any significant change in droplet size, which indicates that only slight coalescence took place.

Oil droplets in water revealed that in many cases emulsions prepared with LBG or guar consist of two populations of droplets. The major portion has a normal size distribution of 2–5 μm, and the other (only 3–5% of the total drop-

Copyright 2002 by Marcel Dekker. All Rights Reserved.

lets) a size distribution of 10–40 μm. Both populations are stable to coalescence. The emulsions prepared with fenugreek had only one normal distribution of droplet size, indicating again a more efficient adsorption process. Another interesting fact is that although the guar and LBG emulsions suffered from severe flocculation when the gum/oil ratio was low (<12), the fenugreek emulsion flocculated only slightly even at low gum/oil ratios, clearly indicating a better adsorption process and better surface coverage.

Surprisingly, close examination under polarized light of the oil droplets of the emulsions prepared with the three gums revealed a strong birefringence effect (Fig. 57). The birefringency was affected by the nature of the oil. For guar, both vegetable and tetradecane oil droplets were birefringent, whereas when fenugreek was used the only pronounced birefringency was detected with vegetable oil. The birefringency was attributed to the formation of a thick, well-oriented gum film on the oil droplet [162–168]. The strong birefringency around the oil droplets can also be interpreted as being due to the formation of a ''gum precipitate around the droplets'' and/or formation of an ''oriented gel-like'' phase around the droplets. The film was formed as a result of a phase separation effect derived from the addition of oil to the aqueous gum solution, which ''precipitated'' the gum on the oil interface. The nature of this adsorption is not clear, but it can be interpreted as ''adsorption of the non-hydrated groups of the reoriented gum onto the oil and dangling of the hydrated groups in the water phase'' (as suggested by Tolstoguzov [174,175]).

The photomicrographs of the O/W emulsions stabilized by galactomannans taken under polarized light (Fig. 57) seem to indicate large surface loads (very strong birefringency with guar gum and strong birefringency with fenugreek gum with soy oil). Unfortunately, to the best of my knowledge, no quantification method is yet available to correlate the birefringency and the surface concentra-

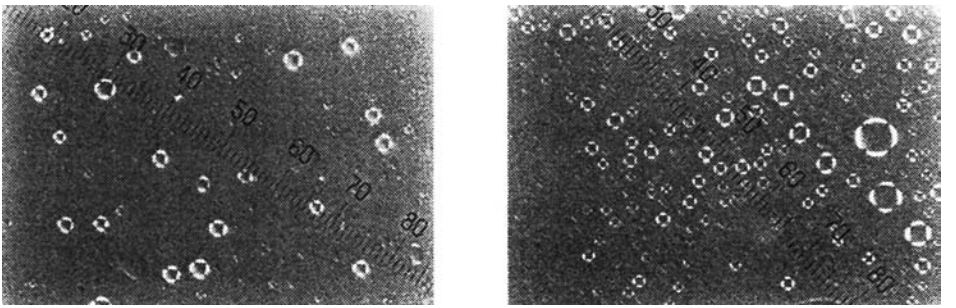

Figure 57 The birefringency effect of 5 wt% tetradecane-in-water emulsions stabilized by (left) 0.5 wt% guar gum and (right) 0.5 wt% fenugreek gum.

Copyright 2002 by Marcel Dekker. All Rights Reserved.

tions of the polymeric emulsifier. The birefringency in fenugreek gum emulsions seems to be similar to that of the guar or LBG emulsions.

Attempts to characterize these birefringent layers were made using small-angle X-ray diffraction methods. The cream phase (strong in birefringency) shows significant one-dimensional swelling, which is characteristic of lamellar liquid crystalline structures [172,176]. More work is required to determine the nature of these thick, organized layers around the droplets.

Figure 58 illustrates the isotherms in the adsorption of guar gum and LBG onto the oil/water interface. The surface load is 4 and 2.8 mg/m^2 for LBG and guar, respectively (at 0.9 g gum per 100 mL emulsion). These surface loadings are somewhat lower than the adsorption loads measured for commercial and/or nitrogen-enriched gum arabic (4 and 7 mg/m^2 so-called equilibrium polymer adsorption concentration, respectively) as measured on latex surfaces [132]. It should be noted that the gum adsorption on the oil/water interface is weak. Dilution of the emulsions with water will cause some gum desorption from the interface. Low molecular weight emulsifiers will compete with the gums on the interface and eventually will displace them completely [172,177].

The adsorption isotherms of fenugreek gum are much more explicit and more characteristic of amphiphilic biopolymers than those of the other gums.

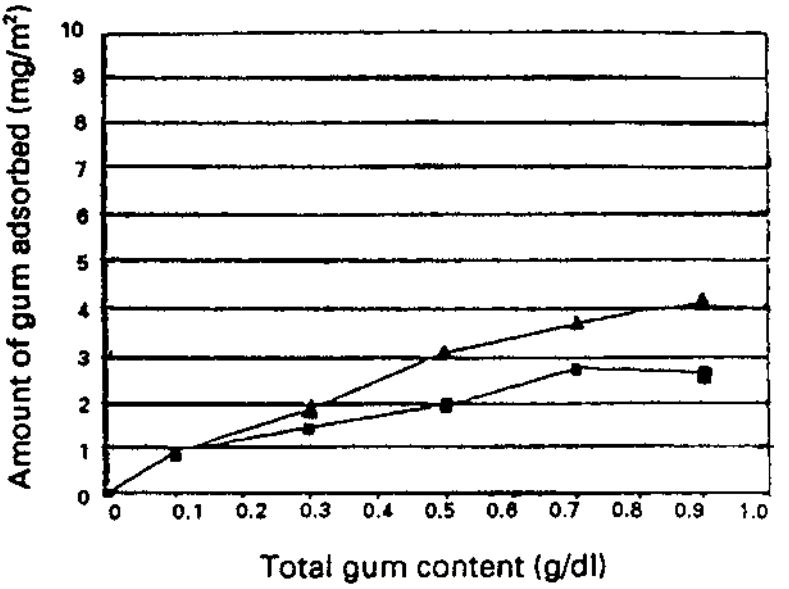

Figure 58 Adsorption isotherms of (■) guar gum and (▲) LBG.

Copyright 2002 by Marcel Dekker. All Rights Reserved.

The total adsorption load is 18 mg/m^2 (compared to 2.8 mg/m^2 for LBG and 4 mg/m^2 for guar) and is achieved with much lower gum solution concentrations.

Much has been written on the effect of protein on the surface activity of certain hydrocolloids, for example, gum arabic. It was therefore essential to establish the nature of the role protein in galactomannan gums plays in the emulsification capabilities of the gum. In our work, after extensive gum purification, it was demonstrated [172,173] that at least the majority of the proteinaceous matter is not an integral component of the polysaccharide and can be almost entirely removed by repeated crystallization. The level of protein contaminating the guar was reduced from 5.95 wt% in the native commercial guar to 0.8 wt% in the ''bipurified fraction.'' However, it should be noted that these techniques were not useful for further reducing the protein from the guar and that some of the gum remained bound to protein.

Surprisingly, the fraction with the lowest nitrogen content had the best surface properties and the fraction with the highest nitrogen levels showed the lowest surface activity. These results might suggest that the protein fraction is not surface-active. In addition it might suggest that hydrophobicity is not a requirement for the gums to adsorb on interfaces. Furthermore, the emulsions with bipurified gums were more stable to coalescence than the emulsions prepared with the native (protein-rich) gums.

Similar results were obtained with fenugreek. No significant improvement in emulsion stability was found when the purified gum was used in place of the one containing proteinaceous matter, in spite of the fact that the droplets seemed to be smaller in size and distribution.

Although ''totally protein-free'' hydrocolloids could not be obtained, it is clear that these gums adsorb onto the oil interface and do not merely contribute to the viscosity of the continuous phase. Series of tests were conducted both on aqueous dispersions of hydrocolloids (heat treatment, dilution, pH change, addition of electrolytes, etc.) and on emulsions (dilution, heat treatment, addition of monomeric emulsifiers, etc.). From these tests it seems that the role of the protein, if any, is insignificant and not similar in any way to its role in gum arabic.

Additional work is required to pinpoint the protein adsorption mechanism and to clarify the role of the protein.

(c) Xanthan Gum. Xanthan gum is an exocellular bacterial polysaccharide. It is a biopolymer of D-glucose, D-mannose, and D-glucuronic acid units in the ratio of 3:3:2. It also contains acetyl and pyruvic acid groups. It consists of a β-D-glucose backbone with a charged trisaccharide side chain consisting of two D-mannose residues and a D-glucuronic acid residue. It dissolves readily in cold or hot water, forming a very viscous solution even if the concentration is low. Xanthan is used as a thickening agent in foods and cosmetics. However, it is known

Copyright 2002 by Marcel Dekker. All Rights Reserved.

also as a film-forming agent. The molecule can undergo a thermally induced conformational change [176,178].

In many previous reports xanthan is mentioned as a stabilizer for oil-in-water emulsions. My coworkers and I [179–183] claim that its activity is derived from the viscosity effect, whereas others have considered different mechanisms. Ikegami et al. [178] explored the interfacial properties of xanthan. The adsorption of xanthan gum onto a model substrate, i.e., monodisperse, spherical polystyrene latex, has been studied. Xanthan gum was found to adsorb onto the latex from both aqueous and 0.5 M NaCl solutions, and low affinity isotherms were obtained in both cases. The nitroxide spin label experimental techniques suggest that the xanthan adsorbs onto the latex surface in the form of ''trains'' from both solutions. The xanthan gum did not affect the stability of the latex in aqueous solution in the absence of electrolytes. In NaCl solutions the latex flocculated at a low polymer surface coverage owing to a bridging mechanism but was stabilized at higher polymer surface coverage through steric repulsive forces. At even higher xanthan concentrations, flocculation was observed that was attributed to depletion phenomena.

The latex adsorption work is the only recent study examining the surface properties of xanthan gum. However, it must be stressed that it was carried out on solid particles and not on liquid interfaces. The reports claiming that the gum has surface activity and that it can stabilize emulsions did not consider the adsorption properties of the gum. The surface activity of the gum is not very clear from its structure, but it is possible that some of it is derived from conformational changes induced by heat treatment [176].

(d) Portulaca oleracea and *Opuntia ficus indica* Gums. Two additional gums that exhibit strong emulsifying capabilities in dilute oil–water emulsions have been isolated. *Portulaca oleracea* gum (POG) [179] and *Opuntia ficus indica* (OFI) [180] were found to (1) reduce surface and interfacial tensions; (2) stabilize oil–water emulsions; (3) form small oil droplets; (4) adsorb onto oil/water interfaces and not contribute to the viscosity of the systems; and (5) exhibit flocculation.

(e) Portulaca oleracea L. is a green annual herb of the Portulacaceae family [179,181–183]. The leaves are sappy and are rich in various salts, proteins, and carbohydrates. The maximum concentration of proteins (23.7 wt%) and carbohydrates (13.8 wt%) was noted during the period of seed period of maturation. Detailed and complicated analytical work helped to isolate two main fractions, the major one (80–90%) resembling cord filaments and the minor one resembling resin fines. The ''resin fines'' are low in acidic sugars and rich in arabinogalactan components and D-xylose. The ''cord filaments'' have high specific gravity and are rich in galacturonic acid. Anion-exchange chromatography was used to fractionate the crude complex into neutral arabinogalactans and polydispersed ''pec-

Copyright 2002 by Marcel Dekker. All Rights Reserved.

tin-like'' polysaccharides. The portulaca gum has a very minor viscosity effect on aqueous solutions [184–187]. The surface tension of POG, after 12 h of equilibrium, was surprisingly low in comparison to the other hydrocolloids (47 mN/m). No critical micellar concentration was detected. The interfacial tension of water and *n*-tetradecane was reduced significantly to 18 mN/m at 0.8 wt% gum. Equilibrium was reached in a shorter time than for the galactomannan gums.

POG does not build much viscosity at low concentrations (10 cSt at 0.8 wt% gum). It seems that at low POG concentration only weak intramolecular gum interactions exist, whereas above 0.8 wt% the gum entangles, overlaps, and imparts opacity to the solution. The low viscosity of the gum is an important factor when one is trying to distinguish between emulsion stabilization resulting from interfacial adsorption and the viscosity effect that gums can impart to the continuous phase in O/W emulsions. Emulsions of 5 wt% *n*-tetradecane and low gum concentrations formed large oil droplets (>14 μm), but droplets are rather small (average 3 μm) at 0.7 wt% gum. The insufficient reduction in droplet size can be explained in terms of shear efficiency restrictions and/or in terms of slow migration of the gum to the oil phase during shear and the rupturing of droplets.

The surface area seems to level off at 0.7 wt% gum, as found by measuring droplet size. Moreover, close examination of the emulsions reveals that at low gum concentrations emulsions have a strong tendency to flocculate, whereas emulsions with high gum concentrations (>0.8 wt%) are free of flocculation.

The emulsification stability index (ESI) reflects the stability of the emulsion to coalescence. An ESI value is the percent by volume of droplets in the range of 2–20 μm immediately after preparation and after 7 days of storage at room temperature (Fig. 59). A high ESI value indicates better stability to coalesce. It should also be stated that all the emulsions stabilized with >0.5 wt% gum are stable to coalescence. No significant change in droplet size was observed after 15 days of aging.

Figure 60 summarizes the adsorption isotherm. A high adsorption efficacy value of 11.8 mg/m^2 was obtained for emulsions stabilized with 0.9 wt% gum in comparison to those of any other hydrocolloids. The high value may suggest that the polymer adsorbs in a mode similar to monomeric emulsifiers with only a few tails (segments) anchoring in the oil and large hydrophilic groups dangling in the water phase.

The pH effect is somewhat surprising and important. The POG hydrocolloid bears a negative charge at any pH above 2. Therefore, it is expected that electrostatic repulsion will contribute significantly to the stabilization even at pH 3. It could be clearly demonstrated that POG adsorbs best at low pH. It seems that the highly charged gum (at pH > 3) is more water-soluble and tends to be more hydrated in the water phase than the gum that has a smaller charge. A similar tendency was observed for certain proteins. The reductions in adsorption load and in zeta-potential values are in good correlation with the emulsification

Copyright 2002 by Marcel Dekker. All Rights Reserved.

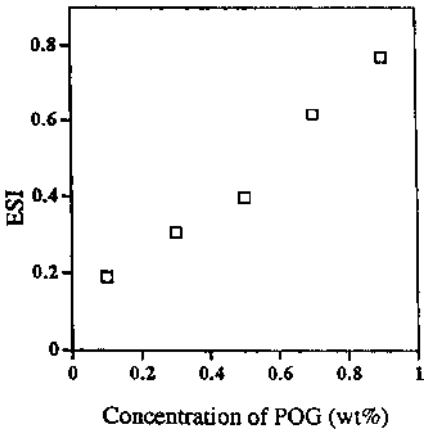

Figure 59 Emulsification stability index (ESI) vs. POG concentration in emulsions of 5 wt% tetradecane in water measured 7 days after preparation.

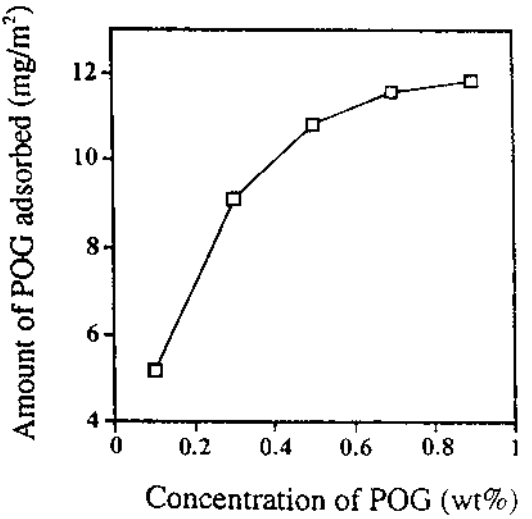

Figure 60 Adsorption isotherm of POG in mg/m^2, using the Tadros and Vincent method.

Copyright 2002 by Marcel Dekker. All Rights Reserved.

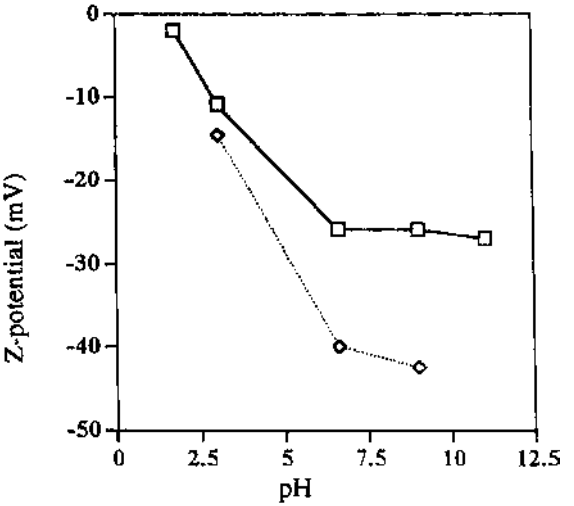

Figure 61 Zeta potential of 5 wt% *n*-tetradecane in water emulsion in the presence of 0.5 wt% POG, vs. pH in the absence (◇) and in the presence (□) of 0.015 M NaCl.

stability index (ESI) values (Fig. 61). It was shown clearly that the ESI values are lower at elevated pH, both in the presence and in the absence of electrolytes. The absence of electrolytes at pH <6.6 does not seem to improve the stability of the emulsions. Microscopic observations carried out on these emulsions confirmed that the best emulsions are formed at pH 3. Emulsions show no flocculation and are very stable for months.

The purified POG contains 3.1 wt% protein and therefore is not protein-free. Gum solutions were heat-treated prior to emulsification. The heat can expose hydrophobic segments of the gum to the oil phase (unfolding) or can cause denaturation of the proteinaceous segment of the gum (or the protein–gum complex). Heat can also reduce emulsification properties of the gum (see gum arabic) or can cleave intramolecular hydrogen bonds and change the hydrophobicity–hydrophilicity balance of the gum.

A decrease in the emulsion stability (decrease in ESI value) was observed for heat-pretreated gum solutions. The authors attributed the loss in emulsification activity to the increase in the hydrophilicity of the gum, with more hydroxyl groups exposed to the water. Such a gum will have a lower tendency to adsorb onto the oil phase and will have weaker steric stabilization effects. The chemical nature of this transformation is the subject of further investigation, and intensive scientific work is presently being carried out in our laboratory.

Copyright 2002 by Marcel Dekker. All Rights Reserved.

The main conclusions from the study are that the natural untreated POG hydrocolloid has a good potential to be an efficient emulsifier in food products.

(f) Pectins. Pectins are plant polysaccharides that have been widely used as gelling and thickening agents in the food industry for many years. The prime sources of industrial pectins are apple pomace and the peel of citrus fruits such as oranges, lemons, limes, and grapefruit. Pectins in which the degree of esterification of the galacturonic acid residues is<50% are known as high methoxy pectins. They require the presence of a low pH and a high concentration of sucrose for gelation. Low methoxy pectins, with a degree of esterification of <50%, gel in the presence of calcium by a different mechanism. Sugar beet pectin differs from other pectins because it contains considerable quantities of acetyl groups. The presence of these groups inhibits the gellation of the high methoxy pectin of sugar beets. The deacetylation will cause a rapid gellation effect. Dea and Madden [188] developed a batch process for isolation of acetylated pectins from sugar beet tissue and from sugar beet pulp (see also Garti et al. [189]). A variety of extraction sequences and fractionation procedures were employed; all the extracts were of the pectin polysaccharide type containing 44–60% uronate, 12–22% neutral sugars, 4–6% methoxy, and 2–9% acetyl groups. Many of the extracts were found to have emulsifying capabilities. The extracts were used to emulsify a model oil-in-water system containing 10% groundnut oil. Oil droplets 1 μm in size were obtained, considerably smaller than those obtained with commercial pectins. The emulsions were stable for at least 36 h at 40°C. Recently we managed to extract the active fractions of pectins from citrus piths and peels and obtained totally natural cloudy emulsifiers. The cloudy emulsifiers are selected fractions of surface-active pectins.

(g) Tragacanth. Several early papers dealt with the stabilization of colloidal suspensions by gum tragacanth [190,191], which exhibits excellent stabilization performance even at relatively low concentrations (on the order of 10 ppm). Adsorption isotherms for the binding of gum tragacanth to polystyrene latex spheres were obtained in solutions of different pH values. It was concluded that the gum adsorbs onto the latex particles and that stabilization results from a steric repulsion force controlled by pH.

6. Protein–Polysaccharide Interactions

Protein–polysaccharide interactions play a significant role in the structure and stability of many processed foods [192]. The control of these macromolecular interactions is a key factor in the development of novel food processes and products as well as in the formulation of fabricated products. Much has been written on the possible interaction between the proteins and hydrocolloids in model and real systems, but very little advantage has been taken of these studies in designing

Copyright 2002 by Marcel Dekker. All Rights Reserved.

new amphiphilic molecules based on these associations. The chemically bound structures as well as the hydrogen-bonded structures or even the ion–dipole or dipole–dipole associates form very balanced amphiphilic structures that can be utilized in fabricated emulsions and that can replace the synthetic low molecular weight emulsifiers. These associates will not require special legislation and will have textural and stability advantages. If one can add to that some nutritional or health benefits (and the hydrocolloids have shown such effects), the fabricated emulsions, food products, or food processes will become more attractive to the food producers.

Dickinson et al. [7] claim that the best way to adsorb hydrocolloids onto interfaces is to link them to proteins. Proteins are surface-active materials that consist of flexible hydrophobic and hydrophilic moieties, preferentially adsorbing onto the interfaces and replacing the hydrocolloids from the surface. Tolstoguzov claims that if a hydrocolloid is thermodynamically incompatible with adsorbed protein (Figs. 62 and 63) (see Refs. 193–198) can be distributed at the interface only if it interacts somehow with the protein. Its distribution on the interface will depend on the nature of these interactions. Strong chemical bonds will cause different surface distributions rather than weak associations between the two.

It was also recognized that polysaccharides can interact at the interface with other polymers (nonproteins and other polysaccharides) as well as with groups residing at the protein/water, oil/water, or air/water interface, forming an aqueous structured material with useful viscoelastic mechanical properties under

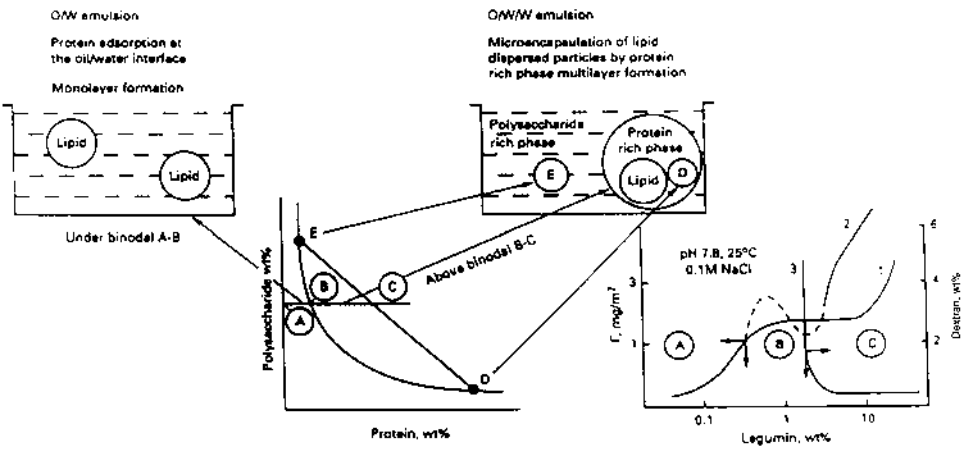

Figure 62 Protein behavior as emulsion stabilizer in the presence of polysaccharides: the effect of thermodynamic incompatibility.

Copyright 2002 by Marcel Dekker. All Rights Reserved.

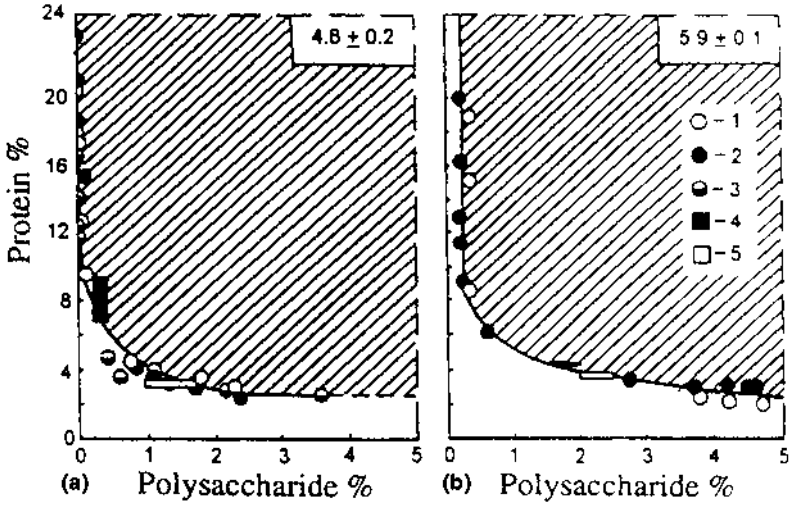

Figure 63 Generalized phase diagrams of some protein (PR) and linear carboxyl-containing polysaccharide (PS)–water systems at (a) pH 9.0, (b) at pH 8–11 (0.1 mol/dm^3 NaOH). PR = SB globulin fraction (a) and casein (b). PS = (○) sodium alginate, (●) carboxymethyl cellulose, and (◒) pectin. Regions of incompatibility are hatched. The regions of localization of critical points and phase separation thresholds are shown as black rectangles and white rectangles, respectively. An average separation threshold in percent is presented at the right upper corner of each diagram. The molecular masses of the polysaccharides are (○) 150, (●) 140, and (◒) kDa. (From Ref. 210.)

conditions of low shear stress. Understanding the detailed chemistry of these polymer–polymer interactions and relating them to the observed rheology is a significant aspect of the study of hydrocolloids.

It is well known that complexation between proteins and polysaccharides at the emulsion droplet surface can improve steric stabilization. Droplet size can be smaller if the polysaccharide is present during homogenization, so the rate of creaming can be reduced as long as there is no bridging flocculation.

Covalent protein–polysaccharide complexation can also provide effective emulsion stabilization. The great improvement in stability arising from the presence of the polysaccharide during emulsification is attributable to the formation of a thicker, stronger steric stabilizing layer around the droplets. Even though both biopolymers carry a net negative charge at pH 7 (BSA–dextran sulfate, 1:3 by weight), a soluble ionic complex can be formed via local electrostatic interaction between the highly charged anionic polymer and positively charged patches on the globular protein. Surface shear viscosity measurements give inde-

Copyright 2002 by Marcel Dekker. All Rights Reserved.

pendent evidence for an interfacial complex between BSA and dextran sulfate [199–201].

It is beyond the scope of this chapter to review the protein–polysaccharide structures.

7. Stabilization by Solid Particles: Colloidal Microcrystalline Cellulose as Emulsifier

The growing concern for personal health and increasing consumer awareness of the importance of a controlled diet in relationship to good health are apparent to most food manufactures. Non-nutritive ingredients that will impart functionality similar to that of their high calorie counterparts are essential in the development of most controlled calorie products. Colloidal microcrystalline cellulose (CMCC, commercially known as Avicel RC-591 or Avicel CL-611) was used in oil-in-water emulsions as a non-nutritive substitute for fat particles [202]. The idea was to use these very small (submicrometer size) solid particles that wet the oil phase as mechanical barriers (known as Pickering stabilizers). The parameters measured included viscosity, yield value, critical stress, flow properties, flow behavior index, and stability index. The result demonstrated that emulsions that incorporate colloidal microcrystalline cellulose have physical properties very similar to those of pure oil-in-water emulsions containing considerably more fat. For example, 20% soy oil with CMCC gave stability behavior and rheological characteristics very similar to those of 60% pure soy oil emulsions without the CMCC, and it is therefore concluded that CMCC is a good emulsifier, stabilizing emulsions in a Pickering mechanism.

It seems that hydrophobic moieties in the hydrocolloid internal structure are not necessary for active adsorption and the formation of a thick birefringent ''get-like'' mechanical barrier onto an oil/water interface.

Nevertheless, hydrocolloids play an important role in stabilizing emulsions when used in conjunction with proteins. The two biopolymers form water-soluble amphiphilic molecules (steric and electrostatic stabilization) or gel-like layers (mechanical barriers) at interfaces.

This new category of naturally occurring hydrocolloid emulsifiers should be reconsidered by food technologists, because these gums can be used instead of some of the synthetic and restricted low molecular weight emulsifiers or chemically modified proteins.

8. Biosurfactants

The term ''biosurfactant'' has been used very loosely to refer to any usable and isolated compound obtained from microorganisms that has some influence on interfaces. Thus, it is used for emulsifying and dispersing agents that do not significantly lower the surface tension of water or exhibit other properties of a

Copyright 2002 by Marcel Dekker. All Rights Reserved.

classical surfactant. Biosurfactants have special advantages over their chemically manufactured counterparts because of their lower toxicity; biodegradable nature; effectiveness at extreme temperatures, pH, and salinity; and ease of synthesis. In addition, they possess surface-active properties differing in many cases from those of synthetic surfactants. Several reviews and monographs have appeared on the properties, chemistry, biosynthesis, and application of biosurfactants [e.g., 203].

Certain hydrocarbon-degrading bacteria and yeast produce appreciable amounts of phospholipids and fatty acids when grown on *n*-alkanes. These surfactants are very interesting from a scientific point of view, and some of them exhibit unique properties including the formation of microemulsions. The structures of two representative phospholipids are shown in Figures 64 and 65. But since the production cost is still very high in comparison to plant (soy) phospholipids, it is difficult to see when these products will become commercially viable.

An interesting example is surfactin, a cyclic lipopeptide, reported first by Armia et al. [204]. It is capable of lowering the surface tension of water to 27.9 mN/m at a concentration of 0.5%. Many similar types of surfactants have been reported and studied. Each has some unique properties and remarkable surface activity. Another interesting surfactant is BL-86, which happens to be a mixture of lipopeptides with the major components ranging in mass from 979 to 1091 Dal. The surfactant is stable at a wide range of pHs and is an excellent emulsifier.

High molecular weight biopolymers generally exhibit useful properties

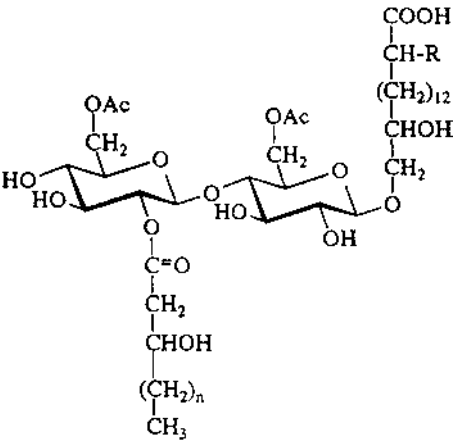

Figure 64 Cellobiose lipid of the corn smut fungus *Ustilago maydis* PRL 119 with R = H or OH and $n = 2$ or 4.

Copyright 2002 by Marcel Dekker. All Rights Reserved.

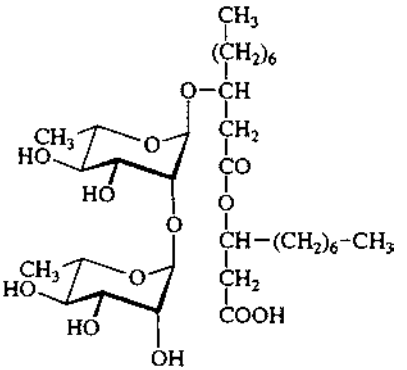

Figure 65 Rhamnose lipid RH1 of *Pseudomonas aeruginosa* DSM 2874.

such as high viscosity, tensile strength, and resistance to shear. Some have found industrial applications. The most studied of these surfactants are surfactin, emulsan, liposan, mannoprotein, and other polysaccharide–protein complexes.

A microbial biopolymer can become a protein look-alike in terms of surface properties if the polysaccharide structure has a large number of hydrophobic side chains attached to the sugar backbone.

The most important microbially derived surfactants are listed in Table 10. In principle, biosurfactants can be used in many food applications. Table 11 lists some important biotechnology products used in the food industry. Some of them are purified end products of fermentation, whereas others are chemically modified.

Emulsan, a microbial biopolymer that has the requisite character to a substantial degree, is an extracellular polysaccharide produced by the oil-degrading bacterium *Acinetobacter calcoaceticus*. RAG-1 was also reported as a naturally occurring surface-active hydrocolloid [205–207]. The biopolymer is called emulsan in recognition of its good emulsifying properties and its strong affinity for the oil/water interface. In part, its emulsifying properties arise from the presence of fatty acids (C_{12}–C_{18}) linked to the amino–sugar backbone of the anionic polysaccharide. Its surface activity is no more than moderate [208], but it exhibits good stabilizing ability for emulsion droplets due to the formation of films that are thick ($\geq$2 nm) and (presumably) viscoelastic. Most important, however, emulsan is known to exist as a complex of lipoheteropolysaccharide (apo-emulsan) and protein. Apo-emulsan, or emulsan treated with proteolytic enzymes, has low surface activity and low emulsifying capacity. The latter is optimized in emulsan samples that contain 5–15% protein, which can be produced by mixing together

Copyright 2002 by Marcel Dekker. All Rights Reserved.

Table 10 Major Types of Biosurfactants Produced by Microorganisms

Biosurfactant type	Producing microbial species
A. Glycolipids	
Trehalose mycolates	*Rhodococcus erythropolis*
	Arthrobacter paraffineus
Trehalose esters	*Mycobacterium phlel*
	Mycobacterium fortitum
	Micromonospora spp.
	Mycobacterium smegmatis
	Mycobacterium paraffinicum
Mycolates of mono-, di-, and trisaccharide	*Rhodococcus erythropolis*
	Corynebacterium diphtheriae
	Mycobacterium smegmatis
Rhamnolipids	*Arthrobacter* spp.
Sophorolipids	*Pseudomonas* spp.
	Torulopsis bombicola
	Torulopsis petrophilum
	Torulopsis apicola
	Candida spp.
B. Phospholipids and fatty acids	
Phospholipids and fatty acids	*Candida* spp.
	Corynebacterium spp.
	Micrococcus spp.
	Acinetobacter spp.
Phospholipids	*Thiobacillus thiooxidans*
	Aspergillus spp.
C. Lipopeptides and lipoproteins	
Gramicidins	*Bacillus brevis*
Polymyxins	*Bacillus polymyxa*
Ornithine-lipid	*Pseudomonas rubescens*
	Thiobacillus thiooxidans
Cerilipin	*Gluconobacter cerinus*
Lysin-lipid	*Agrobacterium tumefaciens*
	Streptomyces sioyaensis
Surfactin, subtilysin	*Bacillus subtilis*
Petide-lipd	*Bacillus licheniformis*
D. Polymeric surfactants	
Lipoheteropolysaccharide	*Arthrobacter calcoaceticus* RAG-1
Heteropolysaccharide	*A. calcoaceticus* A2 Polysaccharide-protein
Polysaccharide-protein	*A. calcoaceticus strains* Manno-protein
Manno-protein	*Candida lipolytica*
	S. cerevisiae
Carbohydrate-protein	*Candida petrophilium*
	Endomycopsis lipolytica
Mannan-lipid complex	*Candida tropicalis*
Mannose/erythrose-lipid	*Shizonella melanogramma*
	Ustilago maydis
Carbohydrate-protein-lipid complex	*Pseudomonas* spp.
	Pseudomonas fluorescens
	Debaryomyces polymorphus
E. Particulate biosurfactants	
Membrane vesicles	*Acinetobacter* sp. H01-N
Fibriae	*A. calcoaceticus*
Whole cells	Variety of microbes

Copyright 2002 by Marcel Dekker. All Rights Reserved.

Table 11 Important Microbial Surfactants and Their Main Products

Surfactant	Producer
Glycolipid	*Arthrobacter* sp.
Glycolipid and/or protein	*Torulopsis petrophilum*
Sophorose lipids	*Torulopsis bombicola*
	Torulopsis apicola
Trehalose dicorynomycolates	*Rhodococcus erythropolis*
Rhamnose lipids	*Pseudomonas* spp.
Sucrose lipids	*Arthrobacter paraffineus*
Fructose lipids	*Arthrobacter paraffineus*
Corynomycolic acids	*Corynebacterium lepus*
Spiculisporic acid	*Penicillium spiculisporum*
Fatty acids, mono- and diglycerides	*Acinetobacter* sp.
Polysaccharide-fatty acid complex	*Candida tropicalis*
''Liposan'' (mostly carbohydrate)	*Candida lipolytica*
Lipoheteropolysaccharide (emulsan)	*Acinetobacter calcoaceticus*
Neutral lipids	*Nocardia erythropolis*
	Corynebacterium salvonicum
Lipoprotein (surfactin)	*Bacillus subtilis*
	Bacillus licheniformis
Peptidolipid	*Candida petrophilum*
Polysaccharide-protein complex	*Corynebacterium hydrocarboclastus*
Whole cell (lipopeptide)	*Acinetobacter calcoaceticus*

protein-rich and deproteinized preparations [207]. The synergistic effect is explained in terms of interfacial tension being lowered by the protein moiety and the stable film formed by the polysaccharide component (MW = 10^6 Da).

IV. CONCLUSIONS

Food colloids and food emulsions are very complex systems consisting of oils, proteins, carbohydrates, and numerous other food ingredients including amphiphilic molecules. Some occur naturally (lecithins, monoglycerides, proteins, and glycolipids), and others are synthetic. Low molecular weight amphiphiles are essential to the stability of food emulsions, foams, and dispersions (beverages, alcoholic emulsions, dressings, margarines, ice cream, etc.). Many natural or manufactured foods are complex micro- and nanostructures in which proteins and polysaccharides are major components.

Much progress has been made in recent years in understanding the texture, rheological properties, and microstructures of food colloids using new and ad-

Copyright 2002 by Marcel Dekker. All Rights Reserved.

vanced techniques. The steric and electrostatic stabilization that amphiphilic macromolecules impart to food emulsions has been elucidated to a great extent. The role hydrocolloids play in stabilizing foods in terms of depletion and steric stabilization was addressed.

The competitive adsorption of different emulsifiers and proteins or hydrocolloids was studied, and it was demonstrated that, with time, the more surface-active surfactant replaces the less active materials.

Health authorities in many countries are constantly enforcing restrictions and limitations on the use of synthetic emulsifiers. As a result, many researchers are constantly looking for new natural sources and amphiphilic molecules to be used in new and advanced food formulations.

The total quantities of surfactants produced in the United States and worldwide in 1999 are estimated at approximately $20 billion and $30 billion US, respectively. Only a small portion of these surfactants is from natural sources.

In spite of the fact that there are so many surfactants, there is great interest in biosurfactants, because they can provide new properties that the classical surfactants are lacking. The U.S. health authorities have so far approved none of the biosurfactants. Some countries, including Japan, do permit the use of some biotechnology products such as the sophorolipids (bakery products), yet the number of countries in which their use is permitted is very limited, and therefore their application is confined to certain cosmetic, pharmaceutical, and industrial applications (oil recovery and oil spillage recovery). However, it must be borne in mind that biosurfactants should be environmentally safe, because they are biodegradable. It is my belief that once the net economic gain becomes clear and the cost performance shows advantages over other surfactants, manufacturers will begin commercial production of biosurfactants.

Chances are slim that new plants or animal tissues rich in emulsifiers as well as major surface-active components will be discovered in the near future, but there are good indications that microbial, algal, and yeast products obtained with improved cultivation and growth techniques and new biosurfactants will be used in future foods.

The aim of every technologist working with food dispersions or food colloids is to be able to select the proper amphiphile for a desired application or, even better, to be able, to design a good blend of emulsifiers and/or stabilizers to achieve the desired stability, texture, rheological properties, and other important characteristics. The aim of the scientists is to provide a good understanding of surfactant activities and capabilities and to be able to predict chemical structure and correlate with surface reactivity.

In spite of the great progress achieved in the last 20 years or so, and in spite of the advanced analytical tools that have been developed, we are still quite far from claiming that we understand the complexity of foods and far from being able to characterize the inter- and intramolecular interactions of surfactants with

Copyright 2002 by Marcel Dekker. All Rights Reserved.

other ingredients. Water and oil are immiscible and difficult to integrate to form stable dispersions. Any additional ingredient will interfere with these dispersions and alter their activity. Surfactant behavior is well understood in simple systems but is difficult to predict for complex systems. It is therefore too ambitious to claim that we can manipulate the surfactant structure and reactivity.

REFERENCES

1. K Esumi, M Ueno, eds. Structure-Performance Relationships in Surfactants. Surfactant Sci Ser. Vol. 70. New York: Marcel Dekker, 1997.
2. DG Dalgleish. In: J Sjöblom, ed. Encyclopedic Handbook of Emulsion Technology. New York: Marcel Dekker, 2001, pp 207–233.
3. MJ Rosen, M Dahanayake. Industrial Utilization of Surfactants: Principles and Practice. Champaign, IL: Am Oil Chem Soc, 2000.
4. RD Bee, P Richmond, J Mingins, eds. Food Colloids. London: Roy Soc Chem 1989.
5. K Larsson, E Friberg, eds. Food Emulsions. New York: Marcel Dekker, 1990.
6. DF Darling, RJ Birkett. In: E Dickinson, ed. Food Emulsions and Foams. London: Roy Soc Chem, 1987, p 1.
7. E Dickinson, BS Murray, G Stainsby. In: E Dickinson, G Stainsby, eds. Advances in Food Emulsions and Foams. London: Elsevier Appl Sci, 1988, pp 123–163.
8. P Walstra. Formation of emulsions. In: P Becher, ed. Encyclopedia of Emulsion Technology, Vol. 1. New York; Marcel Dekker, 1983, p 57.
9. ThF Tadros, B Vincent. In: P Becher, ed. Encyclopedia of Emulsion Technology, Part 1, Vol. 1. New York: Marcel Dekker, 1983, pp 39–70.
10. McCutcheon Division. McCutcheon's Emulsifiers and Detergents. Glen Rock, NJ: MC Pub, 1999.
11. K Shinoda, H Kunieda. In: P Becher, ed. Encyclopedia of Emulsion Technology, Vol 1. New York: Marcel Dekker, 1983, pp 337–367.
12. J Sjoblom, ed. Emulsions and Emulsion Stability. Surfactant Sci. Ser. Vol 61. New York: Marcel Dekker, 1998.
13. AT Florence, D Whitehill. Int J Pharm 11:277, 1982.
14. S Matsumoto, WW Kang. J Dispersion Sci Technol 10:455, 1989.
15. K Shinoda, S Friberg. Emulsions and Double Emulsions. New York: Wiley, 1986, pp 55–81.
16. N Garti, C Bisperink. Curr Opin Colloid Interface Sci 3:657, 1998.
17. N Garti, A Benichou. In: J Sjöblom, ed. Encyclopedic Handbook of Emulsion Technology. New York: Marcel Dekker, 2001, pp 377–407.
18. S Matsumoto. J Texture Stud 17:141, 1986.
19. N Garti. In: M Seiller, JL Grossiord, eds. Multiple Emulsions: Structure, Properties and Applications. Paris: Editions de Sante, 1998, pp 81–116.
20. N Garti, A Aserin. Adv Colloid Interface Sci 65:37, 1996.
21. N Garti, A Benichou. In: J Sjöblom, ed. Encyclopedic Handbook of Emulsion Technology. New York: Marcel Dekker, 2001, pp 377–407.

Copyright 2002 by Marcel Dekker. All Rights Reserved.

22. P Mukerjee. In: KL Mittal, ed. Solubilization and Microemulsions. New York: Plenum Press, 1977, p 171.
23. K Shinoda. Solvent Properties of Surfactants. New York: Marcel Dekker, 1970.
24. TP Hoar, JH Schulman. Nature 152:102, 1943.
25. ThF Tadros. In: KL Mittal, B Lindman, eds. Surfactants in Solution, Vol III. New York: Plenum Press, 1984, pp 1501–1532.
26. PA Winsor. Trans Faraday Soc 44:376, 1984.
27. M Bourrel, RS Schechter. Microemulsions and Related Systems: Formulation, Solvency and Physical Properties. Surfact Sci Seri Vol. 30. New York: Marcel Dekker, 1988, p 127.
28. G Porte. In: WM Gelbart, A Ben-Shaul, D Roux, eds. Micelles, Membranes, Microemulsions and Monolayers. New York: Springer Verlag, 1994, pp 105–151.
29. V Pillai, DO Shah, eds. Dynamic Properties and Association Structures. Champaigns, IL: AOCS Press, 1996.
30. ST Hyde. Langmuir 13:842, 1997.
31. G Porte, J Oberdisse. Colloids Surf A 128:101, 1997.
32. D Roux, CR Safinia, F Nallet. In: WM Gelbart, A Ben-Shaul, D Roux, eds. Micelles, Membranes, Microemulsions and Monolayers. New York: Springer Verlag, 1994, pp 303–346.
33. JM Seddon, RH Templer. In: R Lipowski, E Sackman, eds. Handbook of Biological Physics. Amsterdam: Elsevier, 1995, pp 97–160.
34. JM Seddon. Biochim Biophys Acta 1031:1, 1990.
35. V Luzzati. In: D Chapman, ed. Biological Membranes, Vol. 1. New York: Academic Press, 1968, pp 71–123.
36. GL Kirk, SM Gruner. J Phys 46:761, 1985.
37. SM Gruner, MW Tate, GL Kirk, PTC So, DC Turner, DT Keane, CPS Tilcock, PR Cullis. Biochemistry 27:2853, 1988.
38. Y Hendrikx, J Charvolin. Liq Cryst 3:265, 1988.
39. P-G de Gennes, C Taupin. J Phys Chem 86:2294, 1982.
40. L Ramos, P Fabre. Langmuir 13:862, 1997.
41. JV Selinger, RF Bruisma. Phys Rev A 43:2922, 1991.
42. G Lindblom, L Rilfors. Biochim Biophys Acta 988:221, 1989.
43. K Fontell. Adv Colloid Interface Sci 41:127, 1992.
44. JM Seddon, RH Templer. Phil Trans Roy Soc Lon A 344:377, 1993.
45. V Luzzati, R Vargas, A Gulik, P Mariani, JM Seddon, E Rivas. Biochemistry 31: 279, 1992.
46. V Luzzati, H Delacroix, A Gulik. J Phys II 6:405, 1996.
47. V Luzzati, PA Spegt. Nature 215:701, 1967.
48. SS Funari, G Rapp. J Phys Chem B 101:732, 1997.
49. P Sakya, JM Seddon, RH Templer, RJ Mirkin, GJT Tiddy. Langmuir 13:3706, 1997.
50. S Vauthey, P Visani, Ph Frossard, N Garti, HJ Watzke. J Dispersion Sci Technol 21:263, 2000.
51. L Hernqvist. In: N Garti, K Sato, eds. Crystallization and Polymorphism of Fats and Fatty Acids. New York: Marcel Dekker, 1988, 97.
52. M van den Tempel. SCI (Soc. Chem. Ind.) Monograph 32. London: SCI, 1968, pp 22–33.

Copyright 2002 by Marcel Dekker. All Rights Reserved.

53. N Garti. In: N Garti, K Sato, eds. Crystallization and Polymorphism of Fats and Fatty Acids. Surfactant Sci. Ser. Vol. 31. New York: Marcel Dekker, 1988, p 267.
54. N Garti, J Yano. In: N Garti, K Sato, eds. Crystallization Processes in Fats and Lipid Systems. New York: Marcel Dekker, 2001, pp 211–250.
55. Niiya, T Maruyama, M Imamura, M Okada, T Matsumoto. Jpn J Food Sci Technol 20:182, 1971.
56. J Schlichter-Aronhime, S Sarig, N Garti. J Am Oil Chem Soc 64:529, 1987; 65: 1144, 1988.
57. PR Smith, DJ Cebula, MJW Povey. J Am Oil Chem Soc 71:1367, 1994.
58. PR Smith, MJW Povey. J Am Oil Chem Soc 74:169, 1997.
59. PR Smith. Eur J Lipid Sci Technol 122:2000.
60. TL Harris. SCI Monograph 32. London: SCI, 1968, p 108.
61. S Wahnelt, D Teusel, M Tulsner. Fat Sci Technol 93:117, 1991.
62. S Wahnelt, D Teusel, M Tulsner. Fat Sci Technol 93:174, 1991.
63. NR Easton, DJ Kelly, LR Barton, ST Cross, WC Griffin. Food Technol 6:21, 1952.
64. JW DuRoss, WH Knightly. Proc 19th Conf Pennsylvania Manuf Assoc Conf Sect 15, 1965.
65. JV Ziemba. Food Eng 38:76, 1966.
66. N Garti, J Schlichter, S Sarig. J Am Oil Chem Soc 63:230, 1986.
67. DPJ Moran. Rev Int Choc (RIC) 24:478, 1969.
68. ML Herrera, FJ Marques Rocha. J Am Oil Chem Soc 73:321, 1996.
69. N Kaneko, K Sato. Colloids Surf B 20:229, 2001.
70. H Kunieda, E Ogawa, K Kihara, T Tagawa. Colloid Polym Sci 105:239, 1997.
71. T Katsuragi. In: N Widlak, ed. Physical Properties of Fats, Oils, and Emulsifiers. Champaign, IL: AOCS Press, 2000, p. 209.
72. T Katsuragi, N Kaneko, K Sato. J Jpn Oil Chem Soc (Yakugaku) 49:265, 2000.
73. EH Lucassen-Reynders. PhD Thesis, Agricultural Univ, Wageningen, The Netherlands, 1962.
74. D Johansson, B Bergenstähl. J Am Oil Chem Soc 69:718, 1992.
75. D Johansson, B Bergenstähl. J Am Oil Chem Soc 69:728, 1992.
76. D Johansson, B Bergenstähl, E Lundgren, J Am Oil Chem Soc 72:921, 1995.
77. N Garti, H Binyamin, A Aserin. J Am Oil Chem Soc 75:1825, 1998.
78. N Garti, A Aserin, I Tiunova, H Binyamin. J Am Oil Chem Soc 76:383, 1999.
79. N Garti, D Lichtenberg, T Silberstein. Colloids Surf 128:17, 1997; J Dispersion Sci Technol 20:357, 1999.
80. N Garti. In: NAM Eskin, DS Robinson, eds. Food Shelf Life Stability. Boca Raton, FL: CRC Press, 2001, pp 211–263.
81. GA Reineccius. Encapsulation and Controlled Release of Food Ingredients. ACS Symp Ser Vol 590. Washington, DC: Am Chem Soc, 1995, pp 113–131.
82. JP Cherry. In: BF Szuhaj, GR List, eds. Lecithins. Champaign, IL: Am Oil Chem Soc, 1985, p 57.
83. EJ Weber. In: BF Szuhaj, GR List, eds. Lecithins. Champaign, IL: Am Oil Chem Soc, 1985, p 39.
84. JP Cherry, MS Gray, LA Jones. J Am Oil Chem Soc 58:903, 1981.
85. RK Hommel, C Ratledge. In: N Kosaric, ed. Biosurfactants: Production, Properties and Applications. New York: Marcel Dekker, 1993, pp 3–63.

Copyright 2002 by Marcel Dekker. All Rights Reserved.

86. A Benichou, A Aserin, N Garti. J Dispersion Sci Technol 20:581; 1999.
87. G Charalambous, G Doxastakis. Food Emulsifiers: Chemistry, Technology, Functional Properties and Applications. Dev Food Sci Vol 19. Amsterdam: Elsevier, 1989.
88. RO Feuge, AE Bailey. Oil Soap 23:259, 1946.
89. NS Parker. Properties and functions of stabilizing agents in food emulsions. CRC Crit Rev Food Sci Nutr 25:300, 1987.
90. G Schuster. Emulgatoren fur Lebensmittel. Berlin: Springer-Verlag, 1985.
91. NJ Krog. Cereal Foods World 24:10, 1987.
92. A Meffert. J Am Oil Chem Soc 61:255, 1984.
93. KS Markley. Esters and esterification. In: KS Markley, ed. Fatty Acids: Their Chemistry, Properties and Uses. 2nd ed. Part 2. New York: Interscience, 1961, pp 757–764.
94. J Aronhime, S Sarig, N Garti. Food Struct 9:337, 1990.
95. J Aronhime, S Sarig, N Garti. J Am Oil Chem Soc 65:1140, 1988.
96. RT McIntyre. J Am Oil Chem Soc 56:835A, 1979.
97. VK Babayan, RT McIntyre. J Am Oil Chem Soc 48:307, 1971.
98. N Garti, A Aserin, C Lindner. Baker's Dig 55:19, 1981.
99. N Garti, A Aserin, B Zaidman. J Am Oil Chem Soc 58:878, 1981.
100. N Garti, A Aserin, M Fanun. Colloids Surf A 164:27, 2000.
101. HB Hass, FD Snell, LI Osipow. US Patent 2,893,990 (July 7, 1959).
102. J Colbert, Sugar Esters: Preparation and Applications. Park Ridge, NJ: Noyes Data Corp, 1974.
103. LI Osipow, W Rosenblatt. US Patent 3,644,333 (Feb 22, 1972).
104. RO Feuge, HJ Zeringue Jr, TJ Weiss. US Patent 3,714,144 (Jan. 30, 1973).
105. CC Tsen, EM Peters, T Schaffer, WJ Hoover. Baker's Dig 47:34, 1973.
106. CC Tsen. J Am Oil Chem Soc 51:81, 1974.
107. SE Ebeler, CE Walker, J Food Sci 49:280, 1984.
108. Palsgaard. Technical Memorandum, 1982.
109. HF Bamford, KJ Gardner, GR Howat, AF Thomson. Manuf Confect July: 36, 1970.
110. D Johansson, B Bergenstähl. J Am Oil Chem Soc, 69:705, 1992.
111. PF Fox, JJ Condon. Food Proteins. London: Appl Sci Publ, 1982.
112. E Tornberg, N Ediriweera. In: E Dickinson, ed. Food Emulsions and Foams. London: Royal Soc Chem, 1986, p 52.
113. JL Brash, TA Horbett, eds. Proteins at Interfaces: Physicochemical and Biochemical Studies. ACS Symp Ser 343. Washington, DC: Am Chem Soc 1987.
114. JR Mitchell. In: BJF. Hudson, ed. Development in Food Proteins, Part 4. London: Elsevier Appl Sci, 1982, pp 291–338.
115. G Stainsby. In: JR Mitchell, DA Ledward, eds. Functional Properties of Food Macromolecules. London: Elsevier Appl Sci 1986, p 315.
116. BJF Hudson, ed. Developments in Food Proteins, Vol. 4. New York: Elsevier Appl Sci 1986.
117. E Dickinson, ed. Food Polymers, Gels and Colloids. London: Roy Soc Chem, 1990.
118. JE Kinsella, DM Whitehead. In: E Dickinson, G Stainsby, eds. Advances in Food Emulsions and Foams. London: Elsevier Appl Sci 1988, pp 163–188.

Copyright 2002 by Marcel Dekker. All Rights Reserved.

119. S Arai, M Watanable. In: E Dickinson, G Stainsby, eds. Advances in Food Emulsions and Foams. London: Elsevier Appl Sci, 1988, pp 189–220.
120. PJ Halling. Crit Rev Food Sci Nutr 15:155, 1981.
121. J Mitchell, L Irons, GJ Palmer. Biochim Biophys Acta 200:139, 1970.
122. E Dickinson, DJ Pogson, EW Robson, G Stainsby. Colloids Sur 14:135, 1985.
123. H Mulder, P Walstra. The Milk Fat Globule. Wageningen: Pudoc, 1974.
124. DF Darling, DW Butcher. J Dairy Res 45:197, 1978.
125. E Dickinson, EW Robson, G Stainsby. J Chem Soc Faraday Trans 1 79:2937, 1983.
126. JE Kinsella, DM Whitehead. In: E Dickinson, G Stainsby, eds. Advances in Food Emulsions and Foams. London: Elsevier Appl Sci, 1988, pp 163–188.
127. D Welsby. In: GO Phillips, DJ Wedlock, PA Williams, eds. Gums and Stabilisers for the Food Industry, Vol. 4. Oxford: IRL Press, 1988, pp 355–362.
128. SH Kim, JE Kinsella. J Food Sci 50:1525, 1985.
129. A Kato, S Nakai, Biochim Biophys Acta 624:13, 1980.
130. S Nakai, L Ho, N Helbig, A Kato, MA Tung. Can Inst Food Sci Technol J 13:23, 1980.
131. M Watanabe, S Arai. In: RE Feeney, JR Whitaker, eds. Modification of Proteins: Food Nutritional and Pharmacological Aspects. ACS Adv Chem Ser Vol 198. Washington, DC: Am Chem Soc, 1982, p 199.
132. E Dickinson, G Stainsby, eds. Colloids in Food. London: Appl Sci 1982.
133. E Dickinson, G Stainsby. In: E Dickinson, G Stainsby, eds. Advances in Food Emulsions and Foams. London: Elsevier Appl Sci, 1988, pp 1–45.
134. A Kato, Y Osao, N Matsudomi, K Kobayashi. Agric Biol Chem 47:33, 1983.
135. M Watanabe, S Arai. Emulsifying and foaming properties of enzymatically modified proteins. In: E Dickinson, G Stainsby, eds. Advances in Food Emulsions and Foams. London: Elsevier Appl Sci 1988, pp 189–220.
136. M Watanabe, A Shimada, S Arai. Agric Biol Chem 45:1621, 1981.
137. M Watanabe, A Shimada, E Yazawa, E Kato, S Arai. J Food Sci 46:1738, 1981.
138. N Garti, M Leser. In: DR Karsa, ed. Design and Selection of Performance Surfactants. Annu Surfact Rev, Vol 2. Boca Raton, FL. CRC, 1999, pp 104–166.
139. B Villaudy, G Tilly. In: GO Philips, DJ Wedlock, PA Williams, eds. Gums and Stabilisers for the Food Industry, Vol. 4. Oxford, UK: IRL Press, 1988, pp 309–321.
140. LR Fisher, EE Mitchell. In: RD Bee, P Richmond, J Mingins, eds. Food Colloids. London: Roy Soc Chem, 1989, pp 123–137.
141. V Rosilio, A Baszkin. In: A Baszkin, W Norde, eds. Physical Chemistry of Biological Interfaces. New York: Marcel Dekker, 2000, pp 155–169.
142. E Dickinson. In: GO Phillips, DJ Wedlock, PA Williams, eds. Gums and Stabilisers for the Food Industry, Vol 4. Oxford, UK: IRL Press, 1988, pp 249–263.
143. E Dickinson. In: E Dickinson, D Lorient, eds. Food Macromolecules and Colloids. Cambridge, UK: Royal Soc Chem, 1995, pp 1–19.
144. DF Darling, RJ Birkett. In: E Dickinson, ed. Food Emulsions and Foams. London: Roy Soc Chem, 1987, pp 1–29.
145. S Friberg, K Larsson, eds. Food Emulsions. New York: Marcel Dekker, 1990.
146. RC Randall, GO Phillips, PA Williams. Food Hydrocolloids 2:131, 1988.

Copyright 2002 by Marcel Dekker. All Rights Reserved.

147. M Islam, GO Phillips, A Sljivo, MJ Snowden, PA Williams. Food Hydrocolloids 11:493, 1997.
148. PA Williams, GO Phillips, RC Randall. In: GO Phillips, DJ Wedlock, PA Williams, eds. Gums and Stabilisers for the Food Industry, Vol 5. Oxford, UK: IRL Press, 1990, pp 25–36.
149. CA Street, DMW Anderson. Talanta 30:887, 1983.
150. DMW Anderson. In: GO Phillips, DJ Wedlock, PA Williams, eds. Gums and Stabilisers for the Food Industry, Vol 3. London: Elsevier Appl Sci 1986, pp 79–86.
151. E Dickinson, BS Murray, G Stainsby, DMW Anderson. Food Hydrocolloids 2:477, 1988.
152. SC Churms, EH Merrifield, AM Stephen. Carbohydr Res 123:267, 1983.
153. AM Stephen, SC Churms. In: AM Stephen, ed. Food Polysaccharides and Their Applications. New York: Marcel Dekker, 1995, pp 377–440.
154. E Dickinson, DJ Elverson, BS Murray. Food Hydrocolloids 3:101, 1989.
155. S Connolly, JC Fenyo, MC Vandervelde. Carbohydr Polym 8:23, 1988.
156. M Nakamura. Yakugaku 35:554, 1986.
157. JC Fenyo, MC Vandevelde. In: GO Phillips, DJ Wedlock, PA Williams, eds. Gums and Stabilisers for the Food Industry, Vol 5. Oxford, UK: IRL Press, 1990, pp 17–23.
158. RC Randall, GO Phillips, PA Williams. Food Hydrocolloids 3:65, 1989.
159. E Dickinson, VB Galazka, DMW Anderson, Carbohydr Polym 14:373, 1991.
160. WC Wielinga. In: GO Phillips and PA Williams, eds. Handbook of Hydrocolloids. Cambridge, UK: Woodhead Publishing Ltd., 2000, pp 137–154.
161. B Bergenstähl. In: GO Phillips, DJ Wedlock, PA Williams eds. Gums and Stabilisers for the Food Industry, Vol 4. Oxford, UK: IRL Press, 1988, pp 363–369.
162. B Bergenstähl, S Fogler, P Stenius. In: GO Phillips, DJ Wedlock, PA Williams, eds. Gums and Stabilisers for the Food Industry, Vol. 3. Oxford, UK: IRL Press, 1986, pp 286–295.
163. D Reichman, N Garti. In: E Dickinson, ed. Food Polymers, Gels and Colloids. Cambridge, UK: Roy Soc Chem 1990, pp 549–557.
164. D Reichman, N Garti. In: GO Phillips, DJ Wedlock, PA Williams, eds. Gums and Stabilisers for the Food Industry, Vol. 5. Oxford, UK: IRL Press, 1990, pp 441–446.
165. D Reichman, N Garti. Food Microstruct 12:411, 1993.
166. N Garti, D Reichman. Food Hydrocolloids 8:155, 1994.
167. N Garti, D Reichman. Surface properties and emulsification activity of galactomannans. Proc First World Conf on Emulsions, Paris, 1993, pp 1–11.
168. N Garti. J Dispersion Sci Technol 20:327, 1999.
169. RD Sharma. Nutr Rep Int 30:221, 1984.
170. RD Sharma. Nutr Res 6:1353, 1986.
171. Z Madar, I Shomer. J Agric Food Chem 38: 1535, 1990.
172. K Meiri. PhD Thesis on fenugreek gum: Extraction, characterization and surface properties, Hebrew Univ Jerusalem, Israel, 2000.
173. N Garti, Z Madar, A. Aserin, B Sternheim. Food Sci Technol 30:305, 1997.
174. VB Tolstoguzov. Food Hydrocolloids 4:429, 1991.
175. VB Tolstoguzov. In: GO Phillips, PA Williams, DJ Wedlock, eds. Gums and

Copyright 2002 by Marcel Dekker. All Rights Reserved.

Stabilisers for the Food Industry, Vol 7. Oxford, UK: IRL Press, 1994, pp 115–124.
176. W Liu, T Sato. Carbohydr Res 160:267, 1987.
177. N Garti, A Aserin, L Meiri. New polysaccharides as emulsifiers. Proc 2nd World Cong Emulsions, Bordeaux, 1997, Vol 1, pp 1–17.
178. S Ikegami, PA Williams, GO Phillips. In: GO Phillips, DJ Wedlock, PA Williams, eds. Gums and Stabilisers for the Food Industry, Vol 6. Oxford, UK: IRL Press, 1992, pp 371–377.
179. Y Slavin. New gums as emulsifiers from Portulaca oleracea L. (POG). MSc Thesis, Hebrew Univ Jerusalem, Jerusalem, Israel, 1998.
180. H Rwashda. New gums from Opuntia ficus indica (OFI). MSc Thesis, Hebrew Univ Jerusalem, Jerusalem, Israel, 2000.
181. N Garti, Y Slavin, A Aserin. Food Hydrocolloids 13: 127, 1999.
182. N Garti, Y Slavin, A Aserin. Food Hydrocolloids 13: 139, 1999.
183. N Garti, Y Slavin, A Aserin. Food Hydrocolloids 13:145, 1999.
184. KA Coia, KR Stauffer. J Food Sci 52:166, 1987.
185. AI Mohamed, AS Hussein. Plant Foods Human Nutr 45:1, 1994.
186. ES Amin, SM El-Deeb. Carbohydr Res 56:123, 1977.
187. GE Wenzel, JD Fontana, JBC Correa. Appl Biochem Biotechnol 24/25:341, 1990.
188. ICM Dea, JK Madden. Food Hydrocolloids 1:71, 1986.
189. N Garti, G Agmon, E Pinthus. Israel Patent Appl 123702 (1998).
190. A Yokoyama, KR Srinivasan, HS Fogler. J Colloid Interface Sci 126:141, 1988.
191. M Glicksman. In: M Glicksman, ed. Food Hydrocolloids, Vol II. Boca Raton, FL: CRC Press, 1983, pp 49–60.
192. A Kato, T Sato, K Kobayashi, Agric Biol Chem 53:2147, 1989.
193. VB Tolstoguzov. In: S Damodaran, A Paraf, eds. Protein-Polysaccharide Interactions in Foods and Their Applications. New York: Marcel Dekker, 1997, pp 171–200.
194. VB Tolstoguzov. In: KD Schwenke, R Mothes, eds. Food Proteins, Structure and Functionality. Weinheim: VCH, 1993, pp 203–209.
195. VB Tolstoguzov. In: K Nishinari, E Doi, eds. Food Hydrocolloids: Structure, Properties and Functions. New York: Plenum Press, 1994, pp 327–340.
196. VYa Grinberg, VB Tolstoguzov. Food Hydrocolloids 11:145, 1997.
197. VB Tolstoguzov, VYa Grinberg, AN Gurov. J Agric Food Chem 33:151, 1985.
198. ES Tokaev, AN Gurov, IA Rogov, VB Tolstoguzov. Nahrung 31:825, 1987.
199. E Dickinson. In: GO Phillips, DJ Wedlock, PA Williams, eds. Gums and Stabilisers for the Food Industry, Vol 4. Oxford, UK: IRL Press, 1988, pp 249–263.
200. E Dickinson. In: K Nishinari, E Doi, eds. Food Hydrocolloids: Structure Properties and Functions. New York: Plenum Press, 1993, pp 387–399.
201. E Dickinson, VB Galazka. In: GO Phillips, DJ Wedlock, PA Williams, eds. Gums and Stabilisers for the Food Industry, Vol 6. Oxford, UK: IRL Press, 1992, pp 351–362.
202. EJ McGinley, WR Champion, GO Phillips, PA Williams. In: GO Phillips, DJ Wedlock, PA Williams, eds. Gums and Stabilisers for the Food Industry, Vol 2. Oxford, UK: Pergamon Press, 1985, pp 241–249.
203. JD Desai, AJ Desai. In: N Kosaric, ed. Biosurfactants: Production, Proper-

Copyright 2002 by Marcel Dekker. All Rights Reserved.

ties, Applications. Surfact Sci Ser Vol 48. New York: Marcel Dekker, 1993, pp 65–98.
204. K Arima, A Kakinuma, G Tamura. Biochim Biophys Res Commun 31:488, 1968.
205. DL Gutnick. Biopolymers 26:5223, 1987.
206. Z Zosim, DL Gutnick, E Rosenberg. Biotech Bioeng 24:281, 1982.
207. Z Zosim, E Gutnick, E Rosenberg. Colloid Polym Sci 265:442, 1987.
208. E Rosenberg, C Rubinovitz, A Gottlieb, S Rosenhac, EZ Ron. Appl Environ Microbiol 54:317, 1988.
209. H Kunieda, N Kanei, I Tobita, K Kihara, A Tuki. Colloid Polym Sci 273:584, 1995.
210. VYa Grinberg, VB Tolstoguzov. Food Hydrocolloids 11:145, 1997.

Copyright 2002 by Marcel Dekker. All Rights Reserved.

10
Deodorization

W. Alan Brench
AB Consulting, Hampstead, Maryland

I. INTRODUCTION

In 1869 Mege Mouries, a Frenchman, invented margarine as a substitute for butter, which was in short supply due to the Franco-German war. The product relied on the careful rendering of animal fats to generate fats that were relatively neutral in flavor and odor. Any residual minimal animal flavor associated with the fat was sufficiently reminiscent of butter that it was not perceived as objectionable. With the growth of margarine as an economical alternative to butter the demand for odorless and tasteless animal fats exceeded the supply, leading to interest in the use of vegetable oils in margarine. The major obstacle to their use was the strong natural flavor of oils such as soybean oil and sunflower oil, which can be readily used to distinguish between them. This provided the incentive to generate bland vegetable oils.

Experimental studies showed that it was possible to boil the flavor- and odor-causing components out of the essentially nonvolatile oil but with a severe risk of damaging or burning the oil due to the high temperature employed. In an effort to minimize damage to the oil by lowering processing temperatures, steam was introduced into the distillation as a stripping agent to facilitate the removal of the volatile components. The first application of a modern style deodorization process is attributed to David Wesson [1] who took the existing steam distillation process and added the European practice of operating under vacuum. This allowed further reductions in operating temperatures while minimizing the risks of oxidizing the oil due to air exposure and limiting the level of hydrolysis during

Copyright 2002 by Marcel Dekker. All Rights Reserved.

the stripping process. This improved process allowed the development of cottonseed oil, previously considered to be inedible owing to the presence of highly flavored nontriglyceride components, as a replacement for animal fat in shortenings and liquid oils in the United States and laid the foundation for the current vegetable oil industry.

Long-chain aldehydes and ketones are major contributors to the odoriferous and flavor compounds found in vegetable oils together with breakdown products formed during the thermal decomposition of peroxides caused by exposure of the oil to air. Tracking the large number of odoriferous components found in a crude oil is a major undertaking, and fortunately, from a commercial perspective, it is not necessary, because in general these components exhibit vapor pressures similar to those of the free fatty acids found in vegetable oils that provide a ready marker for the success of the deodorization process. Normally the level of flavor and odor components in an oil prior to deodorization is less than 1000 ppm, and with good handling and refining it can be as low as 200 ppm. Combining this with the human palate's frequent ability to detect such compounds in the 1–10 ppm concentration range, and in some cases the parts per billion (ppb) range, sets a high target for the deodorization process. With normal deodorization practice, by the time the peroxide value of the oil is approaching zero and the free fatty acid level of the oil has been reduced to 0.02%, the majority of the flavor and odor components in the oil have been successfully removed. It must, however, be remembered that the achievement of a low free fatty acid level does not guarantee an acceptable oil flavor, because low levels of air leakage into the deodorizer during processing or high levels of prior oxidative abuse can result in flavor component concentrations that exceed the deodorizer's ability to remove them and generate a bland oil.

By virtue of their geographic location and climate, neither North America nor Europe have any indigenous oilseed crops that generate a solid fat like cocoa butter or palm oil that could be used to provide a hardstock for product formulations. As a consequence, hydrogenation has become the key process for modifying the physical characteristics of vegetable oils. Apart from achieving the desired change in the oil's characteristics, hydrogenation also has a tendency to generate typical off-flavors that are not found in nonhydrogenated oils. Fortunately these flavors are also readily removed by deodorization.

As a by-product of the heat treatment received in the deodorizer, many oils emerge from the deodorizer lighter in color than when they entered owing to the breakdown of pigments, predominantly carotenoids, that are unstable at deodorizer operating temperatures.

In view of the temperatures employed during the deodorization process, the major technical issue associated with the process is to ensure that the hot oil is not exposed to air at any time during the process.

Copyright 2002 by Marcel Dekker. All Rights Reserved.

II. STEAM DISTILLATION THEORY

As the temperature of a liquid mixture is raised, those components of the mixture with the lowest boiling points (and hence highest volatility) evaporate first, leaving behind the less volatile compounds with the higher boiling points. By reducing the pressure of the system the temperature at which the evaporation of the more volatile components occurs can be reduced, although the order in which the components of the mixture distill does not change. The use of an inert (nonreacting) stripping agent effectively enhances the vaporization of the volatile components.

To simplify the derivation of the theoretical description of the deodorization process, assume that an undeodorized oil can be treated simply as a mixture of O moles of a nonvolatile triglyceride and X moles of a volatile component, because the stripping agent, normally steam, is not present in the liquid phase. Assume also that the mixture obeys Raoult's law, i.e., the partial pressure of a component in a mixture is equal to the product of its pure component vapor pressure (P_x) and its mole fraction in the mixture; then

$$P_x = P_x(X/X + O) \tag{1}$$

where P_x is the partial pressure of the volatile component in the mixture. In general the amount of volatile component in the oil represents a very small fraction of the total so that

$$O \gg X$$

and hence

$$O + X \rightarrow O$$

Equation (1) can be simplified for practical purposes to

$$P_x = P_x(X/\mathrm{O}) \tag{2}$$

The vapor phase leaving the deodorizer will comprise only the volatile component and the stripping agent, normally steam, because the triglyceride is effectively nonvolatile. Assuming that the vapor phase leaving the deodorizer obeys Dalton's law, i.e., the molar ratio of the components in the vapor phase will equal the ratio of their partial pressures,

$$\frac{\Delta S}{\Delta X} = \frac{P_s}{P'_x} \tag{3}$$

where ΔS, ΔX are the instantaneous flow rates of steam and the volatile component, respectively, leaving the deodorizer and P_s, P'_x are the partial pressures of the steam and the volatile component at the deodorizer exit. For all practical

Copyright 2002 by Marcel Dekker. All Rights Reserved.

purposes, the partial pressure of the volatile component is very much less than the partial pressure of the steam, so that

$$P'_x \ll P_s$$

and therefore

$$P = P'_x + P_s \rightarrow P_s$$

where P is the total pressure of the system. Equation (3) can thus be modified to give

$$\frac{\Delta S}{\Delta X} = \frac{P}{P'_x} \tag{4}$$

The link between the partial pressure of the volatile component in the liquid phase and the partial pressure of the volatile component in the vapor phase is provided by the mass transfer between the two phases. Classical analysis of gas absorption using the two-film theory [2] shows that the rate of transfer of the volatile component is directly proportional to the difference between the partial pressures of the volatile component in the oil phase and in the steam bubble as follows:

$$\frac{dP'_x}{dt} = kA(P'_x - P_x) \tag{5}$$

where A is the interfacial area of the steam bubbles, k the mass transfer diffusion coefficient, and t the time of contact between the steam bubble and the oil. Given that the duration of the deodorization process is much greater than the mass transfer process in a single bubble, it can be assumed that P_x remains approximately constant during the transfer of volatile component from the oil to the bubble, and Eq. (5) can be integrated to yield

$$kAt = \ln\left[\frac{P'_x}{P_x}\right] \tag{6}$$

Frequently a vaporization efficiency, E, is defined as the ratio of vapor-phase to liquid-phase partial pressures:

$$E = \frac{P'_x}{P_x} \tag{7}$$

which on substitution into Eq. (6) and rearrangement yields

$$E = 1 - e^{-Akt} \tag{8}$$

Copyright 2002 by Marcel Dekker. All Rights Reserved.

Hence as the interfacial area or the length of contact time between the bubble and the oil is increased, the vaporization efficiency increases and the vapor-phase partial pressure of the volatile component approaches the value in equilibrium with the liquid phase. Batch deodorizer studies [3] have suggested that practical values for the vaporization efficiency are in the range of 0.7–0.9, which is consistent with values for steam distillation in other industries.

By assuming that the vaporization efficiency is approximately constant for a given oil–volatile component mixture and a given deodorizer design, the concept of the vaporization coefficient can be combined with Eq. (2) to yield

$$P'_x = \frac{EXP_x}{O} \tag{9}$$

which, when taken with Eq. (4) in the limit, generates

$$\frac{dS}{dX} = \frac{PO}{EXP_x} \tag{10}$$

On integration, Eq. (10) shows that steam consumption is proportional to the concentration reduction achieved in the volatile component:

$$S \propto \ln(X_1/X_2) \tag{11}$$

such that for every order-of-magnitude reduction in the volatile component concentration the steam consumption doubles.

The above analysis, by making use of Raoult's and Dalton's laws, is really applicable only to ideal solutions, which are defined as solutions in which all the molecules interact in the same way. In practical real solutions, the oil and the volatile components differ significantly in chemical structure, which influences their molecular interactions, particularly at low concentrations. Following classical chemical engineering approaches, departures from ideality have been compensated for by introducing an activity coefficient, γ, into Eq. (10) so that it becomes

$$\frac{dS}{dX} = \frac{PO}{EXP_x\gamma} \tag{12}$$

III. NON-IDEAL SOLUTION BEHAVIOR

Detailed descriptions of the thermodynamics of phase equilibrium can be found in a number of standard texts [4]. In principle, equations of state can be used for the calculation of both liquid- and gas-phase properties, but in practice they have found application only in systems comprising nonpolar, nonassociating compounds of low molecular weight such as hydrocarbons and fluorocarbons. For

Copyright 2002 by Marcel Dekker. All Rights Reserved.

real systems, use is made of the thermodynamic excess functions, whose derivation can again be found in a number of standard thermodynamics texts [5]. The excess function of major importance for engineering calculations is the excess Gibbs function, G^E, because its canonical variables of temperature T, pressure P, and composition n figure prominently in design calculations. Given the excess Gibbs function as a function of temperature, pressure, and composition, activity coefficients for component i can be computed from

$$\ln \gamma_i = \left[\frac{d(nG^E/RT)}{dn_i} \right]_{T,P,nj \neq i} \tag{13}$$

where R is the ideal gas constant. Many expressions have been proposed for the excess Gibbs function, but only a handful have found general applicability in the chemical process industries, notably the equations of Margules [6], Van Laar [7], and Wilson [8].

The major application of these equations is frequently found to be in the realm of data correlation rather than prediction, and then mostly in systems of interest to the petrochemical industry with relatively low molecular weight compounds. In the typical deodorization mixture, the volatile component is likely to be a compound with a molecular weight of approximately 200 and a relatively active ketone or aldehyde functional group, while the oil has a molecular weight approaching 900 and predominantly inert ester functional groups. The disparity in molecular size means that this type of system will show both energy interactions and entropy of mixing effects at the molecular level, which the most common of the foregoing equations do not handle well.

One model that has found applicability in the lipids area is the ''regular solution'' theory developed by Hildebrand and Scott [9] and Scatchard [10]. Incorporating a partial molar entropy of mixing term [11–14] into the regular solution theory yields the following expression for the activity of a component a_1 in a liquid mixture:

$$\ln \alpha_1 = \ln \phi_1 + \phi_2 \left(1 - \frac{V_1}{V_2} \right) + V_2 \phi_2^2 \frac{(\delta_1 - \delta_2)^2}{RT} \tag{14}$$

where δ_i is the solubility parameter of component i, V_i is the molar volume of component i, and ϕ_i is volume fraction of component i, given by $\phi_i = x_i V_i/(x_1 V_1 + x_2 V_2)$; with x_i, being the mole fraction of component i.

At very low concentrations of the volatile component, Eq. (14) can be simplified to yield the infinite dilution activity coefficient, γ_1^∞,

$$\ln \gamma_1^\infty = 1 + \ln \left(\frac{V_1}{V_2} \right) - \frac{V_1}{V_2 + V_2} + \frac{(\delta_1 - \delta_2)^2}{RT} \tag{15}$$

Copyright 2002 by Marcel Dekker. All Rights Reserved.

Hence, with a knowledge of the molar volume of a compound and its solubility parameter it is possible to predict the value of its activity coefficient or infinite dilution activity coefficient directly.

Practical attempts at using these equations in the paint industry [15–17] have shown that it is appropriate to replace the solubility parameter term with an expanded set of solubility parameters covering dispersion forces, $\delta_{D,i}$, polar dipole interactions, $\delta_{P,i}$, and hydrogen bond interactions, $\delta_{H,i}$, such that

$$\ln \alpha_1 = \ln \phi_1 + \phi_2\left(1 - \frac{V_1}{V_2}\right) + V_2\phi_2^2 \frac{(\delta_{D,1} - \delta_{D,2})^2 + A(\delta_{P,1} - \delta_{P,2})^2 + (\delta_{H,1} - \delta_{H,2})^2}{RT}$$

where A is a weighting parameter with a value of approximately 0.2–0.25.

Solubility parameters for many common compounds can be found in the literature [16,18,19], and it has been further demonstrated that the solubility parameters for a given compound can be reasonably estimated on the basis of group contributions and a knowledge of the structure of the molecule [20,21]. Adopting this approach for lipid-based systems has proved to be very successful not only in forecasting vapor–liquid equilibrium data but also for selecting the solvent in liquid–liquid extraction [22] and for solid–liquid equilibrium in fractionation.

The regular solution model approach is very similar to the UNIFAC model developed by Fredenslund et al. [23,24], where the interactions between molecules are estimated on the basis of the groups present in each molecule. Extensive tables of interaction parameters [24,25] for vapor–liquid equilibrium data prediction are well developed, and the method has found applicability in the modeling of deodorizer performance [26].

The practical determination of activity coefficients for the volatile components in vegetable oils under normal processing conditions is extremely difficult, and very few data have been reported in the literature. Activity coefficients for free fatty acids have been variously reported, ranging from 0.6 to 1.5 at very low concentrations [27,28], but exact processing conditions and liquid-phase compositions make it difficult to interpret the data.

IV. TYPICAL DEODORIZATION CONDITIONS

The temperature of the oil during steaming is the most critical process parameter during deodorization, and if the temperature falls below 340°F (170°C) very little deodorization actually occurs. For batch deodorization the typical operating temperature ranges from 360 to 465°F (180–240°C). For semicontinuous deodorizers

Copyright 2002 by Marcel Dekker. All Rights Reserved.

typical operating temperatures fall between 430 and 465°F (220–240°C), with an upper limit of 520°F (270°C) to facilitate heat bleaching of the oil or the recovery of valuable by-products such as tocopherols and sterols. The use of very high temperatures for deodorization can have a detrimental effect on oil quality and is economically attractive only if the equipment includes a heat recovery system. Current commercial semicontinuous deodorizers routinely have a heat recovery efficiency of approximately 50%.

Typical headspace pressures range from just below 2 torr to around 6 torr in normal commercial practice. The headspace pressure is a function of the condenser temperature, with the lower pressures requiring either the use of chilled water in the condenser barometric leg or a cryogenic cooling system.

As the temperature of the deodorization is varied, the volatility of the components to be removed varies and hence influences the quantity of steam required to achieve the desired reduction in volatile component concentration. Changing the headspace pressure has the effect of changing the volume of steam flowing into the deodorizer, impacting the interfacial area, etc., thus influencing the stripping performance. Typically with deodorization conditions of 450°F (230°C) and a headspace pressure of 4 torr the steaming rate is approximately 2% (w/w on oil). During deodorization the added steam not only provides the stripping media but also provides the mixing vehicle for the oil.

V. REMOVAL OF FREE FATTY ACIDS

Of the volatile components present in vegetable oils the mostly readily identified and most easily measured is the free fatty acid, which has been widely used to monitor deodorizer performance and confirm the validity of the theoretical analysis. Provided mass transfer is not limiting during the deodorization process, which is normally the case for free fatty acid removal, Eq. (11) shows that the reduction of a free fatty acid during deodorization is a logarithmic function of the amount of stripping steam used. Practical studies of free fatty acid reduction during deodorization have confirmed the validity of this expression, where deviations from ideal behavior are low. As a consequence of this logarithmic relationship, deodorization requires the same amount of stripping steam to reduce the free fatty acid content of an oil from 2% to 1% as to reduce it from 0.2% to 0.1%. Further, this gives each deodorizer a finite ability to reduce the level of a volatile component under a given set of processing conditions, with the following implications:

1. Input oil quality can significantly affect the quality of the final oil.
2. The final oil will always contain a residual level of the volatile component.

Copyright 2002 by Marcel Dekker. All Rights Reserved.

In the latter case, in practice, the free fatty acid content of deodorized oil never falls below 0.005% because of the very low level of hydrolysis that occurs under deodorizer conditions due to the presence of the stripping steam [29].

In comparing the performance of a deodorizer in removing the free fatty acids from a number of different oils, the nature of the free fatty acid has a major impact on the reduction factor achieved, because the volatility of a free fatty acid is a function of its molecular weight. Consequently, under the same processing conditions, palm kernel oil and coconut oil will achieve the highest free fatty acid reduction factors due to the presence of the short-chain fatty acids whereas fish oils will achieve the lowest due to the long-chain acids present. Soybean, sunflower, and canola (rapeseed) oils all tend to exhibit approximately the same free fatty acid reduction factors, because they all comprise predominantly 18-carbon fatty acids, whereas palm oil, with its high level of palmitic acid, exhibits a slightly higher one.

VI. REMOVAL OF OTHER COMPONENTS

In addition to free fatty acids, a number of other compounds present in vegetable oils are influenced by the deodorization process either as a result of the stripping process or due to chemical reaction under the stripping conditions, as summarized in Table 1.

Table 1 Minor Component Removal

Physical Removal	
Odor compounds:	reduced to acceptable levels
Tocopherols:	partially removed
Sterols:	partially removed
Methyl/ethyl esters:	almost completely removed
Antioxidants (BHA, BHT):	completely removed
Pesticides:	partially removed
Polycyclic aromatic hydrocarbons:	partially removed
Monoglycerides:	partially removed
Chemical Reaction	
Oxidized fatty acids:	partially decomposed
Carotene:	partially decomposed
Hydroperoxides:	partially decomposed
Soaps:	completely decomposed
Unsaturated fatty acids:	some cis/trans isomerization

Copyright 2002 by Marcel Dekker. All Rights Reserved.

The important compounds in the volatile odor group are the aldehydes, which either occur naturally in oils or are formed by the breakdown of hydroperoxides, etc., during the deodorization process. The human palate varies in its sensitivity to these compounds, with detection levels ranging from parts per billion to several parts per million depending on both the compound and the individual. Under normal processing conditions, reduction factors achieved for this group of compounds typically range from 10^4 to 10^5 (A. Brench, unpublished).

Today organochloride pesticides are frequently detected in crude vegetable oils and persist in the oil through conventional refining until the oil is deodorized. Precise information on the removal of pesticides by deodorization is difficult to locate because of the range of compounds employed as pesticides and their low initial levels, but in general it appears that pesticide levels are reduced by approximately 70% (a reduction factor of 2–4) under typical batch deodorization conditions (A. Brench, unpublished). Conventional semicontinuous deodorization normally reduces pesticide levels to below their detection limits, and as a consequence pesticide analysis is routinely carried out on batches of oil only on a random basis or when there are grounds for concern about the initial exposure to a pesticide. Local regulations will normally stipulate both which pesticides can be used on a crop and local requirements for pesticide residues in finished products. Pesticides removed from an oil during deodorization will concentrate in the deodorizer distillate recovered from the deodorizer condenser system, with possible implications for the value of products derived from this source.

Among the products found in the deodorizer distillate are tocopherols and phytosterols. The latter have recently found use in margarines and spreads in view of their role in hindering the adsorption of cholesterol by the human metabolism [30]. Tocopherols, normally recovered from soybean oil distillate, are a natural source of antioxidants and vitamin E. Typically tocopherol losses during deodorization at 450°F (230°C) will be of the order of 10%, although the amount can be increased by changing deodorizer conditions. There is, however, a limit to how much tocopherol can be stripped from soybean oil before its shelf life begins to deteriorate. Under normal processing conditions a good deodorized soybean oil will contain approximately 900–1000 ppm tocopherol (A. Brench, unpublished).

Polycyclic aromatic hydrocarbons (PAHs) are sometimes found as contaminants in vegetable oils, chiefly in coconut oil and occasionally in canola (rapeseed) and sunflower oils. The exact origin of this contamination is not clear, but it may stem from the exposure of seeds, during drying, to combustion gases. These compounds have been implicated in some studies [31] as carcinogenic agents, and as a consequence, reductions in their concentration in oils is desirable. Deodorization under typical conditions, 450°F (230°C), will remove approximately 80% of the ''light'' PAH compounds consisting of four condensed aromatic rings or less (A. Brench, unpublished). The ''heavy'' PAH compounds

Copyright 2002 by Marcel Dekker. All Rights Reserved.

consisting of five or more condensed aromatic rings are not volatile under normal deodorizer conditions and thus have to be removed by using carbon treatment.

The elevated temperatures used during deodorization are sufficient to initiate some chemical reactions both on the oil and on some of its minor components. Hydroperoxides, frequently the precursors of off-flavor development, are completely broken down during the deodorization process, so the peroxide value of a freshly deodorized oil is zero. Values other than zero frequently indicate the presence of a small air leak in the equipment, normally in the post-deodorization cooling stages. Volatile products of this thermal decomposition are normally stripped from the oil during the deodorization process, but any nonvolatile fragments will stay with the finished oil, possibly with detrimental effects on its quality.

The high temperature exposure of the oil during deodorization may also impact its color either positively or negatively. If the undeodorized oil contains a significant level of phosphatides, these will break down during the deodorization process, which has an adverse effect on the oil color. In the case of palm oil, however, its bright orange color due to the presence of carotenoids is reduced during the deodorization process owing to the thermal decomposition of these compounds. Normally deodorization above 430°F (220°C) is necessary to trigger the color reduction, and the extent of heat bleaching can be manipulated via the deodorizer temperature and oil residence time. However, chlorophyll, which generates the green color in many oils, is thermally stable in the deodorizer, thus requiring removal by bleaching. Color reversion can be a problem with some oils during deodorization if the initial pretreatment was inadequate.

In terms of the oil itself, above 470°F (240°C) the triglycerides and the fatty acids in them begin to become reactive. With palm oil, cocoa butter, and some of the more exotic tropical oils such as illipe fat and shea butter, some interesterification may occur, possibly catalyzed by residual soap in the oils or the elevated levels of partial glycerides found naturally in these oils. This interesterification adversely affects the melting characteristics of the oils and their application as cocoa butter replacers and extenders.

With the individual fatty acids present in the triglyceride molecules some dimerization does occur with oils that contain very high levels of polyunsaturated fatty acids Typically, however, the level of dimers, from this source, in an oil will be less than 1% (A. Brench, unpublished). Of more recent interest with FDA regulations pending in the United States on the nutritional labeling of trans fatty acids [32] is the generation of trans fatty acids in the deodorizer. Under typical processing conditions, neutralized, bleached, deodorized soybean oil with a 1–2% trans fatty acid level can be regularly obtained, although levels as high as 6.4% trans fatty acid have been recorded, particularly where extensive stripping of tocopherols has taken place. By careful management of, primarily, deodorizer temperature, it is possible to generate neutralized and bleached deodorized oils—

Copyright 2002 by Marcel Dekker. All Rights Reserved.

soybean, canola (rapeseed), and sunflower—with trans fatty acid levels consistently below 1%. Of these three oils, extensive monitoring suggests that canola (rapeseed) oil may present the biggest challenge in keeping the trans fatty acid level below 1% (A. Brench, unpublished).

VII. EQUIPMENT DESIGN AND CONFIGURATION

As a consequence of the processing conditions required during deodorization, the design of the overall process must consider the following critical issues:

1. The generation of the required vacuum
2. The recovery of deodorizer distillate
3. The heating and cooling of the oil to deodorization temperatures
4. The source and supply of the stripping agent
5. Protection of the oil from oxidation at the elevated process temperatures

Current deodorizer installations around the world use, almost exclusively, multistage steam ejectors equipped with barometric intercondensers to generate the necessary vacuum. The design and operation of such units are well documented [33]. The alternative use of a conventional heat exchanger as a condenser and a mechanical vacuum pump is not standard practice owing to the tendency for the fatty material stripped from the oil to condense and solidify, thus fouling the heat exchanger surface and contaminating the pump's lubricating system. Under normal operating conditions a three-stage ejector system is capable of generating a deodorizer working pressure of 5–6 torr, whereas a four-stage system is necessary to achieve a pressure below 3 torr. Purely from an oil quality perspective, there is little advantage in operating below this pressure, but in view of the increasing value of the distillate there is a trend toward pressures of 1–2 torr to achieve higher yields of distillate without increasing the exposure of the oil to the deleterious effects of higher temperatures. This places greater demand on the available cooling source, and there is a move toward the use of cryogenic systems.

Initially deodorizer distillate was not captured during the deodorization process but simply allowed to escape from the plant when the steam and fatty material in it were condensed by using direct contact with cooling water before discharge to the environment. With increasing restrictions on the discharge of organic material to the environment and the recognition that distillate could yield valuable compounds such as tocopherols and sterols, current equipment designs have moved to closed-circuit cooling systems and separate distillate recovery operations. Most deodorizer designs now make use of condensed distillate as the scrubbing liquid to cool and condense the volatiles and entrained oil leaving the

Copyright 2002 by Marcel Dekker. All Rights Reserved.

deodorizer. This is normally carried out in either a spray tower or a packed column using liquid distillate at approximately 140°F (60°C) to avoid condensing the stripping steam. Distillate recovery efficiencies of approximately 95% can be achieved together with a tocopherol content of 10%. In designing the scrubbing system the most critical parameter is the pressure drop over the unit. The lowest pressure drop is achieved by using simple spray condensers in conjunction with cyclone entrainment traps, at the expense, however, of some decrease in distillate recovery. Higher recovery efficiencies are achieved with an acceptable pressure drop by using the current generation of tower packings, particularly the highly efficient structured packings specifically designed for vacuum use. The ultimate decision, however, on whether the distillate can be used for edible purposes will depend on whether it is free of pesticides, which the recovery system does not preferentially remove from the distillate.

With typical deodorization temperatures in the region of 500°F (260°C), preheating the oil is beyond the range of most factory steam supplies [10 atm pressure, 365°F (185°C)]. Typically this has been overcome in the United States by using a vapor-phase heat transfer medium such as Dowtherm A or Therminol VP-1 that allows the elevated temperatures to be achieved without the need to invest in high pressure equipment. In Europe the practice has been to retain steam as the heat transfer medium, accepting the higher investment for boilers and heat exchangers that can withstand the 900 psig pressure generated by steam at 535°F (260°C). Most recent deodorizer installations in the United States, however, have switched to the European practice of using high pressure steam, possibly as a result of concern over the possible impact of contaminating the vegetable oil with heat transfer fluid. The Japanese banned the use of Dowtherm A as a result of an alleged contamination incident in 1973 [34], and materials containing are chlorinated biphenyl compounds no longer acceptable in the United States as heat transfer fluids. Where concern over the use of a heat transfer medium is expressed, the use of level controls and records of heat transfer medium purchase combined with customer audits have been used to confirm the absence of the medium in deodorized oil and the existence of acceptable procedures to give early warning of leaks.

In view of the susceptibility of vegetable oils to oxidation at deodorizer temperatures, the stripping steam must be dry and free of oxygen. This is achieved by deaerating the feed water and generating superheated steam to ensure the availability of dry stream at the deodorizer. The latter requirement is less critical for semicontinuous and continuous operations than for batch ones, where it may have a cooling effect on the oil. Because most boiler systems generate water solids, it is essential that the carryover of these solids into the steam be prevented if mineral contamination of the oil is to be avoided.

The extreme processing temperatures used during the deodorization of vegetable oils mean that any contact between the hot oil and air will lead to very

Copyright 2002 by Marcel Dekker. All Rights Reserved.

rapid oxidation of the oil. To minimize the risks of accidental exposure to air via leaks, a number of commercial deodorizer designs use double-shelled vessels. In comparing single- and double-shelled deodorizers (see Fig. 1), the double-shell system not only reduces the impact of air leaks but also minimizes refluxing on the vessel walls, reduces the vessel insulation requirements, and provides protection against the thermal stresses resulting from semicontinuous operations. The current trend, however, is to install single-shell vessels in view of their lower investment cost and manage the vapor flow to minimize reflux issues. Air leaks at seals, valves, etc., are contained by having the potential leak points above the oil surface and removing any entering air via the vacuum system before it contacts the oil and can initiate a reaction. Stainless steel is normally the construction material of choice, because at deodorization temperatures iron can act as an oxidation catalyst. This is less critical for batch deodorization, where the processing temperatures are typically lower than for the semicontinuous and continuous alternatives, and frequently iron vessels are employed with a layer of polymerized

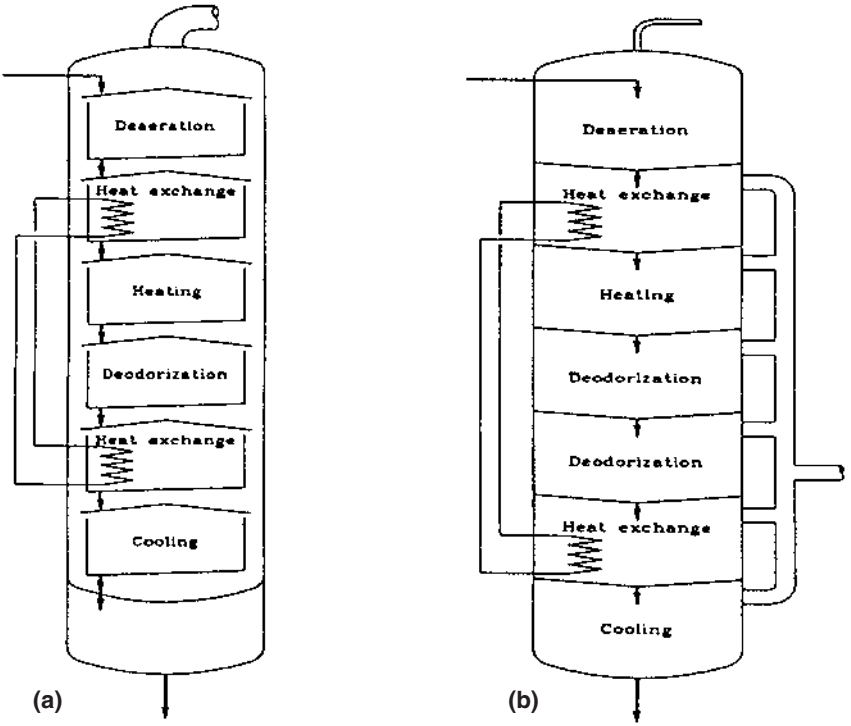

Figure 1 (a) Double-shell and (b) single-shell designs for deodorizer vessels.

Copyright 2002 by Marcel Dekker. All Rights Reserved.

oil providing an inert surface. Because incoming oil can contain up to 2.5% dissolved oxygen it must be deaerated before the oil is heated above 250°F (120°C). Typically a well-designed deaerator using a low level of stripping steam can provide an oil supply for the deodorizer that contains 0.05% oxygen or less.

The critical factor in the design, construction, and operation of a deodorizer will, however, be the flavor of the oil it produces. Air leaks bad enough to influence the flavor of the oil are frequently so small that they cannot be detected by the system's pressure-measuring systems, and reliance is normally placed on oil tasting. Normal deodorization practice to preserve the quality of the oil includes adding 0.005–0.01% of citric acid to the freshly deodorized oil to deactivate any metals present. This addition is frequently carried out as soon as the oil temperature falls below 300°F (150°C) to prevent decomposition of the citric acid. Where legally allowed and relevant to the final use of the oil, antioxidants such as TBHQ and natural tocopherols may be added to the freshly deodorized oil to enhance its stability.

As a matter of good manufacturing practice (GMP), deodorized oils are normally stored and subsequently handled under a nitrogen blanket to minimize further opportunities for oxidation and off-flavor development. The preferred method of generating this inert blanket is to inject the nitrogen directly into the oil by using metal sinters in the piping system and allow the nitrogen escaping from the oil to generate the inert atmosphere in the storage tanks.

VIII. DEODORIZER CHARACTERISTICS

A number of engineering firms around the world design and manufacture deodorizers to meet the needs of the vegetable oil industry, in many instances offering unique equipment designs, detailed descriptions of which can be readily found in the literature [35]. The following sections summarize the general characteristics of the three classes of deodorizers: batch, semicontinuous, and continuous.

A. Batch Deodorizers

Batch deodorization is best suited to low capacity plants where the flexibility of the process can be exploited to handle a multiplicity of oil products with minimal cross-contamination. Vessel oil capacities range from 25,000 to 50,000 lb, and overall refinery throughput will typically be on the order of 250,000 lb/day. The typical issues associated with this type of installation are the high steam usage occasioned by the continual need to reheat the equipment, the poor opportunities for heat recovery, and the peak demands on services that operating a number of batch units in parallel can develop.

Copyright 2002 by Marcel Dekker. All Rights Reserved.

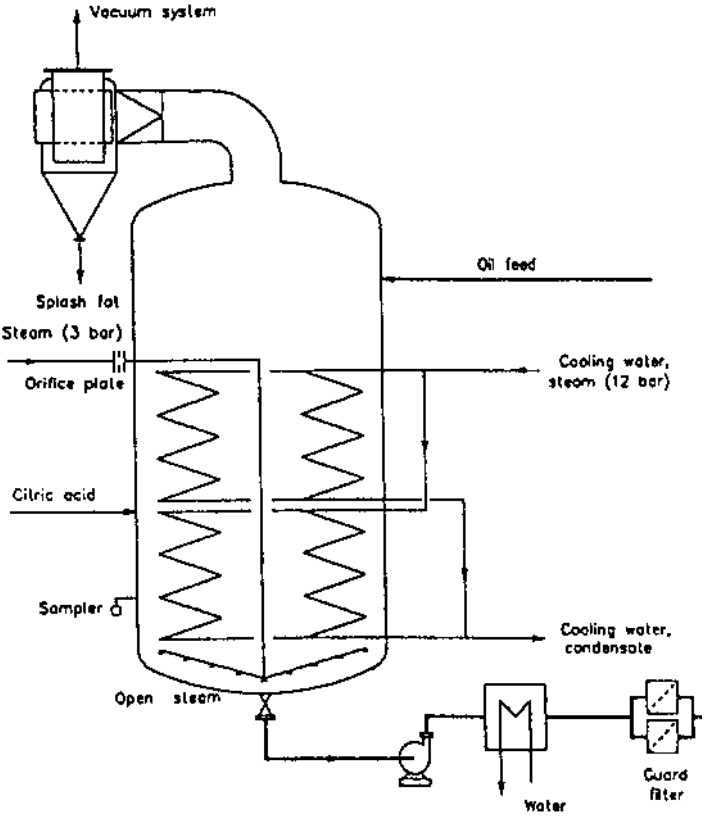

Figure 2 Batch deodorizer.

Figure 2 shows the typical design for a batch deodorizer. The vessel height is approximately two to three times the vessel diameter to provide sufficient volume for de-entrainment of oil droplets from the gas stream. Strategically located baffles and/or packing are also used to enhance the removal of oil droplets from the gas stream. The stripping steam is normally introduced into the vessel via a circular sparger ring located at the bottom of the deodorizer. An alternative approach, drawn from the field of fermenter design, uses a gas lift tube in the center of the vessel to force the oil to circulate, continually pumping it back to the stripping steam injection point to increase the efficiency of the process.

Heating and cooling of a batch deodorizer are normally achieved by way of either internal coils or external forced circulation heat exchangers. The latter

Copyright 2002 by Marcel Dekker. All Rights Reserved.

option offers the quickest process route and facilitates cleaning of the vessel and equipment but does suffer from enhanced opportunities for cross-contamination. The refluxing of distillate that condenses on the upper walls of the vessel and runs back into the oil can be an issue, again due to the continual heating and cooling of the vessel with each batch. Current practice to minimize this effect involves insulating the vessel and possibly externally heating the upper sections of the vessel. The batch nature of the operation makes heat recovery very difficult without resorting to significant investment to hold up either the incoming or outgoing oil stream.

In general, batch deodorizers have a typical turnaround time of approximately 8 h, with the oil being subjected to approximately 4 h of stripping.

B. Semicontinuous Deodorizers

Effectively a semicontinuous deodorizer can be considered as a number of batch operations interlinked to handle a larger throughput than can be processed by the individual batch units. The strong point of the design is that it can readily handle changes in feedstocks while minimizing cross-contamination. Figures 3 and 4 show a conventional vertically arranged unit and a less common horizontal one, respectively.

A preweighed batch of oil is moved through the deodorizer from section to section after preset timed intervals, being deaerated, heated, deodorized, and cooled, all under vacuum, in the sequential compartments. Typically the liquid level in each compartment ranges from 1 to 3 ft (0.3–0.8 m) with a holding time in each compartment of 15–30 min. The actual exposure of the oil to high temperatures depends on the number of deodorizing trays or compartments and the heating and cooling capability of the unit and could effectively be up to 60 min.

Heat recovery is achieved by using a thermosyphon system between the heating and cooling compartments, with distilled water as the carrying fluid. Steam is injected in a manner similar to that used in the batch process, primarily in the deodorization compartment, although a low level may be added in the deaeration section to aid in the removal of air. In the horizontal configuration some steam may be used for agitation in the heating and cooling sections.

The semicontinuous deodorizer possesses a number of advantages over the truly continuous unit. By virtue of its discontinuous operation, the location of a batch of oil is always discretely known, which aids product changeovers and minimizes cross-contamination, particularly if blank or empty trays are used in the processing cycle to segregate batches of oil. The major disadvantages of the semicontinuous deodorizer compared to its continuous counterpart are its higher investment cost and complexity, its poorer heat recovery performance, and its higher steam consumption due to the agitation requirement.

Copyright 2002 by Marcel Dekker. All Rights Reserved.

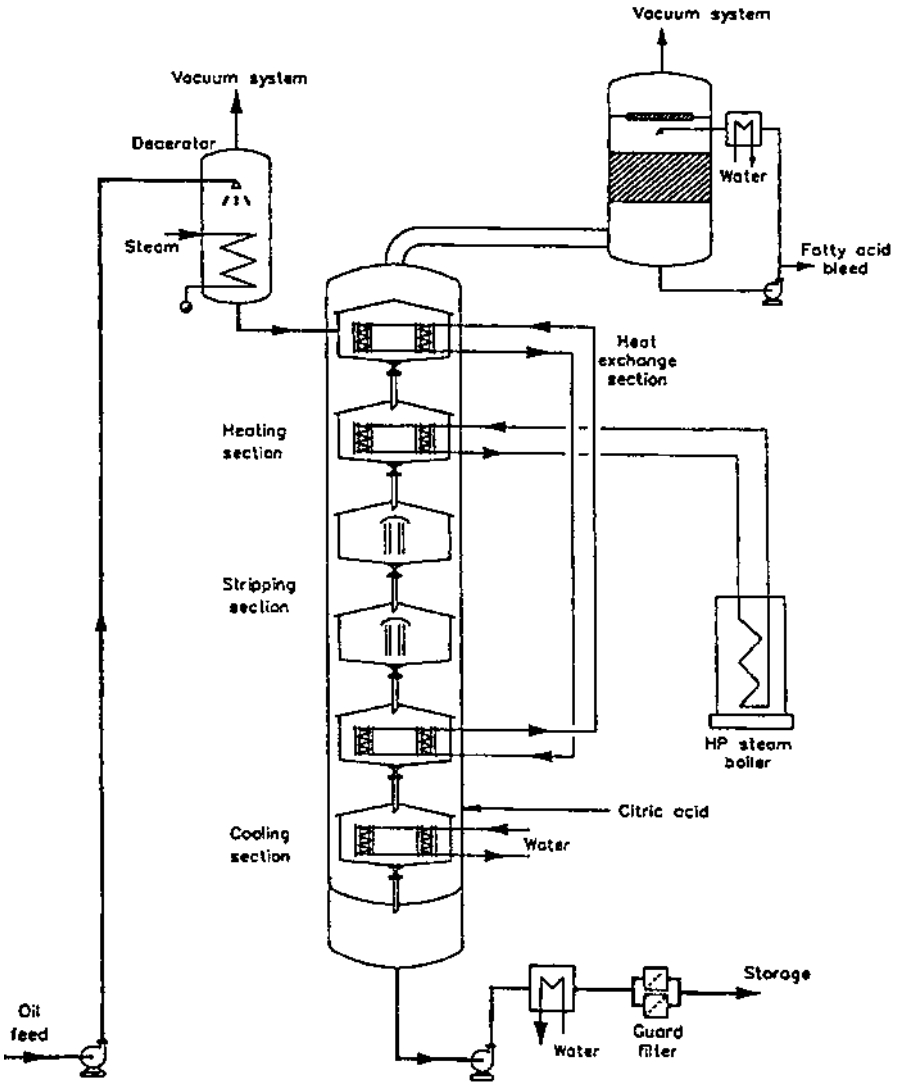

Figure 3 Conventional vertical semicontinuous deodorizer (Girdler type).

Copyright 2002 by Marcel Dekker. All Rights Reserved.

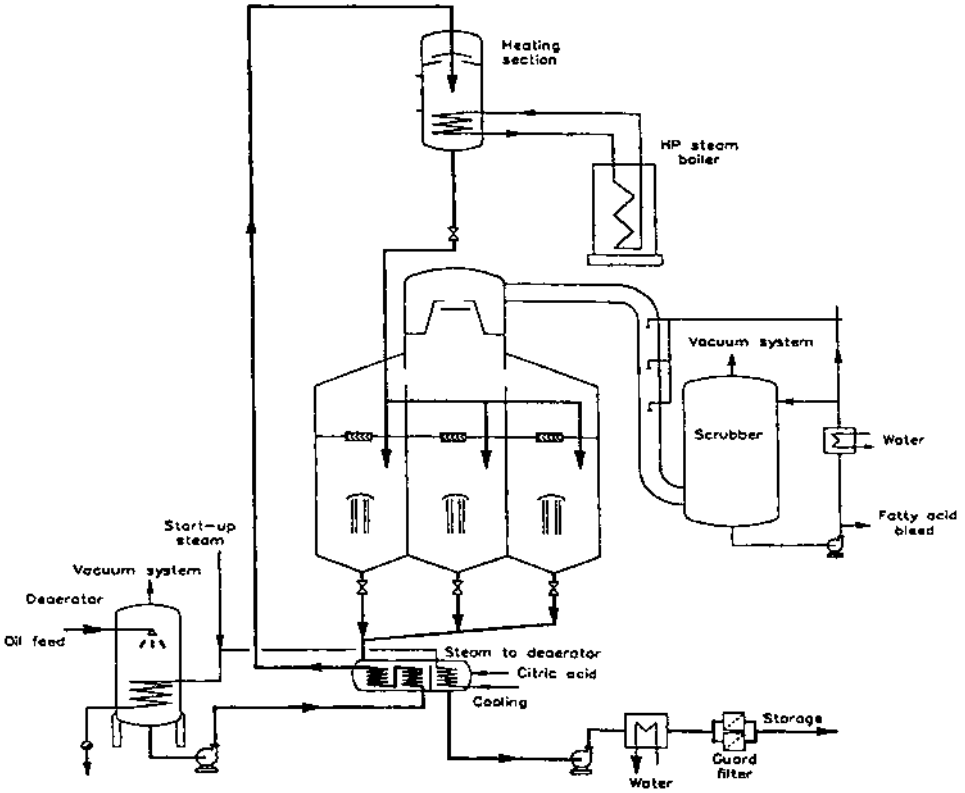

Figure 4 Horizontal semicontinuous deodorizer (De Smet MTD type).

C. Continuous Deodorizers

There are two basic configurations of continuous deodorizers. The first, shown in Figure 5, is very similar to the design of the semicontinuous units with a number of trays or compartments in which the oil is deodorized. As distinct from the semicontinuous deodorizers, the flow of oil through the unit is continuous, with the oil retention time on each tray or in each compartment simply being a function of the volume of the tray or compartment. Valve or sieve trays are most commonly employed in this deodorizer configuration. Typically tray or compartment residence times are comparable with those of semicontinuous units.

The second configuration of the continuous deodorizer (Fig. 6) relies on the use of a packed column design to generate a thin film system. The packing

Copyright 2002 by Marcel Dekker. All Rights Reserved.

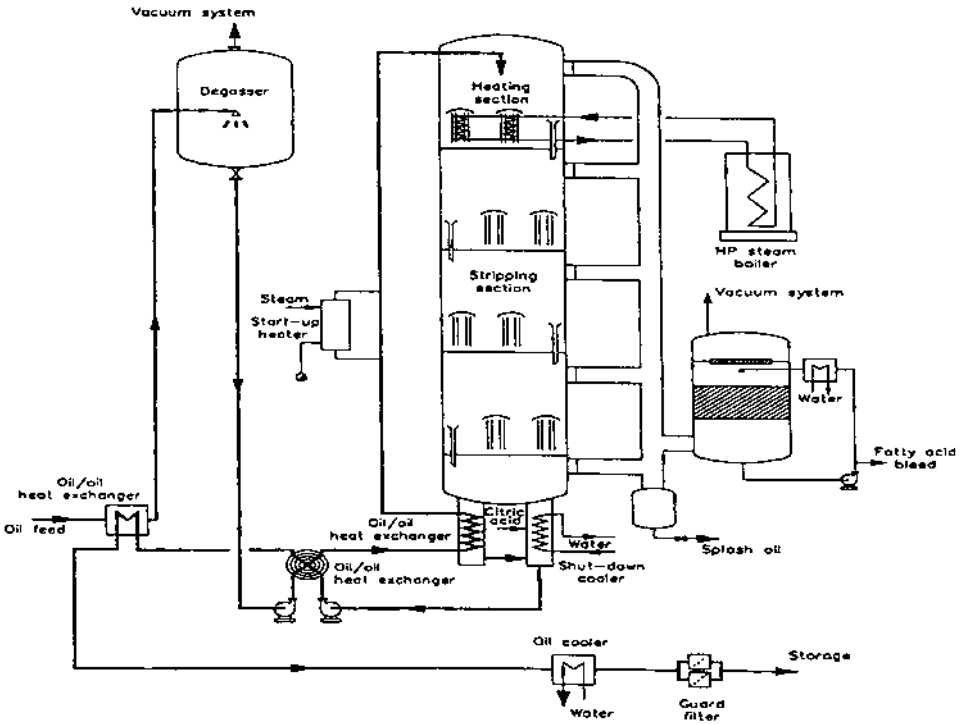

Figure 5 Lurgi-type continuous deodorizer.

is chosen to maximize the surface-to-volume ratio of the oil consistent with a low pressure drop across the packed section. The deodorization is achieved by exposing the thin oil film on the packing to a countercurrent flow of stripping steam. Modern packing designs can achieve surface areas of 75 ft^2/ft^3 (250 m^2/m^3) with pressure drops of approximately 1.5 torr over a packed height of 12–16 ft (4–5 m).

The typical residence time in a packed column deodorizer is on the order of 5 min, which is too short to initiate any heat-sensitive reactions, so it does not have a noticeable heat bleaching effect but does tend to keep trans fatty acid formation to a low level. This type of unit is particularly suited to handling extended production runs of nonhydrogenated liquid oils.

Both types of continuous deodorizers can be configured via external heat exchangers to readily achieve 75–80% heat recovery.

Copyright 2002 by Marcel Dekker. All Rights Reserved.

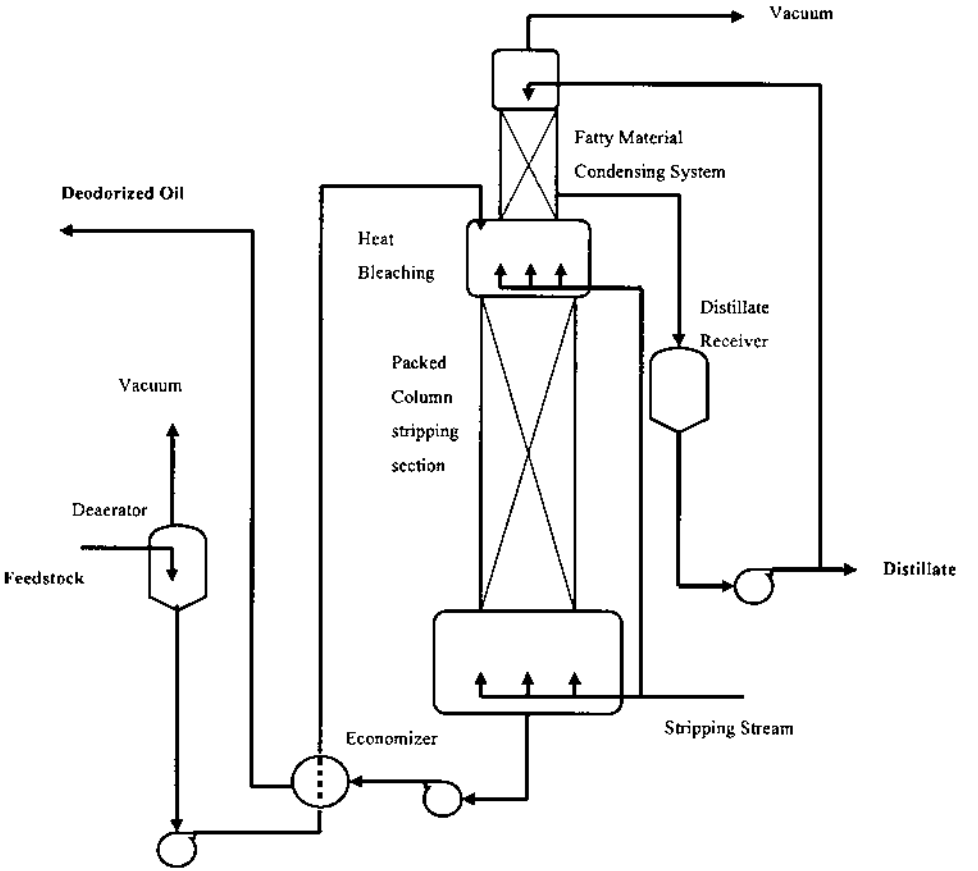

Figure 6 Continuous thin film deodorizer.

IX. PHYSICAL REFINING

Apart from the conventional use of deodorization to improve the flavor and keepability of vegetable oils, the process can be employed primarily as a steam distillation operation that removes the free fatty acid from the crude oil in preference to the conventional alkali neutralization process. The change in emphasis for the process can lead to the potential removal of a much larger amount of free fatty acid than was considered in the customary theoretical analysis of the deodorization process, and the non-ideal solution variation of free fatty acid activity can have a greater impact on the performance of the unit in this role. From

Copyright 2002 by Marcel Dekker. All Rights Reserved.

the practical perspective, the need to evaporate a much greater amount of free fatty acid during physical refining greatly increases the demands on both the heating and condensing systems associated with the deodorizer and dictates the use of stainless steel as the construction material of choice. The success of physical refining, however, depends less on the deodorization step of the process than on the degumming and bleaching step that precede it to remove phosphatides, metals, etc., and generate an oil suitable for stripping that will not be vulnerable to flavor reversion or color problems.

The major reasons for adopting physical refining in preference to conventional alkali refining are:

1. The lower oil losses achieved, due to the absence of the soap stock generated in the conventional alkali refining process and associated entrained oil.
2. The elimination of a chemical reaction step.
3. A reduction in effluent problems due to elimination of the need to dispose of soap stock. This is less of an issue for refineries associated with an extraction facility, because customary practice at these locations is to add the soap stock back to the animal feed. The use of silica to remove residual soap while avoiding a final water wash contributes further to the effluent reduction.

Hence, with their typically high crude oil content, free fatty acid levels, and low levels of nonhydratable phosphatides, both palm oil and palm kernel oil are excellent candidates for physical refining, and the technique finds extensive use in the Malaysian refining of these oils. The quality of these oils is a little inferior to that produced by alkali refining, but this is offset by the processing cost advantage and continued progress on quality improvements. At the opposite end of the scale, neither cottonseed oil nor fish oils are candidates for physical refining because they require treatment with caustic soda to remove impurities that have a deleterious effect on oil quality, particularly after exposure to high temperatures.

REFERENCES

1. AP Lee, WG King. Oil Soap 14:263, 1937.
2. WG Whitman. Chem Met Eng 29:146, 1923.
3. E Bailey. Ind Eng Chem 33:404, 1941.
4. K Lin, HC Van Ness, MN Abbott. Perry's Chemical Engineer's Handbook. 6th ed. (RH Perry, DW Green, JD Maloney, eds.) New York: McGraw-Hill, 1984, pp 4–78 to 4–81.
5. K Lin, HC Van Ness, MN Abbott. Perry's Chemical Engineer's Handbook. 6th ed.

Copyright 2002 by Marcel Dekker. All Rights Reserved.

(RH Perry, DW Green, JD Maloney, eds.) New York: McGraw-Hill, 1984, pp 4–60 to 4–67.
6. M Margules. Sitzber Akad Wiss Wien Math Naturewiss Kl II 104:1243, 1985.
7. JJ Van Laar. Z Physik Chem 72:723, 1910.
8. GM Wilson. J Am Chem Soc 86:127, 1964.
9. JH Hildebrand, RL Scott. Regular Solutions. Englewood Cliffs, NJ: Prentice-Hall, 1962.
10. G Scatchard. Chem Res 8:321, 1931.
11. G Scatchard. J Am Chem Soc 56:995, 1934.
12. G Scatchard. Trans Faraday Soc 33:160, 1937.
13. PJ Flory. J Chem Phys 9:660, 1941.
14. ML Higgins. Chem Phys 9:440, 1941.
15. AE Van Arkel. Trans Faraday Soc 42B: 81, 1946.
16. CM Hansen, A Beerbower. Kirk-Othmer Encyclopedia of Chemical Technology. 2nd ed. Suppl Vol (A Standen, ed.). New York: Wiley-Interscience, 1971, pp 889–909.
17. RF Blanks, JM Prausnitz. Ind Eng Chem Fundam 3:1, 1964.
18. BL Karger, LR Snyder, C Horvath. An Introduction to Separation Science. New York: Wiley, 1973, pp 268–276.
19. CM Hansen. Ind Eng Chem Proc Des 8:2, 1969.
20. J Small. Appl Chem 3:71, 1953.
21. KL Hoy. J Paint Technol 42(541):76, 1970.
22. TC Lo, MH Baird, C Hanson. Handbook of Solvent Extraction. New York: Wiley, 1983, pp 17–31.
23. A Fredenslund, RL Jones, JM Prausnitz. J Am Inst Chem Eng 21:1086, 1975.
24. A Fredenslund, J Gmehling, P Rasmussen. Vapor-Liquid Equilibria Using UNIFAC. Amsterdam: Elsevier, 1977.
25. S Skjold-Jorgensen, B Kolbe, J Gmehling, P Rasmussen. Ind Eng Chem Process Des 18:714, 1979.
26. GH Crapiste et al. JAOCS Annual Meeting, Prediction of Equilibrium Properties of Fatty Acids for Deodorization Modeling, 2000.
27. DSS Sarkadi. J Am Oil Chem Soc 35:479, 1958.
28. H Stage. Seifen Oele Fatte Wachse 104:445, 1978.
29. KF Mattil. In: Bailey's Industrial Oils and Fats Products. (D Swern, ed.). New York: Wiley, 1964, Chap 18.
30. Federal Register Notice, Interim Final Rule, ''FDA authorizes new coronary heart disease health claim for plant sterol and plant stanol esters,'' Sept 8, 2000.
31. YH Hui. Bailey's Industrial Oil and Fat Products, 5th ed. New York: Wiley, 1996, Vol 1, Chapter 8 (O Kitts): Toxicity and safety of fats and oils, pp 251–254.
32. 21 CFR Part 101. Food Labeling: Trans Fatty Acids in Nutrition Labeling, Nutrient Content Claims, and Health Claims. Proposed Rule, FDA Docket No. 94P-0036, Nov 12, 1999.
33. RB Power. Steam Ejectors for the Process Industries. New York: McGraw-Hill, 1994.
34. CH Imai, H Watanabe, H Haga, T Li. J Am Oil Chem Soc 51:495, 1974.
35. YH Hui. Bailey's Industrial Oil and Fat Products, 5th ed. New York: Wiley, 1996. Vol 4, Chap 6 (KF Carlson): Deodorization, pp 367–382.

Copyright 2002 by Marcel Dekker. All Rights Reserved.

11
Fractionation of Fats

David Illingworth
New Zealand Dairy Research Institute, Palmerston North, New Zealand

I. HISTORY OF FRACTIONATION

Oils and fats with a diverse range of physical properties are derived from vegetable, animal, or marine origins. However, in spite of this wide range of properties, the oils and fats as extracted are not always suitable for many applications in the food industry. For example, oils used in salad dressings must remain clear at 5°C. Other oils are highly unsaturated and need some form of modification to improve their oxidative stability. This is usually done by hydrogenation to harden the oil and is often followed by fractionation to obtain the most desirable properties. In addition, fats may be interesterified, to modify their triacylglycerol (TAG) composition, and this too may be followed by fractionation to procure ideal properties for the end application. Fractionation remains the only modification process that can be described as completely physical. Apart from the special case where organic solvents are used for fractionation, the process involves a completely physical separation of a fat into component fractions that are still fats or oils by definition but have different physical properties than the parent fat from which they were derived.

The earliest form of fractionation was called winterization, simply because tanks of semisolid fats were left quiescent over the northern winter. The higher melting TAGs crystallized in the low ambient temperatures and sedimented in the tanks, leaving liquid olein, suitable for use as a salad or frying oil, to be drawn from the top of the tank.

Nowadays, the term ''winterization'' is used for the process of crystallizing wax esters that occur in oils such as sunflower oil. If they were left in the oil, the waxes would begin to precipitate even at ambient temperatures, giving a

Copyright 2002 by Marcel Dekker. All Rights Reserved.

cloudy appearance. Practices similar to those that are used for modern commercial fractionation can be used to crystallize the waxes, which are then separated from the oil by filtration or centrifugation. The term winterization is also still applied to some conventional fractionation practices. For example, the highest melting TAGs may be removed from partially hydrogenated oils such as cottonseed oil, as a way of improving both the oil's cold stability and its oxidative stability. In addition, fish oils that are rich in omega-3 fatty acids may be winterized after partial hydrogenation to increase the concentrations of the fatty acids eicosapentaenoic acid (EPA; C20:5, $n-3$) and docosahexaenoic acid (DHA; C22:6, $n-3$) [1]. This process will not be discussed further in this chapter.

Fat fractionation as we know it today has its origins in the late nineteenth century with the invention of margarine in 1869. The secret was the careful crystallization of freshly rendered edible tallow at temperatures between 25°C and 30°C [2]. The resultant grainy mass was then hydraulically pressed to obtain a crude 60:40 separation of a soft fraction (olein) and a hard fraction (stearin). This has remained the basic principle of the modern process. The softer fraction had physical properties similar to those of anhydrous milkfat (AMF) and was easily rendered into a plastic product that could be used in place of butter.

In the early part of the twentieth century, coconut oil was commonly fractionated to produce hardstock for margarine [3], but as the demand for margarine grew, the fractionation technology of the day was unable to keep up [4], and hydrogenation replaced it.

Fractionation saw an amazing revival in the late 1950s and early 1960s following the rapid increase in the production of palm oil, particularly in Malaysia. In the succeeding years, the technology has been applied not only to palm oil but also to an increasing range of oils and fats. The confectionery industry has provided much of the impetus with the increasing desire to have cheaper fats with physical properties similar to those of cocoa butter without some of the disadvantages such as bloom—the powdery appearance that can occur on chocolate products because of recrystallization of the cocoa butter. Fats such as palm oil, shea nut oil (indigenous to West Africa), sal (found mainly in India), and hydrogenated cottonseed oil can be fractionated to obtain fractions that can be blended with or replace cocoa butter in confectionery. Palm kernel and coconut oils, both rich in C_{12} lauric acid are also fractionated to obtain stearins that have a wide range of applications in confectionery, mainly as coating fats.

Probably the most rapid growth of the application of fractionation has occurred in the dairy industry over the past 30–40 years. The physical properties of AMF and butter have many disadvantages compared with modern margarines, which can be formulated precisely for a given application, be it for specialist bakery use or for spreading. Fractionation has allowed AMF to become more competitive in these areas. By the end of the twentieth century, AMF in its frac-

Copyright 2002 by Marcel Dekker. All Rights Reserved.

tionated forms was widely used commercially for a variety of end uses in many countries [5,6].

In this chapter the principles of fractionation are discussed and some of the processes that are currently in use are described. In addition, advances in processing, suggested during the last decade of the twentieth century, as well as applications for fractions from selected fats and oils are covered. The costs of fractionation have been extensively reviewed by Kellens [7] and are not discussed here.

II. THE TECHNOLOGY OF FRACTIONATION

A. Crystallization Theory

Fractionation, or more accurately fractional crystallization, requires two distinct steps. First there is a crystallization step, which is followed by a separation step. Although they are distinct, the efficiency of the separation step may be partly dependent on how the crystallization step proceeds. Timms [8] discusses the principles of crystallization by analogy with ideal solubility. Basically, when an oil or fat is cooled, a solid phase separates out. The amount of solid and its composition are determined in general by the temperature to which the fat or oil is cooled to effect the crystallization. Timms's analogy works well for simple systems such as fully saturated TAGs, e.g., glycerol tripalmitate (PPP) or glycerol tristearate (StStSt) in glycerol trioleate (OOO), glycerol trilinoleate (LiLiLi), or paraffin oil, as shown in Figure 1. It is clearly evident that the solubility of the higher melting component is independent of the lower melting component. Effectively these act like the solute and solvent, respectively, in an ideal solution. There is no interaction between the solute and solvent, and no solid solutions are formed if the melting points of the two differ by more than 20°C.

However, although simple binary or tertiary systems can be used to demonstrate the basic principles, they are of little use in understanding more complex real systems such as palm oil or AMF. In a real fat there are always solid solutions, and these affect the ideal solubility curve, causing it to deviate from the straight line as shown in Figure 2, which demonstrates this in terms of the phase behavior of PPP and 2-oleodipalmitate (POP). At all temperatures, the actual solubility is higher than the ideal solubility.

To achieve crystallization at any temperature it is necessary for the concentration of the crystallizing species to exceed its solubility or saturation in the lower melting species at that temperature. This does not imply immediate crystallization. Solutions can exist indefinitely in the supersaturated state without forming crystals. Fats can also remain liquid or supersaturated at temperatures below those at which they would be expected to begin crystallizing.

Copyright 2002 by Marcel Dekker. All Rights Reserved.

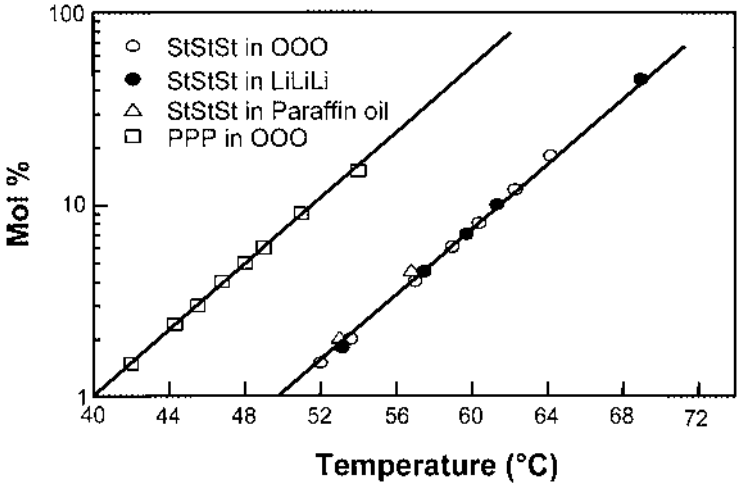

Figure 1 The solubility curves for PPP and StStSt in OOO, LiLiLi, and paraffin oil. (Redrawn from Ref. 8.)

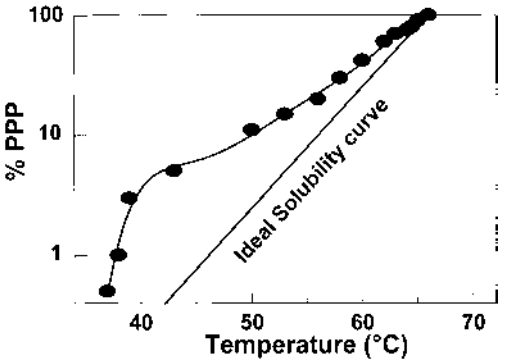

Figure 2 The solubility curve (concentration vs. temperature) of PPP in POP showing the deviation from ideal solubility that occurs in this instance. (Redrawn from Ref. 8.)

Copyright 2002 by Marcel Dekker. All Rights Reserved.

What this implies is that a solubility curve forms a distinct boundary between crystallization and solution but that the transition from solution to crystallization is not abrupt. The slope and position of the solubility curve on a temperature–concentration plot varies, depending on the composition of the crystallizing oil or fat. Close to the solubility curve, there is a metastable zone where thermodynamics suggests that crystallization should occur but it does not unless some external assistance such as seeding is used. Beyond the metastable zone is an unstable zone where crystallization will occur spontaneously, without any external assistance. The extent of the metastable zone is dictated by processing conditions such as the speed of agitation and the cooling rate. As might be expected, the slower the cooling rate, the wider the metastable zone. As might be expected, time comes into play as well, because the existence of a metastable zone implies that there is a finite induction period before crystallization actually begins.

This concept is demonstrated by using a saturation–supersaturation diagram as illustrated in Figure 3. From this it can be seen that there are two ways of increasing the supersaturation (the concentration of crystallizing species in solution) to induce crystallization. First, the temperature can be reduced as along line *A-B-C*, and second, lower melting species, which act as a solvent for the higher melting species, can be removed, for example by evaporation, as along line *A-D-E*. Evaporation is applicable only to solvent fractionation, whereas reducing the temperature is the only option for melt or dry fractionation. Both of these effectively move the system through the metastable zone into the unstable zone. The idea of a metastable zone is justified if crystallization is considered as a two-step process—nucleation followed by crystal growth.

A crystal nucleus may be defined as the smallest stable crystal that can exist at any given concentration–temperature combination for a crystallizing me-

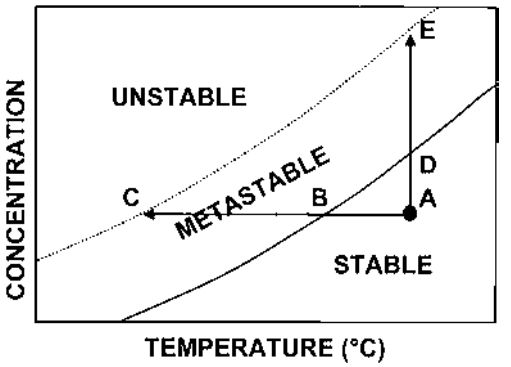

Figure 3 Saturation–supersaturation diagram. (Redrawn from Ref. 8.)

Copyright 2002 by Marcel Dekker. All Rights Reserved.

dium. Thus a nucleus must consist of a finite number of molecules that have collided to form a stable crystal. Crystals that have fewer than this finite number of molecules will redissolve. Thus, in the metastable zone, conditions may exist that would favor crystallization as molecules collide and stick together as subnuclear crystallites. Unless these crystallites continue to collide with other molecules and gain sufficient mass to become stable nuclei, they redissolve.

When TAG molecules in liquid fat collide under conditions that will allow crystallization, two opposing forces come into play. One is the latent heat of crystallization, which has a positive effect as energy is evolved, reducing the entropy of the system. Second, for the crystal to grow and expand, energy is required to overcome the increasing surface tension. When the former exceeds the latter, a stable crystal nucleus is formed.

Triacylglycerol molecules, by their very nature, are complex, so attaining their correct attachment on a growing crystal is a very complicated process. Once a stable crystal nucleus is apparent, it can begin to grow by addition of further molecules incorporated from the surrounding liquid by diffusion. In turn, more molecules enter the diffusion zone from the surrounding liquid. Thus, in the immediate vicinity of the growth surface one can imagine a seething mass of TAG molecules, some being driven toward crystallization because the temperature conditions dictate they should be solid, and others tending to move away because the temperature is still above their solidification point. As a result, the attachment of new molecules can be a random affair, with many molecules attaching momentarily. They then either become dislodged or move across the surface until they lock into the correct configuration and place on the surface.

Thus, the rate-determining step for crystal growth is not the diffusion process but the attachment of a molecule in the correct orientation at the correct site on the growth face. Only when a molecule becomes firmly bonded on at least two sides to similar molecules can it be considered a part of the crystal.

If the degree of supercooling is the driving force toward crystallization, the processes described above will occur in different ways as the degree of supercooling changes. For a small degree of supercooling, the incorporation of a new molecule is entirely dependent on its becoming attached in exactly the correct orientation and place on the growth surface. The opportunity for crystalline defects or dislocations or for a molecule of the wrong type (wrong melting point) to become part of the crystal is slight. Thus, small degrees of supercooling tend to favor larger, more perfect crystals.

On the other hand, greater degrees of supercooling may allow molecules to become less perfectly attached by allowing second and subsequent molecules to attach before the first one is properly in place. The frequency of dislocations becomes greater with an increased tendency toward the formation of a larger number of smaller crystals. In addition, the incorporation of different TAGs of similar chain lengths and melting points into a crystal, giving rise to mixed crys-

Copyright 2002 by Marcel Dekker. All Rights Reserved.

tals, is more likely. Under normal circumstances, these mixed crystals or solid solutions are unstable and will tend to rearrange to a more stable configuration if conditions are adjusted to allow it.

For solvent fractionation (see Section II.D) the picture changes completely. The solvents used for fractionation such as acetone and hexane have smaller molecules than TAGs. In addition they have very low melting points and are thus unlikely to crystallize. The addition of solvent to a fat or oil reduces the viscosity of the resulting miscella, and this allows greater freedom of mobility for the TAG molecules. Consequently, they are more likely to become attached in the correct configuration on the growing crystal face. The result is larger crystals with fewer dislocations and a lesser tendency to form mixed crystals than could be achieved from crystallization of the melted fat on its own. It also means that solvent fractionation lends itself more readily to a continuous process rather than the batch processes favored for melt fractionation.

It should not be forgotten that the two processes described thus far are parallel events. The nucleation rate determines how many crystals form in unit time, and crystal growth determines how fast the crystals will then grow. The rate at which new crystals are formed can be manipulated to control the crystal size. This is usually accomplished by changing the temperature differential between the crystallizing fat and the cooling medium in the jacket around the crystallizer. If the desire is for large crystals, then nucleation must be suppressed in some way to allow the crystals to grow. As it happens, the kinetic order for growth in fat crystals is an order of magnitude higher than for nucleation [9], resulting in higher degrees of supercooling and increasing crystal size without forming too many more nuclei.

If the fat to be fractionated is allowed to crystallize in the quiescent state, not only will the process take a much longer time than necessary, but also the result may be less than satisfactory. The heat transfer between the fat and the heat transfer surface would be poor under such conditions. It is certain that agitation both assists and improves heat transfer in a crystallizer, but little else is understood about it. It has little effect on crystal growth because it influences only the diffusion of TAG molecules toward the growing surfaces of crystals. This is not rate-determining, so any effect can be ignored. In some instances, the stirrer used in the crystallizer can be fitted with scraper blades, allowing contact with the heat transfer surface. This can result in relatively uncontrolled heterogeneous nucleation, which in turn may lead to difficulties in the later process of separation.

The most important effect that agitation in crystallizers has is that of agglomeration. Agglomerates are formed when individual crystals in a stirred mass collide and adhere to each other, growing into masses that can be up to 100 μm in diameter. The degree of aggregation is affected by agitation in two ways. In the destructive phase, when a crystal exceeds a certain size the torque forces can

Copyright 2002 by Marcel Dekker. All Rights Reserved.

cause pieces to break off it. When fat crystallizes in well-formed spherulites, as shown in Figure 4, they can be easily damaged.

On the other hand, smaller crystals (say, 1–10 μm in diameter) can more easily withstand these destructive forces. Rather than being broken, these crystals are more likely to be driven together and combine into larger clusters or agglomerates. As will be seen later, the control of crystallization during the fractionation process has a major bearing on the success of the separation of the crystals from the slurry that results.

1. Entrainment

Before leaving the discussion of crystallization, consider another phenomenon that is common in fat fractionation—entrainment. The very nature and shape of the spherulitic crystals that occur in fat dictates that the crystal cake entrain a certain proportion of the liquid olein when the stearin and olein are separated. The scanning electron micrograph of an AMF crystal shown in Figure 5 clearly demonstrates that spherulites have many voids and channels that hold olein much like sponge holds water.

The most efficient method for eliminating entrainment is to resort to solvent fractionation (see Section II.D) Entrained olein can be displaced from the cake by washing with fresh solvent. Separation by detergents (see Section II.B.3) and

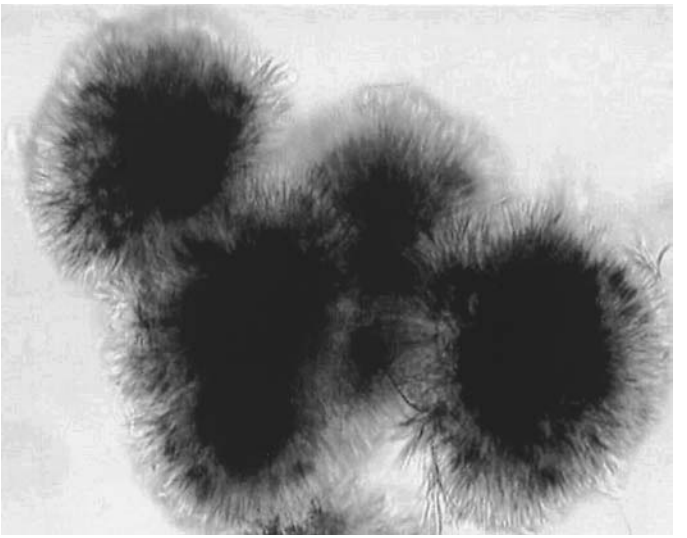

Figure 4 Spherulites of high melting TAGS of AMF growing from the melt.

Copyright 2002 by Marcel Dekker. All Rights Reserved.

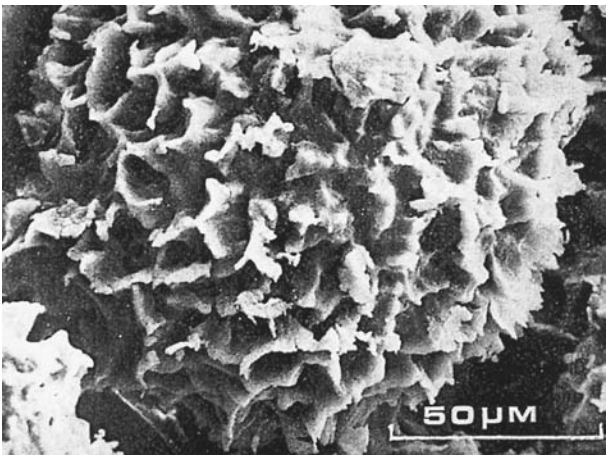

Figure 5 Scanning electron micrograph of a typical AMF spherulite grown from acetone solution.

membrane filtration (see Section II.B.2) for dry fractionation have also played a major part in reducing entrainment.

Entrainment is also reduced by the use of additives during melt crystallization. Three Unilever patents describe the use of additives to produce crystals that are easier to filter and separate with high efficiency. The addition of mono- or diglyceride, optionally esterified with citric acid as a crystal-modifying agent [10], is claimed to change the crystal form of the stearin fraction such that entrainment is reduced compared with conventional melt fractionation. In a second patent [11], it is suggested that bovine brain membrane lipids—complex phospholipids that, like the previous additives, are polar and surface-active—have a similar effect. Both patents lay claim to being applicable to a wide range of oils and fats, including AMF. Recent controversy over bovine spongiform encephalopathy (BSE) probably precludes any further use of this processing aid. Polysaccharides and peptide esters [12] have also been used to modify crystallization behavior to reduce entrainment.

2. Oil Quality

The quality of an oil or fat has a major effect on the way in which it crystallizes and subsequently on the efficiency of any fractionation. Probably the most likely contaminant is water, which can affect the nucleation. Water will dissolve in fats and oils at very low concentrations. If the water level is too high, it can be liberated from solution as very fine droplets that act as nuclei. As the temperature is

Copyright 2002 by Marcel Dekker. All Rights Reserved.

reduced, solid fat coats the water droplets. This solid is not necessarily of the same composition as that which would crystallize from a dry fat. In addition, the number of nuclei is likely to be much higher than is desirable.

However, the composition of the fat is also of concern in fractionation. If the fat has been held under conditions that promote saponification, the free fatty acid (FFA) level is raised. As a consequence, the level of mono- and diacylglycerols is also raised. It has been well established that the presence of diacylglycerols in particular, retards nucleation in both vegetable oils [13] and AMF [14].

B. Conventional Dry (Melt) Fractionation

1. Crystallization Stage

Dry fractionation or fractionation from the melt is the most common of all fat fractionation technologies. Two commercial processes dominate, and both follow the same basic principle. The melted fat is first crystallized carefully, and then the stearin crystals are separated from the olein in some way.

S.A. Fractionnement Tirtiaux has developed its Tirtiaux process into one of the most widely used fractionation processes. It has been used to fractionate a wide variety of oils and fats, particularly palm oil, tallow, and AMF. Its proponents were among the first people to recognize both the importance of controlling the temperature of the crystallizing fat and the value of using this to dictate the overall efficiency of the process [15]. A schematic layout of the crystallization process appears as Figure 6. Constant monitoring of the temperature of the fat in the crystallizer allows precise control of the amount of cooling required, with

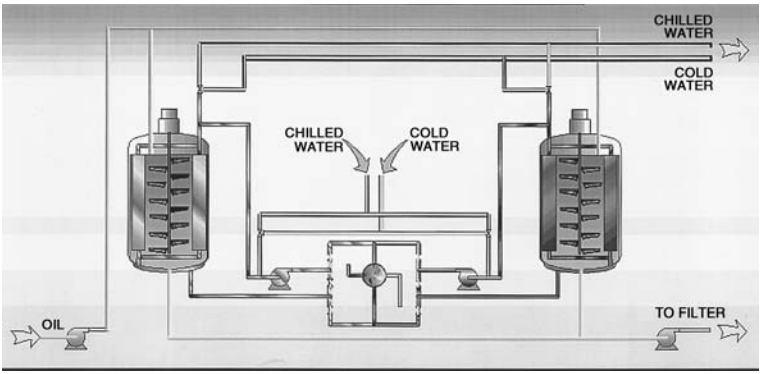

Figure 6 Schematic layout of crystallizers in a Tirtiaux fractionation plant. (Courtesy of S.A. Fractionnement Tirtiaux, Fleurus, Belgium.)

Copyright 2002 by Marcel Dekker. All Rights Reserved.

the flows of cold and chilled water being adjusted to maintain the temperature differential between the fat and the coolant at a predetermined value. The main objective of the crystallization stage is to produce a crystal slurry with just the right amount of crystals and a tight but precise crystal size distribution to allow efficient filtration. The agitation rate in the crystallizers can also be adjusted throughout the crystallization process to assist in obtaining crystals of the ideal size and habit to suit the separation process. The process inherently requires long crystallizing times (up to 24 h) to achieve the optimum crystallization.

In contrast, the de Smet process uses a similar control principle but applies it in a different way [16]. The temperature of the liquid in the crystallizer jacket is lowered stepwise in precise and precalculated steps to bring the temperature of the crystallizing fat down to the desired level within a set time period. According to de Smet, this allows the fat to be first conditioned prior to the nucleation step that occurs during the early part of the cooling process. This is followed by crystal growth, which continues up to the final filtration temperature, when the stearin is separated from the olein by filtration.

The cooling rate applied to the oil mass is the most critical factor in ensuring that the crystals formed are both distinct and filterable. Ideally, if a fractionation is performed at a temperature of, for example, 20°C, all the solid that is crystallized will consist of TAGs that have melting points greater than 20°C, leaving those with melting points below 20°C as the olein. The concentric crystallizers in a de Smet plant are designed to achieve this. An example of cooling profiles for the oil and coolant for fractionation of palm oil to produce a low cloud point palm olein in a single step is shown as Figure 7. Crude as well as refined palm oil can be fractionated using this process. In addition, with changes to the temperature profiles for cooling, the process can be readily adapted for fractionation of other oils and fats. Figure 8 shows crystallizers in a de Smet fractionation plant, with Figure 9 showing the details of a concentric crystallizer in such a plant. Figure 10 shows a schematic layout of a complete fractionation plant. The de Smet process achieves its optimum crystallization in much less time than the Tirtiaux process.

2. Filtration Stage

Once fat has been crystallized in a form that enables the crystals to be separated from the remaining liquid oil, the most common separation method is to use one of the various filter systems that are available commercially.

Vacuum filtration in commercial plants can be likened to the standard operation that is used in any laboratory to separate solids and liquids. In the laboratory the slurry is poured into a Buchner funnel fitted with a filter paper, over a flask that is attached to a vacuum system. The suction draws the liquid through the filter paper, which acts as a support for the crystals; the crystals build up on the

Copyright 2002 by Marcel Dekker. All Rights Reserved.

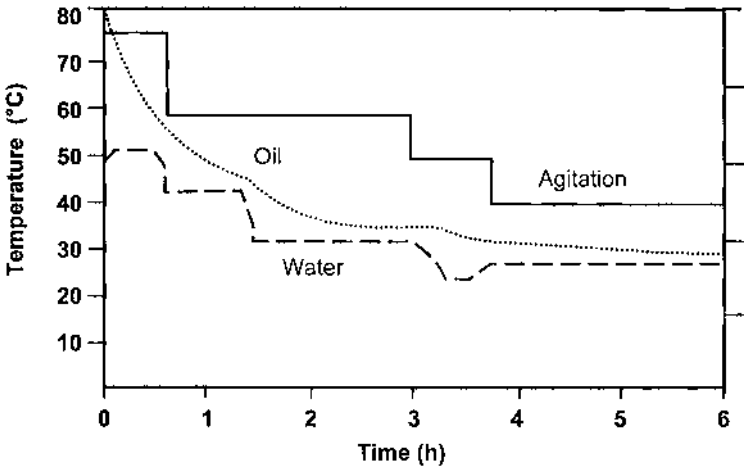

Figure 7 Cooling profile used for the manufacture of a low-cloud-point olein from palm oil. [Courtesy of Extraction de Smet N.V./S.A., Edegem (Antwerp), Belgium.]

Figure 8 View of crystallizers in a de Smet fractionation plant. [Courtesy of Extraction de Smet N.V./S.A., Edegem (Antwerp), Belgium.]

Copyright 2002 by Marcel Dekker. All Rights Reserved.

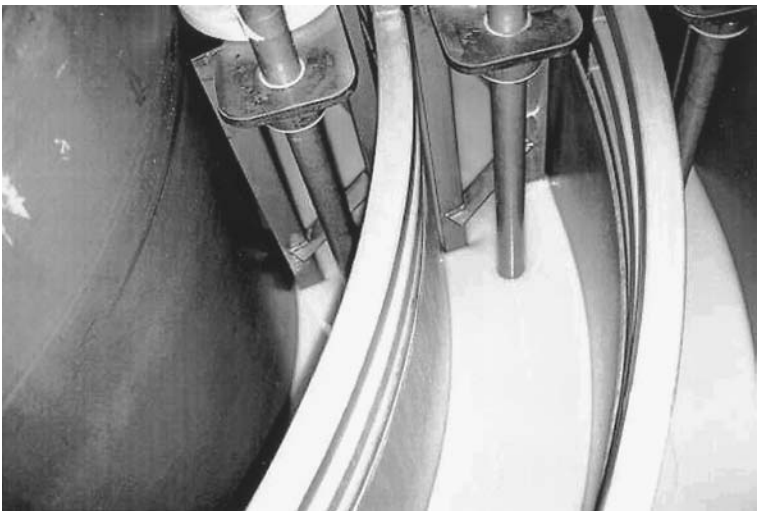

Figure 9 Detail of a de Smet concentric crystallizer. [Courtesy of Extraction de Smet N.V./S.A., Edegem (Antwerp), Belgium]

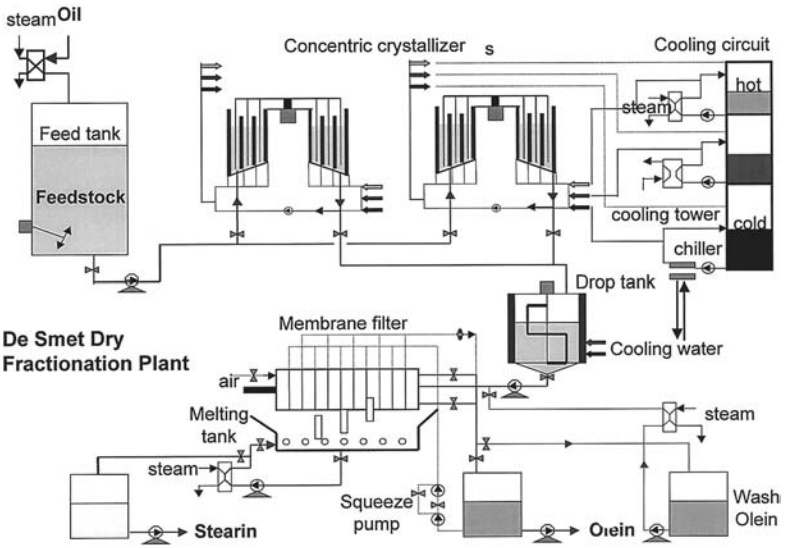

Figure 10 Schematic layout of a de Smet fractionation plant. [Courtesy of Extraction de Smet N.V./S.A., Edegem (Antwerp), Belgium.]

Copyright 2002 by Marcel Dekker. All Rights Reserved.

paper as a cake. When filtration is completed, the cake may be removed, or in some cases it can be washed with solvent. Commercially this process is made continuous by having a moving filter cloth and a device for continuously removing the filtered crystal cake.

Such a device is a rotary vacuum filter of the type shown in Figure 11. In this, the crystal slurry is introduced into a tank in which a rotating drum, holding the filter medium, is partially immersed. Vacuum is applied to the interior of the drum, and this draws the olein fraction through, causing the stearin crystals to build up as a cake on the outer surface. A scraping device removes the filter cake, revealing a clean filter surface that allows the process to repeat itself.

As an alternative to the rotary filter drum, the filter may be stretched into a horizontal continuous belt, around two rotating drums, as shown in the diagram in Figure 12 of a Florentine filter from a Tirtiaux plant. Filtration takes place on the upper, horizontal surface of the belt, which has a vacuum chamber beneath it. In the diagram shown, the first portion of the filter belt, which in this case is perforated stainless steel, allows for any crystal fines to be recycled so they do not contaminate the olein fraction.

Probably the most common filter used today in dry fractionation is some form of plate-and-frame membrane filter. The increasing demand worldwide for salad and frying oils, particularly those derived from palm oil, led to the introduc-

Figure 11 Rotary vacuum filter. [Courtesy of Extraction de Smet N.V./S.A., Edegem (Antwerp), Belgium.]

Copyright 2002 by Marcel Dekker. All Rights Reserved.

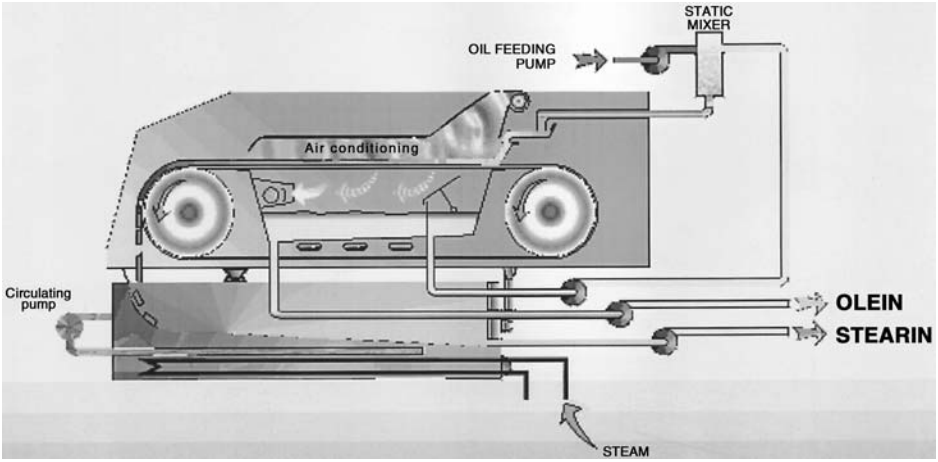

Figure 12 Schematic of a Florentine horizontal belt vacuum filter. (Courtesy of S.A. Fractionnement Tirtiaux, Fleurus, Belgium.)

tion of these filters as replacements for detergent fractionation plants (see Section II. B. 3).

Membrane filters are similar to the plate-and-frame filters that were once common in bleaching plants. A number of manufacturers offer these for fractionation, and each has its own particular preferences regarding the feed position and the materials used in manufacturing the plates. For example, Tirtiaux plants can be coupled with membrane filters as an alternative to the Florentine filter, as shown in Figure 13.

A typical membrane filter is shown in Figure 14. The frame that supports the plates is heavy because the pressure holding the plate stack together is necessarily high (the actual pressure depends on the pressure rating of the press squeeze). The membrane plates are often made entirely from polypropylene, but some manufacturers use synthetic rubbers for the membranes that support the filter cloths. The slurry is fed into the filter either at one corner or through the center. Figure 15, for example, shows a center-feed membrane filter in cross section. The crystal slurry is pumped through the center channel, which opens into the chambers between the filter elements, gradually filling the chambers with stearin crystals that pack into a cake. The feed pressure forces the olein through the filter cloths into drain holes in each plate that are in turn connected to the corner channels. The principle is to fill the chambers just sufficiently that liquid continues to percolate through the cakes without overfilling the chambers with

Copyright 2002 by Marcel Dekker. All Rights Reserved.

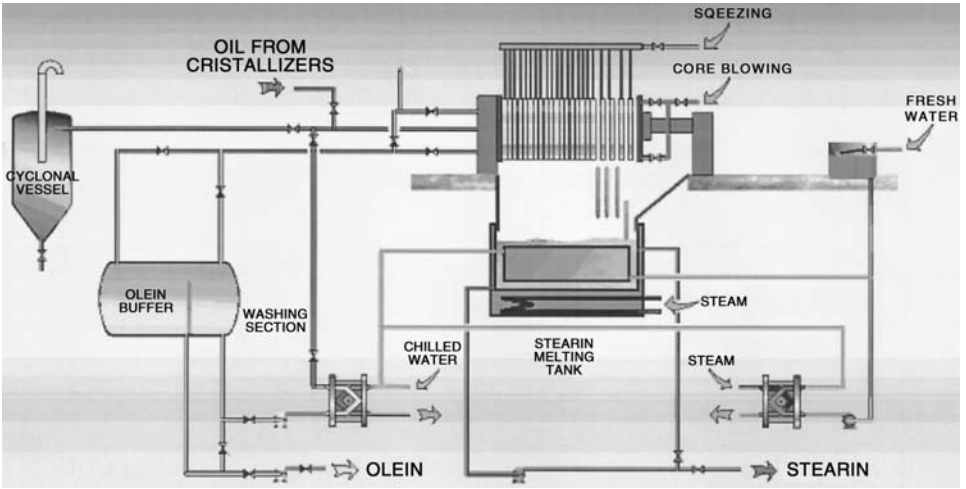

Figure 13 Layout of a Tirtiaux fractionation plant with a membrane filter. (Courtesy of S.A. Fractionnement Tirtiaux, Fleurus, Belgium.)

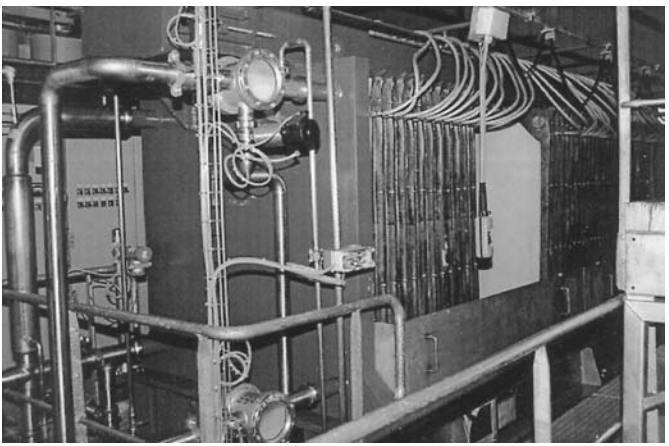

Figure 14 Membrane filter in a de Smet fractionation plant. [Courtesy of Extraction de Smet N.V./S.A., Edegem (Antwerp), Belgium.]

Copyright 2002 by Marcel Dekker. All Rights Reserved.

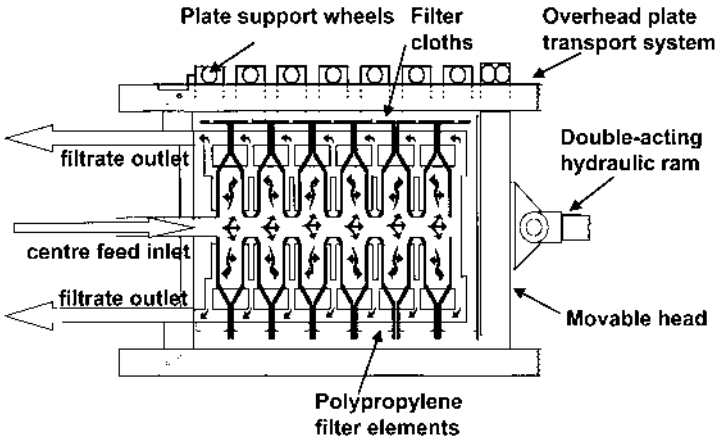

Figure 15 Cross section of a center-feed membrane filter.

solid. If that happens, the second part of the operation cannot be carried out. Once there is sufficient stearin in each chamber, but while the mass is still porous, the flexible membranes supporting the filter cloths can be expanded under pressure to squeeze excess olein out of the cakes. Once sufficient olein has been squeezed out, usually determined by time, the pressure is relaxed and the filter may be opened, as shown in Figure 16, to release the filter cakes into a hopper for melting and pumping to storage.

Early membranes were only capable of reaching pressures of 600 kPa, but modern filters such as the Statofrac filter manufactured by Krupp [17] can be used at pressures up to 3000 kPa. As a result, the quality of stearins that can be obtained from dry fractionation coupled with membrane filtration is comparable with the quality of those obtained from solvent fractionation, and, as might be expected, the yield of olein is markedly increased over vacuum or detergent separation.

3. Detergent Separation

In 1905, Lanza demonstrated that slurries of crystals of stearin in liquid olein could be separated by mixing the slurry with an aqueous solution of detergent (sodium lauryl sulfate) containing an electrolyte such as magnesium sulfate. The detergent encourages the olein fraction to break into droplets, allowing the detergent to attach itself to the surface of the crystals, then move from the oil phase into the aqueous phase. The electrolyte is there to prevent the olein from completely emulsifying and to assist the coalescence of the olein droplets. In addition, the

Copyright 2002 by Marcel Dekker. All Rights Reserved.

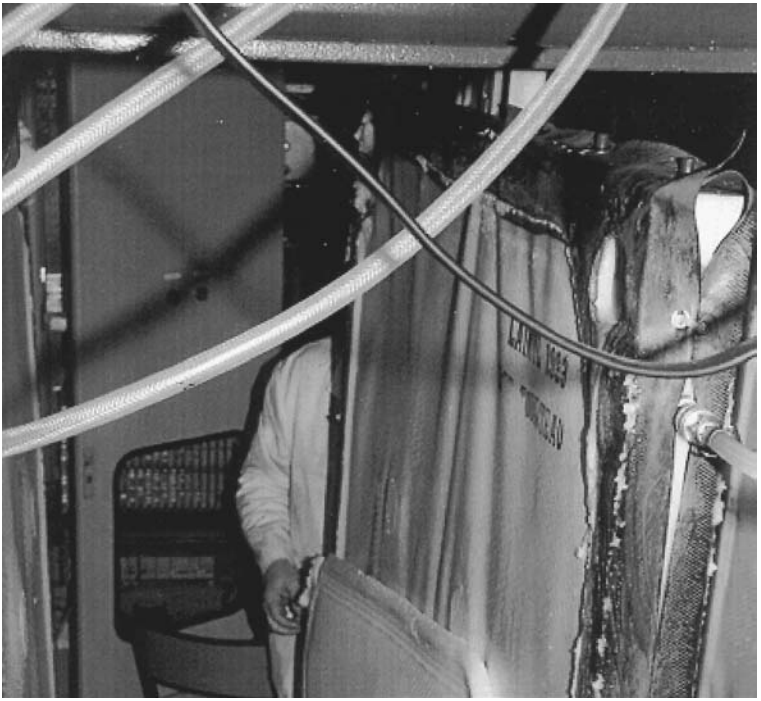

Figure 16 Membrane filter in a de Smet plant being opened for removal of the filter cakes. [Courtesy of Extraction de Smet N.V./S.A., Edegem (Antwerp), Belgium.]

entrapment of oil droplets by the crystals is discouraged. Once the crystals have moved into the aqueous phase, a centrifugal separator is used to separate the aqueous and olein phases. The aqueous phase containing the crystals is then heated to melt the stearin, and a second separator completes the separation. Both fractions can then be dried, and the aqueous phase may be recycled for reuse but is more likely to be discarded. A simple diagrammatic layout of the process is shown in Figure 17.

Tetra Pak (formerly Alfa-Laval) has marketed the process as the Lipofrac process [18,19] for many years. It can be used for both palm oil and palm kernel oil. Early AMF fractionation research in New Zealand also used the Lipofrac process [20], and in the 1970s and early 1980s both commercial and pilot plants were operated in New Zealand. However, the process fell out of favor when the International Dairy Federation discouraged the use of detergent-separated fractions, with a number of countries, including the former Federal Republic of Germany and Japan, legislating against their use in spreads and other fat products.

Copyright 2002 by Marcel Dekker. All Rights Reserved.

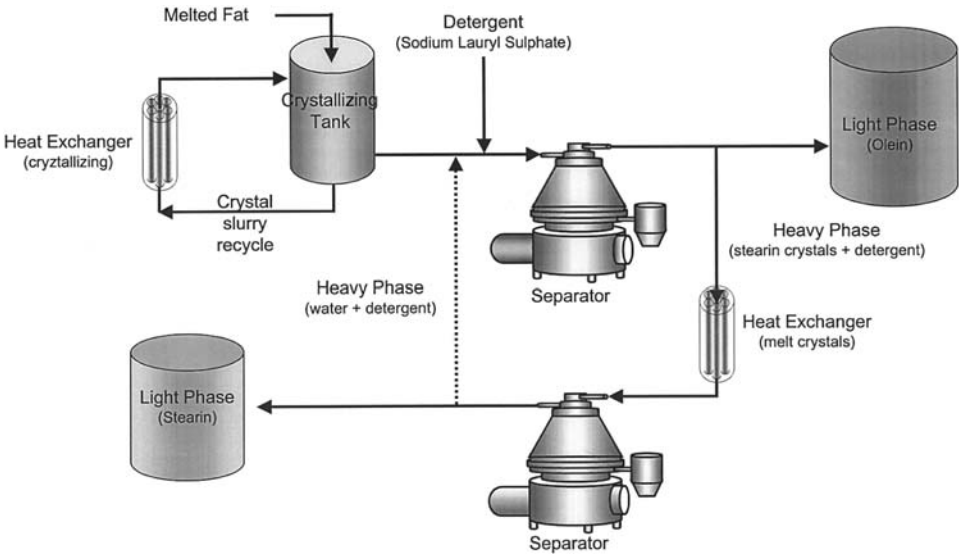

Figure 17 Schematic layout of a detergent fractionation plant.

Efficient detergent separation requires crystals that are smaller and more needle-like than the spherulite crystals common for a dry fractionation process coupled with filtration [21], because the detergent more easily wets such crystals. In addition, the formation of crystals agglomerates is discouraged, because they tend to hold olein that is then drawn into the stearin phase. However, even conventional spherulites can be separated using detergents. When stearin crystals in olein, as a slurry (Fig. 18a), are contacted by the aqueous detergent solution, the crystals begin to enter the aqueous phase (Fig. 18b). The olein phase first separates into droplets (Fig. 18c), which then coalesce into a continuous oil phase (Fig. 18d). A simple stirred jacketed tank is all that is necessary as a crystallizer for detergent fractionation, because most of the crystallization actually takes place in an external heat exchanger, with continuous recycle through it and back to the crystallizer. Once steady-state operation is achieved, the slurry can be pumped continuously from the crystallizer for detergent separation at a rate that is equivalent to the addition of fresh feedstock oil.

4. Centrifugal Separation

Several workers have advocated separating stearins and oleins by the use of centrifugation, but only a relatively few commercial installations are known to exist. For example, Westfalia offers a nozzle centrifuge as an alternative to membrane

Copyright 2002 by Marcel Dekker. All Rights Reserved.

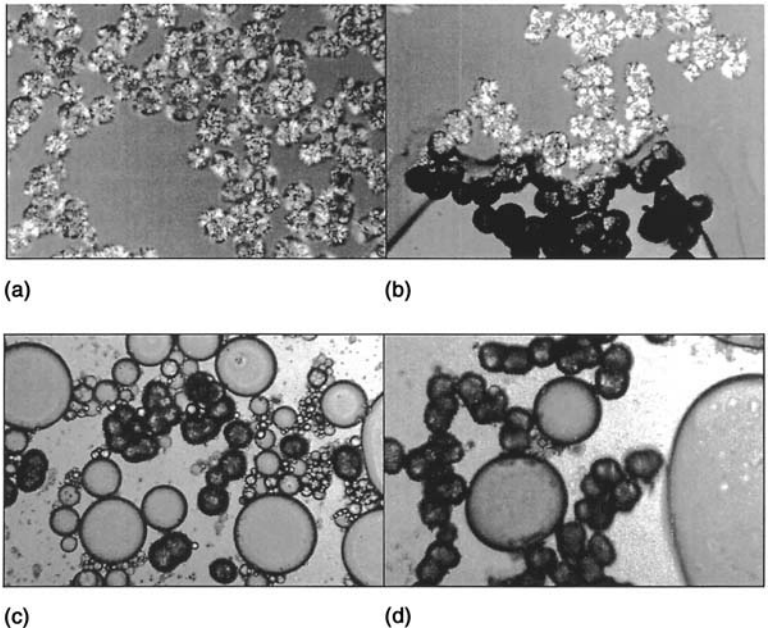

Figure 18 Detergent fractionation: (a) crystal slurry; (b) crystal slurry contacting aqueous detergent and crystals moving into the aqueous phase; (c) olein separating into droplets; (d) olein droplets coalescing into a continuous oil phase.

filtration for AMF fractionation. Figure 19 shows an example of the Westfalia device. The nozzle size may be changed to effect different degrees of separation. The advantage of this type of separation is that not only is it continuous, it is also totally enclosed. This is very important when fractionating fats such as AMF that may deteriorate if exposed to oxygen or light. Nozzle centrifuges are being used in at least one AMF fractionation plant in Switzerland [22], and Tirtiaux also offers one for the production of what it terms a ''soft stearin.''

Others have also advocated centrifugation as a means of separating stearin crystals from oleins. Dijkstra and Maes [23,24], for example, described processes that use a basket centrifuge process for this purpose. A typical basket centrifuge with a horizontal basket and continuous removal of the filter cake is shown in cross section in Figure 20. A photograph of the centrifuge is shown in the inset. I have evaluated a laboratory-scale basket centrifuge for AMF fractionation (D. Illingworth, unpublished results, 1999) and found the yield and quality of the fractions obtained in a single-stage fractionation at 20°C to be comparable to those from a test pressure filter.

Copyright 2002 by Marcel Dekker. All Rights Reserved.

Figure 19 A nozzle centrifuge used for separating fat crystals from liquid oil. (Courtesy of GEA-Westfalia Separators, Oelde, Germany.)

Deffense [25] also patented a centrifugal separation process for fat crystals, based on a hydroejector, and Breeding and Marshall [26] successfully fractionated AMF using a filter centrifuge.

C. Advances in Melt Fractionation

Were any of the early pioneers in fat fractionation able to visit a modern dry fractionation plant they would still recognize the basic process. Melted fat is crystallized batchwise in large tanks, and then the crystals are filtered or separated from the remaining liquid oil in some way. It has always been assumed that batch processes are inefficient in their use of resources compared with continuous processes. As will be seen in the next sections, improvements have been sought in two main areas; first, the final elimination of entrainment, and second the key to continuous fractionation from the melt. A selection of the most recent attempts to achieve these aims follows.

Copyright 2002 by Marcel Dekker. All Rights Reserved.

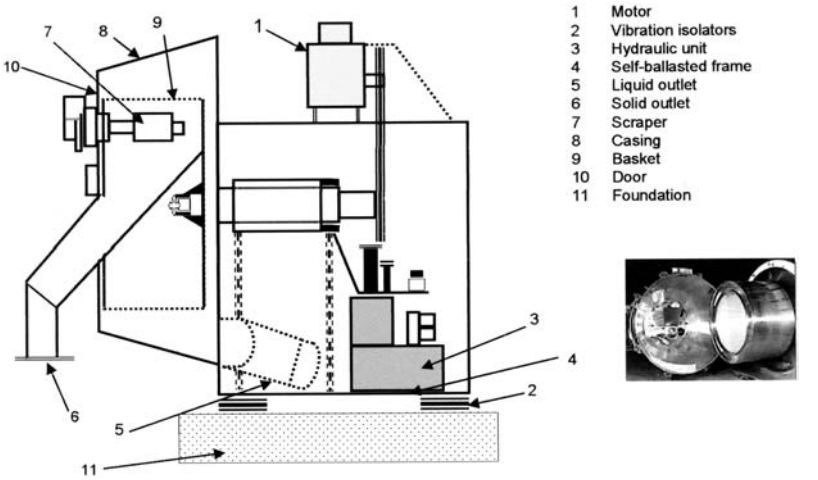

Figure 20 Cross section of a basket centrifuge that may be used for separating stearin and olein. Inset Photograph of the centrifuge with the door open to reveal the basket. (Courtesy of Rousselet Centrifuges, Annonay, France.)

1. Batch Fractionation Processes

In the 1990s several new melt fractionation techniques were suggested, many of them in the field of AMF fractionation. The STAR crystallizer [27] overcomes the limitations of conventional crystallizers, particularly with regard to crystallizing time and the minimum temperature that can be reached without the crystal suspension becoming too thick to filter. The crystallizer has cooled stirring surfaces that increase the heat transfer rate and exert a lower mechanical stress on the crystals. This allows lower temperatures to be reached in palm oil fractionation than with conventional crystallizers. Yields of stearin are thus higher without compromising the quality, and the olein has a higher iodine value.

A new process for a rapid multistage AMF fractionation [28] uses a sintered stainless steel dynamic microfiltration system with a pore size of 10 μm. The crystal slurry is formed rapidly compared with the conventional melt fractionation process, and the slurry is pumped at 200 mL/min at a pressure of 360 kPa. A filtrate flow of 140 mL/min is achieved for fractionation at 28–30°C. However, the SFC profiles given in the accompanying examples suggest that the retentate from this process may be highly contaminated with soft fraction.

Another method for separating high and low melting fat fractions [29] involves dispersing the fat in a hydrophilic medium followed by tangential filtration through a semipermeable hydrophobic membrane, similar to those used in ultrafiltration.

Copyright 2002 by Marcel Dekker. All Rights Reserved.

Fat may also be crystallized for later fractionation by using pressure filtration, according to Tirtiaux and Schmitz [30]. The fat is melted and then dispersed as small droplets into a stirred tank containing a precooled aqueous medium. This can be purely water or may contain an antioxidant such as citric acid. Another option is to dissolve a nonionic detergent in the water.

The size of the beads is critical, and the crystallizer tank is specially designed to allow fat to be introduced as droplets through a specially designed distributor at the bottom. The temperature and rate of addition are adjusted to maintain the temperature of the beads that form. The temperature of the mix is held until the crystallization has reached equilibrium, and then the mix is transferred to a membrane filter press. The aqueous phase is separated from the fat beads using low pressure, and then the liquid fraction of the fat is squeezed from the beads by increasing the pressure. Unlike conventional batch crystallization from the melt, where the crystallization may not have reached equilibrium by the time the crystals are filtered, this process allows the crystals to reach equilibrium before filtration. The result is a more efficient separation than that achieved by conventional filtration.

Conventional melt fractionation of vegetable and animal fats may be enhanced by the addition of seed material [31]. During the crystallization growth stage of the fractionation process, TAG material that is different in composition from the material being crystallized and would crystallize readily is added to prevent the formation of unfilterable paste-like crystals. The seed material must be added continuously in the melted state in such a way that the temperature equilibrium in the crystallizer is not compromised. Filtration becomes easier, and there is less entrainment.

Another melt fractionation process [32] is designed to produce a kinetically stable crystalline form of stearin that results in a high yield of olein. The process requires long crystallizing times and slow stirring and results in crystals that filter readily and have less entrainment than in a conventional process.

2. Continuous Fractionation Processes

Continuous crystallization applied to AMF fractionation was the subject of considerable research during the last decade of the twentieth century. One such continuous fractionation process [33] requires that melted AMF be held in a tank and then cooled rapidly at 20°C/min by being pumped through an external heat exchanger such that the AMF becomes supercooled. The supercooled fat then passes into a nucleation chamber that is small in volume and then into a crystallizer where the nuclei grow into crystals. The nucleation chamber is used to provide energy input sufficient for the nucleation threshold of the desired crystallizing species to be reached, by using multiple agitators. The AMF then passes into the crystallizer, where the crystals are formed from the nuclei and allowed

Copyright 2002 by Marcel Dekker. All Rights Reserved.

to sediment. Part of the olein is removed from the top of the crystallizer, and the crystal slurry is removed from the bottom and transferred to a filtration system. By replenishing the holding tank the process may be made continuous. The fractions are obtained in yields equivalent to those obtained from conventional fractionation processes and have equivalent physical properties.

Breitschuh [34] proposed that AMF can be fractionated continuously by using a scraped-surface heat exchanger (SSHE). Unlike the conventional use of SSHE for fat processing, the temperature of the coolant is carefully controlled to within $\pm 0.5°C$ by ensuring that the mass flow through the jacket is maintained at a high rate. Both the coolant temperature and the amount of shear in the SSHE are critical, and according to Breitschuh the shear has a major influence on the crystallization kinetics. The temperature differential between the crystallizing fat and the coolant should be as low as possible to ensure minimum formation of mixed crystals. The soft fraction is uncontaminated with hard fraction TAGs, because the crystallization stage is at more of an equilibrium than in conventional batch crystallization.

Cross-flow filtration allows the olein fraction to be recovered continuously. However, this type of filtration only concentrates the crystal slurry and does not separate the crystals. There is a tendency for the smaller, needle-like crystals to pass through the filter medium, contaminating the liquid fraction. Complete separation of the fractions still requires conventional filtration such as with a membrane filter.

The method has been scaled up [35] and has the advantage that the fat is cooled rapidly to the crystallizing temperature compared with conventional stirred-tank fractionation. Moreover, the crystal size is uniform (and small), as is the TAG composition of the crystals. This leads to less entrainment of liquid in the mass because no large spherulites are present.

Keulemans and van den Oever [36] demonstrated that countercurrent crystallization from the melt can be applied to any semisolid TAG mixture. The principle of their process requires a minimum of two stages, with recycle of the hard fraction from the second stage back to the beginning of the process. This results in a purer highest melting fraction once steady state is reached.

A novel means of crystallizing and separating in the same apparatus was described by Onwulata and Goldberg [37]. The equipment is in the form of a cylindrical pipe fitted with an agitator. The pipe has a series of temperature-controlled zones, with the coolest at the top. The highest melting fraction is deposited near the top, and the lower melting fraction is drained from the bottom after batch crystallization. By adjusting the thermal profile up the tube, fractions with different melting points can be obtained. Although this may appear to have some drawbacks because the solid has to be scraped from the surfaces, it cannot be discounted. Their method has some similarity to thin-layer crystallization techniques that have been the subject of studies by American, German, and New

Copyright 2002 by Marcel Dekker. All Rights Reserved.

Zealand researchers [38–40]. Thin-layer crystallization results in a high degree of efficiency with low entrainment, particularly if a ''gas sweating'' stage is applied to reduce entrainment even further.

D. Solvent Fractionation

Solvent fractionation is the most efficient of all the fractionation processes. It is also the most expensive. The crystallizers used for solvent fractionation may be scraped-surface heat exchangers (SSHEs), such as the one shown schematically in Figure 21, with a typical commercial filter shown in Figure 22. The miscella of melted fat and solvent passes into the SSHE, where the high shear and temperature differential and relatively low viscosity encourage rapid crystallization. The mean residence time in the crystallizer is often on the order of 30 min, compared with up to 24 h for the Tirtiaux process.

The most important aspect of solvent fractionation is the washing stage during filtration, which allows entrained olein TAGs in the stearin cake to be washed out into the olein filtrate stream. Horizontal belt filters, as shown diagrammatically in Figure 23, readily allow the filter cake to be washed after the main filtration. By removing entrained olein from the stearin cake, the washing process improves the separation of stearin and olein. Figure 24 shows a filter assembly that is designed especially for solvent fractionation. These filters are totally enclosed so they can operate in a flameproof environment. The wash streams can be segregated from the main filtrate stream, which contains the majority of the olein. The early wash streams contain olein that is displaced from the filter cake, but later wash streams may contain desirable TAGs that would usually be part of the stearin and that may be dissolved during washing. The concentration of

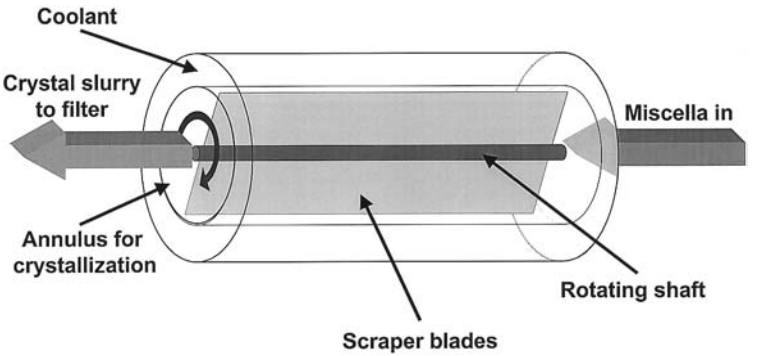

Figure 21 Schematic of an SSHE crystallizer.

Copyright 2002 by Marcel Dekker. All Rights Reserved.

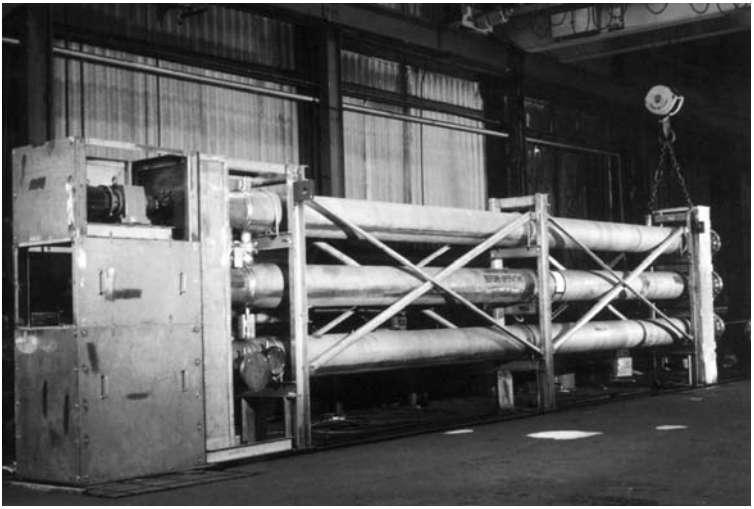

Figure 22 Armstrong-Chemtec scraped-surface crystallizer used in the solvent fractionation of fats. (Courtesy of Chemtec Pte. Ltd. Singapore.)

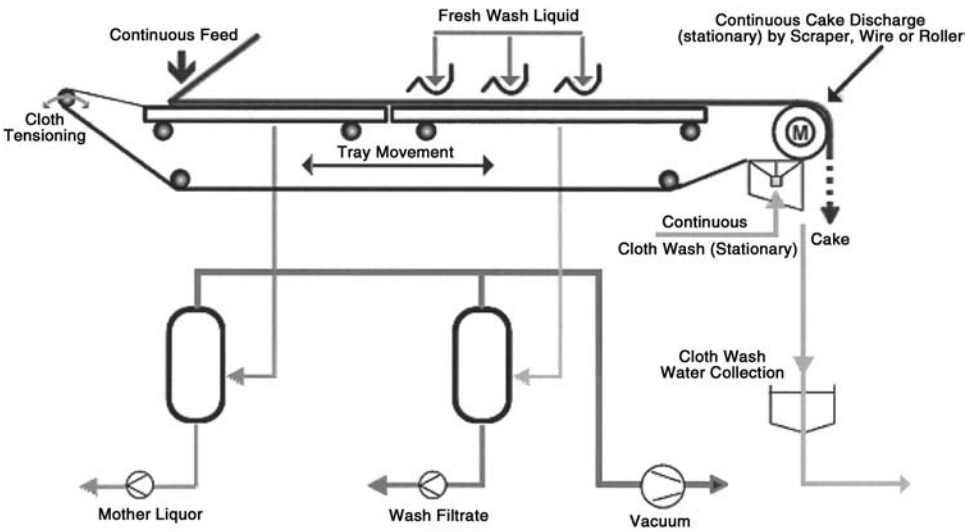

Figure 23 Schematic of a continuous moving-belt filter with wash sprays as used for the solvent fractionation of fats. (Reproduced courtesy of Pannevis BV, Utrecht, Netherlands.)

Copyright 2002 by Marcel Dekker. All Rights Reserved.

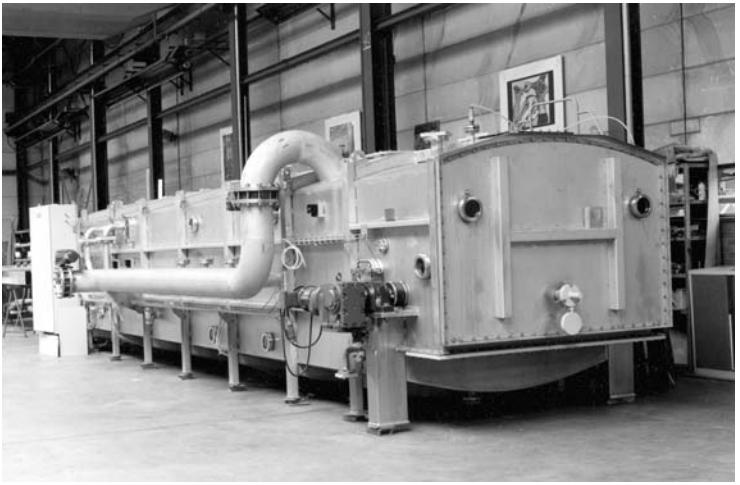

Figure 24 Pannevis continuous moving-belt filter for the solvent fractionation of oils and fats. (Reproduced courtesy of Pannevis BV, Utrecht, Netherlands.)

fat in the final wash stream is usually low. Rather than sending these streams to solvent recovery, recycling to the front of the process allows a second chance to recover the final traces of an often valuable fraction. This has a major effect in lowering the overall energy requirements because of the reduction of the amount of solvent in the plant at any one time. Either a single-stage or a multistage process, as shown in Figure 25, can be used for solvent fractionation.

The merits or otherwise of solvent fractionation were studied thoroughly by Hamm [41]. He concluded that the use of solvent fractionation was limited by the fact that there are no ''standard'' plants—each plant has to be designed for a specific purpose.

The main solvents used for fractionation are acetone and hexane. However, only the Bernadini process [42] was designed around the use of the latter. Although it requires lower crystallization temperatures, hexane has a much lower latent heat of evaporation than acetone. The solvent-to-oil ratio required for hexane fractionation is lower than that for acetone because the solubility of fats in hexane is higher. However, its drawback is that hexane has a lower selectivity for triglycerides than acetone. In addition, hexane, unlike acetone, does not require rectification for drying after recovery. Thus the energy required for solvent recovery is about half of that required for acetone.

Solvent fractionation of palm oil from acetone has been used extensively for manufacture of high quality palm midfractions (PMFs) for confectionery use, particularly in cocoa butter equivalents or extenders (CBEs) [43]. Acetone frac-

Copyright 2002 by Marcel Dekker. All Rights Reserved.

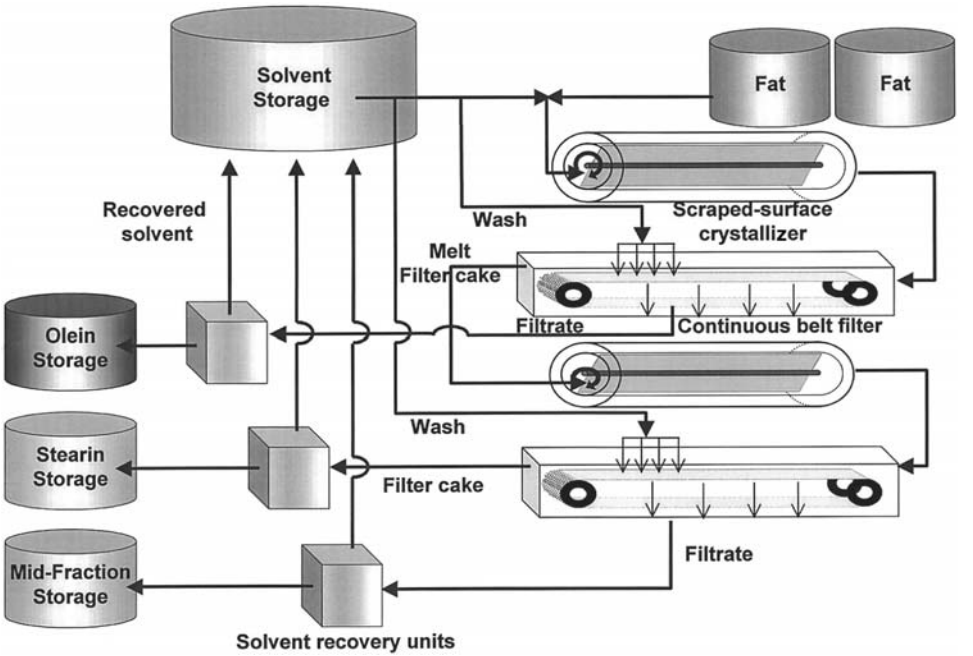

Figure 25 Schematic layout for multistage solvent fractionation.

tionation of AMF was the basis of a New Zealand patent for a spreadable butter in the 1970s [44].

E. Supercritical and Other Fractionation Technologies

Supercritical fractionation has been touted for many years as an ideal process for fractionation of AMF [45–47], but no studies of its use for other oils and fats have been published. One of the main attractions for AMF was that it is possible to efficiently remove cholesterol from it [48]. Such studies came about at a time when cholesterol was first linked specifically to heart disease and arterial deterioration. The majority of people now recognize that this is only one factor in a very complex situation, and thus the need for cholesterol reduction is less important. Much of the published work has revolved around the use of carbon dioxide, this being the most common of the gases with a supercritical stage in their liquid state. The choice of carbon dioxide for this purpose is a mystery,

Copyright 2002 by Marcel Dekker. All Rights Reserved.

because the solubility of TAGs in supercritical carbon dioxide is not very high. TAGs have a higher solubility in other supercritical solvents such as ethylene or propane [49]. The latter is more expensive and requires the same flameproofing precautions as solvent fractionation (see Section II. D).

In spite of the volume of published studies, the practical use of supercritical fractionation now appears to be limited to the extraction of high value components, e.g., the removal of something that may render a product more salable yet maintain a high value, such as the decaffeination of coffee. Such an application is unlikely for fats, unless specific TAGs can be identified as having some nutritional or other high value application. Current commercial fractionation technologies are far cheaper and easier to operate to obtain fractions with specific physical properties. Even the push to use it for AMF fractionation has lost its impetus. One of the attractions for fractionating AMF this way was to produce a cold-spreadable butter [50]. However, it has been demonstrated commercially that this can be achieved easily and cheaply by using one of the standard melt fractionation methods (see Section II.B) [51,52]. The result is that supercritical fractionation of fats is now only a scientific curiosity, along with other technologies such as short-path distillation [53]. The latter was studied in relation to AMF fractionation, but its major drawback is its destructive effect on the flavor of AMF.

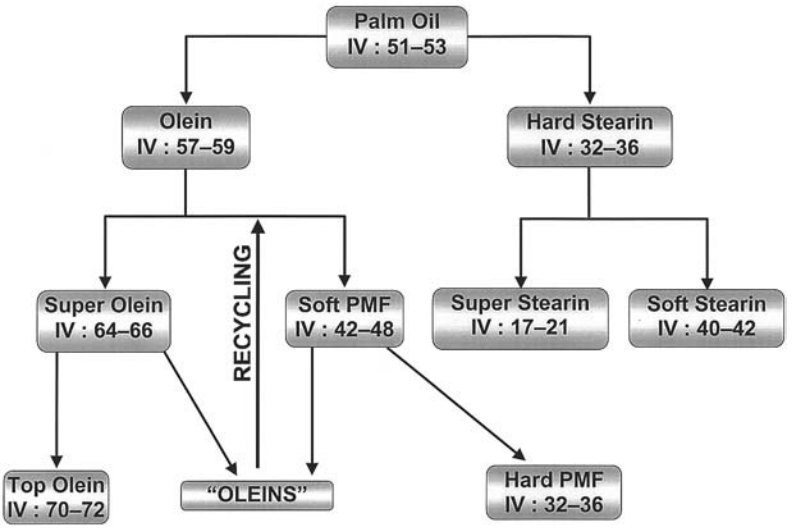

Figure 26 Multistep fractionation of palm oil. (Courtesy of S.A. Fractionnement Tirtiaux, Fleurus, Belgium.)

Copyright 2002 by Marcel Dekker. All Rights Reserved.

Table 1 Properties of Palm Oleins

	Iodine Value	Cloud point (°C)	β-Carotene (mg/kg)
Neutralized palm oil	51.9	21.6	382
Olein	56.7	8.1	409
Super olein	63.2	3.3	670
Top olein	71.3	−2.4	854

Source: Reproduced courtesy of S.A. Fractionnement Tirtiaux, Fleurus, Belgium.

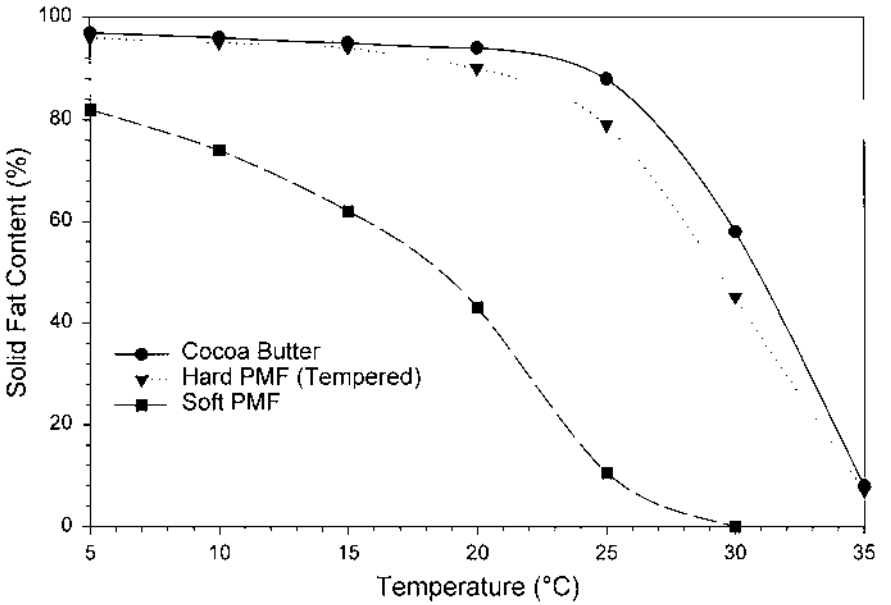

Figure 27 SFC profiles of PMFs compared with cocoa butter. (Courtesy of S.A. Fractionnement Tirtiaux, Fleurus, Belgium.)

Copyright 2002 by Marcel Dekker. All Rights Reserved.

III. APPLICATIONS FOR FAT FRACTIONS

Fat fraction applications are best illustrated by reference to specific oils and fats that are regularly fractionated.*

A. Palm Oil

Palm oil may be fractionated in a multistep process as shown in Figure 26 to give a range of products with different melting and crystallization characteristics.

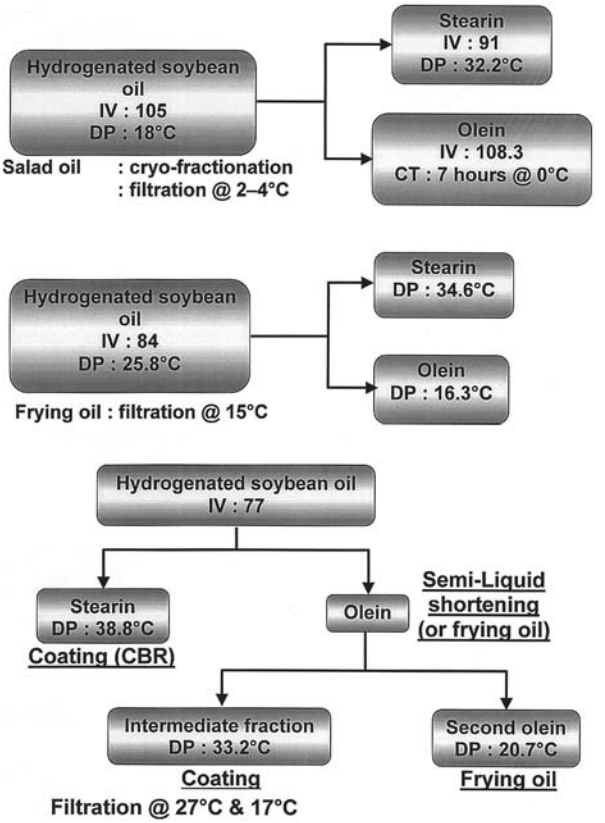

Figure 28 Fractionation of hydrogenated soybean oil at various temperatures. (Courtesy of S.A. Fractionnement Tirtiaux, Fleurus, Belgium.)

* The examples given here are a selection from those which may be found on the web-site of S.A. Fractionnement Tirtiaux at www.tirtiaux.com.

Copyright 2002 by Marcel Dekker. All Rights Reserved.

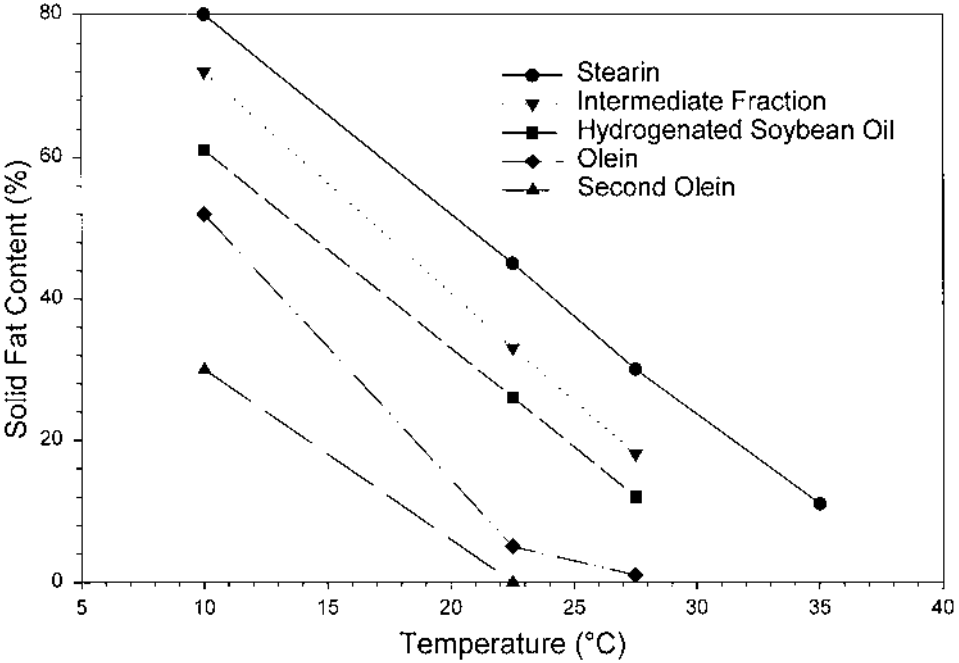

Figure 29 SFC profiles for hydrogenated soybean oil fractions. (Courtesy of S.A. Fractionnement Tirtiaux, Fleurus, Belgium.)

The hard palm midfraction (PMF) may be used either on its own or in admixture with StOSt fractions from shea butter or sal fat to produce cocoa butter equivalents such as Coberine, which is highly compatible with cocoa butter [54]. At one time the hard stearin was of little use and tended to end up as a feedstock for soap manufacture. However, it has become an important starting material for oleochemical production and has also found use in margarine manufacture, where, after further modification, its zero-trans status makes it useful for replacing hydrogenated oils.

If the palm oil is subjected to only a ''soft'' pretreatment and low temperature deodorization, much of the naturally occurring β carotene is retained in the oil and tends to concentrate in the olein fractions during fractionation, as shown in Table 1. The various oleins are used in salad and frying oils with a high oxidative stability. The stearins and soft PMF find use in the manufacture of margarines and shortenings.

The solid fat content (SFC) profile may be used to compare the physical properties of the various fractions. SFC can be measured by using one of the standard pulsed nuclear magnetic resonance (pNMR) methods [55,56]. In Figure

Copyright 2002 by Marcel Dekker. All Rights Reserved.

27 the SFC profiles of the soft and hard palm midfractions are compared with that of cocoa butter.

B. Hydrogenated Soybean Oil

Hydrogenated oils can also provide fractions for confectionery use. In this case the function is to replace cocoa butter as the fat used in enrobing or coating. Various fractionation schemes for hydrogenated soybean oil are shown in Figure 28, with the SFC profiles shown in Figure 29. The oleins in these examples make good frying or salad oils with high oxidative and cold stabilities, with the stearin being used in margarine as a hardstock ingredient. The term cryofractionation is used to describe fractionation where the filtration step is carried out at very low temperature. In these instances, the filter is shrouded to maintain the low temperature.

C. Milkfat

Figure 30 shows a typical scheme from Tirtiaux for multistage fractionation of AMF, complete with a recycle stage requiring cryofractiona-

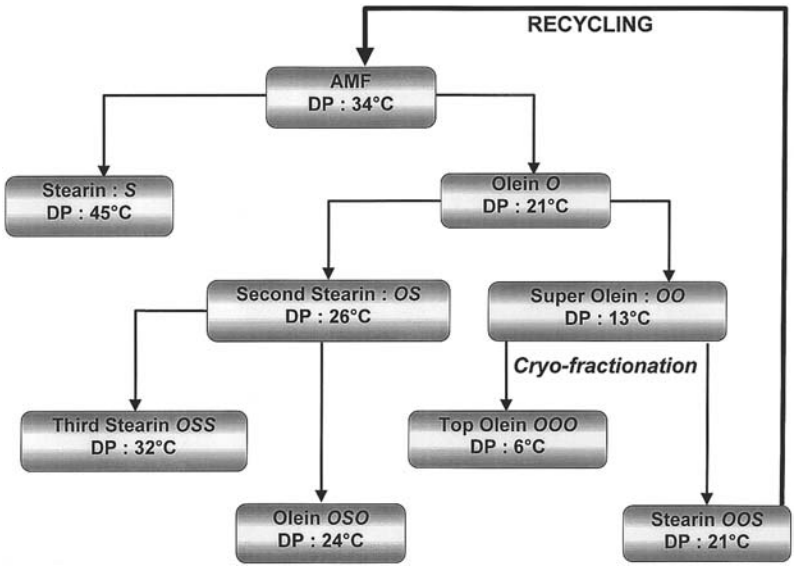

Figure 30 Multistep fractionation of AMF. (Courtesy of S.A. Fractionnement Tirtiaux, Fleurus, Belgium.)

Copyright 2002 by Marcel Dekker. All Rights Reserved.

Figure 31 Florentine filter, shrouded and air-conditioned for cryofractionation.

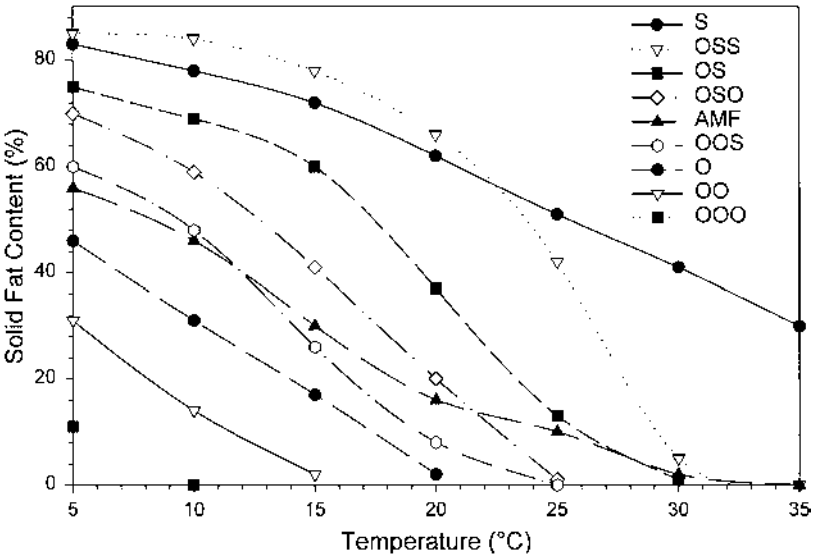

Figure 32 SFC profiles of AMF fractions. (Courtesy of S.A. Fractionnement Tirtiaux, Fleurus, Belgium.)

Copyright 2002 by Marcel Dekker. All Rights Reserved.

tion is the standard process with the refinement that the Florentine filter is shrouded and air-conditioned to maintain the low temperature during filtration, as shown in Figure 31. This effectively produces five fractions from the parent AMF, all with different applications dictated by their SFC profiles as shown in Figure 32. The high melting stearin may be used in applications such as pastry making (Puff pastry, croissants, and Danish) and confectionery, as an antibloom inhibitor in chocolate, a constituent of cold-spreadable butter [57], and a hardstock for margarine in place of hydrogenated fats [58]. The softer second stearin is an excellent puff pastry fat for low temperature use, with its low dropping point imparting good mouthfeel to the baked goods. The various oleins may be used in making both butter and cheese. For example, butter for creaming applications may be softened by the addition of olein to improve its performance. The oleins can also be combined with the hard stearin in cold-spreadable butter.

REFERENCES

1. V Gibon, A Tirtiaux. Winterisation, dewaxing, fractionation—Crystal clear. World Conference and Exhibition on Oilseed Processing and Utilization, Cancun, November 2000.
2. AJC Anderson, PN Williams. Margarine. Oxford, UK: Pergamon Press, 1965, pp 1–2.
3. JB Rossell. J Am Oil Chem Soc 62(2):385–390, 1985.
4. KK Rajah. In: AS Grandison, MJ Lewis, eds. Separation Processes in the Food and Biotechnology Industries: Principles and Applications. Cambridge, UK: Woodhead, 1996, pp 207–241.
5. KE Kaylegian, RC Lindsay. Handbook of Milkfat Fractionation Technology and Applications. Champaign, IL: AOCS Press, 1994.
6. RW Hartel, KE Kaylegian. In: N Garti, K Sato, eds. Crystallization Processes in Fats and Lipid Systems. New York: Marcel Dekker, 2001, pp 381–428.
7. M Kellens. In: W Hamm, RJ Hamilton, eds. Edible Oil Processing. Sheffield: Sheffield Academic Press, 2000, pp 161–166.
8. RE Timms. Theory and kinetics of fractional crystallisation of fats. Presented at Palm Oil Research Institute of Malaysia Course on Palm and Palm Kernel Oils, Malaysia, 1985.
9. G Singh. Am Inst Chem Eng (Symp Ser) 72:100–109, 1974.
10. M van den Kommer, A Visser, P van Dam, J Henricus. Fractional crystallisation of triglyceride oils using monoglyceride or diglyceride for separation enhancement. Patent WO 9526391, 1995.
11. M van den Kommer, PR Smith, A Visser, C Winkel. Dry fractionation of triglyceride oils and crystallizing modifying substance. Patent WO 9504122, 1995.
12. PH van Dam, JJ Eshuis, W Hogervorst, S Noomen. Fractional crystallization of triglyceride fats. Patent WO 9835001, 1998.
13. M Kellens. In: W Hamm, RJ Hamilton, eds. Edible Oil Processing. Sheffield: Sheffield Academic Press, 2000, p 158.

Copyright 2002 by Marcel Dekker. All Rights Reserved.

14. D Illingworth, RW Hartel. Crystallisation kinetics studies on anhydrous milkfat. Presented at 23rd World Congress, Int Soc Fat Research, Brighton, 1999.
15. F Tirtiaux. Ol Corps Gras Lipides 79:279, 1976.
16. M Kellens. Developments in fat fractionation technology. Paper No. 0042. Society of Chemical Industry, London, 1994.
17. T Willner, W Sitzmann, E-W Munch. Cocoa butter replacers produced by dry fractionation. Presented at 81st Annual Meeting Am Oil Chem Soc, Baltimore, 1990.
18. A Fjaervoll, Svenska Mejeritidningen 61:491–496, 1969.
19. A Fjaervoll. XVIII International Dairy Congress, Vol. IE. Sydney, 1970, 239.
20. RS Jebson. XVIII International Dairy Congress, Vol IE. Sydney, 1970, 240.
21. DA Glassner, EA Grulke, JI Gray. J Am Oil Chem Soc 61(12):1919, 1984.
22. H Eyer. Schweiz Milchztg/Le Laitier Romand 38:19, 2000.
23. AJ Dijkstra, PJ Maes. Separating solid and liquid phases in edible oils by centrifugal sieving or decantation with short residence time. Eur Patent EP 88949, 1983.
24. PJ Maes, AJ Dijkstra. Process for separating solids from oils. US Patent 4542036, 1985.
25. E Deffense. Process for separation of vegetable or animal fats including a step of aspirating the fatty material using a hydro-ejector to form a mixture of microcrystals. US Patent Appl WO 99423545, 1999.
26. CJ Breeding, RT Marshall. J Am Oil Chem Soc 72:449–453, 1995.
27. K Weber, T Homann, T Willner, Ol Corps Gras Lipides 5(5):381–384, 1998.
28. PJ Degen, T Alex, JW Dehn Jr. Fractionation of fatty materials by crystallisation. Eur Patent DE 4330256, 1994.
29. M Parmentier, S Bornaz, B Joumet. Process for separation of anhydrous fat into fractions with high and low m.p. and equipment for implementation of this process. Fr Patent Appl FR2 and 13 656 A1, 1995.
30. A Tirtiaux, Y Schmitz. Fat crystallisation method and apparatus therefore./Procede de crystallisation de matieres grasses et installation pour la mise en oevre ce procedet. Int Patent WO 97/14777, 1997.
31. PJ Maes, AJ Dijkstra, P Seynaeve. Method for dry fractionation of fatty substances. Eur Patent EP 651046, 1995.
32. JB Harris, CN Keulemans, LA Milton, EJG Roest. Dry fractionation process for separation of polymorphic fats and oils as stable crystals. Patent WO 9605279, 1996.
33. RW Hartel, L Baomin, S Yuping. Continuous crystallisation system with controlled nucleation for milk fat fractionation. Patent Appl WO 9851753 [US 46166 (19970512)], 1998.
34. B Breitschuh. Continuous dry fractionation of milk fat—Application of high shear fields in crystallization and solid-liquid separation. Doctor of Tech Sci Dissertation, Swiss Fed Inst Technol, Zürich, 1998.
35. H Eyer. Schweiz Milchztg/Le Laitier Romand 42:17, 2000.
36. CNM Keulemans, CE van den Oever. Counter current dry fractionation. Eur Patent Appl EP 0 399 597 A2, 1990.
37. CI Onwulata, N Goldberg. J Am Oil Chem Soc 74(6):697–683, 1997.
38. M Tiedtke, J Ulrich, RW Hartel. In: AS Myerson, DA Green, P Meenan, eds. Crystal Growth of Organic Materials. Washington DC: Am Chem Soc, 1995, pp 137–144.

Copyright 2002 by Marcel Dekker. All Rights Reserved.

39. S Peters-Erjawetz, J Ulrich, M Tiedtke, RW Hartel. J Am Oil Chem Soc 76(5):579–584, 1999.
40. X Chen. Layer crystallisation of milkfat in a shear field. M Eng Dissertation, Auckland Univ, Auckland, 2000.
41. W Hamm. Fette Seifen Anstrichm 88(suppl):533–537, 1986.
42. M Bernadini, E Bernardini. Olx Corps Gras Lipides 30:121–128, 1975.
43. W Hamm. Trends Food Sci Technol 6(4):121–126, 1995.
44. R Norris. Improvements in or relating to milk fat containing products and processes therefore. NZ Patent 172 101, 1974.
45. AR Bhaskar. Supercritical fluid processing of milk fat: Modelling fractionation and applications. PhD Dissertation, Cornell Univ, Ithaca, NY, 1997.
46. AR Bhaskar, SSH Rizvi, JW Sherbon. J Food Sci 58(4):748–752, 1993.
47. AR Bhaskar, SSH Rizvi, C Betoli, LB Fay, B Hug. J Am Oil Chem Soc 75(10): 1249–1264, 1998.
48. A Boudreau, J Arul. J Dairy Sci 76(6):1772–1781, 1993.
49. YC Wang, RW Hartel, J Woon, RS Jebson. J Food Process Pres 19(6):409–425, 1995.
50. D Dalemans. Lait et Nous 3:5–10, 1994.
51. KE Kaylegian, RC Lindsay. J Dairy Sci 75(12):3307–3317, 1992.
52. E Deffense. Fett Wiss Technol 89(suppl 13):502–507, 1987.
53. J Arul, A Boudreau, J Makhlouf, R Tardif, T Bellavia, J Am Oil Chem Soc 65(10): 1642–1646, 1988.
54. BW Minifie. Chocolate, Cocoa and Confectionery: Science and Technology. 3rd ed. New York: AVI, 1989, pp 101–103.
55. AOCS. Official Method Cd 16b-93, Solid Fat Content (SFC) by Low-Resolution Nuclear Magnetic Resonance—The Direct Method. Champaign, IL: Am Oil Chem Soc, 1999.
56. IUPAC. Official Method 2. 150. Solid Content Determination in Fats (Low Resolution Nuclear Magnetic Resonance). Oxford: Blackwell Scientific Publications, 1987, pp 59–70.
57. DS Munro, PAE Cant, AKH MacGibbon, D Illingworth, P Nicholas. In: R Early, ed. The Technology of Dairy Products. 2nd ed. Glasgow: Blackie, 1998, pp 198–227.
58. D Illingworth, TG Bissell. In: KK Rajah, DPJ Moran, eds. Fats in Foods. Glasgow: Blackie, 1991, pp 111–154.

Copyright 2002 by Marcel Dekker. All Rights Reserved.

12
Crystallization of Hydrogenated Sunflower Oil

María Lidia Herrera
University of Buenos Aires, Buenos Aires, Argentina

I. INTRODUCTION

Two distinct processes take place during crystallization: nucleation and growth. Nucleation involves the formation of molecular aggregates, which, above a certain size, are stable and can grow and develop into crystals. The nucleation process depends only on the degree of supersaturation or supercooling, the thermodynamic driving force for crystallization. As a crystal starts to grow, the difference in chemical potential between a molecule in solution or in the melt and one at a site in the crystal will determine the crystal's growth rate. This difference is directly related to the supercooling of an oil or the supersaturation of a solution. Growth also depends on the state of the crystal surface, on factors such as viscosity, molecular conformation, surface defects, presence of impurities, shear rates, and so on. In fact, nucleation and growth can happen simultaneously; the system is therefore in continuous evolution. New nuclei may form by primary or secondary nucleation. Additional changes in the crystals can occur as stable crystals modify their habit and metastable crystals undergo polymorphic transformations.

Rates of nucleation, growth, and polymorphic transformation are important factors that strongly influence the processing and storage characteristics of oils and fats. For example, fat crystals with a platelet-like shape must be below 30 μm in order to avoid a ''sandy'' mouthfeel in food products containing fat. Another challenging problem is the control of crystallization conditions so as to minimize the amount of solid fat required to create a fat crystal network in shortenings used in the manufacture of bakery products. In some food manufacturing processes, it is necessary that the fat crystallization process be complete by the end of the

Copyright 2002 by Marcel Dekker. All Rights Reserved.

production line. In this case, it is necessary to understand the crystallization behavior of the particular fat(s) used and the effects that processing as well as chemical and physical modification such as hydrogenation, interesterification, and fractionation may have.

The aim of this study is to investigate the nucleation and isothermal crystallization behavior of sunflower seed oil hydrogenated under selective and nonselective conditions. Two methods were used to measure induction times of crystallization and compared. Measurements of solid fat content by nuclear magnetic resonance (NMR) and a description of the growth behavior in terms of number and size of the crystals formed are also reported.

II. HYDROGENATION PROCESS

Hydrogenation and interesterification are two important industrial processes used to give fats and oils a desired functionality for specific products. Currently, formulators can raise the melting point and solid fat content of fats by (1) hydrogenating oils to different degrees of hardness or (2) interesterifying a liquid oil with a more saturated oil [1]. The aim of the hydrogenation process is to fully or partially saturate the double bonds in unsaturated fats and oils in order to obtain plastic fats and/or improve oxidative stability. The final product depends on the nature of the starting oil, the type and concentration of the catalyst used, the concentration of hydrogen, and the experimental conditions under which the reaction takes place [2]. Heterogeneous catalysts are known to catalyze undesirable side reactions such as cis–trans and positional isomerization of double bonds [3]. Geometric isomerism of the double bonds affects the melting behavior and general physical properties of fats to a greater extent than positional isomerism of the double bonds [4].

In this study, hydrogenation was performed in a batch slurry reactor using a supported nickel catalyst at a concentration of 0.05% (w/w). Two different hydrogenation conditions were selected: (1) high reaction temperature and low hydrogen gas pressure (463 K, 1 kg/cm^2) and (2) low temperature and high pressure (443 K, 2.5 kg/cm^2). There is general agreement that high reaction temperatures promote formation of trans isomers. High concentrations of hydrogen gas result in low selectivity and low trans isomer content, and low concentrations of hydrogen gas result in high selectivity and high trans isomer content. By using these two temperature and pressure conditions, we intended to obtain two oils with different chemical compositions in order to determine the effects of structure on crystallization behavior. Samples were collected every 15 min, beginning 45 min after the start of the reaction. Reactions were stopped after 145 and 150 min, respectively. Samples collected at the same time in both processes had similar iodine values and had a solid fat content that made them suitable for use as plastic

Copyright 2002 by Marcel Dekker. All Rights Reserved.

Table 1 Iodine Values and Mettler Dropping Points (MDPs) of Samples Taken During the Two Hydrogenation Processes

First hydrogenation				Second hydrogenation			
Sample	Time (min)	Iodine value	MDP (K)	Sample	Time (min)	Iodine value	MDP (K)
1	45	102	292.4	9	45	98	293.1
2	60	96	295.1	10	60	94	295.7
3	75	86	296.3	11	75	86	296.7
4	90	83	298.0	12	90	78	299.3
5	105	77	300.4	13	105	74	301.3
6	120	70	303.0	14	120	68	305.4
7	135	69	305.2	15	135	67	309.8
8	145	62	306.8	16	150	64	313.4

fats in different industrial applications, e.g., margarines or shortenings. The starting sunflower seed oil had an iodine value of 134. Iodine values and Mettler dropping points (MDPs) of all collected samples are reported in Table 1.

III. CHEMICAL COMPOSITION OF SAMPLES

Samples were analyzed for their fatty acid composition by gas–liquid chromatography (GLC) as described in Herrera et al. [5]. Results of the GLC analysis are shown in Figures 1 and 2. Only fatty acids present in percentages higher than 1% were included. The behavior of sunflower oil during hydrogenation is unusual [6]. The degree of isomerization is highest during the early stages of the reaction, steadily decreasing as the reaction proceeds. It is reasonable to assume that double-bond migration begins before hydrogenation occurs. As a result of double-bond migration, more reactive conjugated dienes are formed. These dienes are quickly hydrogenated, and therefore the degree of isomerization decreases. The original sunflower oil had the following composition: 0.1% 14:0, 6.7% 16:0, 3.6% 18:0, 0.7% trans-18:1, 21.9% cis-18:1, 66.3% cis-18:2, 0.2% 20:0, and 0.5% 22:0.

As can be observed in Figures 1 and 2, cis-18:2 (L) content was high in the starting oil and decreased with hydrogenation time. Concomitantly, trans-18:2 (Ln) content increased in the early stages of hydrogenation and remained constant thereafter. Stearic acid [18:0 (S)] and elaidic acid [trans-18:1 (E)] contents always increased as a function of hydrogenation time, 18:0 content being slightly higher in the second hydrogenation, whereas trans-18:1 content was slightly higher in the first hydrogenation.

Copyright 2002 by Marcel Dekker. All Rights Reserved.

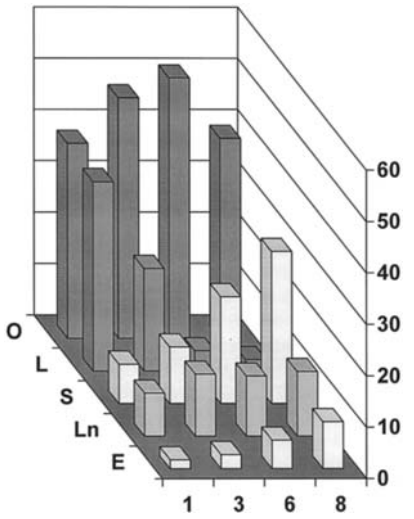

Figure 1 Fatty acid composition (%) of samples collected after 45 (sample 1), 75 (sample 3), 120 (sample 6), and 145 (sample 8) min of the first hydrogenation process. O, oleic acid; L, linoleic acid; S, stearic acid; Ln, linoleic acid, E, elaidic acid.

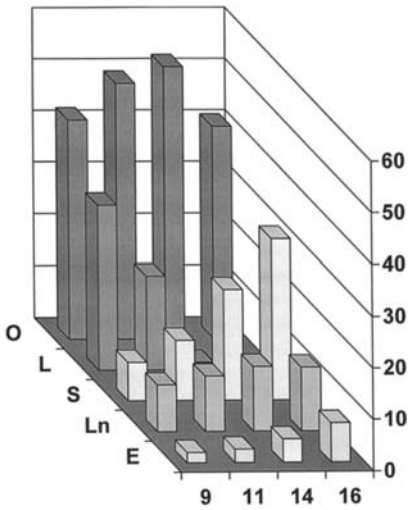

Figure 2 Fatty acid composition (%) of samples collected after 45 (sample 9), 75 (sample 11), 120 (sample 14), and 150 (sample 16) min of the second hydrogenation process. Abbreviations as for Figure 1.

Copyright 2002 by Marcel Dekker. All Rights Reserved.

No significant differences were observed in the global trans fatty acid content between the two hydrogenation processes, which is surprising taking into account the behavior of other systems such as soybean oil. We expected to obtain a higher trans isomer content when selective hydrogenation conditions were used. To obtain further information on the chemical composition of the samples, these were analyzed for their triacylglycerol (TAG) composition. TAGs were analyzed by using high-performance liquid chromatography (HPLC) as previously described [5].

When the starting oil was analyzed, 40 peaks could be discerned (Fig. 3). The six main TAGs were identified as OOO, PLO, OLO, PLL, LLO, and LLL, present in percentages of 9.9, 10.1, 7.5, 11.7, 23.5, and 29.1, respectively. Their retention times (t_R) are reported in Figure 3. The others were minor components with percentages less than 1.5.

Figures 4 and 5 show changes in the relative concentrations of these TAGs with hydrogenation time. Figures 6 and 7 show the trends for those TAGs that varied the most with hydrogenation time, between hydrogenation processes. Sam-

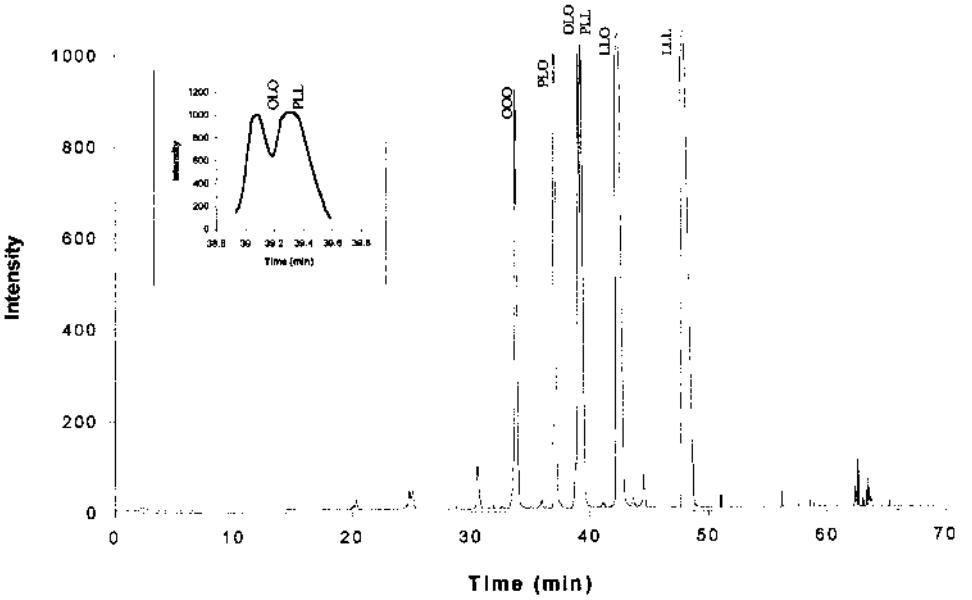

Figure 3 Typical HPLC chromatogram of the initial triacylglycerol (TAG) composition of sunflower seed oil. A magnification of the area in the vicinity of 39 min is also shown in the figure.

Copyright 2002 by Marcel Dekker. All Rights Reserved.

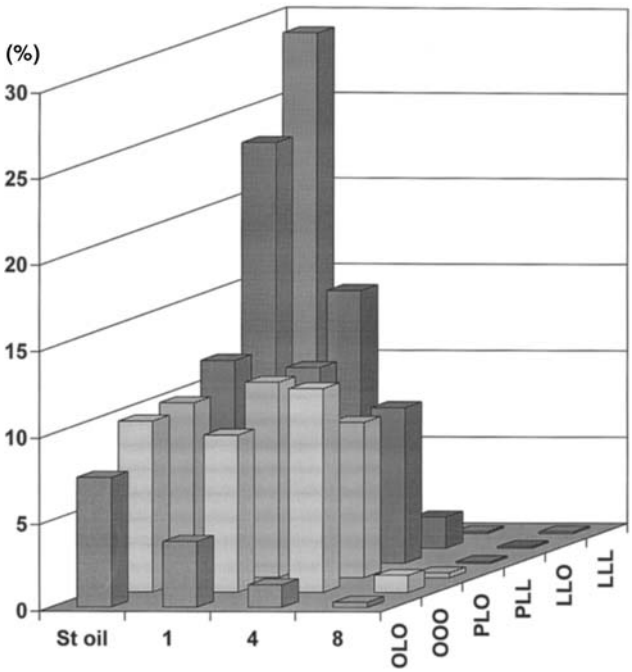

Figure 4 Changes in TAG composition (%) with hydrogenation time during the first hydrogenation. St oil, starting oil; 1, sample 1 (45 min); 4, sample 4 (90 min); 8, sample 8 (145 min).

ples 6–8 were taken during the first hydrogenation process (Fig. 6), and samples 14–16 were collected during the second hydrogenation process (Fig. 7).

The percentages of OLO, PLL, LLO, and LLL were greater in the starting oil and, as can be observed in Figures 4 and 5, decreased with hydrogenation time. After 105 min they could no longer be detected. Samples 5–8 and 13–16 did not contain these TAGs, in agreement with the decrease in cis-18:2 (L) shown in Figures 1 and 2. PLO and OOO relative contents started to increase after 45 min of hydrogenation; however, after 90 min they diminished to 1.0% or less (first hydrogenation). For the second hydrogenation, PLO and OOO levels initially increased, and then they diminished to nondetectable levels (samples 15 and 16). During both hydrogenation processes, TAGs with more saturated and trans fatty acids were formed. Only the TAG species that varied the most between hydrogenation processes were included in Figures 6 and 7. At the beginning of the hydrogenation reaction, TAGs with long retention times diminished whereas those with

Copyright 2002 by Marcel Dekker. All Rights Reserved.

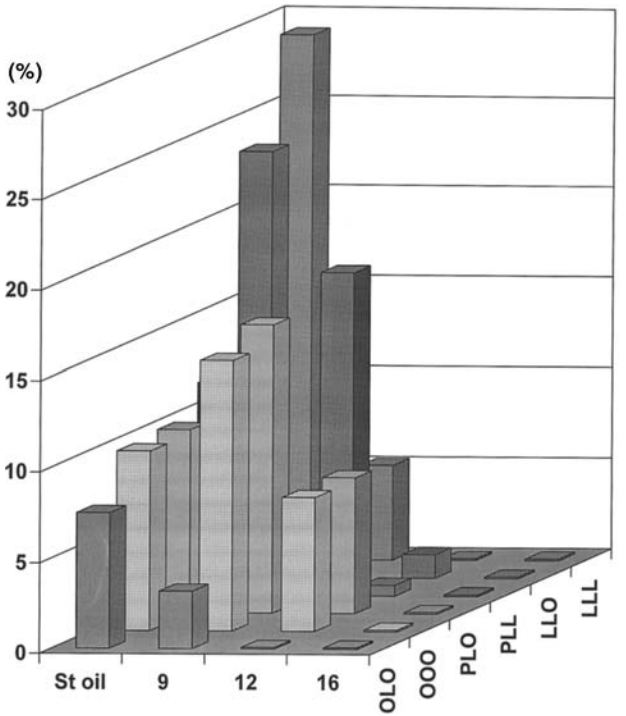

Figure 5 Changes in TAG composition (%) with hydrogenation time during the second hydrogenation. St oil, starting oil; 9, sample 9 (45 min); 12, sample 12 (90 min); 16, sample 16 (150 min).

intermediate retention times increased (Figs. 8 and 9). These TAGs were present in high proportions in samples 1–4 and 9–12. Then, 90 min after the start of the reaction, intermediate retention time TAG content diminished as short retention time TAG contents increased. The TAG compositions of samples 6–8 and 14–16 were, as expected, different. OSE, EEE, and EEO values, especially, were different, as shown in Figures 6 and 7. OSE and EEE were present in much higher percentages in samples 14–16 compared to the percentages found for samples 6–8. EEO was the main TAG present in samples 6–8. Sample 14 had higher percentages of OSE and EEE than sample 8 but lower ones than samples 15 and 16. It also had the highest EEO content of the three last samples taken during the second hydrogenation process (Samples 14–16).

Even though fatty acid composition was similar for the two hydrogenation

Copyright 2002 by Marcel Dekker. All Rights Reserved.

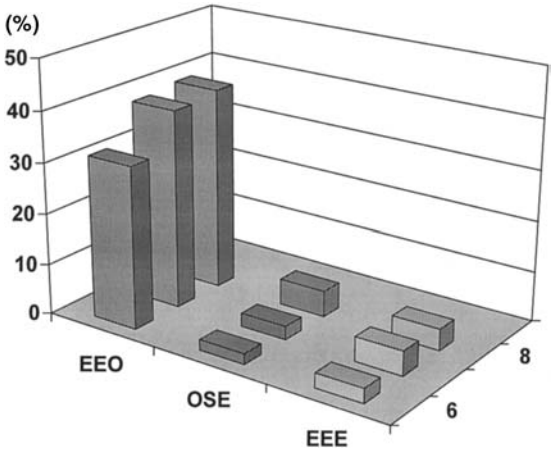

Figure 6 TAG species (%) that show the greatest variation between hydrogenation processes—first hydrogenation.

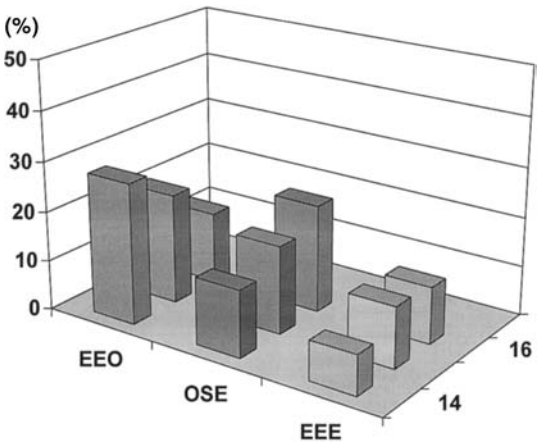

Figure 7 TAG species (%) that show the greatest variation between hydrogenation processes—second hydrogenation.

Copyright 2002 by Marcel Dekker. All Rights Reserved.

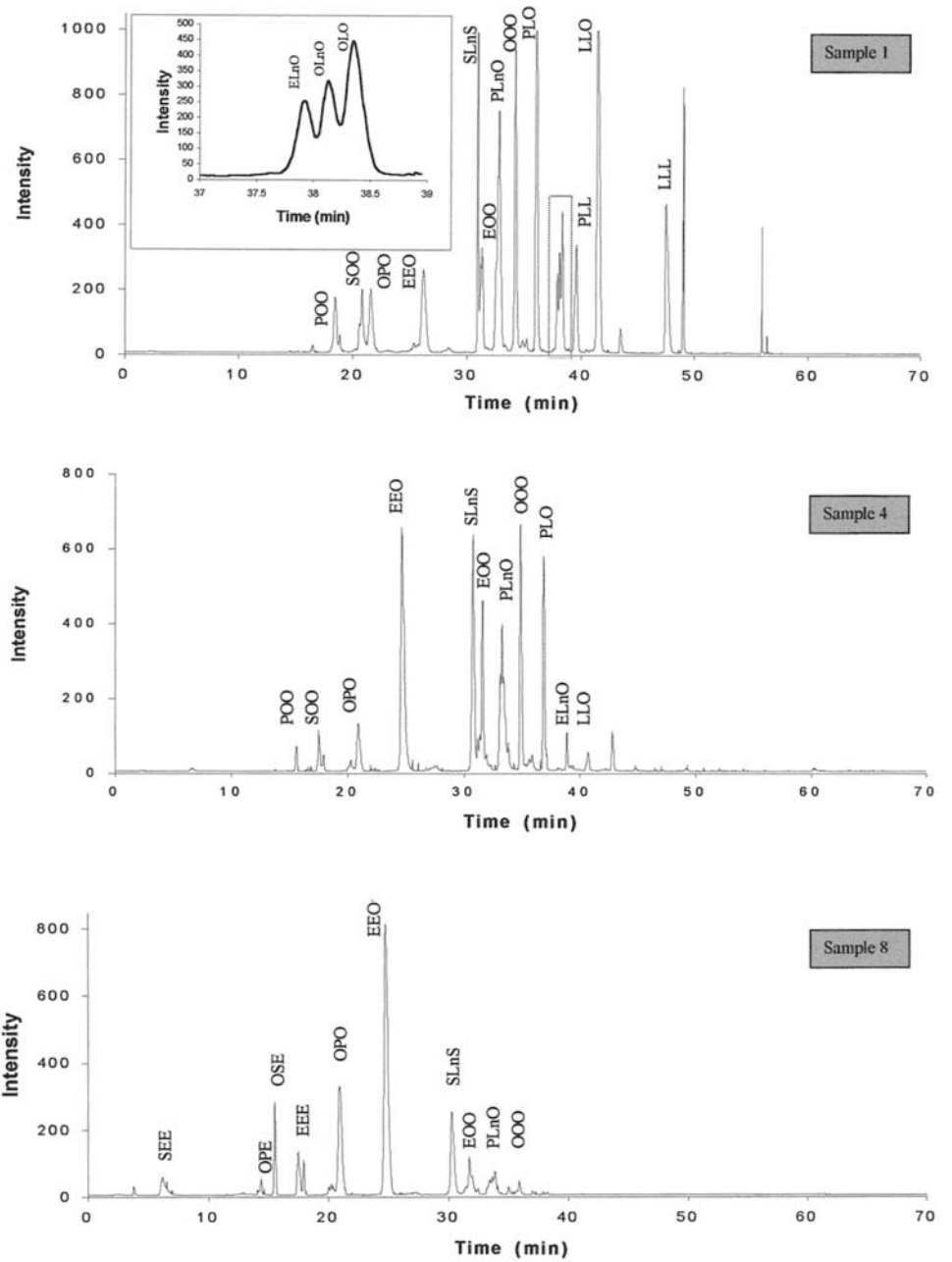

Figure 8 HPLC TAG chromatograms of samples 1, 4, and 8.

Copyright 2002 by Marcel Dekker. All Rights Reserved.

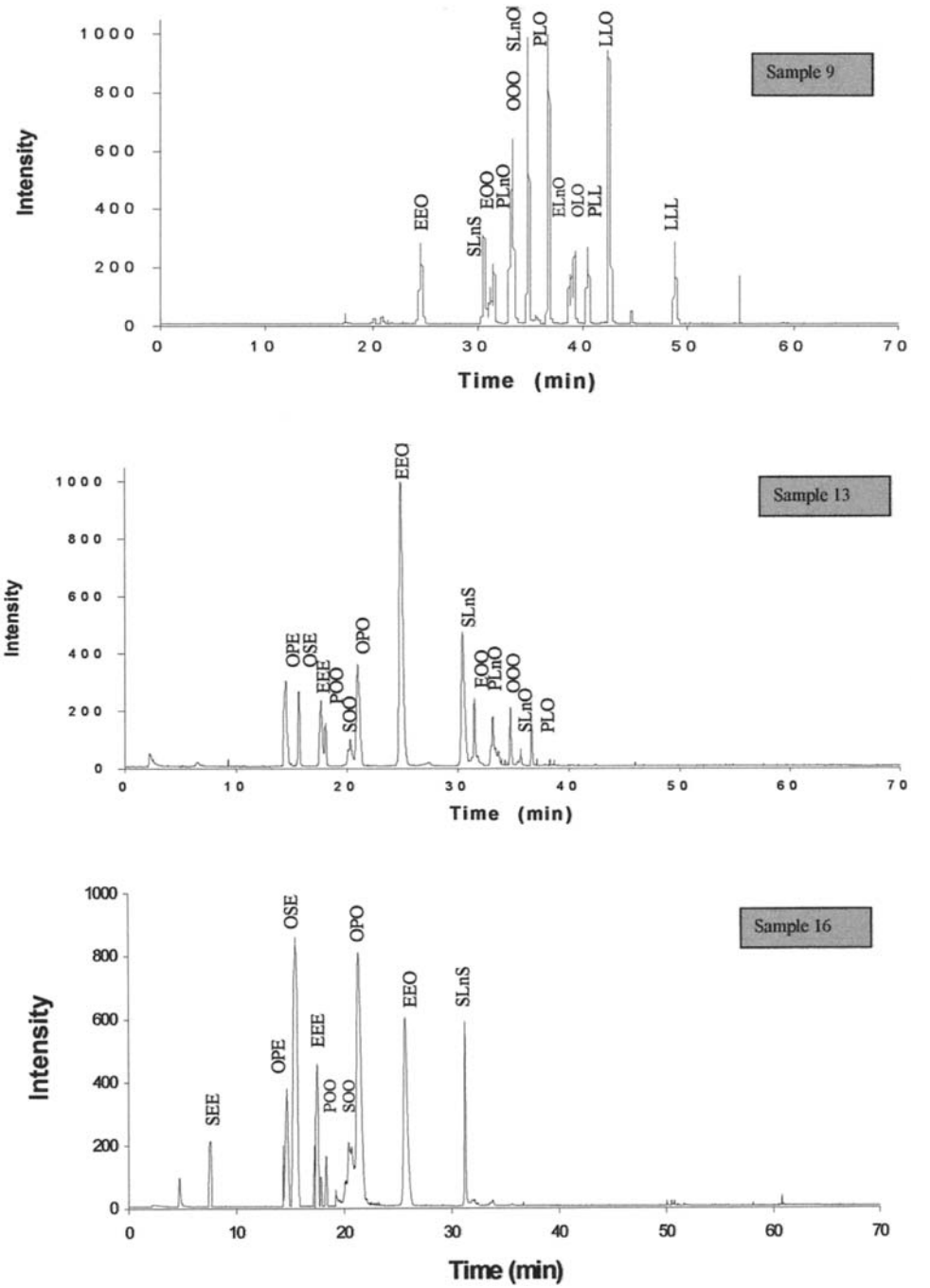

Figure 9 HPLC TAG chromatograms of samples 9, 13, and 16.

Copyright 2002 by Marcel Dekker. All Rights Reserved.

processes, TAG structure was markedly different. The differences in TAG structures were responsible for the observed differences in crystallization behavior (see Section V).

IV. EFFECTS ON NUCLEATION

Two methods were used to measure crystallization induction times: polarized light microscopy and laser polarized light turbidimetry, as described in Herrera et al. [5]. This polarized light laser turbidimetric technique (setup shown diagramatically in Fig. 10) was developed by our group.

The induction time is defined as the interval between the time at which the crystallization temperature is reached and the start of the crystallization process. A typical chart recorder output of the detected light intensity as well as the thermocouple's temperature record for the crystallization of hydrogenated sunflower seed oil are shown in Figure 11. The induction time for crystallization was defined as the time interval between the attainment of a particular crystallization temperature and the first detection of crystalline mass. Samples were melted and held at 353 K for 10 min. They were then crystallized by reducing the temperature to the crystallization temperatures reported in Table 2, at a cooling rate of 5°C/min. Samples 6–8 and 14–16 were also crystallized to all temperatures reported in Figures 12 and 13. The results shown in Table 2 represent the average of seven runs. Induction times obtained by the two methods were compared using a paired Student's *t*-test.

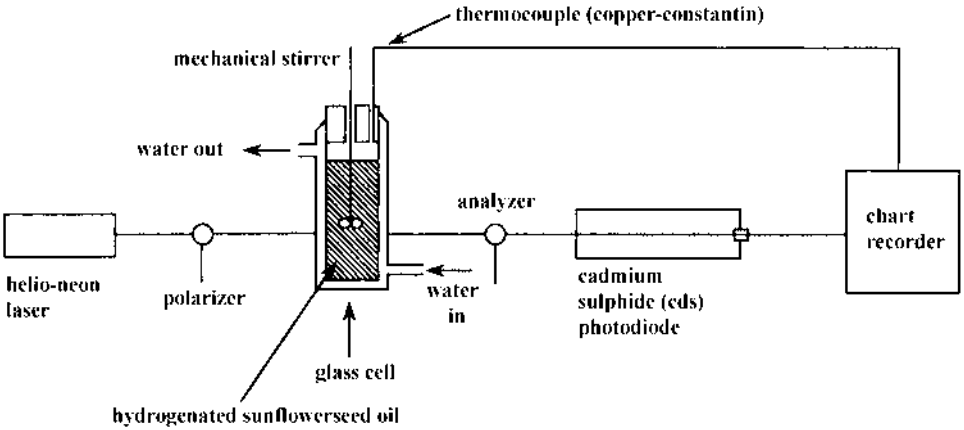

Figure 10 Schematic of the laser-polarized light turbidimetry equipment.

Copyright 2002 by Marcel Dekker. All Rights Reserved.

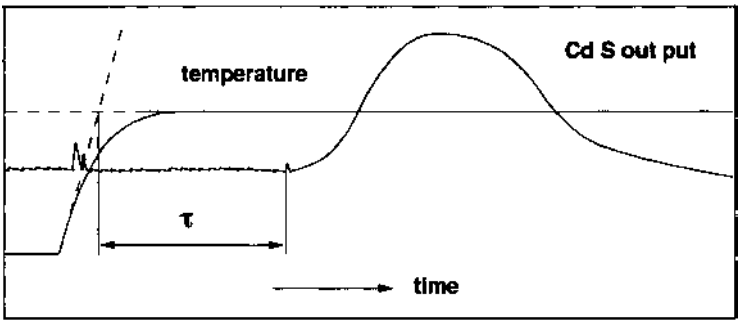

Figure 11 Typical chart recorder output for scattered light intensity and the thermocouple's temperature signal during the crystallization of hydrogenated sunflower seed oil. τ = induction time.

Table 2 Comparison of Nucleation Induction Times Determined by Microscopy and Polarized Laser Light Turbidimetry

Sample	Temperature (K)	Laser optical setup, $n = 7$	Microscopy, $n = 7$
A	290.2	60.0 ± 1.7	65.3 ± 3.5[a,b]
B	289.9	17.3 ± 1.0	22.2 ± 1.6[a,b]
C	293.8	31.6 ± 1.0	33.6 ± 1.8[a]
D	295.1	20.7 ± 0.8	25.2 ± 2.3[a,b]
E	295.4	10.9 ± 0.5	15.7 ± 1.1[a,b]
F	298.3	12.1 ± 0.5	17.6 ± 1.5[a,b]
G	300.4	14.6 ± 0.6	15.3 ± 0.8
H	303.2	23.3 ± 0.9	29.8 ± 1.9[a,b]
I	290.6	46.7 ± 0.9	50.1 ± 2.9[a]
J	291.6	32.7 ± 1.2	35.6 ± 2.3[a]
K	293.3	32.6 ± 0.9	34.8 ± 2.0[a]
L	295.6	26.9 ± 0.8	29.0 ± 1.5[a]
M	296.3	9.8 ± 0.3	12.2 ± 0.8[a,b]
N	302.1	16.4 ± 0.5	20.1 ± 1.2[a,b]
O	305.7	14.1 ± 0.7	17.0 ± 1.5[a,b]
P	307.1	11.4 ± 0.4	13.2 ± 1.0[a,b]

n = number of analyses.

[a] Value (mean ± SD) is significantly different ($P < 0.05$, paired Student's t-test) from the optical setup value.

[b] $P < 0.01$.

Copyright 2002 by Marcel Dekker. All Rights Reserved.

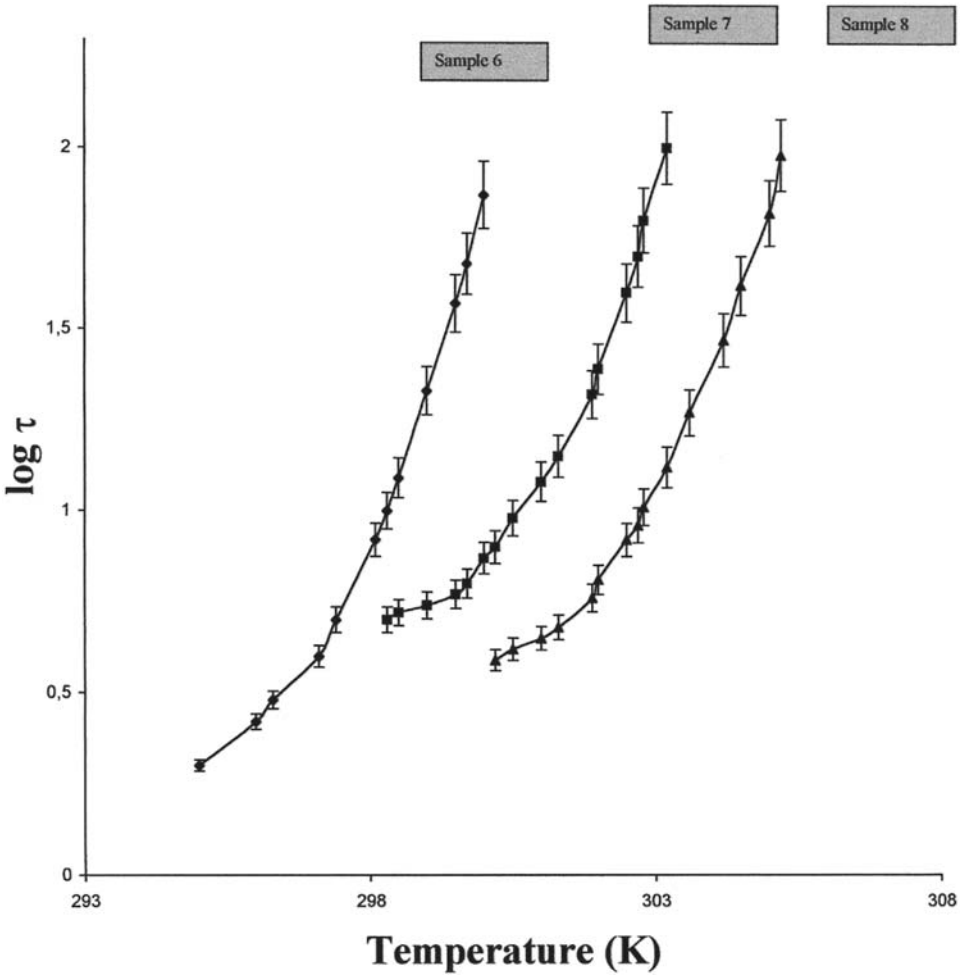

Figure 12 Semilogarithmic plot of induction times of crystallization (τ) vs. temperature (K) for (◆) sample 6, (■) sample 7, and (▲) sample 8 collected during the first hydrogenation process.

Results of the analysis of 16 samples by the two methods (microscopy and laser polarized turbidimetry) are shown in Table 2, with the temperatures selected in each case. Temperatures were selected taking into account their MDPs, because at low temperatures no induction period was detected because the sample crystallizes before it reaches the crystallization temperature. Induction times varied from

Copyright 2002 by Marcel Dekker. All Rights Reserved.

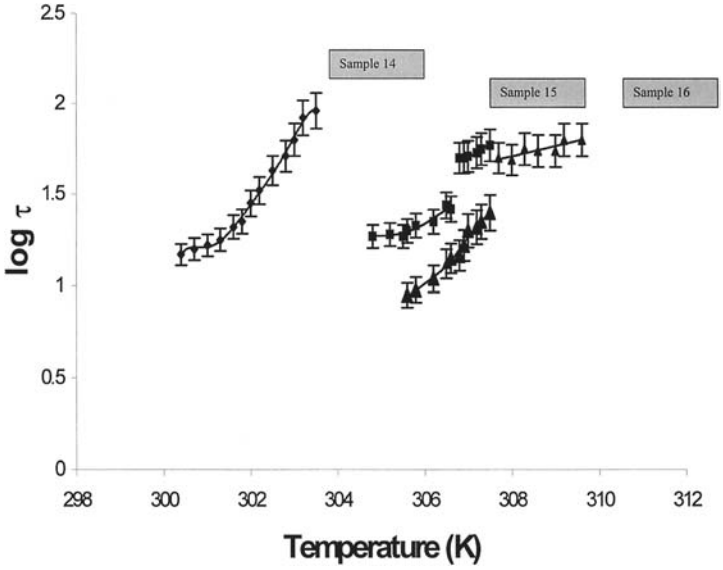

Figure 13 Semilogarithmic plot of induction times of crystallization (τ) vs. temperature (K) for (◆) sample 14, (■) sample 15, and (▲) sample 16 collected during the second hydrogenation process.

about 10 min to 60 min. Every sample was measured seven times by polarized light laser turbidimetry and microscopy. Means and standard deviations are shown in Table 2. The same crystallization temperatures, degrees of supercooling, and cooling rates were used in both cases. This procedure was carried out for the 16 samples analyzed.

Standard deviations were higher when induction times were measured by microscopy. Significant differences between methods were detected ($P < 0.01$). Induction times determined by microscopy were not equivalent to those measured by laser turbidimetry. Crystals must reach a minimum size of 0.2 μm to be detected by microscopy, whereas the laser turbidimetric technique is able to detect smaller nuclei [5].

Induction times (τ) at different crystallization temperatures (T_c) were measured for samples 6–8 and 14–16. Curves of log τ vs. temperature are shown in Figures 12 and 13. No crystallization was detected at 293 K, 295 K, or 297 K for samples 6, 7, and 8 or at 297 K, 303 K, and 304 K for samples 14, 15, and 16, respectively. These values are consistent with the trends in MDPs within the same hydrogenation process. The higher the MDP, the higher the critical temperature for nucleation. Sample 14 should have had induction times closer

Copyright 2002 by Marcel Dekker. All Rights Reserved.

to those obtained for sample 7. However, the times were intermediate between the times found for samples 7 and 8. Nucleation behavior was different for the two hydrogenation processes because even if the MDPs were similar the TAG composition of the samples was different. Two distinct crystallization behaviors were observed. For samples 6–8 and 14, a continuous trend could be observed, whereas for samples 15 and 16 discontinuities at 306.8 K and 307.7 K, respectively, could be observed. This suggested that when samples 6–8 and 14 were crystallized from the melt, a single polymorphic form was obtained that was the same at every temperature. On the other hand, the discontinuities observed in samples 15 and 16 were indicative of the presence of two polymorphic forms. The β′ polymorph forms at lower crystallization temperatures, whereas the β polymorph forms at higher temperatures. To confirm this hypothesis, crystals were analyzed by X-ray diffraction to determine their polymorphic state. The diffraction patterns of samples 6–8 and 14 showed two strong signals at 3.9 Å and 4.3 Å (Fig. 14). These samples were found to nucleate in the β′ form even

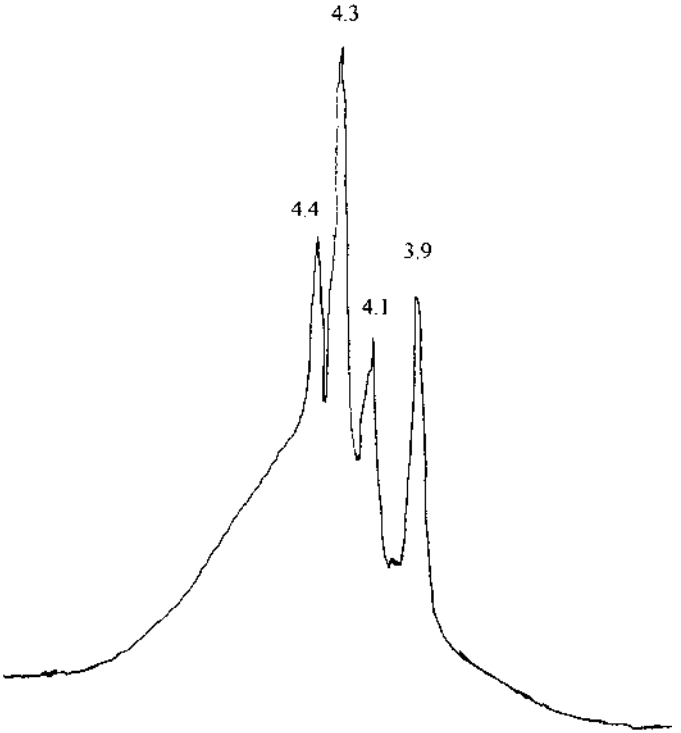

Figure 14 X-ray diffraction pattern of sample 6 (β′ form) crystallized at 298 K.

Copyright 2002 by Marcel Dekker. All Rights Reserved.

at the highest crystallization temperatures, close to their melting points. Samples obtained from the lower crystallization temperature region of curves 15 and 16 also crystallized in the β′ form. Samples obtained from the higher crystallization temperature regions were found to have crystallized in the β form (Fig. 15). A characteristic pattern of the β form with a strong signal at 4.6 Å was obtained by powder X-ray diffraction for samples 15 and 16.

During hydrogenation, the percentage of OSE and EEE always increased with time for both hydrogenation processes, but their accumulation patterns differed. EEO always increased in the first hydrogenation, whereas for the second hydrogenation EEO initially increased, reached the highest value (sample 13), and then decreased to a value markedly lower (sample 16) than the one of sample 8. Samples 15 and 16 had higher EEE and OSE and lower EEO contents than the others. No reports of a stable β′ form of EEE were found in the literature. When EEE is mixed with another TAG, such as PPP, the β′ form is destabilized [7]. The crystallization behavior of samples 15 and 16, as far as polymorphism is concerned, is more similar to the behavior of plastic fats such as palm oil. The polymorphic form in which these samples crystallized was a function of the crystallization temperature, and both β′ or β could be obtained from the melt.

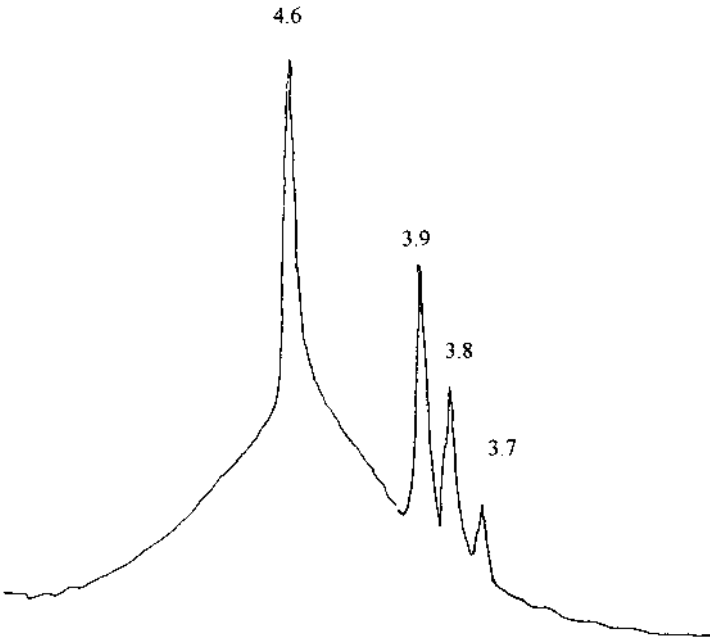

Figure 15 X-ray diffraction pattern of sample 16 (β form) crystallized at 309 K.

Copyright 2002 by Marcel Dekker. All Rights Reserved.

Samples with lower EEE contents crystallized in the β′ form, and no β form was obtained from the melt even at crystallization temperatures very close to their melting points. The crystallization behavior was closely related to the TAG species present in the oil, especially to those containing elaidic acid.

A. Activation Free Energy of Nucleation

The activation free energy of nucleation, ΔG_c, was evaluated using the Fisher–Turnbull equation [8],

$$J = \frac{NkT}{h} \exp\left[-\frac{\Delta G_d}{kT}\right] \exp\left[-\frac{\Delta G_c}{kT}\right] \tag{1}$$

where J is the rate of nucleation; ΔG_d, activation free energy of diffusion; k, Boltzmann's constant; T, temperature; N, number of molecules per cubic centimeter in the liquid phase; and h, Planck's constant. J can be taken as being proportional to the inverse of the induction time (τ) of nucleation. For a spherical nucleus, the activation free energy of nucleation is related to the surface free energy of the crystal/melt interface, σ, and the degree of supercooling (melting point minus crystallization temperature) ($\Delta T = T_m - T_c$) by

$$\Delta G_c = \frac{16}{3}\left(\frac{\pi\sigma^3 T_m^2}{(\Delta H)^2(\Delta T)^2}\right) \tag{2}$$

where ΔH corresponds to the enthalpy of fusion.

Assuming the temperature independence of ΔG_d within the relatively narrow crystallization temperature range studied, combining Eqs. (1) and (2) and rearranging, we obtain

$$\tau T = B \exp\left[\frac{16}{3}\left(\frac{\pi\sigma^3 T_m^2}{kT}\right)(\Delta H)^2(\Delta T)^2\right] \tag{3}$$

where B is a constant. From a plot of in τT vs. $1/T(\Delta T)^2$, a slope s can be evaluated that allows the calculation of the activation free energy of nucleation from the expression

$$\Delta G_c = \frac{sk}{(T_m - T_c)^2} \tag{4}$$

The Fisher–Turnbull equation [Eq. (1)] was originally derived for single-component systems; however, it was proved to be applicable to palm oil and milkfat, which are multicomponent systems [9,10]. A fairly good linearity of the plots shows that the Fisher–Turnbull equation can be used to study such systems.

Copyright 2002 by Marcel Dekker. All Rights Reserved.

The activation free energies of these samples are reported in Tables 3 and 4 along with the crystallization temperatures and degree of supercooling $\Delta T = T_m - T$. MDPs for samples 6–8 and 14–16 are reported in Table 1, and the slopes (s) were 0.048×10^5, 0.017×10^5, 0.006×10^5, 0.111×10^5, 0.093×10^5, and 0.115×10^5, respectively, for the β′ forms and 0.033×10^5 and 0.008×10^5 for the β forms of samples 15 and 16.

For the same degree of supercooling, the β′ form of sample 14 had a greater activation free energy of nucleation than samples 6–8. Sample 8 had the lowest values of ΔG_c. Nucleation of the β′ crystal was the fastest in sample 8 and the slowest in sample 14. Samples 15 and 16 crystallized in the β form above 306.7 and 307.6 K, respectively. At these high temperatures, ΔG_c values were very low for the β form; therefore nucleation in this form was preferred. From induction times of crystallization data, ΔG_c can be calculated, and from its values the possible occurrence of a polymorphic form can be deduced. The crystallization behavior was found to be closely related to elaidic acid TAG content. Samples 15 and 16, with high contents of EEE, had a low activation free energy of nucleation for the β form at crystallization temperatures close to their melting points, whereas samples with low EEE contents and a higher mixed elaidic acid TAG content did not crystallize in the β form. In samples 15 and 16, high EEE contents resulted in a β-mediated crystallization at temperatures in the vicinity of the melting point.

Short induction times for hydrogenated sunflower oil indicate that nucleation in sunflower oil occurs readily even at low degrees of supercooling com-

Table 3 Activation Free Energy of Nucleation as a Function of Temperature and Degree of Supercooling for the First Hydrogenation Process

Sample 6			Sample 7			Sample 8		
Temp (K)	ΔG_c (kJ/mol)	ΔT (K)	Temp (K)	ΔG_c (kJ/mol)	ΔT (K)	Temp (K)	ΔG_c (kJ/mol)	ΔT (K)
295.0	0.6	8	298.3	0.3	6.9	300.2	0.1	6.6
296.0	0.8	7	299.0	0.3	6.4	301.9	0.2	4.9
296.6	1.0	6.4	300.0	0.5	5.2	302.8	0.3	4
297.1	1.1	5.9	300.5	0.6	4.9	303.2	0.4	3.6
297.5	1.3	5.5	301.0	0.7	4.4	303.6	0.5	3.2
298.1	1.7	4.9	301.3	0.8	4.1	304.2	0.7	2.6
298.5	2.0	4.5	302.0	1.2	3.4	304.5	0.9	2.3
299.0	2.5	4	302.7	1.9	2.7	305.0	1.5	1.8
299.5	3.3	3.5	303.2	2.9	2.2	305.5	2.9	1.3
299.7	3.7	3.3						
300.0	4.4	3						

Copyright 2002 by Marcel Dekker. All Rights Reserved.

Table 4 Activation Free Energy of Nucleation as a Function of Temperature and Degree of Supercooling for the Second Hydrogenation Process

Sample 14			Sample 15			Sample 16		
Temp (K)	ΔG_c (kJ/mol)	ΔT (K)	Temp (K)	ΔG_c (kJ/mol)	ΔT (K)	Temp (K)	ΔG_c (kJ/mol)	ΔT (K)
300.4	3.7	5	304.8	3.1	5	305.6	1.6	7.8
300.7	4.2	4.7	305.2	3.6	4.6	305.8	1.6	7.6
301.0	4.8	4.4	305.5	4.2	4.3	306.0	1.7	7.4
301.3	5.5	4.1	305.8	4.8	4	306.2	1.8	7.2
301.6	6.4	3.8	306.2	5.9	3.6	306.5	2.0	6.9
301.8	7.1	3.6	306.5	7.1	3.3	306.6	2.1	6.8
302.0	8.0	3.4	306.7	8.0	3.1	306.9	2.2	6.5
302.2	9.0	3.2	306.8	3.0	3	307.0	2.3	6.4
302.5	11.0	2.9	307.0	3.5	2.8	307.3	2.5	6.1
302.8	13.6	2.6	307.2	4.1	2.6	307.5	2.7	5.9
303.0	16.0	2.4	307.5	5.2	2.3	307.7	0.2	5.7
303.2	19.1	2.2	307.8	6.9	2	308.0	0.2	5.4
303.5	25.5	1.9	308.1	9.5	1.7	308.3	0.2	5.1
			308.2	10.7	1.6	308.6	0.3	4.8
						309.0	0.3	4.4
						309.2	0.4	4.2
						309.6	0.5	3.8

pared to other fats [9]. These results are also very important from a practical point of view for process design, especially for processes in which fats should be completely crystallized by the end of the process line.

V. EFFECTS ON CRYSTAL GROWTH—ISOTHERMAL CRYSTALLIZATION

A. Solid Fat Content

Solid fat contents (SFCs) of the samples were measured by pulsed nuclear magnetic resonance (pNMR). The number of hydrogen nuclei in the liquid and the total number of hydrogen nuclei in liquid and solids were measured. The percentage of solid content is given by the equation

$$\text{Solids } (\%) = \frac{(A_1 - A_2)f}{(A_1 - A_2)f + A_2} \times 100 \tag{5}$$

Copyright 2002 by Marcel Dekker. All Rights Reserved.

where A_1 is the signal amplitude proportional to the total number of hydrogen nuclei, A_2 is the signal amplitude proportional to the hydrogen nuclei in liquid, and f is a factor to correct the dead time of the receiver because it is not possible to measure the samples at time zero. f was previously determined by using standards with a known percentage of solids. Samples were run in triplicate, and the values were averaged. The SFC of the samples was determined by using the following thermal treatment: Samples were melted at 353 K for 30 min, transferred to NMR tubes, and placed in a bath at different crystallization temperatures: 293 K, 288 K, 283 K, 279 K, and 276 K. Solid fat content was then measured as a function of time (Figs. 16 and 17). The Avrami–Erofeev model [Eq. (6), see below] was then fitted to the experimental data using standard least squares regression procedures. Means of k_n estimates and the r^2 statistic (goodness of fit) are reported in Tables 5 and 6 [11].

B. Mathematical Interpretation

The modified Avrami model was derived for the case of three-dimensional random nucleation followed by uniform linear growth of the nuclei. In its linearized form,

$$-\ln(1 - f) = (k_n t)^n \tag{6}$$

where n represents the index of the reaction, t is time, k_n is the rate constant for crystallization, and f is the fractional crystallization. In this treatment, the value on n is fixed as an integral number. Patterns obtained for samples 6–8 and 14, crystallized at 293 K, and sample 6, crystallized at 288 K, were evaluated with this model by fixing $n = 3$. The rate constants obtained are shown in Tables 5 and 6. As can be appreciated from these tables, the model fit the data well over the range of fractional crystallizations 0–0.7 ($r^2 > 0.9$ in all cases). Sample 8 had the highest rate constant, followed by samples 7 and 6. The rate constant for sample 14 was similar to that of sample 7.

Hyperbolic curves can also be described by the modified Avrami equation, but in this case n should set to 1. The resulting equation is an exponential growth curve. There also was a good fit of the model to the data over the same range of fractional crystallizations. Tables 5 and 6 show the values of k_n and the correlation coefficients for samples 16, 15, and 14 (second hydrogenation process) and 8, 7, and 6 (first hydrogenation process), respectively.

C. Optical Microscopy

A polarized light microscope with a temperature-controlled stage was used to monitor crystallization. In the crystallization tests, samples were melted at 353 K and held at this temperature for 30 min. Samples were then placed on a slide

Copyright 2002 by Marcel Dekker. All Rights Reserved.

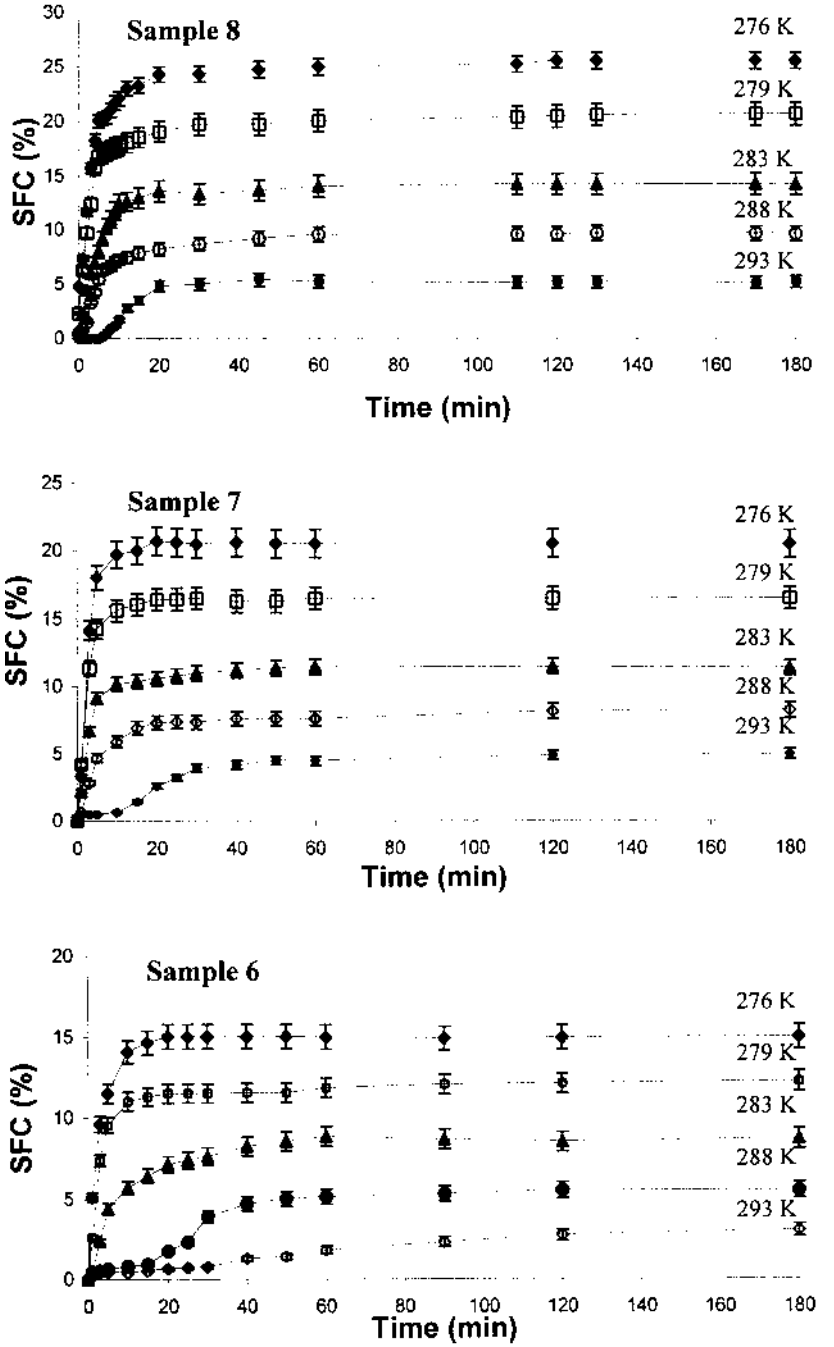

Figure 16 Solid fat content vs. crystallization for samples 6, 7, and 8 at indicated temperatures.

Copyright 2002 by Marcel Dekker. All Rights Reserved.

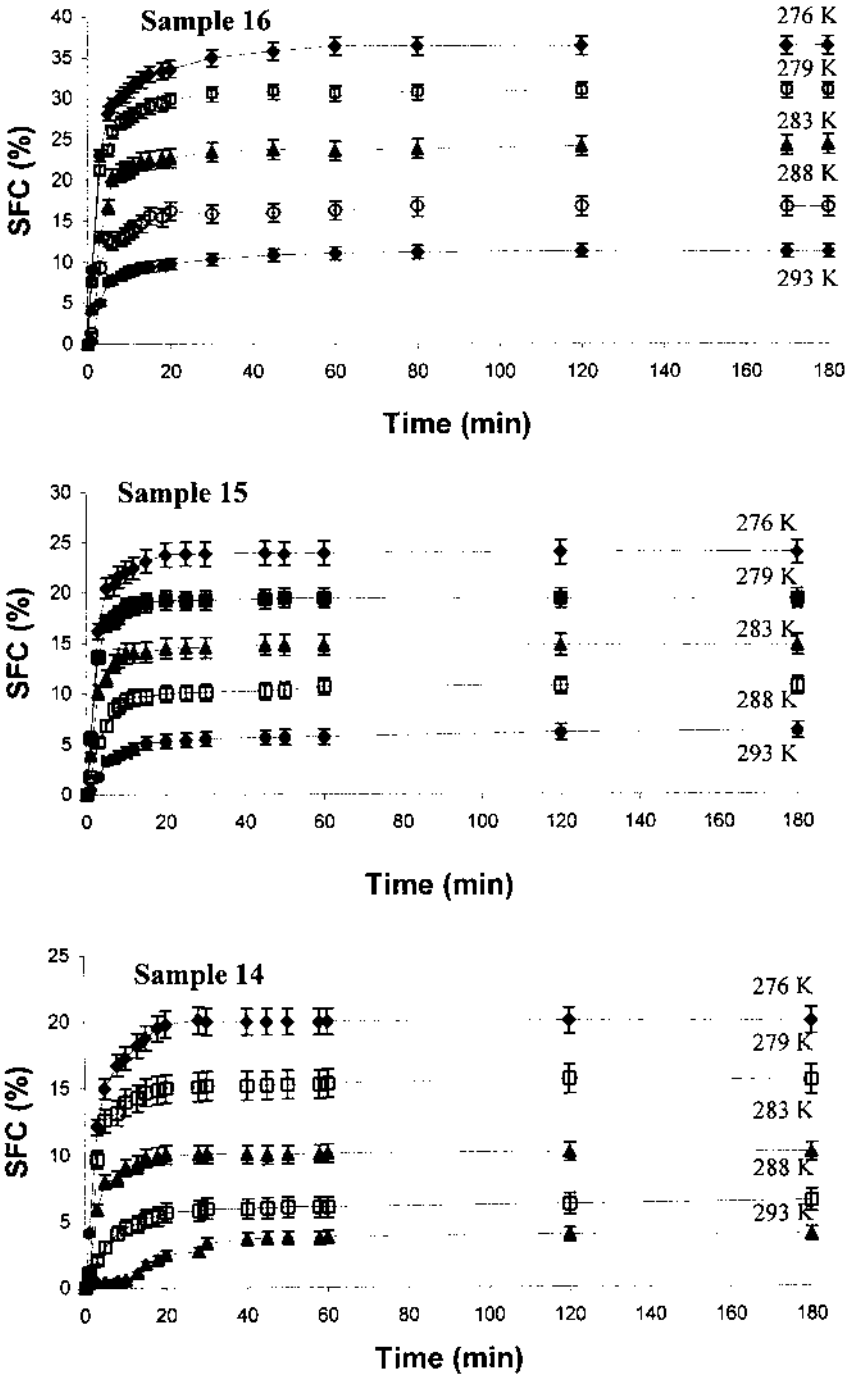

Figure 17 Solid fat content vs. crystallization for samples 14, 15, and 16 at indicated temperatures.

Copyright 2002 by Marcel Dekker. All Rights Reserved.

Table 5 Rate Constants of Crystallization Derived from Fits of Solid Fat Content vs. Time Data to the Modified Avrami Model for the Second Hydrogenation Process

Temperature (K)	n	k_n (min^{-1})	r^2
Sample 16			
293	1	0.209	0.934
288	1	0.283	0.953
283	1	0.293	0.980
279	1	0.321	0.955
276	1	0.303	0.988
Sample 15			
293	1	0.137	0.935
288	1	0.216	0.998
283	1	0.316	0.965
279	1	0.315	0.994
276	1	0.294	0.988
Sample 14			
293	3	0.025	0.986
288	1	0.136	0.983
283	1	0.310	0.967
279	1	0.338	0.945
276	1	0.284	0.986

heated to the desired crystallization temperature, and covered with a cover slip. Photographs of the crystals were taken every 15 s for 15 min, then every 5 min for 45 min. Photographs were digitized using a flat-bed scanner, and the number and size of the crystals were determined using a standard image analysis software program [11]. Crystal size was arbitrarily considered as the longest dimension of the crystal—the diameter for spherical shape crystals and the length for needle-shaped crystals.

1. Crystal Number, Size, and Size Distribution

Samples 6–8 and 14–16 were photographed as a function of time, and their crystal numbers were determined. At 293 K, the number of crystals per field found for sample 16, 15 after it was placed on the slide, was 674, and after 60 min it was 728. (Sample crystal size distributions are shown in Figure 18.) At this degree of supercooling (20.4 K), the number of crystals per field increased slightly with time. Values for sample 15 were 751 and 788 crystals per field at the same times and temperature. This number also increased slightly in time. Sample 14 showed

Copyright 2002 by Marcel Dekker. All Rights Reserved.

Table 6 Rate Constants of Crystallization Derived from Fits of Solid Fat Content vs. Time Data to the Modified Avrami Model for the First Hydrogenation Process

Temperature (K)	n	k_n (min^{-1})	r^2
Sample 8			
293	3	0.037	0.995
288	1	0.136	0.968
283	1	0.154	0.962
279	1	0.266	0.951
276	1	0.258	0.989
Sample 7			
293	3	0.026	0.989
288	1	0.163	0.957
283	1	0.111	0.982
279	1	0.240	0.990
276	1	0.232	0.967
Sample 6			
293	3	0.008	0.963
288	3	0.022	0.976
283	1	0.134	0.937
279	1	0.201	0.993
276	1	0.209	0.957

a different behavior. The first crystals that could be seen appeared 4 min 45 s after the sample had been placed. The number of crystals was initially 124 and grew to 282 after 7 min and to 784 after 60 min. In this case there was a marked increase in crystal number. Sample 8 had 481 and 845 crystals per field after 3 and 60 min, respectively. (Sample crystal size distribution is reported in Figure 19.) Before 3 min, crystals could not be detected. Sample 7 showed 657 and 919 crystals per field after 4 and 60 min, respectively. Sample 6 crystals appeared after 7 min, with 98 per field. After 9 min, the number increased to 179, and after 60 min, to 651.

The same general behavior was found at all temperatures. For hyperbolic curves, the number of crystals increased slightly from the onset of crystallization to 60 min. On the other hand, samples with sigmoidal fractional crystallization curves showed a rapid increase in crystal number with time.

Sample 16 was also crystallized at 288, 283, 279, and 276 K. The crystal numbers at 15 s and 60 min were, respectively, 776, 791; 788, 859; 790, 870; and 796, 882. The number of crystals increased slightly with degree of supercooling. This result was found for all samples.

Copyright 2002 by Marcel Dekker. All Rights Reserved.

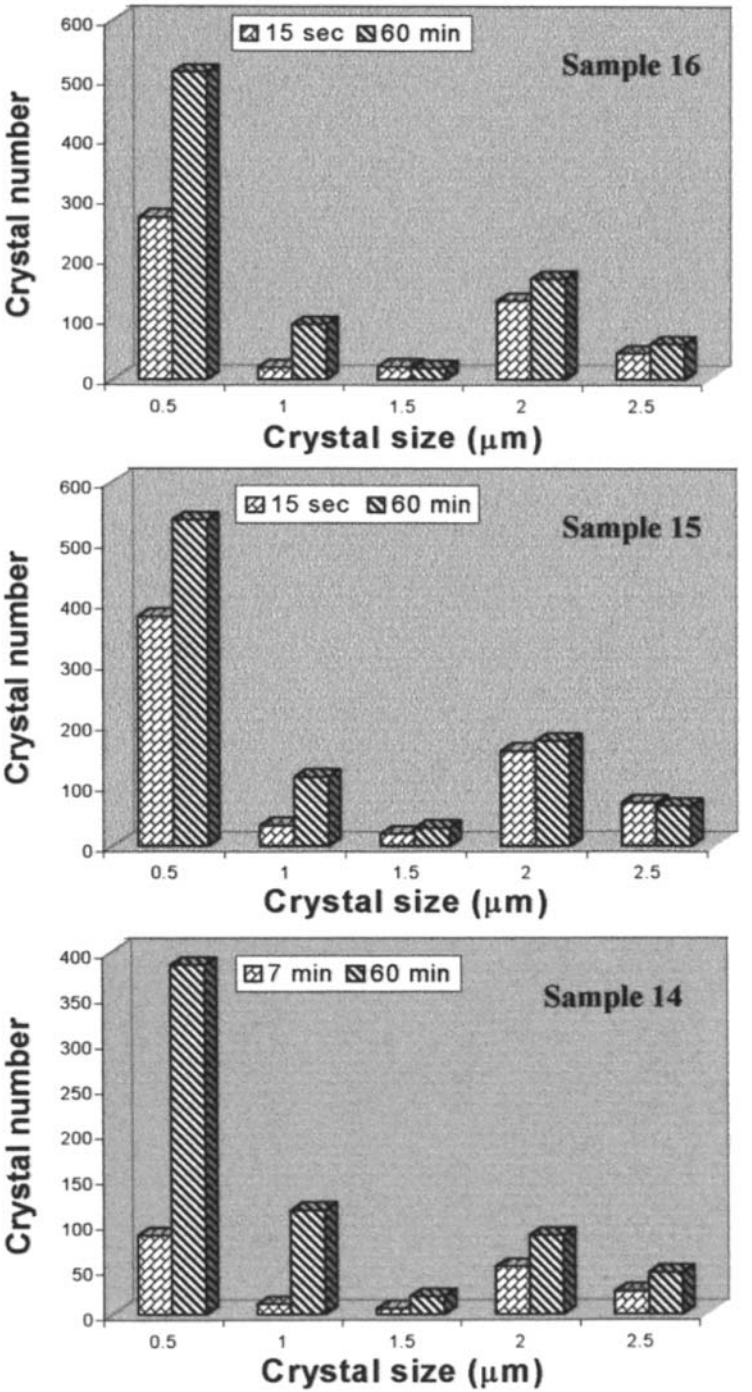

Figure 18 Crystal size distribution of samples 14, 15, and 16.

Copyright 2002 by Marcel Dekker. All Rights Reserved.

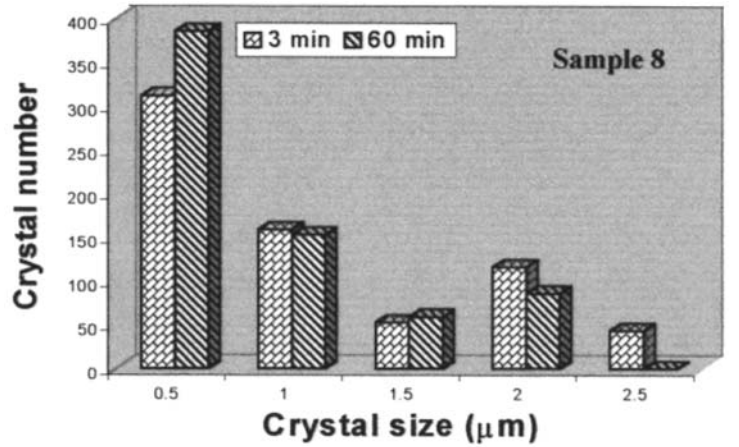

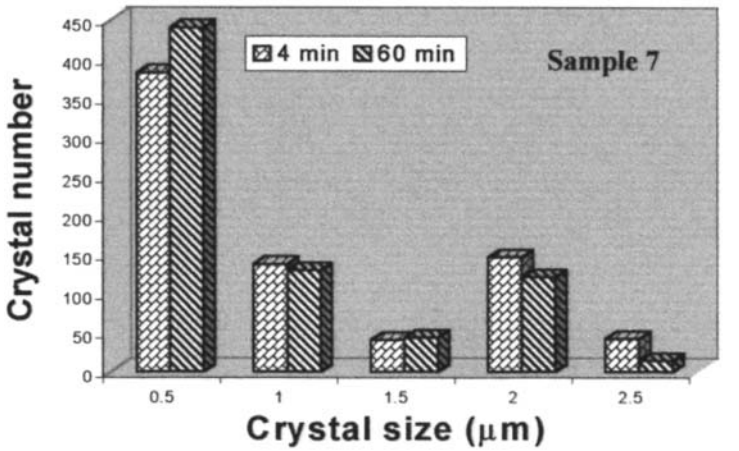

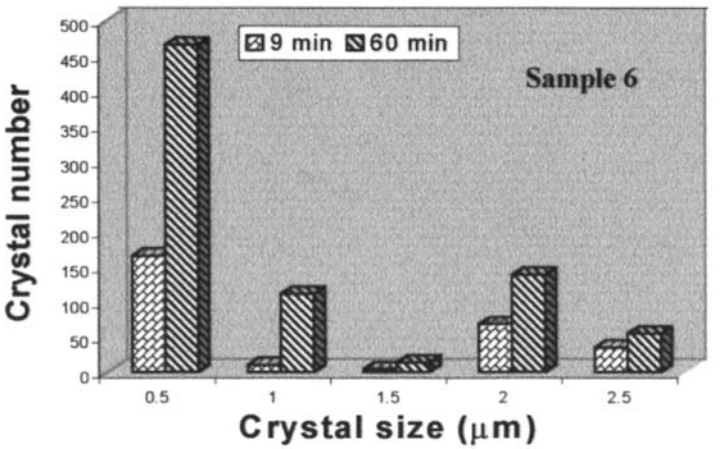

Figure 19 Crystal size distribution of samples 6, 7, and 8.

Copyright 2002 by Marcel Dekker. All Rights Reserved.

Changes in crystal size distribution during the crystallization process are reported in Figures 18 and 19. No clear differences were evident between the two hydrogenation processes [11].

2. Crystal Morphology

Two different morphologies were found in agreement with the shape of the SFC curves. Samples with hyperbolic curves showed needle-like crystals (Fig. 20a), and samples with sigmoidal curves showed spherical crystals (Fig. 20b).

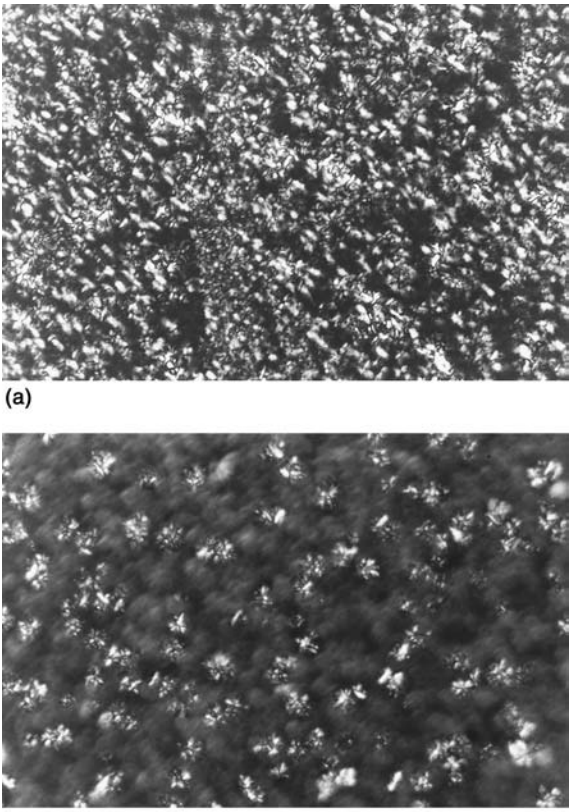

Figure 20 Crystal morphology of (a) sample 15, crystallized at 15°C, 5 min after having been placed on the slide; (b) sample 6, crystallized at 15°C, 5 min after having been placed on the slide.

Copyright 2002 by Marcel Dekker. All Rights Reserved.

Depending on the degree of supercooling, two different crystallization behaviors were observed. When supercooling was high, the initial number of crystals was high and small changes in size were detected over time (hyperbolic curves). On the other hand, when the degree of supercooling was low, an induction period before the onset of crystallization was evident (sigmoidal curves). Crystal number increased significantly with time, and a slight change in size was also detected [11].

Crystallization behavior could be related to the chemical composition of the samples. Samples 14 and 7 had very similar MDPs. As can be observed in Figures 1 and 2, the maximum solid fat contents attained (S_{max}) in sample 14 were slightly lower at all crystallization temperatures than those in sample 7. However, there is a systematic tendency for SFC values to be lower for sample 14. These samples had a different chemical composition, and therefore different interactions between triacylglycerols could have taken place, which could be responsible for the lower SFC values. In addition, samples 15 and 16, which had the highest content of high melting triacylglycerols (especially OSE and EEE), showed only hyperbolic curves. Samples 14,8,7, and 6, with lower MDPs and higher percentages of EEO, showed both behaviors, depending on the supercooling.

Supercooling is an important parameter that defines the way in which nucleation takes place. Depending on the initial number of nuclei, two different growth modes were observed: uniform linear crystal growth for a small initial number of nuclei (sigmoidal curves), and an aggregate-type crystal growth for a high initial number of nuclei (hyperbolic curves).

VI. CONCLUSION

In this work we have explored the effects of chemical composition on the crystallization behavior of hydrogenated sunflower oil. Interestingly, hydrogenation did not alter the global fatty acid composition of the oil but rather induced changes in the molecular species of triacylglycerols present. This in turn led to profound changes in the crystallization behavior of hydrogenated sunflower oil.

ACKNOWLEDGMENTS

Thanks to W. Atencio, A. Colavita, and A. Campana for expert technical assistance. This work was supported by funds from SECYT (Secretaria de Ciencia y Technologia), Argentina.

Copyright 2002 by Marcel Dekker. All Rights Reserved.

REFERENCES

1. BF Haumann. INFORM 5:668–678, 1994.
2. MT Rodrigo, S Mendioroz. J Am Oil Chem Soc 69:802–805, 1992.
3. RR Allen. J Am Oil Chem Soc 58:166–169, 1981.
4. H Lawson. Food Oils and Fats. New York: Chapman & Hall, 1995, p 29.
5. ML Herrera, C Falabella, M Melgarejo, MC Anon. J Am Oil Chem Soc 75:1273–1280, 1998.
6. M Naglic, A Smidovnik, T Koloini. J Am Oil Chem Soc 75:629–633, 1998.
7. A Desmedt. Etude des propriétés structurales et thermiques de triglycérides purs et en présence d'emulsifiants. Influence de la nature de la chai//ne en C18 et application au phénomène de blanchiment PhD Thesis. Facultés Universitaires, Notre-Dame de la Paix, Namur, 1993.
8. RF Strickland-Constable. Kinetics and Mechanism of Crystallization. London: Academic Press, 1968, pp 74–129.
9. WL Ng. J Am Oil Chem Soc 67:879–882, 1990.
10. ML Herrera, M de León Gatti, RW Hartel. Food Res In 32:289–298, 1999.
11. ML Herrera, C Falabella, M Melgarejo, MC Anon. J Am Oil Chem Soc 76:1–6, 1999.

Copyright 2002 by Marcel Dekker. All Rights Reserved.

13

The Effects of Interesterification on the Physical Properties of Fats

Dérick Rousseau
Ryerson University, Toronto, Ontario, Canada

Alejandro G. Marangoni
University of Guelph, Guelph, Ontario, Canada

I. INTRODUCTION

The physical properties of a fat or oil depend on its inherent triacyglycerol (TAG) structure, that is, its fatty acid composition and stereospecific positional distribution. Modification of a lipid's physical properties is usually achieved using three processes. Roughly 30% of all edible fats and oils in the world are hydrogenated, whereas ~10% are either fractionated or interesterified (Haumann, 1994). These unit operations rely on different principles to attain their goals. Fractionation is a physical separation process based on TAG crystallization behavior, primarily the differences in the melting points of different TAGs (Deffense, 1993; Makhlouf et al., 1987). Hydrogenation, on the other hand, relies on the addition of hydrogen molecules at high temperature and pressure in the presence of a catalyst to saturate the double bonds that are present in unsaturated fatty acids, which increases their melting points. Hydrogenated fats are extensively used as margarine and shortening base stocks as well as in many processed foods (Nawar, 1996a). Interesterification, used industrially for many years to modify the physical properties of lard (Lutton et al., 1962; Luddy et al., 1955; Hoerr and Waugh, 1950), is also used in the production of margarines (List et al., 1995), palm oil and palm kernel oil derivatives (Laning, 1985; Sreenivasan, 1978), and fat substitutes (Smith et al., 1994; Gunstone and Harwood, 1994). This process redistributed fatty acids within and among TAG molecules, which can lead to substantial

Copyright 2002 by Marcel Dekker. All Rights Reserved.

changes in lipid functionality. The fatty acid distribution is changed without changing the fatty acids' inherent properties. Unsaturation levels stay constant, and there is no cis–trans isomerization (Kaufmann and Grothues, 1959), such as is encountered during hydrogenation.

Two types of interesterification are presently in use: chemical and enzymatic. Enzymatic modifications rely on the use of random or regiospecific (1,3- or 2-specific) and fatty acid–specific lipases as catalysts, whereas for chemical modifications metal alkali catalysts are usually employed.

II. MECHANISMS OF CHEMICAL INTERESTERIFICATION

Prior to examining the effects of chemical interesterification on the physical properties of fats, we briefly review the mechanisms and reaction conditions. Existing reviews on chemical interesterification include those of Kaufmann et al. (1958), Going (1967), Hustedt (1976), Sreenivasan (1978), Rozenaal (1992), and Marangoni and Rousseau (1995). Acidolysis, alcoholysis, glycerolysis, and transesterification all fall under the heading interesterification (Sonntag, 1982; Feuge, 1962). Acidolysis involves a reaction between a fatty acid and a triacylglycerol. Reactions can produce an equilibrium mixture of reactants and products or can be driven to completion by physically removing one of the reaction products. For example, coconut oil can be reacted with stearic acid to partially replace the short-chain fatty acids of coconut oil with higher melting stearic acid (Going, 1967). Alcoholysis involves the reaction of a triacylglycerol and an alcohol and has several commercial applications, primarily the production of partial acylglycerols. Glycerolysis is an alcoholysis reaction in which glycerol acts as the alcohol (Sonntag, 1982). Finally, transesterification is the most widely used type of interesterification in the food industry. During the reaction, the ester bonds linking fatty acids to the glycerol backbone are split; the newly liberated fatty acids are randomly shuffled within a fatty acid pool and are then re-esterified onto a new position either on the same glycerol (intraesterification) or on another glycerol (interesterification) (Sreenivasan, 1978). Intraesterification occurs at a faster rate than interesterification owing to kinetic considerations (Freeman, 1968). Once the reaction has reached equilibrium, a complex, random mixture of triacylglycerol species is obtained.

Regardless of the type of interesterification used, the extent of the effects of interesterification on the physical properties of a fat will depend on the composition of the starting material. If a single starting material (e.g., vegetable oil) is randomized, the effects will not be as great as if a hardstock (e.g., palm stearin) is randomized with a vegetable oil (Rousseau et al., 1996a). Furthermore, if a material has a quasi-random distribution prior to randomization, randomization will not lead to notable modifications.

Copyright 2002 by Marcel Dekker. All Rights Reserved.

Chemical interesterification has been in industrial use since the 1940s to improve the spreadability and baking properties of lard (Wiedermann et al., 1961; Weiss et al., 1961). In the 1970s there was renewed interest in this process, particularly as a hydrogenation replacement for the manufacture of zero-trans margarines. Today, it plays a key role in the production of low calorie fat replacers, such as Olestra and Salatrim (Smith et al., 1994; Jandacek and Webb, 1978).

A. Reaction Mechanisms

The interesterification reactions consist of three main steps: catalyst activation, ester bond cleavage, and fatty acid interchange. The exchange of fatty acids between triacylglycerol hydroxyl sites does not occur directly but via a series of alcoholysis reactions involving partial acylglycerols (Naudet, 1976). Interesterification depends on the properties of the carbonyl group (C═O), which is predisposed to nucleophilic attack, the electronegative oxygen pulls electrons away from the carbon, leading to a partial positive charge on the carbon.

Steric considerations also come into play. The carbonyl carbon is joined to three other groups by σ bonds (sp^2 orbitals); these bonds lie in a flat plane at angles of 120° to each other. The remaining *p* orbital from the carbon overlaps with a *p* orbital from the oxygen to form a π bond. This flat plane and the absence of neighboring bulky groups permit easy access for nucleophiles to approach and react with the carbonyl carbon.

The transition state of the reaction is a relatively stable tetrahedral intermediate with a partial negative charge on the oxygen. As the reaction progresses, a group leaves and the structure reverts to the planar carbonyl structure. Strong evidence supports the cleavage of the carbonyl carbon–oxygen bond as the mechanism for the release of the leaving group.

For acid-catalyzed nucleophilic acyl substitution, a hydrogen easily associates with the carbonyl oxygen because of the polarization of the carbonyl function and the presence of free electron pairs on the oxygen, imparting a positive charge to this atom (Vollhardt, 1987). The carbonyl carbon is then even more susceptible to nucleophilic attack because oxygen can accept π electrons without gaining a negative charge. Acid-catalyzed interesterification will not be discussed further, because it is not used for the chemical interesterification of food lipids.

1. Carbonyl Addition

As an alkaline environment is encountered during interesterification, the catalyst (which is nucleophilic) attacks the slightly positive carbonyl carbon at one of three fatty acid–glycerol ester bonds to form a tetrahedral intermediate. A fatty acid methyl ester is released, leaving behind a glycerylate anion. Kinetics of base-catalyzed hydrolysis of esters are second-order reactions dependent on both ester

Copyright 2002 by Marcel Dekker. All Rights Reserved.

and base concentration. This newly formed glycerylate anion is the nucleophile for subsequent intra- and intermolecular carbonyl carbon attacks, which continue until a thermodynamic equilibrium is reached. This process continues until all available fatty acids have exchanged positions and an equilibrium composition of acylglycerol mixture is achieved (Sreenivasan, 1978).

2. Claisen Condensation

In the Claisen condensation mechanism, the sodium methoxide removes an acidic hydrogen from the carbon α to the carbonyl carbon, resulting in the formation of an enolate ester (Wiedermann et al., 1961). This reaction produces a carbanion, a powerful nucleophile. This nucleophile will attack carbonyl groups, forming a β-keto ester intermediate and a glycerylate. The glycerylate is now free to attack other carbonyl carbons and exchange esters intra- and intermolecularly. Once this carbanion is created, the same considerations as for the usual carbonyl carbon chemistry apply.

B. Reaction Conditions

Interesterification can proceed without catalyst at high temperatures (300°C); however, equilibrium is attained slowly, and isomerization, polymerization, and decomposition reactions can occur (Going, 1967; Eckey, 1948). Addition of catalyst allows for significantly lower reaction temperatures and shortens reaction time (Joly and Lang, 1978). Other important considerations include the type and concentration of catalyst (Täufel et al., 1958).

III. ENZYMATIC INTERESTERIFICATION

In recent years, increased availability of lipases for the food industry has increased the feasibility and attractiveness of enzyme-mediated biotransformations. Although such lipid synthesis is still in its infancy, the inherent specificity of lipases provides flexibility in manipulating lipid structure. This has led to varied applications in the production of value-added lipids (Mukherjee, 1992), including low calorie triacylglycerols (TAG) (McNeill and Sonnet, 1995), confectionary fat substitutes (Macrae, 1985, 1983; Lazar and Henkel, 1985), nutraceuticals (Quinlan and Moore, 1993; Yamane et al., 1992; Haraldsson et al., 1993), incorporation of long-chain fatty acids into TAGs (Akoh et al., 1995; Kosugi and Azuma, 1994b; Huang and Akoh, 1994), margarine hardstocks (Foglia et al., 1993), lipid hydrolysis (McNeill and Sonnet, 1995; de Renobales et al., 1992), emulsifier production (Garcia et al., 1992, 1996), and reuse of waste oils (Kosugi and Azuma, 1994a).

Copyright 2002 by Marcel Dekker. All Rights Reserved.

Unlike chemical interesterification, the catalytic action of lipases is reversible. In aqueous conditions lipases promote lipolysis, whereas in a water-poor environment synthesis reactions predominate. Lipase-catalyzed synthesis reactions have been studied since the 1970s, when Tsujisaka et al. (1977) showed that lipases could catalyze the formation of TAGs from partial acylglycerols and free fatty acids. Hydrolysis reactions have been studied since the 1950s (Brockerhoff and Jensen, 1974).

Of the many industrial procedures used for lipid transformations, lipases have processing advantages over many chemical or physical processes (Al-Duri et al., 1995):

1. Their specificity leads to product control, and reduction of side product formation leads to increased yields.
2. Mild operating conditions (e.g., low temperature) reduce energy expenditures.
3. Lowered waste cost helps to assuage environmental concerns.
4. In contrast to chemical catalysts such as sodium methoxide, lipases are not deactivated by water or moisture in the air.

However, there are also disadvantages to using lipases (Yamane, 1987):

1. Lipases can be very costly.
2. Given that lipases must operate at lipid/water interfaces, there are engineering difficulties associated with the heterogeneity of the system.

A. The Catalyst

Lipases (glycerol ester hydrolases) are digestive enzymes generally found in fungi, bacteria, or the pancreas; they consist of 199–641 amino acid residues (Malcata et al., 1992) that act as biological catalysts by selectively lowering the activation energy of chemical reactions (Segel, 1976). The natural substrates of lipases are TAGs, which are normally not soluble in water. Normally, lipases catalyze the hydrolysis of ester bonds at the interface the between aqueous phase (where the lipase is dissolved) and the nonaqueous phase. The pH optima of most animal lipases are basic (pH 8–9), whereas microbial lipase optima lie between pH 5.6 and 8.5 (Kilara, 1985). Generally, free (nonimmobilized) lipases are optimally active between 30 and 40°C (Kilara, 1985). Thermostability of lipases depends strongly on their origin, with animal and plant lipases generally being less thermostable than microbial lipases (Yamane, 1987).

For the fat and oil industry, there are potentially four synthesis reactions (often grouped under the term interesterification)—alcoholysis (alcohol–TAG), glycerolysis (glycerol–TAG), acidolysis (fatty acid–TAG), or ester–ester (trans-

Copyright 2002 by Marcel Dekker. All Rights Reserved.

esterification)—and hydrolysis reactions that lead to the production of free fatty acids, partial acylglycerols (mono- and diacylglycerols), and glycerol (Marangoni and Rousseau, 1995; Malcata et al., 1990). An enzyme's environmental conditions, such as available water, pH level, and temperature, will dictate whether hydrolysis or synthesis predominates (Elliott and Parkin, 1991).

Lipases vary in their specificity. Jensen et al. (1983) noted four types of specificity: substrate [TAG vs. DAG (diacylglycerols) vs. MAG (monoacylglycerols)], positional (primary vs. secondary esters), fatty acid (butyric vs. oleic acid, for example), and stereospecificity (random vs. *sn*-1,3, for example). Most lipases will preferentially react at the 1- and 3-positions of TAGs, yet many can hydrolyze all three positions. Examples of the former include lipases from *Rhizopus arrhizus*, porcine pancreas, *Aspergillus niger*, *Mucor miehei*, and *Rhizopus delemar*, whereas nonspecific lipases include those from *Pseudomonas cepacia*, *Pseudomonas fluorescens*, *Candida rugosa* (formerly *Candida cylindracae*), and *Chromobacterium viscosum*. Some lipases are fatty acid–specific. An interesting case is the lipase from *Geotrichum candidum*, which is highly specific toward unsaturated 18-carbon fatty acids (oleic and linoleic acid) at the *sn*-2 position of TAGs (Nielsen, 1985; Jensen et al., 1965). Complicating matters is the possibility of acyl migration, a strictly chemical phenomenon that leads to the spontaneous exchange of fatty acids from one ester site to another (e.g., from the *sn*-2 position to the *sn*-1 or *sn*-3 positions). So, depending of the reaction conditions, both types of enzymes can completely hydrolyze TAGs (Tombs, 1990). Kalo (1988), studying the interesterification of butterfat by *A. niger* and *M. miehei*, found that both enzymes hydrolyzed fatty acids at the *sn*-2 position of butterfat TAGs under the conditions used, although both lipases were normally *sn*-1,3-specific.

B. Reaction Mechanisms

As opposed to esterases, which cleave the ester bonds of water-soluble TAGs such as tributyrin, lipases function at the interface separating the hydrophilic and lipophilic components of a mixture (Tombs, 1990). Lipases are water-soluble even if they act primarily on nonaqueous substrates. To be fully functional, lipases undergo a conformational change to allow a substrate to diffuse into an active site consisting of the catalytic triad Asp/Glu-His-Ser, with the Ser being the nucleophile necessary for catalysis (Derewenda and Sharp, 1993; Derewenda et al. 1992; Winkler et al., 1990; Brady et al., 1990). This triad is concealed under a surface loop known as the ''flap,'' which consists of a short helical fragment of a long surface loop held in place by electrostatic and hydrophobic interactions (Derewenda et al., 1992). During interfacial activation, the flap becomes displaced upon binding to an interface, exposing the substrate to the active site (Tilbeurgh et al., 1992; Winkler et al., 1990). Simultaneously, the hydrophobic

Copyright 2002 by Marcel Dekker. All Rights Reserved.

environment around the active site becomes exposed and forms a strong binding site for the interface (Winkler et al., 1990). During catalysis, the triad is involved in a charge relay mechanism.

Kinetic studies of emulsified lipid hydrolysis systems have shown that the interfacial area strongly influences the reaction rate (Benzonana and Desnuelle, 1965). Macrae (1985) showed that rapid interesterification rates were obtained only if there was a large interfacial area between the oil and water phases. Garcia et al. (1991) studied the influence of emulsion particle size on the reaction rate of *Aspergillus niger* lipase-catalyzed milkfat hydrolysis. An increase in surface area led to greater enzyme activity.

Lipase hydrolysis is believed to follow a Ping-Pong Bi-Bi reaction mechanism consisting of two steps: (1) the nucleophilic attack of the serine hydroxyl group on the ester bond leading to the formation of an acyl-enzyme intermediate and release of the alcohol moiety of the original substrate and (2) hydrolysis of the acyl-enzyme intermediate (Marangoni and Rousseau, 1995). The reader is referred to the review by Marangoni and Rousseau (1995) for a full description of the reaction mechanisms.

Kinetic models to describe lipase-catalyzed reaction mechanisms have been proposed, and most have been extensions of the model developed by Michaelis and Menten (1913). However, normal Michaelis–Menten kinetics do not apply to lipase-induced changes, because the substrates (lipids) are not water-soluble and the enzyme operates at an interface (Brockman, 1984). However, rate expressions for the hydrolysis of emulsified lipids catalyzed by immobilized lipases resemble the rate expressions modeled with Michaelis–Menten mechanisms (Benzonana and Desnuelle, 1965). The kinetics and mechanisms of reactions catalyzed by immobilized lipases have been reviewed by Malcata et al. (1990; 1992).

C. Lipase Environmental Conditions

The specificity and stability of a lipase will be dictated primarily by its microenvironmental conditions: temperature, pH, ionic strength, water content, dispersing solvent, presence of inhibitors or promoters, and whether the lipase is in the free state or immobilized. Here we discuss the paramount roles of water content and solvent in detail.

1. Water Content

A small amount of water is necessary for the lipase to display catalytic activity (Elliott and Parkin, 1991; Macrae, 1983). During transesterification, water is crucial for the production, via hydrolysis, of intermediate acylglycerols (mono- and

Copyright 2002 by Marcel Dekker. All Rights Reserved.

diacylglycerols) that can subsequently react with released fatty acids to produce new TAGs (Adlercreutz, 1991). How much water is used will determine the amounts of by-products (partial acylglycerols and free fatty acids) formed (Macrae, 1985). Optimal control of moisture content is a key element of lipase biocatalysis, because it affects reaction rate, product yield, product selectivity, and operational stability (Yamane, 1987). At low water content, interesterification product yield may be high, but reactions will be slower, whereas at high water content, the reaction rate would be high and the yield lower (Goderis et al., 1987). In between lies an optimal water content that results in an adequate reaction rate and adequate yield (Reyes et al., 1994).

2. Nonaqueous Solvents

Zaks and Klibanov (1988) showed that enzymes could be catalytically active in nonaqueous solvents. Greater activity was found in hydrophobic solvents than in hydrophilic solvents because water partitions to the enzyme in hydrophobic solvents. Enzyme-bound water can be stripped in nonaqueous media, particularly with polar solvents acting as the continuous phase (Gorman and Dordick, 1992). Sufficient water is required by the enzyme in a nonaqueous environment to provide a monolayer, which allows for the conformational flexibility needed for catalysis, such as the structural unfolding mentioned previously. Mechanistically, water's role as a lubricant stems from its ability to form hydrogen bonds with functional groups of the protein that were previously bound to each other, thereby unlocking the structure. Essential water is tightly bound (thermodynamically) (Halling, 1994).

Lipases used in aqueous solutions are thermostable up to ~40°C, above which they rapidly lose activity (Kang and Rhee, 1989). In solvents with a very low water content, however, lipases are known to remain catalytically active at temperatures as high as 100°C and to have much longer half-lives (Elliott and Parkin, 1991). This is due to the inability of the enzyme to unfold (Zaks and Klibanov, 1984).

Another offshoot of the discovery that enzymes are active in solvents was that prior lyophilization also affects reaction rate. Elliott and Parkin (1991) found that porcine pancreatic lipase activity diminished by 37% following freeze-drying, and Monot et al. (1993) found that *Rhizomucor miehei* lipase activity was enhanced. In fact, this group found that activity was greatly enhanced when substrates were incorporated into the reaction mixture before lyophilization. Activity enhancement was described as a rigidification of the lipase in its active conformation (Dabulis and Klibanov, 1992). Addition of some water was found to enhance this effect whereas greater amounts led to lower activity. This method could be of great use in synthetic reaction.

Copyright 2002 by Marcel Dekker. All Rights Reserved.

IV. HOW DOES INTERESTERIFICATION AFFECT THE PHYSICAL PROPERTIES OF FATS?

This section examines the effects of chemical interesterification on the physical properties of butterfat–canola oil, palm oil–soybean oil, and lard–canola oil blends as well as the effects of enzymatic interesterification of butterfat–canola oil blends.

A. Chemical Interesterification of Butterfat–Canola Oil Blends

Butterfat consists of several thousand different TAGs with melting points ranging from −40°C to +40°C. Jensen et al. (1991) noted the presence of approximately 400 different fatty acids in butterfat, 25% of which were short-chained saturates and 45% long-chained (Deffense, 1993). Such variety in composition is responsible for butterfat's unique physical properties (DeMan, 1961), such as its abrupt drop in solid fat content (SFC) between 10 and 20°C. In stark contrast, canola oil is predominantly (>85%) oleic acid (18:1 $n-9$). The mixing of these dissimilar lipids can lead to the creation of median fats with substantially altered physical properties. In the studies reported here, butterfat and canola oil were mixed in proportions ranging from 100% butterfat to 100% canola oil in 10% (w/w) increments. Details on the methodology used in this study can be found elsewhere (Rousseau et al., 1996a).

As previously mentioned, chemical interesterification is not well understood. In the literature, most studies dealing with chemical interesterification do not show why a specific reaction time was chosen. Coenen (1974) and Weiss et al. (1961) both remarked that the reaction is entropically driven and that once it has begun it is a quick process. However, other workers (Konishi et al., 1993) have shown that the reaction can continue for many hours without reaching equilibrium. Many have shown that the reaction is extremely temperature-dependent. Given this uncertainty, in this study we determined the reaction time that maximized the change in solid fat content. Reaction onset was considered to correspond to the appearance of the brown intermediate commonly associated with the beginning of interesterification (Sreenivasan, 1978; Coenen, 1974).

Much research has been carried out on the chemical interesterification of milkfat. Milkfat, like most fats, does not have a random distribution. Butyric and caproic acids, for example, are predominantly located at the *sn*-3 position, whereas palmitic acid is mostly at *sn*-1 and *sn*-2 positions (Kuksis et al., 1973). Interesterification of milkfat can be a powerful means of modifying its functional properties.

Weihe and Greenbank (1958) presented the first paper dealing with the

Copyright 2002 by Marcel Dekker. All Rights Reserved.

chemical interesterification of milkfat, with details appearing in Weihe (1961). They performed randomization of milkfat at 40–45°C for 20 min to 6 h with 0.1–0.3% Na/K alloy. For directed interesterification, xylene or hexane was added before the start of the reaction, which was begun at 25–38°C and dropped in three to five steps to 10–25°C. Directed interesterification led to more substantial changes than random interesterification, for example, on the content of solid fat. Increases in melting point were greater in the presence of a solvent than without solvent, and directed interesterification generated larger increases in melting point than random interesterification.

Interesterification increased the softening point of milkfat by 3.7–4.2°C, which was explained by higher proportion (5–7%) of high melting triacylglycerol, which translated into greater hardness. Mickle (1960), on the other hand, found that interesterification reduced the hardness of butter and also led to a rancid, metallic flavor. The removal of free fatty acids and the injection of steam under vacuum removed the undesirable flavor, yet the final product was tasteless. Finally, an in-depth study by Mickle et al. (1963) revealed the effects of three interesterification reaction parameters—time (5–55 min), temperature (40–90°C), and catalyst concentration (0.5–5%)—on the hardness of a semisolid resembling butter. All three parameters were statistically significant ($p < 0.05$), with catalyst having the greatest influence on hardness, which diminished by 45–55% using 1–2% catalyst. DeMan (1961a) observed, using polarized light microscopy, that the crystal habit of interesterified milkfat was markedly changed from that of native milkfat. The effects of cooling procedures on the consistency, crystal structure, and solid fat content of milkfat were also examined (deMan, 1961b, 1964b). Parodi (1979) examined the relationship between trisaturates and the softening point of milkfat and found that interesterification increased the softening point from ~32.5°C to ~36.5°C. Timms (1979) found that milkfat and beef tallow interesterified blends lacked milkfat flavor. Timms and Parekh (1980) explored the possibility of incorporating milkfat into chocolate. Interesterified milkfat appeared better suited for addition to chocolate than noninteresterified milkfat, but the improvement gained was too small given the investment and loss of flavor resulting from interesterification.

1. Comparing TAG and SFC Evolution

In order to understand the influence of chemical interesterification on the physical properties of butterfat, it is imperative to understand the changes in composition. Shown in Figure 1 are the changes in butterfat TAG and canola oil composition following 2 h of interesterification. On average over a period of two hours, TAG species C_{24}–C_{32} and C_{44}–C_{48} increased at the expense of species C_{36}–C_{40} and C_{52}–C_{54}, which decreased. Results indicated that interesterification was incom-

Copyright 2002 by Marcel Dekker. All Rights Reserved.

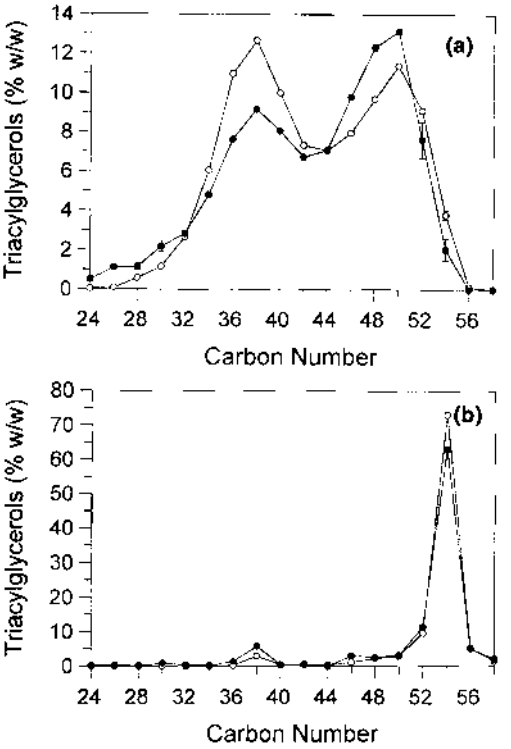

Figure 1 Effect of chemical interesterification on the relative proportions (w/w) of (a) butterfat and (b) canola oil TAGs as function of TAG species carbon number.

plete after 2 h, because noteworthy changes were still observed in the TAG profile between 90 and 120 min, mostly in the C_{46} species.

Canola oil interesterification generated only small changes in TAG composition compared to butterfat. Canola oil is composed of about 90% unsaturated C_{18} fatty acids, so there will always be production of C_{54} (tri-C_{18}) species regardless of treatment duration. After 2 h, the TAG profile was not greatly altered (Fig. 1b). Species with 54 carbons diminished, and C_{36} species increased. Small changes were also observed in the C_{52} species. The increased proportion of C_{36} species, most likely C_{18} diacylglycerols, suggests the presence of unwanted moisture in the system leading to hydrolysis.

Physically, the SFC modifications did not change substantially after 30 min of treatment (Fig. 2). In Figure 2 the SFC evolution of butterfat is plotted against

Copyright 2002 by Marcel Dekker. All Rights Reserved.

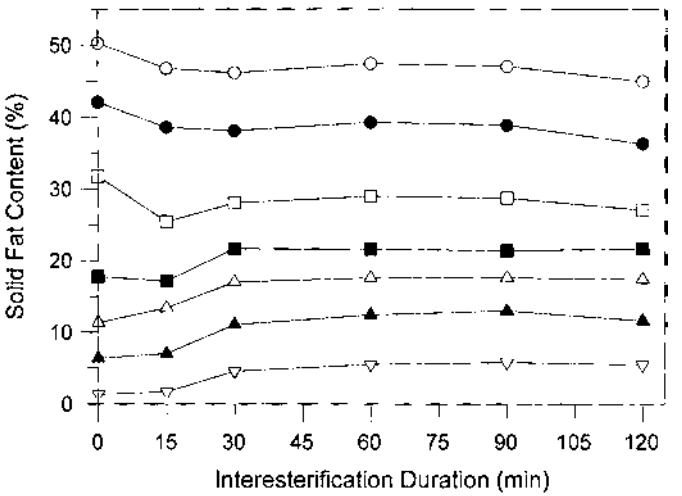

Figure 2 Solid fat content of butterfat as a function of chemical interesterification duration (minutes). Symbols represent the SFC at different temperatures, ranging from 5°C (○) to 35°C (▽) in five degree increments.

chemical interesterification duration. After 15 min, the SFC at 5, 10, 15, and 20°C dropped, whereas it increased at 25, 30, and 35°C. After 30 min, the SFC at 15 and 20°C increased 3% and 5%, respectively. SFC values at 5 and 10°C decreased by an additional 1% between 15 and 30 min, whereas SFCs at 25, 30, and 35°C increased 2–4%. After 30 min, the SFC variations were small (<1% SFC) except at 10°C, where a 2% drop was registered.

It was difficult to determine which species are responsible for the observed SFC evolution. TAG species C_{24}–C_{32} and C_{44}–C_{48} increased, as did the SFC between 25 and 35°C. TAG species C_{36}–C_{40} and C_{52}–C_{54} decreased, as did the SFC, at 5 and 10°C. The variable SFC pattern at 15 and 20°C may be correlated with the variable patterns of TAG species C_{34} and C_{50}.

Random interesterification is usually conducted until equilibrium is reached. There are many conflicting reports in the literature concerning interesterification reaction rate. Coenen (1974) stated that once a sufficient concentration of catalyst in solution was reached in the reaction mixture, the actual interesterification reaction was extremely fast, requiring only a few minutes unless operating at very low temperatures. The kinetics were modeled in several ways to support this theory. The first example was a model system consisting of short-chain fatty esters (8:0, 10:0) of ethylene glycol. The induction period was long, yet the reaction itself was rapid, even at 30°C. In the second example, interesterification of palm oil was evaluated using solid fat content determinations. The

Copyright 2002 by Marcel Dekker. All Rights Reserved.

reaction rate was faster at higher temperatures. These data confirm that an activation period is indeed required, and they agree with Weiss et al. (1961) and Rozenaal (1992), who reported that the catalyst formation phase was longer than the interesterification reaction itself because of the activation energy being higher than for the interesterification reaction itself. Lo and Handel (1983) observed that interesterification of soybean oil and beef tallow was complete after 30 min. Reaction completion was determined by lipase hydrolysis analysis. Results by Konishi et al. (1993) showed that in certain cases the interesterification reaction can progress for as long as 24 h, even with catalyst preactivation. Thus, depending on conditions, randomization can proceed for many hours. Other factors that may influence interesterification onset include agitation intensity, catalyst particle size, and temperature. Studies by many, including Konishi et al. (1993), Laning (1985), and Wiedermann et al. (1961), have shown that interesterification kinetics are temperature-dependent.

2. Solid Fat Content

The solid fat content (SFC) profiles as a function of temperature for noninteresterified (NIE) and chemically interesterified (CIE) butterfat to 20–80% (w/w) butterfat–canola oil blends are shown in Figure 3. All blend SFC profiles (Fig. 3a) were significantly different from each other ($p < 0.0001$), and the rate of SFC evolution was dependent on both temperature and the proportion of butterfat in the blend ($p < 0.0001$). Gradual replacement of butterfat with canola oil led to lower initial SFCs at 5°C.

A nonlinear profile was evident for all blends. Noninteresterified butterfat (NIEBF) and the NIE90:10 and NIE80:20 blends had very similar melting profiles. The NIEBF blend had an SFC of 49% at 5°C that progressed downward nonlinearly until no solid fat was present at 40°C. The NIE90:10 and NIE80:20 blends were also completely melted at 40°C but had lower SFCs at 5°C. Other groups of blends with similar profiles included the NIE70:30 and NIE60:40 blends, the NIE50:50 and NIE40:60 blends, and the NIE30:70 and NIE20:80 blends. The largest decline in SFC occurred from 15 to 20°C, owing to the large proportion of TAGs that liquefy and solubilize in this range. However, as the proportion of oil was increased, this sharp drop became less pronounced. For the NIE50:50 and NIE40:60 blends, the rate of melting was slower at 15–20°C than between 10 and 15°C. The NIE60:40 and NIE70:30 blends have similar melting behavior between 10 and 20°C. Progressively lower concentrations of butterfat led to a reversal of melting behavior between 10 and 20°C.

The SFC profiles of the chemically interesterified (CIE) blends differed from those of the NIE blends (Fig. 3b). The most striking feature was the disappearance of the sharp SFC drop in the range 15–20°C, which shifted to 10–15°C for most of the CIE blends.

Copyright 2002 by Marcel Dekker. All Rights Reserved.

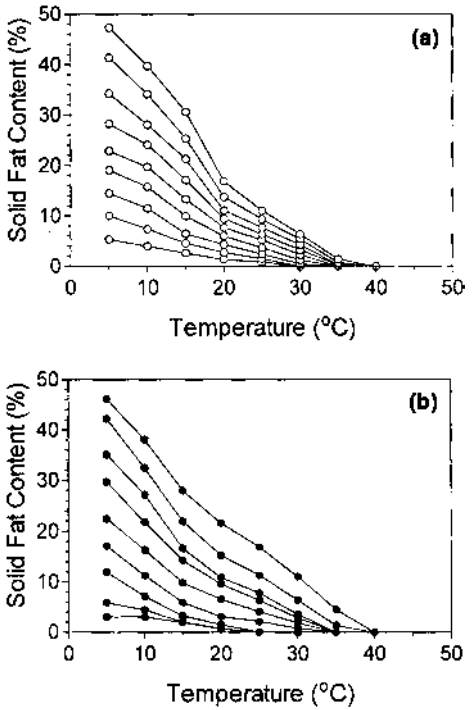

Figure 3 Evolution of solid fat content of butterfat–canola oil blends as a function of temperature (a). SFC evolution of chemically interesterified butterfat–canola oil blends as a function of temperature (b).

The profile of the CIE blends mimicked that of CIEBF but at lower SFC values. As with simple blending, the complexity of the profile diminished as the percentage of oil increased and became quasilinear for the CIE20:80 and CIE30:70 blends. The increased linearity was due to the greater variation of TAGs resulting from interesterification.

The proportion of butterfat and interesterification duration (in the 5–20°C range only) had a significant effect on SFC ($p < 0.0001$). SFC was not significantly affected by chemical interesterification at 25 and 30°C ($p > 0.05$).

Figure 4 displays the effect of chemical interesterification on blend SFC. No SFC changes greater than ±6% resulted from this treatment. The largest SFC increase was produced by interesterification of butterfat at 25°C, for the 80:20 blend at 15°C, and for the 40:60 and 50:50 blends at 10°C. Obviously, no large change in SFC occurred at higher temperatures. The SFC drops upon interesterification are due to the replacement of saturated fatty acids with unsaturated fatty

Copyright 2002 by Marcel Dekker. All Rights Reserved.

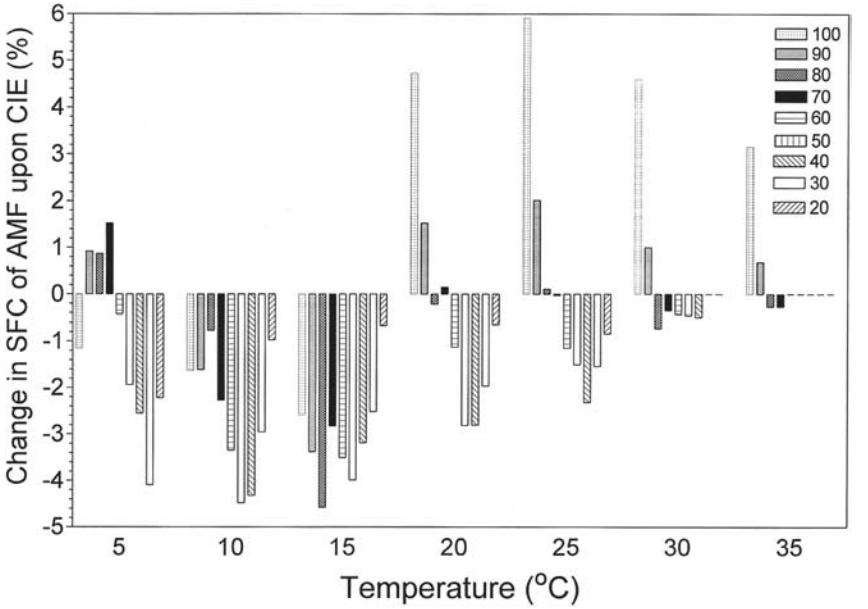

Figure 4 Profile of the effect of chemical interesterification on the SFC of butterfat–canola oil blends. AMF = anhydrons milkfat.

acids in the butterfat TAGs, which contain many di- and trisaturates. Owing to the presence of double bonds, unsaturated fatty acids have lower melting points.

A look at the isosolids diagram (Fig. 5) reveals continuous solid solutions for both NIE and CIE butterfat–canola oil blends. Isosolid lines represent the temperature at constant SFC for various blends of fats. For all linear regressions, the correlation coefficients (r) were greater than 0.95. Trends in isolines indicated the dilution effect generated by blending and chemical interesterification. Ouite visible is the greater dilution effect for NIE blends than for CIE blends, due to the greater intersolubility of ''butterfat'' TAGs following interesterification. A crossover occurred between the 80:20 and 70:30 blends for the 5%, 10%, and 15% isolines. Large differences in slope exist between these sets of linear regressions, but the difference between the slopes diminished with increasing iso-SFC value. By 20% SFC, the isolines were parallel. No crossover was observed at the 25% SFC lines, but the lines were not parallel.

3. Differential Scanning Calorimetric Analysis of Restructured Butterfat

Differential scanning calorimetric (DSC) thermograms, which revealed transition temperatures and heats of fusion, provided results complementary to the pNMR

Copyright 2002 by Marcel Dekker. All Rights Reserved.

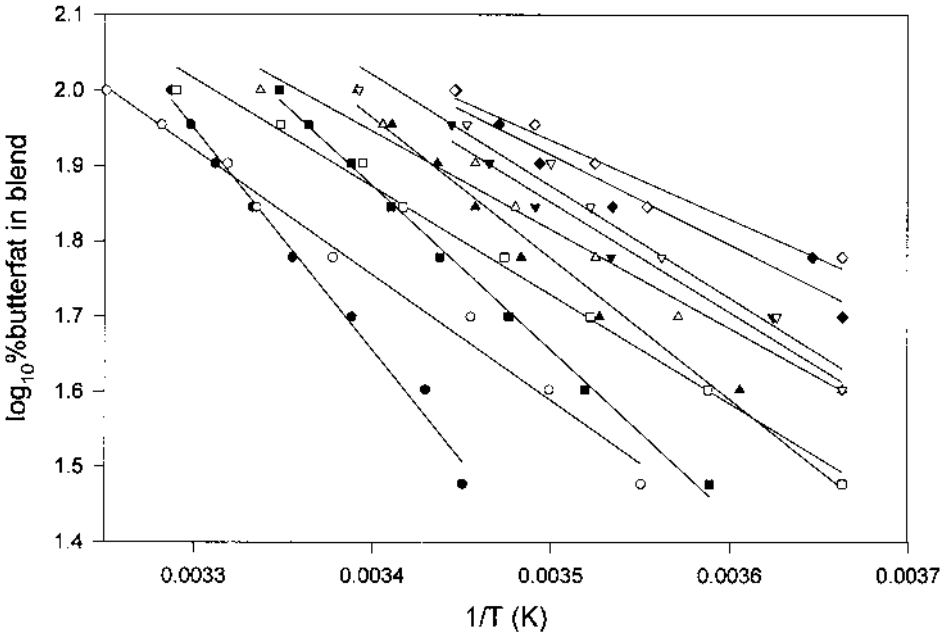

Figure 5 Isosolid lines as a function of the logarithm of percent butterfat in each butterfat–canola oil blend. (○) 5% isoline, NIE; (●) 5% isoline, CIE; (□) 10% isoline, NIE; (■) 10% isoline, CIE; (△) 15% isoline, NIE (▲) 15% isoline, CIE (▽) 20% isoline, NIE; (▼) 20% isoline, CIE; (◇) 25% isoline, NIE; (◆) 25% isoline, CIE.

data. Thermograms representative of NIE and interesterified (IE) butterfat and the 90:10 and 50:50 butterfat–canola oil blends are shown in Figure 6, with the shaded area representing the IE blends. As with pNMR, interesterification produced noteworthy changes in melting profile, whereas blending alone resulted in a dilution effect.

The melting thermograms for butterfat were similar to previously published ones (Timms, 1979). Because butterfat is a mixture of many compounds, it exhibited a broad melting range composed of the low melting TAGs (LMTAGs), the middle melting TAGs (MMTAGs), and the high melting TAGs (HMTAGs). Smaller peaks were also resolved in the thermogram, suggesting possible polymorphic subforms due to lack of thermodynamic equilibrium. Interesterification of the butterfat caused the proportion of HMTAGs to increase at the expense of the MMTAGs. The LMTAGs' endotherms diminished following interesterification. The butterfat thermogram shows that the LMTAG end of melt was at ~19°C, the MMTAG fraction at ~35°C, and the HMTAG fraction at ~48°C.

Copyright 2002 by Marcel Dekker. All Rights Reserved.

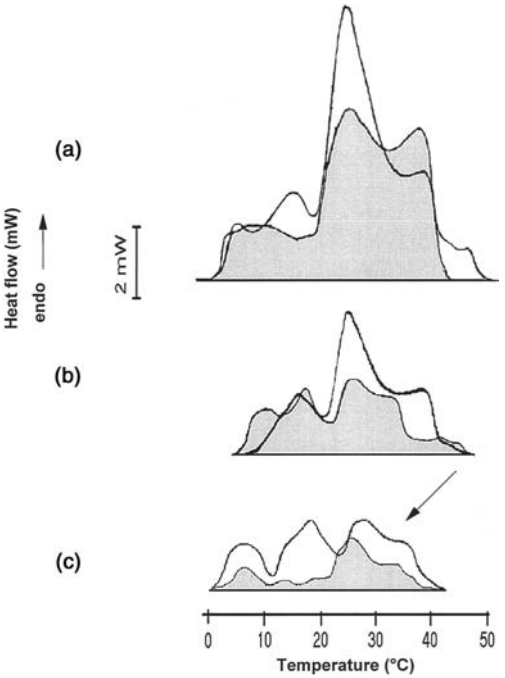

Figure 6 Differential scanning calorimetric melting thermograms of NIE and CIE butterfat–canola oil blends. (a) Butterfat; (b) 90:10; (c) 50:50. The shaded area represents the CIE blends.

Thus, at refrigerator temperature, butterfat was composed of all three fractions, whereas at room temperature the solid butterfat contained mainly the MMTAG and HMTAG fractions. The same analysis could apply to CIEBF.

Addition of 10% canola oil (NIE90:10) produced a dilution effect of the profile of the NIEBF (Fig. 6b). Interesterification, however, created a much-altered thermogram. The MMTAG fraction diminished, the HMTAG fraction shifted a few degrees down, and the LMTAG peak became more pronounced.

Incorporation of 50% canola oil led to peak separation (Fig. 6c) of the remaining solid fat, whereas interesterification dramatically altered the melting profile as the MMTAG fraction disappeared.

Onset of melting, peak maxima for the three main peaks, and end-of-melting temperatures for the DSC thermograms as a function of butterfat proportion are shown in Figure 7. The peak maxima did not change very much as the canola oil content increased. Onset of melting temperatures for NIE blends was at 1.7°C for NIEBF and between 4.3 and 4.8°C for all the other blends (NIE90:10 to

Copyright 2002 by Marcel Dekker. All Rights Reserved.

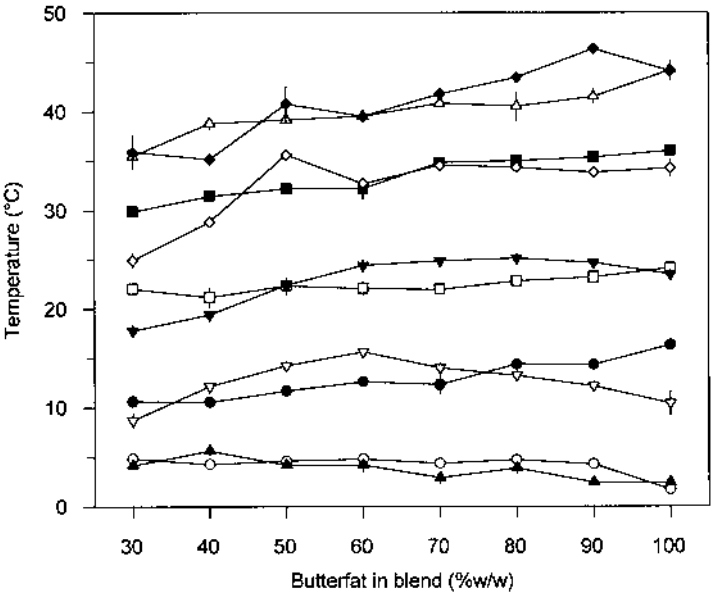

Figure 7 Transition temperatures (onset of melt, peak maxima, and end of melt) for CIE and NIE blends of butterfat and canola oil. (○) Onset of melt, NIE; (●) onset of melt, CIE; (□) peak 1 maximum, NIE; (■) peak 1 maximum, CIE; (△) 2 maximum, NIE; (▲) peak 2 maximum, CIE; (▽) peak 3 maximum, NIE; (▼) peak 3 maximum, CIE; (◇) end of melt, NIE; (◆) end of melt, CIE.

NIE30:70). NIEBF onset temperature was statistically significantly different ($p < 0.05$) from all other blend onset temperatures. For IE blends, the onset temperature was more variable. CIEBF, CIE90:10, and CIE70:30 blends had onset temperatures between 2 and 3°C, and the CIE80:20 blend's onset temperature was 3.9°C. The CIE60:40, CIE50:50, and CIE30:70 blends had an onset temperature of 4.2°C, whereas the CIE40:60 blend began to melt at 5.6°C. Onset temperatures should probably have been lower for CIE blends because the integrity of the butterfat TAGs was altered and they were more unsaturated.

The profile of onset temperatures for NIE blends was not expected to change dramatically as the percentage of oil increased. The enthalpy should drop linearly while the temperatures of onset and end of melting remain unchanged. However, with the incorporation of 10% or more canola oil, the onset temperature increased by ~2°C. This meant that there were less TAGs crystallizing at low temperature, possibly indicative of increased solubility of the LMTAGs in the

Copyright 2002 by Marcel Dekker. All Rights Reserved.

canola oil. This increased solubility was constant between 10% and 70% canola oil in the blend, because there was no subsequent increase in onset temperature. For the CIE blends, a general upward trend was observed. This was expected as more intermediate TAGs were produced. Similar TAGs are more likely to dissolve in one another (''like dissolves like''). Statistically, butterfat content had a significant effect ($p < 0.0001$) on onset of melting and interesterification did not ($p > 0.2$).

The same analysis can be applied to the end-of-melt temperatures. For NIEBF, end of melting was observed at 44.2°C; addition of 10% canola oil resulted in a 2.7°C drop to 41.5°C. Between NIE90:10 and NIE40:60, the end-of-melt temperature dropped only 2.6°C. Finally, the NIE30:70 blend finished melting at 35.5°C, 3.3°C lower than the 40:60 blend. There appeared to be three regions of miscibility: NIEBF, NIE90:10-NIE40:60, and NIE30:70. The miscibility was dependent on the proportion of butterfat TAGs. Butterfat concentration had a significant effect ($p > 0.0001$) on end-of-melt temperatures areas interesterification did not ($p > 0.35$).

A comparison of all peak maxima trends between the CIE and NIE blends revealed similar results. CIEBF had lower maxima than NIEBF. With gradual incorporation of oil, an inversion occurred and the CIE blends had higher maxima than NIE blends. This inversion occurred at different butterfat–canola oil proportions, depending on the peak: peak 1, between 80:20 and 70:30; peak 2, between butterfat and 90:10; and peak 3, between 70:30 and 60:40. Another crossover occurred at higher canola oil concentrations: peak 1, between 60:40 and 30:70; peak 2, 50:50, and peak 3, between 50:50 and 40:60.

Heat of fusion (enthalpy) was proportional to sample SFC at a specific temperature (Fig. 8). As expected, the enthalpy decreased as canola oil was added. Canola oil does not crystallize at refrigerator temperatures and cannot be directly implicated in the crystallization of the blends per se. However, it mingled intimately with the butterfat TAGs. The enthalpy for NIE blends was much higher than for IE blends, and the drop in enthalpy observed with addition of oil was not linear. For blends with 70% or more butterfat, the enthalpy diminished slowly in an almost linear fashion. NIEBF to NIE70:30 enthalpies were not statistically significantly different from each other ($p > 0.05$). With 50% or less butterfat, the enthalpy drop was much sharper. These results suggest that the butterfat TAG matrix could harbor a large amount of liquid oil and retain a structured network. The NIE60:40 region may represent an important region in the crystallization pattern of these blends.

The drop in enthalpy of the IE blends was not linear as oil content increased, and there was no obvious break point as with NIE blends, due to the randomization of the TAG structure. With fewer trisaturates a strong network could not form; hence less heat was required to melt the crystal network.

Copyright 2002 by Marcel Dekker. All Rights Reserved.

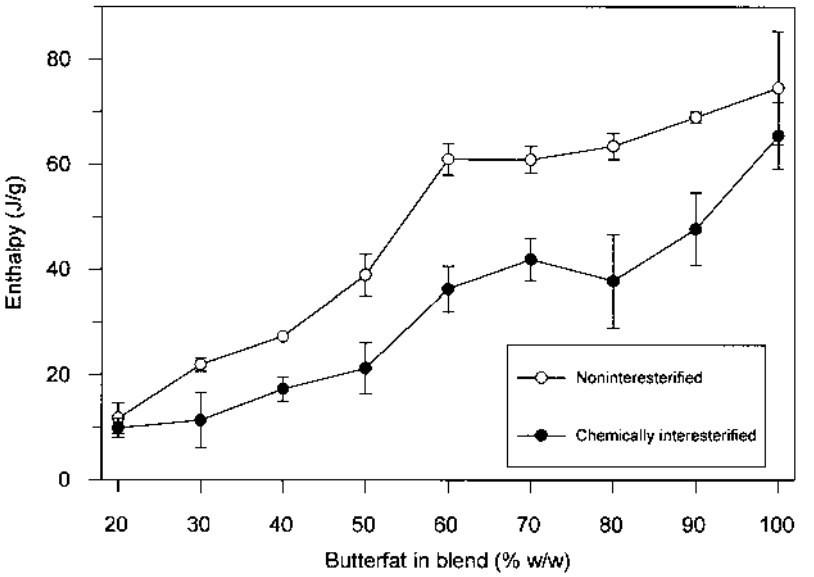

Figure 8 Enthalpy of melting (J/g) of CIE and NIE butterfat–canola oil blends as a function of percent (w/w) butterfat in the blend.

In any fat, there is a direct relationship between the TAG composition and physical properties. The types of fatty acids dictate the melting behavior of a TAG. Also important is the FA positioning along the glycerol backbone, which affects structure and thereby melting. TAGs with a more asymmetrical distribution tend to have lower melting points. Given butterfat's complex composition, determination of the melting pattern is complicated.

The proportion of butterfat had a significant effect ($p < 0.05$) on TAG composition, except for C_{42} species. Chemical interesterification produced statistically significant changes in TAG composition for most carbon species in most samples, except C_{32}, C_{34}, C_{38}, and C_{42} ($p > 0.05$). For species with 24–30 or 58 carbons, no changes greater than 1.5% were observed.

Butterfat TAGs were divided into two groups (Fig. 1a), the first composed of C_{26}–C_{40} species and the second composed of C_{44}–C_{54}. The predominant TAGs in butterfat were C_{36} (11.0%), C_{38} (12.7%), C_{40} (10%), C_{48} (9.7%), C_{50} (11.4%), and C_{52} (9.1%). According to Timms (1979), the LMTAG fraction is composed of TAGs containing one long-chain saturated acid with two short-chain or cis-unsaturated acids. The MMTAG fraction TAGs contain two long-chain saturated acids plus one one short-chain or cis-unsaturated acid. Finally, the HMTAG fraction contains only long-chain saturated acids.

Copyright 2002 by Marcel Dekker. All Rights Reserved.

This great variety in TAGs was not found in canola oil, which was predominantly composed of C_{54} (73.2%) and C_{56} (9.6%) species (Fig. 1b). Canola oil consists primarily of oleic acid (>80%).

Small TAG distribution changes occurred with the addition of 10% canola oil (Fig. 9a), which correlated with the small drop in enthalpy from 100% butterfat (Fig. 8). Interesterification led to a substantial drop (31%) in the enthalpy of CIE90:10.

Gradual TAG modifications were observed for the 80:20 to 60:40 blends (Figs. 9b–9d). The C_{34}–C_{40} and C_{54} species diminished whereas the C_{46}–C_{52} species increased following interesterification. These gradual TAG changes accounted for the steady changes in enthalpy and melting temperatures.

The notable change in enthalpy for the 50:50 blend cannot be readily explained by the TAG behavior, which underwent a gradual change from NIE60:40 to NIE50:50 (Fig. 9e). Perhaps there is a limit of saturated TAGs required to hold the crystal network together. The most notable changes occurred in the C_{50}–C_{54} species.

For all the other blends (Figs. 9f–9i), TAG modifications were gradual, except for the 40:60 and 20:80 blends, which underwent substantial changes, mostly in the C_{54} species. With the loss of C_{54}s, there were large increases in the C_{48}–C_{52} species. This exchange was not reflected in the enthalpy changes, which had a constant rate of decline for these blends.

4. Solution Behavior

Using the Hildebrand solubility law, predicting the melting point of a higher melting lipid component in a lower melting component is possible (Hildebrand and Scott, 1962). This equation is applicable to ideal mixtures (Birker and Padley, 1987). In the liquid state, all TAGs are miscible. As the temperature is decreased from the melt and the lipid is supercooled, the solubility of the crystallizing TAGs becomes negligible (Knoester et al., 1968). An approximation of the melting of the butterfat component in canola oil (T_c), assuming it behaves as an ideal solution is given by the equation

$$\ln x = \frac{\Delta H_f}{R}\left(\frac{1}{T_m} - \frac{1}{T_c}\right)$$

where

X = mole fraction of the high melting lipid
ΔH_f = molar enthalpy of fusion of the higher melting fat
R = universal gas constant
T_m = melting temperature of higher melting component in butterfat
T_c = melting temperature of blend as evaluated by DSC

Copyright 2002 by Marcel Dekker. All Rights Reserved.

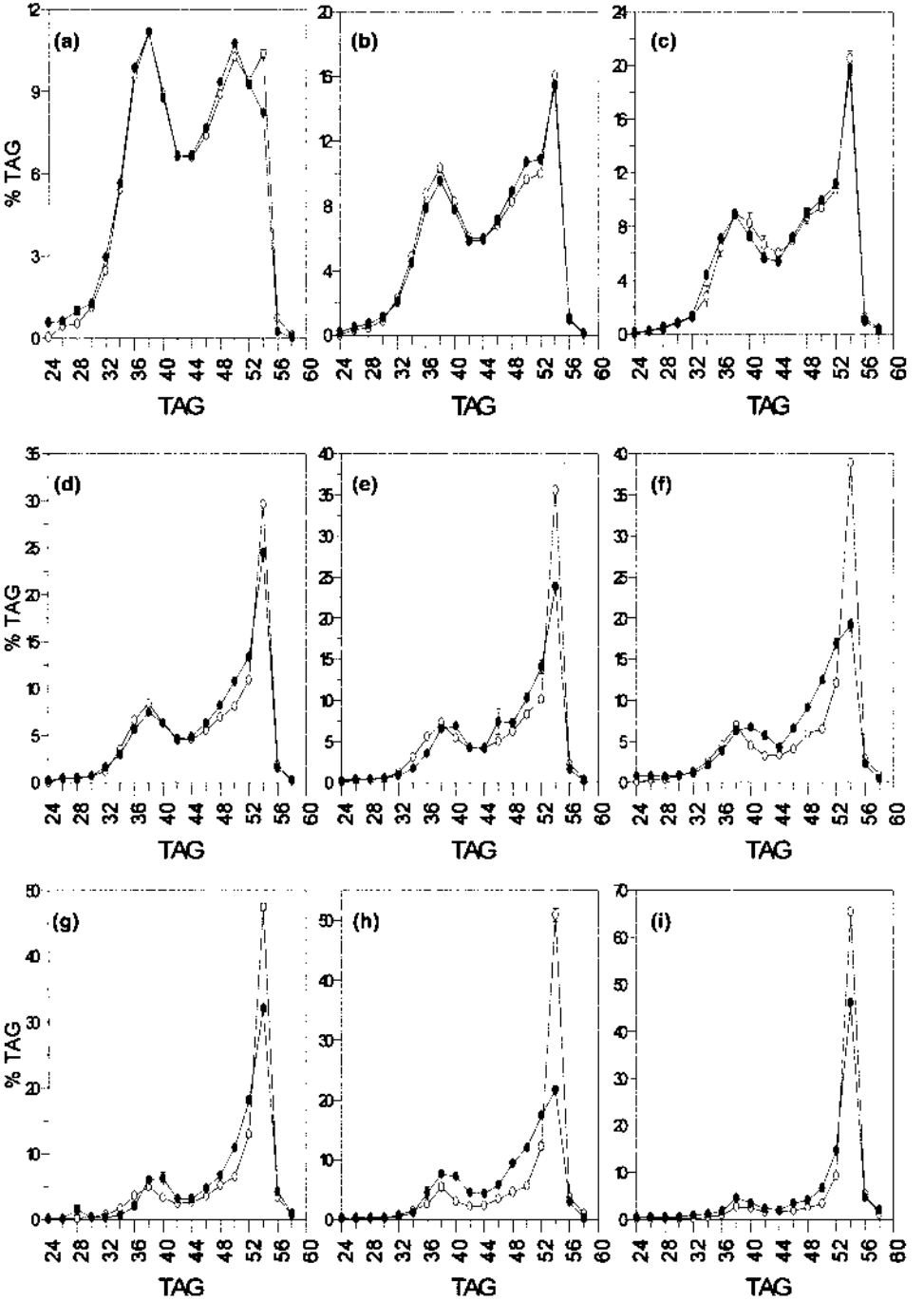

Copyright 2002 by Marcel Dekker. All Rights Reserved.

Table 1 Temperature Deviations (±Standard Error) from Ideal Solubility for Butterfat to Form 20:80 Blends Before and After Interesterification as Evaluated by Hildebrand Solubility Law for Ideal Mixtures

Percent butterfat in blend	Deviation (°C) from ideal solubility	
	Noninteresterified	Interesterified
90	−1.29 ± 0.01	−1.51 ± 0
80	−2.84 ± 0.03	−3.30 ± 0
70	−4.48 ± 0.01	−5.12 ± 0.03
60	−6.49 ± 0.03	−7.37 ± 0.02
50	−8.80 ± 0.02	−10.09 ± 0.11
40	−11.60 ± 0.04	−12.84 ± 0.05
30	−14.95 ± 0.03	−16.96 ± 0.18

The molecular weight of butterfat has been approximated as 731 g/mol, and that of canola oil as 876 g/mol (Timms, 1978).

Temperature deviations from ideal solubility for butterfat to 20:80 blends before and after interesterification are shown in Table 1. Comparison of the end-of-melt temperatures for the NIE and CIE butterfat–canola oil blends and that calculated with the Hildebrand equation indicated that the solubility of butterfat became progressively higher than predicted by the Hildebrand equation for both CIE and NIE samples, as the proportion of canola oil increased. As expected, deviations were higher for CIE samples as the butterfat component (HMTAG) was altered through interesterification, leading to more similarily between TAGs and hence greater intersolubility.

Statistically, both interesterification and blending had significant effects ($p < 0.0001$) on deviation from ideal solubility. All deviations from ideal solubility for all blends were significantly different from one another ($p < 0.05$).

Bailey (1950) discusses entropy in fat systems. In the solid state, order predominates. Solid–liquid transformations result in greater entropy due to increased atomic and electronic motion. Heating of fat samples by DSC likewise results in increased structural disorder. However, as the temperature does not

Figure 9 Relative TAG proportion (% w/w) evolution as a function of TAG species carbon number (C) for CIE and NIE butterfat–canola oil blends. (○) Noninteresterified blends and (●) chemically interesterified blends (a) 90:10; (b) 80:20; (c) 70:30; (d) 60:40; (e) 50:50; (f) 40:60; (g) 30:70; (h) 20:80; (i) 10:90.

Copyright 2002 by Marcel Dekker. All Rights Reserved.

increase during the solid-to-liquid transformation, the energy absorbed is strictly entropic. TAGs encased in a crystal matrix with reduced molecular motility become free to move upon liquefaction, resulting in higher entropy. According to Hildebrand and Scott (1962), the following equation can be used to calculate the enthalpy change upon melting:

$$\Delta S_m = \frac{\Delta H_m}{T_m}$$

where ΔS_m = entropy change, ΔH_m = enthalpy change, and T_m = melting temperature.

Table 2 lists the entropy of melting of butterfat to 30:70 blends. NIE100 had the highest change in entropy (most order lost during melting) upon melting. As oil was gradually added to the blends, ΔS_m dropped nonlinearly. At 50% butterfat, there was a large drop in ΔS_m indicative of a much less ordered system. Depending on the blend, the entropy was one-half to one-fourth as much for the CIE blends as for the NIE blends. Greater changes in entropy were obtained for the NIE blends because of their greater initial order.

5. Crystal Morphology via Polarized Light Microscopy

Plastic fats consist of a crystal network in a continuous oil matrix. Fat crystals, which consist of interacting triacylglycerol (TAG) molecules in an asymmetrical tuning fork geometry (Jensen and Mabis, 1963), exhibit polymorphism. TAGs with identical fatty acids can show large differences in polymorphic behavior

Table 2 Entropy of Melting for Butterfat to 20:80 Blends Before and After Interesterification

Percent butterfat in blend	Entropy of melting[a] [kJ/(mol · K)]	
	NIE	IE
100	0.1720	0.1511
90	0.1605	0.1092
80	0.1480	0.0874
70	0.1419	0.0973
60	0.1427	0.0849
50	0.0912	0.0496
40	0.0642	0.0410
30	0.0519	0.0268

[a] Standard error was $<10^{-4}$ kJ/(mol · K).

Copyright 2002 by Marcel Dekker. All Rights Reserved.

(Rossell, 1967). The current crystal polymorph nomenclature, proposed by Lutton (1950), consists of three main forms: α, β′, and β. The α-form chain packing is hexagonal; the β′ form, orthorhombic; and the β form, triclinic (Chapman, 1962). Crystal subforms include sub-α, β_1', β_2', pseudo-β′, sub-β, β_1, and β_2 (D'Souza et al., 1990).

Both blending of canola oil and chemical interesterification substantially altered the crystal morphology of butterfat. Figure 10a shows the noninteresterified butterfat (NIEBF) crystal network following 1 day of crystallization. A very dense network of spherulites and ill-defined needles with no discernible regular pattern was visible. Most structural elements measured 10–25 μm in size. Figure 10b reveals that the interesterified butterfat (CIEBF) crystal network was composed of spherulites of varying density measuring ~15 μm with a lacy network of small crystals. These results agree with the results of deMan (1961a), who found that milkfat interesterification caused a decrease in crystal size. The spheru-

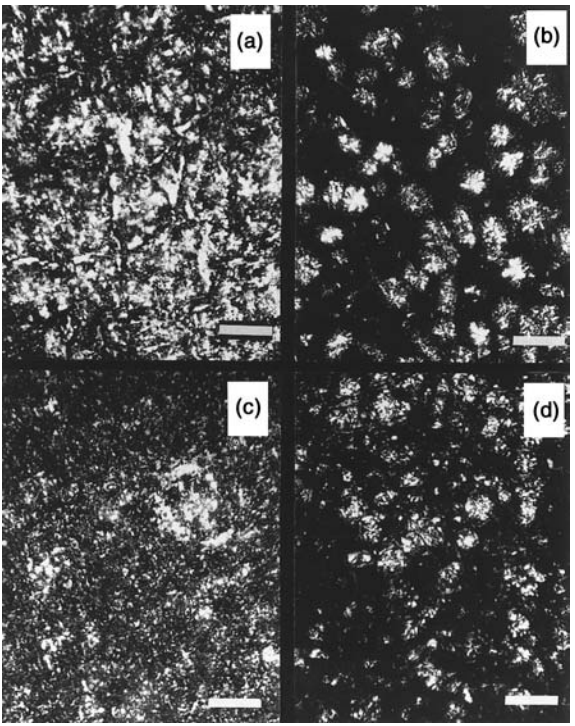

Figure 10 Polarized light microscopic photomicrographs of samples tempered 24 h at 5°C. (a) NIE100; (b) CIE100; (c) NIE90:10; (d) CIE90:10. The bar represents 25 μm.

Copyright 2002 by Marcel Dekker. All Rights Reserved.

lites were structurally weak—slight agitation led to their dismemberment. Addition of 10% canola oil to butterfat (NIE90:10) resulted in a dilution of the butterfat structure with no substantial change in morphology (Fig. 10c). Fewer large crystals were visible with only a few irregularly shaped aggregates present. Small needles measuring only a few micrometers in size composed most of the crystals. Chemical interesterification of the 90:10 blend (CIE90:10) (Fig. 10d) resulted in a morphology very similar to that of CIEBF.

Addition of 20% canola oil generated substantial morphological changes for the noninteresterified 80:20 blend (NIE80:20), the crystal network consisting of large and dense spherulites measuring ~20 μm (Fig. 11a). Interesterification of the 80:20 blend (CIE80:20) led to larger, more loosely packed spherulites that measured approximately. 30–40 μm in size (Fig. 11b). Small, disordered platelets

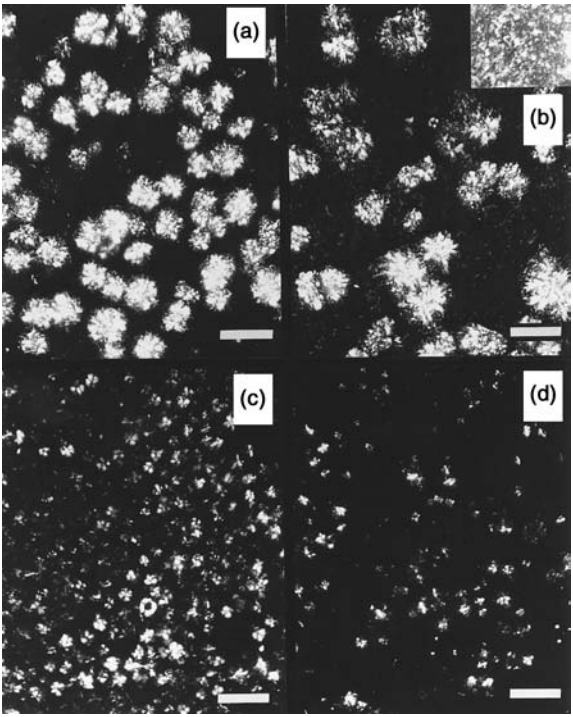

Figure 11 Polarized light microscopic photomicrographs of samples tempered 24 h at 5°C. (a) NIE80:20; (b) CIE80:20; (c) NIE50:50; (d) CIE50:50. The bar represents 25 μm.

Copyright 2002 by Marcel Dekker. All Rights Reserved.

were also discernible (Fig. 11b inset), a commonality of chemically interesterified fats.

The 50:50 blend (NIE50:50) (Fig. 11C) was composed of small spherulites measuring only 5–10 μm in diameter. The interesterified sample (CIE50:50) contained fewer crystals. At the magnification used, these crystals lacked structure and measured only a few micrometers in size (Fig. 11d).

In a perfect crystal, the surface free energy is close to zero. An increase in imperfection results in an increase in free energy. Larger crystals have lower surface energy than smaller crystals (Hoerr and Waugh, 1950). Crystals aggregates have even lower surface energy (Larsson, 1994). This phenomenon, known as Ostwald ripening, is evident in Figures 10 and 11. The migration of crystals to form aggregates was most likely facilitated by the addition of canola oil, because less solid fat is present to impede migration toward other crystals.

6. Crystal Network Structure via Scanning Electron Microscopy and Confocal Laser Scanning Microscopy

Figure 12 shows the structure of NIE100 and CIE100 tempered for 1 day or 8 days at 5°C. Figures 12a–12d and 12f were viewed by scanning electron microscopy (SEM), and Figure 12e by confocal laser scanning microscopy (CSLM). The surface structure of butterfat following 1 day of crystallization (Fig. 12a) was poorly defined. High magnification (photomicrograph not shown) showed that the visible ridges were structured but not well ordered. Tempering for 8 days (Fig. 12b) revealed extensive mottling, indicative of crystal growth.

CIE100 following 1 day and 8 days of crystallization (Figs. 12c and 12d, respectively) was comparatively more structured than NIE100. After 8 days of crystallization, the surface of CIE100 (Fig. 12d) was more finely detailed than the surface of NIE100 after 8 days. This may be due to greater recrystallization in the NIE100 compared with CIE100.

Figure 12e reveals a cross-sectional view of a butterfat aggregate viewed with CLSM. The image suggests a well-resolved dendritic structure of the butterfat with microstructure in the submicrometer range visible. The large aggregate measured 90 μm by 70 μm and consisted of three or four different component aggregates within the main structure. From all groups, wispy filaments emanated from a central nucleus with extensive branching. It is quite possible that this branching was responsible for the formation of crystal bridges between different aggregates. The interacting aggregates may suggest how larger aggregates form. Clear areas between the aggregates where only liquid oil was visible may have arisen due to steric hindrance or may have represented areas in the initial stages of sintering. Figure 12f shows an isobutanol-extracted butterfat crystal. As with the CLSM results, a central nucleus was visible with outwardly radiating arms.

Copyright 2002 by Marcel Dekker. All Rights Reserved.

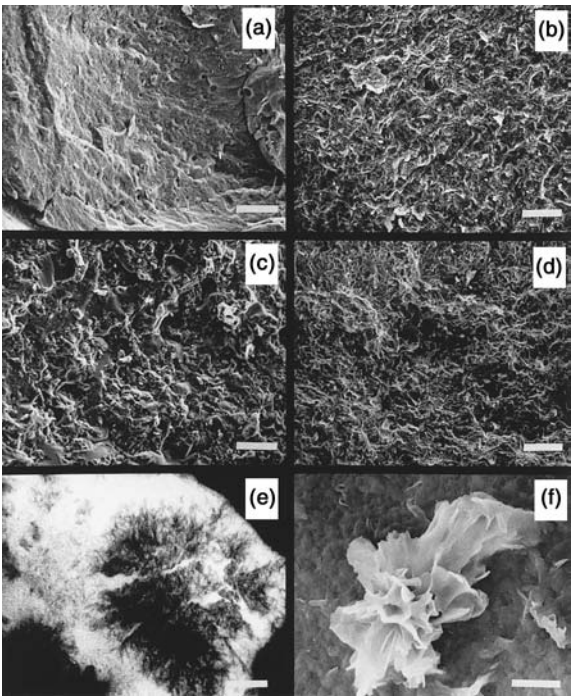

Figure 12 Scanning electron microscopic (SEM) and confocal laser scanning microscopic (CLSM). Photomicrographs of butterfat tempered for 1 or 8 days at 5°C. (a) SEM, NIE100, 1 day; (b) SEM, NIE100, 8 days; (c) SEM, CIE100, 1 day; (d) SEM, CIE100, 8 days; (e) CLSM, NIE100, 8 days; (f) SEM, isobutanol-extracted NIE100, 8 days. The bar represents 25 μm for (a)–(e) and 5 μm for (f).

The structure appeared as an oblong spherulite. Although the isobutanol-extracted crystal and the CLSM images are on different scales, definite similarities are evident because both structures show a dense, well-defined nucleus with tenuous crystalline matter surrounding the central region.

Figure 13 shows the surface structure of various samples examined by SEM. Figures 13a and 13b show the NIE90:10 blend following 1 and 8 days of tempering, respectively. Structure increased from day 1 to day 8. Figures 13c and 13d show NIE80:20 and CIE80:20, respectively, following 8 days of tempering. Surface structure was very different for the two blends. In the noninteresterified blend, a definite segregation of liquid and solid was visible that was not visible in the interesterified equivalent. Figures 13e and 13f show NIE50:50 and CIE50:50, respectively, following 1 day of tempering. The two samples appeared equally

Copyright 2002 by Marcel Dekker. All Rights Reserved.

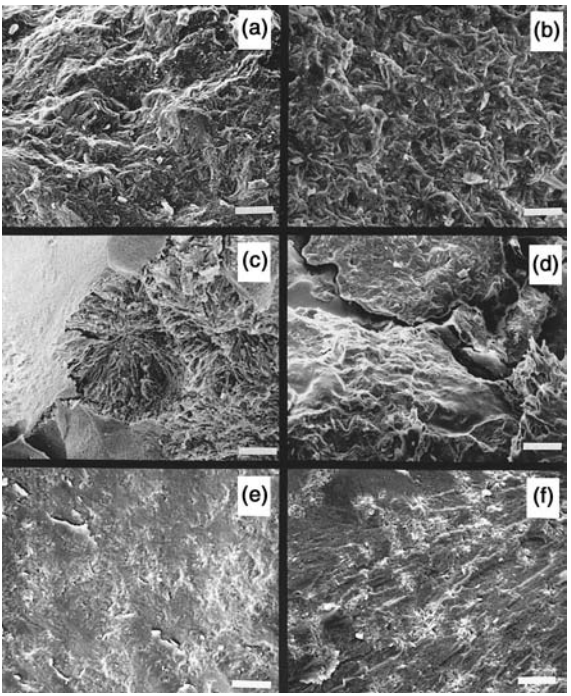

Figure 13 SEM photomicrographs of blends tempered for 1 or 8 days at 5°C. (a) CIE90:10, 1 day; (b) CIE90:10, 8 days; (c) NIE80:20, 8 days; (d) CIE80:20, 8 days; (e) NIE 50:50, 1 day; (f) CIE50:50, 1 day. The bar represents 25 μm.

detailed, but their structure was different. The NIE50:50 blend showed a relatively smooth surface, whereas the CIE50:50 blend (Fig. 13f) revealed segregation of spherulitic agglomerates.

Figure 14a shows a high magnification view of NIE90:10 following 8 days of crystallization, and Figure 14b shows a close-up of butterfat structure following 8 days of crystallization. The NIE90:10 blend presented an extensive, haphazardly arranged structure. In Figure 14b, there appears to be layering in the butterfat crystal structure. This phenomenon was explored in great detail by Precht and Buchheim (1980), who examined the fine structure of butter using transmission electron microscopy (TEM). Although there was a 100-fold difference in scale between the present work and the work of Precht and Buchheim (1980), definite layering pattern is visible in both cases. This shows that the repeating layer order in the structure may be partly responsible for the structure of three-dimensional crystal networks.

Copyright 2002 by Marcel Dekker. All Rights Reserved.

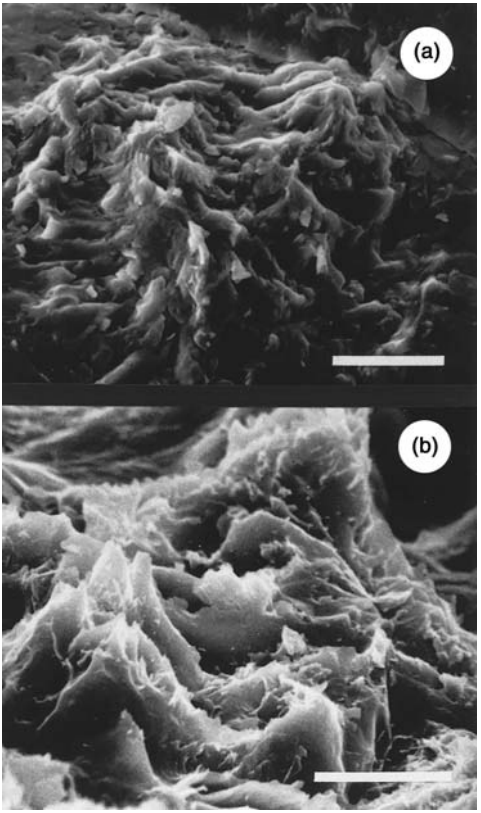

Figure 14 Higher magnification SEM photomicrographs of blends tempered for 8 days at 5°C. (a) NIE100, 8 days; (b) NIE90:10, 8 days. The bar represents 10 μm.

The examples of the effect of tempering and composition shown here represent an accurate cross section of all examined specimens. The spherulites observed in the PLM photomicrographs were also present in the SEM equivalents; however, they were embedded in the solid–liquid matrix. This effect is particularly evident for the CIE50:50 blend (Fig. 11d vs. Fig. 13f) and the CIE90:10 blend (Fig. 10d vs. Fig. 13a).

During the cryopreparation with liquid nitrogen, the cooling was rapid enough to prevent the formation of noticeable crystals in the liquid oil. This minimized artifacts created upon freezing as the liquid oil is solidified in an amorphous fine structure, void of detail. Jewell and Meara (1970) observed the same phenomenon with cryofixed samples of lard and shortening viewed with TEM.

Copyright 2002 by Marcel Dekker. All Rights Reserved.

For all the samples examined, the tempering was meticulously controlled. Even with identical tempering, great variations in morphology were apparent among all samples. Thus, the fatty acid and TAG composition were responsible for the variations in microstructure. Different proportions of canola oil followed by randomization resulted in different final morphologies. A more random TAG distribution resulted in less organized structure as exemplified in both PLM and SEM results.

7. Polymorphic Behavior of Butterfat–Canola Oil Blends

X-ray diffraction, used to identify crystal polymorphs, is based on the determination of the long and short spacings of crystals. The α form has a single short spacing near 4.15 Å and the β′ form, spacings at 3.8 and 4.2 Å or three at 4.27, 3.97, and 3.71 Å, whereas the β form does not correspond to either of these forms and shows a single strong spacing at 4.6 Å (Nawar, 1996; deMan, 1992; Larsson, 1966).

Table 3 details the polymorphic modifications engendered by blending and chemical interesterification. Other extremely weak bands appeared but were not considered in the final analysis. The X-ray diffraction data reveal that most samples were combinations of β′ and β crystals. Natural butterfat consisted primarily of β′ crystals, with a small proportion of β crystals, indicated by a weak spacing at ~4.6 Å. Interesterification of butterfat resulted in the removal of the band at 4.6 Å. Woodrow and deMan (1961) and Timms (1979) both reported X-ray diffraction results for NIE and CIE milkfat. Natural milkfat had strong short spacings at 3.8 and 4.2 Å, indicative of β′, plus a weak short spacing at 4.6 Å, indicative of the β polymorph. Following interesterification, the short spacing at 4.6 Å almost completely disappeared.

Replacement of 10% (w/w) butterfat with canola oil increased the relative

Table 3 Polymorphic Forms and Short Spacings of NIE and CIE Butterfat and the 90:10 and 80:20 Butterfat–Canola Oil Blends[a]

	Short spacings (Å)				
Blend	4.6	4.2	3.8	3.7	Polymorph
NIE100	4.62 (w)	4.19 (s)	3.80 (m)	3.75 (w)	$\beta' \gg \beta$
NIE90	4.57 (w)	4.19 (s)	3.80 (m)	3.71 (w)	$\beta' \gg \beta$
NIE80	4.60 (w)	4.23 (s)	3.83 (m)	—	$\beta' > \beta$
IE100	4.61 (vw)	4.22 (s)	3.80 (m)	—	$\beta' \ggg \beta$
IE90	4.57 (w)	4.21 (s)	3.81 (m)	—	$\beta' \gg \beta$
IE80	4.57 (w)	4.24 (s)	3.80 (m)	—	$\beta' \gg \beta$

[a] Intensities: v, very; w, weak; m, medium; s, strong.

Copyright 2002 by Marcel Dekker. All Rights Reserved.

intensity of the band at 4.6 Å, indicating a higher proportion of the β polymorph. Interesterification of the 90:10 blend generated β crystals with the appearance of a very weak band at 4.6 Å only in very small proportions. The reappearance of β crystals in the interesterified 90:10 blend is possible due to lack of variety in chain length. One means of stabilizing the β′ modification is to have TAGs with varying chain lengths. As stated by Larsson (1994), variations in chain length result in more disordered packing near the methyl end regions, leading to less chance of a tightly knit crystal lattice. Because β crystals have the most ordered structure, less variation in the chain length will increase their likelihood.

For both NIE100 and NIE90:10, there was a weak band at ~3.73 Å, indicative of a possible crystal subform. Both 80:20 blends contained larger amounts of β crystals than the 90:10 blends. The increased canola oil content led to an increase in β content in both NIE and CIE blends.

Crystal polymorph plays a key role in final product consistency and acceptability. Smaller crystals lead to firmer fat products, whereas larger fats give a sense of sandiness in the mouth. Incorporation of large amounts of liquid oil increases the tendency of the desirable β′ polymorphic form to convert to the β form (deMan et al., 1995). In the production of butterfat–canola oil spreads, preserving the β′ form would be essential in order to avoid a sandy mouthfeel.

8. Linking Structure to Polymorphic Form

Tempel (1961) surmised that fat crystal network structure consisted of an assembly of chains, each chain being an assembly of a linear array of closely aligned particles. The chains were considered to be branched and interlinked to form a three-dimensional network, with liquid fat filling the voids. Unfortunately, this theory did not successfully account for the nonlinear dependence of rheological phenomena such as yield stress and elastic modulus on the proportion of solid fat. Fat crystal networks are now viewed as being composed of haphazardly interlinked aggregates (Tempel, 1979).

Examination of Figures 10 and 11 reveals aggregated structure for many samples. This aggregation behavior represents reality in terms of network structure.

Beta crystals are considered the most stable crystal polymorph (Lutton, 1950). In the examined samples, as the proportion of oil increased, so did the presence of β crystals. Microstructurally, aggregation in the form of spherulites became more pronounced. Aggregation behavior was more apparent in the CIE samples than in the NIE samples. CIE100 was almost devoid of β crystals, yet it demonstrated substantial aggregation. Thus, aggregation in fat crystals cannot be readily explained by polymorphic form. Other factors such as the rheological properties of the spreads must have come into play.

Copyright 2002 by Marcel Dekker. All Rights Reserved.

9. Rheological Properties of the Fats

The rheological behavior of plastic fats is governed by interactions between fat crystals in an aggregated three-dimensional solid–liquid fat matrix (deMan and Beers, 1987). The prime forces leading to network formation are van der Waals attractive forces, because electrostatic and steric repulsion are absent (Walstra and Jenness, 1984). The liquid portion of the fat, interspersed throughout the aggregated fat network, serves as a continuous phase and, in conjunction with the solid fraction, is responsible for viscoelastic behavior (Drake et al., 1994). Of primary importance to the rheological behavior of fat is the amount of crystalline fat and the type of crystal present in the fat crystal network (Haighton, 1976).

Rheological measurements of fats can be performed at low or high deformation. In the latter, the fat crystal network undergoes irreversible deformation, whereas in the former, viscoelasticity is measured below the yield point, is reversible, and approaches the state of the sample at rest (Rohm and Weidinger, 1993; Rohm, 1993). Single-point empirical measurement methods such as cone penetrometry, extrusion, and simple compression are commonly used for measuring large deformations (deMan, 1983), and more complex methods such as controlled stress rheometry are generally used for measuring small deformations.

(a) Cone Penetrometry. Cone penetrometry (CP) is a rapid, yet empirical, method used in the evaluation of texture (deMan, 1983). The hardness index (HI) is a simple expression of consistency calculated by dividing the mass M of the penetrating cone assembly by the depth of penetration p in millimeters (Hayakawa and deMan, 1982):

$$HI = \frac{M}{p} \quad (g/mm)$$

During penetration of the cone assembly, the cone sinks into the fat sample until the stress exerted by the increasing contact surface of the cone is balanced by the hardness of the fat (deMan, 1983). In the process, the crystal aggregate network is partially and irreversibly destroyed (Lefèbvre, 1983). Cone penetrometry is a large-deformation rheological method.

Figure 15 displays blend HI as a function of butterfat proportion (% w/w) measured by cone penetrometry at 5°C. The HI of CIE100 was 20.8% lower than that of the NIE butterfat. The HI of the NIE 90:10 (NIE90:10) blend was only 2.9% lower than that of NIE100. Interesterification of the 90:10 blend (CIE90:10) led to a 54.4% decline in HI compared with CIE100, whereas a difference of 62.8% was observed between the HIs of NIE90:10 and CIE90:10. Addition of 20% canola oil (NIE80:20 blend) produced a 51.4% drop in HI relative to butterfat and a 50% drop in HI relative to NIE90:10. Interesterification of the 80:20 blend led to a 75% drop in HI relative to CIE100 and a 45.1% drop in HI

Copyright 2002 by Marcel Dekker. All Rights Reserved.

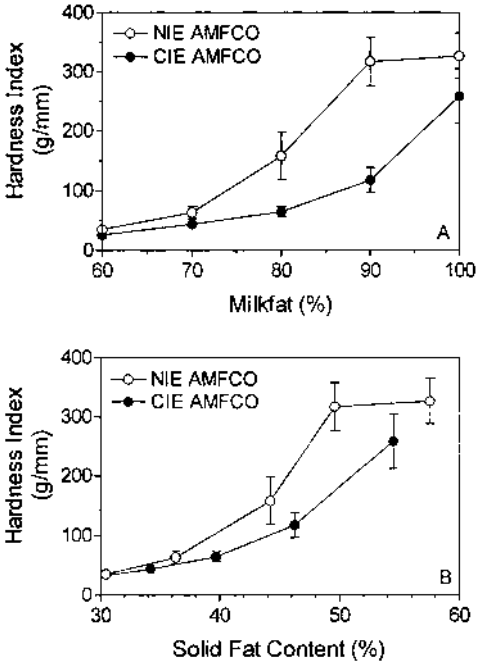

Figure 15 Hardness index (g/mm) of NIE and CIE butterfat–canola oil blends as a function of percent butterfat (w/w) in the blend.

relative to NIE90:10. A 59.1% drop in HI was observed between NIE80:20 and CIE80:20.

With 70% butterfat or less, the HIs of both CIE and NIE blends were similar. The HI of the NIE70:30 blend was 6 g/mm, and that of the CIE70:30 blend was 4.5 g/mm, a 30% reduction. The HI difference became even smaller for blends containing 60%, 50%, and 40% butterfat. At such low HIs, the cone penetrometer was insensitive to structural differences between the CIE and NIE blends.

Statistically, both the proportion of butterfat and chemical interesterification had significant effects on HI ($p < 0.0001$). The HIs of NIE100 and NIE90:10 were not significantly different ($p > 0.05$), but the NIE80:20 HI differed significantly from all other blends. Blends with 70% or less butterfat were not significantly different from one another ($p > 0.05$). The HIs of CIE100, CIE90:10, and CIE80:20 were all significantly different from each other ($p < 0.05$). However, those of CIE80:20 and all CIE blends containing less butterfat were not significantly different from one another ($p > 0.05$).

Copyright 2002 by Marcel Dekker. All Rights Reserved.

Blending and chemical interesterification altered the rheology of the fats via different mechanisms. Blending alone resulted in a dilution of the butterfat crystal network. At 5°C, butterfat is ~50% solid and 50% liquid (Rousseau et al., 1996a). Replacement of 10% butterfat with canola oil did not substantially diminish the HI, indicating that butterfat could accommodate a larger proportion of oil at 5°C without losing structural integrity. Addition of 20% canola oil resulted in a large decrease in HI. This was interpreted as being due to a structurally weaker network, given the lower solid fat content (SFC). Furthermore, because the growth of fat crystals is very slow (Walstra and Jenness, 1984) and tempering was of short duration, interparticle interactions (e.g., sintering) were not as strong. The replacement of 30% butterfat with canola oil resulted in a low HI. Finally, with larger butterfat replacements, the HI was very low. For the CIE blends, the dilution effect of blending was compounded by the incorporation of unsaturated canola oil fatty acids into butterfat TAGs, resulting in a lower hardness.

All CP results were obtained at 5°C. Correlation of SFC values at 5°C with CP data indicated that a small difference in SFC led to large variations in rheological behavior. Thus, the role of solid fat appeared to be secondary when it came to CP. The small changes in SFC were not solely responsible for the substantial differences in HI observed for the CIE butterfat–canola oil blends with 70–100% butterfat. Other mechanisms were definitely at play. As stated by Mahklouf et al. (1987), fats with identical SFCs can have vastly different rheological properties.

(b) Dropping Point. Another method to examine the rheological properties of fats is via use of the dropping point (DP). DP is a simple yet effective method of measuring the effect of interesterification. It is the temperature at which a fat begins to flow under its own weight. DPs for NIE and CIE blends as a function of butterfat content (w/w) are shown in Figure 16. Blends with 10% or less butterfat did not solidify sufficiently to yield reproducible DPs. The proportion of butterfat and the interesterification process both had significant effects on the DP of the blends ($p < 0.0001$).

According to Borwanker et al. (1992) and Borwankar and Buliga (1990), DPs are not solely related to the melting point of a fat but can also reveal information on its rheological properties. In a study of margarines and table spreads, both groups found that DP was not a function of crystallinity. Instead, it correlated well with the complex viscoelastic modulus. In this study, DP was considered a rheological parameter describing the flow that occurs at a temperature at which the fat crystal network lacks sufficient cohesion to hold oil in its matrix.

NIE100 had a DP of 34.4°C whereas that of CIE100 was 37.0°C. The higher DP for CIE100 suggested a more structured, denser crystal network than that of natural butterfat. Samples with 60–90% butterfat did not exhibit notable differences between the DPs of NIE and CIE samples, indicating that interesterification resulted in rheologically similar flow patterns for both NIE and CIE sam-

Copyright 2002 by Marcel Dekker. All Rights Reserved.

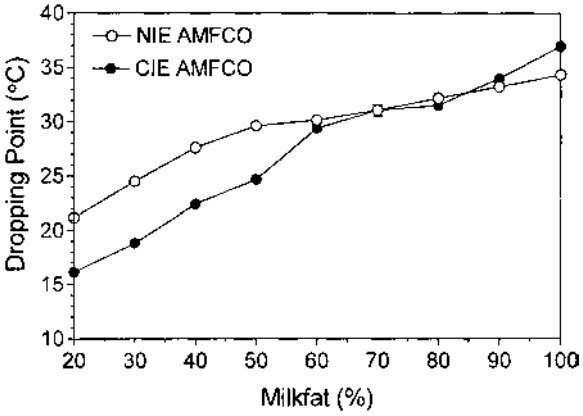

Figure 16 Dropping point evolution of NIE and CIE butterfat–canola oil blends as a function of percent milkfat (w/w) in the blend.

ples. Samples with 50% canola oil displayed differences of 5–6°C between the CIE and NIE samples. This suggested that the crystal network of the CIE fats was weaker than that of NIE samples.

Statistically, all NIE samples were significantly different from one another ($p < 0.05$), except for NIE60:40 and NIE50:50 ($p > 0.05$). CIE80:20 and CIE70:30 did not differ from each other. Neither did CIE70:30 and CIE60:40 ($p > 0.05$). All other samples were significantly different from one another ($p < 0.05$). The DP of CIE samples demonstrated greater change as the proportion of oil increased compared with NIE samples.

As the sample temperature is raised during a DP measurement, solid fat melts. The progressive reduction of crystalline matter means that at a certain temperature the oil cannot be enclosed any further within the fat matrix and begins to flow out. According to deMan et al. (1983), the DP of butter occurs at an SFC of ~2.5%. In terms of rheological properties, only a small amount of solid fat is required for butterfat to maintain a cohesive network of fat crystals and oil.

(c) Constant Stress Rheometry.

Viscosity. All fats (in the liquid state at 70°C) exhibited Newtonian behavior (Timms, 1985) and had viscosities of 26 ± 3 mPa·s.

Figure 17 shows the onset of crystallization temperatures of NIE and CIE blends (60–100% butterfat in the blend). At the crystallization onset temperature, viscosity increased dramatically. All CIE samples had a higher crystallization onset temperature than their NIE counterparts. Both the proportion of butterfat and interesterification had significant effects on crystallization onset temperature

Copyright 2002 by Marcel Dekker. All Rights Reserved.

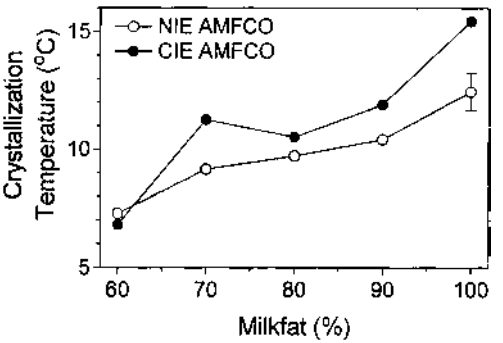

Figure 17 Crystallization temperature (°C) as a function of viscosity of NIE and CIE butterfat–canola oil blends as a function of percent milkfat (w/w) in the blend.

($p < 0.0001$). NIE100 and NIE90:10 were not significantly different ($p > 0.05$). Nor were NIE90:10, NIE80:20, and NIE70:30. Finally, NIE80:20, NIE70:30, and NIE60:40 did not differ significantly ($p > 0.05$). For the CIE blends, only CIE80:20 and CIE70:30 were not significantly different from all other CIE blends ($p > 0.05$).

The higher crystallization onset temperatures of the CIE blends are not readily explainable. A plausible explanation is that the randomization of saturated fatty acids created a greater number of potential nucleation sites in the CIE blends than were present in the NIE blends. For example, dilution of butterfat with 10% canola oil led to a a drop in crystallization onset temperature. This was due to a lower proportion of TAGs containing saturated fatty acids, which reduced the number of nucleation sites. Interesterification of the 90:10 blend increased the onset temperature. Quite possibly, the UUU TAGs present in the canola oil were restructured and now contained a saturated fatty acid (SUU), thereby increasing the number of nucleation sites. Although not examined, the crystallization rate would have probably been slower for the CIE blends than for NIE blends.

Viscoelastic properties. The parameters measured were storage modulus (G'), loss modulus (G''), dynamic viscosity (η'), and tan δ (dimensionless). The storage modulus (G') is a measure of the energy stored and recovered per cycle of sinusoidal deformation and is indicative of the elastic nature of a substance; the loss modulus (G'') is a measure of the energy lost per cycle of sinusoidal deformation and is indicative of the viscous nature of a substance (Ferry, 1970). Dynamic viscosity (η') is related to G'' by

$$\eta' = \frac{G''}{\omega}$$

Copyright 2002 by Marcel Dekker. All Rights Reserved.

where ω is the angular frequency (rad/s). In regions where G'' is flat, η' is inversely proportional to frequency (slope $= -1$). The viscoelastic nature was evaluated with tan δ, a dimensionless factor relating the energy lost to the energy stored per cycle of deformation. It is calculated from

$$\tan \delta = \frac{G''}{G'}$$

and indicates whether elastic or viscous behavior predominates in a structure (Ferry, 1970). Lower tan δ values indicate a more elastic sample.

Figure 18 shows the effect of interesterification on G' of the blends. The G' of NIE blends was consistently higher than the G'' of their CIE counterparts, suggesting that interesterification led to a loss of elasticity. G'' was also lower for the CIE blends than for their NIE counterparts. G' was frequency-dependent, a phenomenon in many food systems (Kokini and Plutchok, 1987) and is in agree-

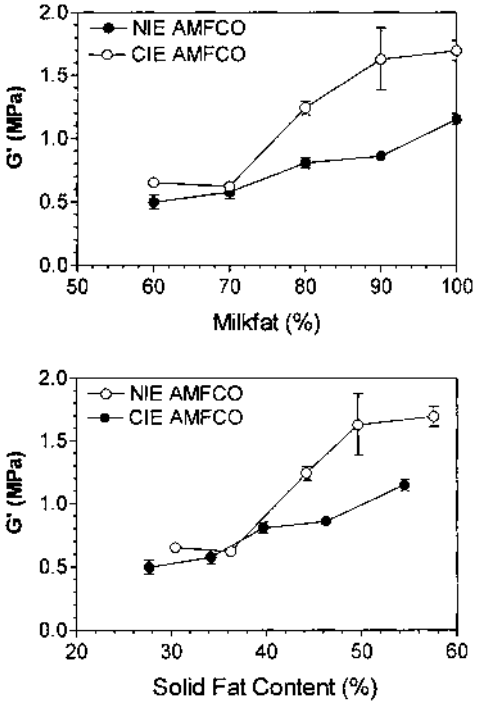

Figure 18 Effect of interesterification on the storage modulus (G') of (○) NIE and (●) CIE butterfat–canola oil blends.

Copyright 2002 by Marcel Dekker. All Rights Reserved.

ment with the results of Shukla and Rizvi (1995) and Rohm and Weidinger (1993), who examined the viscoelastic properties of butter. According to Kokini and Plutchok (1987), G' frequency dependence at high frequency is the result of interchain entanglements not having enough time to come apart within the period of one oscillation. These results indicated that the crystal network could maintain a rheologically cohesive structure.

10. The Fractal Nature of the Butterfat Crystal Network

The formation of a network of crystallized fat particles is of key importance in the manufacture of plastic fats because it provides firmness or solidlike properties (viscoelasticity) (Vreeker et al., 1992). This network can be visualized as being built from aggregates of fat particles (Vreeker et al., 1992) rather than from straight chains of particles (Tempel, 1961) and can be thought of as a colloidal aggregate, analogous to a protein gel. Each of these fat particles in turn comprises several aggregated fat crystals. The quantitative description of a complex, aggregated ''random'' system is difficult. Recently, fractal geometry has proven extremely helpful in the characterization of these fractal objects (Mandelbrot, 1982).

An examination of the results on the chemical interesterification of butterfat has revealed some interesting trends. First, chemical interesterification of butterfat or butterfat–canola oil blends did not substantially decrease the solid fat content (SFC) of butterfat or the blends, the maximum decrease being 5% for CIE blends. Second, melting characteristics, as determined by differential scanning calorimetry, were similar for chemically interesterified and noninteresterified butterfat–canola oil blends. However, when the rheological properties of butterfat and butterfat–canola oil blends are studied, the hardness (determined by cone penetrometry) of the blends containing 100%, 90%, and 80% (w/w) butterfat dropped sharply following CIE compared to their noninteresterified counterparts. These drastic changes could not be correlated with their SFC values. Furthermore, the storage modulus (G'), or elasticity, of the interesterified blends was lower compared to their noninteresterified counterparts. Light and scanning electron microscopy of the blends showed us that the fat crystal morphology (size and shape) and crystal arrangement changed drastically owing to interesterification. In general, both the incorporation of canola oil and interesterification led to the creation of larger spherulitic particles. X-ray diffraction studies of the blends confirmed that the predominant crystal form of butterfat and butterfat–canola oil blends was the β' form. Even though small changes were observed in butterfat crystal polymorphism due to canola oil incorporation and/or interesterification, no drastic changes in the polymorphic behavior of the fat crystals were observed.

All of these results pointed toward the possibility that it is not the actual SFC and/or crystal polymorphic form that determines the mechanical properties

Copyright 2002 by Marcel Dekker. All Rights Reserved.

of butterfat–canola oil blends but rather the macroscopic structure of the network of fat crystals in liquid oil.

(a) Scaling Behavior of the Elastic Properties of Colloidal Gels. What follows are highlights of the theories used to characterize the fractal nature of colloidal aggregates in terms of their mechanical properties taken from the paper by Shih et al. (1990). The elastic constant of a colloidal aggregate (in our case the fat crystal network in liquid oil) as a function of particle concentration (in our case, the SFC or volume fraction of crystals) is dictated by the fractal nature of the colloidal flocs. The colloidal aggregate is considered a collection of fractal flocs that are closely packed throughout the sample. Depending on the strength of the links between flocs relative to that of the flocs themselves, we can have strong-link behavior or weak-link behavior.

Strong-link regime. Strong-link behavior is observed at low particle concentrations (low SFC or low crystal volume fraction). This regime can be achieved by allowing the individual flocs to grow very large so that each floc is considered a weak spring. In this case, the links between flocs have a higher elastic constant than the flocs themselves. Therefore, the elastic constant of the system as a whole (K) as a function of particle concentration (φ) is dominated by the elastic constant of the flocs. For this case;

$$K \sim \varphi^{(d+x)/(d-D)}$$

where d is the Euclidean dimension (usually 3), D is the fractal dimension, and x is the backbone fractal dimension, usually a constant between 1 and 1.3. In the case of low SFC plastic fats, the elastic modulus of the fat crystal network increases as a function of the SFC in a power law fashion with a slope $(d + x)/(d - D)$.

Weak-link regime. Weak-link behavior is observed at high particle concentrations (high SFC or high crystal volume fraction). Small flocs are stronger springs than large flocs, and therefore the elastic constant of the system as a whole is dominated by the elastic constants of the interfloc links rather than by the elastic constants of the flocs, as for the strong-link regime. For this case,

$$K \sim \varphi^{(d-2)/(d-D)}$$

where d is the Euclidean dimension (usually 3) and D is the fractal dimension.

In the case of high SFC plastic fats, the elastic modulus of the fat crystal network increases as a function of the solid fat content in a power law fashion with a slope of $(d - 2)/(d - D)$. The elastic constant K for the weak-link regime increases more slowly as a function of particle concentration than for the strong-link regime.

The fractal dimension for the noninteresterified butterfat–canola oil blends was calculated as 2.46. The fractal dimension for the chemically interesterified

Copyright 2002 by Marcel Dekker. All Rights Reserved.

butterfat–canola oil blends was 2.15. There was a noticeable decrease in the fractal dimension of a colloidal aggregate, in our case the fat crystal network. It is this large change in the ''structure'' of the fat crystal network that is responsible for the drastic decrease in hardness observed by cone penetrometry.

Pioneering work in the application of fractal geometry principles to the study of fat crystal networks (Vreeker et al., 1992) showed how the fractal dimension of tristearin crystal aggregates in olive oil could be determined from light scattering measurements. These authors also determined the fractal dimension of tristearin crystals in paraffin oil using small-amplitude oscillatory shear measurements and yield stress measurements from literature values. These authors reported good agreement among all techniques used and determined the fractal dimension (D) of tristearin in olive oil to be about 1.7–1.8. This value increased upon aging of the fat to $D = 2$. Low fractal dimensions are indicative of low-density open structures. Upon aging, the crystallization, aggregation, and network formation processes continue, creating a more dense, compact, more tightly packed structure with a higher fractal dimension. Aggregates with low fractal dimensions are prone to restructuring.

In summary, chemical interesterification of butterfat changed the structure of triacylglycerols. This in turn led to a change in the kinetics of crystal formation and therefore of the resulting fat crystal network responsible for the macroscopic structure of the plastic fat. The fractal dimension is a better parameter for predicting rheological behavior of plastic fats than the SFC and appears to have great potential for targeting specific rheological properties of plastic fats such as spreadability.

B. Enzymatic Interesterification of Butterfat

Kalo and coworkers were among the first researchers to realize important findings on lipase-catalyzed interesterification of butterfat [or butterfat–vegetable (or tallow)] blends. Although their results primarily involved elucidation of changes in composition as a result of interesterification, they also reported findings on the changes to butterfat's physical properties following enzymatic interesterification. Kalo et al. (1986a, 1987a) compared the changes in the TAG composition of butterfat interesterified using either sodium methoxide (chemical interesterification) or random lipase as catalysts and found minimal differences in both chemical and physical properties.

Kalo et al. (1986b) studied the changes in TAG composition and melting properties of butterfat and butterfat solid fat fraction–rapeseed oil mixtures interesterified by *Candida cylindracae* lipase. They found that the proportion of trisaturated TAGs with 42–52 carbons was distinctly lower in the interesterified product. They also noticed that DAGs were responsible for the changes in acyl species with 30–38 carbons. Kalo et al. (1987b) subjected butterfat to *Candida cylindra-*

Copyright 2002 by Marcel Dekker. All Rights Reserved.

cae lipase–catalyzed interesterification. The enzyme was immobilized onto celite and was activated with glycerol or with variable amounts of water to produce fats with different contents of lipolysis products. Emphasis was placed on the separation of TAGs, DAGs, MAGs, and free fatty acids. Physical behavior was followed with pulsed nuclear magnetic resonance. SFC was higher above 20°C and lower below 20°C for the interesterified butterfat. Kalo (1988) studied lipase-catalyzed interesterification of butterfat with either *A. niger* or *M. miehei* lipases, two *sn*-1,3-specific lipases. The evolution of changes in SFC was very similar to that obtained by interesterification with a random lipase (*C. cylindracae*). Kalo et al. (1989a, 1989b) examined the enzymatic interesterification of butterfat dissolved in hexane at variable water content and in isooctane in medium and low water content at variable temperatures. In both cases, TAG composition of the interesterified product was close to random distribution. Results also showed that temperature did not affect positional specificity or hydrolytic side reactions. Finally, Kalo et al. (1990) examined the *Pseudomonas fluorescens* lipase–catalyzed interesterification of butterfat in a solvent-free system. Under reaction conditions where the hydrolysis is minimal, interesterification in the absence of solvent yielded a modified product that required only mild refining. The proportion of saturated TAGs with 48–54 acyl carbons were higher in fats interesterified at 40°C than in those interesterified at 50 or 60°C. Reactions were allowed to continue until equilibrium was reached (8–10 days). Oba and Wilholt (1994) interesterified milkfat and oleic acid to improve butter's nutritional properties. Melting and crystallization profiles of the interesterified butterfat, analyzed by differential scanning calorimetry, showed that interesterification yielded a fat with lower enthalpy of melting and shifted melting peaks.

Nevertheless, little work has been published on the physical properties of interesterified blends. In this research, we reported on the melting, crystallization, rheological, and crystal properties of butterfat and butterfat–canola oil blends following interesterification with an *sn*-1,3-specific lipase from *Rhizopus arrhizus* as a means of understanding the physical and rheological properties of fats. Furthermore, the complex relationship between composition, rheology, and microstructure could be further clarified.

1. Comparing TAG and SFC Evolution

As with the chemical interesterification study, in order to understand the effects of enzymatic interesterification (EIE) on the physical properties of butterfat, it is necessary to understand changes in composition.

Enzymatic interesterification proceeds much more slowly than chemical interesterification. As interesterification progressed, TAG 34–42 and 54-carbon species decreased while 46-, 48-, 50-, and 52-carbon species increased. The midpoint was C_{44} which did not change noticeably. Most of the TAG changes occurred within the first 24 h of enzymatic interesterification. The trends in carbon

Copyright 2002 by Marcel Dekker. All Rights Reserved.

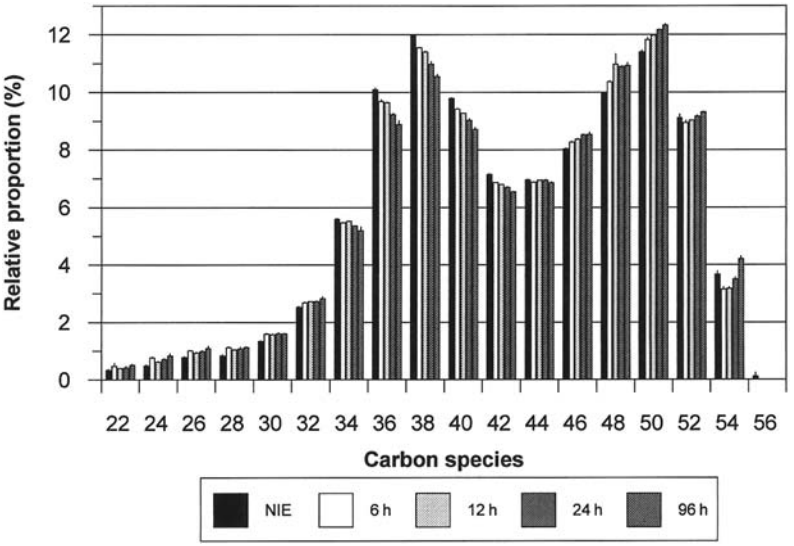

Figure 19 Relative proportions of species of various carbon numbers in butterfat as a function of enzymatic interesterification duration.

species modifications resulting from EIE mimicked those of chemically interesterified butterfat, although with smaller relative changes. Figures 19–23 show the changes in TAG composition for butterfat, the 90:10 blend, the 80:20 blend, the 70:30 blend, and the 60:40 blend, respectively. The previously mentioned species of various carbon numbers behaved similarly regardless of the proportion of butterfat replaced by oil. As the proportion of oil in the blend increased, greater changes in TAG composition arose. Generally, a sharper drop in the 54-carbon species led to a larger increase in 48–52-carbon species. The large drop in 54-carbon species in the blends is attributed to the loss of TAGs containing unsaturated 18-carbon fatty acids in canola oil, which represent the majority of its fatty acid make-up. As shown by Kalo et al. (1986b), following interesterification of a blend of butterfat solid fraction and rapeseed oil, there was a drop in trisaturates. This is due to the shuffling of unsaturated fatty acids found in the oil, which take the place of saturated fatty acids in butterfat TAGs.

2. Melting and Crystallization Properties

(a) Solid Fat Content. The solid fat content (SFC) of all interesterified blends was consistently lower than that of the NIE blends at all temperatures measured. Figure 24a shows the evolution of SFC for NIE blends ranging from NIEBF to NIE60:40. A sharp drop in SFC occurred between 15 and 20°C for NIEBF,

Copyright 2002 by Marcel Dekker. All Rights Reserved.

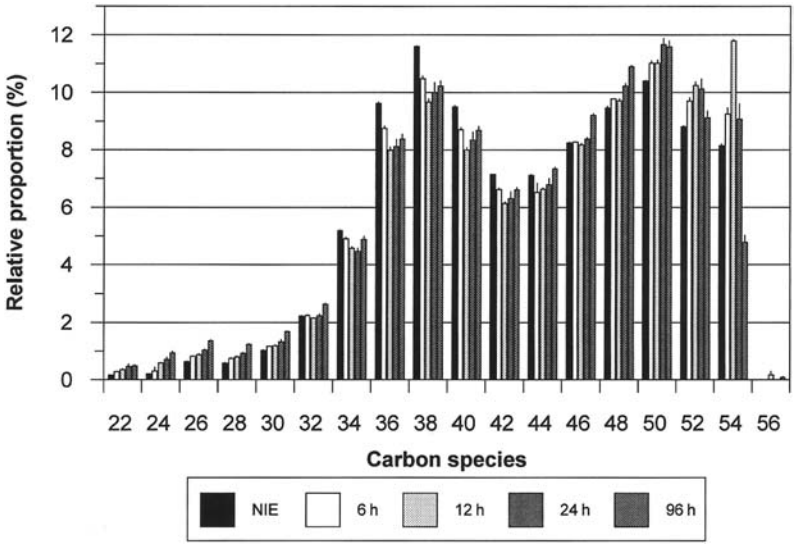

Figure 20 Relative proportions of species of various carbon numbers in the 90:10 blend as a function of enzymatic interesterification duration.

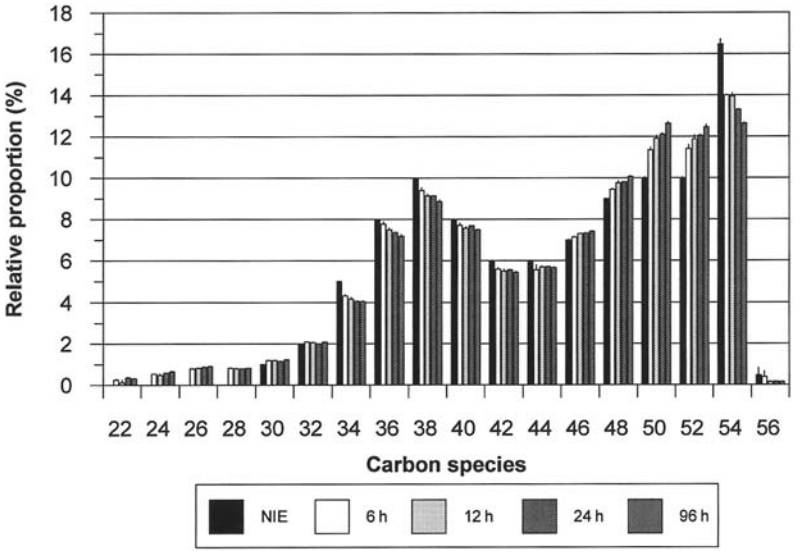

Figure 21 Relative proportions of species of various carbon numbers in the 80:20 blend as a function of enzymatic interesterification duration.

Copyright 2002 by Marcel Dekker. All Rights Reserved.

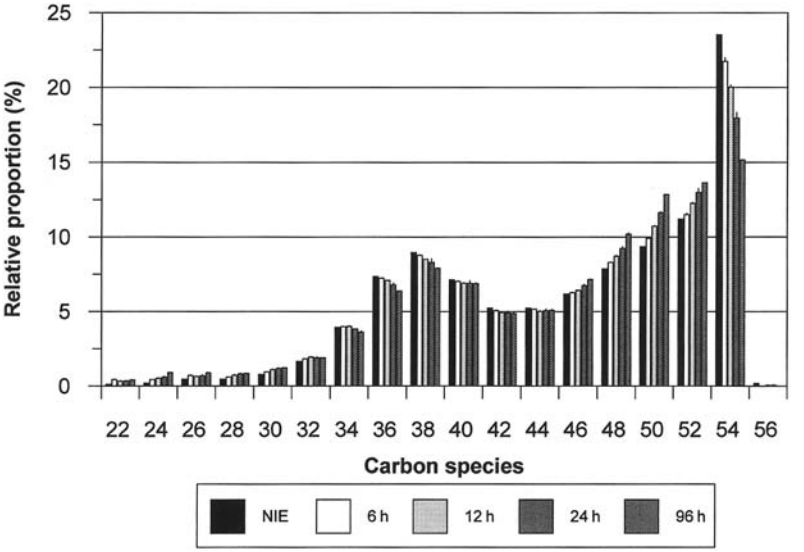

Figure 22 Relative proportions of species of various carbon numbers in the 70:30 blend as a function of enzymatic interesterification duration.

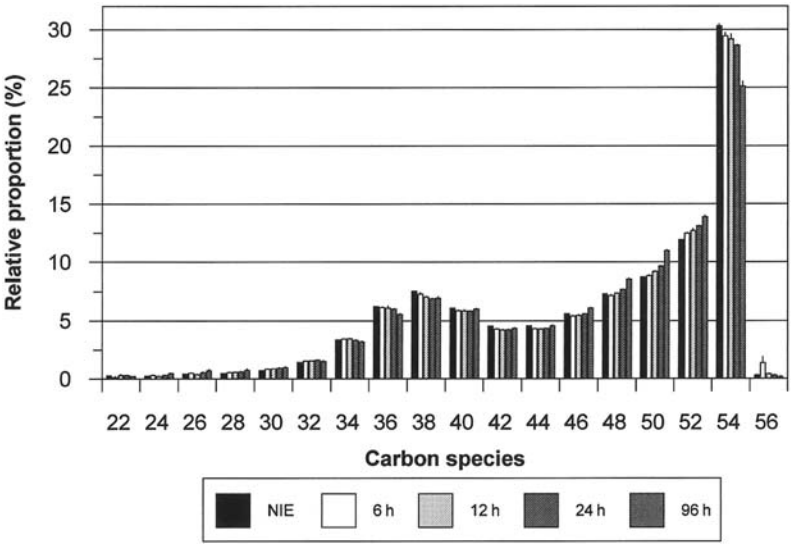

Figure 23 Relative proportions of species of various carbon numbers in the 60:40 blend as a function of enzymatic interesterification duration.

Copyright 2002 by Marcel Dekker. All Rights Reserved.

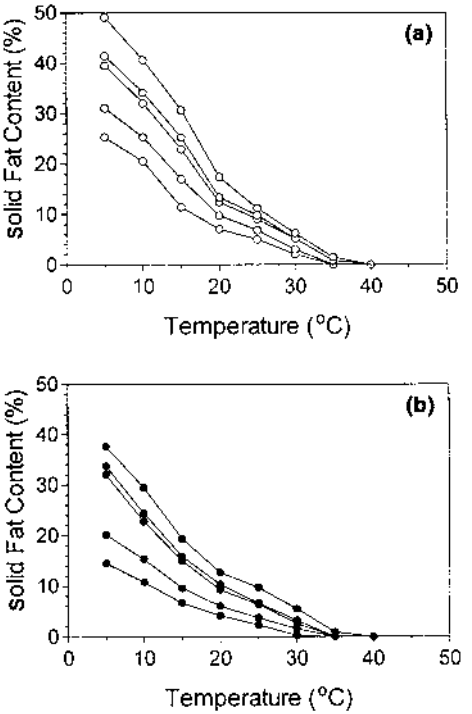

Figure 24 (a) SFC evolution of butterfat–canola oil blends as a function of temperature (°C). (b) SFC evolution of EIE butterfat–canola oil blends as a function of temperature (°C).

NIE90:10, and NIE80:20. Above 20°C, the drop in SFC was less pronounced. Addition of canola oil progressively lowered SFCs and somewhat linearized the melting profile. Enzymatic interesterification (EIE) of the blends (Fig. 24b) caused a drop in SFC at all temperatures relative to NIE samples and altered melting profiles. The largest drops in SFC as a result of EIE occurred with butterfat at 5 and 10°C and for the 60:40 and 70:30 blends below 10°C. Between 10 and 20°C, differences in SFC between NIE blends and their interesterified counterparts decreased such that, above 20°C, the differences in SFC were small. These results are similar to those reported by Foglia et al. (1993), who enzymatically interesterified a 50%–50% butterfat–sunflower oil blend and noticed a drop in SFC (measured between −10°C and 30°C) following EIE. However, these results contrast with the changes in SFC obtained from chemically interesterified milkfat, which have been shown to be higher than those from NIE butterfat from 15 or 20°C to the end of melt (Rousseau et al., 1996a; Becker, 1959). Further-

Copyright 2002 by Marcel Dekker. All Rights Reserved.

more, these results conflicted with those of other researchers who enzymatically interesterified butterfat with either random or regiospecific lipases. Bornaz et al. (1994) increased the SFC (measured by DSC) of butterfat from ~21% to ~40% (at 20°C) following 10 h of EIE with an *sn*-1,3-specific lipase. Kalo et al. (1990) found that the SFC (at 20°C) of butterfat interesterified at 50°C with an *sn*-1,3-specific lipase in the absence of solvent increased from 21.3% to 30.3%. Reactions were carried for 8–10 days, in contrast to 24 h for our system. Kalo et al. (1986b) enzymatically interesterified a butterfat solid fraction–rapeseed oil blend to discover that the latter has a narrower melting range than the former. Globally, interesterification had a highly significant effect on SFC ($p < 0.0001$), and there was also a highly significant interaction effect of interesterification and blend composition on SFC ($p < 0.0001$).

Figure 25 illustrates the effect of enzymatic interesterification on blend SFC. SFC changes of up to 12% were observed. The largest change in SFC occurred with the butterfat at 5, 10, and 15°C, whereas only small changes occurred at higher temperatures.

(b) Dropping Point. Figure 26 shows the evolution of the dropping point (DP) for blends ranging from 100% to 60% butterfat before and after EIE. The decrease in the DP of EIE blends was sharper than that of NIE blends (0.16°C/wt% vs. 0.10°C/wt%, respectively). DPs dropped by ~4.4°C between NIE100 and NIE60 blends, whereas for EIE blends the drop was 6.3°C. The blend DP temperature difference between NIE and EIE blends increased from 1.2°C for 100% butterfat

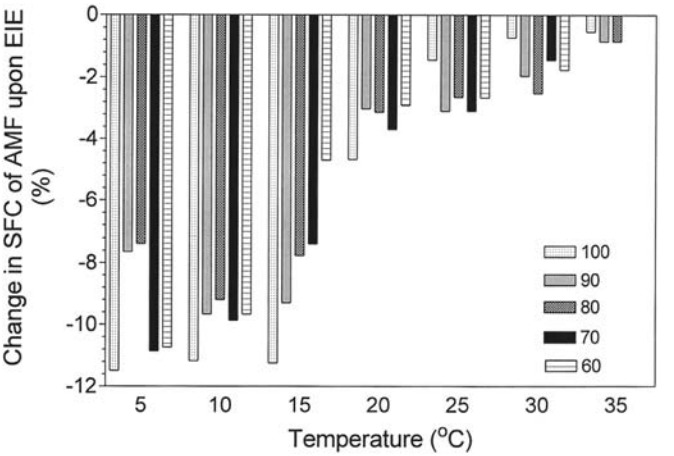

Figure 25 Profile of the effect of enzymatic interesterification on the SFC of butterfat–canola oil blends.

Copyright 2002 by Marcel Dekker. All Rights Reserved.

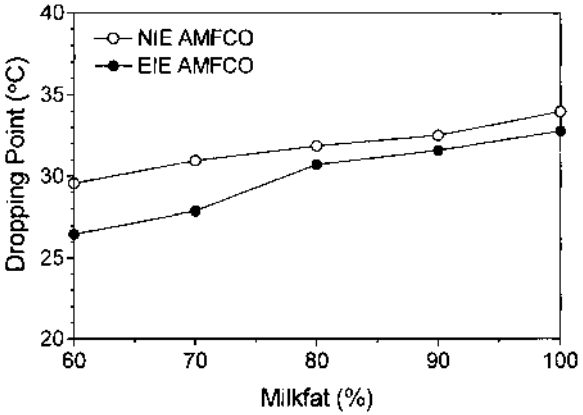

Figure 26 Dropping point (°C) evolution of NIE and EIE butterfat–canola oil blends as a function of butterfat (% w/w) in the blend.

to 3.1°C for the 60%–40% blend. EIE of a 50%–50% butterfat–sunflower blend has been reported to increase its melting point, even though the SFCs were lower from −10°C to 30°C (Foglia et al., 1993). Larger changes in DP for EIE blends can be attributed to either the large decrease in SFC or rearrangement of the fat crystal structure (shown later) resulting from changes in TAG distribution after interesterification. The incorporation of unsaturated fatty acids from canola oil into butterfat TAGs results in a disruption of crystal structure, leading to a lower melting temperature (Norton et al., 1985).

The SFC value corresponding to the DP was between 1.7% and 3.2% for all blends, suggesting that little crystalline matter was necessary to maintain sufficient cohesion to trap liquid oil within the crystalline matrix. These SFC values agree with previous results (deMan et al., 1983). All DPs were significantly different from each other ($p < 0.001$).

(c) Crystallization Curves. Isothermal fat crystallization for all NIE and EIE blends are shown in Figure 27. The spectrophotometric method allows detection of initial crystal nucleation in a supercooled environment by observing the change in turbidity. Nucleation can be defined as a chain reaction that advances through a multitude of clusters with the result that some of them reach macroscopic dimensions (Toschev, 1973). The increase in observed optical density can be the result of either additional nucleation or crystal growth but is probably a combination of both (Boistelle, 1988). Under the conditions used, there was no statistically significant difference in crystallization behavior between NIEBF, EIEBF, and NIE90:10 ($p > 0.4$). For statistical analysis, the crystallization onset was taken as the time at which the absorbance exceeded 0.1. Crystallization for these blends

Copyright 2002 by Marcel Dekker. All Rights Reserved.

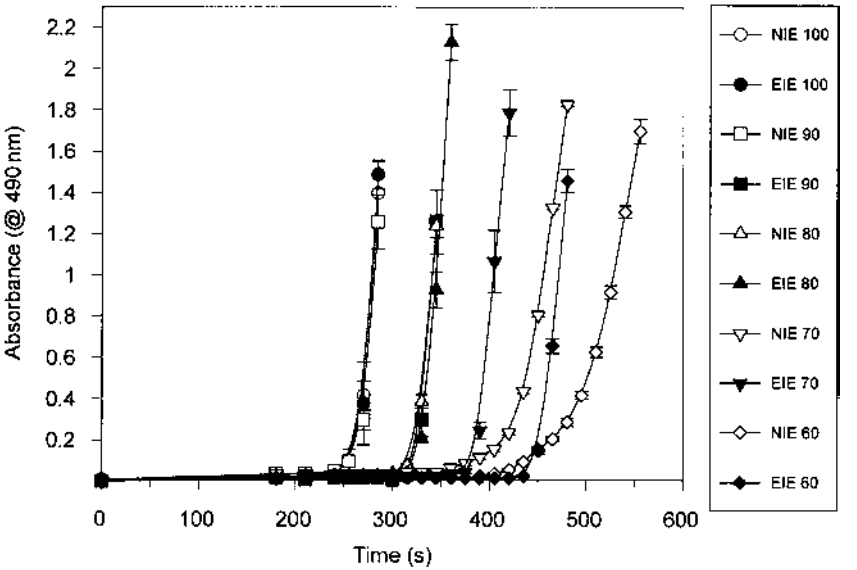

Figure 27 Effect of blending and enzymatic interesterification on isothermal (10°C) crystallization behavior of butterfat as measured by optical density.

began at ~250 s and progressed rapidly. Crystallization onset for the EIE90:10, NIE80:20, and EIE80:20 blends was close to ~325 s ($p > 0.05$). Unexpected behavior was observed for blends with 60% and 70% butterfat. It was expected that interesterification would lead to earlier nucleation and slower crystallization during the isothermal runs due to the randomization of saturated fatty acids. However, the NIE blends (70:30 and 60:40) had earlier onset of crystallization and slower crystallization rates than their EIE blend counterparts.

3. Rheology

(a) Cone Penetrometry. The hardness indices (HIs) for NIE and EIE blends as a function of butterfat (w/w) and EIE duration are shown in Figure 28a. Most of the changes in HI for all samples occurred within 12 h of enzymatic interesterification. The HI of 100% butterfat dropped 34% following 3 h of EIE and 63% after 12 h. A similar pattern was observed for the 90% and 80% butterfat blends, which both underwent ~30% decreases in HI following 3 h of interesterification. Hardness indices after 24 h are shown in Figure 28b.

The rapid change in hardness suggested that only limited structural rearrangement was necessary to lead to large changes in rheological properties

Copyright 2002 by Marcel Dekker. All Rights Reserved.

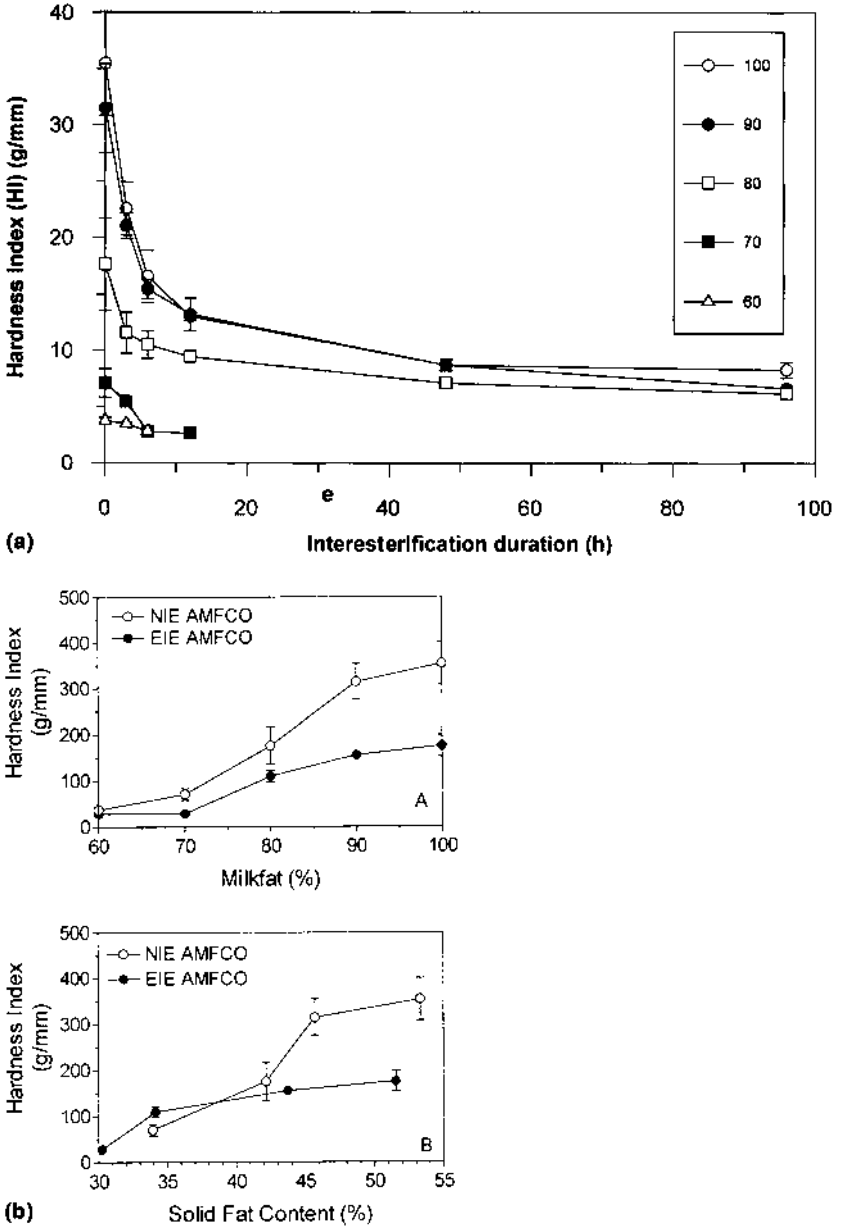

Figure 28 (a) Effect of interesterification duration on hardness index (g/mm) of butterfat–canola oil blends as a function of percent butterfat (w/w) in the blend. (b) Hardness index of the blends after 24 h of enzymatic interesterification.

Copyright 2002 by Marcel Dekker. All Rights Reserved.

(Rousseau and Marangoni, 1998a,b). These results complemented those of the SFC evolution as a function of interesterification duration, which indicated that the largest changes in SFC occurred within 3 h of EIE (results not shown). For the blends examined, the softening effect produced by the addition of liquid oil only was caused by dissolution of solid TAGs in the additional oil, leading to a lower SFC at a given temperature (Timms, 1978). This may explain the nonlinear change in HI of the NIE blends as a function of the proportion of canola oil added. That effect combined with EIE dramatically altered this aspect of the blends.

Other factors influencing the HI of blends may have been the modification, albeit small, in the proportion of long-chain trisaturates present in the butterfat, which influence the rheology of butterfat (Simoneau et al., 1994).

(b) Controlled Stress Rheometry. Figure 29 shows the effect of gradual replacement of butterfat with canola oil and/or enzymatic interesterification on the storage modulus (G') of the blends. For all systems examined, G' was substantially higher than G'' (Rousseau et al., 1996c; Shukla and Rizvi, 1995; Drake et al., 1994). Even though the solid fraction necessarily contributes the majority of the structural network in plastic fats, fats with similar SFCs can have very differ-

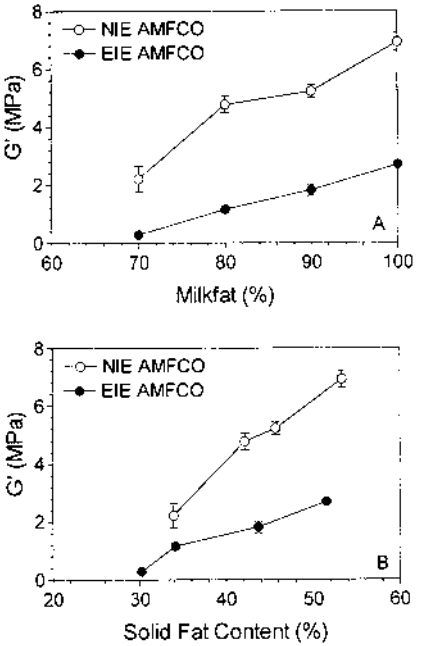

Figure 29 Effect of enzymatic interesterification on the storage modulus (G') of butterfat–canola oil blends.

Copyright 2002 by Marcel Dekker. All Rights Reserved.

ent textural properties (Rousseau et al., 1996c; Haighton, 1976). For example, the SFCs (at 5°C) for NIE80:20 and EIEBF were very close at 39.5% and 37.6%, respectively. Rheological data show, however, that the G' of EIEBF was half that of NIE80:20. However, the opposite trend was observed for HI, with EIEBF's HI being higher than that of NIE80:20, irrespective of EIE duration.

Both blending and interesterification had significant effects on G' and G'' ($p < 0.0001$). There was also a significant interaction between blend and interesterification on G' and G'' ($p < 0.0001$).

4. Fat Crystal Morphology

(a) Polarized Light Microscopy. Enzymatic interesterification dramatically altered the crystal morphology of all blends. Figure 30a shows the small needle-like crystals found in butterfat following 24 h of tempering at 5°C with no signs of spherulitic aggregation. Based on size alone, these are β′ crystals, which normally measure <5 μm (Sato, 1988). Interesterification of butterfat resulted in a vastly different crystal morphology (Fig. 30b), where many large spherulites were scat-

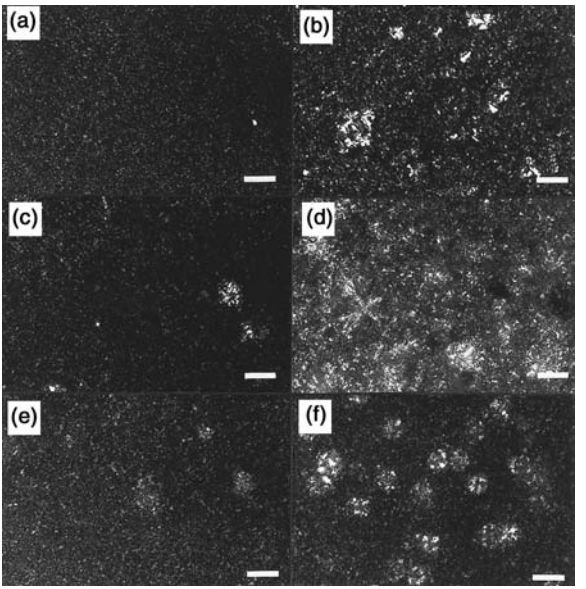

Figure 30 Polarized light microscopic photomicrographs of samples tempered 24 h at 5°C. (a) Noninteresterified butterfat; (b) enzymatically interesterified butterfat; (c) noninteresterified 90:10 blend; (d) enzymatically interesterified 90:10; (e) noninteresterified 80:20; (f) enzymatically interesterified 80:20. The bar represents 25 μm.

Copyright 2002 by Marcel Dekker. All Rights Reserved.

tered among small crystals. These results agree with those of other researchers (Rousseau et al., 1996b; deMan, 1961a). Blending (Fig. 30C: NIE90:10, 30E–NIE80:20) resulted in a morphology similar to that of NIEBF, whereas interesterification of the blends (Figs. 30D, 30F) led to crystal habits similar to that of EIEBF. However, the spherulites in the interesterified blends appeared more organized than those of EIEBF. It is also possible that we are seeing the crystals at different states of aggregation. The samples examined in this study were viewed after only 24 h of tempering at 5°C. Foley and Brady (1984) examined temperature-induced effects on the crystallization behavior of milkfat. They showed that a sample of milkfat crystallized for 7 days at 5°C consisted of very large spherulites not unlike those found in the EIEBF image. Hence, it is possible that the butterfat examined in this study would aggregate to a similar state after a few more days of tempering. Overall, enzymatic interesterification led to the formation of spherulites, whereas blending alone resulted in little change except for the presence of a few spherulites.

Distinguishing polymorphic forms based solely on crystal habit is difficult, because, visually, many morphologies can exist for a single polymorph (Kellens et al., 1992; Chapman, 1965). However, from crystal size alone, it would appear that the small platelets visible in each image are β′ crystals. The large agglomerates may be simply groupings of β′ or β crystals.

(b) X-Ray Diffraction. The long and short spacings of the NIE and EIE blends were determined with powder X-ray diffraction. X-ray diffraction patterns of milkfat produce broad peaks due to the large proportion of oil present in the samples, the small size of crystals, and the probable interchain disorder (Timms, 1980). Table 4 shows the short spacings and long spacings for the examined samples. The spacing at ~4.6 Å is associated with β-form crystals, and the others

Table 4 Short and Long Spacings of NIE and EIE Butterfat–Canola Oil Blends[a]

Blend	Long spacings (Å)	Short spacings (Å)
NIE100	42.0 (vvs), 20.8 (vw), 13.6 (w)	3.73 (w), 4.00 (s), 4.33 (vs), 4.64 (m)
NIE90:10	40.8 (vvs), 20.3 (vw), 13.5 (w)	3.73 (w), 4.00 (s), 4.36 (vs), 4.64 (m)
NIE80:20	42.7 (vvs), 20.8 (vw), 13.6 (w)	3.73 (w), 4.01 (s), 4.36 (vs), 4.64 (m)
NIE70:30	41.4 (vvs), 20.8 (vw), 13.6 (w)	3.73 (w), 4.01 (s), 4.36 (vs), 4.64 (m)
NIE60:40	42.0 (vvs), 20.8 (vw), 13.7 (w)	3.73 (w), 4.02 (s), 4.43 (vs), 4.68 (m)
EIE100	45.4 (vvs), 22.8 (w), 14.7 (w)	3.92 (s), 4.29 (vs), 4.61 (m)
EIE90:10	44.6 (vvs), 23.5 (w), 14.4 (w)	3.85 (s), 4.29 (vs), 4.61 (m)
EIE80:20	44.6 (vvs), 22.8 (w), 14.3 (w)	3.84 (s), 4.25 (vs), 4.61 (m)
EIE70:30	44.6 (vvs), 23.7 (w), 14.2 (w)	3.84 (s), 4.26 (vs), 4.61 (m)

NIE = noninteresterified; EIE = enzymatically interesterified.

[a] Intensities: v, very; w, weak; m, medium; s, strong.

Copyright 2002 by Marcel Dekker. All Rights Reserved.

are associated with β′ crystals (Larsson, 1966). All samples were combinations of β and β′ crystals. Gradual replacement of butterfat with canola oil increased the relative proportion of β crystals. The presence of canola oil is known to the promote β′-to-β transition (deMan et al., 1995; deMan, 1989). The effect of enzymatic interesterification on butterfat polymorphism was opposite that of chemical interesterification. It has been shown by many (Rousseau et al., 1996b; Timms, 1979; deMan, 1961a) that the β crystal form in butterfat is lost upon chemical interesterification. This is usually explained by the randomization of all fatty acids among all available glycerol-binding sites. With an *sn*-1,3-specific lipase promoting interesterification, however, there was an increase in the proportion of β crystals. This may be interpreted as a loss of mixed crystals present in butterfat (Walstra and Van Beresteyn, 1975; Mulder, 1953). Mixed crystals incorporate disparate fatty acids into an imperfect matrix. Enzymatic interesterification probably removed some of that variety, leading to a more homogeneous crystal network. The changes in proportions of β′ and β crystals were very small for the EIE blends compared to the NIE blends. Long spacings were also examined. Work by Timms (1980) showed that butterfat had long spacings of 42 and 65 Å. Our work showed long spacings of 41.5 ± 1 Å for all NIE blends. Interesterification increased the first-order long spacings by 2–3 Å for all blends. These long spacings correspond to a double-layer TAG structure. deMan (1961b) also examined long spacings and obtained similar data resulting from the chemical interesterification of milkfat. The reason for the increase in long spacings is unclear. What is clear, however, is that the change in long spacings was strictly associated with interesterification. In the range of blends examined, the addition of canola oil did not alter the short or long spacings of the crystalline butterfat. Interesterification altered the long spacings of *all* the interesterified blends similarly, regardless of the proportion of butterfat replaced with oil. The only mention in the literature of the changes observed in long spacings following interesterification is that of Hernqvist et al. (1984), who examined the polymorphic transitions of interesterified blends of triolein, tristearin, and trielaidin and compared them with the behavior of the component TAGs.

If we assume that long spacings are roughly a function of the combined lengths of the fatty acid chains (Bailey, 1950), and knowing that the C—C bond measures ~2.5 Å (Chapman, 1962), then we can assume that the average chain length increases by two carbons, passing from 14 to 16. The change in long spacing may also be due to tilt variations (Kodali et al., 1984). Changes in the tilt of the chain with respect to the endgroup plane can shorten the observed long spacing (Lutton, 1950). It is possible that longer unsaturated fatty acids are replacing shorter saturated fatty acids, leading to a combined effect of chain replacement and tilt.

When all changes in the physical properties are considered together, some interesting trends emerge. Given that there is a slightly higher proportion of β

Copyright 2002 by Marcel Dekker. All Rights Reserved.

crystals in the EIE samples, it may be expected that they would have higher G' or HI values than NIE blends. However, EIE samples also have significantly lower SFCs at 5°C. These effects result in a net decrease in G' and HI.

5. Effects of Enzymatic Interesterification on the Fractality of Butterfat–Canola Oil Blends

The fractal dimension (D) of butterfat–canola oil blends diminished from 2.59 to 2.50 as a result of enzymatic interesterification. This drop in D was smaller than for chemically interesterified butterfat–canola oil blends, where D dropped from 2.46 to 2.15 upon chemical interesterification (CIE). Changes in D are normally attributed to changes in the structure of the solid network (Shih et al., 1990). These results showed a small reduction in D, suggesting only a slight change in the fat crystal network structure. However, a large reduction in SFC was observed. Hence, the large changes observed in storage modulus (G') were likely due to the large reduction in solid fat content (SFC).

C. Effects of Chemical Interesterification on the Physical Properties of Lard–Canola Oil Blends and Palm Oil–Soybean Oil Blends

A study was carried out to evaluate the physical, crystal, and rheological properties of palm oil–soybean oil (POSBO) and lard–canola oil (LCO) systems after blending and chemical interesterification.

1. Effect of Interesterification Duration

Figure 31a shows the changes in 48–54 carbon palm oil (PO) TAG species as a function of CIE duration. Palm oil predominantly consisted of 50- (~40%) and 52-carbon (~36%) (excluding glycerol) TAG species with lesser amounts of 54- (~11%) and 48-carbon (~8%) TAG species. CIE for 30 min led to 6% and 1% decreases in the 50- and 52-carbon TAG species, respectively, and 3% and 4% increases for the 54- and 48-carbon species, respectively. Subsequent CIE did not noticeably alter the PO TAG composition further. Wiedermann (1978) reported that palm oil was a fat that was not much altered by CIE.

Lard consisted primarily (~54%) of 52-carbon TAG species with lesser amounts of 48- (4%), 50- (~16%), and 54-carbon (~25%) TAG species. Interesterification substantially altered lard TAG composition (Fig. 31b). Lard CIE for 1 h and longer periods altered the distribution as follows: C_{48}, +1%, C_{50}, +5%, C_{52}, −12%, and C_{54}, +6%. The TAG evolution of POSBO blends ranging from 90:10 to 60:40 (% w/w) POSBO and LCO are shown in Figures 32 and 33, respectively. POSBO TAG changes were dependent on the proportion of added oil. For example, with the addition of 20% oil (Fig. 32c), CIE led to large in-

Copyright 2002 by Marcel Dekker. All Rights Reserved.

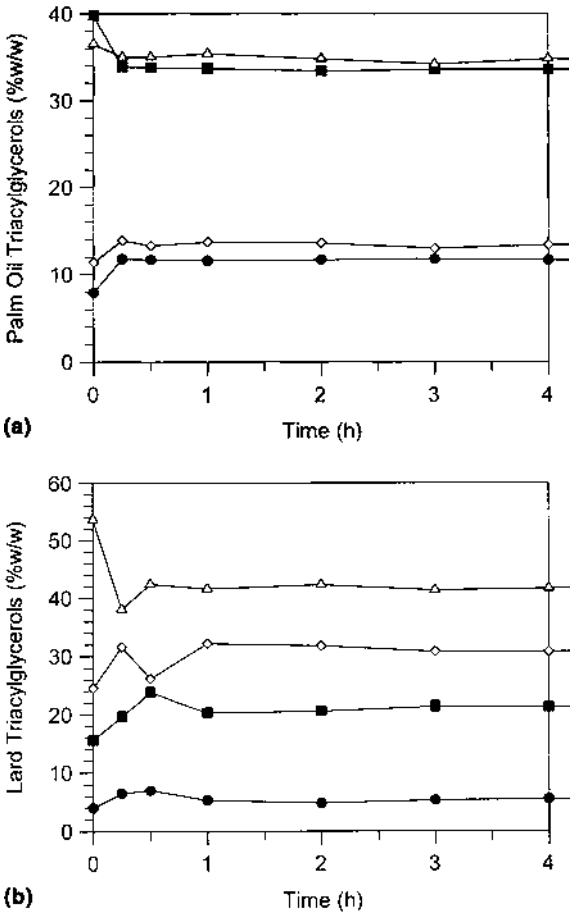

Figure 31 Evolution of TAG species as a function of chemical interesterification duration (minutes). (a) Palm oil; (b) Lard. (●) C_{48} ; (■) C_{50} ; (△) C_{52} ; (◇) C_{54}.

creases of C_{48} and C_{50} TAGs and decreases in C_{52} and C_{54} TAG species. However, addition of 30% or 40% oil (Figs. 32d and 32e), changes in TAG proportions were markedly smaller, with increases in C_{52} TAG species and decreases in C_{48}, C_{50}, and C_{54} species. Observed changes in TAG composition were smaller than those reported in other studies (Al-Rashood et al., 1996).

On the other hand, changes in SFC as a function of interesterification duration for lard are shown in Figure 34. Note that even though TAG modifications stopped after 1 h, the SFC kept dropping for 3–4 h. Similar qualitative trends were observed for samples crystallized for three different time periods. This result highlights the importance of measuring several parameters during interesterifica-

Copyright 2002 by Marcel Dekker. All Rights Reserved.

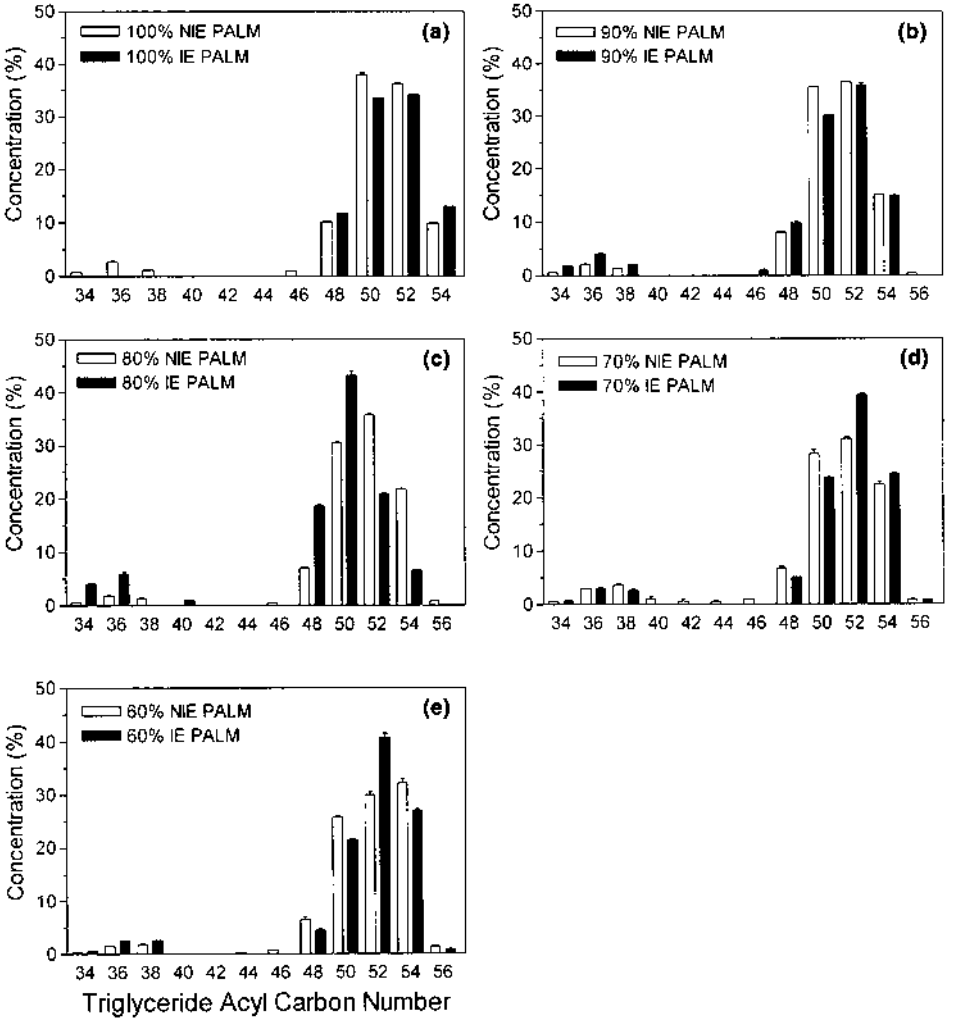

Figure 32 Effect of CIE on the relative TAG proportion (% w/w) for NIE and CIE POSBO blends. (a) 100:0; (b) 90:10; (c) 80:20; (d) 70:30; (e) 60:40.

tion in order to judge whether the desired endpoint of the reaction has been reached. It is curious to note that the opposite effect was observed for butterfat. In that case, the SFC stopped changing after 30 min to 1 h of interesterification, whereas TAG profiles kept on changing for several hours.

It is important to understand compositional modifications through interesterification because the generation of new TAG species can profoundly affect the physical properties of fats (Jakubowski, 1971).

Copyright 2002 by Marcel Dekker. All Rights Reserved.

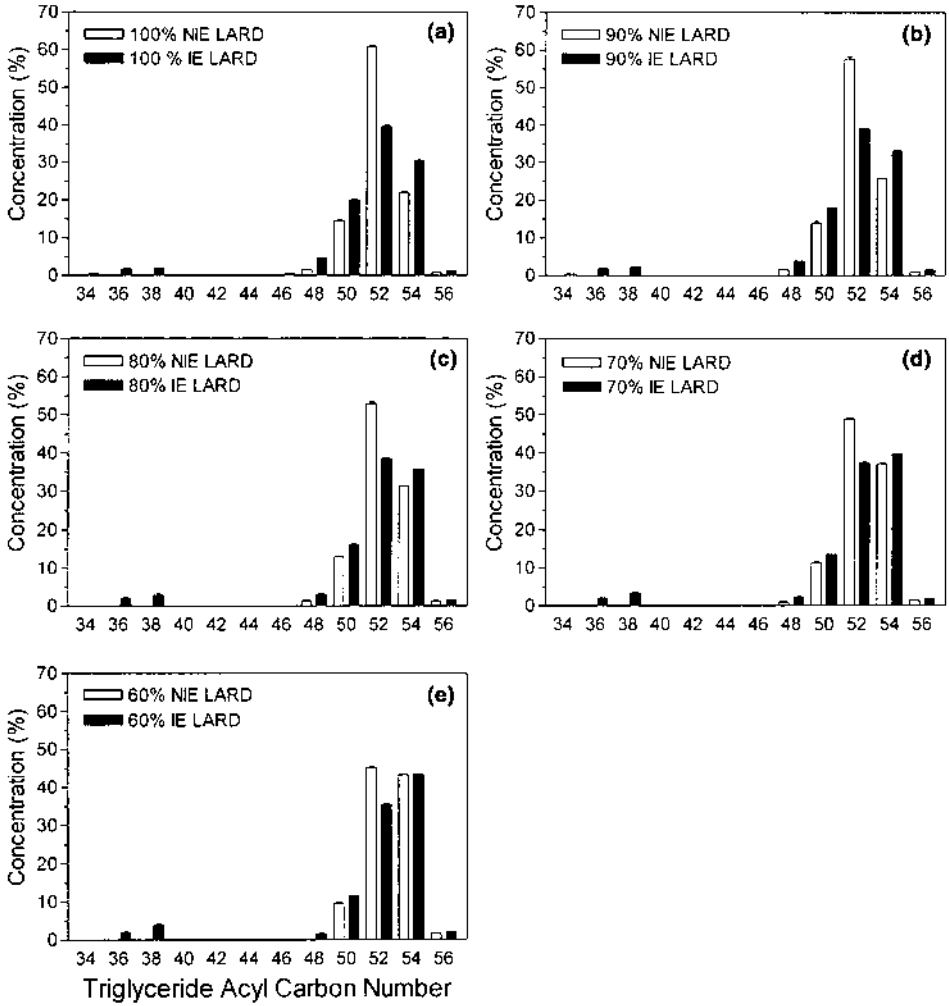

Figure 33 Effect of CIE on the relative TAG proportion (% w/w) for NIE and CIE LCO blends. (a) 100:0; (b) 90:10; (c) 80:20; (d) 70:30; (e) 60:40.

2. Solid Fat Content

The SFC profiles as a function of temperature for NIE and CIE blends of POSBO are shown in Figures 35a and 35b, respectively, and those for NIE and CIE blends of LCO are shown in Figures 36a and 36b, respectively. The SFC profiles of all blends were significantly different from each other ($p < 0.0001$).

Palm oil had an SFC of 68% at 0°C, with a ~30% decrease between 10

Copyright 2002 by Marcel Dekker. All Rights Reserved.

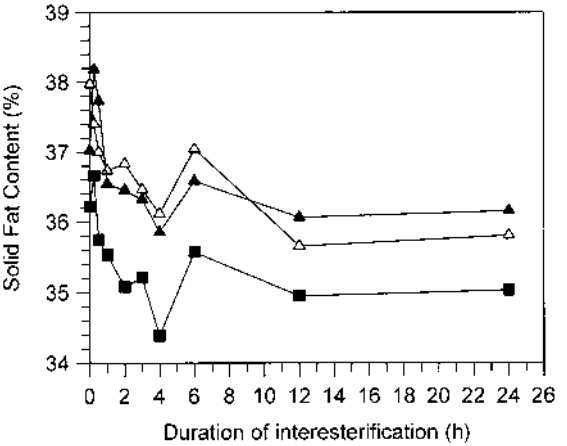

Figure 34 SFC evolution of lard as a function of chemical interesterification duration (minutes). Samples were crystallized for (■) 22 h, (△) 68 h, and (▲) 167 h.

and 20°C (Fig. 35a). Dilution of PO with soybean oil gradually lowered the initial SFC at 0°C, which continued until the end of melt. CIE linearized PO and 90% PO blend melting profiles by lowering SFC at 15°C and increasing it at 20°C, analogous to the behavior of milkfat in response to CIE (Fig. 35b). With 80% or less PO, SFC was lowered from 0°C to end of melt due to CIE.

The SFC of native lard (Fig. 36a) decreased linearly from 0 to 25°C. Dilution with canola oil gradually led to the appearance of two distinct melting zones—0–10°C and 15–25°C—possibly indicating increased intersolubility of the lower melting (0–10°C) TAGs of lard in the canola oil. This may be explained by the greater likelihood of finding unsaturated fatty acids in the lower melting TAGs of lard than in the higher melting TAGs. CIE of lard and lard–canola oil blends led to less linear profiles and narrowed the melting range substantially (Fig. 36b). For example, the SFC of native lard at 25°C was ~20%, whereas that of CIE lard was ~10%. Relative changes in SFC for the POSBO and LCO blends are shown in Figures 37 and 38, respectively. The largest SFC changes occurred for PO and the 90:10 POSBO blend at 5 and 10°C and for all LCO blends at 15–25°C. Others have shown that the physical properties of lard can be substantially altered by CIE (Quimby et al., 1953).

3. TAG Solution Behavior

The isosolid diagrams of NIE and CIE POSBO and LCO (Fig. 39) indicate the monotectic solution behavior, which is prevalent in mixed systems consisting of

Copyright 2002 by Marcel Dekker. All Rights Reserved.

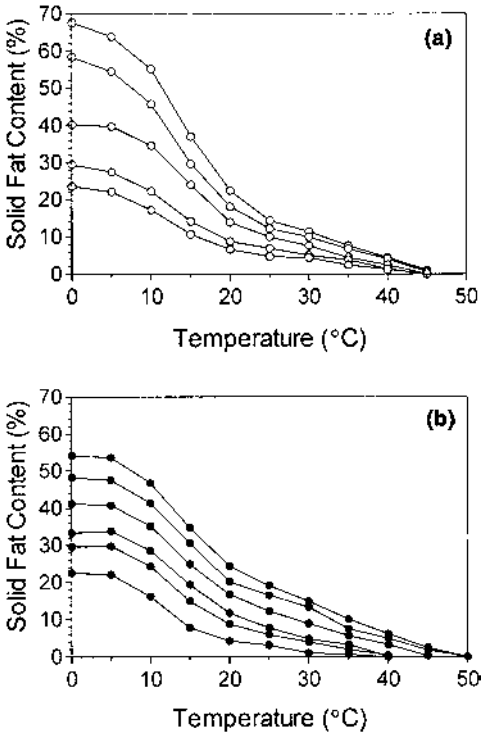

Figure 35 (a) SFC evolution of NIE POSBO blends as a function of temperature (°C). (b) SFC evolution of CIE POSBO blends as a function of temperature (°C).

fats with widely different melting points (Knoester et al., 1968). Monotectic behavior occurs when the higher melting TAGs of a fat are solubilized in the liquid TAG component (Timms, 1984). For example, the lower than expected isosolid temperatures observed for 5% SFC in the POSBO system (Fig. 39a) with increased soybean oil content indicates greater intersolubility of the palm oil in the soybean oil as the proportion of soybean oil is increased. Furthermore, the generally lower temperatures for the CIE blends (both POSBO and LCO) indicate greater solubility of the higher melting TAGs in the liquid following interesterification (Figs. 39b and 39d, respectively). The mixing behavior of PPP and SSS with OOO was discussed by Norton et al. (1985), who also observed changes in solubility.

Our results suggest that TAG intersolubility strongly influences the mechanical properties of the fat crystal network, because there is a substantial lard and PO TAG solubilization in the canola oil and soybean oil, respectively. This

Copyright 2002 by Marcel Dekker. All Rights Reserved.

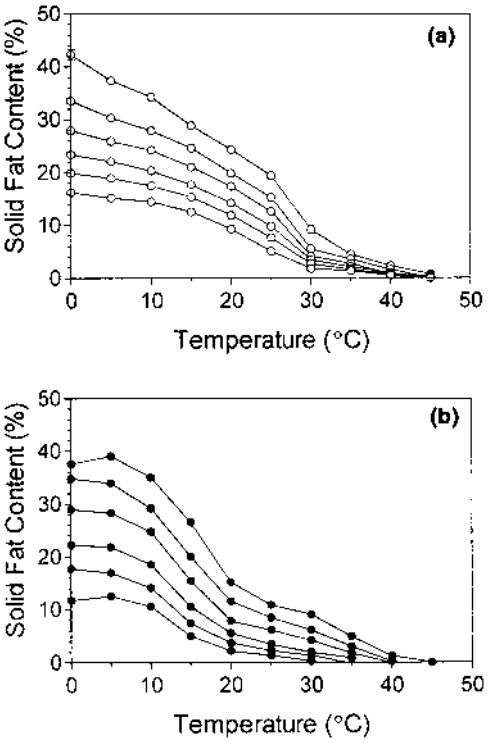

Figure 36 (a) SFC evolution of NIE LCO blends as a function of temperature (°C). (b) SFC evolution of CIE LCO blends as a function of temperature (°C).

solubilization increases relatively as the proportion of oil is increased in the blends, as shown in previous work (Herrera et al., 1992). For example, PO has an SFC of ~68% at 5°C. Assuming negligible PO solubility in SBO, we would predict an SFC of ~34% for a blend containing 50% PO and 50% SBO; however, the measured SFC was ~23%. This decrease in the amount of supersaturation will affect crystallization behavior. The decreased final SFC will also lead to a weaker network and impaired oil-holding capacity.

4. Melting Behavior

Dropping point measurements have traditionally been used to study the melting behavior of fats. Changes in DP in the POSBO and LCO systems are shown in Figures 40a and 40b. The measured DP of PO was 38°C, similar to other studies (deMan and deMan, 1994). CIE increased PO DP by 5.5°C. Others have also

Copyright 2002 by Marcel Dekker. All Rights Reserved.

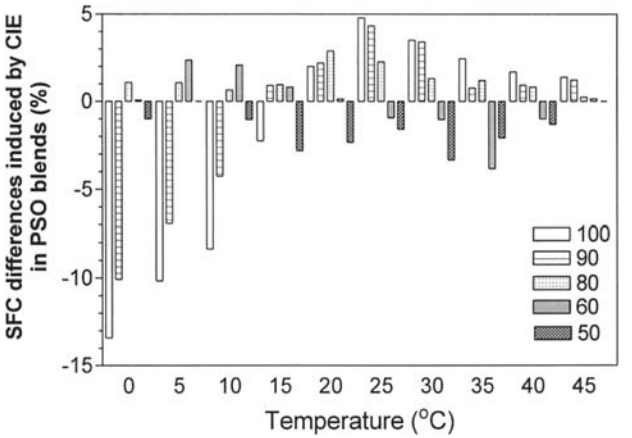

Figure 37 Profile of the effect of chemical interesterification on the SFC of POSBO blends.

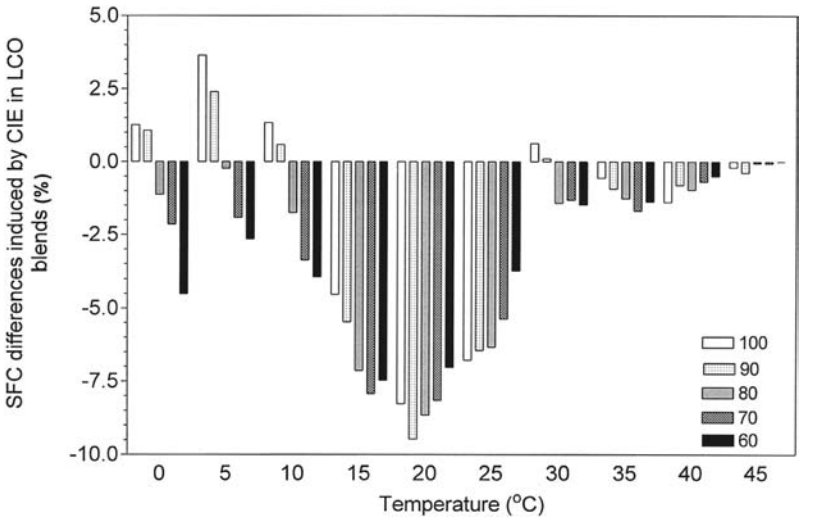

Figure 38 Profile of the effect of chemical interesterification on the SFC of LCO blends.

Copyright 2002 by Marcel Dekker. All Rights Reserved.

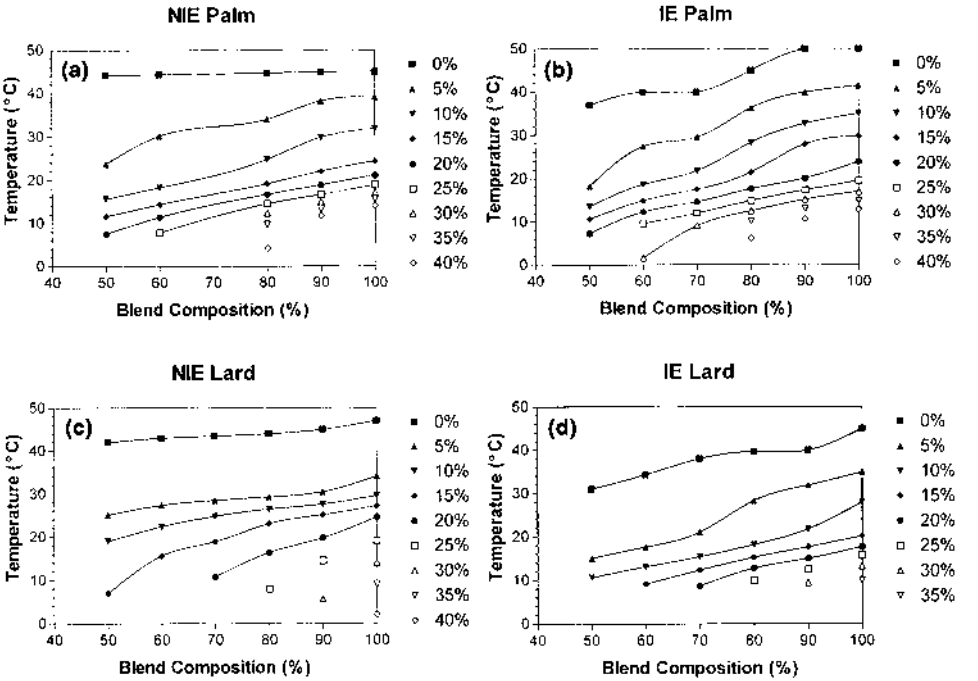

Figure 39 Isosolids lines for POSBO and LCO blends. (a) NIE POSBO; (b) CIE POSBO; (c) NIE LCO; (d) CIE LCO.

found that CIE increased the PO DP (Laning, 1985). CIE POSBO blends with 80% PO had higher DPs and those with 70% had lower DPs than NIE blends. From 100% PO to 50% PO in the blend, there was a 5–6°C drop for NIE blends and an 18°C drop for CIE blends.

The change in DP for PO can be correlated to changes in both SFC and TAG composition. CIE increased the content of 48-carbon species, which are likely trisaturated palmitic acid TAGs, by ~5%. For both POSBO and LCO systems, changes in DP could be correlated to changes in SFC profiles. For example, native PO had a DP of 38°C, which increased to 44°C after CIE. Figures 41a and 41b show the SFC vs. temperature profiles of palm oil and lard, respectively. Note that upon CIE, the SFCs of PO around its DP temperature are higher. This explains the increase in DP for palm oil upon CIE. No differences in SFC were noted for lard upon CIE, in agreement with the absence of change in its DP.

The DPs of NIE and CIE LCO blends were similar, with differences of 0.4–1.6°C between all NIE and CIE equivalents, indicating that CIE did not

Copyright 2002 by Marcel Dekker. All Rights Reserved.

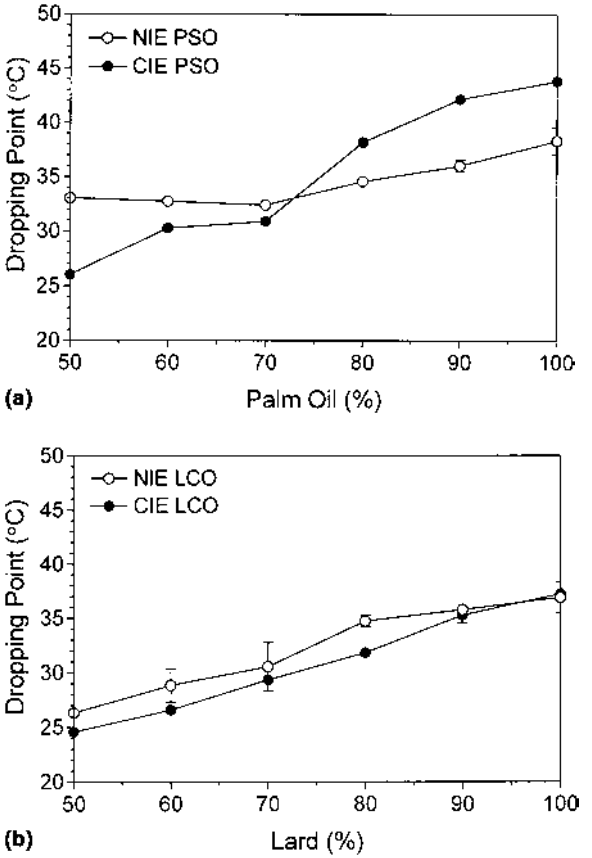

Figure 40 Changes in dropping point (°C) for (a) palm oil–soybean oil blends and (b) land–canola oil blends. Open symbols correspond to NIE blends and solid symbols to CIE blends.

greatly affect lard DP. Luddy et al. (1955) and Kaufmann and Grothues (1960) also found that CIE of lard did not affect its melting point. Incremental dilution of lard with canola oil lowered DPs by 10.5°C for NIE blends and by 12.7°C for CIE blends, again indicating greater lard–CO TAG intersolubility for the CIE blends.

Interesterification leads to partial or total randomization of TAGs present within a fat or fat blend. This randomization produces more similar TAGs, which are then more intersoluble because of their similarity. Hence, it is easier for interesterified fat blends to form solid solutions (mixed crystals). Solid solutions do

Copyright 2002 by Marcel Dekker. All Rights Reserved.

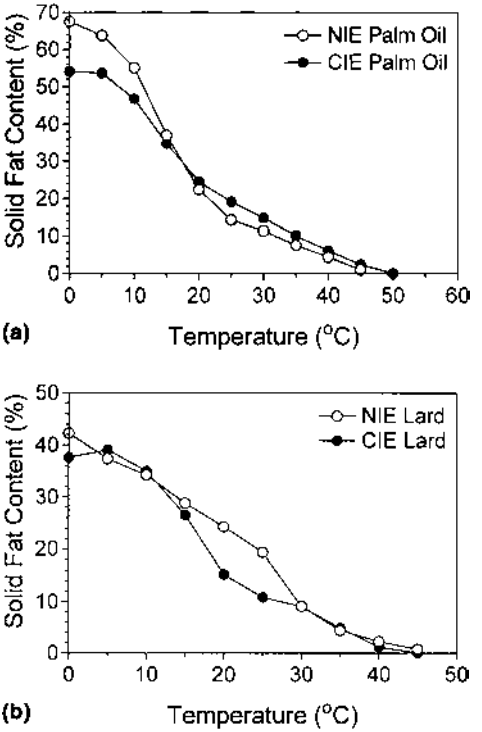

Figure 41 Changes in SFC for (a) palm oil and (b) lard. Open symbols correspond to NIE blends and solid symbols to CIE blends.

not readily form in mixtures of single acid and symmetrical mixed TAGs (Lutton, 1967). The production of more similar crystals leads to lower DPs. As with other systems, the blending of a hardstock with large amounts of oil (30% oil) and subsequent interesterification will lower the DP or melting point (Lo and Handel, 1983).

The changes in DPs in the blends following CIE could not be directly related to the changes in composition. CIE of lard and LCO blends led to greater TAG compositional changes than CIE of PO and POSBO blends but to a smaller difference in DP than for the PO blends. Furthermore, each system was influenced differently by the addition of oil. The POSBO systems underwent only a 5–6°C drop from 100% PO to 50% PO in the blend, whereas lard blend DPs diminished by 9–10°C within the same range. From a solubility standpoint, this indicates that the compatibility of lard with canola oil was greater than that of palm oil with soybean oil because the lard TAGs were more soluble in the oil than the palm oil TAGs.

Copyright 2002 by Marcel Dekker. All Rights Reserved.

Table 5 Effect of Blending and CIE on the Crystallization Peak Temperatures (°C) of POSBO and LCO Blends, as Measured by DSC

Hardstock in blend (% w/w)	Lard–canola oil blends		Palm oil–soybean oil blends	
	NIE (°C)	CIE (°C)	NIE (°C)	CIE (°C)
100	21.4[a,1]	21.2[a,1]	18.3[a,1]	21.9[b,1]
90	18.0[a,2]	22.6[b,1]	18.8[a,1]	21.0[b,1]
80	18.5[a,2]	21.0[b,1]	21.2[a,1]	19.3[b,1]
70	17.1[a,1,2]	15.8[a,2]	18.9[a,1]	20.0[b,1]
60	21.6[a,3]	13.5[b,3]	16.0[a,1]	16.5[a,2]

[a,b] Comparisons between NIE and CIE treatments, separately for each lard and PO blend. Means with the same letter are not significantly different as determined by the protected LSD test ($p > 0.05$).
[1,2,3] Comparisons between blends within a column. Means with the same number are not significantly different as determined by the protected LSD test ($p > 0.05$).

The DP of fats corresponds to an SFC of 3–5%. Studies of water-in-oil emulsions have shown that coalescence of the aqueous phase does not occur with as little as 3–4% SFC (29). Structurally, fats can form a network even at very low SFCs. This behavior was evident in all blends before and after interesterification. This would seem to indicate that a continuous fat crystal network is present and is responsible for much of the solidlike behavior of plastic fats. Without the presence of such a network, DPs would be expected to be much lower.

Table 6 Difference Between Onset and Peak Crystallization Temperatures (ΔT_{o-p}) of NIE and CIE POSBO and LCO Blends

Hardstock in blend (% w/w)	Lard–canola oil blends		Palm oil–soybean oil blends	
	ΔT_{o-p} NIE (°C)	ΔT_{o-p} CIE (°C)	ΔT_{o-p} NIE (°C)	ΔT_{o-p} CIE (°C)
100	1.07[a,1]	2.00[b,1]	0.60[a,1]	1.13[b,1]
90	1.03[a,1]	1.50[b,1]	0.93[a,1]	1.67[a,1]
80	1.03[a,1]	1.70[a,1]	0.93[a,1]	1.37[b,1]
70	0.57[a,1]	1.80[a,1]	1.23[a,1]	0.93[a,1]
60	0.83[a,1]	1.03[a,1]	1.17[a,1]	1.33[a,1]

[a,b] Comparisons between NIE and CIE treatments, separately for each lard and PO blend. Means with the same letter are not significantly different as determined by the protected LSD test ($p > 0.05$).
[1,2] Comparisons between blends within a column. Means with the same number are not significantly different as determined by the protected LSD test ($p > 0.05$).

Copyright 2002 by Marcel Dekker. All Rights Reserved.

5. Crystallization Behavior

Crystallization consists of two steps: nucleation and crystal growth. Modification of a hardstock via blending and/or chemical interesterification can alter the kinetics of both of these processes. LCO blend peak crystallization temperatures decreased with addition of 10% (w/w) CO (Table 5). Further addition of oil did not affect peak crystallization temperature. Interesterification of the LCO blends increased crystallization peak temperatures for the LCO blends with 80% (w/w) and 90% (w/w) lard. Peak temperatures of blends with 60% (w/w) or 70% (w/w) CO decreased relative to their noninteresterified counterparts as a result of CIE. The crystallization peak temperature of pure lard was not affected by CIE (21.4°C vs. 21.2°C)—an unexpected result given the noticeable change in TAG distribution following interesterification. Palm oil crystallization temperatures were generally higher for the interesterified blends than for their noninteresterified counterparts, and was not greatly affected by addition of SBO (Table 5). Variability was observed, though, in all these general trends. Table 6 outlines the differences between crystallization onset and peak temperatures (ΔT_{o-p}) for the NIE and CIE LCO and POSBO blends. This parameter is proportional to the rate of crystal growth. As shown in Table 2, the ΔT_{o-p} are larger for the CIE blends than for the NIE blends in both systems. This effect may be due to the randomization of saturated fatty acids among all TAG species present, potentially leading to increased nucleation and decreased crystallization rates. In terms of crystal packing, the random rearrangement of fatty acids in the TAGs would destroy any structural complementarity among TAGs which would favor crystal growth. Chemical interesterification in both PO and lards results in a kinetically and/or thermodynamically less favorable crystal growth.

6. Polarized Light Microscopy

Figures 42 and 43 show the effects of blending and chemical interesterification on lard fat crystal morphology. PLM examination of native lard (Fig. 42a) shows that it consisted of dense, asymmetrical spherulitic particles and small crystals. Interesterification caused a decrease in the number of spherulites, and low density aggregates of fine crystals were observed instead (Fig. 42b). The grainy texture of native lard is often attributed to the presence of large spherulites, or spherulitic aggregates, and more specifically to the presence of tristearin (Hannewijk, 1972). Many studies have shown that interesterification reduces the spherulitic nature of the native lard crystal structure (Wiedermann et al., 1961; Herb et al., 1956; Hoerr and Waugh, 1950).

Addition of 20% canola oil to lard led to the formation of larger and more highly asymmetrical particles (Fig. 42c). Similar spherulitic size increases have been reported in butterfat–canola oil blends Rousseau et al. (1996b). CIE of the 80% LCO blend led to a reduction in size of the spherulites. Spherulites also

Copyright 2002 by Marcel Dekker. All Rights Reserved.

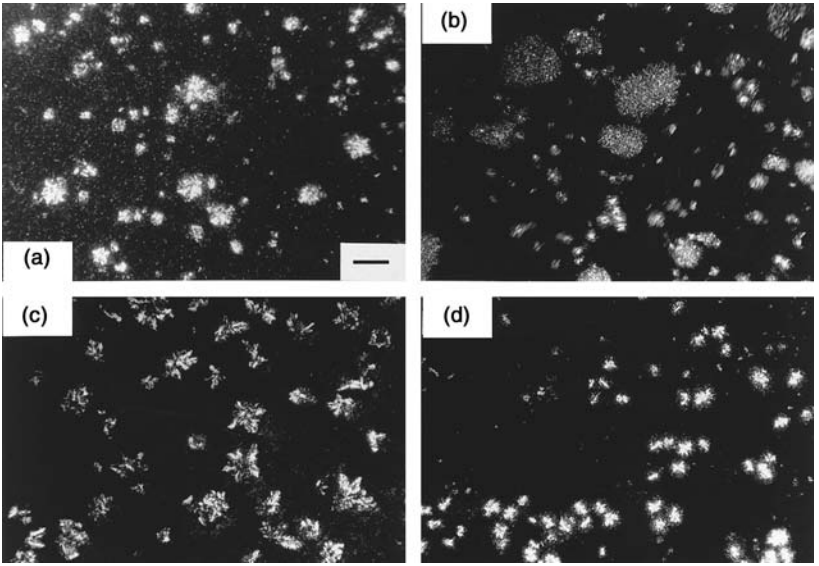

Figure 42 Polarized light microscopic photomicrographs of lard–canola oil blends tempered 24 h at 5°C. (a) NIE lard; (b) CIE lard; (c) NIE80:20; (d) CIE80:20. The bar represents 25 μm.

became more symmetrical, and a distinct high density core surrounded by a lower density halo region became evident (Fig. 42d). Addition of 30% CO resulted in the formation of symmetrical spherulites (Figs. 43a and 43c). CIE led to a further reduction in the size of the spherulites, accompanied by an increase in the halo-to-core ratio within the spherulites (Figs. 43b and 43d). In general, incorporation of canola oil into lard led to a decrease in the size of spherulites, and spherulitic particles became more symmetrical. CIE led to a decrease in the size of the spherulites and to an increase in their halo-to-core ratio. CIE spherulites in lard were also more symmetrical than their NIE counterparts.

Mulder and Walstra (1974) showed that fat crystal morphology can substantially affect rheology. For example, they reported that slowly crystallized milkfat, with an SFC greater than 20%, contained large spherulites and was pourable. On the other hand, acceptable spreads with SFCs of ~10–15% can be manufactured (Chrysam, 1996; deMan et al., 1995). Hence, the formation of the fat crystal network is strongly influenced by the structure of the individual crystals or crystal aggregates (e.g., spherulites).

Palm oil (PO) crystal morphology was not greatly altered by either blending or chemical interesterification (Figs. 44 and 45). Palm oil spherulites were large,

Copyright 2002 by Marcel Dekker. All Rights Reserved.

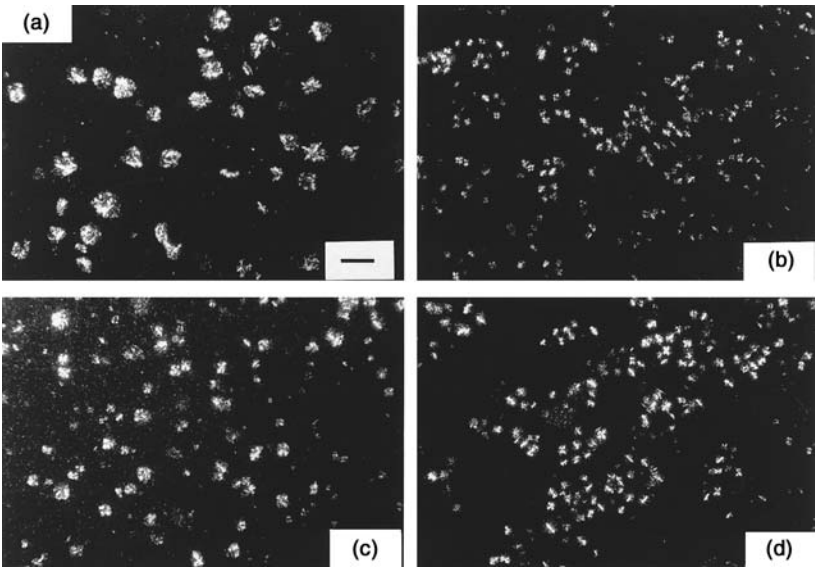

Figure 43 Polarized light microscopic photomicrographs of lard–canola oil blends tempered 24 h at 5°C. (a) NIE70:30; (b) CIE70:30; (c) NIE60:40; (d) CIE60:40. The bar represents 25 μm.

with a dense core and a lower density halo region around the core. As for the LCO blends, incremental addition of soybean oil (SBO) to PO led to a decrease in the size of the spherulites. Interesterification of native PO and POSBO blends did not appear to alter crystal morphology significantly.

Palm oil contains a high proportion of DAGs (~6%) (Goh and Timms, 1985; Siew and Ng, 1995), which influence its crystallization behavior (Jacobsberg and Ho, 1976). Upon storage, PO develops a grainy texture that adversely affects organoleptic properties such as mouthfeel. Watanabe et al. (1992) found that PO granules predominantly consisted of POP (1,3-dipalmitoyl 2-oleoyl glycerol) in the β_1 form with a triple-chain-length structure. The main component of palm oil TAGs is POP, a symmetrical TAG (Okawachi et al., 1985). In a study of the kinetics of palm oil crystallization, Ng (1990) found that the initial nuclei probably consisted of PPP and PPS. It is possible that this small fat fraction dictates the overall crystallization behavior. In complex fat systems, however, it is difficult to establish exactly which TAGs, or other lipid components, dominate the crystallization behavior (Hernqvist et al., 1984).

In the NIE LCO blends, the interfacial boundary between the spherulites and liquid is much sharper than in the NIE POSBO blends, where spherulites

Copyright 2002 by Marcel Dekker. All Rights Reserved.

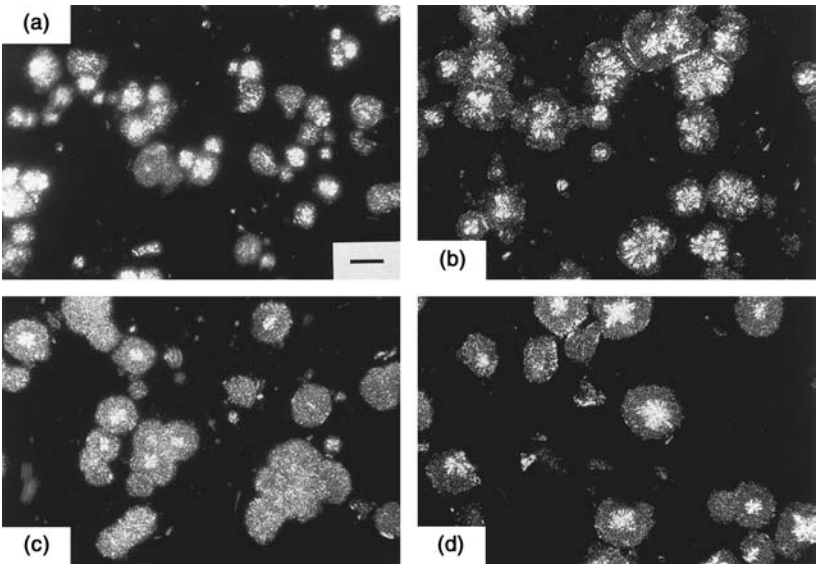

Figure 44 Polarized light microscopic photomicrographs of palm oil–soybean oil blends tempered 24 h at 5°C. (a) NIEPO; (b) CIEPO; (c) NIE90:10; (d) CIE90:10. The bar represents 25 μm.

consist of a dense core surrounded by a lower density halo. The PO and POSBO spherulite boundary can be described as macroscopically diffuse. In practice, most of the available data on crystal growth kinetics strictly consider sharp interfaces (Brice, 1973). This is at a microscopic level, however. Macroscopically, the presence of either sharp (lard) or diffuse (palm oil) interfaces may influence the interaction between spherulitic particles and affect the strength of the three-dimensional crystal network. The presence of greater halo-to-core ratios in the PO and POSBO spherulites relative to lard and LCO spherulites translates into a greater surface area being available for spherulite–spherulite interactions, leading to a stronger network. The hardness indices (HIs) of PO and POSBO blends were much higher than those for lard and LCO blends, corroborating this hypothesis. Further support for this hypothesis comes from the fact that CIE of lard and LCO blends led to the formation of more symmetrical spherulites with higher halo-to-core ratios and the HI of lard and LCO blends increased.

These results suggest that fat crystal networks composed of spherulites with high halo-to-core ratios are stronger than fat crystal networks composed on spherulites with low halo-to-core ratios. A potential strategy for the modification of

Copyright 2002 by Marcel Dekker. All Rights Reserved.

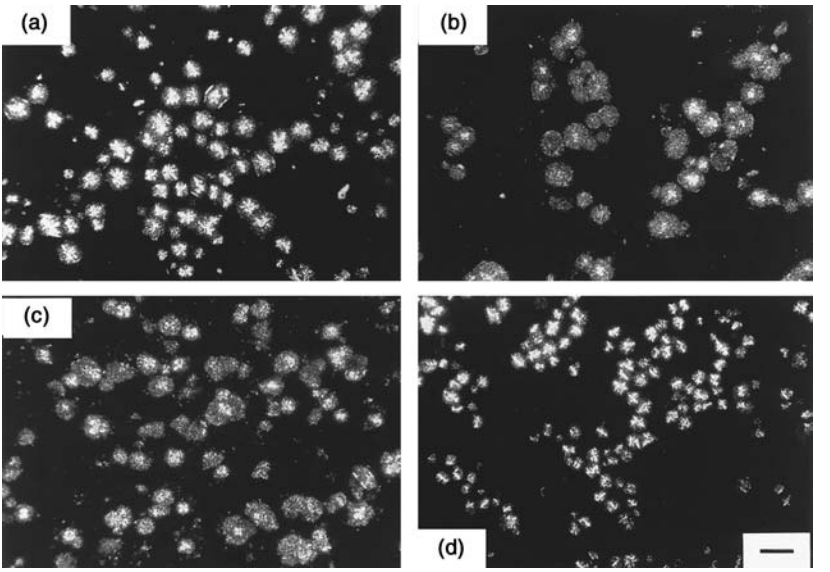

Figure 45 Polarized light microscopic photomicrographs of palm oil–soybean oil blends tempered 24 h at 5°C. (a) NIE70:30; (b) CIE70:30; (c) NIE50:50; (d) CIE50:50. The bar represents 25 μm.

the macroscopic physical properties of fat-containing products could involve alterations in crystal morphology by blending or CIE.

7. Polymorphism

Long and short spacings of the NIE and CIE LCO and POSBO blends were determined by powder X-ray diffraction (XRD). Diffraction patterns of natural fats produce broader peaks than pure compounds (e.g., tristearin) owing to the presence of multiple fatty acid families within the unit cells (Timms, 1980) and the presence of oil. Lard has been reported to be a β-tending fat, whereas PO has been reported to be a β′-tending fat (deMan et al., 1991; Wiedermann, 1978).

Tables 7 and 8 summarize XRD results on short and long spacings of fat crystals in the PO and POSBO blends and in the lard and LCO blends. Short spacing reflections of native PO fat crystals were centered at 4.46 Å with shoulders at 3.92 and 4.30 Å, characteristic of a mixture of β and β′ polymorphs. Rapid cooling of PO results in the formation of β′ crystals, whereas slow cooling at relatively high temperatures, which gives rise to palm stearin, will result pri-

Copyright 2002 by Marcel Dekker. All Rights Reserved.

Table 7 Short and Long Spacings of NIE and CIE POSBO Blends

Blend	Long spacings (Å)	Short spacings (Å)
NIE100	47.7 (vvs), 14.4 (vw)	3.92 (w), 4.30 (m), 4.46 (s)
NIE90	46.8 (vvs), 14.5 (w)	3.90 (m), 4.20 (s)
NIE80	46.8 (vs), 14.4 (w)	3.89 (m), 4.20 (s)
NIE70	46.8 (vs), 14.4 (w)	3.90 (m), 4.20 (s)
CIE100	45.0 (s), 14.3 (vvw)	3.90 (m), 4.22 (m), 4.46 (s)
CIE90	45.0 (vvs), 14.3 (w)	3.82 (m), 4.2 (s), 4.43 (m)
CIE80	41.9 (vs), 13.7 (w)	3.72 (m), 4.10 (s), 4.30 (m)
CIE70	45.0 (vs), 14.5 (w)	3.88 (m), 4.25 (m), 4.47 (s)

POSBO = palm oil–soybean oil.

marily in the crystallization of trisaturated TAGs and hence in the formation of β crystals. The formation of β crystals is promoted by the presence of trisaturates (e.g., PPP, SSS) containing fatty acids of similar chain lengths.

Upon dilution of PO with SBO, β polymorphs disappeared (Table 9). CIE PO and CIE POSBO blends contained mixtures of both polymorphs. Hence, we conclude that CIE induced the formation of β polymorphs in PO and POSBO systems. Long spacings were not altered upon dilution of PO with SBO (Table 7). However, CIE led to an approximately 2 Å decrease in long spacings in PO and POSBO blends. These results were in agreement with short spacing results, which suggested the CIE-induced transformation of some of the fat crystals to the β form. A transformation to a β form can be accompanied by a decrease in long spacings. This effect was observed in our study of PO and POSBO blends.

In our study, lard fat crystals were mainly β′-tending (Table 9). Incremental

Table 8 Short and Long Spacings of NIE and CIE LCO Blends

Blend	Long spacings (Å)	Short spacings (Å)
NIE100	44.5 (vvs), 22.7 (vw), 14.4 (w)	4.08 (m), 4.41 (s), 4.64 (vw)
NIE90	44.5 (vs), 35.7 (s), 22.7 (vw), 14.3 (w)	4.02 (m), 4.35 (s), 4.63 (m)
NIE80	44.5 (vs), 35.7 (s), 22.7 (vw), 14.1 (w)	4.01 (m), 4.39 (s), 4.66 (m)
NIE70	44.5 (vs), 35.7 (s), 22.7 (vw), 13.6 (w)	4.00 (m), 4.36 (m), 4.65 (m)
CIE100	39.9 (vvs), 13.6 (w)	3.84 (s), 4.17 (m), 4.44 (vs), 5.15 (mw)
CIE90	39.6 (vs), 14.2 (w)	3.80 (m), 4.19 (s), 4.42 (m)
CIE80	40.2 (vs), 14.1 (w)	3.78 (w), 4.21 (m), 4.43 (m)
CIE70	39.0 (vs), 13.8 (w)	3.80 (w), 4.21 (m), 4.40 (m)

LCO = lard–canola oil.

Copyright 2002 by Marcel Dekker. All Rights Reserved.

Table 9 Polymorphs of Palm Oil–Soybean Oil and Lard–Canola Oil Blends

	Lard–canola oil blends		Palm oil–soybean oil blends	
Blend	NIE	CIE	NIE	CIE
100	$\beta' \ggg \beta$	$\beta > \beta'$	$\beta' = \beta$	$\beta > \beta'$
90	$\beta' \gg \beta$	$\beta' > \beta$	β'	$\beta' > \beta$
80	$\beta' > \beta$	$\beta' = \beta$	β'	β'
70	$\beta' = \beta$	$\beta' = \beta$	β'	$\beta > \beta'$

addition of vegetable oil led to an increased presence of β crystals, and CIE led to an increase in the proportion of β polymorphs in all blends. NIE lard crystals had long spacings of 44.5 Å, whereas the crystals in the LCO blends with 10–30% canola oil had long spacings of 35.7 and 44.5 Å. The 44.5 Å spacing corresponds to a double-layer structure, and similar first-order long spacings have been observed in the past (Lutton, 1962; Wiedermann et al., 1961). The 35 Å spacing could correspond to the triclinic unit cell of an 18-carbon TAG bilayer tilted at 53.3° (Kodali et al., 1984). This is surprisingly close to the tilt observed for an oleic acid bilayer triclinic unit cell (56.3°). Another plausible explanation could be that addition of Canola oil induced the formation of triple-chain unit cells in lard fat crystals, which has been observed in the past (Lutton, 1962; Wiedermann et al., 1961). In both cases, addition of canola would have decreased system viscosity, permitting the crystallizing TAGs to adopt a more thermodynamically favorable conformation.

Chemical interesterification of lard and LCO blends caused a large change in long spacings (Tables 7 and 8). Only a single reflection at ~40 Å was observed after CIE. Lutton (1962) reported that hydrogenation or interesterification alone did not remove the triple structure of the unit cells of lard fat crystals but that a combination of the two did. In double-layer structures, the odd-order long spacings are much stronger than the even-order long spacings (Chapman, 1962), and such behavior has been observed in lard (Lutton, 1962) and simple TAGs (Gibon et al., 1986). In triple-layer structures, the first-order spacing can be absent (Fahey et al., 1985). Lutton (1962) reported that only the Second- and Fifth-order reflections of a triple-layer structure were detected in lard fat crystals. We observed this effect in our work as well. Singleton (1955) explained this effect as acyl chains butting end to end, leading to a decrease in electron density between the layers.

As shown by deMan and deMan (1994) and others (Desmedt et al., 1990; Gray et al., 1976), the more a fat is diluted with liquid oil, the more likely it is that β-crystal polymorphs will form. This was generally the case in both fat systems.

Copyright 2002 by Marcel Dekker. All Rights Reserved.

Table 10 Cone Penetrometry Penetrating Cone Assembly Characteristics Used for Determining the Hardness Index of Lard–Canola Oil Blends and Palm Oil–Soybean Oil Blends

Characteristic	Palm oil–soybean oil blends	Lard–canola oil blends
Cone weight (g)	45	57.7
Cone angle (°)	10	30
K factor	42,970	9670

Lutton (1945) reported on the progressive decrease in long spacings of some saturated monoacid TAG crystals, where, generally, a 1–2 Å decrease was associated with a β′-to-β polymorph transformation. In the systems examined, a slight decrease in long spacings with increasing dilution was observed in NIE POSBO and CIE LCO. The CIE POSBO and NIE LCO systems, however, did not exhibit changes in long spacings as a function of dilution.

8. Hardness

The hardness index (HI) of a fat can be directly correlated to its yield stress. A different cone was used for the analysis of each system, because each fat had large differences in penetration depths. For direct comparison of the penetration depths, a conversion factor was determined:

$$K_f = \frac{\text{weight}_{\text{cone}_{\text{palm}}} K_{\text{palm}}}{\text{weight}_{\text{cone}_{\text{lard}}} K_{\text{lard}}}$$

where K_{palm} and K_{lard} are constants based on cone angle, established by Haighton (1959). Cone characteristics are shown in Table 10.

A modified version of the equation developed by Hayakawa and deMan (1982) was used to convert the penetration data into hardness index (HI):

$$HI = K_f \left(\frac{\text{mass of cone(g)}}{\text{depth of penetration(mm)}} \right) \times 0.1$$

The HI of both POSBO and LCO blends gradually decreased as the proportion of canola oil in the mixture increased ($p < 0.0001$) (Fig. 46). Upon CIE, the HIs of the POSBO blends were largely unaffected by CIE ($p > 0.05$), whereas for the LCO blends the HIs increased significantly ($p < 0.0001$). All HIs are

Copyright 2002 by Marcel Dekker. All Rights Reserved.

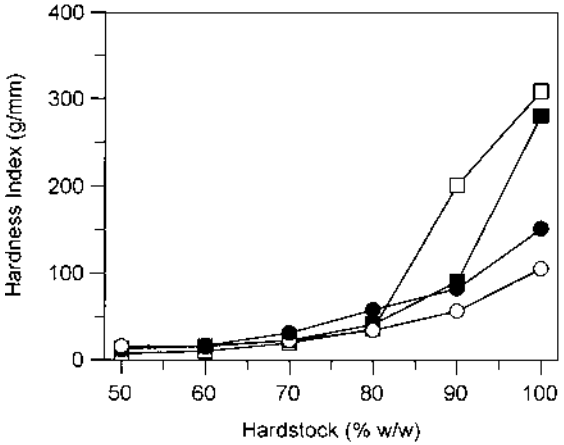

Figure 46 Hardness index (g/mm) of palm oil–soybean and lard–canola oil blends as a function of amount of hardstock present (% w/w). (□) POSBO NIE blends; (■) POSBO IE blends; (○) LCO NIE blends; (●) LCO CIE blends.

reported as a function of SFC; therefore, any changes in hardness index induced by CIE are due to non-SFC-related factors.

The crystal habit (polymorphism and morphology) of CIE lard crystals differed substantially from that of native lard, as shown earlier. Differences in crystal habit and aggregation behavior could have led to an alteration in the structure of the fat crystal network in lard and resulted in altered rheological properties such as HI. Examination of margarines by Stern and Cmolik (1976) showed that rheological properties depended partially on the shape and amount of fat crystals. The observed changes in the crystal habit of lard shown earlier could be responsible for the diverse effects observed in this study.

9. Viscoelastic Properties

Viscoelasticity studies provide valuable data that can be correlated with fat crystal network structure. Parameters derived from such studies include the storage (solidlike or elastic) modulus (G') and the loss (liquidlike or viscous) modulus (G'') (Davis, 1973). Small-deformation measurements take place below a critical value of deformation (yield point). In plastic fats, G' is substantially higher than G'' (Rousseau et al., 1996c; Drake et al., 1994).

Spectra of PO showed a decrease in G' of 23% as a result of CIE (Fig. 47). Blends with 60–90% PO saw their G'' increase by 5–77% due to CIE. The

Copyright 2002 by Marcel Dekker. All Rights Reserved.

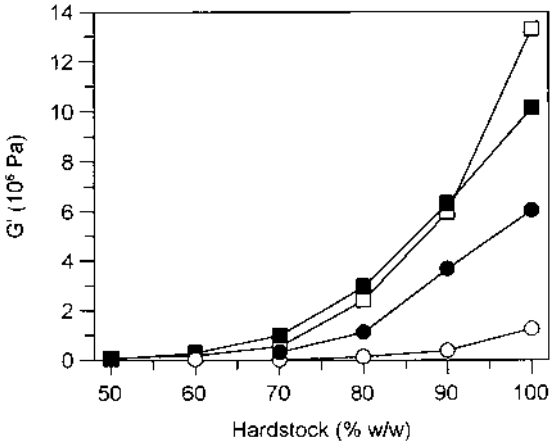

Figure 47 Elastic modulus, G' (Pa), of palm oil–soybean oil and lard–canola oil blends as a function of amount of hardstock present (% w/w). (□) POSBO NIE blends; (■), POSBO IE blends; (○) LCO NIE blends; (●) LCO CIE blends.

50/50 POSBO blend G'' decreased 32%. A nonlinear response of G' vs. SFC was observed.

Lard viscoelastic behavior was different from that of PO (Fig. 47). The G′ values of all lard blends increased as a result of CIE and also displayed a nonlinear response with blend SFC. Cornily and Le Meste (1985) studied the flow behavior of lard and of its fractions at 15°C and attempted to establish relationships between thermal, compositional, and rheological behavior.

10. Fractal Geometry

The effects of chemical interesterification on the fractal dimension (D) of LCO and POSBO blends were examined. A power law relationship between the elastic modulus and the solid fat content for NIE and CIE blends (at 5°C) was established:

$$G' = \gamma(\text{SFC})^m$$

where m represents the slope used to derive the fractal dimension, and the constant γ, we propose, represents an undefined element representing the effect of crystal habit (morphology and polymorphism) on the mechanical properties of the particles that make up the network, e.g., the spherulites. This concept is borrowed from Bremer et al.'s (1990) study of acid casein gels. The fractal dimension D can be established within either the strong-link or weak-link regime, where

Copyright 2002 by Marcel Dekker. All Rights Reserved.

the latter generally applies to high-SFC systems and the former to low-SFC systems. According to the relationship between the strain at the limit of linearity (γ_0) and the SFC, it is possible to define the regime: γ_0 increases for weak-link regimes and decreases for strong-link regimes.

The fractal dimensions of palm oil ($D = 2.82$) and lard ($D = 2.86$) did not change upon chemical interesterification. However, the factor γ, which is related to properties of the particles that make up the network (Bremer et al., 1990), increased four fold in the CIE LCO system. The factor γ did not, however, change in the POSBO system. This means that the spatial distribution of mass is not affected by CIE in these fats. Rather, it is the properties of the particles that make up the network that play a key role. The factor γ increased four fold in lard upon CIE. Polarized light microscopic results showed a stark alteration in crystal size and shape following interesterification of lard. In addition, large changes were observed in the long spacings, as noted earlier. Examination of the PLM crystal morphology in the POSBO system showed little variation in the spherulitic structure. No drastic changes in polymorphic behavior were observed either.

Therefore, it would seem that the rheological properties of palm oil and lard-based fats are controlled predominantly by the properties of the particles that make up the network (*i.e.*, the spherulites), which are influenced by crystal habit (morphology and polymorphism). In contrast, the rheological properties of butterfat are influenced by both the spatial distribution of the fat crystals in the network and the properties of the particles that make up the network (as noted in the CIE butterfat section).

REFERENCES

Adlercreutz, P. (1991). On the importance of the support material for enzymatic synthesis in organic media. Eur J Biochem 199:609–614.

Akoh, CC, BH Jennings, DA Lillard. (1995). Enzymatic modification of trilinolein: Incorporation of n−3 polyunsaturated fatty acids. J Am Oil Chem Soc 72:1317–1321.

Al-Duri, B, E Robinson, S McNerlan, P Bailie. (1995). Hydrolysis of edible oils by lipases immobilized on hydrophobic supports: Effects of internal support structure. J Am Oil Chem Soc 72:1351–1359.

Al-Rashood, KA, RRA Abou-Shaaban, EM Abdel-Moety, A Rauf. (1996). Compositional and thermal characterization of genuine and randomized lard: a comparative study. J Am Oil Chem Soc 73:303–309.

Bailey, AE. (1950). Melting and Solidification of Fats. New York: Interscience.

Becker, E. (1959). Der Einfluss der Umesterung auf das Kristallizationsverhaltern von Fetten bzw. Fettmischungen. Fette, Seifen, Anstrichtm 61:1040–1046.

Benzonana, G, P Desnuelle. (1965). Étude cinétique de l'action de la lipase pancréatique

Copyright 2002 by Marcel Dekker. All Rights Reserved.

sur des triglycérides enémulsion. Essai d'une enzymologie en milieu hétérogène. Biochim Biophys Acta 105:121–136.
Birker, PJMWL, FB Padley. (1987). Physical properties of fats and oils. In: RJ Hamilton, A Bhati, eds. Recent Advances in Chemistry and Technology of Fats and Oils. New York: Elsevier.
Boistelle, R. (1988). Fundamentals of nucleation and crystal growth. In: N Garti, K Sato, eds. Crystallization and Polymorphism of Fats and Fatty Acids. New York: Marcel Dekker, pp 189–226.
Bornaz, S, J Fanni, M Parmentier. (1994). Limit on the solid fat modification of butter. J Am Oil Chem Soc 71:1373–1380.
Borwankar, RP, GS Buliga. (1990) Emulsion properties of margarines and lowfat spreads. Am Inst Chem Eng Symp Ser 86:44–52.
Borwankar, RP, LA Frye, AE Blaurock, FJ Sasevich. (1992). Rheological characterization of melting of margarines and tablespreads. J Food Eng 16:55–74.
Brady, L, AM Brzozowski, ZS Derewenda, E Dodson, G Dodson, S Tolley, JP Turkenburg, L Christiansen, B Huge-Jensen, L Norskov, L Thim, U Menge. (1990). A serine protease triad forms the catalytic centre of a triglyceride lipase. Nature (Lond) 343:767–770.
Bremer, LGB, BH Bijsterbosch, R Schrijvers, T van Vliet, P Walstra. (1990). On the fractal nature of the structure of casein gels. Colloids Surf 51:159–170.
Brice, JC. (1973). The Growth of Crystals from Liquids. New York: American Elsevier Publishing Co., Inc., pp 79–127.
Brockerhoff, H, RG Jensen. (1974). Lipolytic Enzymes. New York: Academic Press.
Brockman, HL. (1984). General features of lipolysis: Reaction scheme, interfacial structure and experimental approaches. In: B Borgström, HL Brockman, eds. Lipases. Amsterdam: Elsevier Science, pp 3–46.
Chapman, D. (1962). The polymorphism of glycerides. Chem Rev 62:433–456.
Chapman, D. (1965). X-ray diffraction studies. In: The Structure of Lipids by Spectroscopic and X-ray Techniques. New York: Wiley, pp 221–315.
Chrysam, MM. (1996). Margarines and spreads. In: YH Yui, ed. Bailey's Industrial Oil and Fat Products, Vol. 3, 5th edition. Toronto: John Wiley and Sons, pp 65–114.
Coenen, JWE. (1974). Fractionnement et interestérification des corps gras dans la perspective du marché mondial des matières premières et des produits finis. II. Interestérification. Rev franç corps gras 21:403–413.
Cornily, G, M Le Meste. (1985). Flow behaviour of lard and of its fractions at 15C. Relationship with thermal behaviour and chemical composition. J Texture Stud 16:383–402.
D'Souza, V, JM deMan, L deMan. (1990). Short spacings and polymorphic forms of natural fats and commercial solid fats: A review. J Am Oil Chem Soc 67:835–843.
Dabulis, K, AM Klibanov. (1992). Other macromolecules resulting in new adsorbents. Biotechnol Bioeng 39:176–185.
Davis, SS. (1973). Rheological properties of semi-solid foodstuffs. J Texture Stud 4:15–40.
Deffense, E. (1993). Milk fat fractionation today: A review. J Am Oil Chem Soc 70:1193–1201.

Copyright 2002 by Marcel Dekker. All Rights Reserved.

deMan, L, JM deMan, B Blackman. (1995). Effect of tempering on the texture and polymorphic behavior of margarine fats. Fat Sci Technol 97:55–60.
deMan, L, JM deMan. (1994). Functionality of palm oil, palm oil products and palm kernel oil in margarine and shortening. PORIM Occ Paper, Palm Oil Res Inst Malaysia No 32.
deMan, JM. (1992). X-ray diffraction spectroscopy in the study of fat polymorphism. Food Res Int 25:471–476.
deMan, L, CF Shen, JM deMan. (1991). Composition, physical and textural characteristics of soft (tub) margarines. J Am Oil Chem Soc 68:70–73.
deMan, L. (1989). Polymorphic behavior of some fully hydrogenated oils and their mixture with liquid oil. J Amer Oil Chem Soc 66:1777–1788.
deMan, JM, AM Beers. (1987). Fat crystal networks: Structure and rheological properties. J Texture Stud 18:303–318.
deMan, JM. (1983). Consistency of fats: A review. J Am Oil Chem Soc 60:6–11.
deMan, JM, L deMan, B Blackman. (1983). Melting-point determination of fat products. J Am Oil Chem Soc 60:91–94.
deMan, JM. (1964a). Physical properties of milk fat. J Dairy Sci 47:1194–1200.
deMan, JM. (1964b). Effect of cooling procedures on consistency, crystal structure and solid fat content of milk fat. Dairy Ind 29:546–548.
deMan, JM. (1961a). Physical properties of milk fat. I. Influence of chemical modification. J Dairy Res 28:81–86.
deMan, JM. (1961b). Physical properties of milk fat. II. Some factors influencing crystallization. J Dairy Res 28:117–123.
de Renobales, M, I Agud, JM Lascaray, JC Múgica, LC Landeta, R Solozábal. (1992). Hydrolysis of animal fats by lipase at temperature below their melting points. Biotechnol Lett 14:683–688.
Derewenda, ZS, AM Sharp. (1993). News from the interface: The molecular structure of triacylglyceride lipases. Trends in Biochemical Sciences 18:20–25.
Derewenda, ZS, U Derewenda, GG Dodson. (1992). The crystal and molecular structure of the Rhizomucor miehei triacylglyceride lipase at 1.9 Å resolution. J Mol Biol 227:818–839.
Desmedt, A, C Culot, C Deroanne, F Durant, V Gibson. (1990). Influence of *cis* and *trans* double bonds on the thermal and structural properties of monoacid triglycerides. J Am Oil Chem Soc 67:653–660.
Drake, MA, L Ma, BG Swanson, GV Barbosa-Cánovas. (1994). Rheological characteristics of milkfat and milkfat-blend sucrose polyesters. Food Res Int 27:477–481.
Eckey, EW. (1948). Directed interesterification of glycerides. Ind Eng Chem 40:1183–1190.
Elliott, JM, KL Parkin. (1991). Lipase-mediated acyl-exchange reactions with butteroil in anhydrous media. J Am Oil Chem Soc 68:171–175.
Fahey, DA, DM Small, DR Kodali, D Atkinson, TG Redgrave. (1985). Structure and polymorphism of 1,2-dioleoyl-3-acyl-*sn*-glycerols. Three- and six-layered structures. Biochem 24:3757–3764.
Ferry, JD. (1970). Viscoelastic Properties of Polymers. New York: Wiley.
Feuge, RO. (1962). Derivatives of fats for use as foods. J Am Oil Chem Soc 39:521–527.

Copyright 2002 by Marcel Dekker. All Rights Reserved.

Foglia, TA, K Petruso, SH Feairheller. (1993). Enzymatic interesterification of tallow–sunflower oil mixtures. J Am Oil Chem Soc 70:281–285.
Foley, J, JP Brady. (1984). Temperature-induced effects on crystallization behaviour, solid fat content and the firmness values of milkfat. J Dairy Res 51:579–589.
Freeman, IP. (1968). Interesterification. I. Change of glyceride composition during the course of interesterification. J Am Oil Chem Soc 45:456–460.
Garcia, HS, CH Amundson, CG Hill Jr. (1991). Partial characterization of the action of an Aspergillus niger lipase on butteroil emulsions. J Food Sci 56:1233–1237.
Garcia, HS, FX Malcata, CG Hill, CH Amundson. (1992). Use of Candida rugosa lipase immobilized in a spiral wound membrane reactor for the hydrolysis of milkfat. Enz Microb Technol 14:535–545.
Garcia, HS, B Yang, KL Parkin. (1996). Continuous reactor for enzymatic glycerolysis of butteroil in the absence of solvent. Food Res Int 28:605–609.
Gibon, V, F Durant, CI Deroanne. (1986). Polymorphism and intersolubility of some palmitic, stearic and oleic triglycerides: PPP, PSP and POP. J Am Oil Chem Soc 63: 1047–1055.
Goderis, HL, G Ampe, MP Feyten, BL Gouwe, WM Guffnes, SM van Canwenbergh, PP Toback. (1987). Lipase-catalyzed ester exchange reactions in organic media with controlled humidity. Biotechnol Bioeng 30:258–266.
Goh, EM, RE Timms. (1985). Determination of mono- and diglycerides in palm oil, olein and stearin. J Am Oil Chem Soc 62:730–734.
Going, LH. (1967). Interesterification products and processes. J Am Oil Chem Soc 44: 414A–422A, 454A–456A.
Gorman, LAS, JS Dordick. (1992). Organic solvents strip water off enzymes. Biotechnol Bioeng 39:392–397.
Gray, MS, NV Lovegren, RO Feuge. (1976). Effect of 2-oleodipalmitin and 2-elaidopalmitin on polymorphic behavior of cocoa butter. J Am Oil Chem Soc 53:727–731.
Gunstone, FD, JL Harwood. (1994). Synthesis. In: FD Gunstone, JL Harwood, FB Padley, eds. The Lipid Handbook. 2nd ed. London: Chapman and Hall, pp 359–399.
Haighton, AJ. (1959). The measurement of the hardness of margarine and fats with cone penetrometers. J Am Oil Chem Soc 36:345–348.
Haighton, AJ. (1976). Blending, chilling and tempering of margarines and shortenings. J Am Oil Chem Soc 53:397–399.
Halling, PJ. (1994). Thermodynamic predictions for biocatalysis in nonconventional media: Theory, tests, and recommendations for experimental design and analysis. Enz Microb Technol 16:178–206.
Hannewijk, MJ. (1972). L'utilisation du saindoux et du suif dans l'alimentation humaine. Rev franç corps gras. 19:677–685.
Haraldsson, GG, BÖ Gudmundsson, Ö Almarsson. (1993). The preparation of homogeneous triglycerides of eicosapentanoic acid and docosahexanoic acid by lipase. Tetrahedron Lett 34:5791–5794.
Haumann, B. (1994). Tools: Hydrogenation, interesterification. INFORM 5:668–674.
Hayakawa, M, JM deMan. (1982). Interpretation of cone penetrometer consistency measurements of fats. J Texture Stud 13:201–210.
Herb, SF, MC Audsley, RW Riemenschneider. (1956). Some observations on the microscopy of lard and rearranged lard. J Am Oil Chem Soc 33:189–193.

Copyright 2002 by Marcel Dekker. All Rights Reserved.

Hernqvist, L, B Herslöf, M Herslöf. (1984). Polymorphism of interesterified triglycerides and triglyceride mixtures. Fette, Seifen, Anstrichtm 86:393–397.
Herrera, ML, JA Segura, GJ Rivarola, MC Añon. (1992). Relationship between cooling rate and crystallization behavior of hydrogenated sunflower-seed oil. J Am Oil Chem Soc 69:898–907.
Hildebrand, JH, RL Scott. (1962). Regular Solutions. Englewod Cliffs, NJ: Prentice-Hall.
Hoerr, GW, DF Waugh. (1950). Some physical characteristics of rearranged lard. J Am Oil Chem Soc 32:37–41.
Huang, K-h, CC Akoh. (1994). Lipase-catalyzed incorporation of n−3 polyunsaturated fatty acids into vegetable oils. J Am Oil Chem Soc 71:1277–1280.
Hustedt, HH. (1976). Interesterification of edible oils. J Am Oil Chem Soc 53:390–392.
Jacobsberg, B, OC Ho. (1976). Studies in palm oil crystallization. J Am Oil Chem Soc 53:609–617.
Jakubowski, A. (1971). L'interestérification entre corps gras animaux et huiles végétales. Rev franç corps gras 18:429–437.
Jandacek, RJ, MR Webb. (1978). Physical properties of pure sucrose octaesters. Chem Phys Lipids 22:163–176.
Jensen, LH, AJ Mabis. (1963). Crystal structure of β-tricaprin. Nature 197:681–682.
Jensen, RG, J Sampugna, JG Quinn, DL Carpenter, TA Marks, JA Alfords. (1965). Specificity of a lipase from Geotrichum candidum for cis-octadecanoic acid. J Am Oil Chem Soc 42:1029–1035.
Jensen, RG, FA Dejong, RM Clark. (1983). Determination of lipase specificity. Lipids 18:239–252.
Jensen, RG, AM Ferris, CJ Lammi-Keefe. (1991). Symposium: Milkfat—composition, function and potential for change. J Dairy Sci 74:3228–3243.
Jewell, GG, ML Meara. (1970). A new and rapid method for the electron microscopic examination of fats. J Am Oil Chem Soc 47:535–538.
Joly, F, J-P Lang. (1978). Interestérification des corps gras. Mise au point de travaux sur les corps gras animaux. Rev franç corps gras 25:423–429.
Kalo, P. (1988). Modification of butter fat by interesterifications catalysed by Aspergillus niger and Mucor miehei lipases. Meijeritiet Aikak 66:36–47.
Kalo, P, P Parviainen, K Vaara, S Ali-Yrrkö, M Antila. (1986a). Changes in the triglyceride composition of butter fat induced by lipase and sodium methoxide catalysed interesterification reactions. Milchwissenschaft 41:82–85.
Kalo, P, K Vaara, M Antila. (1986b). Changes in triglyceride composition and melting properties of butter fat fraction/rapeseed oil mixtures induced by lipase catalysed interesterification. Fette, Seifen, Anstrichtm 88:362–365.
Kalo, P, A Kemppinen, M Antila. (1987a). Lipase- and sodium methoxide-catalysed interesterification in the modification of Finnish fats. Meijeritiet Aika 66:36–47.
Kalo, P, A Kemppinen, M Antila. (1987b). Candida cylindracae lipase-catalyzed interesterification of butter fat. In: TH Applewhite, ed. Proceedings—World Conference on Biotechnology for the Fats and Oils Industry. Champaign, IL: Am Oil Chem Soc, pp 323–327.
Kalo, P, H Huotari, M Antila. (1989a). Chemical composition of butter fat interesterified

Copyright 2002 by Marcel Dekker. All Rights Reserved.

with Pseudomonas fluorescens lipase at various temperatures. Meijeritiet Aikak 48: 29–38.
Kalo, P, H Huotari, M Antila. (1989b). Pseudomonas fluorescens lipase-catalysed interesterification of butter fat. Fat Sci Technol 91:276–281.
Kalo, P, H Huorati, M Antila. (1990). Pseudomonas fluorescens lipase-catalysed interesterification of butter fat in the absence of a solvent. Milchwissenschaft 45:281–285.
Kang, ST, JS Rhee. (1989). Characteristics of immobilized lipase-catalyzed hydrolysis of olive oil of high concentration in reverse phase system. Biotechnol Bioeng 33: 1469–1476.
Kaufmann, HP, B Grothues. (1959). Umesterungen auf dem Fettgebiet. III. Über den Einfluss verschiedener Umesterungs-Katalysoren auf ungesättigte Fettsäuren. Fette, Seifen, Anstrichtm 61:425–429.
Kaufmann, HP, B Grothues. (1960). Umesterungen auf dem Fettgebiet IV: Tropfpunktsänderungen bei der Ein- und Mehrfett-Umesterung. Fette, Seifen, Anstrichtm 62: 489–495.
Kaufmann, HP, F Grandel, B Grothues. (1958). Umesterungen auf dem Fettgebiet I: Theoretische Grundlagen und Schriftum; die Hydrier-Umesterung. Fette, Seifen, Anstrichtm 60:919–930.
Kellens, M, W Meeussen, H Reynaers. (1992). Study of the polymorphism and the crystallization kinetics of tripalmitin: A microscopic approach. J Am Oil Chem Soc 69: 906–911.
Kilara, A. (1985). Enzyme-modified lipid food ingredients. Proc Biochem 20:35–45.
Knoester, M, P de Bruyne, M van den Tempel. (1968). Crystallization of triglycerides at low supercooling. J Crystal Growth 3:776–780.
Kodali, DR, D Atkinson, TR Redgrave, DM Small. (1984). Synthesis and polymorphism of 1,2-dipalmitoyl-3-acyl-sn-glycerols. J Am Oil Chem Soc 61:1078–1084.
Kokini, JL, GJ Plutchok. (1987). Viscoelastic properties of semisolid foods and their biopolymeric component. Food Technol 40:89–95.
Konishi, H, WE Neff, TL Mounts. (1993). Chemical interesterfication with regioselectivity for edible oils. J Am Oil Chem Soc 70:411–415.
Kosugi, Y, N Azuma. (1994a). Continuous and consecutive conversion of free fatty acid in rice bran oil to triacylglycerol using immobilized lipase. Appl Microb Biotechnol 41:407–412.
Kosugi, Y, N Azuma. (1994b). Synthesis of triacylglycerol from polyunsaturated fatty acid by immobilized lipase. J Am Oil Chem Soc 71:1397–1403.
Kuksis, A, L Marai, JJ Myher. (1973). Triglyceride structure of milk fats. J Am Oil Chem Soc 50:193–201.
Laning, SJ. (1985). Chemical interesterification of palm, palm kernel and coconut oils. J Am Oil Chem Soc 62:400–405.
Larsson, K. (1966). Classification of glyceride crystal forms. Acta Chem Scand 20:2255–2260.
Larsson, K. (1994). Molecular arrangements in glycerides. Fette Seifen Anstrichtm 74: 136–142.
Lazar, G, K Henkel. (1985). Estersynthesen mit Lipasen. Fette, Seifen, Anstrichtm 87: 394–400.

Copyright 2002 by Marcel Dekker. All Rights Reserved.

Lefèbvre, J. (1983). Finished product formulation. J Am Oil Chem Soc 60:295–300.
List, GR, TL Mounts, F Orthoefer, WE Neff. (1995). Margarine and shortening oils by interesterification of liquid and trisaturated triglycerides. J Am Oil Chem Soc 72: 379–382.
Lo, YC, AD Handel. (1983). Physical and chemical properties of randomly interesterified blends of soybean oil and tallow for use as margarine oils. J Am Oil Chem Soc 60:815–818.
Luddy, FE, SG Morris, P Magidman, RW Riemenschneider. (1955). Effect of catalytic treatment with sodium methylate on glycerine composition and properties of lard and tallow. J Am Oil Chem Soc 32:522–525.
Lutton, ES. (1945). The polymorphism of tristearin and some of its homologues. J Am Oil Chem Soc 67:524–527.
Lutton, ES. (1950). Review of the polymorphism of saturated even glycerides. J Am Oil Chem Soc 27:276–281.
Lutton, ES. (1962). Interesterification of lard. J Am Oil Chem Soc 359:233–235.
Lutton, ES. (1967). Binary systems from palmitic-stearic triglycerides. J Am Oil Chem Soc 44:303–304.
Lutton, ES. (1972). Lipid structures. J Am Oil Chem Soc 49:1–9.
Lutton, ES, MF Mallery, J Burgers. (1962). Interesterification of lard. J Am Oil Chem Soc 39:233–238.
Macrae, AR. (1983). Lipase-catalyzed interesterification of oils and fats. J Am Oil Chem Soc 60:291–294.
McNeill, GP, PE Sonnet. (1995). Isolation of erucic acid from rapeseed oil by lipase-catalyzed hydrolysis. J Am Oil Chem Soc 72:213–217.
Macrae, AR. (1985). Enzyme-catalysed modification oils and fats. Phil Trans Roy Soc Lond B310:227–233.
Makhlouf, J, J Arul, A Boudreau, P Verret, MR Sahasrabudhe. (1987). Fractionnement de la matière grasse laitière par cristallisation simple et son utilisation dans la fabrication de beurres mous. Can Inst Food Sci Technol J 20:236–245.
Malcata, FX, HR Reyes, HS Garcia, CG Hill Jr, CH Amundson. (1990). Immobilized lipase reactors for modifications of fats and oils: A review. J Am Oil Chem Soc 67:890–910.
Malcata, FX, HR Reyes, HR Garcia, CG Hill Jr. CH Amundson. (1992). Kinetics and mechanisms of reactions catalysed by immobilized enzymes. Enz Microb Technol 14:426–446.
Mandelbrot, BB. (1982). The Fractal Geometry of Nature. New York: WH Freeman.
Marangoni, AG, D Rousseau. (1995). Engineering triacylglycerols: The role of interesterification. Trends Food Sci Technol 6:329–335.
Michaelis, L, ML Menten. (1913). Die Kinetik der Invertinwirkung. Biochem Z 49:333–369.
Mickle, JB. (1960). Flavor problems in rearranged milkfat. J Dairy Sci 43:436–437.
Mickle, JB, RL von Gunten, RD Morrison. (1963). Rearrangement of milkfat as a means for adjusting hardness of butterlike products. J Dairy Sci 46:1357–1361.
Monot, F, E Paccard, F Borzeix, M Bardin, JP Vandercasteele. (1993). Effect of lipase conditioning on its activity in organic media. Appl Microbiol Biotechnol 39:483–486.

Copyright 2002 by Marcel Dekker. All Rights Reserved.

Mukherjee, KD. (1992). Gewinnung wertvoller Lipide mit Hilfe enzymatischer Reaktionen. Fat Sci Technol 94:542–545.
Mulder, H. (1953). Melting and solidification of milkfat. Neth Milk Dairy J 7:149–174.
Mulder, H, P Walstra. (1974). The Milk Fat Globule. Wageningen, The Netherlands: Centre for Agricultural Publishing and Documentation.
Naudet, M. (1976). Interestérification et estérification. Mécanismes réactionnels et conséquences sur la structure. Rev franç corps gras 23:387–391.
Nawar, WW. (1996). Lipids. In: OR Fennema, ed. Food Chemistry. 3rd ed. New York: Marcel Dekker, pp 225–319.
Nielsen, T. (1985). Industrial application possibilities for lipase. Fette, Seifen, Anstrichtm 87:15–19.
Norton, IT, CD Lee-Tuffnell, S Ablett, SM Bociek. (1985). A calorimetric, NMR and X-ray diffraction study of the melting behavior of tripalmitin and tristearin and their mixing behavior with triolein. J Am Oil Chem Soc 62:1237–1244.
Oba, T, B Wilholt. (1994). Interesterification of milk fat with oleic acid catalyzed by immobilized Rhizopus oryzae lipase. J Dairy Sci 77:1790–1797.
Okawachi, T, N Sagi, H Mori. (1985). Confectionary fats form palm oil. J Am Oil Chem Soc 62:421–425.
Parodi, PW. (1979). Relationship between trisaturated glyceride composition and the softening point of milk fat. J Dairy Res 46:633–639.
Precht, D, W Buchheim. (1980). Elektronenmikroskopische Untersuchungen über die physikalische Struktur von Streichfetten. II: Die Mikrostruktur des zwischenglobularen Fettphase in Butter. Milchwissenschaft 35:393–398.
Quimby, OT, RL Wille, ES Lutton. (1953). On the glyceride composition of animal fats. J Am Oil Chem Soc 30:186–190.
Quinlan, P, S Moore. (1993). Modification of triglycerides by lipases: Process technology and its application to the production of nutritionally improved fats. INFORM 4: 580–585.
Reyes, HR, CG Hill Jr, CH Amundson. (1994). Interesterification reactions catalyzed by a lipase immobilized on a hydrophobic support. J Food Process Pres 18:119–132.
Rohm, H. (1993). Rheological behaviour of butter at large deformations. Milchwissenschaft 24:139–155.
Rohm, H, K-H Weidinger. (1993). Rheological behaviour of butter at small deformations. J Texture Stud 24:157–172.
Rossell, JB. (1967). In: R Padetti, D Kritchevsky, eds. Advances in Lipid Research. New York: Academic Press, pp 353–408.
Rousseau, D, AG Marangoni. (1998). Tailoring the textural attributes of butterfat-canola oil blends via *Rhizopus arrhizus* lipase-catalyzed interesterification I. Compositional modifications. J Agric Food Chem 46:2368–2374.
Rousseau, D, AG Marangoni. (1998). Tailoring the textural attributes of butterfat-canola oil blends via *Rhizopus arrhizus* lipase-catalyzed interesterification II. Modification of physical properties. J Agric Food Chem 46:2375–2381.
Rousseau, D, K Forestière, AR Hill, AG Marangoni. (1996a). Restructuring butter fat through blending and chemical interesterification. 1. Melting behavior and triacylglycerol modifications. J Am Oil Chem Soc 73:963–972.
Rousseau, D, AR Hill, AG Marangoni. (1996b). Restructuring butter fat through blending

Copyright 2002 by Marcel Dekker. All Rights Reserved.

and chemical interesterification. 2. Morphology and polymorphism. J Am Oil Chem Soc 73:973–981.
Rousseau, D, AR Hill, AG Marangoni. (1996c). Restructuring butter fat through blending and chemical interesterification. 3. Rheology. J Am Oil Chem Soc 73:983–989.
Rozenaal, A. (1992). Interesterification of fats. INFORM 3:1237–1236.
Sato, K. (1988). Crystallization of fats and fatty acids. In: N Garti, K Sato, eds. Crystallization and Polymorphism of Fats and Fatty Acids. New York: Marcel Dekker, pp 227–263.
Segel, IH. (1976). Biochemical Calculations. 2nd ed. Toronto: Wiley.
Shih, WH, WY Shih, SI Kim, J Liu, IA Aksay. (1990). Scaling behavior of the elastic properties of colloidal gels. Phys Rev A 42:4772–4779.
Shukla, A, SSH Rizvi. (1995). Viscoelastic properties of butter. J Food Sci 60:902–905.
Siew, W-L, W-L Ng. (1995). Partition coefficient of diglycerides in crystallization of palm oil. J Am Oil Chem Soc 72:591–595.
Simoneau, C, P Fairley, JM Krochta, JB German. (1994). Thermal behavior of butter fat fractions and mixtures of tripalmitin and butter fat. J Am Oil Chem Soc 71:795–801.
Singleton, WS. (1955). X-ray spectroscopy. J Am Oil Chem Soc 32:612–615.
Smith, RE, JW Finley, GA Leveille. (1994). Overview of SALATRIM, a family of low-calorie fats. J Agric Food Chem 42:432–434.
Sonntag, NOV. (1982). Glycerolysis of fats and methyl esters: Status, review and critique. J Am Oil Chem Soc 59:795A–802A.
Sreenivasan, B. (1978). Interesterification of fats. J Am Oil Chem Soc 55:796–805.
Stern, P, J Cmolik. (1976). Study of rheological properties of margarine. J Am Oil Chem Soc 53:644–647.
Täufel, K, C Franzke, M Achtzehn. (1958). Über die Umestrung unter Acyl-Austausch bei natürlichen Fetten und gehärteten Fetten sowie bei Fett-Mischungen. Fette, Seifen, Anstrichtm 60:456–461.
Tempel, M van den. (1961). Mechanical properties of plastic disperse systems at very small deformations. J Colloid Sci 16:284–296.
Tempel, M van den. (1979). Rheology of concentrated suspensions. J Colloid Interface Sci 71:18–20.
Tilbeurgh, H van, L Sarda R Verger, C Cambillau. (1992). Structure of the pancreatic lipase-procolipase complex. Nature 359:159–162.
Timms, RE. (1978). The solubility of milk fat, fully hardened milk fat and milk fat hard fractions in liquid oils. Aust J Dairy Technol 33:130–135.
Timms, RE. (1979). The physical properties of blends of milk fat with beef tallow and beef tallow fractions. Aust J Dairy Technol 34:60–65.
Timms, RE. (1980). The phase behaviour and polymorphism of milk fat, milk fat fractions and fully hardened milk fat. Aust J Dairy Tech 35:47–53.
Timms, RE. (1984). Phase behavior of fats and their mixtures. Prog Lipid Res 23:1–38.
Timms, RE. (1985). Physical properties of oils and mixtures of oils. J Am Oil Chem Soc 62:241–249.
Timms, RE, JV Parekh. (1980). The possibilities for using hydrogenated, fractionated or interesterified milk fat in chocolate. Lebensm Wiss Technol 13:177–182.
Tombs, MP. (1990). Biotechnology in the Food Industry. Buckingham: Open Univ Press.

Copyright 2002 by Marcel Dekker. All Rights Reserved.

Toschev, S. (1973). Homogeneous nucleation. In: P Hartman, ed. Crystal Growth: An Introduction. New York: American Elsevier, pp 1–49.
Tsujisaka, Y, S Okumura, M Iwai. (1977). Glyceride synthesis by four kinds of microbial lipase. Biochim Biophys Acta 489:415–422.
Vollhardt, KPC. (1987). Organic Chemistry. New York: WH Freeman.
Vreeker, R, LL Hoekstra, DC den Boer, WGM Agterof. (1992). The fractal nature of fat crystal networks. Colloids Surf 65:185–189.
Walstra, P, R Jenness. (1984). Dairy Chemistry and Physics. New York: Wiley.
Walstra, P, ECH van Beresteyn. (1975). Additional evidence for the presence of mixed crystals in milk fat. Neth Milk Dairy J 29:238–241.
Watanabe, A, I Tashima, N Matsuzaki, J Kurashige, K Sato. (1992). On the formation of granular crystals in fat blends containing palm oil. J Am Oil Chem Soc 69:1077–1080.
Weihe, HD. (1961). Interesterified butter oil. J Dairy Sci 44:944–947.
Weihe, HD. GR Greenbank. (1958). Properties of interesterified butter oil. J Dairy Sci 41:703.
Weiss, TJ, GA Jacobson, LH Wiedermann. (1961). Reaction mechanics of sodium methoxide treatment of lard. J Am Oil Chem Soc 38:396–399.
Wiedermann, LH. (1978). Margarine and margarine oil, formulation and control. J Am Oil Chem Soc 55:823–829.
Wiedermann, LH, TJ Weiss, GA Jacobson, KF Mattil. (1961). A comparison of sodium methoxide treated lards. J Am Oil Chem Soc 38:389–395.
Winkler, FK, A D'Arcy, W Hunziker. (1990). Structure of human pancreatic lipase. Nature 343:771–774.
Woodrow, IL, JM deMan. (1961). Polymorphism in milk fat shown by X-ray diffraction and infrared spectroscopy. J Dairy Sci 51:996–1000.
Yamane, T. (1987). Enzyme technology for the lipids industry: An engineering overview. J Am Oil Chem Soc 64:1657–1662.
Yamane, T, T Suzuki, Y Sahashi, L Vikersveen, T Hoshino. (1992). Production of n−3 polyunsaturated fatty acid-enriched fish oil by lipase-catalyzed acidolysis without solvent. J Am Oil Chem Soc 69:1104–1107.
Zaks, A, AM Klibanov. (1984). Enzymatic catalysis in organic media at 100°C. Science 224:1249–1251.
Zaks, A, AM Klibanov. (1988). The effect of water on enzyme action in organic media. J Biol Chem 263:8017–8021.

Copyright 2002 by Marcel Dekker. All Rights Reserved.